

December 2018

Inducible DNA Cross-Linking Agents: Design, Synthesis, Mechanism, and Anticancer Activity

Heli FAN

University of Wisconsin-Milwaukee

Follow this and additional works at: <https://dc.uwm.edu/etd>

 Part of the [Toxicology Commons](#)

Recommended Citation

FAN, Heli, "Inducible DNA Cross-Linking Agents: Design, Synthesis, Mechanism, and Anticancer Activity" (2018). *Theses and Dissertations*. 1986.

<https://dc.uwm.edu/etd/1986>

This Dissertation is brought to you for free and open access by UWM Digital Commons. It has been accepted for inclusion in Theses and Dissertations by an authorized administrator of UWM Digital Commons. For more information, please contact open-access@uwm.edu.

INDUCIBLE DNA CROSS-LINKING AGENTS: DESIGN, SYNTHESIS, MECHANISM,
AND ANTICANCER ACTIVITY

by

Heli Fan

A Dissertation Submitted in
Partial Fulfillment of the
Requirements for the Degree of

Doctor of Philosophy
in Chemistry

at

The University of Wisconsin-Milwaukee

December 2018

ABSTRACT

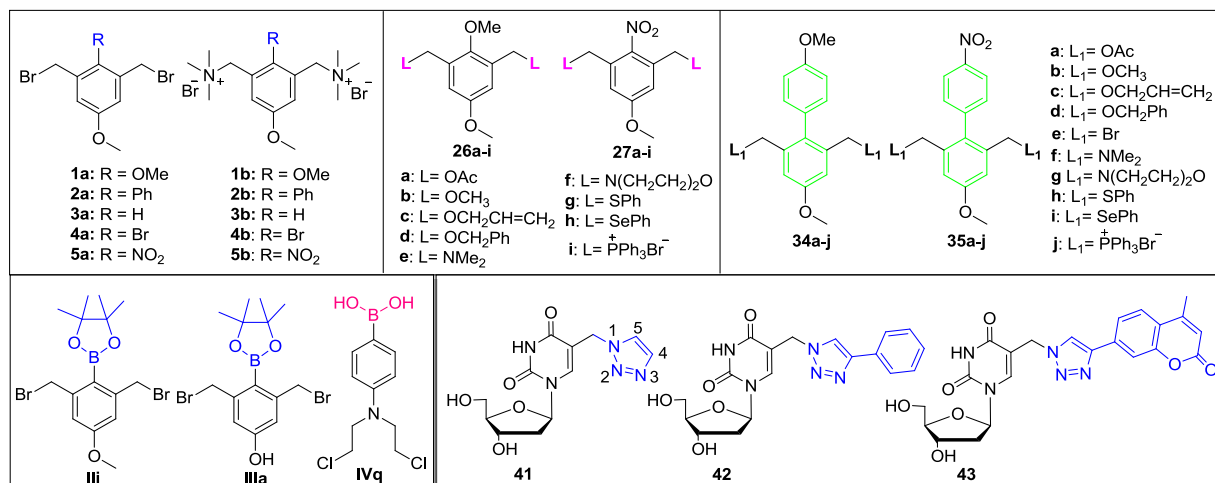
INDUCIBLE DNA CROSS-LINKING AGENTS: DESIGN, SYNTHESIS, MECHANISM, AND ANTICANCER ACTIVITY

by

Heli Fan

The University of Wisconsin-Milwaukee, 2018
Under the Supervision of Professor Xiaohua Peng

This thesis focuses on investigating the reactivity of DNA towards a wide variety of aromatic compounds as novel DNA cross-linking agents and exploring their biomedical applications.



In the first part, we synthesized three series of bifunctional aromatic compounds with various core structures, aromatic substituents, and benzylic leaving groups and investigated their reactivity towards DNA. Most of these compounds efficiently form DNA interstrand cross-links (ICLs) via carbocations generated upon irradiation at 350 nm. The efficiency of DNA ICL formation and the pathway of carbocation formation strongly depend on core structures, aromatic substituents and leaving groups. Mono benzene analogues bearing an electron donating substituent showed higher DNA cross-linking efficiency than those with an electron withdrawing

substituent while an opposite trend was observed for the biphenyl compounds. In most cases the carbocations were generated through oxidation of the corresponding benzyl radicals. However, photo irradiation of the ammonium salt **5b** generated the carbocation via direct heterolysis of the C-N bond. Surprisingly, both path ways were observed for compound **4b**.

The second part is *in vivo* efficacy study of H₂O₂-activated quinone methide (**III**, **IIIa**) and nitrogen mustard (**IVq**) precursors. Compounds **III** and **IIIa** inhibited the tumor growth in nude mice xenografted with MDA-MB-468 breast cancer cells without obvious toxicity, such as no weight loss and other unusual behaviors, while they were less effective towards renal cancer cells. Compound **IVq** greatly shrank the tumor size in nude mice xenografted with MDA-MB-468.

The third part focused on investigating the influences of triazole-moieties and the substituents at the position-4 of triazole ring on the thermal stability of DNA duplexes by testing the melting temperature of the DNA•DNA and DNA•RNA duplexes containing triazole-modified thymidines (**41-43**). The introduction of triazole-modified thymidines decreased the stability of DNA•DNA and DNA•RNA duplexes. Bulky substituent at the position-4 of triazole ring further destabilized DNA duplex possibly due to steric hindrance interfering with efficient Watson-Crick base-pair formation. Due to noncoplanar conformation between substituents and thymine groups, two or three consecutive modifications further destabilized the DNA duplex even in the presence of efficient π -stacking induced by modified-triazole moieties.

TABLE OF CONTENTS

Abstract	ii
Table of Contents	iv
List of Figures	vii
List of Tables	xi
List of Schemes	xii
List of Abbreviations	xv
Acknowledgements	xvii
1. Introduction	1
1.1. The Structure and Functions of DNA	1
1.2. DNA Alkylation and Commonly Used Chemotherapeutic Agents	2
1.3. Inducible DNA Interstrand Cross-linking Agents	10
1.3.1. Photo-induced DNA ICLs via Three Mechanisms.....	10
Photo-induced DNA ICL formation via [2+2] cycloaddition reaction	10
Photo-induced DNA cross-linking via quinone methide formation	15
Photo-induced DNA cross-linking via carbon cation formation	18
1.3.2. DNA Interstrand Cross-linking Induced by Chemical Agents.....	23
Fluoride Inducible DNA Cross-linking Agents	23
NaIO ₄ or ¹ O ₂ Inducible DNA Cross-linking Agents.....	26
NBS Inducible DNA Cross-linking Agents	28
H ₂ O ₂ Inducible DNA Cross-linking Agents	29
1.4. References.....	35
2. The Effects of Substituents on Photochemical Generation of Benzyl Cations and DNA Cross-linking	43
2.1. Introduction	43
2.2. Bifunctional Benzylic Derivatives as Photo-inducible DNA Cross-linking Agents	46
2.2.1. Synthesis of Compounds with Various Substituents.....	46
2.2.2. Preparation of DNA Duplex	49
2.2.3. DNA Interstrand Cross-linking Assay	52
2.2.4. Correlation Between UV Absorbance and The Photo-reactivity	60
2.2.5. Correlation Between Heterolytic Cleavage Energy and The Photo-reactivity	62
2.2.6. Mechanism of DNA ICL Formation and Substituent Effects	63
2.2.7. Determination of DNA Alkylation Sites and Alkylation Products ..	69
2.2.8. Conclusions	74

2.3. Experimental Section.....	75
2.4. References	88
3. Substituents and Benzylic Leaving Groups Have a Large Effect on Photo-Induced DNA Cross-linking.....	93
3.1. Introduction.....	93
3.2. Synthesis of Compounds with Various Leaving Groups.....	94
3.3. DNA Interstrand Cross-linking Assay.....	97
3.4. Mechanism of DNA ICL Formation.....	105
3.5. Determination of DNA Alkylation Sites.....	112
3.6. Conclusions.....	119
3.7. Experimental Section.....	119
3.8. References	132
4. The Effects of Core Structure and Leaving Groups on Photo-induced DNA Cross-linking	134
4.1. Introduction	134
4.2. Core Structure Modification to Improve DNA Cross-linking Efficiency ..	135
4.2.1. Synthesis of Compounds with Different Core Structure and Various Leaving Groups.....	135
4.2.2. DNA Interstrand Cross-linking Assay	138
4.2.3. Mechanism of DNA ICL Formation	146
4.2.4. Determination of DNA Alkylation Sites	151
4.2.5. Conclusions	159
4.3. Experimental Section.....	160
4.4. References	174
5. <i>In Vivo</i> Efficacy Study for Several Hydrogen Peroxide Activated Precursors	175
5.1. Introduction	175
5.2. <i>In Vivo</i> Efficacy of H ₂ O ₂ -activated Nitrogen Mustard Precursor.....	178
5.2.1. Toxicity Study with CD-1 Mice.....	178
5.2.2. <i>In Vivo</i> efficacy Study with Athymic Nude Mice Xenografted with Breast Cancer Cell Line MDA-MB-468.....	180
5.3. <i>In Vivo</i> Efficacy of H ₂ O ₂ -activated QM Precursors	182
5.3.1. Toxicity Study with CD-1 Mice.....	182
5.3.2. <i>In Vivo</i> Efficacy Study with Athymic Nude Mice Xenografted with Breast cancer cell line MDA-MB-468.....	184
5.3.3. <i>In Vivo</i> Efficacy Study with Athymic Nude Mice Xenografted with Renal Cancer Cell Lines (UO-31, 786-O or A-498).....	186
5.4. Conclusions.....	192
5.5. Experimental Protocol	193
5.5.1. Protocol for Cell Preparation.....	193
5.5.2. Protocol for Cell Injection to Nude Mice	195
5.5.3. Protocol for Compound Injection to Nude Mice.....	196
5.6. References.....	197

6. The Effect of Triazole-modified Thymidines on DNA and RNA Duplex Stability	201
6.1. Introduction	201
6.2. Synthesis of Triazole-modified Pyrimidine Nucleosides and Oligodeoxyribonucleotides Containing Triazole-modified Thymidines	203
6.3. Determination of pK_a Values by UV Spectroscopy	206
6.4. The Effect of pH Values on The Stability of DNA Duplexes	212
6.5. Substituent Effects on The Thermal Stability of DNA Duplexes	214
6.6. Thermal Stability of the DNA Duplexes with Multiple Incorporations	216
6.7. DNA Computational Study	218
6.8. Conclusions	221
6.9. Experimental Section	221
6.10. References	231
Appendices:	234
Appendix A: Phosphor Image Autoradiograms	234
Appendix B: ODN Characterization	290
Appendix C: Copy Licenses	295
Curriculum Vitae	302

LIST OF FIGURES

Figure 1-1. Three types of DNA alkylation.....	3
Figure 1-2. Photo-induced DNA cross-linking formation (A) and fluorescence intensity change (B)	12
Figure 1-3. Photoreversible DNA cross-linking formation (A) and reversibility of the DNA interstrand cross-linking (B)	13
Figure 1-4. Photoreversible DNA cross-linking formation (A) and fluorescence intensity change (B)	14
Figure 2-1. DNA ICL efficiency of three classes of existing compounds upon UV irradiation	45
Figure 2-2. The structure of [γ - 32 P] ATP and 5'-end oligonucleotide labeling	52
Figure 2-3. Time dependence of DNA ICL formation of duplex 17 for 1a-5a and 1b-5b upon photo-irradiation	53
Figure 2-4. Concentration dependence of DNA ICL formation of duplex 17 for 1a-5a and 1b-5b upon 350 nm irradiation	56
Figure 2-5. Photo-induced DNA ICL formation for 1a-5a and 1b-5b	59
Figure 2-6. UV absorption spectra for 1a-5a and 1b-5b with 1.0 mM concentration	60
Figure 2-7. Carbocation and radical trapping with DNA ICL formation for 1a-5a and 1b-5b	65
Figure 2-8. Determination of the reaction sites of 1a	71
Figure 3-1. Photo-induced DNA ICL formation for 26a-i and 27a-i	101
Figure 3-2. UV absorption spectra for 26a-i and 27a-i (500 μ M).....	104
Figure 3-3. Carbocation and radical trapping during DNA ICL formation for 26a-i and 27a-i	107

Figure 3-4. LC-MS chromatogram for the reaction mixture of 3i and methoxyamine hydrochloride upon 350 nm irradiation.....	111
Figure 3-5. Determination of the reaction sites of 26a-i and 27a-i	113
Figure 4-1. Photo-induced DNA ICL formation for 34a-j and 35a-j	142
Figure 4-2. UV absorption spectra for 34a-j and 35a-j (500 μ M)	144
Figure 4-3. Carbocation and radical trapping during DNA ICL formation for 34a-j and 35a-j	147
Figure 4-4. Determination of the reaction sites of 34a-j and 35a-j	152
Figure 5-1. DNA ICL formation with/without H ₂ O ₂ for compounds IIIi , IIIa and IVq	177
Figure 5-2. The result of one dose treatment for compound IVq	179
Figure 5-3. The result of five dose treatment for compound IVq	180
Figure 5-4. The volume of tumors for control and IVq -treated mice from 1 st to 9 th week.....	181
Figure 5-5. Body weight of mice for control and IVq -treated mice from 1 st to 9 th week.....	182
Figure 5-6. Final harvested tumor weight average for control, Chlorambucil and IVq -treated mice after nine weeks' treatment.....	182
Figure 5-7. The result of one dose treatment for compounds IIIi and IIIa	183
Figure 5-8. The result of five dose treatment for compounds IIIi and IIIa	184
Figure 5-9. The volume of tumors for control and IIIi -treated mice from 1 st to 8 th week	185
Figure 5-10. Body weight of mice for control and IIIi -treated mice from 1 st to 8 th week	185
Figure 5-11. Final harvested tumor weight average for control and IIIi -treated mice after eight weeks' treatment	186

Figure 5-12. The volume of tumors for control, III and IIIa -treated mice from 1 st to 6 th week.....	187
Figure 5-13. Body weight of mice for control, III and IIIa -treated mice from 1 st to 6 th week.....	188
Figure 5-14. The volume (A) or percentage growth (B) of tumors for control and III -treated mice from 1 st to 7 th week.....	189
Figure 5-15. Body weight of mice for control and III -treated mice from 1 st to 7 th week.....	190
Figure 5-16. Final harvested tumor weight average for control and III -treated mice after seven weeks' treatment	190
Figure 5-17. The volume of tumors for control, III and IIIa -treated mice from 1 st to 7 th week.....	191
Figure 5-18. Body weight of mice for control, III and IIIa -treated mice from 1 st to 7 th week.....	192
Figure 5-19. Final harvested tumor weight average for control, III and IIIa -treated mice after seven weeks' treatment.....	192
Figure 6-1. UV-spectra changes of compound 41 in phosphate buffer solution from pH 2.7 to 12.1	208
Figure 6-2. UV-absorbance of compound 41 as a function of pH values measured at 265 nm	208
Figure 6-3. UV-absorbance of compound 41 as a function of pH values measured at 237 nm	209
Figure 6-4. UV-spectra changes of compound 42 in phosphate buffer solution from pH 2.4 to 11.3	209
Figure 6-5. UV-absorbance of compound 42 as a function of pH values measured at 254 nm	210
Figure 6-6. UV-absorbance of compound 42 as a function of pH values measured at 240 nm	210

Figure 6-7. UV-spectra changes of compound 43 in phosphate buffer solution from pH 2.5 to 12.5	211
Figure 6-8. UV-absorbance of compound 43 as a function of pH values measured at 326 nm	211
Figure 6-9. UV-absorbance of compound 43 as a function of pH values measured at 236 nm	212
Figure 6-10. Comparison of the melting temperatures of ds DNAs containing 41 , 42 , or 43 in a buffer (pH =7.0)	215
Figure 6-11. T_m decrease per modification in different DNA·DNA or DNA·RNA duplexes in phosphate buffer (pH =7.0)	218
Figure 6-12. The Geometries of (un)substituted-dT ₃ /dA ₃ in duplexes 49 (A), 56 (B), 57 (C) and 58 (D) optimized by DFT computation	220

LIST OF TABLES

Table 2-1. The optimized conditions, ICL yields, heterolytic cleavage energy (ΔE_{HCE}) and UV absorption data for 1a-5a and 1b-5b	63
Table 3-1. The optimized conditions, ICL yields and UV absorption data for 26a-i and 27a-i	98
Table 4-1. The optimized conditions, ICL yields and UV absorption data for 34a-j and 35a-j	140
Table 6-1. T_m values of oligonucleotides in different pH values	213
Table 6-2. T_m values of oligonucleotides in pH 7.0 buffer	217

LIST OF SCHEMES

Scheme 1-1. Structure of DNA double helix and Watson-Crick base pairing	1
Scheme 1-2. Possible alkylation sites on dA, dG, dC, and dT	2
Scheme 1-3. Monofunctional methylating agents and mechanism of action.	5
Scheme 1-4. Commonly used bi-functional alkylating agents as chemotherapeutic agents.	6
Scheme 1-5. Cisplatin compounds and the mechanism of ICL formation	7
Scheme 1-6. The mechanism of action for mitomycin C	8
Scheme 1-7. Nitrogen mustards and the mechanism of action.	9
Scheme 1-8. Photo-inducible DNA cross-linking agents via [2+2] cycloaddition....	11
Scheme 1-9. The mechanism of action for Psoralen.....	12
Scheme 1-10. Site-specific conversion of cytosine to Uracil in target DNA using the ^{CNV} K-modified oligonucleotide	15
Scheme 1-11. Photo-generation of QMs and substituent effects	16
Scheme 1-12. General structure of three classes of photo-inducible QM precursors.	16
Scheme 1-13. Mechanism for photo-induced DNA ICL formation	17
Scheme 1-14. Photo-induced DNA cross-linking via modified thymidines.....	19
Scheme 1-15. Three classes of photo-inducible DNA cross-linking agents via a carboncation mechanism	19
Scheme 1-16. Photo-induced DNA cross-linking by binitroimidazoles via a carbon cation mechanism	20
Scheme 1-17. Photo-induced DNA ICL by naphthalene analogues via a carbon cation mechanism and the trapping products	21

Scheme 1-18. Photo-induced DNA cross-linking by benzyl boronates via a carbon cation mechanism	22
Scheme 1-19. Four types of chemical agents inducible cross-linking agents.....	23
Scheme 1-20. Fluoride-induced QM precursors and mechanism of action.....	25
Scheme 1-21. Active sites and monoadducts formed by fluoride-inducible QM precursors	25
Scheme 1-22. Fluoride-induced nitrogen mustard precursors and the mechanism for ICL formation	26
Scheme 1-23. NaIO ₄ or ¹ O ₂ inducible DNA cross-linking agents.....	27
Scheme 1-24. Mechanism of action for ICL formation.....	28
Scheme 1-25. NBS inducible DNA cross-linking agents.	29
Scheme 1-26. Mechanism of action for furan-containing analogues.	29
Scheme 1-27. H ₂ O ₂ inducible QM precursors.	31
Scheme 1-28. Mechanism of action for H ₂ O ₂ inducible QM precursors.....	32
Scheme 1-29. H ₂ O ₂ -inducible DAN cross-linking agents	34
Scheme 1-30. Mechanism of action for H ₂ O ₂ inducible nitrogen mustard precursors	35
Scheme 2-1. Three classes of photo-induced DNA cross-linking agents via a carbocation mechanism	45
Scheme 2-2. Structure of 1a-5a and 1b-5b	46
Scheme 2-3. Synthesis of 1a-5a and 1b-5b	48
Scheme 2-4. The sequence of DNA duplex 17	49
Scheme 2-5. Automated DNA synthesis cycle (A) and structures of phosphoramidites (B)	50
Scheme 2-6. DNA deprotection.....	51

Scheme 2-7. Proposed mechanism for DNA ICL formation	68
Scheme 2-8. Cation and free radical trapping products obtained with 1a-5a and 1b-5b upon 350 nm irradiation.....	69
Scheme 2-9. Monomer reactions of 1a and the nucleosides dG, dA, dC	73
Scheme 2-10. The proposed structures for the minor adducts detected by LC-MS ..	74
Scheme 3-1. Structures of 26a-i and 27a-i	93
Scheme 3-2. Synthesis of 26a-i	95
Scheme 3-3. Synthesis of 27a-i	96
Scheme 3-4. Proposed mechanism for DNA ICL formation	110
Scheme 3-5. Cation and free radical trapping products obtained with 3i upon 350 nm irradiation	110
Scheme 4-1. Structures of 34a-j and 35a-j	135
Scheme 4-2. Synthesis of 34a-j	137
Scheme 4-3. Synthesis of 35a-j	138
Scheme 4-4. Proposed mechanism for DNA ICL formation	150
Scheme 5-1. Compounds used for <i>in vivo</i> study	177
Scheme 6-1. Structure of triazole-modified pyrimidine nucleosides	203
Scheme 6-2. Synthesis of compounds 41-43 and the corresponding phosphoramidites 41c-43c	204
Scheme 6-3. Structures of regular phosphoramidites used during DNA (A) or RNA (B) oligonucleotide synthesis.....	205
Scheme 6-4. Double-stranded DNAs and RNA·DNAs used for this study	206
Scheme 6-5. Watson-Crick base pair motifs of dA-dT/ 41/42/43	214

LIST OF ABBREVIATIONS

A	Adenosine
AIBN	Azobisisobutyronitrile
ATP	Adenosine triphosphate
C	Cytidine
dA	Deoxyadenosine
dC	Deoxycytidine
dG	Deoxyguanosine
dT	Deoxythymidine
DIPEA	<i>N,N</i> -Diisopropylethylamine
DMF	Dimethylaminomethylene
DMSO	Dimethyl sulfoxide
DMTr	4',4'-Dimethoxytrityl
DNA	2'-Deoxyribonucleic acid
ds DNA	Double-stranded DNA
EDTA	Ethylenediaminetetraacetic acid
ESI	Electrospray
EtOAc	Ethyl acetate
EtOH	Ethanol
G	Guanosine
HPLC	High-performance liquid chromatography
HRMS	High-resolution mass spectrometry
ICLs	Interstrand cross-links
LC-MS	Liquid chromatography–mass spectrometry
MALDI-TOF	Matrix-assisted laser desorption/ionization – time of flight

MeCN	Acetonitrile
MeOH	Methanol
MS	Mass spectrometry
NBS	N-Bromosuccinimide
NMR	Nuclear magnetic resonance
ODN	Oligodeoxyribonucleotide
Pac	Phenoxyacetyl
PAGE	Polyacrylamide gel electrophoresis
ⁱ Pr	Isopropyl
QM	Quinone methide
ROS	Reactive oxygen species
RNA	Ribonucleic acid
T	Thymidine
TBAF	Tert-n-butylammonium fluoride
TEA	Triethylamine
TEMPO	2,2,6,6-Tetramethylpiperidin-1-yl)oxyl
THF	Tetrahydrofuran
T_m	Melting temperature
TMS	Trimethylsilyl
U	Uridine
UV	Ultraviolet
UVA	Ultraviolet A

ACKNOWLEDGMENTS

First of all, I would like to acknowledge my advisor, Prof. Xiaohua Peng, an outstanding scholar and supervisor, for her kind mentorship. She has done great efforts in selecting projects and helped in trouble shooting on these projects. Dr. Peng's profound knowledge, excellent advice, patient mentoring, and professional training led me to become a real chemist. She generously shared her expertise and fostered me to be a distinguished student fellow and a distinguished dissertation fellow at University of Wisconsin-Milwaukee. I am greatly honored to have Dr. Peng as my supervisor and carry deep respect, admiration, and appreciation for her.

I greatly appreciate my committee members: Prof. Alexander Arnold, Prof. Andy Pacheco, Prof. M. Mahmum Hossain and Prof. Jorg Woehl for their nice support, encouragement, insightful comments and valuable advice for my research. It is my great honor to have them as my committee members. I admire their talents and appreciate their generosity in sharing their expertise. Especially thank Professor Alexander Arnold for his fruitful collaboration and professionally training in cell culture and animal study. Especially thank Prof. Andy Pacheco for his insightful comments and valuable advice for my paper.

It is my great pleasure to be a member of Prof. Peng's Lab, which offers perfect opportunities to discuss science with talented coworkers. Thanks to all members in our group: Dr. Huabing Sun, Dr. Wenbing Chen, Dr. Yibin Wang, Dr. Zechao Lin, Anahit Campbell, Asad Uz Zaman and Qi Zhang for their kind assistance and support both in my study and life. I especially thank Dr. Huabing Sun, Dr. Wenbing Chen, and Dr. Yibin Wang for their kind collaboration and efforts to help me to solve problems.

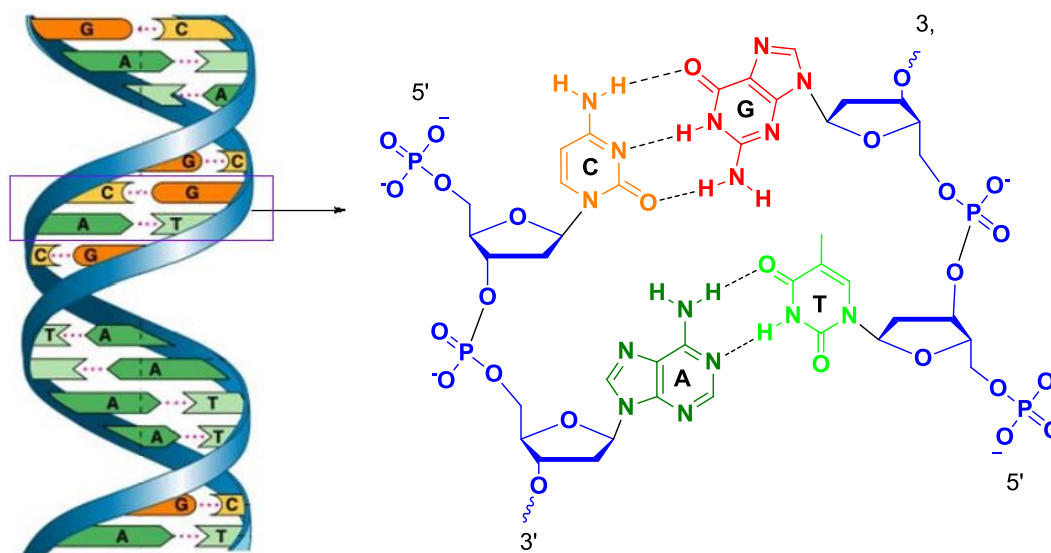
Sincere gratitude to the faculty members and staffs in the department of Chemistry & Biochemistry at University of Wisconsin-Milwaukee. Especially thank Anna Benko for her kind help for compounds analysis.

Last but not the least, I would like to thank my family for their constant encouragement and support in these years: my parents, Fubang Fan and Yurong Yin provided trust and great support all the time; my husband, Huabing Sun, provided encouragement and support during these years; and my lovely kids, Fan Sun and Yirong Sun gave me endless happiness and energy.

Chapter 1. Introduction

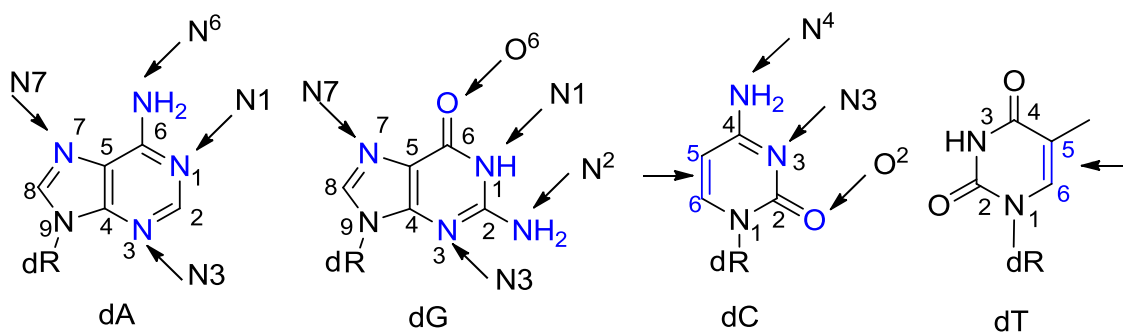
1.1. The Structure and Functions of DNA

Deoxyribonucleic acid (DNA) is a hereditary material carrying genetic information in an organism for its development, functions, and reproduction. The structure of DNA was first discovered by Watson and Crick in 1953. It is a double helix structure consisting of two complementary polynucleotide chains (Scheme 1-1).¹ Each polynucleotide strand is constructed by nucleotides containing a phosphate group, a deoxyribose, and one of four nitrogen-containing nucleobases (adenine [A], thymine [T], guanine [G] and cytosine [C]). The two complementary strands are bound together via hydrogen bonding with Watson-Crick base pair, namely A always pairs with T and C pairs with G (Scheme 1-1). Hydrogen bond formation allows temporarily dissociation of two DNA strands that enable the process of DNA replication and transcription, while specific recognition of Watson-Crick base pairs is essential for maintaining high fidelity of DNA replication and transcription.



Scheme 1-1. Structure of DNA double helix and Watson-Crick base pairing.

However, DNA can react with a wide variety of chemical agents or undergo photo reactions, which disrupt the normal function of DNA. For example, both DNA base moieties and the phosphate backbone can be alkylated by a wide variety of electrophiles including alkyl halides, quinone methide, and carbocation precursors. The cyclic nitrogens, exocyclic amino groups, and carbonyl group in cytosine, guanine or adenine can act as nucleophiles reacting with many alkylating agents (Scheme 1-2).²⁻⁴ On the other hand, the unsaturated C=C bond of thymine and cytosine can react with other unsaturated molecules via [2+2] cycloaddition. All these reactions may lead to DNA interstrand cross-link (ICL) formation that inhibits DNA replication and transcription. As the carrier of genetic information, understanding the chemical reactivity and function of DNA is extremely important. This thesis focuses on investigating the reactivity of DNA towards a wide variety of aromatic compounds as novel DNA cross-linking agents and exploring their biomedical applications. We use the tools of synthetic and physical organic chemistry, as well as biochemistry, and molecular biology for the mechanistic studies of these novel DNA cross-linking agents.



Scheme 1-2. Possible alkylation sites on dA, dG, dC, and dT (dR = 2'-deoxyribose).

1.2. DNA Alkylation and Commonly Used Chemotherapeutic Agents

DNA alkylation is one of the most important chemical modifications used in nucleic acid research as well as chemotherapy. There are three major types of alkylation: mono-alkylation, intrastrand cross-link, and interstrand cross-link (ICL). Mono-alkylation modifies single bases on one DNA strand; intrastrand cross-link is formed by alkylating two DNA bases in the same strand; and ICL is produced by alkylation on two bases on opposite strands (Figure 1-1).⁵

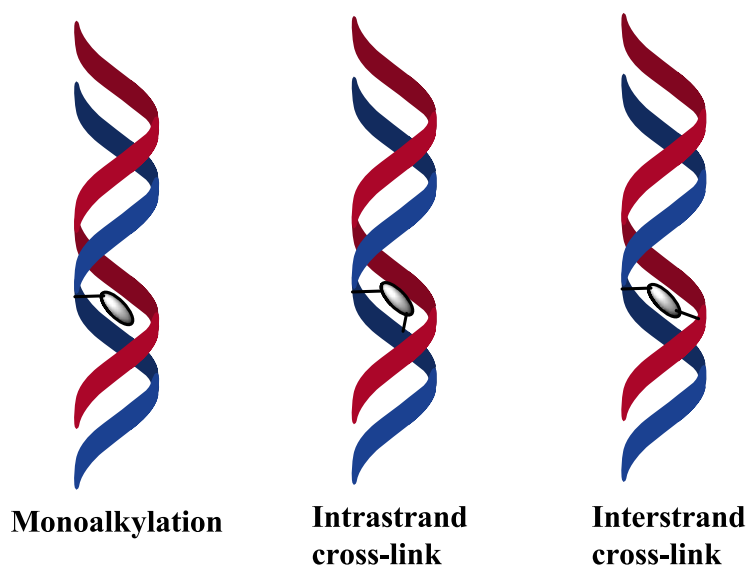
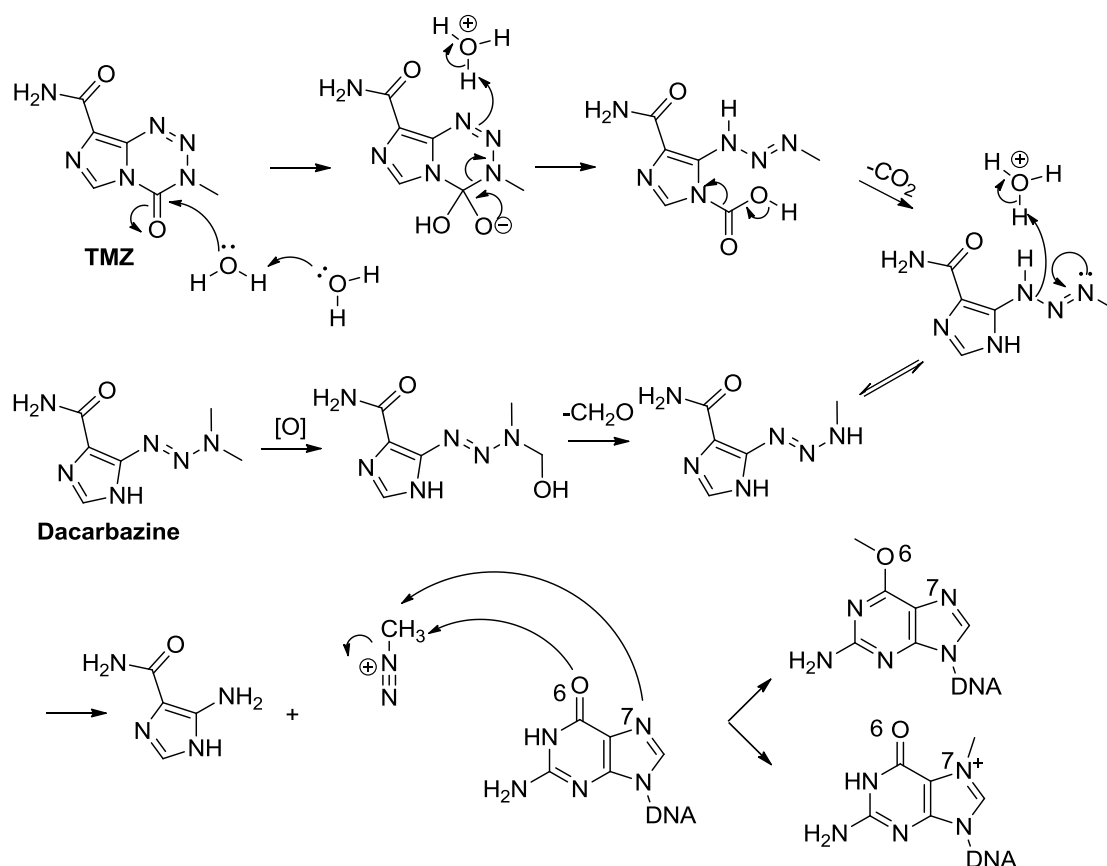


Figure 1-1. Three types of DNA alkylation.

DNA alkylating agents are widely used in cancer chemotherapy as they can prevent DNA from functioning properly by changing the original structure of the DNA. DNA alkylation is the source of the cytotoxicity of many antitumor and anticancer agents. It can cause gene mutations or block DNA replication and transcription eventually leading to cell death. DNA alkylating agents were grouped in two major categories such as mono-functional alkylating and bi-functional alkylating agents. They have been considered to be one of the significant classes of compounds that have been widely utilized or have great potential in cancer treatments.^{5,6}

The first type of DNA alkylating agents is methylating agents that are one of the most important monoalkylating agents. DNA methylating agents have been well studied and used for DNA damage and repair study as well as for cancer treatment, such as Temozolomide (TMZ) and dacarbazine (Scheme 1-3).⁷ In general, methylation occurred either at the N- or O-positions of nucleobases. N-Methylation products are the major adducts formed (~80%). TMZ is one of the earliest oral alkylating drugs approved for cancer therapy. TMZ showed two advantages over other existing drugs. It has small size and good lipophilicity so that it can efficiently go through the blood-brain barrier and can be used for the treatment of brain cancer. TMZ also showed perfect bioavailability (100%) leading to improved efficacy.⁸ Dacarbazine is a chemotherapeutic agent for skin cancer, namely melanoma. The mechanism of their function involved the methylation of DNA at the N⁷ or O⁶ of guanine moiety (Scheme 1-3), which damaged the DNA and led to cell death.⁹ The damaged DNA double helix stacked together which prevented it from functioning.^{9,10} However, alkylated DNAs can be efficiently repaired by direct reversal proteins and base excision repair (BER), which reduced the toxicity of the methylating agents.¹¹

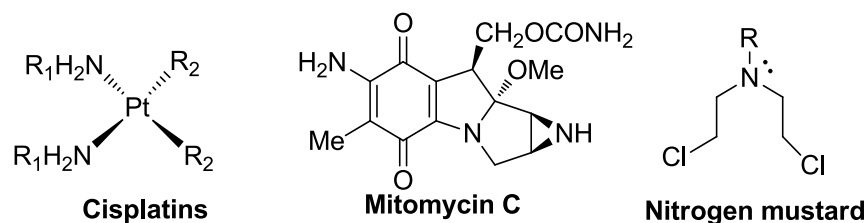


Scheme 1-3. Monofunctional methylating agents and mechanism of action.

Later on, a variety of bi-functional alkylating agents have been developed that can lead to intra or interstrand cross-link formation. The intrastrand cross-links can induce bends in DNA, which may affect the binding affinity to DNA binding proteins, and inhibit DNA normal function.¹²

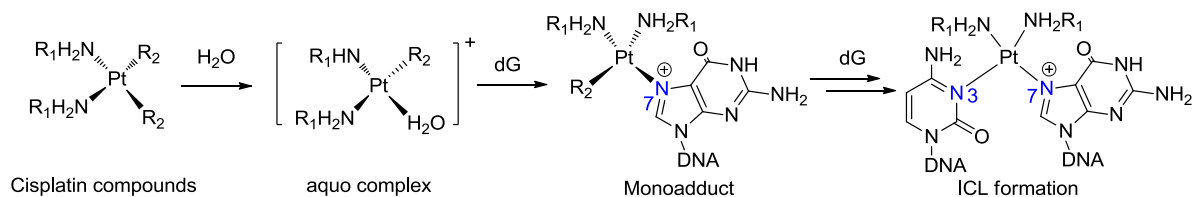
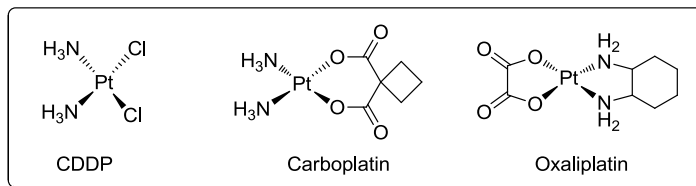
ICLs covalently bond two complementary DNA strands, which prevents their separation and block DNA replication and/or transcription finally leading to cell death. However, the intrastrand cross-links are readily repaired by nucleotide excision repair (NER), which decreases its toxicity and confines its usage for cancer treatment. DNA ICLs cannot be easily repaired by NER, therefore are more toxic than the intrastrand cross-links.¹³ More attentions have been paid on development of DNA interstrand cross-linking agents for cancer treatment and other biological applications.⁶

A variety of bi-functional alkylating agents have been employed for the treatment of cancer disease, such as cisplatin, mitomycin C and nitrogen mustard analogues (Scheme 1-4). These three classes of compounds have been well studied and widely used for cancer treatment.



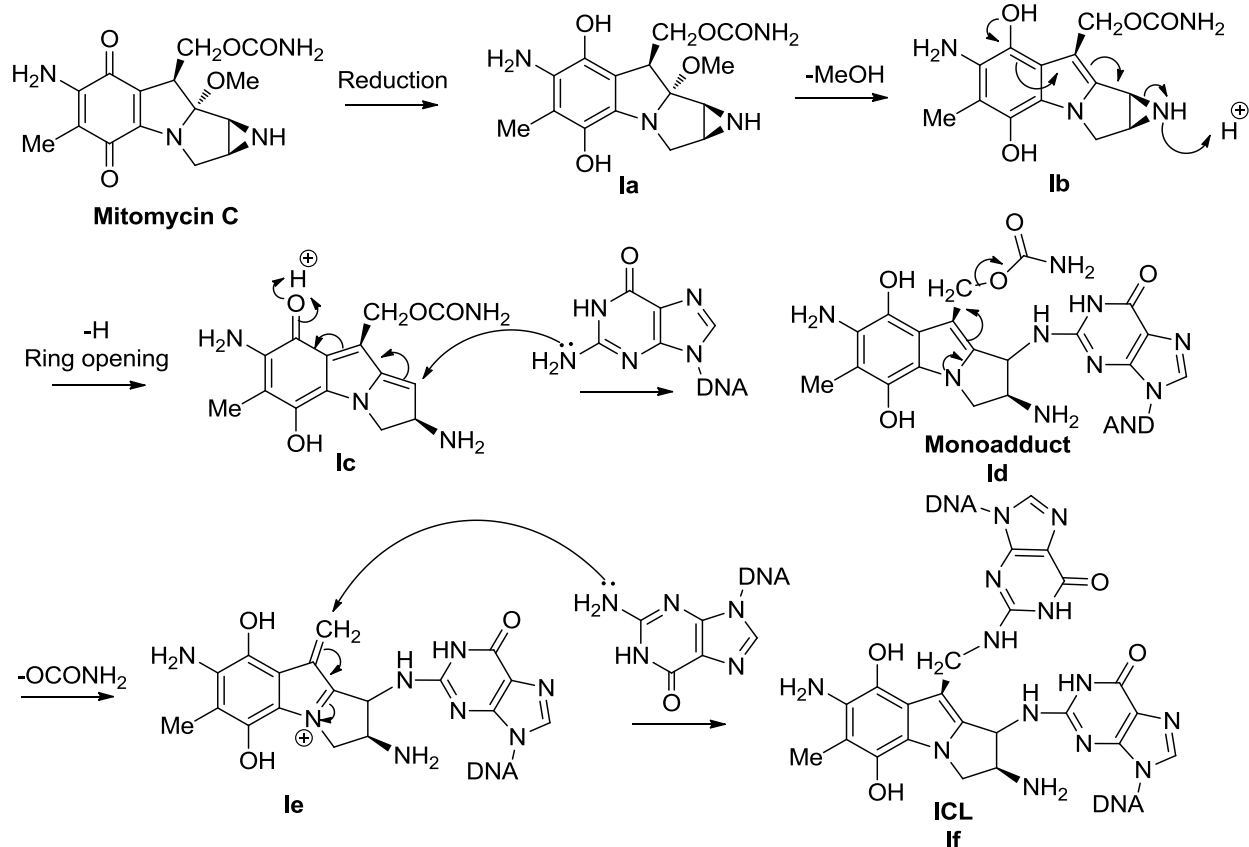
Scheme 1-4. Commonly used bi-functional alkylating agents as chemotherapeutic agents

Cisplatin is a well-known anticancer drug approved for medical use. It has been used for half cancer patients who have ever received chemotherapy.¹⁴ For instance, cis-diamminedichloridoplatinum (II) (CDDP), carboplatin, and oxaliplatin (Scheme 1-5) are medicines used to treat various types of cancers, such as lung cancer, bladder cancer, germ cell tumors, sarcomas and cervical cancer.^{15,16} These platinum compounds are commonly made up of platinum (II), two neutral ammonium molecules, and two ligands with negative charge. Cisplatin forms both inter- and intrastrand cross-links. The mechanism of ICL formation involved the replacement of one of the negatively charged ligands with a neutral water, leading to the formation of the positively charged aquo complex that acts as a good electrophile. The water molecule in the aquo complex can be easily exchanged by N-heterocyclic bases in the DNA, resulting in the formation of the monoadduct. The following replacement of the second ligand (chloride or R₂) by the nucleobase in the opposite strand led to the formation of the ICLs. N7 of guanine and cytosine of N3 were reported to be the major cross-link sites for this class of compounds (Scheme 1-5).^{15,17-18} However, cisplatin can cause a number of side effects, including kidney damage, hearing loss, bone marrow suppression and vomiting.¹⁹



Scheme 1-5. Cisplatin compounds and the mechanism of ICL formation.

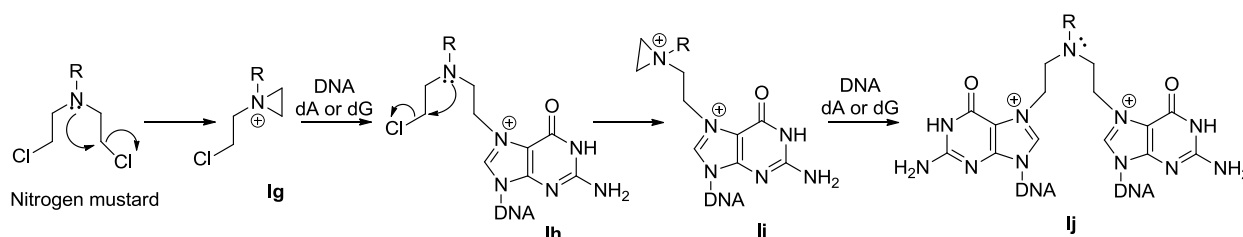
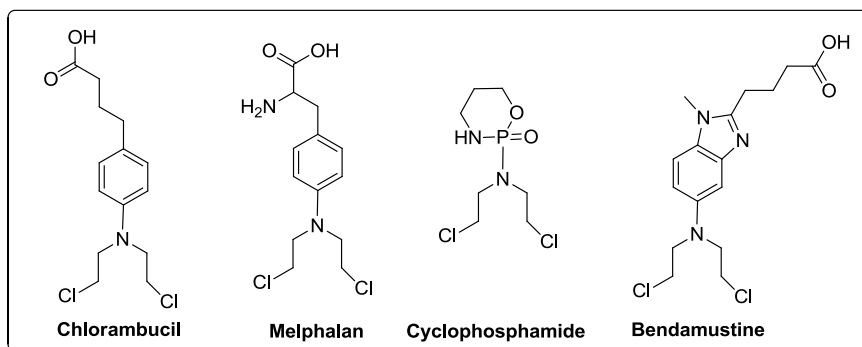
Mitomycin C belongs to a family of azidine-containing natural products. It was originally isolated from *streptomyces caespitosus*. It has been used as DNA alkylating agent for treatment of anal cancers, breast cancers and bladder cancers.²⁰ Mitomycin C is inert towards DNA, but can be activated by enzymatic reduction of quinone, leading to the formation of methide intermediates that cross-link DNA via alkylating dGs.^{15,21} The detailed mechanism was shown in scheme 1-6. Mitomycin C was first reduced to biphenol **Ia** that was easily converted to **Ib** by releasing one molecule of methanol. Compound **Ib** was further converted to the methide intermediate **Ic** that alkylated guanine at N2 position to form the monoadduct **Id**. Elimination reaction with the carbamoyl as a leaving group generated the methide **Ie** that reacted with a second guanine in the opposite strand to form ICL products **If**. Even though Mitomycin C has been widely used for cancer treatment, its side effects cannot be overlooked. The common side effects included mouth sore, poor appetite, nausea, hair loss and bone marrow toxicity.



Scheme 1-6. The mechanism of action for mitomycin C.

Nitrogen mustard and its analogs are a major kind of synthetic DNA alkylating agents which are still widely used for cancer therapy, such as chlorambucil, melphalan, cyclophosphamide, and bendamustine (Scheme 1-7). These nitrogen mustard analogues contain a highly reactive N,N-bis-(2-chloroethyl)amine functional group, which can cross-link DNA by alkylating the N7 position of adenine or guanine residues.¹⁵ The mechanism of action involves the formation of a highly reactive aziridinium intermediate **Ig** that reacts with N7 of adenine or guanine to form a monoadduct **Ih**, followed by the formation of a second aziridinium intermediate **Ii** that reacts with a second adenine or guanine on the opposite strand to produce the ICL product **Ij** (Scheme 1-7). Nitrogen mustards were highly reactive DNA alkylating agents which showed poor

selectivity and caused serious side effects, such as nausea, hair loss, mouth sores and loss of fertility.



Scheme 1-7. Nitrogen mustards and the mechanism of action.

Even though these traditional chemotherapeutic agents are powerful drugs for cancer treatment, most of these drugs showed poor selectivity. These agents could not differentiate between cancer cell DNA and normal cell DNA causing serious side effects. For instance, the use of cisplatin may lead to kidney damage, hearing loss, bone marrow suppression and vomiting.¹⁹ Mitomycin C can cause mouth sore, poor appetite, nausea, hair loss, and permanent bone marrow toxicity with long term usage. Nitrogen mustards lead to nausea, hair loss, mouth sores and loss of fertility. All these side effects limited their usage in cancer therapy. One effective way to reduce the toxicity of DNA alkylating agents towards normal cells is to develop inducible DNA alkylating agents that are inert to normal cells but can be activated under tumor specific conditions. Such agents can be used to target malignant cells with the unique conditions while leaving normal cells untouched, therefore minimizing the side effects. Inducible DNA cross-

linking agents, being non-toxic and selective, can be also used in other biological applications. Great efforts have been made to develop novel strategies to induce DNA ICL formation. Examples include photo induction, chemical agent induction, and enzymes induction.

1.3. Inducible DNA Interstrand Cross-linking Agents

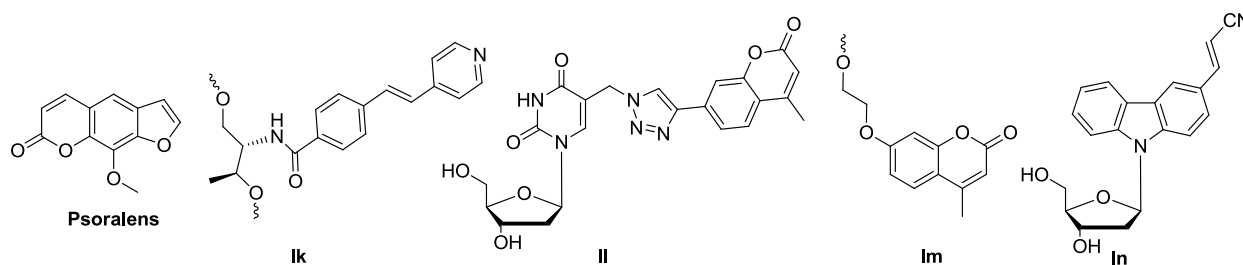
1.3.1. Photo-induced DNA ICL formation via three mechanisms

Photo-induction attracted attention for its unique properties, such as biocompatibility and orthogonality. Such method is clean and non-invasive and doesn't require additional chemical reagents. Various photo-inducible DNA crosslinking agents have been developed to induce ICL formation. In general, three common mechanisms are involved in the ICL formation process, including photocycloaddition, alkylation via quinone methides (QMs), or alkylation via carbocations. The photo-induced DNA ICL formation via cycloaddition and QMs mechanisms has been extensively studied.²² For instance, psoralens²³, p-stibaolze,²⁴ coumarin,^{25,26} 3-cyano-vinylcarbazole²⁷ can induce DNA ICL formation via [2+2] photocycloaddition, while phenol,²⁸ biphenol,²⁸ or binol analogues²⁹⁻³¹ induce DNA cross-linking through a QM mechanism. However, photo-induced DNA ICL formation via carbocation mechanism was less explored. Recently, it was reported by Li³² and Greenberg³³ that photoirradiation of modified thymidines generated both the radical and cation, but only the cation directly cross-linked DNA.

Photo-induced DNA ICL formation by [2+2] cycloaddition reaction

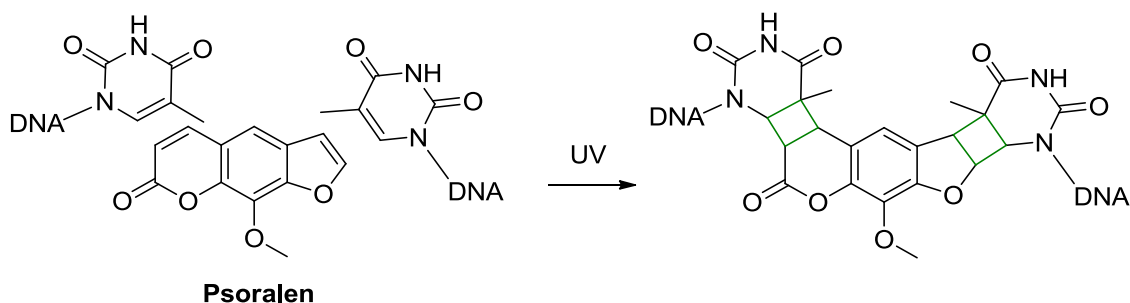
[2+2] Photocyclization takes place between two unsaturated molecules that are photo-sensitive and can be activated by light with specific wavelength, resulting in the formation of a new cyclobutane adduct. Such reaction has been widely used as a strategy for inducing DNA interstrand cross-linking because of its orthogonality. [2+2] Photocyclization is a clean reaction

and can easily occur with pyrimidine bases and other compounds containing unsaturated bonds. In addition to psoralens, several modified nucleosides with unsaturated bonds were developed and incorporated into DNA, which can induce DNA ICL formation upon UV irradiation through [2+2] cycloaddition reaction, including p-stilbazole analogs^{24,34,35}, coumarin analogs^{26,36} and 3-cyanovinylcarbazole-modified nucleosides³⁷⁻³⁹ (Scheme 1-8).



Scheme 1-8. Photo-inducible DNA cross-linking agents via [2+2] cycloaddition.

Psoralens, a class of natural products isolated from plants, are a type of photo-induced DNA cross-linking agents. These compounds consist of a coumarin moiety fused with a furan ring. The psoralens can be selectively activated by the ultraviolet A (UVA) light (320-410 nm) to react with thymidine residues in DNA to form DNA ICLs.²¹ Due to this unique property, combination of psoralens and UVA have been widely used for treatment of skin disorder, such as skin cancer and psoriasis.^{40,41} The mechanism of action involves formation of two cyclobutene products via [2+2] cycloadditions, one of which was formed between the pyrone and a thymine, while the other was formed between the furan ring and another thymine moiety on the complementary strand (Scheme 1-9).



Scheme 1-9. The mechanism of action for Psoralen.

The p-stilbazole analogue **Ik** was developed by Kashida's group.²⁴ The DNA cross-linking occurred between two complementary ODNs that contain p-stilbazole moiety that undergo a [2+2] cycloaddition reaction upon UV irradiation causing rapid DNA cross-linking (completed within 5 min). The DNA cross-linking process can be monitored by UV absorbance (Figure 1-2B). The p-stilbazole modified ODNs have strong UV absorbance at 323 nm, which became weaker upon the formation of the [2+2] cycloaddition adduct and finally disappeared (Figure 1-2), illustrating the formation of DNA ICL products.

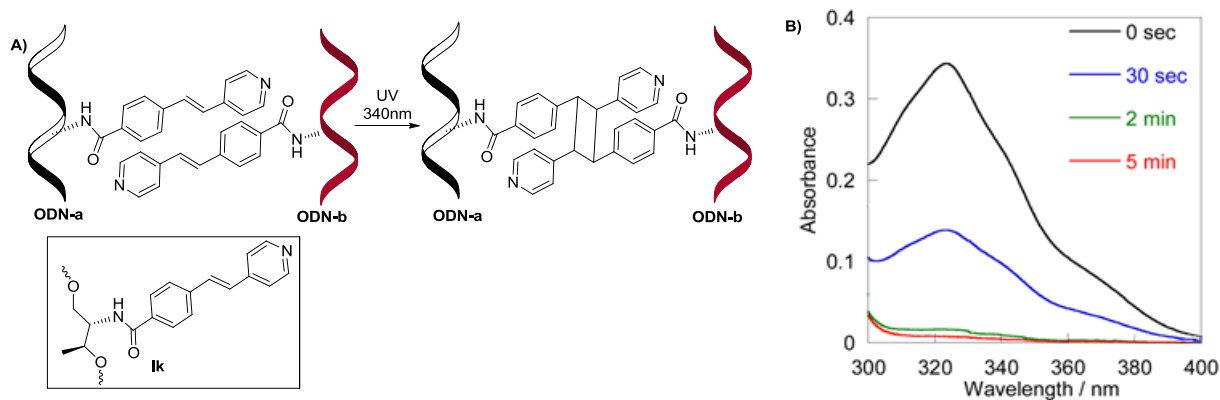


Figure 1-2. Photo-induced DNA cross-linking formation (A) and fluorescence intensity change (B)

Recently, a coumarin-modified nucleotide **II** was developed and incorporated into DNA by Peng and co-workers.³⁶ Efficient DNA ICL formation was observed upon UV irradiation at 350 nm with a maximum yield of about 90%. The DNA cross-linking occurred between the coumarin moiety and the opposing thymidine (dT) or 2'-deoxycytidine (dC) via a [2+2] cycloaddition mechanism (Figure 1-3A). Most importantly, the photo-induced ICL formation between **II** and pyrimidines were photo-switchable, which can be cleaved by 254 nm light and reversed into single stranded ODNs. Consistent photo-reversible behaviors can be achieved over six cycles by switching the UV light between 350 nm and 254 nm (Figure 1-3B).

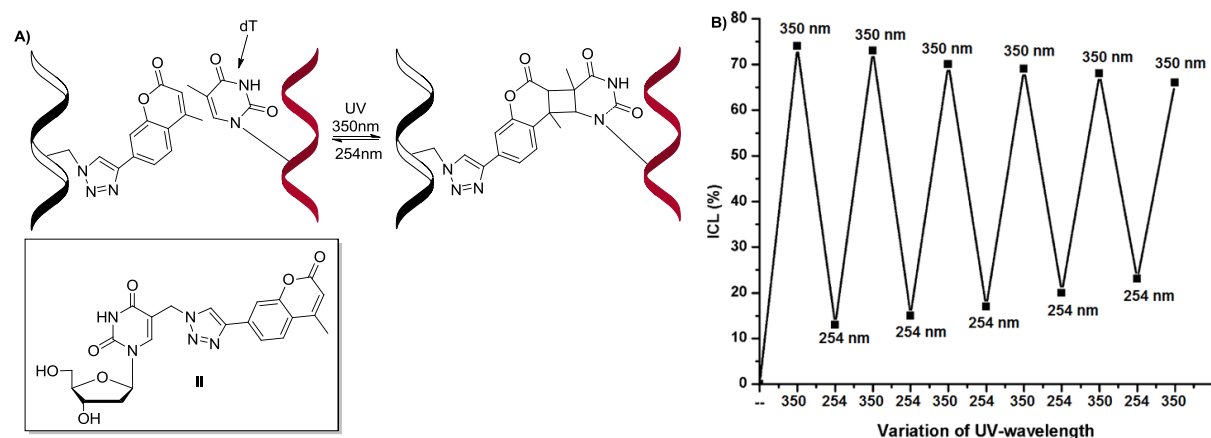


Figure 1-3. Photoreversible DNA cross-linking formation (A) and reversibility of the DNA interstrand cross-linking (B)

A detailed study on the DNA ICL formation using different coumarin analogues was carried out in Peng's group.²⁶ The linker units at the 4-position of coumarin moieties affect the efficiency of DNA ICL formation. A linker with two or more carbons is favored and led to quantitative DNA ICL formation. The DNA sequences also affect the efficiency of ICL formation. Higher DNA cross-linking efficiency was obtained when coumarin moiety was flanked by an A:T versus G:C base pair. This may be due to the efficient photo-induced electron transfer between coumarin and

dG that makes the ICL formation process less efficient. The DNA ICL formation process can be monitored by fluorescence spectroscopy. The coumarin moiety in DNA has strong fluorescence at 380 nm, which became weaker and disappeared after the formation of the [2+2] photo-induced cycloaddition adduct, suggesting the formation of the DNA ICLs (Figure 1-4).

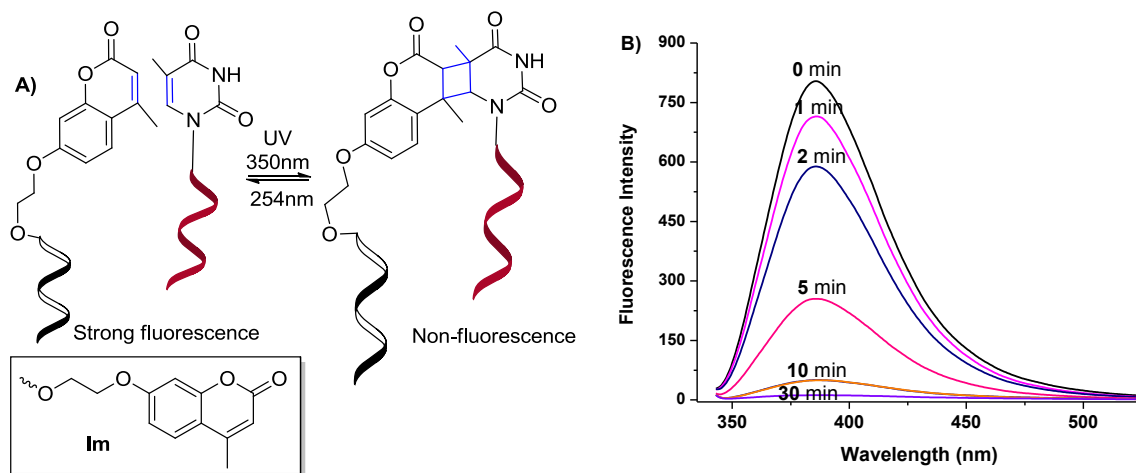
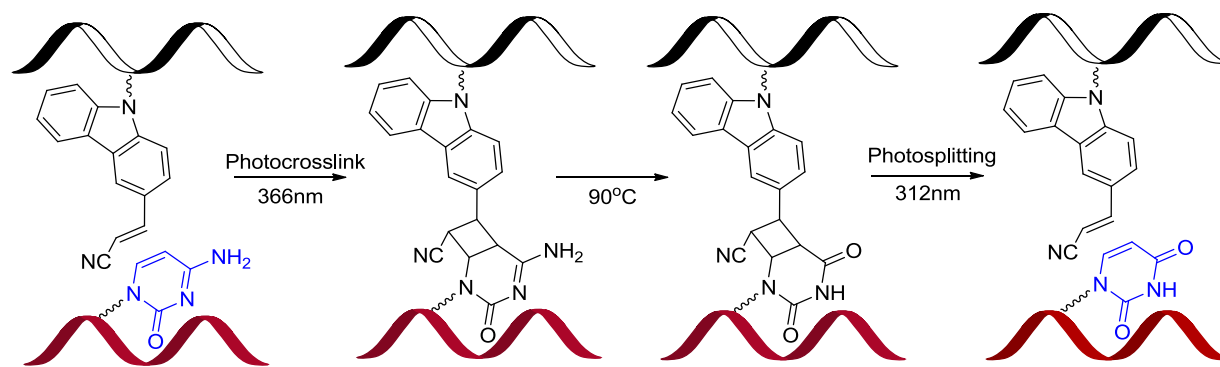


Figure 1-4. Photoreversible DNA cross-linking formation (A) and fluorescence intensity change (B)

Fujimoto's group developed a 3-cyanovinylcarbazole-modified nucleoside **In** that was incorporated into DNA.³⁷⁻³⁹ The photo-induced DNA cross-linking process is ultrafast and photo reversible. The photo-cross-link can be done within 1 s upon 366 nm irradiation via a [2+2] cycloaddition mechanism. The ICL products can be split into single strands within 60 s upon UV irradiation at 312 nm. More interestingly, the target cytosine can be selectively converted to uracil by heating the ICL product at 90 °C for 3.5 h, followed by photo-splitting at 312 nm for 60 s.³⁹ Such selective conversion is very important and can be used for gene therapy (Scheme 1-10).



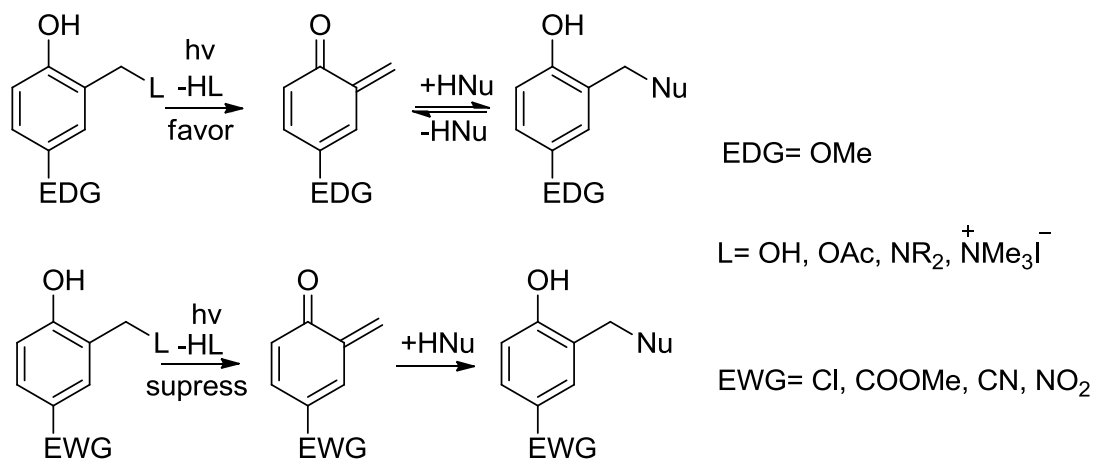
Scheme 1-10. Site-specific conversion of cytosine to Uracil in target DNA using the ^{CNV}K-modified oligonucleotide.

Photo-induced DNA cross-linking via quinone methide formation

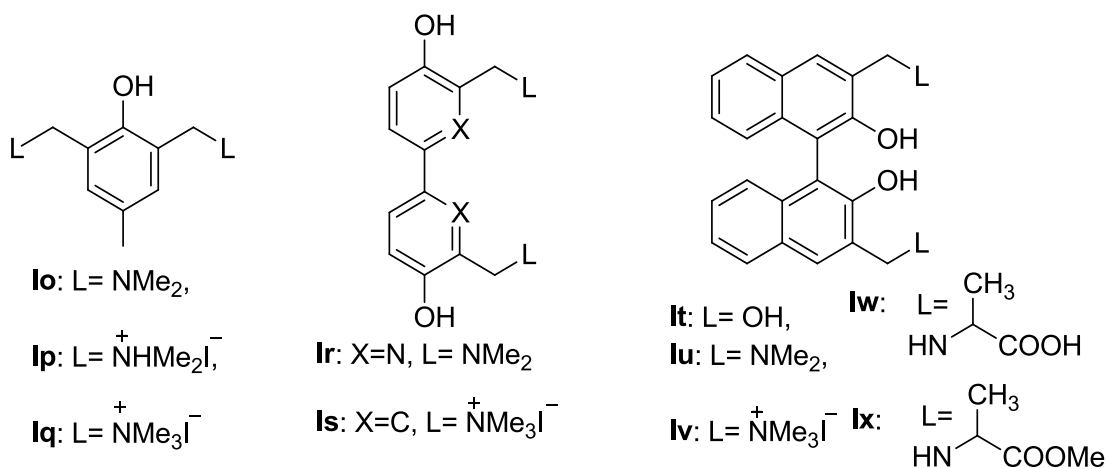
Quinone methides (QMs) are electrophiles with high reactivity with nucleophiles, such as nucleobases. The cyclic nitrogens, exocyclic amino groups and oxygens in the cytosine and guanine are good nucleophiles that can efficiently react with QMs.²⁻⁴ Various kinds of QM precursors were developed for inducing DNA ICL formation. Some of them are chemical inducible (F^- , $NaIO_4$, H_2O_2) while others are photo-inducible. Photo activated QM formation is clean and biorthogonal, which can be carried out under physiological condition.

QM precursors with various benzylicleaving groups ($L = OH, NR_2, NMe_3I$) and aromatic substituents ($R = OMe, H, Cl, COOMe, CN, NO_2$) were developed and the structure effects of precursors were investigated. Both leaving groups (L) and aromatic substituents affect QM formation. The ammonium salts are considered as better leaving groups because they do not react with QMs and have higher quantum yield.⁴² In addition, electron-donating groups favored the QM formation and regeneration from formed adducts. Electron-withdrawing groups suppressed the QM formation and regeneration. The stability of QM decreased with the

increasing strength of the electron withdrawing property for the substituents (Cl, COOMe, CN, NO₂). This is consistent with the electron-deficient property of the QMs (Scheme 1-11).



Scheme 1-11. Photo-generation of QMs and substituent effects.

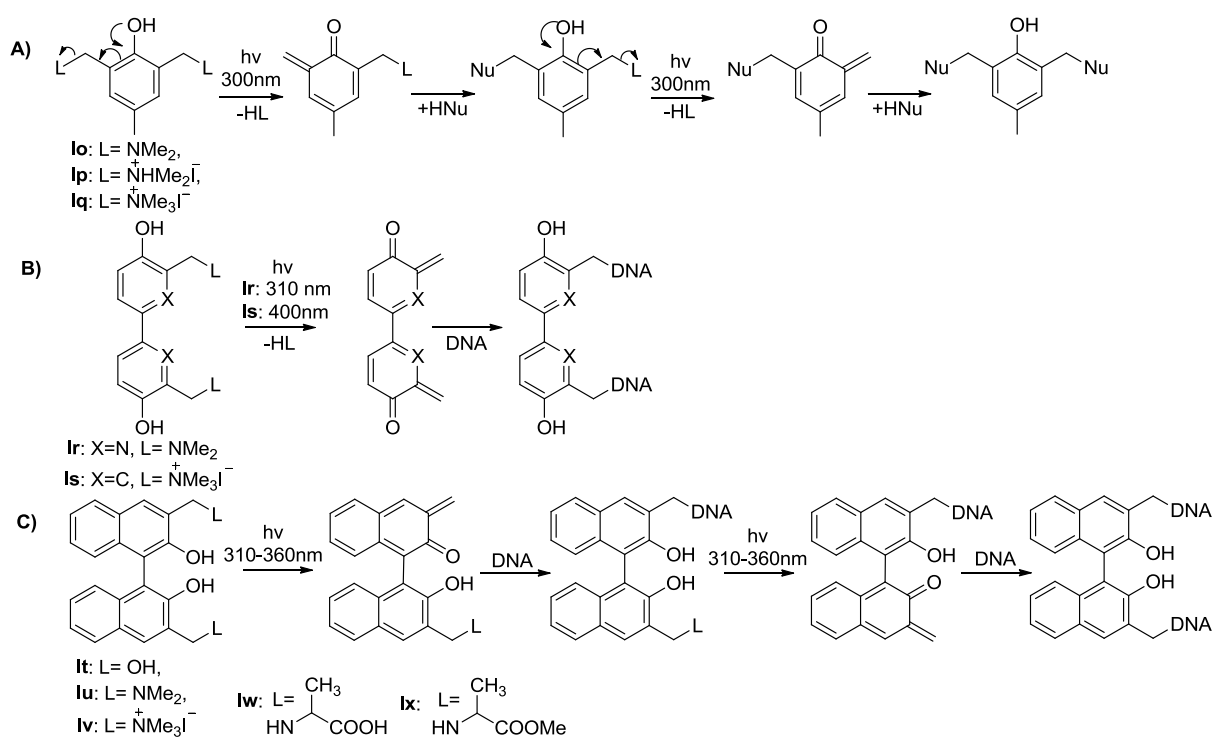


Scheme 1-12. General structure of three classes of photo-inducible QM precursors.

Recently, several classes of bifunctional QM precursors have been developed as DNA cross-linking agents, such as phenols, biphenols and binol quinone methide (BQM) precursors (scheme 1-12).^{28-31, 43-46} It was reported by Zhou²⁸ and Basaric⁴³ that the bifunctional phenols generated QM under UV irradiation at 300 nm, which can react with various kinds of nucleophiles (scheme 1-13A). Such bifunctional phenols were capable of inducing DNA ICL formation. Nevertheless,

they have limited usage in biological system due to the short activation wavelength (300 nm). The light with a wavelength longer than 350 nm was considered to be safe in bio-system.⁴⁴ To expand their application in biological context, extended conjugation systems were investigated for achieving longer wavelength for activation.

Heterocyclic bifunctional pyr-QM precursor **Ir** was synthesized by Freccero and co-workers.⁴⁵ Such compound can be activated by UV light at 310 nm to generate QMs that efficiently cross-linked DNA. A water-soluble biphenol ammonium salt **Is** was developed by Zhou's group,²⁸ which could generate the reactive QM intermediate upon UV irradiation at 400 nm. The cross-linking efficiency of **Is** is 100 fold higher than that of the prototype phenol ammonium salt **Iq**, suggesting that extending conjugation system is an efficient way to make the activation wavelength red-shift and to improve the DNA cross-linking efficiency (Scheme 1-13).

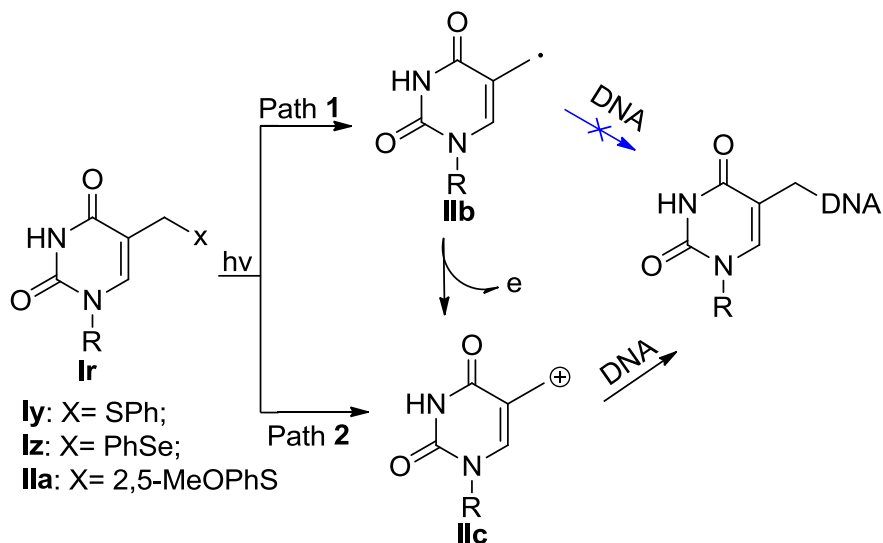


Scheme 1-13. Mechanism for photo-induced DNA ICL formation.

A series of binol analogues containing extended conjugation system were developed by Freccero and co-workers (Scheme 1-13C).^{29-31,46} All these compounds could be activated by UV light (310-360 nm) to produce binol quinone methide (BQM) to cross-link DNA. Among these compounds, **Iv** containing ammonium salts as leaving groups showed better photosensitivity. However, the positive charge in **Iv** made it impossible to go through cell membrane thereby confined its usage in bio-system. In order to use them in biological context, the ammonium salt was replaced by an amino acid (ester) resulting in **Iw** and **Ix** that had higher cell membrane permeability than **Iv**. Compound **Iw** can be activated upon 360 nm photoirradiation to induce DNA ICL formation with high efficiency. Compound **Iw** showed an ICL efficiency that was comparable to that of **Iv**. Compounds **Iw,x** can successfully reach the DNA targets in the cells.⁴⁶

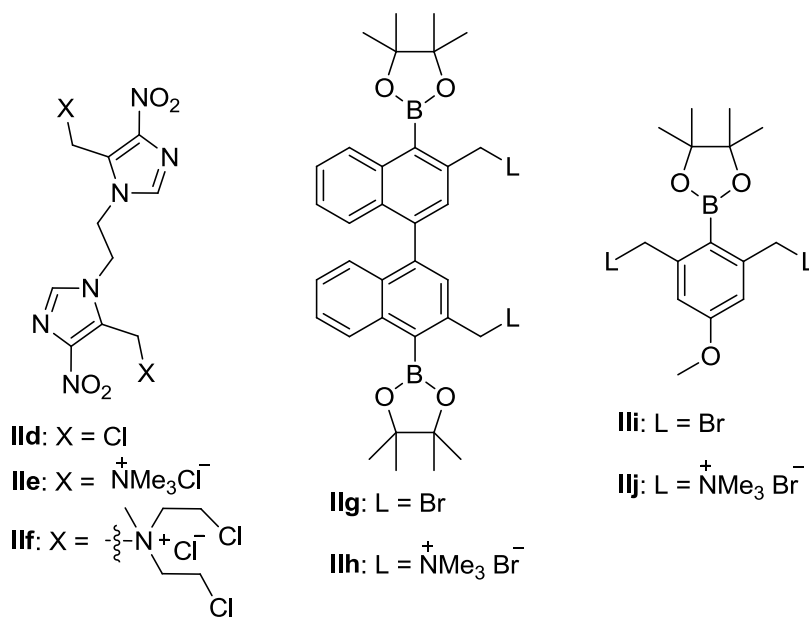
Photo-induced DNA cross-linking via carbon cation formation

In comparison to DNA cross-linking via photo-induced [2+2] cycloaddition and QM formation, the DNA ICL formation via a photo-induced carbocation generation is relatively novel and less explored. Recently, Li³² and Greenberg³³ group reported that the modified thymidines (**Iy,z** and **Ila**) produced both radical **Iib** and cation **Iic** under UV irradiation but only the cation **Iic** directly cross-linked DNA (Scheme 1-14).



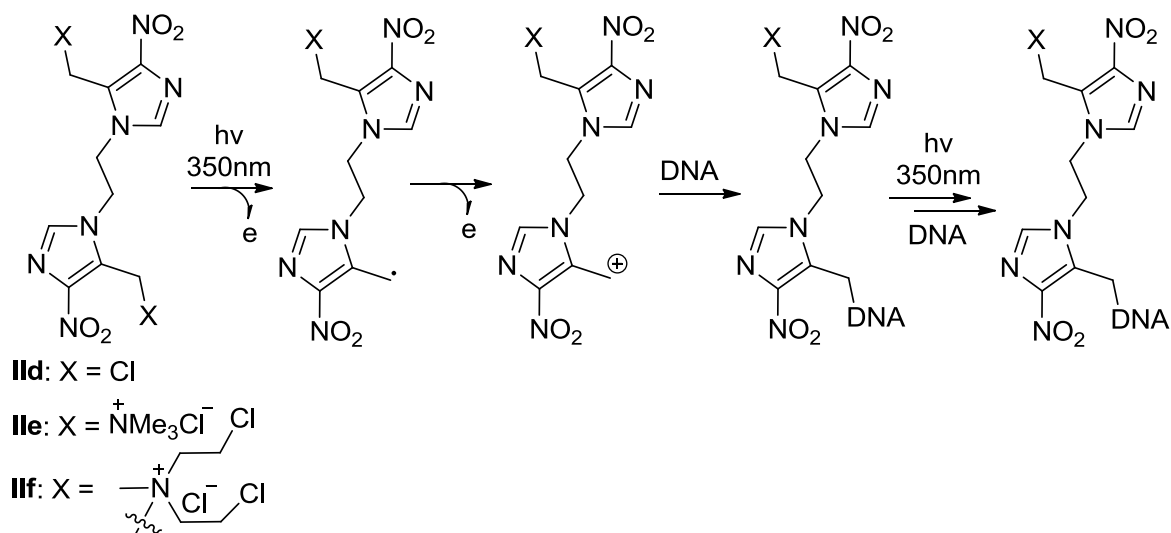
Scheme 1-14. Photo-induced DNA cross-linking via modified thymidines.

Most recently, a series of biaryl bifunctional compounds **IId-j** (Scheme 1-15) have been developed as photo-inducible DNA cross-linking agents.⁴⁷⁻⁴⁹ All these compounds cross-linked DNA efficiently upon UV irradiation at 350 nm. The DNA cross-linking process involved a carbocation mechanism. The carbocations can be produced either through oxidation of the corresponding radicals or direct heterolysis of C-L bond (Scheme 1-16, 1-17, 1-18).^{32,33,47-49}



Scheme 1-15. Three classes of photo-inducible DNA cross-linking agents via a carbon cation mechanism.

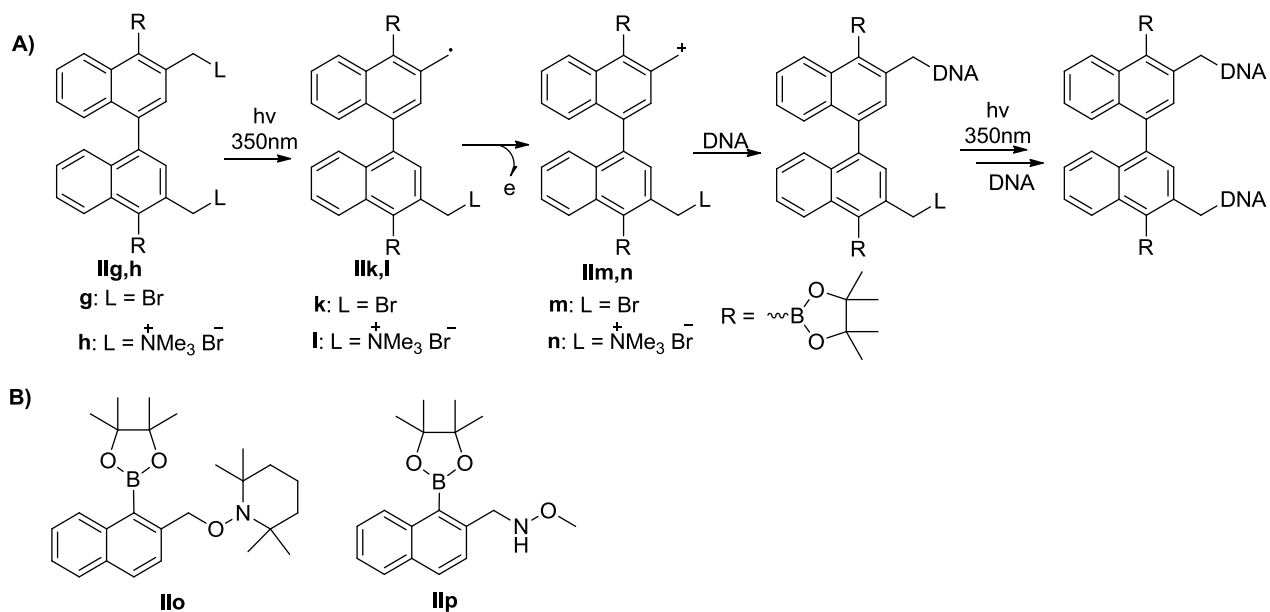
Binitroimidazole analogues **IId-f** were observed to generate DNA ICL formation and direct strand breaks (DSB) upon UV irradiation at 350 nm.⁴⁷ Free radicals were involved in the DNA cross-linking process but not the species that directly cross-linked DNA, since the presence of O₂, which would quench the free radicals, did not affect the ICL formation. Carbon cation was proposed to be the key intermediate cross-linking DNA. However there was no direct evidence obtained due to the low reactivity of **IId-f** (scheme 1-16).



Scheme 1-16. Photo-induced DNA cross-linking by binitroimidazoles via a carbon cation mechanism.

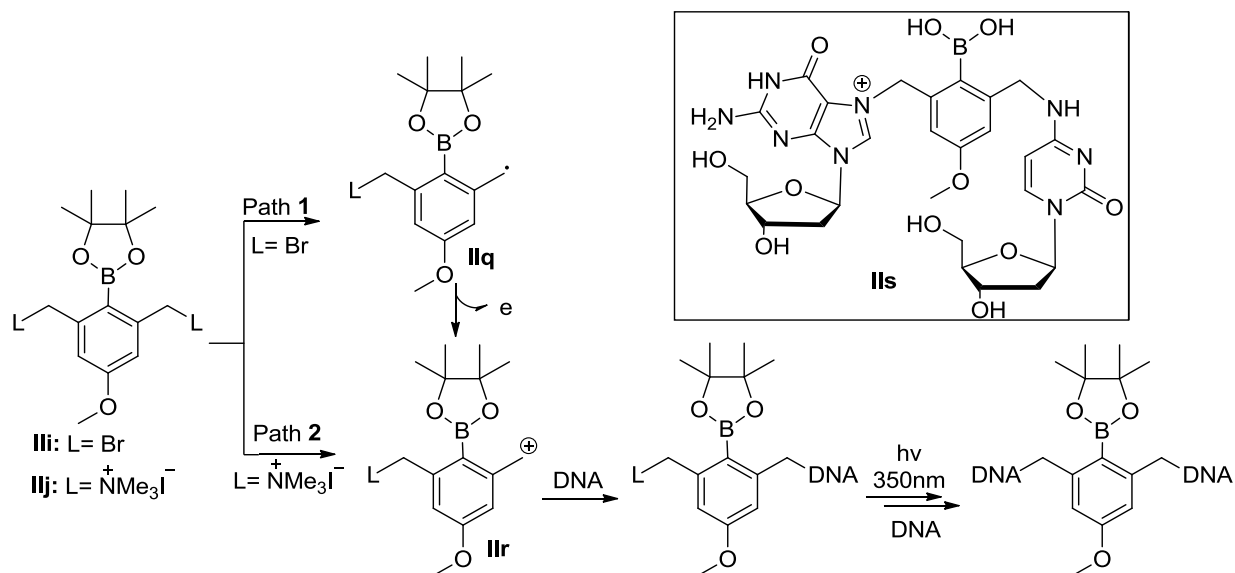
Very recently, bifunctional naphthalene compounds **IIf,h** have been developed in our group as photo-inducible DNA cross-linking agents via a carbocation mechanism (Scheme 1-15, 1-17A).⁴⁸ All these compounds underwent the same mechanism, namely free radicals **IIf,i** were first formed and then converted to carbocations **IIf,m,n** that directly cross-linked DNA. The mechanism was determined by free radical and cation trapping using 2,2,6,6-

tetramethylpiperidin-1-oxyl (TEMPO) and methoxyamine, respectively. Both TEMPO and methoxyamine inhibited DNA ICL formation induced by **Ilg,h**, indicating that both free radical and carbocation were involved in the cross-linking process for compound **Ilg,h**. Direct evidence was gained by isolation and determination of the radical and cation trapping adducts formed with the monomers (Scheme 1-17B). To determine whether the carbocations are produced from direct heterolysis of C-L bond or through free radical oxidation, two distinct monomer trapping experiments were carried out. One used methoxyamine for the cation trapping while the other used co-existence of TEMPO and methoxyamine as trapping agents. The cation trapping product **Ilp** was observed in the presence of methoxyamine. But the presence of TEMPO greatly reduced the yield of the cation trapping product **Ilp** and produced radical trapping product **Ilo**, suggesting that the carbocation was produced from the free radical oxidation. Complete inhibition of the ICL formation for **Ilg,h** by addition of methoxyamine, indicated that the carbocations cross-linked DNA but not the free radicals.⁴⁸



Scheme 1-17. Photo-induced DNA ICL by naphthalene analogues via a carbon cation mechanism and the trapping products.

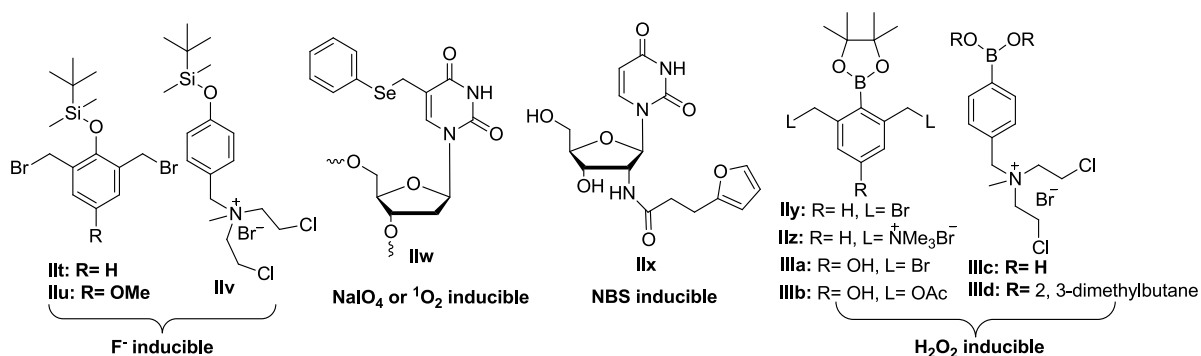
Bifunctional benzyl boronates **III,j** are another class of DNA cross-linking agents developed by our group that cross-link DNA via carbocations under UV irradiation.⁴⁹ Benzyl cations, generated from **III,j**, cross-linked DNA at guanine (dG) and cytosine (dC). The cross-linking product **IIIs** was confirmed by LC-MS-MS. The leaving groups have a large effect on the pathways of carbocation formation. Bromide **IIIi** would undergo a radical-cation pathway (path 1, Scheme 1-18), namely free radical **IIq** was first formed, and then converted to carbocation **IIr** via the oxidation. The ammonium salt **IIIj** underwent path 2 in which direct heterolysis of C-N bond generated carbocation **IIr**. The mechanism was proved by trapping experiments using TEMPO and methoxyamine as a radical and cation trapping reagent, respectively. Methoxyamine completely quenched DNA ICL formation for both compounds **IIIi** and **IIIj**, indicating that carbocations were involved in the DNA cross-linking process. On the other hand, TEMPO showed inhibitory effect on bromide **IIIi** but not for ammonium salt **IIIj**, suggesting that free radicals were involved in the DNA ICL formation process for **IIIi** but not for **IIIj**.



Scheme 1-18. Photo-induced DNA cross-linking by benzyl boronates via a carbon cation mechanism.

1.3.2. DNA Interstrand Cross-linking Induced by Chemical Agents

Chemical agents, such as fluoride (F^-), $NaIO_4$ or 1O_2 , N-bromosuccinimide (NBS), and hydrogen peroxide (H_2O_2) were employed to activate various precursors to induce DNA ICL formation. Fluoride-inducible DNA cross-linking agents contain a silyl-protecting group that can be selectively cleaved by fluoride ion (**II**t,u and **II**v) (Scheme 1-19).^{50,51} $NaIO_4$ or 1O_2 inducible DNA cross-linking agents are phenyl selenide-containing compounds. In the presence of $NaIO_4$ or 1O_2 , these selenides can be converted to the methide intermediates that cross-link DNA (**II**w).⁵² Some furan-containing nucleosides can be activated by NBS to form enal species that cross-link DNA (**II**x).⁵³ Hydrogen peroxide inducible DNA cross-linking agents contain an arylboronate or boronic acid trigger that selectively reacts with H_2O_2 to release DNA cross-links (**II**y,z and **III**a-d).^{54,55} (scheme 1-19).



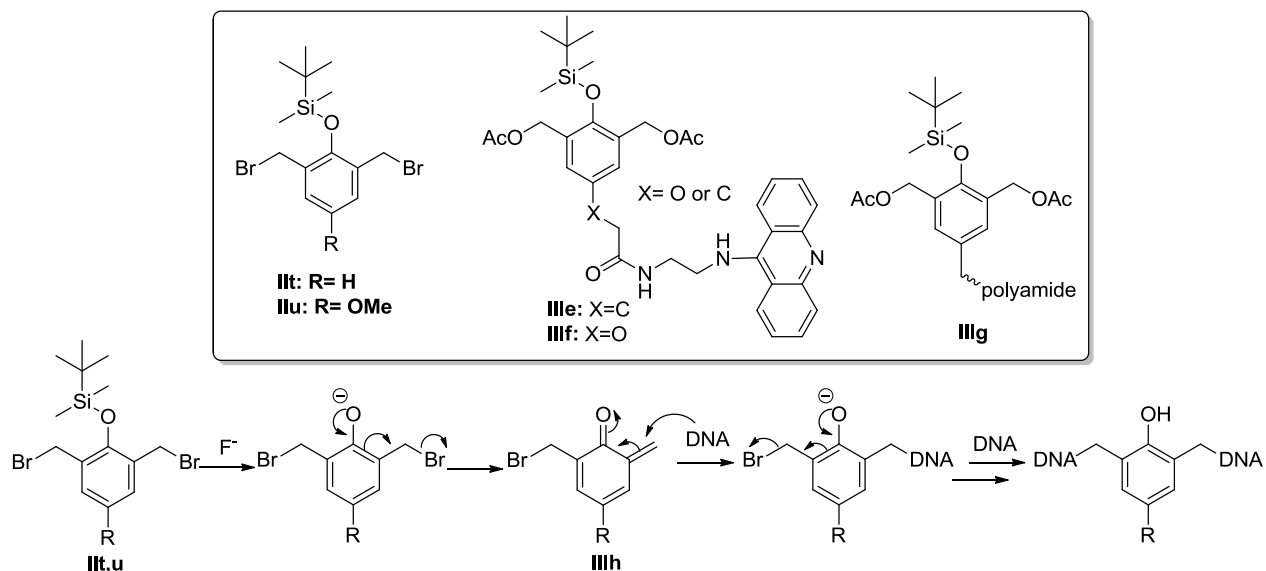
Scheme 1-19. Four types of chemical agents inducible cross-linking agents.

Fluoride (F^-)-inducible DNA Cross-linking Agents

Fluoride-induced desilylation is a very important chemical reaction since it can selectively and efficiently remove the silyl-protection and release the free alcohols. This reaction has been used for designing fluoride inducible DNA cross-linking agents. Recently, a large number of tert-

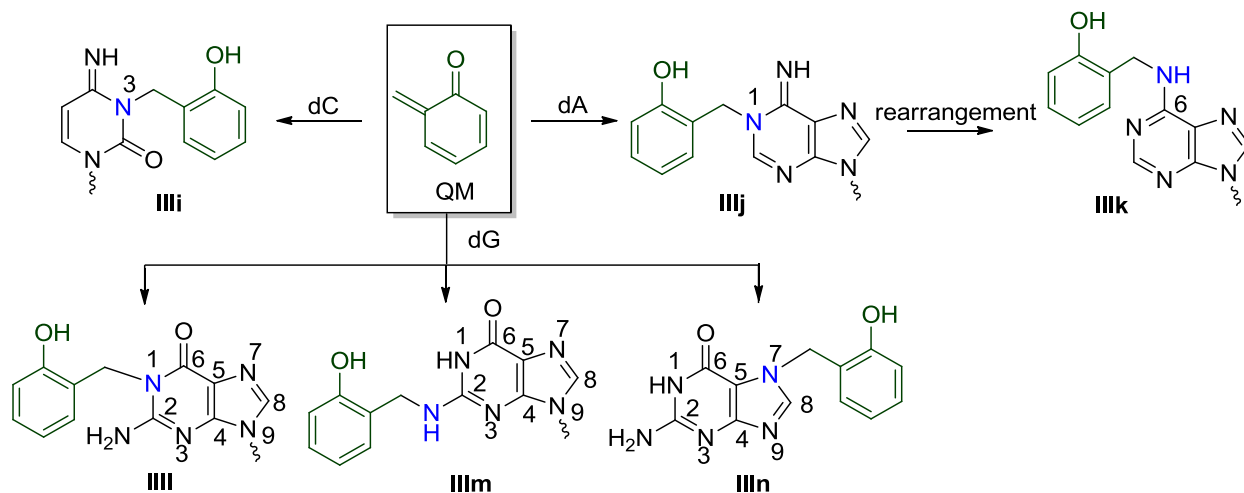
butyldimethylsilyl (TBDMS)-containing precursors have been developed as fluoride inducible DNA cross-linking agents.^{50,51,56} Two common mechanisms are involved in the DNA cross-linking process, either via quinone methide (QM) or nitrogen mustard formation.

The fluoride inducible quinone methide precursors (QMs) were first reported by Rokita and co-workers (Scheme 1-20).^{50,56} Compound **III**t was the first bifunctional silyl-containing QM precursor reported by Rokia group. It could be activated by fluoride ion to form interstrand cross-linking. However, the ICL efficiency for this compound was very poor (less than 10%) even with high concentration of KF (10 mM).⁵⁰ Modification of **III**t by introducing a strong electron donating OMe group *para* to the silyl group led to compound **III**u. The electron donating groups were reported to facilitate the QM formation.⁴² Further modification led to **III**e,f and **III**g containing a DNA major (acridine) or minor groove (polyamide) binding group with the goal of increasing the delivery selectivity.^{57,58} As expected, compound **III**e was successfully delivered to the cross-linking sites in the major groove, and showed higher DNA ICL yield (64%) than **III**t.⁵⁷ However, **III**g led to very low ICL yield (only 4%) due to the formation of the intramolecular adduct.⁵⁸ The mechanism of action for this class of compounds involved the cleavage of the Si-O bond, leading to the formation of the active QM intermediate (**III**h) that directly produced DNA ICL products (scheme 1-20).



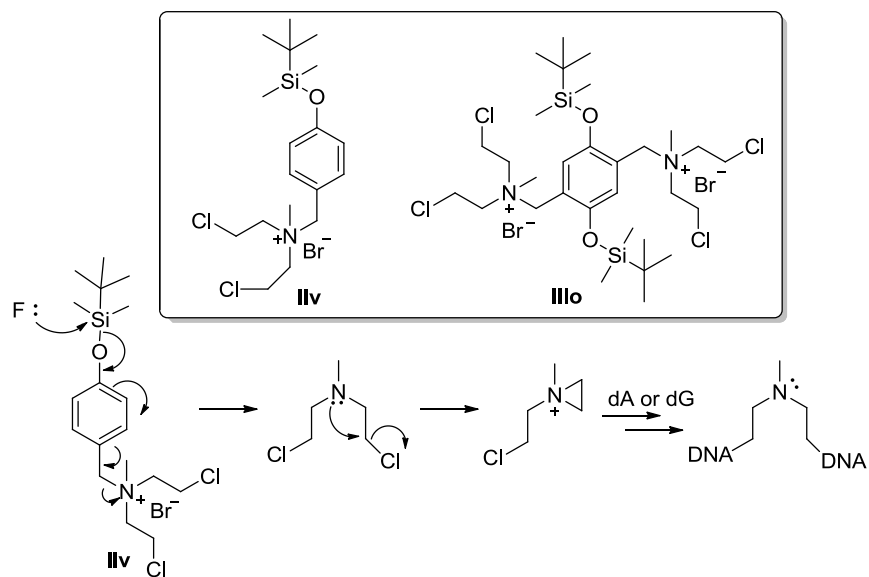
Scheme 1-20. Fluoride-induced QM precursors and mechanism of action.

The reaction sites for DNA ICL formation were dC, dA and dG.^{3,59,60} The dC residue reacted with QM at N3 position (**IIIi**),³ and dA mainly reacted at N1 position to form monoadduct (**IIIj**)⁵⁹ that was not stable and converted to dA-N⁶ adduct (**IIIk**), while multiple active sites (N1, N² or N7) were found in dG residue (**III-n**) (Scheme 1-21).⁶⁰



Scheme 1-21. Active sites and monoadducts formed by fluoride-inducible QM precursors.

Fluoride-activated nitrogen mustard analogues (**IIv**, **IIIo**) were also reported, both of which contain a trigger unit (TBDMS-protected phenol) and an effector (nitrogen mustard).⁵¹ The trigger unit can be selectively removed by fluoride ion that cleaved the Si-O bond releasing the active nitrogen mustard that directly cross-linked DNA (scheme 1-22). These compounds (**IIv**, **IIIo**) showed high selectivity toward fluoride ion. No ICL formation was observed in the absence of fluoride, while efficient DNA ICLs were obtained for **IIv** (73%) and **IIIo** (99%) in the presence of fluoride (10 mM). DNA cross-linking occurred mainly at the N7 of adenine or guanine residues.^{15,51}



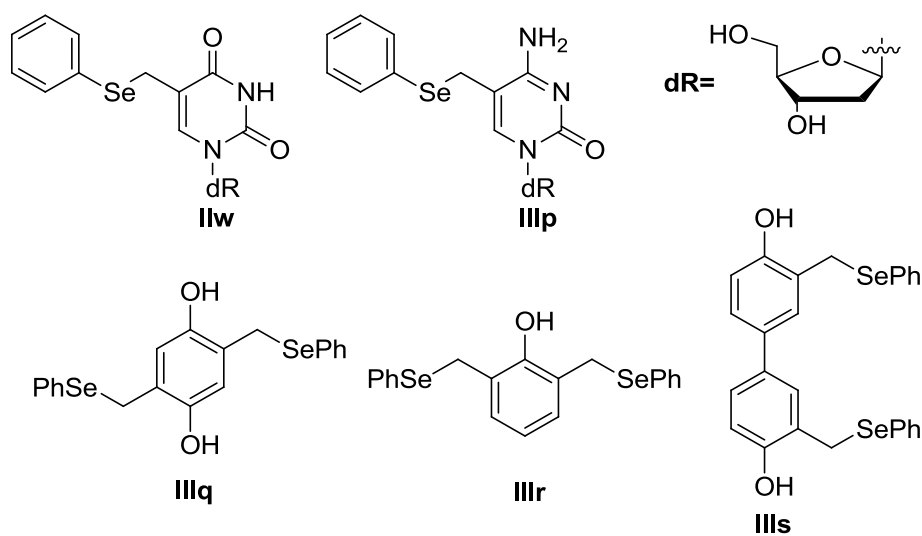
Scheme 1-22. Fluoride-induced nitrogen mustard precursors and the mechanism for ICL formation.

NaIO₄ or ¹O₂-inducible DNA Cross-linking Agents

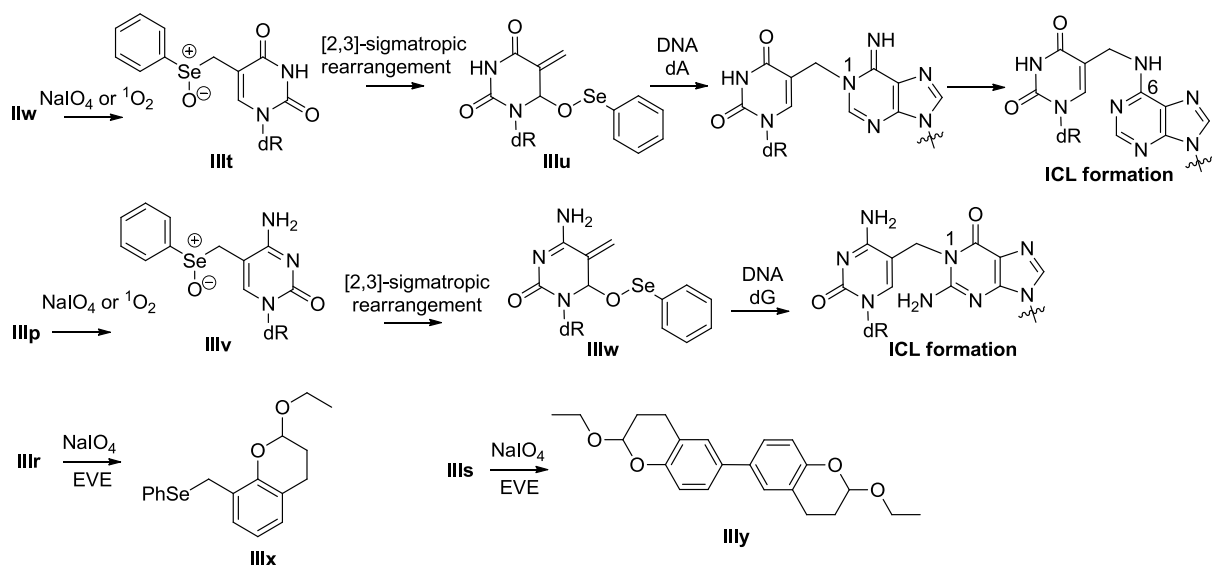
There are two kinds of selenide-containing DNA alkylating agents. One type is phenylselenide-modified pyrimidine nucleosides (**IIw**, **IIIp**), and the other type is the phenol derivatives that contain two phenylselenide groups as benzylic leaving groups (**IIIq-s**) (scheme 1-23). Both can

be activated by NaIO_4 or $^1\text{O}_2$ to generate highly reactive methides that directly alkylate DNA.⁶¹⁻

⁶³ The mechanism of action for compounds **IIw**, **IIIp** involved the oxidization of selenide to selenoxide, which was converted to the reactive methide intermediates via [2,3]-Sigmatropic rearrangement that directly cross-link DNA (Scheme 1-24). The ICL formation by the phenol derivatives **IIIq-s** was also related with the QM formation, which was confirmed via ethyl vinyl ether (EVE) trapping. The QM trapping adducts **IIIx** and **IIIy** were observed for compounds **IIIr** and **IIIs** (Scheme 1-24). The dA and dG residues were found to be the major cross-link sites for both classes of compounds.⁶¹⁻⁶⁴



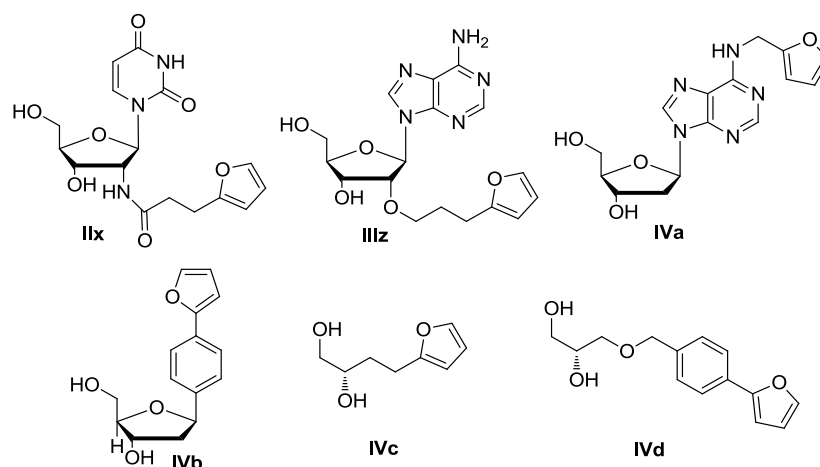
Scheme 1-23. NaIO_4 or $^1\text{O}_2$ inducible DNA cross-linking agents.



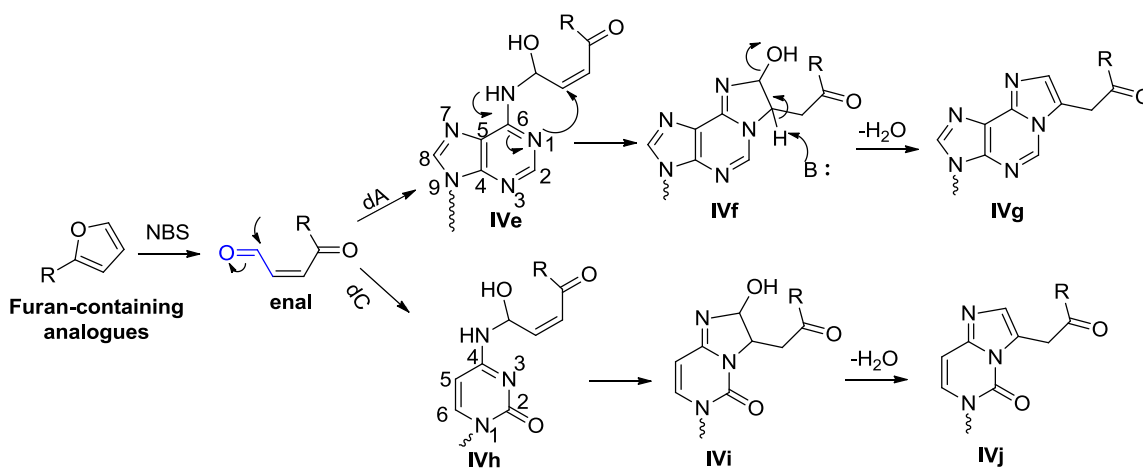
Scheme 1-24. Mechanism of action for ICL formation.

NBS-inducible DNA Cross-linking Agents

The furan-containing analogues were developed by Madder and co-workers (Scheme 1-25).^{53,65-70} After incorporating into DNA, the furan moiety can be oxidized by NBS to generate a reactive enal species that directly cross-link DNA. The dA or dC residues were found to be the major cross-linking sites.^{53,65-70} The aldehyde group of the enal was attacked by N⁶ of dA or N⁴ of dC to form the adduct **IVe** or **IVh** that underwent Michael addition to afford the intermediate **IVf** or **IVi**. Spontaneously, the elimination reaction occurred with **IVf** or **IVi** generating more stable ICL product **IVg** or **IVj** (Scheme 1-26).^{53,65-70}



Scheme 1-25. NBS-inducible DNA cross-linking agents.



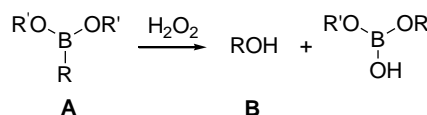
Scheme 1-26. Mechanism of action for furan-containing analogues.

H₂O₂-inducible DNA Cross-linking Agents

The key problem for most DNA cross-linking agents is the poor selectivity toward cancer cells over normal cells. They are not only toxic to the cancer cells but also toxic to the normal cells. In order to improve the selectivity and reduce the toxicity of the DNA cross-linking agents, prodrugs that can only be activated under tumor-specific conditions were developed. Due to the faster growth of cancer cells than normal cells, higher level of reactive oxygen species (ROS),

such as superoxide (O_2^-), hydroxyl radicals ($OH\cdot$) and hydrogen peroxide (H_2O_2), was observed in cancer cells.⁷¹⁻⁷⁴ The higher level of ROS is a unique property of cancer cells that can be used to develop novel anticancer drugs.

Hydrogen peroxide (H_2O_2) as a normal ROS is well known to react selectively with boronic acid or boronic esters (A) that are converted to the HO-

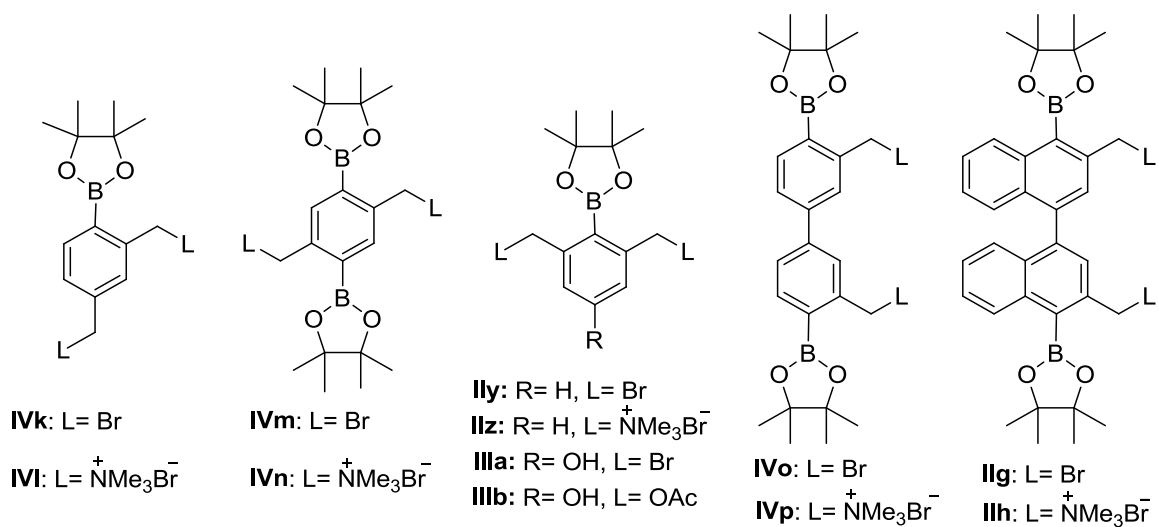


containing compounds (B).⁷⁵ The huge change from a

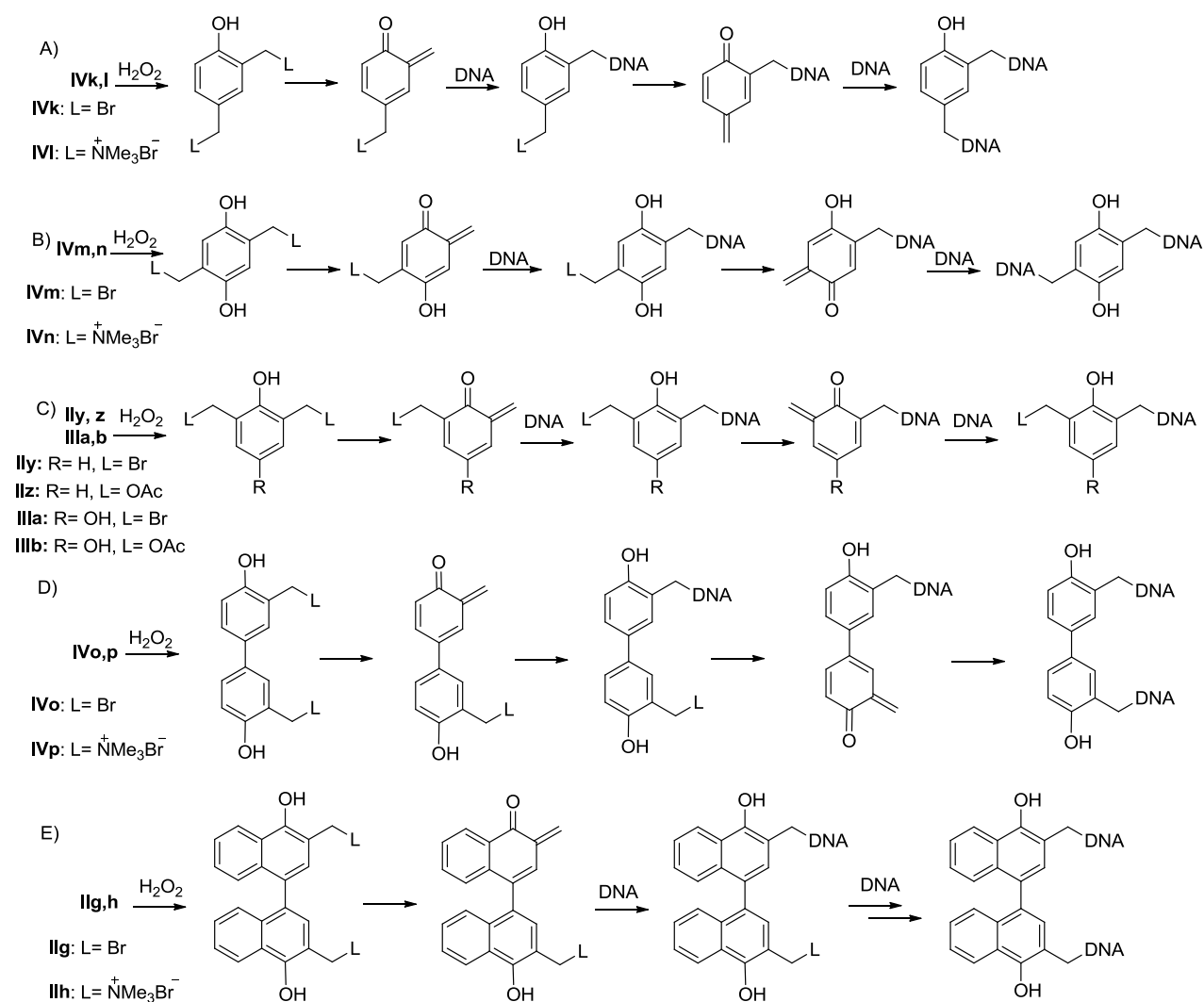
strong electron withdrawing boron group to a strong electron donating hydroxyl group can greatly alter the reactivity of the compounds. Based on this understanding, several H_2O_2 -inducible DNA cross-linking agents have been developed, with the purpose to reduce the toxicity toward normal cells,^{48,54,55,76-80} including H_2O_2 -activated QM precursors (scheme 1-27)^{48,54,76-78} and H_2O_2 -activated nitrogen mustard precursors (scheme 1-29).^{55,79,80} All these molecules contain a boronic acid or boronic ester as the trigger unit. The strong electron withdrawing boron group in the trigger unit deactivates these molecules, but can selectively react with H_2O_2 to produce a strong electron donating hydroxyl group therefore activating the prodrugs to release DNA alkylating agents, QM or nitrogen mustard that cross-link DNA.

Compounds **IVk-p**, **IIIa,b**, **IIg,h** and **Ily,z** (scheme 1-27) can be activated by H_2O_2 to form highly reactive QM intermediates (scheme 1-28) that directly cross-link DNA. Among them, compound **IIg,h**, **Ily,z** and **IIIa,b** have higher DNA cross-linking efficiency, and were chosen as novel scaffolds for anticancer drug development. The leaving group L and the aromatic substituent R greatly affected DNA cross-linking efficiency. In comparison with the ammonia salts **IVl** and **IIz**, compounds **IVk** and **Ily** with bromo as the leaving group facilitated QM formation and showed higher ICL efficiency.⁵⁴ The presence of an electron donating aromatic

substituent (R) favored QM formation and afforded higher ICL yield, while the electron withdrawing groups inhibited QM formation.⁷⁷



Scheme 1-27. H₂O₂-activated QM precursors.



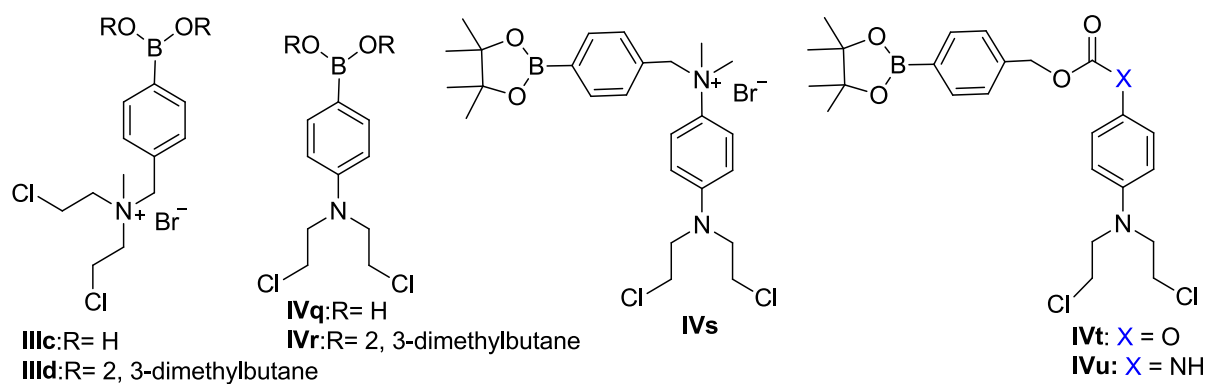
Scheme 1-28. Mechanism of action for H_2O_2 -activated QM precursors.

Peng and coworkers have developed several classes of H_2O_2 -activated nitrogen mustard processors that contain a boronic or boronic ester as a trigger unit (scheme 1-29).^{55, 79, 80} The strong electron withdrawing boron group can deactivate the nitrogen mustard, but selectively react with H_2O_2 to generate a strong electron donating OH group releasing the highly active nitrogen mustard. Three ways were employed to bridge nitrogen mustard and the trigger unit, including nitrogen directly bonded with the benzene ring (**IVq,r**),⁷⁹ via a positively charged linker (**IVs**)⁵⁵ or a neutral electron withdrawing linker (**IVt,u**).⁸⁰

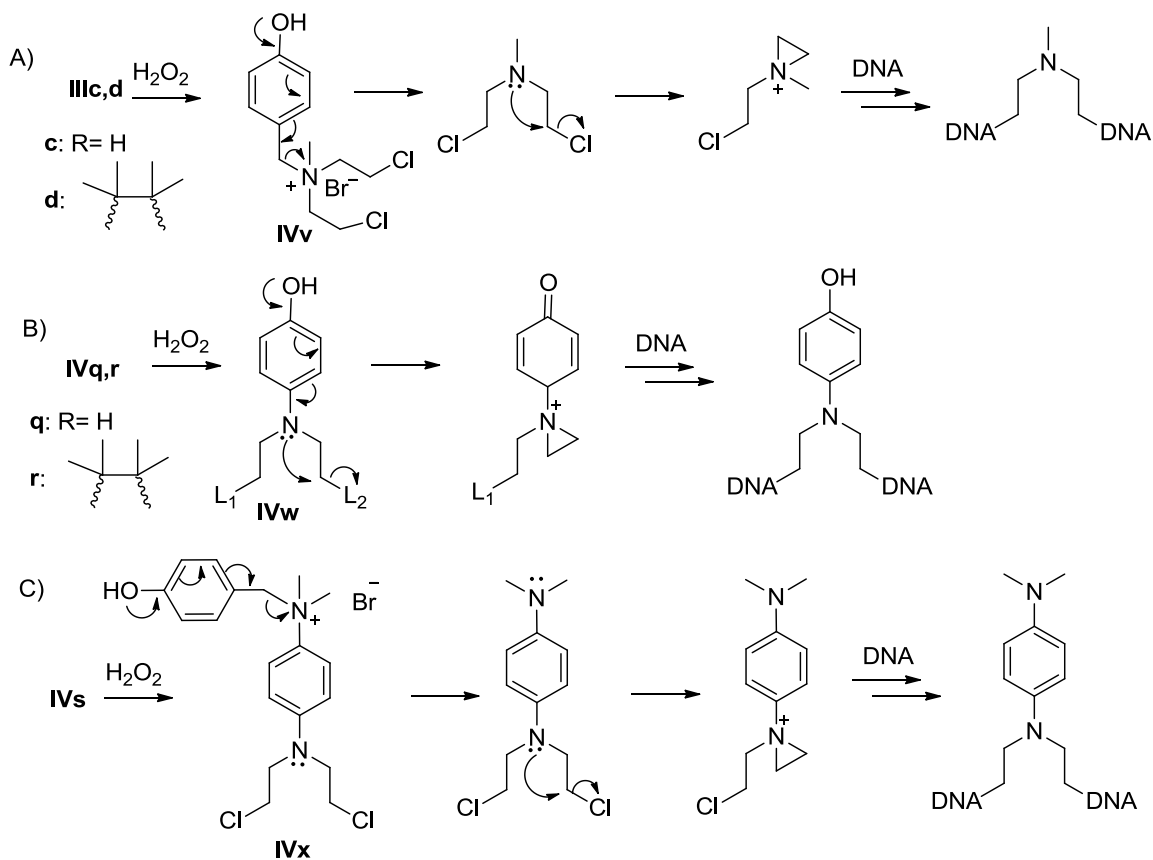
Compounds **IIIc,d** were the first generation of H₂O₂ activated nitrogen mustard precursors, which contain a boronic acid (or ester) and a nitrogen mustard with a positive charge. The positively charged nitrogen greatly decreased the activity of nitrogen mustard therefore masking the toxicity of these prodrugs. The boronic acid (or ester) in **IIIc,d** can selectively react with H₂O₂ to form an intermediates **IVv** containing a hydroxyl group, which spontaneously released free nitrogen mustard that directly cross-link DNA. Compounds **IIIc,d** showed good selectivity toward H₂O₂. High ICL yield was obtained in the presence of H₂O₂ while no ICL formation was observed without H₂O₂. They also showed selective toxicity towards cancer cells with great inhibitory effect for cancer cell growth, while normal cells were less affected.⁵⁵ However, low activity was found for compounds **IIIc,d** possibly due to the positive charge of the molecule that prevented them from going through the cell membrane.

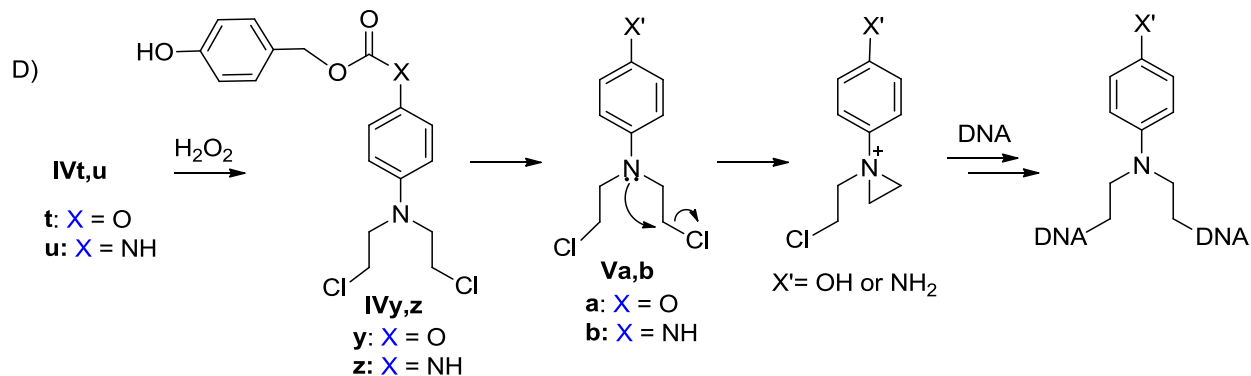
In order to increase the cell membrane permeability, two classes of neutral compounds (**IVq,r**, **IVt,u**) were designed. Compounds **IVq,r** contain the nitrogen of nitrogen mustard directly bonded to the benzene ring with a boronic acid (or ester) group on the para-position. The electron withdrawing boronic acid (or ester) can greatly pull the electron away from the nitrogen to boron via both inductive and resonance effects, therefore deactivating the nitrogen mustard. On the other side, the boronic acid (or ester) can selectively react with H₂O₂, which convert **IVq,r** to **IVw** with an electron donating OH group that push the electron to the nitrogen of the nitrogen mustard therefore activating the prodrug for ICL formation. Compounds **IVt,u** were designed to study the effect of linker units on the selectivity of these prodrugs towards hydrogen peroxide (scheme 1-29). The aromatic nitrogen mustard moiety and the trigger unit were connected via an electron withdrawing carboxamide or carbonate linker, which decreased the electron density of the nitrogen therefore deactivating the nitrogen mustard. In the presence of

H₂O₂, compound **IVt,u** can be activated to form **Va,b** containing a strong electron donating group (OH or NH₂) that can efficiently cross-link DNA (scheme 1-30). For all these H₂O₂-activated nitrogen mustard precursors, dG, dC, and dA were found to be the possible cross-linking sites.^{55, 79, 80}



Scheme 1-29. H₂O₂-inducible DAN cross-linking agents.





Scheme 1-30. Mechanism of action for H₂O₂-activated nitrogen mustard precursors.

Most of the existing methods for inducing DNA ICL formation require chemical reagents, leading to the complexity for the *in vivo* application. Some require additional chemical reagents (Cu^I) that are highly toxic to the cells, which limited their applications under cellular conditions. Among these methods, photo-induction and H₂O₂-induction are most attractive due to their bioorthogonal properties. Photo-induction is a green method that is clean, non-invasive, and doesn't require additional chemical reagents. H₂O₂ is endogenously generated. More importantly, cancer cells produce higher level of H₂O₂ than normal cells, which enable selectively targeting cancer cells by using H₂O₂-activated DNA cross-linking agents. This thesis mainly focus on photo- and H₂O₂-inducible DNA cross-linking agents.

1.3. References

1. Watson JD, Crick FHC. Molecular Structure of Nucleic Acids: A Structure for Deoxyribose Nucleic Acid. *Nature*. 1953;171:737–8.
2. Pande P, Shearer J, Yang J, Greenberg WA, Rokita SE. Alkylation of Nucleic Acids by a Model Quinone Methide. *Journal of the American Chemical Society*. 1999;121:6773–9.
3. Rokita SE, Yang J, Pande P, Greenberg WA. Quinone Methide Alkylation of Deoxycytidine. *The Journal of Organic Chemistry*. 1997;62:3010–2.

4. Cao S, Peng X. Exploiting Endogenous Cellular Process to Generate Quinone Methides In Vivo. *Current Organic Chemistry*. 2014;18:70–85.
5. Helleday T, Petermann E, Lundin C, Hodgson B, Sharma RA. DNA repair pathways as targets for cancer therapy. *Nature Reviews Cancer*. 2008;8:193–204.
6. Ralhan R, Kaur J. Alkylating agents and cancer therapy. *Expert Opinion on Therapeutic Patents*. 2007;17:1061-75.)
7. Kondo N, Takahashi A, Ono K, Ohnishi T. DNA Damage Induced by Alkylating Agents and Repair Pathways. *Journal of Nucleic Acids*. 2010;2010:1–7.
8. Agarwala SS. Temozolomide, a Novel Alkylating Agent with Activity in the Central Nervous System, May Improve the Treatment of Advanced Metastatic Melanoma. *The Oncologist*. 2000;5:144–51.
9. Mouhri ZS, Goodfellow E, Kelley S, Stein R, Rogers R, Jean-Claude BJ. ¹⁵N-, ¹³C- and ¹H-NMR Spectroscopy Characterization and Growth Inhibitory Potency of a Combi-Molecule Synthesized by Acetylation of an Unstable Monoalkyltriazene. *Molecules*. 2017;22:1183.
10. Kewitz S, Stiefel M, Kramm CM, Staeger MS. Impact of O6-methylguanine-DNA methyltransferase (MGMT) promoter methylation and MGMT expression on dacarbazine resistance of Hodgkins lymphoma cells. *Leukemia Research*. 2014;38:138–43.
11. Wyatt MD, Pittman DL. Methylating Agents and DNA Repair Responses: Methylated Bases and Sources of Strand Breaks. *Chemical Research in Toxicology*. 2006;19:1580–94.
12. Kowalczyk A, Carmical JR, Zou Y, Houten BV, Lloyd RS, Harris CM, et al. Intrastrand DNA Cross-Links as Tools for Studying DNA Replication and Repair: Two-, Three-, and Four-Carbon Tethers between the N2 Positions of Adjacent Guanines†. *Biochemistry*. 2002;41:3109–18.
13. Huang Y, Li L. DNA crosslinking damage and cancer - a tale of friend and foe. *Translational Cancer Research*. 2013; 2:144-154.
14. Johnstone TC, Park GY, Lippard S J. Understanding and Improving Platinum Anticancer Drugs – Phenanthriplatin. *Anticancer Research*. 2014; 34:471–476.
15. Noll DM, Mason TM, Miller PS. Formation and Repair of Interstrand Cross-Links in DNA. *Chemical Reviews*. 2006;106:277–301.

16. Florea A-M, Büsselberg D. Cisplatin as an Anti-Tumor Drug: Cellular Mechanisms of Activity, Drug Resistance and Induced Side Effects. *Cancers*. 2011;3:1351–71.
17. Trzaska S. "Cisplatin". *Chemical & Engineering News*. 20 June 2005; 83 (25).
18. Brulikova L, Hlavac J, and Hradil P. DNA Interstrand Cross-Linking Agents and their Chemotherapeutic Potential. *Current Medicinal Chemistry*, 2012;19:364-385.
19. Oun R, Moussa YE, Wheate NJ. The side effects of platinum-based chemotherapy drugs: a review for chemists. *Dalton Transactions*. 2018;47:6645–53.
20. Danshiitsoodol N, Pinho CAD, Matoba Y, Kumagai T, Sugiyama M. The Mitomycin C (MMC)-binding Protein from MMC-producing Microorganisms Protects from the Lethal Effect of Bleomycin: Crystallographic Analysis to Elucidate the Binding Mode of the Antibiotic to the Protein. *Journal of Molecular Biology*. 2006;360:398–408.
21. Rajski SR, Williams RM. DNA Cross-Linking Agents as Antitumor Drugs. *Chemical Reviews*. 1998;98:2723–96.
22. Fan H, Peng X. Novel DNA Cross-Linking Reagents. *Advances in Molecular Toxicology*. 2016;10:235–92.
23. Momtaz TK, Fitzpatrick TB. The Benefits And Risks Of Long-Term Puva Photochemotherapy. *Dermatologic Clinics*. 1998;16:227–34.
24. Kashida H, Doi T, Sakakibara T, Hayashi T, Asanuma H. p-Stilbazole Moieties As Artificial Base Pairs for Photo-Cross-Linking of DNA Duplex. *Journal of the American Chemical Society*. 2013;135:7960–6.
25. Sun H, Fan H, Eom H, Peng X. Coumarin-Induced DNA Ligation, Rearrangement to DNA Interstrand Crosslinks, and Photorelease of Coumarin Moiety. *ChemBioChem*. 2016;17:2046–53.
26. Sun H, Fan H, Peng X. Quantitative DNA Interstrand Cross-Link Formation by Coumarin and Thymine: Structure Determination, Sequence Effect, and Fluorescence Detection. *The Journal of Organic Chemistry*. 2014;79:11359–69.
27. Fujimoto K, Yamada A, Yoshimura Y, Tsukaguchi T, Sakamoto T. Details of the Ultrafast DNA Photo-Cross-Linking Reaction of 3-Cyanovinylcarbazole Nucleoside: Cis–Trans Isomeric Effect and the Application for SNP-Based Genotyping. *Journal of the American Chemical Society*. 2013;135:16161–7.

28. Wang P, Liu R, Wu X, Ma H, Cao X, Zhou P, et al. A Potent, Water-Soluble and Photoinducible DNA Cross-Linking Agent. *Journal of the American Chemical Society*. 2003;125:1116–7.
29. Verga D, Nadai M, Doria F, Percivalle C, Antonio MD, Palumbo M, et al. Photogeneration and Reactivity of Naphthoquinone Methides as Purine Selective DNA Alkylating Agents. *Journal of the American Chemical Society*. 2010;132:14625–37.
30. Richter SN, Maggi S, Mels SC, Palumbo M, Freccero M. Binol Quinone Methides as Bisalkylating and DNA Cross-Linking Agents. *Journal of the American Chemical Society*. 2004;126:13973–9.
31. Colloredo-Mels S, Doria F, Verga D, Freccero M. Photogenerated Quinone Methides as Useful Intermediates in the Synthesis of Chiral BINOL Ligands. *The Journal of Organic Chemistry*. 2006;71:3889–95.
32. Lin G, Li L. Oxidation and Reduction of the 5-(2'-Deoxyuridinyl)methyl Radical. *Angewandte Chemie International Edition*. 2013;52:5594–8.
33. Weng L, Horvat SM, Schiesser CH, Greenberg MM. Deconvoluting the Reactivity of Two Intermediates Formed from Modified Pyrimidines. *Organic Letters*. 2013;15:3618–21.
34. Doi T, Kashida H, Asanuma H. Efficiency of [2+2] photodimerization of various stilbene derivatives within the DNA duplex scaffold. *Organic & Biomolecular Chemistry*. 2015;13:4430–7.
35. Kamiya Y, Iishiba K, Doi T, Tsuda K, Kashida H, Asanuma H. Terminus-free siRNA prepared by photo-crosslinking activated via slicing by Ago2. *Biomaterials Science*. 2015;3:1534–8.
36. Haque MM, Sun H, Liu S, Wang Y, Peng X. Photoswitchable Formation of a DNA Interstrand Cross-Link by a Coumarin-Modified Nucleotide. *Angewandte Chemie International Edition*. 2014;53:7001–5.
37. Sakamoto T, Tanaka Y, Fujimoto K. DNA Photo-Cross-Linking Using 3-Cyanovinylcarbazole Modified Oligonucleotide with Threoninol Linker. *Organic Letters*. 2015;17:936–9.
38. Yoshimura Y, Fujimoto K. Ultrafast Reversible Photo-Cross-Linking Reaction: Toward in Situ DNA Manipulation. *Organic Letters*. 2008;10:3227–30.

39. Fujimoto K, Konishi-Hiratsuka K, Sakamoto T, Yoshimura Y. Site-Specific Cytosine to Uracil Transition by Using Reversible DNA Photo-crosslinking. *ChemBioChem*. 2010;11:1661–4.
40. Wu Q, Christensen LA, Legerski RJ, Vasquez KM. Mismatch repair participates in error-free processing of DNA interstrand crosslinks in human cells. *EMBO reports*. 2005;6:551–7.
41. Stern RS, Nichols KT, Väkevä LH. Malignant Melanoma in Patients Treated for Psoriasis with Methoxsalen (Psoralen) and Ultraviolet A Radiation (PUVA). *New England Journal of Medicine*. 1997;336:1041–5.
42. Weinert EE, Dondi R, Colloredo-Melz S, Frankenfield KN, Mitchell CH, Freccero M, et al. Substituents on Quinone Methides Strongly Modulate Formation and Stability of Their Nucleophilic Adducts. *Journal of the American Chemical Society*. 2006;128:11940–7.
43. Škalamera Đ, Bohne C, Landgraf S, Basarić N. Photodeamination Reaction Mechanism in Aminomethyl p-Cresol Derivatives: Different Reactivity of Amines and Ammonium Salts. *The Journal of Organic Chemistry*. 2015;80:10817–28.
44. Percivalle C, Doria F, Freccero M. Quinone Methides as DNA Alkylating Agents: An Overview on Efficient Activation Protocols for Enhanced Target Selectivity. *Current Organic Chemistry*. 2014;18:19–43.
45. Verga D, Richter SN, Palumbo M, Gandolfi R, Freccero M. Bipyridyl ligands as photoactivatable mono- and bis-alkylating agents capable of DNA cross-linking. *Org. Biomol. Chem*. 2007;5:233–5.
46. Doria F, Richter SN, Nadai M, Colloredo-Mels S, Mella M, Palumbo M, et al. BINOL–Amino Acid Conjugates as Triggerable Carriers of DNA-Targeted Potent Photocytotoxic Agents. *Journal of Medicinal Chemistry*. 2007;50:6570–9.
47. Han Y, Chen W, Kuang Y, Sun H, Wang Z, Peng X. UV-Induced DNA Interstrand Cross-Linking and Direct Strand Breaks from a New Type of Binitroimidazole Analogue. *Chemical Research in Toxicology*. 2015;28:919–26.
48. Wang Y, Lin Z, Fan H, Peng X. Photoinduced DNA Interstrand Cross-Link Formation by Naphthalene Boronates via a Carbocation. *Chemistry - A European Journal*. 2016;22:10382–6.
49. Wang Y, Liu S, Lin Z, Fan Y, Wang Y, Peng X. Photochemical Generation of Benzyl Cations That Selectively Cross-Link Guanine and Cytosine in DNA. *Organic Letters*. 2016;18:2544–7.

50. Zeng Q, Rokita SE. Tandem Quinone Methide Generation for Cross-Linking DNA. *The Journal of Organic Chemistry*. 1996;61:9080–1.
51. Wu J, Huang R, Wang T, Zhao X, Zhang W, Weng X, et al. Fluoride as an inducible DNA cross-linking agent for new antitumor prodrug. *Organic & Biomolecular Chemistry*. 2013;11:2365-9.
52. Peng X, Hong IS, Li H, Seidman MM, Greenberg MM. Interstrand Cross-Link Formation in Duplex and Triplex DNA by Modified Pyrimidines. *Journal of the American Chemical Society*. 2008;130:10299–306.
53. Halila S, Velasco T, Clercq PD, Madder A. Fine-tuning furan toxicity: fast and quantitative DNA interchain cross-link formation upon selective oxidation of a furan containing oligonucleotide. *Chemical Communications*. 2005;936-8.
54. Cao S, Wang Y, Peng X. The Leaving Group Strongly Affects H₂O₂-Induced DNA Cross-Linking by Arylboronates. *The Journal of Organic Chemistry*. 2014;79:501–8.
55. Kuang Y, Balakrishnan K, Gandhi V, Peng X. Hydrogen Peroxide Inducible DNA Cross-Linking Agents: Targeted Anticancer Prodrugs. *Journal of the American Chemical Society*. 2011;133:19278–81.
56. Fakhari F, Rokita SE. A walk along DNA using bipedal migration of a dynamic and covalent crosslinker. *Nature Communications*. 2014;5:5591.
57. Veldhuyzen WF, Pande P, Rokita SE. A Transient Product of DNA Alkylation Can Be Stabilized by Binding Localization. *Journal of the American Chemical Society*. 2003;125:14005–13.
58. Kumar D, Veldhuyzen WF, Zhou Q, Rokita SE. Conjugation of a Hairpin Pyrrole-Imidazole Polyamide to a Quinone Methide for Control of DNA Cross-Linking. *Bioconjugate Chemistry*. 2004;15:915–22.
59. Veldhuyzen WF, Shallop AJ, Jones RA, Rokita SE. Thermodynamic versus Kinetic Products of DNA Alkylation as Modeled by Reaction of Deoxyadenosine. *Journal of the American Chemical Society*. 2001;123:11126–32.
60. Veldhuyzen WF, Lam Y-F, Rokita SE. 2'-Deoxyguanosine Reacts with a Model Quinone Methide at Multiple Sites. *Chemical Research in Toxicology*. 2001;14:1345–51.
61. Peng X, Pigli YZ, Rice PA, Greenberg MM. Protein Binding Has a Large Effect on Radical Mediated DNA Damage. *Journal of the American Chemical Society*. 2008;130:12890–1.

62. Hong IS, Greenberg MM. DNA Interstrand Cross-Link Formation Initiated by Reaction between Singlet Oxygen and a Modified Nucleotide. *Journal of the American Chemical Society*. 2005;127:10510–1.
63. Weng X, Ren L, Weng L, Huang J, Zhu S, Zhou X, et al. Synthesis and Biological Studies of Inducible DNA Cross-Linking Agents. *Angewandte Chemie International Edition*. 2007;46:8020–3.
64. Bastia D, Zzaman S, Krings G, Saxena M, Peng X, Greenberg MM. Replication termination mechanism as revealed by Tus-mediated polar arrest of a sliding helicase. *Proceedings of the National Academy of Sciences*. 2008;105:12831–6.
65. Stevens K, Madder A. Furan-modified oligonucleotides for fast, high-yielding and site-selective DNA inter-strand cross-linking with non-modified complements †. *Nucleic Acids Research*. 2009;37:1555–65.
66. Stevens K, Claeys DD, Catak S, Figaroli S, Hocek M, Tromp JM, et al. Furan-Oxidation-Triggered Inducible DNA Cross-Linking: Acyclic Versus Cyclic Furan-Containing Building Blocks-On the Benefit of Restoring the Cyclic Sugar Backbone. *Chemistry - A European Journal*. 2011;17:6940–53.
67. Jawalekar AM, Beeck MOD, Delft FLV, Madder A. Synthesis and incorporation of a furan-modified adenosine building block for DNA interstrand crosslinking. *Chemical Communications*. 2011;47:2796-8.
68. Carrette LLG, Madder A. A Synthetic Oligonucleotide Model for Evaluating the Oxidation and Crosslinking Propensities of Natural Furan-Modified DNA. *ChemBioChem*. 2014;15:103–7.
69. Beeck MOD, Madder A. Unprecedented C-Selective Interstrand Cross-Linking through in Situ Oxidation of Furan-Modified Oligodeoxynucleotides. *Journal of the American Chemical Society*. 2011;133:796–807.
70. Gyssels E, Carrette LLG, Vercruyssen E, Stevens K, Madder A. Triplex Crosslinking through Furan Oxidation Requires Perturbation of the Structured Triple-Helix. *ChemBioChem*. 2015;16:651–8.
71. Zhou Y, Hileman EO, Plunkett W, Keating MJ, Huang P. Free radical stress in chronic lymphocytic leukemia cells and its role in cellular sensitivity to ROS-generating anticancer agents. *Blood*. 2003;101:4098–104.

72. Kamiguti AS, Serrander L, Lin K, Harris RJ, Cawley JC, Allsup DJ, et al. Expression and Activity of NOX5 in the Circulating Malignant B Cells of Hairy Cell Leukemia. *The Journal of Immunology*. 2005;175:8424–30.
73. Chou F-T, Khan AH, Driscoll JS. Potential central nervous system antitumor agents. Aziridinybenzoquinones. 2. *Journal of Medicinal Chemistry*. 1976;19:1302–8.
74. Szatrowski T P, Nathan CF. Production of large amounts of hydrogen peroxide by human tumor cells. *Cancer research*. 1991;51:794-798.
75. Kuivila HG, Armour AG. Electrophilic Displacement Reactions. IX. Effects of Substituents on Rates of Reactions between Hydrogen Peroxide and Benzenboronic Acid1-3. *Journal of the American Chemical Society*. 1957;79:5659–62.
76. Cao S, Wang Y, Peng X. ROS-Inducible DNA Cross-Linking Agent as a New Anticancer Prodrug Building Block. *Chemistry - A European Journal*. 2012;18:3850–4.
77. Cao S, Christiansen R, Peng X. Substituent Effects on Oxidation-Induced Formation of Quinone Methides from Arylboronic Ester Precursors. *Chemistry - A European Journal*. 2013;19:9050–8.
78. Wang Y, Fan H, Balakrishnan K, Lin Z, Cao S, Chen W, et al. Hydrogen peroxide activated quinone methide precursors with enhanced DNA cross-linking capability and cytotoxicity towards cancer cells. *European Journal of Medicinal Chemistry*. 2017;133:197–207.
79. Chen W, Balakrishnan K, Kuang Y, Han Y, Fu M, Gandhi V, et al. Reactive Oxygen Species (ROS) Inducible DNA Cross-Linking Agents and Their Effect on Cancer Cells and Normal Lymphocytes. *Journal of Medicinal Chemistry*. 2014;57:4498–510.
80. Chen W, Han Y, Peng X. Aromatic Nitrogen Mustard-Based Prodrugs: Activity, Selectivity, and the Mechanism of DNA Cross-Linking. *Chemistry - A European Journal*. 2014;20:7410–8.

Chapter 2. The Effects of Substituents on Photochemical Generation of Benzyl Cations and DNA Cross-linking

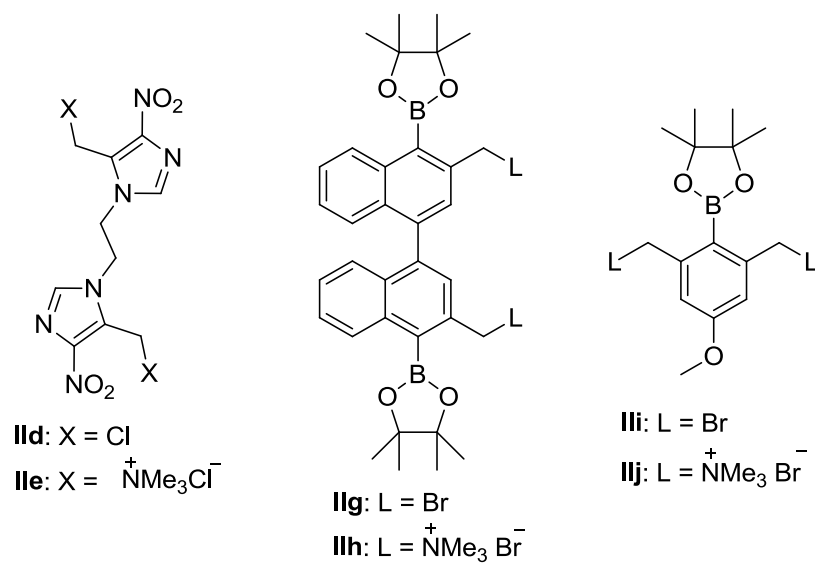
2.1. Introduction

DNA interstrand cross-linking agents have wide applications. They are used as probes for sequence-specific DNA detection,¹⁻³ for DNA damage and repair studies,⁴⁻⁷ for DNA nanostructure construction,⁸ and for cancer treatment.⁹⁻¹² However, the traditional DNA cross-linking agents are too reactive and showed poor selectivity. Apart from reacting with DNA, they can also interact with other cellular components and lead to unexpected side reactions and cellular toxicity, which confined their usage in biological system. To improve the selectivity and extend the biological applications of DNA cross-linking agents, various methods have been developed to induce DNA ICL formation, including fluoride (F⁻) induction,¹³⁻¹⁵ sodium periodate (NaIO₄),¹⁶⁻¹⁸ hydrogen peroxide (H₂O₂),¹⁹⁻²² or photo induction.²³⁻²⁵ Among these strategies, photo induction is an important method and attracts attentions because of its biocompatibility and potential applications in biological system. Photo induction is clean, non-invasive and does not require additional chemical reagents.

Various photo-inducible DNA cross-linking agents have been developed, which induce DNA ICL formation via different mechanisms. Some cross-link DNA via photocycloaddition, others alkylate DNA via photo-generated quinone methides (QMs) or carbocations. The photo-induced DNA cross-linking via photocycloaddition or QM mechanism have been extensively studied. For instance, p-stilbene,²⁶ coumarin,²⁷⁻²⁹ psoralen^{30,31} and 3-cyano-9-vinylcarbazole^{32,33} were reported to induce DNA ICL formation via [2+2] photocycloaddition while phenol, biphenol, or binol analogues were described to induce DNA cross-linking through QM mechanism.³⁴⁻³⁷ Moreover,

the effects of the chemical structure of the precursors for QM activity and subsequent DNA ICL formation have been well investigated.³⁸⁻⁴¹ In contrast, photo-induced DNA ICL formation via a carbocation mechanism was less explored. Recently, the research groups of Li⁴² and Greenberg⁴³ reported that photo irradiation of the modified thymidines led to the formation of both 5-(2'-dexoyuridiny)methyl radical and cation, while only cation can directly cross-link DNA. Most recently, several bifunctional aromatic boronates were developed in our group, which were found to cross-link DNA via a carbocation mechanism upon UV irradiation at 350 nm.^{23,24}

To date, there are three classes of photo-induced DNA cross-linking agents with limited structure variations that induce DNA ICL formation through a photo-generated carbocation. These are binitroimidazole analogues (**IId**, **IIE**), binaphthalene boronates (**IIG**, **IIf**), and bifunctional benzyl boronates (**III**, **IIj**) (Scheme 2-1). Among these compounds, compounds **III** and **IIj** showed better DNA cross-linking efficiency than **IId,e** and **IIG,h** (Figure 1). Thus, **III** and **IIj** were chosen as lead compounds for further modification. Even though the DNA cross-linking capability of **III,j** is higher than other existing compounds, their photo reactivity towards DNA is still low. They took more than 8 hours to complete the cross-linking reaction.^{23,24} It appears that the strong electron withdrawing boronate ester on the benzene ring played a very important role in controlling formation of the cationic intermediates and subsequent DNA interstrand cross-linking. The goal of this work is to understand the generality of the photo-induced DNA ICL formation via a carbocation mechanism, investigate the role of the aromatic substituents in carbocation formation and subsequent DNA ICL formation, and find ways to improve the efficiency of photo-induced DNA cross-linking and expand its potential biological applications.



Scheme 2-1. The existing photo-induced DNA cross-linking agents via a carbocation mechanism.

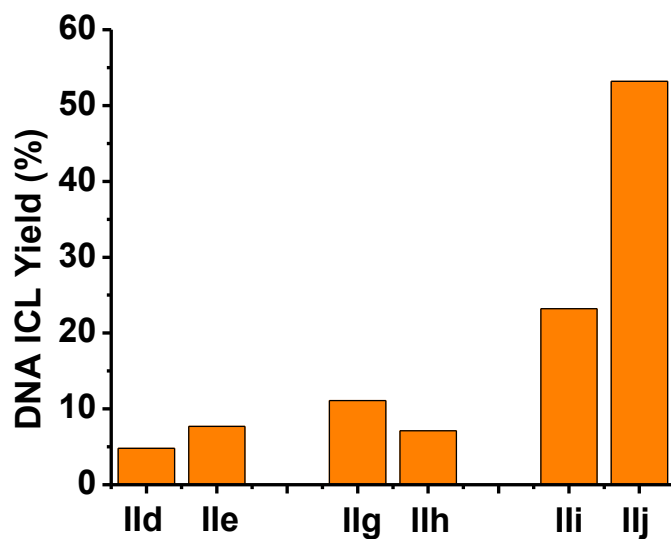
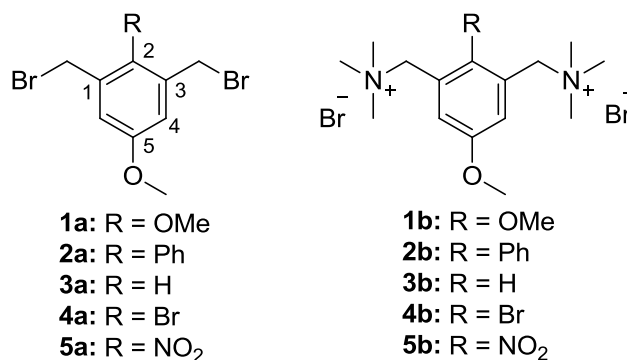


Figure 2-1. DNA ICL efficiency of three classes of the existing compounds upon UV irradiation.

To achieve these goals, we developed a series of compounds via chemical modifications on the lead compounds (**IIIi**, **IIIj**). The boronate ester group was replaced by a variety of other functional groups. As the carbocation intermediates are electron deficient, an electron donating group may

offset the electron deficient property therefore facilitating the carbocation formation. In contrast, the electron withdrawing groups may destabilize the carbocation intermediate thus suppressing the carbocation formation. In addition, the incorporation of auxochromic groups into the aromatic rings, either electron-donating or withdrawing groups, may affect the UV absorption of the compounds, which in turn may affect compounds' sensitivity towards UV light. Based on this understanding, a series of compounds with various aromatic substituents (**1a-5a**, and **1b-5b**) were designed and synthesized by replacing the boronate ester group of the lead compounds (**III,j**) with different functionalities (Scheme 2-2). We further investigated the influence of chemical structure on carbocation generation and subsequent DNA cross-linking formation, DNA cross-linking sites and the mechanism for DNA ICL formation.



Scheme 2-2. The structures of **1a-5a**, and **1b-5b**.

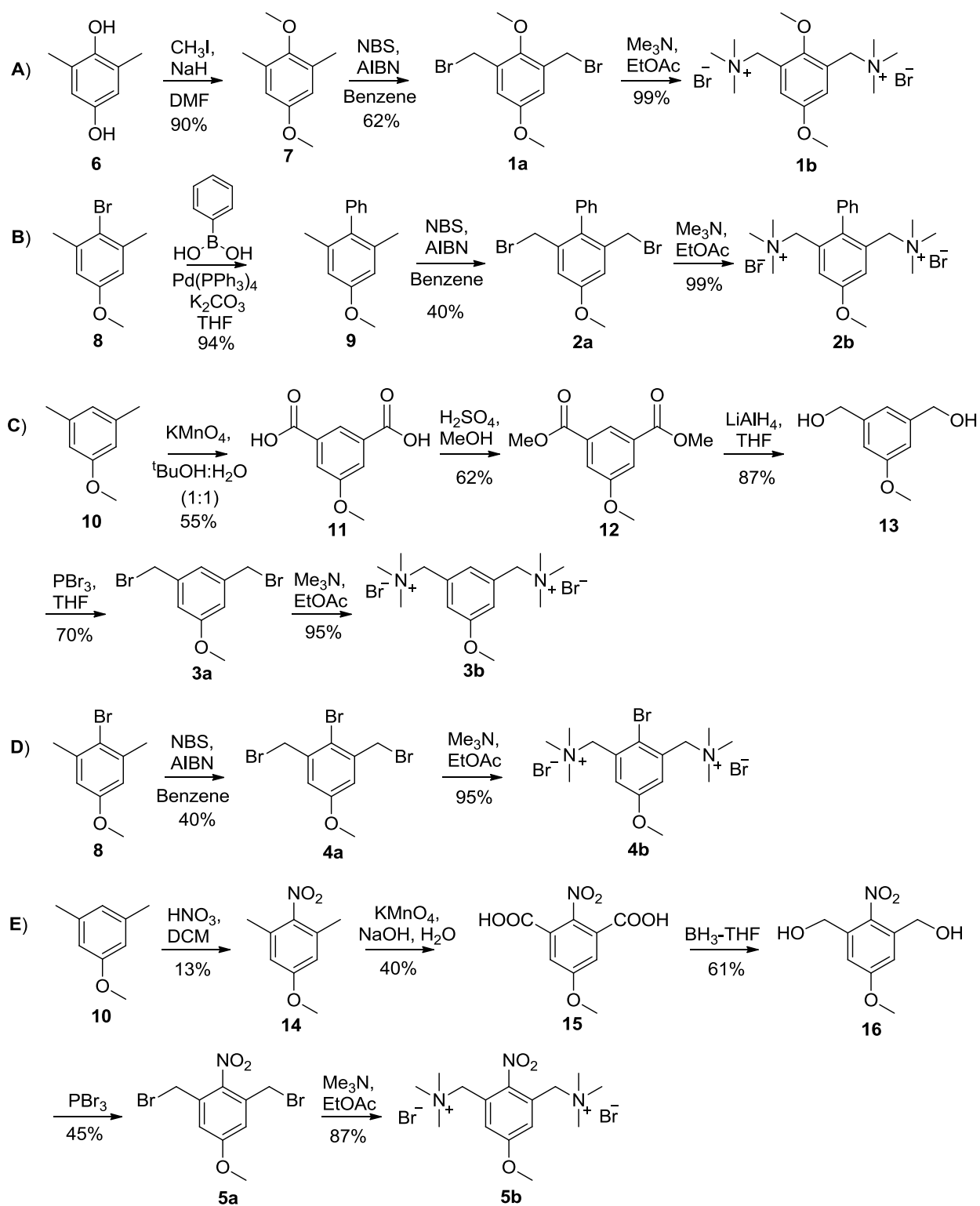
2.2. Bifunctional Benzylic Derivatives as Photo-inducible DNA Cross-linking Agents

2.2.1. Synthesis of compounds with various substituents

The general synthetic route is based on our previous work.^{23,44} Meta-xylene precursors **6**, **8**, and **10** were used as starting materials for the preparation of bromides **1a-5a** (scheme 2-3).

Methylation of **6** with methyl iodide (MeI) afforded 2,5-dimethoxy-1,3-dimethylbenzene (**7**) that

was converted to **1a** via bromination with *N*-bromosuccinimide (NBS) using azobisisobutyronitrile (AIBN) as a radical initiator (Scheme 2-3A). Compound **2a** was synthesized using commercially available **8** as starting material via Suzuki coupling reaction (\rightarrow **9**), followed by bromination (\rightarrow **2a**) (Scheme 2-3B). Compound **4a** was produced from direct bromination of **8** using NBS/AIBN (Scheme 2-3D).⁴⁵ A different synthetic route was used for the synthesis of **3a** and **5a**, since direct bromination of **10** or **14** with NBS/AIBN did not afford the desired products. Instead of **3a**, a mixture of **8** and **4a** was obtained by treating **10** with NBS/AIBN while bromination product was not observed with **14** possibly due to the deactivating effect of the strong electron withdrawing nitro group. To synthesize bromide **3a**, we started with **10**. Compound **10** was first converted to dibenzoic acid **11**, which was then converted to bifunctional benzyl alcohol **13** via esterification (\rightarrow **12**) and reduction (\rightarrow **13**).⁴⁶ The dialcohol **13** was then further converted to **3a** by PBr₃ bromination (Scheme 2-3C).⁴⁷ To synthesize compound **5a**, the nitro functionality was first introduced using nitration reaction in the presence of HNO₃. Followed by oxidation (\rightarrow **15**), reduction (\rightarrow **16**) and bromination (\rightarrow **5a**) (Scheme 2-3E). Finally, the bromides **1a-5a** were converted to corresponding ammonium salts **1b-5b** by treating with trimethylamine in nearly quantitative yields (Scheme 2-3).

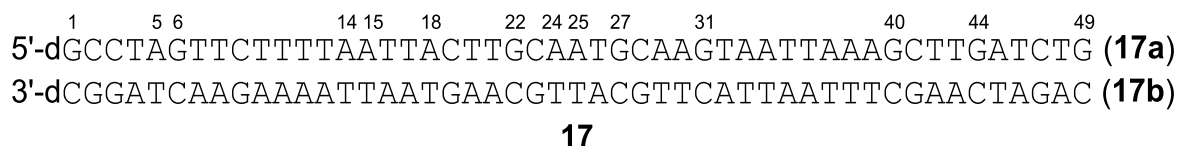


Scheme 2-3. Synthesis of **1a-5a** and **1b-5b**.

2.2.2. Preparation of DNA duplex

ODN sequence design

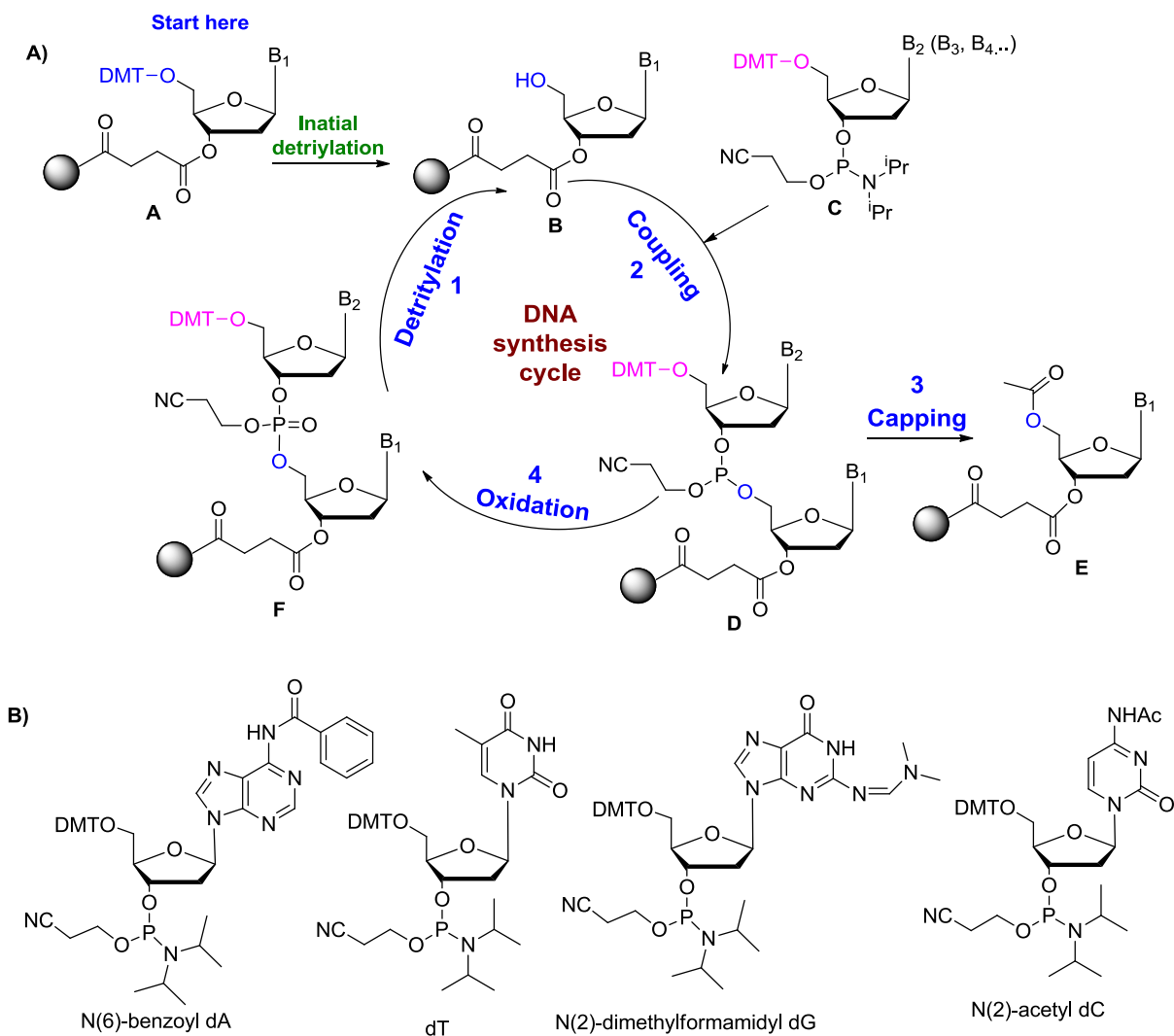
DNA duplex **17** (Scheme 2-4) is part of a p53 gene that plays an important role in cell cycle control and apoptosis. Damaged p53 gene may lose its function leading to uncontrolled cell cycles, where abnormal cells grow rapidly leading to cancer eventually. There are more than 50% human cancers caused by p53 gene mutation.^{48,49}



Scheme 2-4. The sequence of DNA duplex **17**.

ODN synthesis

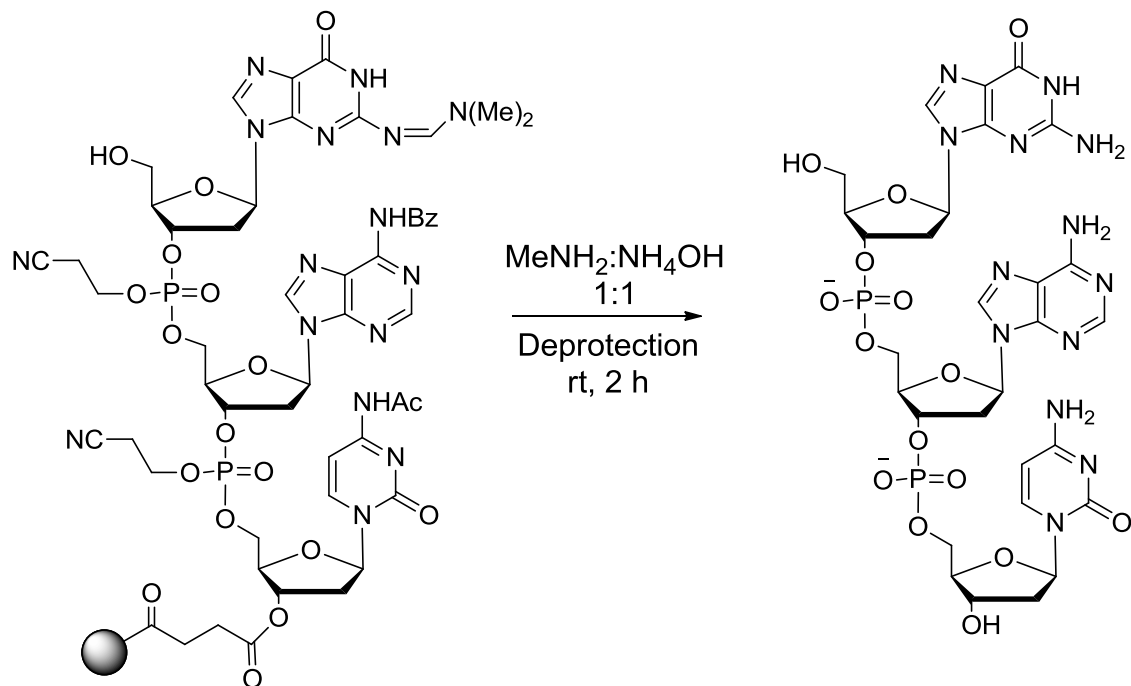
Oligonucleotides were synthesized via standard solid-phase oligonucleotide DNA synthesis techniques using commercially available phosphoramidites (Scheme 2-5). Phosphoramidite oligo synthesis goes from the 3'- to 5'-direction. One nucleotide is attached per synthesis cycle. Each cycle contains four steps: **(1)** detritylation (removal of 4,4'-dimethoxytrityl group), **(2)** activation (protonation of diisopropylamino group of the incoming phosphoramidite building block **C**) and coupling (the terminal 5'-hydroxyl group of the growing ODN chain (**B**) attacks the phosphorus atom of the incoming phosphoramidite building block (**C**) to form a new P-O bond), **(3)** capping (block the unreacted 5'-end hydroxyl groups (**E**)), and **(4)** oxidation (convert P (III) to P (V)).



Scheme 2-5. Automated DNA synthesis cycle (A) and structures of phosphoramidites (B).

ODN deprotection

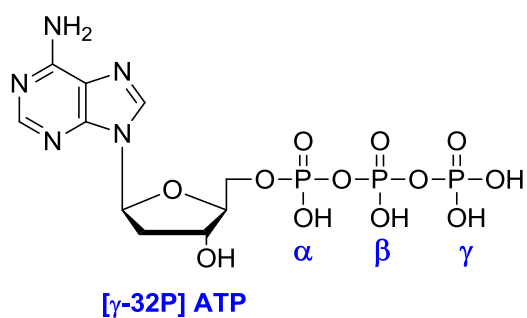
Deprotection of the synthesized ODN was performed under mild deprotection conditions using a mixture of 40% aqueous MeNH_2 and 28% aqueous NH_3 (1:1) at room temperature for 2 h via a β -elimination mechanism. 20% Denaturing polyacrylamide gel electrophoresis (PAGE) was used for DNA purification.



Scheme 2-6. DNA deprotection

^{32}P -Labeling at the 5'-end of oligodeoxyribonucleotides

$[\gamma\text{-}^{32}\text{P}]$ ATP was used for DNA labeling with standard protocol. ODN **17a** was 5'-end labeled using gamma ^{32}P ATP ($[\gamma\text{-}^{32}\text{P}]$ ATP) and T4 polynucleotide kinase (T4 PNK), where T4 PNK transfers the gamma-phosphate from ATP to the 5'-OH group (Figure 2-2).



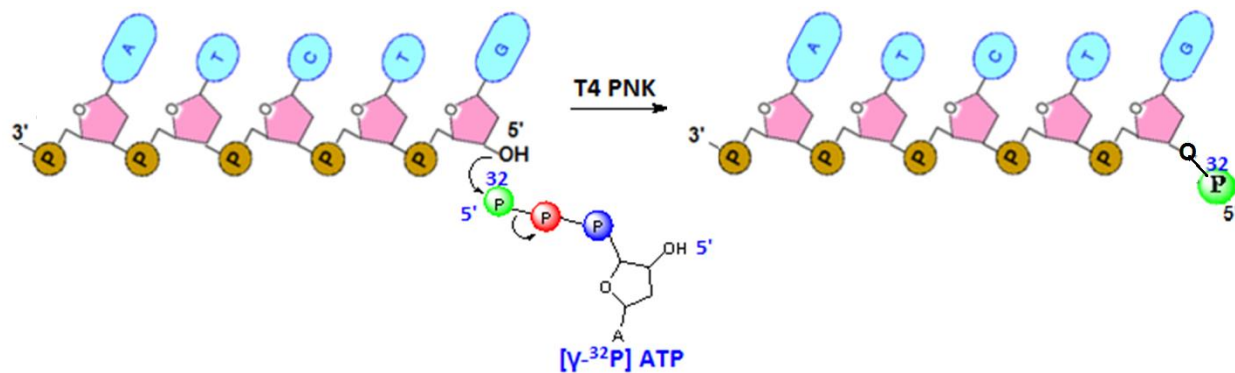


Figure 2-2. The structure of $[\gamma\text{-}^{32}\text{P}]$ ATP and 5'-end oligonucleotide labeling.

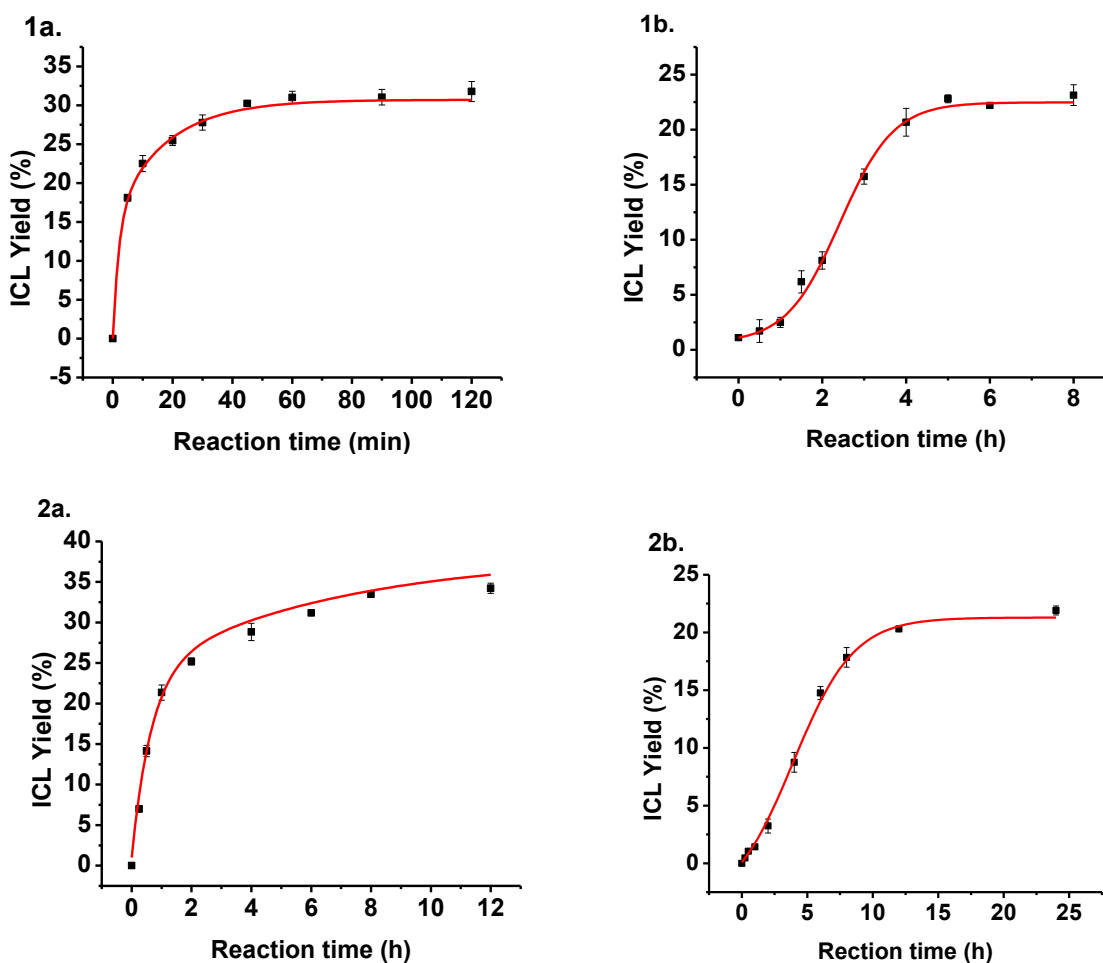
2.2.3. DNA interstrand cross-linking assay

After synthesizing compounds **1a-5a** and **1b-5b**, we investigated their DNA cross-linking ability using a 49-mer DNA duplex (**17**) in a phosphate buffer (pH 8.0) under UV irradiation at 350 nm.^{23,24} PAGE was used for DNA ICL analysis. The cross-linked and the single-stranded DNA can be distinguished by PAGE because they migrate differently in the polyacrylamide gel due to different molecular size. The cross-linked products with larger molecular size migrate slower than the single-stranded ODN. Molecular Dynamics phosphorimager (ImageQuant, version 5.2) was used for quantification of DNA ICL yields, where the ICLs and the single strands show different bands on the image plate. Origin 8.0 software was used for data plot and curve fitting.

Initially, we tested the DNA cross-linking ability of **1a-5a** and **1b-5b** in the presence or absence of 350 nm light. These compounds did not induce DNA ICL formation without photo irradiation while efficient DNA cross-linking was achieved upon UV irradiation at 350 nm. Previous study showed that the DNA cross-linking efficiency strongly depended on the irradiation time and the concentration of the substrates.²³ To fully understand how the aromatic substituents and benzylic leaving groups affect the DNA cross-linking ability, we first optimized the reaction time and concentration to obtain optimal DNA cross-linking efficiency for **1a-5a** and **1b-5b**.

Time-dependent DNA cross-link study

We carried out the time-dependent DNA cross-link study with **1a-5a** and **1b-5b** to determine the time needed to achieve the highest DNA ICL yield. In general, the DNA ICL yields gradually enhanced with the increased reaction time, and then reached a balance at specific time points. Further increasing reaction time did not increase ICL yield. This time was then defined as optimal reaction time for the compound. The optimal time for **1a-5a** is 0.75 h, 8 h, 35 h, 6 h, and 24 h, while that is 6 h, 12 h, 40 h, 24 h and 12 h for **1b-5b** respectively (table 2-1 and Figure 2-3).



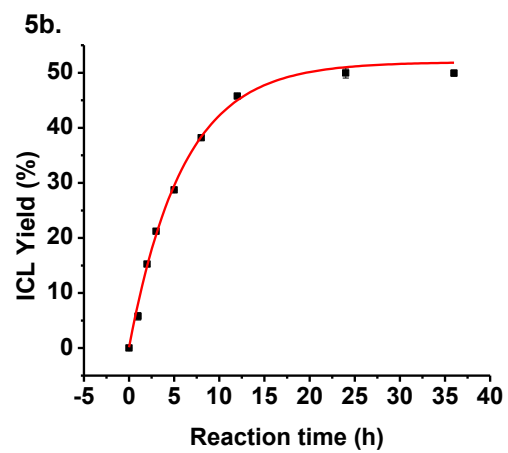
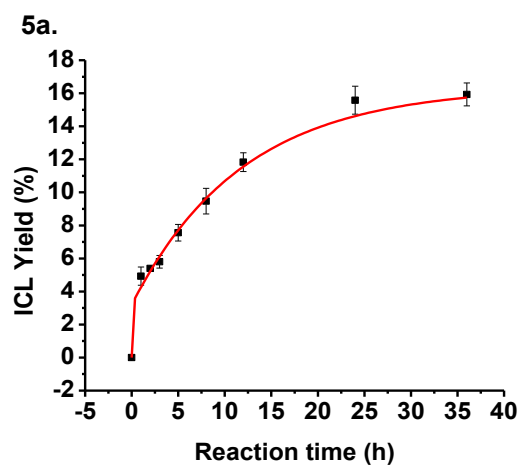
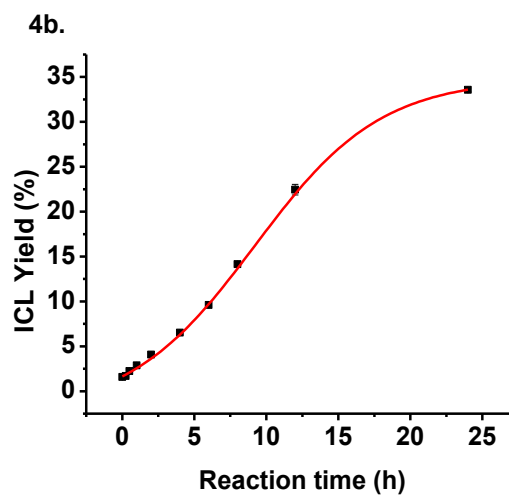
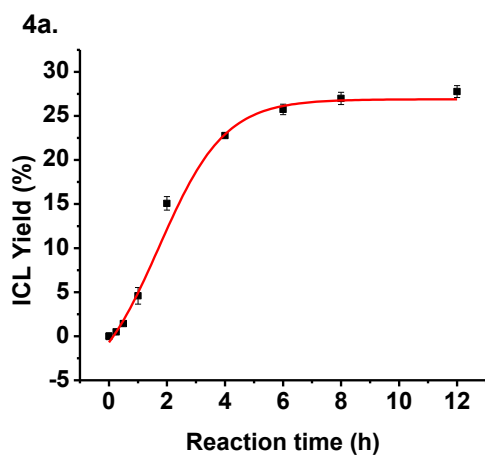
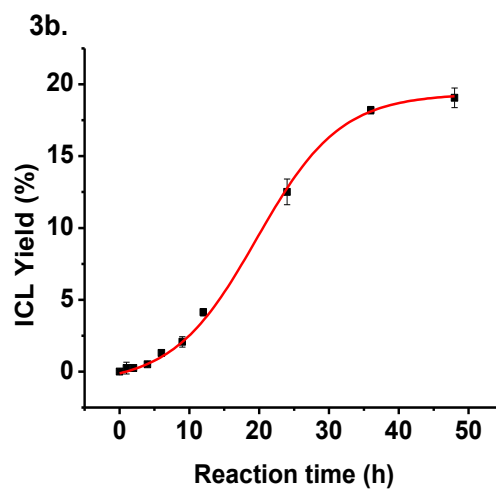
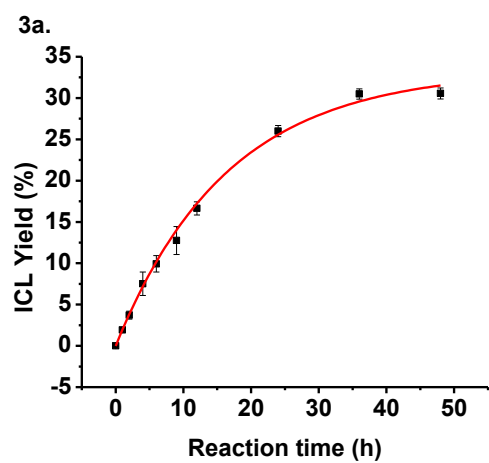
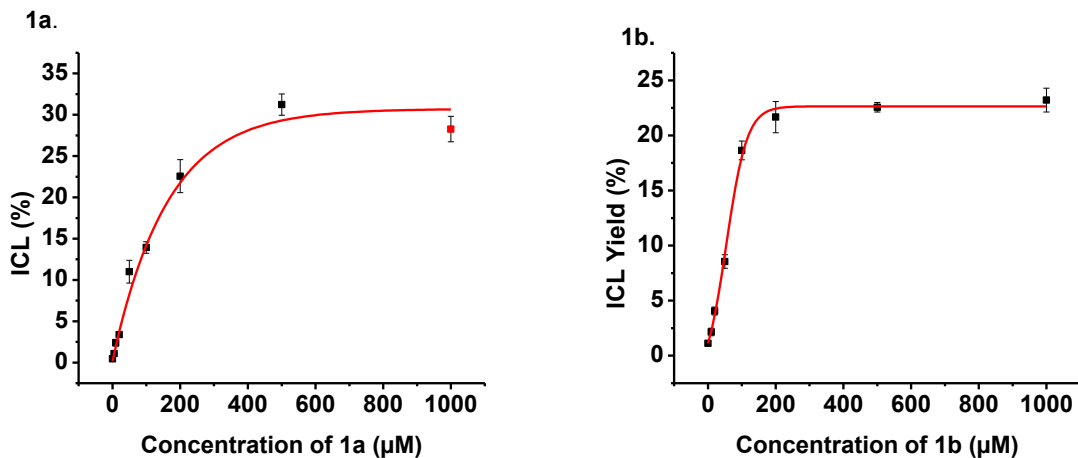


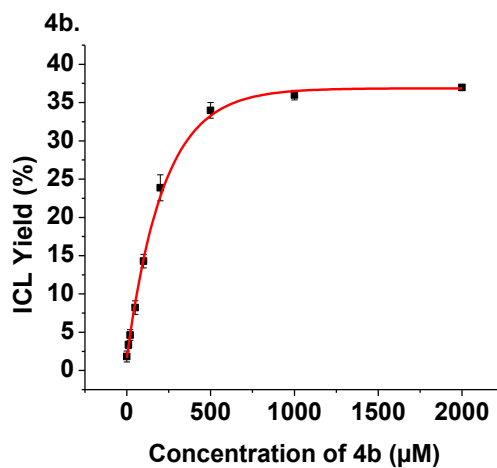
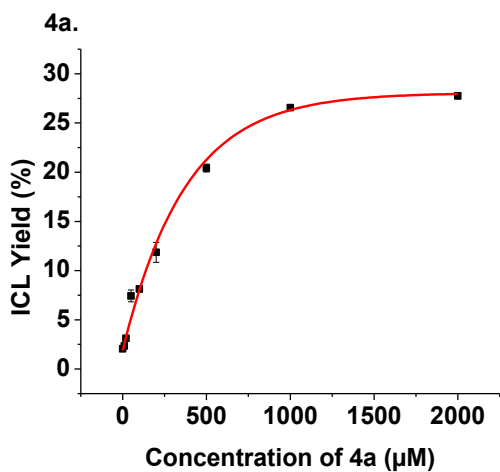
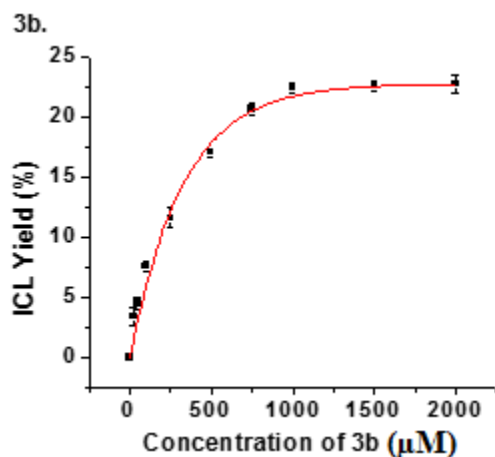
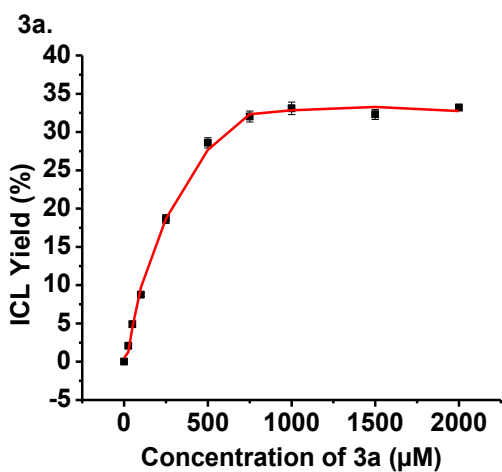
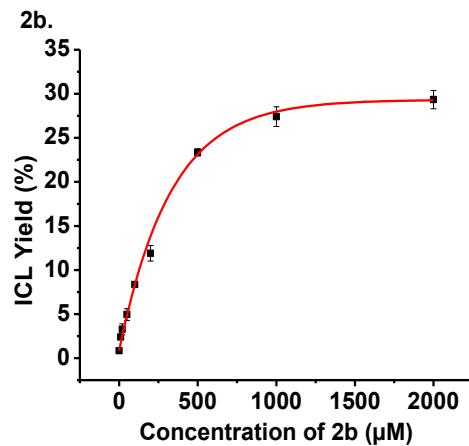
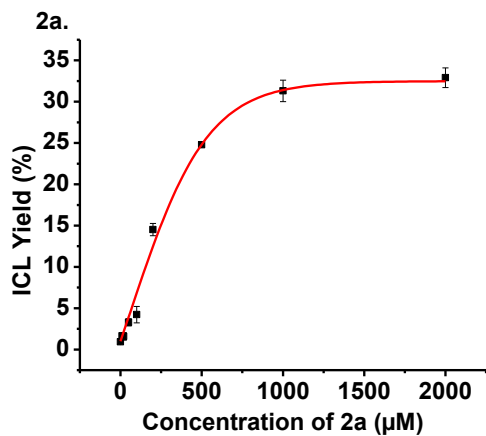
Figure 2-3. Time-dependence of DNA ICL formation of duplex **17** for **1a-5a** and **1b-5b** upon photo-irradiation. **1a** at time points 0', 5', 10', 20', 30', 45', 1 h, 1.5 h, 2 h. [**1a**] = 500 μ M; **1b** at time points 0, 30', 1 h, 1.5 h, 2 h, 3 h, 4 h, 5 h, 6 h, 8 h, [**1b**] = 500 μ M; **2a** at time points 0', 15', 30', 1 h, 2 h, 4 h, 6 h, 8 h, 12h, [**2a**] = 1mM; **2b** at time points 0', 15', 30', 1 h, 2 h, 4 h, 6 h, 8 h, 12h, 24h, [**2b**] = 1 mM; **3a** at time points 0', 1 h, 2 h, 4 h, 6 h, 9 h, 12 h, 24 h, 36 h, 48 h, [**3a**] = 1 mM; **3b** at time points 0, 1 h, 2 h, 4 h, 6 h, 9 h, 12 h, 24 h, 36 h, 48 h, [**3b**] = 1 mM; **4a** at time points 0', 15', 30', 1 h, 2 h, 4 h, 6 h, 8 h, 12h, [**4a**] = 1.0 mM; **4b** at time points 0', 15', 30', 1 h, 2 h, 4 h, 6 h, 8 h, 12h, 24h, [**4b**] = 1mM; **5a** at time points 0', 1 h, 2 h, 3h, 5 h, 8 h, 12 h, 24 h, 36 h, [**5a**] = 1 mM; **5b** at time points 0', 1 h, 2 h, 3h, 5 h, 8 h, 12 h, 24h, [**5b**] = 1.0 mM. Reaction mixtures were irradiated with UV at 350 nm.

It was observed that the bromides (**1a-4a**) showed faster photo-induced DNA cross-linking reaction rate than that for the trimethyl ammonium salts (**1b-4b**), while opposite trend was observed for **5a** and **5b** possibly because they undergo different mechanisms. We also observed that the introduction of a substituent on the benzene ring promoted photo-induced DNA ICL formation rate regardless of the presence of an electron donating or withdrawing group (OMe, Ph, Br, and NO₂). Namely, all compounds (**1a-4a**) needed shorter reaction time to complete the DNA cross-linking reactions than the parent compound **3a**, indicating the poorest photo-reactivity for **3a** towards DNA. Among all introduced substituents, the methoxy group (OMe) (a strong electron donating group) displayed the greatest promoting effect. For instance, **1a** with a methoxy required the shortest reaction time (~ 0.7 h) to complete the photo-induced DNA cross-linking reaction, suggesting the fastest reaction rate. For **2a**, **4a**, and **5a** with weak electron donating (Ph) or electron withdrawing groups (Br and NO₂), moderate reactivity was observed. Similar trend was found for the ammonia salts **1b-5b**.

Concentration-dependent DNA cross-linking study

Having determined the optimal reaction time for **1a-5a** and **1b-5b**, we performed the concentration-dependent DNA cross-linking study to determine the optimized concentration to reach the highest DNA cross-linking yields. In general, the DNA ICL yields were gradually raised by increasing the concentration of compounds. The DNA cross-linking reaction reached a balance at specific concentrations, and further increase of compounds' concentration did not increase the ICL yields. This concentration was defined as optimal concentration for the compound. For example, the DNA ICL yield reached the highest at 0.2 mM concentration for **1b**, and the concentration higher than 0.2 mM did not further increase the DNA ICL yield. Thus, 0.2 mM was the optimal concentration for **1b**. The optimal concentration is 0.5 mM for **1a** and **5a**, 1.0 mM for **2a-4a** and **2b-4b**, and 3.5 mM for **5b** (Table 2-1 and Figure 2-4).





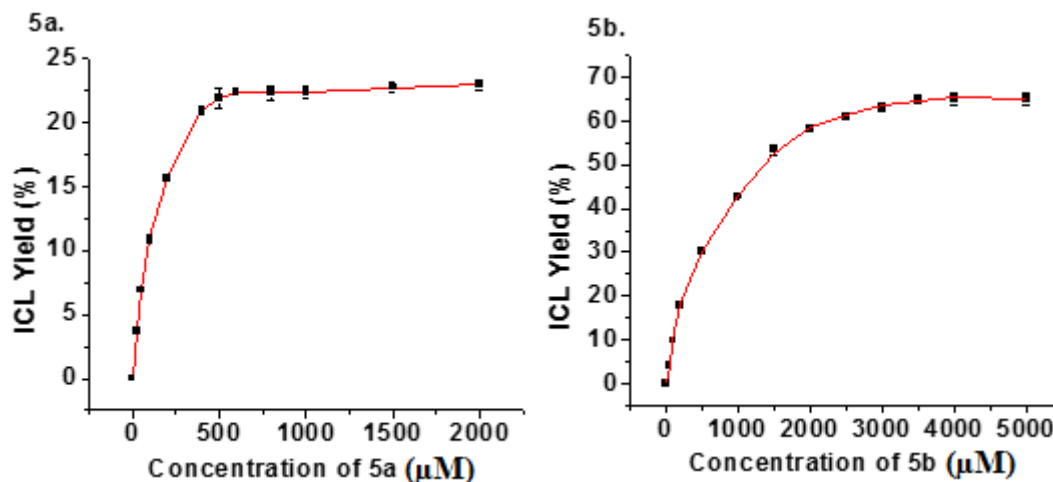


Figure 2-4. The concentration dependence of DNA ICL formation of duplex **17** for **1a-5a** and **1b-5b** upon 350 nm irradiation. **1a** with an irradiation of 0.75 h; **1b** with an irradiation of 6 h; **2a** with an irradiation of 8 h; **2b** with an irradiation of 12 h; **3a** with an irradiation of 35 h; **3b** with an irradiation of 40 h; **4a** with an irradiation of 6 h; **4b** with an irradiation of 24 h; **5a** with an irradiation of 24 h; **5b** with an irradiation of 12 h. The reaction mixtures were irradiated with UV at 350 nm.

For compounds with the bromide as a leaving group (**1a-5a**), the electron donating groups in the benzene ring slightly increased the DNA ICL yields (**1a** and **2a**), while the electron withdrawing groups decreased the ICL yields (**4a** and **5a**). This is consistent with the electron-deficient property of the carbocations that were stabilized by the electron donating groups while destabilized by the electron withdrawing ones. However, an opposite trend was found for the ammonium salts (**1b-5b**). Higher ICL yields were obtained for compounds with electron withdrawing groups (**4b** and **5b**) in comparison with those with electron donating functionalities (**1b** and **2b**), even though withdrawing groups were expected to suppress the carbocation generation and subsequent DNA ICL formation.

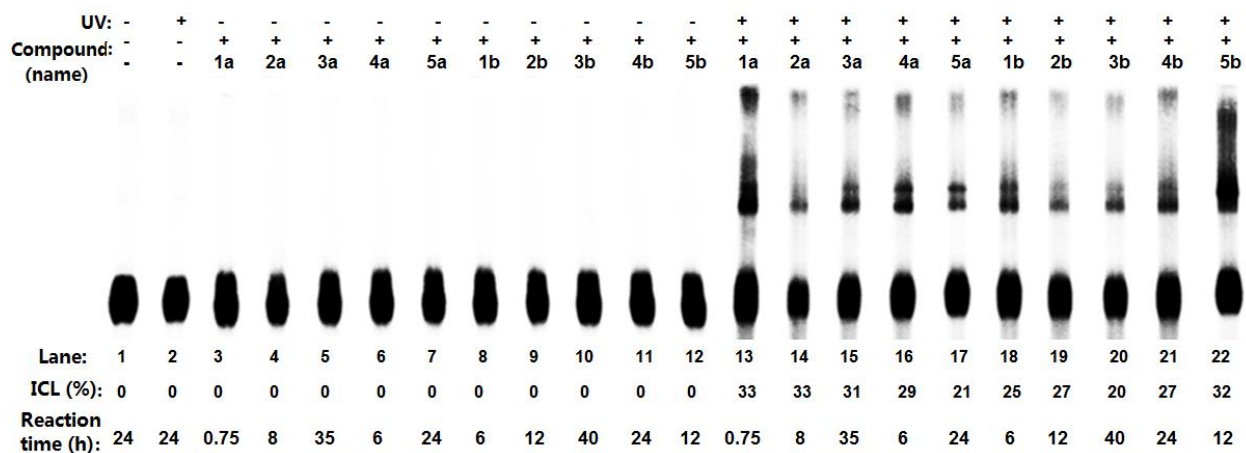


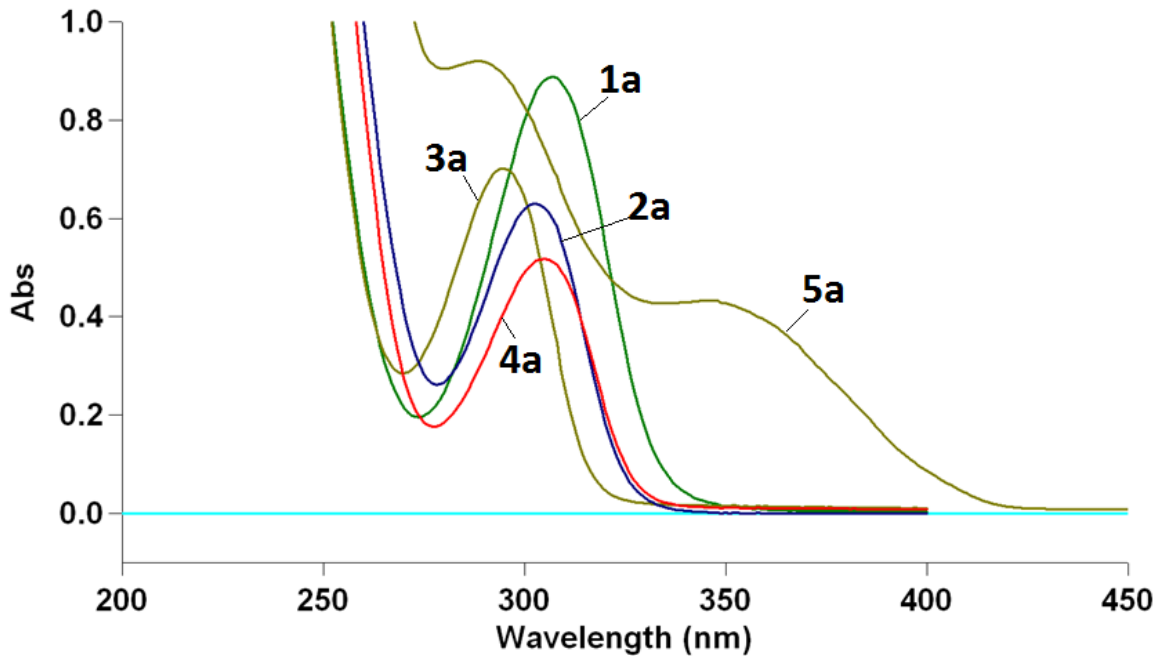
Figure 2-5. Photo-induced DNA ICL formation for **1a-5a** and **1b-5b**. Lane 1: DNA without UV irradiation; lane 2: DNA with 24 h UV irradiation at 350 nm; lanes 3-12: DNA with the compound (500 μ M) but no UV irradiation at 350 nm for designed time; lanes 13-22: DNA with the compound (500 μ M) upon 350 nm irradiation for designed time: lane 13: **1a** (ICL yield, $33 \pm 5\%$); lane 14: **2a** (ICL yield, $33 \pm 3\%$); lane 15: **3a** (ICL yield, $31 \pm 3\%$); lane 16: **4a** (ICL yield, $29 \pm 4\%$); lane 17: **5a** (ICL yield, $21 \pm 3\%$); lane 18: **1b** (ICL yield, $25 \pm 3\%$); lane 19: **2b** (ICL yield, $27 \pm 4\%$); lane 20: **3b** (ICL yield, $20 \pm 4\%$); lane 21: **4b** (ICL yield, $27 \pm 3\%$); lane 22: **5b** (ICL yield, $32 \pm 5\%$). All DNA ICL yields were obtained by triplicate experiments and shown as average \pm standard deviation.

As all compounds studied have different optimal concentrations to achieve an highest DNA cross-linking yield, it is hard to make a conclusion on how the substituents affect the DNA ICL efficiency based on the ICL yields under optimized conditions. For better comparison, we performed DNA cross-linking assay under the same concentration (500 μ M) and the optimized reaction time for each compound (Figure 2-5). For all compounds (**1a-5a**, and **1b-5b**) tested, the trend of ICL yields at 500 μ M (Figure 2-5) was consistent with that achieved under optimized conditions (Table 2-1). All these results suggested that for the bromides (**1a-5a**), electron

donating groups promoted the DNA ICL formation (**1a**, **2a**), while electron withdrawing groups suppressed the process (**4a**, **5a**). However, from the electronic effect point of view no conclusive data was obtained for the ammonium salts (**1b-5b**).

2.2.4. Correlation between UV absorbance and the photo-reactivity

Apart from the electronic effect, the aromatic substitutions could also affect the UV absorption which in turn might influence the reactivity and DNA cross-linking ability. Therefore the UV absorbance of the target compounds were investigated (Figure 2-6).



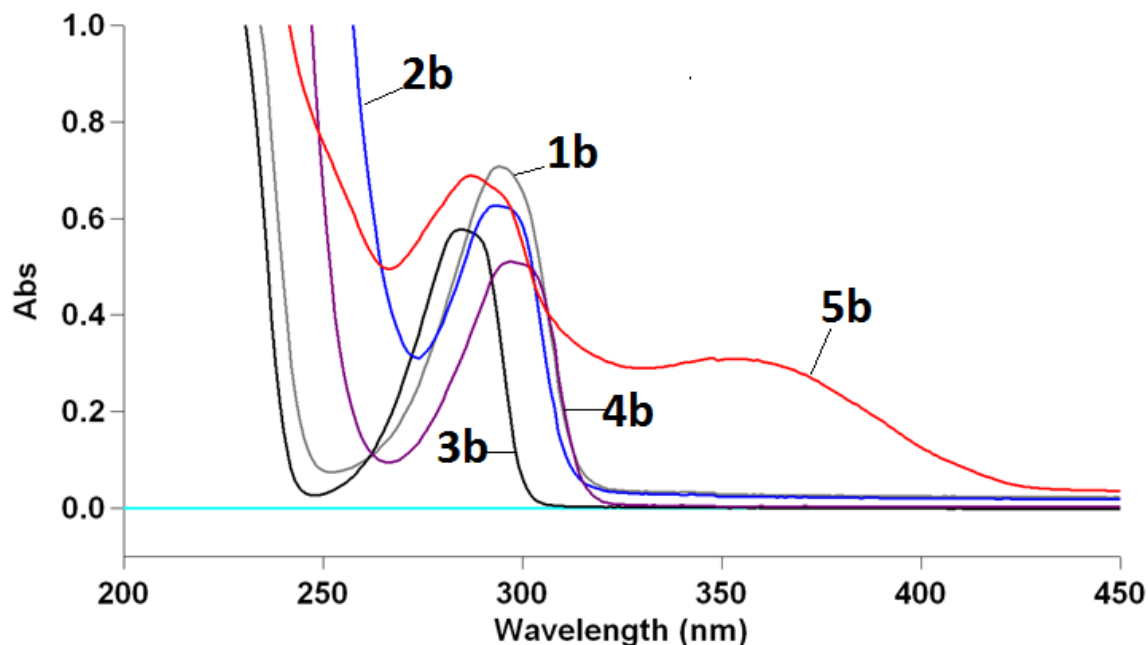


Figure 2-6. UV absorption spectra for **1a-5a** and **1b-5b** at 1.0 mM concentration.

UV-Vis spectra of target compounds were determined at 1.0 mM concentration in acetonitrile (**1a-5a**) or water (**1b-5b**) as the solvent. A clear correlation was observed between the UV absorption and the photo reactivity of these compounds. In general, compounds with a UV absorption closer to 350 nm (maximum output for rayonet photoreactor used in the study) and/or stronger UV absorbance exhibited higher DNA cross-linking reactivity. For instance, the bromides (**1a-4a**) whose maximum UV absorption showed red shift (~ 300 nm) have higher DNA cross-linking efficiency than that of the corresponding ammonium salts (**1b-4b**) with shorter maximum UV absorption (~ 290 nm). For compounds with the same leaving group, the ones with the maximum absorption band closer to 350 nm and the stronger absorbance showed higher DNA ICL efficiency. For example, **1a** bearing a maximum absorption at 307 nm with an extinction coefficient ($\epsilon_{\lambda_{\max}}$) of $4000 \text{ M}^{-1} \cdot \text{cm}^{-1}$ has higher DNA cross-linking efficiency in comparison with the parent compound **3a** that has a maximum absorption at 295 nm with the biggest $\epsilon_{\lambda_{\max}}$ of $2700 \text{ M}^{-1} \cdot \text{cm}^{-1}$. The photo-induced DNA ICL reaction rates follows the order of

1a > **4a** > **2a** > **3a**, which correlates well with the order of bathochromic shift (**1a** > **4a** > **2a** > **3a**). Similarly, the DNA cross-linking rates of **1b-3b** follows the order of **1b** > **2b** > **3b**, which is consistent with their maximum absorption trend (**1b** > **2b** > **3b**). However, the photo-induced DNA cross-linking reactivity of **4b**, **5a**, and **5b** (electron withdrawing) does not correlate with their bathochromic shift. Although these compounds have their maximum absorption shift to longer wavelength, none of them showed the highest DNA ICL reaction rates. This is possibly due to the electron withdrawing property of the substituents that offsets the increased photo sensitivity of **4b**, **5a**, and **5b** resulted from bathochromic shift, which hindered the carbocation generation and subsequent DNA ICL formation. Our data indicated that the introduction of aromatic substituents not only affect compounds' electronic properties but also their absorption properties. Both of them influenced the photo-induced DNA cross-linking reactivity of these compounds.

2.2.5. Correlation between heterolytic cleavage energy and the photo-reactivity

The bond-dissociation energy may also play an important role in compounds' photoreactivity. Thus, we calculated the heterolytic cleavage energy (ΔE_{HCE}), defined as the energy needed to release the first leaving group to form a carbocation. The ΔE_{HCE} (5.01–6.52 eV) is higher for the compounds with bromo (-Br) as a leaving group than that with trimethylamine as a leaving group (2.22–3.42 eV). This indicated that the direct bond cleavage via heterolysis is harder for C-Br in **1a-5a** than for C-N in **1b-5b**. The bromides (**1a-5a**) have similar heterolytic cleavage energy with the exception of **5a**, which has lower ΔE_{HCE} than other bromides. Similar phenomenon was found for the ammonium salts. Compounds **1b-4b** have similar heterolytic cleavage energy while **5b** has much lower ΔE_{HCE} . In comparison with all other compounds, **5b** has the lowest ΔE_{HCE} .

Table 2-1. The optimized conditions, ICL yields, heterolytic cleavage energy (ΔE_{HCE}) and UV absorption data for **1a-5a** and **1b-5b**.

Bromides	Reaction Time (h)	Con. ^b (mM)	ICL (%) ^c	ΔE_{HCE} (eV)	λ_{max} (nm)	$\epsilon_{\lambda_{\text{max}}}$ (M ⁻¹ ·cm ⁻¹)
1a (R = OMe)	0.75	0.5	36 ± 3	6.07	307	4000
2a (R = Ph)	8	1.0	34 ± 4	6.16	303	2850
3a (R = H)	35	1.0	30 ± 3	6.42	295	2700
4a (R = Br)	6	1.0	29 ± 4	6.52	305	2500
5a (R = NO ₂)	24	0.5	23 ± 2	5.01	288, 347	3400, 1550
Ammonia Salts						
1b (R = OMe)	6	0.2	25 ± 2	3.30	295	3400
2b (R = Ph)	12	1.0	27 ± 3	3.26	294	2950
3b (R = H)	40	1.0	21 ± 3	3.42	285	2800
4b (R = Br)	24	1.0	33 ± 4	3.24	298	2600
5b (R = NO ₂)	12	3.5	65 ± 3	2.22	287, 356	3100, 1300

^a The DNA cross-linking reaction was performed in a pH 8 phosphate buffer with 50 nM DNA duplex **17** upon 350 nm irradiation.

^b The minimum compound concentration needed to obtain the highest DNA cross-linking efficiency.

^c The maximum DNA ICL yield obtained for each compound under optimized conditions (all data are the average of three experiments).

2.2.6. Mechanism of DNA ICL formation and substituent effects.

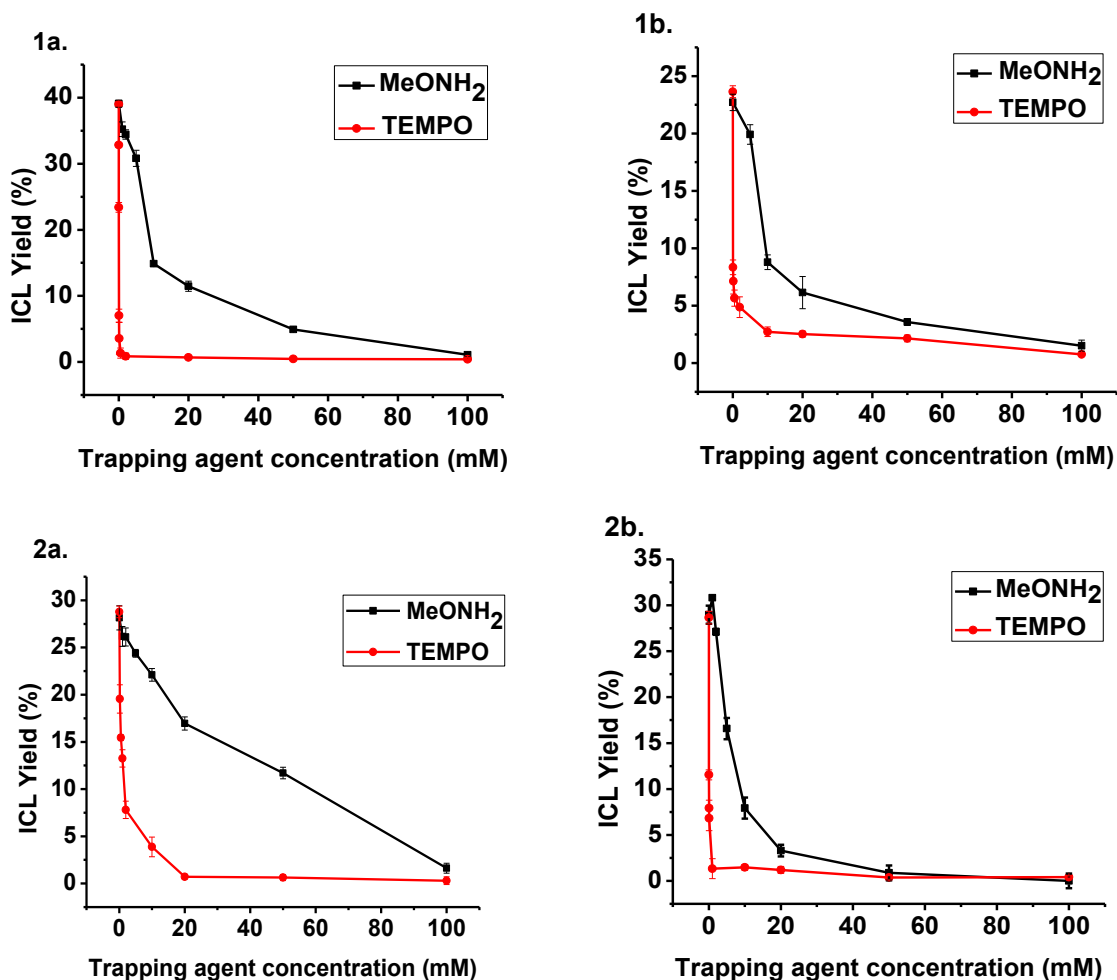
Our previous study showed that the phenyl boronates with bromo or trimethyl amine as a leaving group undergoes different pathways for the generation of carbocations.²³ The carbocations were generated from initial radicals via free radical oxidation for phenyl boronate esters with bromo as a leaving group, while carbocations were formed via direct heterolysis of C-N bond for those with trimethyl ammoniums as leaving groups. However, it is hard to conclude that this is a general phenomenon due to the limited literature data. Only few compounds with limited

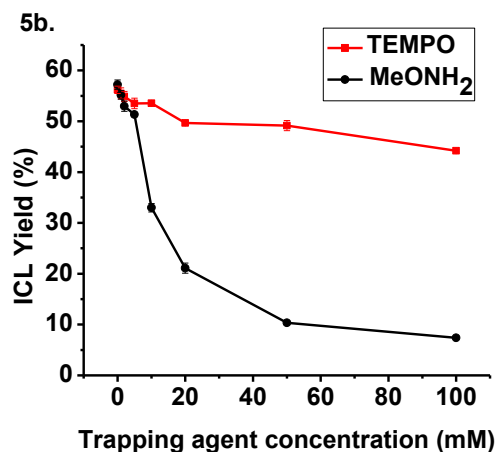
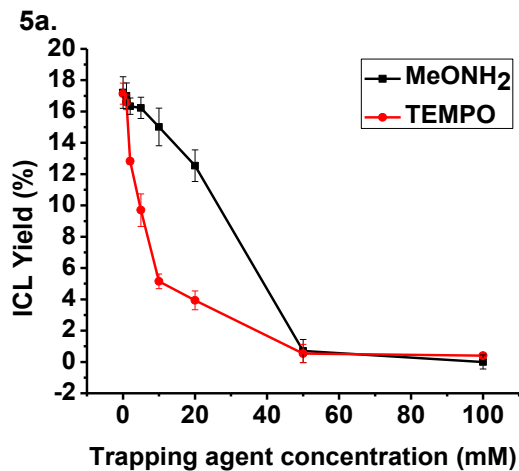
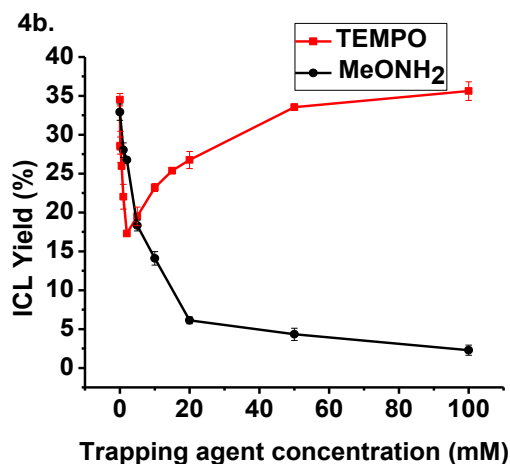
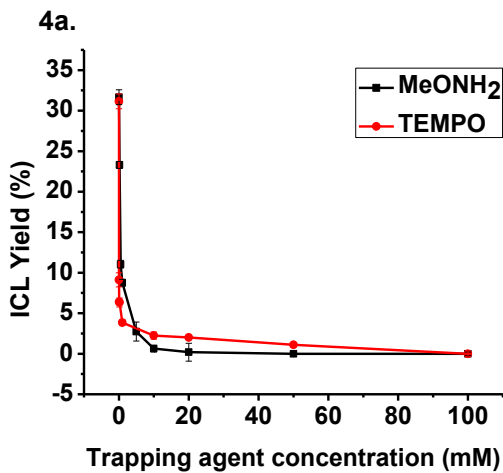
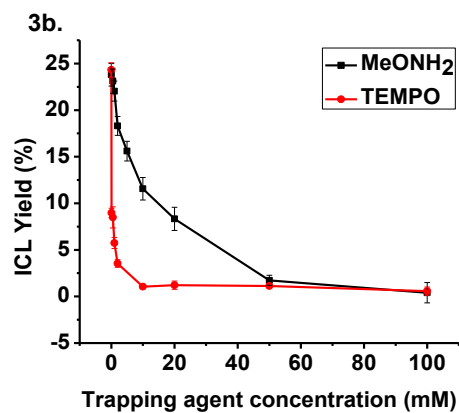
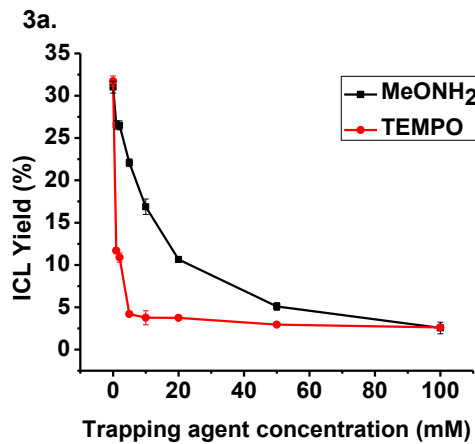
structure variations have been reported to cross-link DNA via a carbocation mechanism upon photo irradiation. The study on photo inducible DNA ICL formation via a carbocation mechanism is still in its nascent stage. To understand the generality of such a mechanism and fully understand how the aromatic substituents (R) affect the DNA cross-link mechanism, radical and cation trapping experiments were carried out for **1a-5a** and **1b-5b** under the optimized DNA ICL formation conditions. The 2,2,6,6-tetramethylpiperidin-1-oxyl (TEMPO) was used as a radical trap while methoxyamine was used as a carbocation trapping agent.²³ The results are shown in Figure 2-7.

In general, the DNA ICL yield gradually decreased for all compounds (**1a-5a**, **1b-5b**) with increased concentration of methoxyamine. The complete inhibition of DNA ICL formation was observed when the concentration of methoxyamine was increased to 100 mM, indicating that the carbocations were involved in the photo-induced DNA ICL formation process. To figure out whether carbocations were generated from the radical oxidation or via direct heterolysis of C-X bonds, we performed radical trapping experiments using TEMPO as a trapping agent. For all compounds tested (**1a-5a** and **1b-5b**), **1a-5a** and **1b-3b** showed similar phenomenon. The addition of TEMPO hindered the DNA cross-linking process, and complete inhibition was obtained at 100 mM TEMPO. These results indicated that photo-induced DNA ICL formation for **1a-5a** and **1b-3b** was via a radical-cation pathway (defined as first to generate radicals, then the radicals were converted to cations via free radical oxidation) where the radicals were first formed upon photo irradiation of these compounds, then oxidized to cations that directly cross-link DNA (Scheme 2-7). Different from **1a-5a** and **1b-3b**, no obvious decrease of DNA ICL yield was observed for **5b** even with high concentration of TEMPO (100 mM), suggesting that free radicals were not involved in the DNA ICL formation process for **5b**. The slight decrease of

DNA ICL yields was possibly due to the inner filter effect or interaction blockage of TEMPO.⁵⁰

Only carbocations were involved for the photo-induced ICL formation for **5b**, where the carbocations were generated via direct heterolysis of the C-N bond. The result is consistent with our previous results obtained for **IIj**. Apart from that, the lowest heterolytic cleavage energy (ΔE_{HCE}) for **5b** provided another evidence that **5b** might undergo a different mechanism.





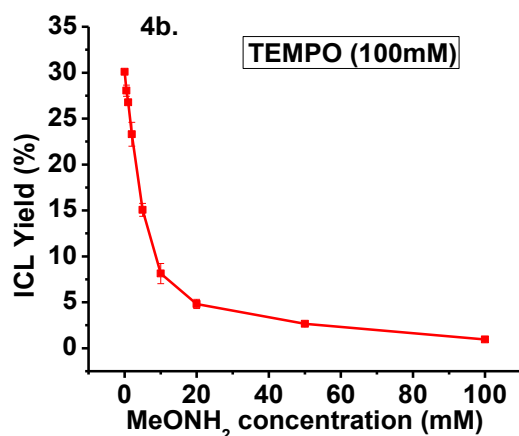
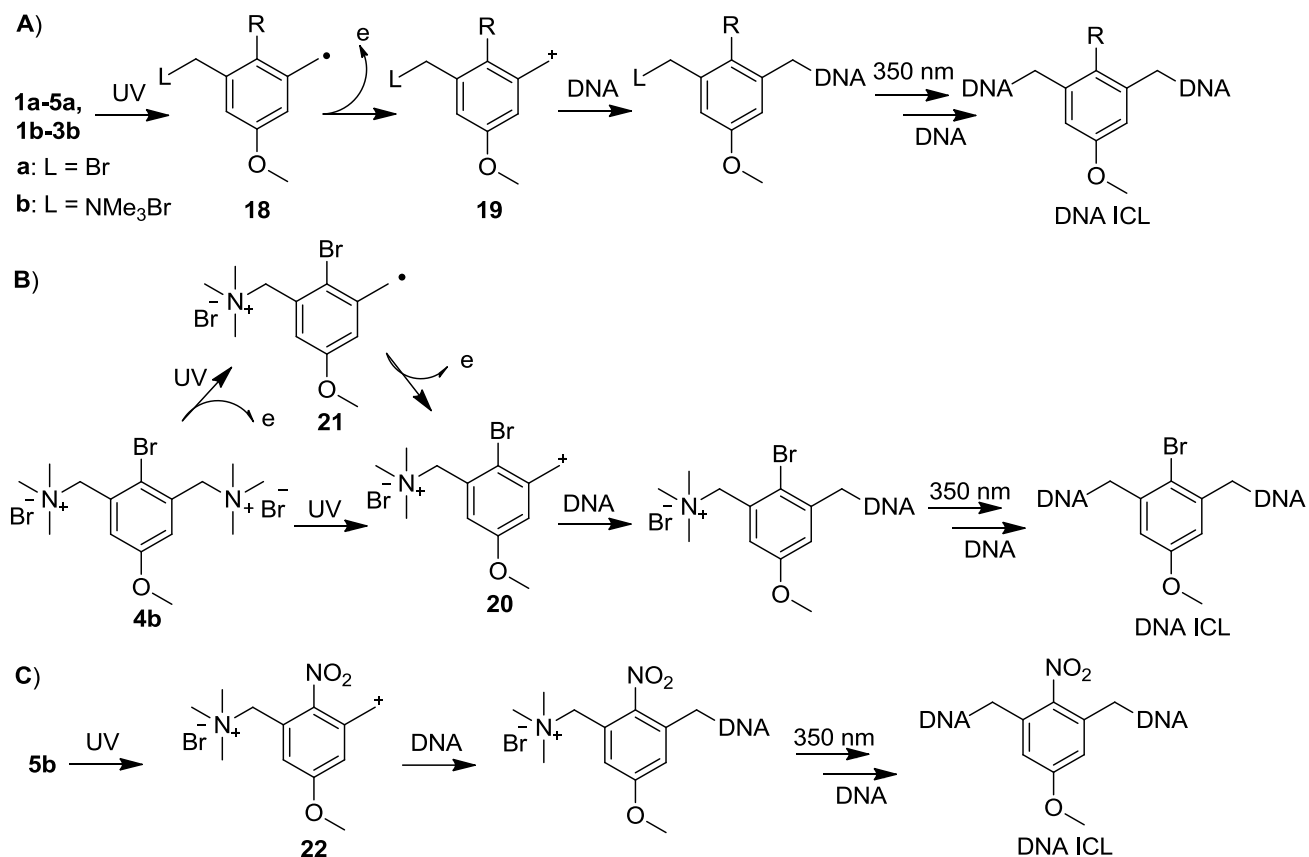


Figure 2-7. Carbocation and radical trapping with DNA ICL formation for **1a-5a**, and **1b-5b**.

Interestingly, different results were obtained for the trapping reaction of **4b**. The DNA ICL yield of **4b** first decreased with addition of TEMPO (0-2.0 mM), then gradually increased with higher concentration of TEMPO (5.0-100 mM), eventually reached the highest one with 50-100 mM TEMPO (Figure 2-7). The decreased DNA ICL yield with 0-2.0 mM TEMPO indicated that the free radicals were involved in the DNA ICL formation process while later increased ICL yield may suggest a more complicate mechanism. Thus, we proposed that the carbocations might be produced via two different pathways for **4b**, either through direct C-N bond heterolysis (path 1) or via free radial oxidation (path 2) (Scheme 2-7). The concentration of TEMPO might have a huge effect on the pathway for carbocation generation. However, we do not have a good explanation at this stage. On the other hand, the efficient DNA ICL formation at 50-100 mM TEMPO indicated that path 1 is predominant, where the carbocation was produced via direct C-N bond heterolysis. To provide evidence for our proposal, we performed the cation trapping experiment in the presence of 100 mM TEMPO. The DNA ICL yield gradually decreased by the addition of methoxyamine and reached the background level with 100 mM methoxyamine, which provided further evidence for the proposed mechanism.

Overall, our results showed that the mechanism pathway for photo-induced DNA cross-link by these bifunctional phenyl compounds was not only influenced by the leaving groups but also by the aromatic substituents.



Scheme 2-7. Proposed mechanism for DNA ICL formation.

In order to provide direct evidence that free radicals and carbocations were formed, the carbocation and radical trapping reactions were carried out with monomers **1a-5a** and **1b-5b** using large excesses of methoxyamine and TEMPO as trapping agents, respectively.

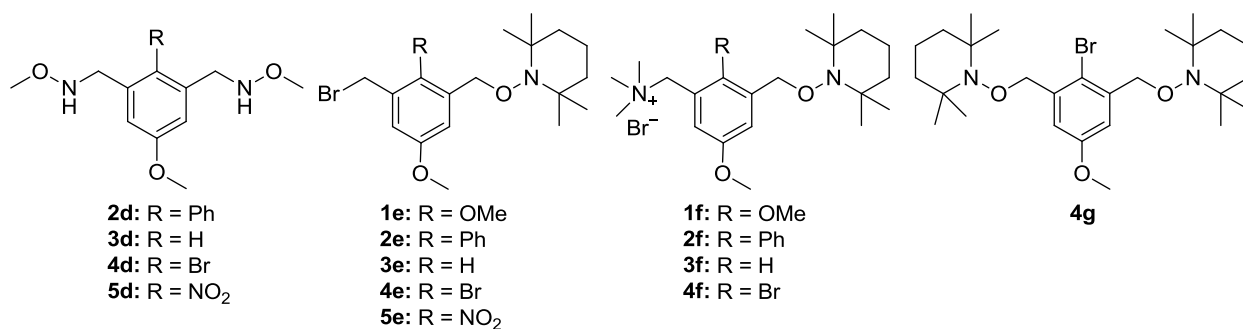
The cation trapping adducts (**2d-4d**) were obtained for compounds **2a-4a** and **2b-4b** upon UV irradiation, which was confirmed by NMR and HRMS analysis, suggesting the generation of carbocations. However, the cation trapping adducts of **1a** and **1b** were not observed due to the complexity of the trapping reactions. The trapping reactions completed within 60 min under UV

irradiation at 350 nm while more than 8 new products were formed. This might be due to the strong electron donating effect of the methoxy group that highly improved the reactivity of the compounds leading to a lot of side reactions. Similar situation was found for **5a** and **5b**.

Compound **5a** was completely consumed after UV irradiation for 6 h, while a very complex reaction occurred and no expected trapping adduct was obtained. For compound **5b**, the cation trapping adduct was formed but not sufficient for NMR analysis, so it was confirmed by HRMS analysis.

The free radical trapping adducts **1e-5e** and **1f-4f** were obtained for compound **1a-5a** and **1b-4b** upon UV irradiation in the presence of the excess of TEMPO, suggesting that the free radicals were generated by UV irradiation of **1e-5e** and **1f-4f**. Apart from **4e**, the trapping adduct **4g** was also isolated from the reaction of **4a** or **4b** with TEMPO. Different from **5a**, photo irradiation of **5b** in the presence of large excess of TMEPO did not produce the trapping adduct. This provided further evidence that free radicals were not involved in the DNA ICL formation process for **5b**.

The free radicals and carbocations were generated via a stepwise manner, which was confirmed by the formation of mono-trapping products **1e-5e** and **1f-4f**. (Scheme 2-8)



Scheme 2-8. Cation and free radical trapping products obtained with **1a-5a** and **1b-5b** upon 350 nm irradiation.

2.2.7. Determination of DNA alkylation sites and alkylation products.

In order to identify the DNA alkylation sites for **1a-5a** and **1b-5b** upon UV irradiation at 350 nm, we performed the heat stability study under basic or neutral conditions, which allowed us to determine heat-labile and/or alkaline-labile DNA alkylation sites. It was reported that N7-alkylated purines can be cleaved by piperiding treatment. The heat stability experiment for alkylated products formed by **1a** is shown in Figure 2-8, and the rest are shown in Appendix A. The DNA ICL products formed by **1a** were damaged by 1.0 M piperidine treatment upon heating at 90 °C for 30 min while they were stable in a pH 7.0 phosphate buffer. The cleavage bands were observed at dAs and dGs, such as dG₂₇, dG₂₂, dG₆, and dA₅. These data indicated that dAs and dGs were the major alkylation sites for **1a**. Similar phenomenon was observed for other compounds (Appendix A). Apart from dAs and dGs, cleavage bands were also found at dCs and dTs for **5b**, which possibly due to the formation pyrimidine glycol as a result of nitro group. It is reported that the electron-affinic nitro compounds greatly facilitated thymine glycol formation.⁵¹

¹ 5'-dGCCTAGTTCTTTTAATTACTTGCAATGCAAGTAATTAAAGCTTGATCTG (**17a**)
^{5 6 14 15 18 22 24 25 27 31 40 44 49}
 3'-dCGGATCAAGAAAATTAATGAACGTTACGTTTCATTAATTTTCGAACTAGAC (**17b**)

17

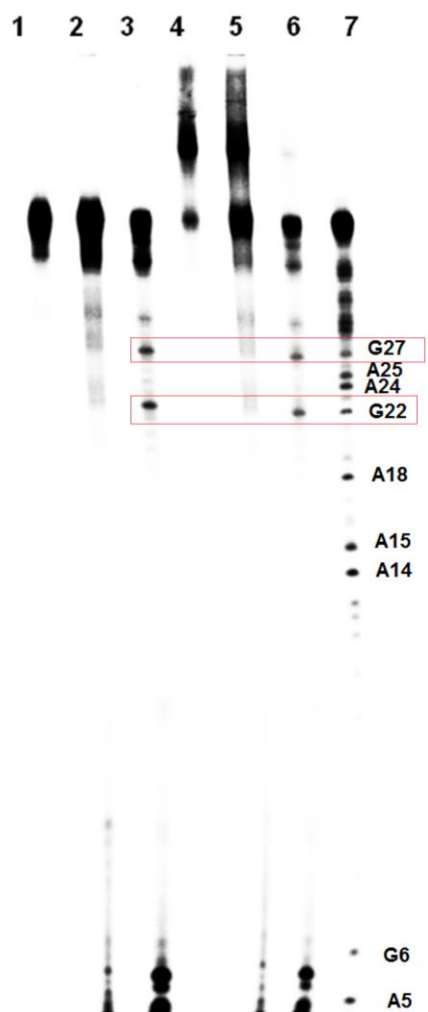
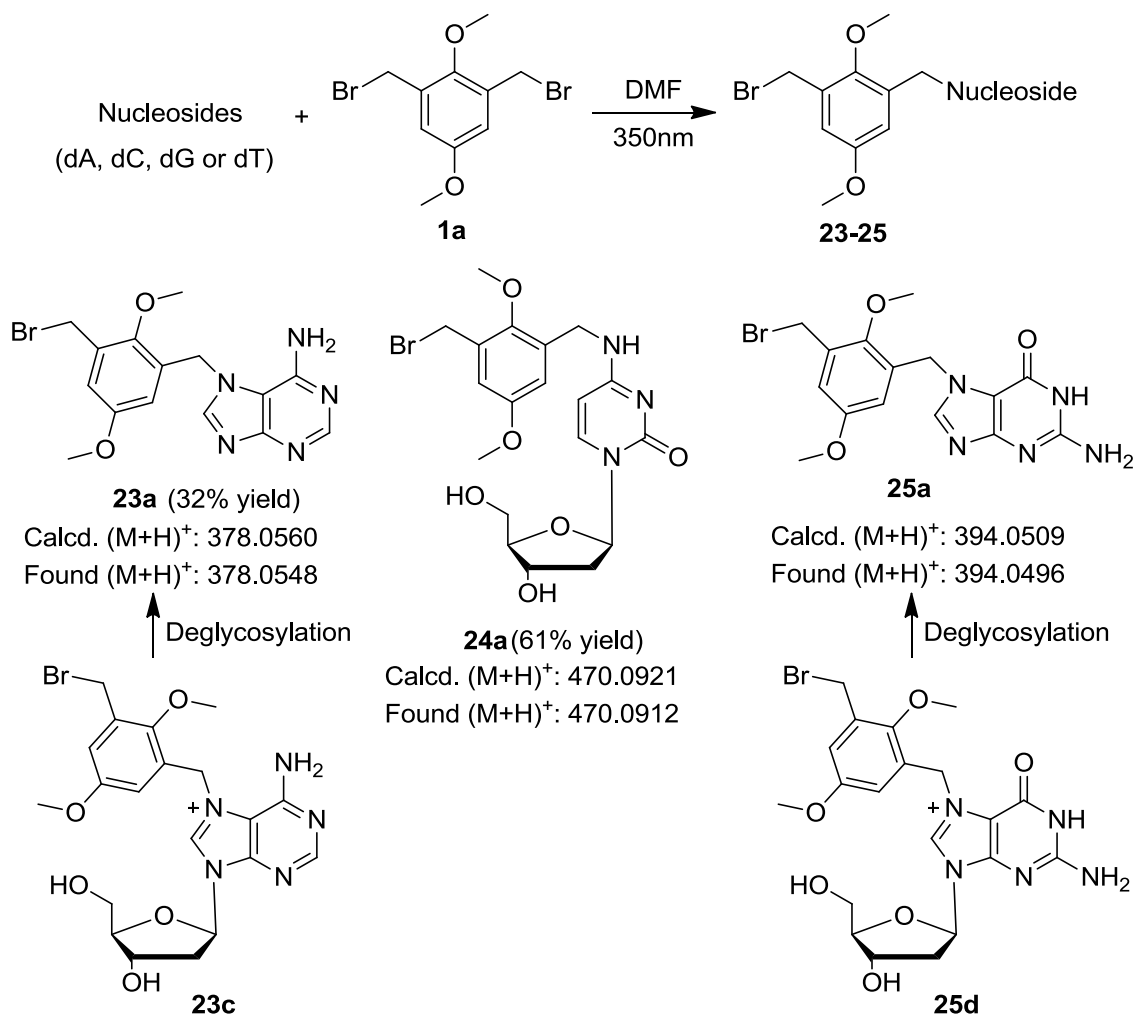


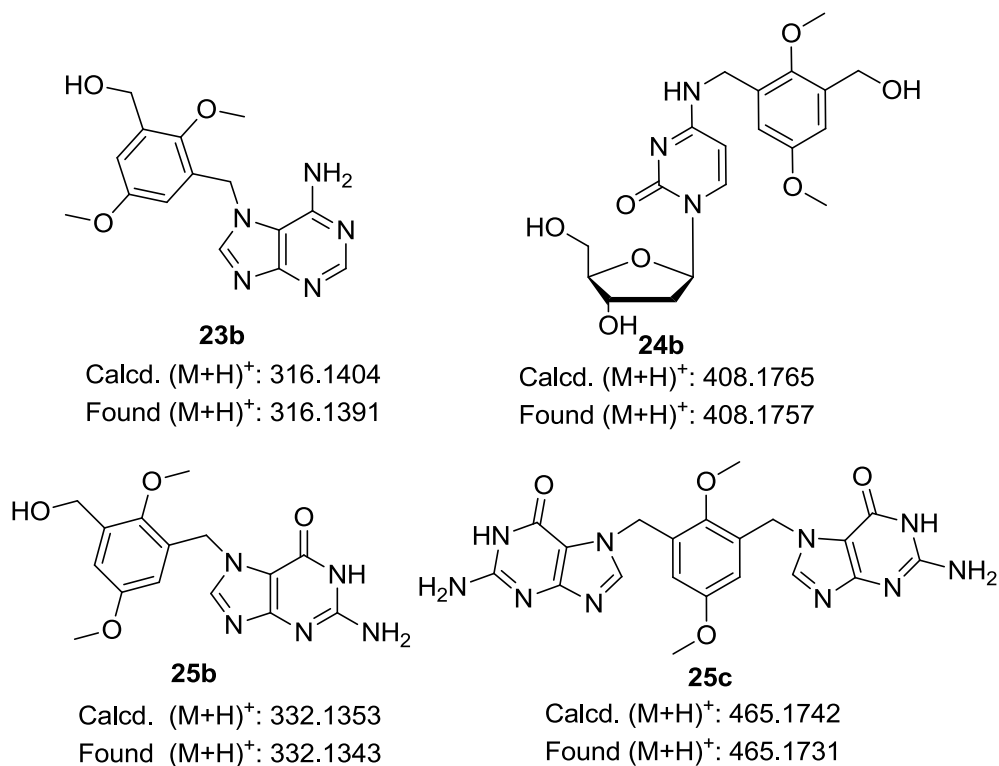
Fig 2-8. Determination of the reaction sites of **1a**. Phosphorimage autoradiogram of 20% denaturing PAGE analysis of the isolated DNA ICL products and alkylated single-stranded DNA (**17a'**) upon heating in piperidine or phosphate buffer. The ICL product and **17a'** were produced by 350 nm irradiation of duplex **17** in the presence of **1a** (500 μ M). **17a** was radiolabeled at the 5'-terminus. Lane 1: isolated alkylated single stranded DNA (**17a'**). Lane 2: **17a'** was heated in a pH 7 phosphate buffer at 90 °C for 30 min. Lane 3: **17a'** was heated in 1.0 M piperidine at 90 °C for 30 min. Lane 4: Isolated DNA ICL products. Lane 5: the DNA ICL products were heated in a pH 7 phosphate buffer at 90 °C for 30 min. Lane 6: the DNA ICL products were heated in 1.0 M piperidine at 90 °C for 30 min. Lane 7: G+A sequencing.

Even though the heat-stability study of the DNA ICL products provided evidences for that dAs and dGs were the possible alkylation sites, it is hard to determine the alkylation sites that are stable in heating. In addition, the structure of the DNA alkylating adducts formed by these compounds could not be determined by heat stability study. Previously, the LC-MS was used to determine the DNA ICL adducts formed by a photo-generated carbocation.²³ However, the detailed structure could not be fully determined because it was impossible to isolate sufficient amount of adducts for NMR analysis. To further investigate the possible DNA cross-linking sites and test the reactivity of the benzyl cations towards four nucleoside, monomer reactions were carried out by treating **1a** with four nucleosides (dA, dC, dG and dT) using DMF as the solvent. Compound **1a** was chosen as a representative for the monomer reaction because it exhibited the highest DNA cross-linking reactivity. HPLC was used to monitor reactions. After one day reaction, new products were observed with dA, dC, and dG but not with dT. The photoreaction of **1a** and dA provided a major adduct (**23a**) with a retention time of about 41 min. Similarly, a major adduct (**24a**) with a retention time of around 41 min was observed for the reaction between **1a** and dC (Scheme 2-9). The structures of **23a** and **24a** were determined based on NMR and HRMS analysis. In addition to the major adducts, the hydrolyzed products of **23a** and **24a** were also observed based on LC-MS analysis (Scheme 2-10). The photoreaction of **1a** with dG was too complex to obtain the pure adducts for NMR analysis. In addition, decomposition was observed during the purification process. Thus, the major adduct isolated was analyzed by HRMS, indicating formation of **25a**. In addition, LC-MS analysis suggested that two minor adducts formed with dG (retention time of around 37 min) corresponded to **25b** and **25c**, caused by the hydrolysis of **25a** and substitution of bromo in **25a** with the second guanine base, respectively. We propose that **23a** and **25a** resulted from a deglycosylation of the corresponding N7 adduct

23c and **25d**, respectively (Scheme 2-9). Deglycosylation of N-7 alkylated purine nucleosides is well-documented.²¹ These data suggested that the benzyl cations mainly alkylate N7 of purines and NH₂ of dC. Thus, we conclude that the DNA interstrand crosslinking induced by these benzyl cations took place with both dG and dC, whereas mono-alkylation would also occur with dA, dG, and dC.



Scheme 2-9. Monomer reactions of **1a** and the nucleosides dG, dA, and dC.



Scheme 2-10: The proposed structures for the minor adducts detected by LC-MS. (LCMS 2020 Single Quad and IT-TOF)

2.2.8. Conclusions

Recently, several bifunctional aryl compounds were reported to undergo photo activation to induce DNA ICL formation via a carbocation mechanism. To better understand the generality of such a mechanism and investigate the effect of chemical structures on carbocation formation and subsequent DNA interstrand cross-linking, we synthesized a series of bifunctional phenyl compounds (**1a-5a** and **1b-5b**) containing a variety of substituents and tested their DNA cross-linking capability. Upon UV irradiation, all bifunctional phenyl compounds (**1a-5a** and **1b-5b**) generated carbocations that directly cross-link DNA. The mechanism pathways for carbocation and subsequent DNA ICL formation highly depend on the aromatic substitutions and leaving groups. For compounds with bromo as a leaving group, the benzyl cations were produced via

free radical oxidation, no matter what substituents are present. Different from bromide compounds, two pathways were involved for the ammonium salts, either via free radical oxidation or through direct C-N bond heterolysis, which highly relies on the aromatic substituents. The ammonium salts with an electron withdrawing group preferred direct C-N bond heterolysis but suppressed the radical formation. Generally speaking, the introduction of substituents to the benzene ring led to red shift of the maximum UV absorption (closer to 350 nm UV light), which in turn increased the photo-sensitivity of these compounds, therefore promoting their DNA cross-linking ability. An electron-donating group exhibited a stronger promoting effect than the electron withdrawing ones, which is consistent with the electron-deficient property of the carbocations. This study provides systematic data regarding how the aromatic substituents and leaving groups affect the photo-induced carbocation mechanism pathways and DNA cross-linking efficiency, which are important mechanistic fundamentals for developing novel photo-induced drugs.

2.3. Experiment Section

General Information. All chemicals from commercial available source were directly used without further purification. Oligonucleotides were synthesized via standard automated DNA synthesis techniques. Deprotection of the synthesized DNA were performed under mild deprotection conditions using a mixture of 40% aqueous MeNH₂ and 28% aqueous NH₃ (1:1) at room temperature for 2 h. 20% denaturing polyacrylamide gel electrophoresis was used for DNA purification. [γ -³²P] ATP was used for DNA labeling with standard method. Quantification of radiolabeled oligonucleotides was carried out using a Molecular Dynamics phosphorimager equipped with ImageQuant, version 5.2, software. ¹H NMR and ¹³C NMR spectra were taken on

a Bruker DRX 300 MHz spectrophotometer with TMS as internal stander. High-resolution mass spectrometry IT-TOF was used for molecular measurement.

Synthesis of 2,5-dimethoxy-1,3-dimethylbenzene (7): The 2,6-dimethylhydroquinone (2.0 g, 14.47 mmol) was added to a solution of NaH (60%, 2.3 g, 57.88 mmol) in DMF (20 mL). The reaction mixture was stirred at rt for 10 min and cooled to 0 °C. Methyl iodide (8.22 g, 57.88 mmol) was added dropwise into the reaction mixture, which was allowed to warm to rt naturally, stirred at rt overnight, and then diluted with ethyl acetate (3 × 40 mL). The organic layer was combined, washed with brine, and dried over anhydrous Na₂SO₄. Solvent was removed and the residue was purified by column chromatography (Hexane: Ethyl acetate = 10:1, R_f = 0.7) to afford **7** as a colorless liquid (2.16 g, 13 mmol). ¹H NMR (300 MHz, CDCl₃): δ. 6.60 (s, 2H), 3.78 (s, 3H), 3.72 (s, 3H), 2.31 (s, 6H) (the NMR spectra were in agreement with those reported).⁵²

1,3-Bis(bromomethyl)-2,5-dimethoxybenzene (1a): Into a solution of compound **7** (1.66 g, 10 mmol) in benzene (40 mL), *N*-bromosuccinimide (3.56 g, 20 mmol) and azobisisobutyronitrile (164.21 mg, 1 mmol) were added. The reaction mixture was refluxed for 3 h. Solvent was removed and the residue was purified by column chromatography (Hexane: DCM= 5:1, R_f= 0.24) to afford **1a** as a white solid (1.70 g, 5.28 mmol): m.p. 92-93 °C; ¹H NMR (300 MHz, CDCl₃): δ.6.92 (s, 2H), 4.55 (s, 4H), 3.99 (s, 3H), 3.82 (s, 3H) (the NMR spectra were in agreement with those reported).⁵⁰

1,1'-(2,5-Dimethoxy-1,3-phenylene)bis(*N,N,N*-trimethylmethanaminium) bromide (1b): Into a solution of compound **1a** (200 mg, 0.62 mmol) in ethyl acetate (10 mL), trimethylamine (4.2 M, 2.2 mL, 9.3 mmol) was added. The reaction mixture was stirred at rt overnight. The mixture was filtrated to afford **1b** as a white solid (270 mg, 0.61 mmol): m.p. 270-271 °C; ¹H NMR (300

MHz, Methanol-*d*₄): δ . 7.40-7.38 (d, J = 6.0 Hz, 2H), 4.62-4.60 (d, 4H), 3.92 (s, 3H), 3.88 (s, 3H), 3.21 (s, 18H). ¹³C NMR (75 MHz, Methanol-*d*₄): δ . 156.37, 153.87, 123.69, 122.94, 63.75, 63.05, 55.39, 52.31. HRMS-ESI (+) (m/z): [M-2Br]²⁺ calcd. for C₁₆H₃₀N₂O₂²⁺, 141.1148; found: 141.1139.

4-Methoxy-2,6-dimethyl-1,1'-biphenyl (9): To a mixture of compound **8** (2.14 g, 10 mmol), phenylboronic acid (2.2 g, 18 mmol), and tetrakis(triphenylphosphine)palladium(0) (1.15 g, 2 mmol) in a two-neck round-bottom flask (100 mL), THF (60 mL) was added under N₂. Then, a solution of K₂CO₃ (6.9 g, 50 mmol) in water (20 mL) was added using syringe. The reaction mixture was refluxed for 24 h, diluted with DCM (3 × 40 mL), washed with brine, and dried over anhydrous Na₂SO₄. Solvent was removed and the residue was purified by column chromatography (Hexane: Ethyl acetate = 10:1, R_f = 0.3) to obtain **9** as a colorless oily product (2 g, 9.4 mmol) that was solidified at -20 °C. ¹H NMR (300 MHz, CDCl₃): δ . 7.48-7.34 (m, 3H), 7.20-7.17 (d, J = 9.0, Hz, 2H), 3.87 (s, 3H), 2.08 (s, 6H) (the NMR spectra were in agreement with those reported).⁵³

2,6-Bis(bromomethyl)-4-methoxy-1,1'-biphenyl (2a): Into a solution of compound **9** (1.4 g, 6.6 mmol) in benzene (50 mL), *N*-bromosuccinimide (2.35 g, 13.2 mmol) and azobisisobutyronitrile (108 mg, 0.66 mmol) were added. The reaction mixture was refluxed for 2 h. Solvent was removed and the residue was purified by column chromatography (Hexane: DCM = 5:1, R_f = 0.33) to obtain **2a** as a white solid (1.4 g, 3.81 mmol): m. p. 75-76 °C; ¹H NMR (300 MHz, CDCl₃): δ . 7.52-7.36 (m, 5H), 7.05 (s, 2H), 4.21 (s, 4H), 3.89 (s, 3H). ¹³C NMR (75 MHz, CDCl₃): δ . 159.04, 137.97, 136.56, 134.31, 129.88, 128.37, 127.93, 115.98, 55.48, 31.91. HRMS-ESI (+) (m/z): [M-Br]⁺ calcd. for C₁₅H₁₄OBr, 289.0223; found: 289.0205.

1,1'-(4-Methoxy-[1,1'-biphenyl]-2,6-diyl)bis(N,N,N-trimethylmethanaminium) bromide

(2b): To a solution of compound **2a** (200 mg, 0.54 mmol) in ethyl acetate (10 mL), 4.2 M trimethylamine solution in ethanol (1.93 mL, 8.11 mmol) was added. The reaction mixture was stirred at rt overnight and then filtrated to afford **2b** as a white solid (260 mg, 0.53 mmol): m.p. 261-262 °C; ¹H NMR (300 MHz, Methanol-*d*₄): δ. 7.68-58 (m, 5H), 7.45-7.43 (d, *J* = 6.0 Hz, 2H), 4.64 (s, 4H), 4.02 (s, 3H), 2.89 (s, 18H). ¹³C NMR (75 MHz, Methanol-*d*₄): δ. 158.72, 139.17, 135.84, 131.98, 129.47, 128.81, 122.31, 66.27, 55.30, 52.52. HRMS-ESI (+) (*m/z*): [M-2Br]²⁺ calcd. for C₂₁H₃₂N₂O²⁺, 164.1252; found: 164.1241.

2-Bromo-1,3-bis(bromomethyl)-5-methoxybenzene (4a): To a solution of compound **8** (1.90 g, 8.88 mmol) in benzene (25 mL), *N*-bromosuccinimide (3.32 g, 18.65 mmol) and azobisisobutyronitrile (145 mg, 0.89 mmol) was added. The reaction mixture was refluxed for 2 h, then the second portion of *N*-bromosuccinimide (0.33 g, 1.86 mmol) and azobisisobutyronitrile (14.5 mg, 0.089 mmol) were added and refluxed for another 0.5 h. Solvent was removed. The residue was diluted with ethyl acetate (3 × 30 mL), washed with brine, and dried over anhydrous Na₂SO₄. Solvent was removed, and the residue was purified by column chromatography (Hexane: Ethyl acetate = 25:1, *R_f* = 0.4) to obtain **4a** as a white solid (1.2 g, 3.25 mmol): m. p. 126-127 °C; ¹H NMR (300 MHz, CDCl₃): δ. 7.00 (s, 2H), 4.62 (s, 4H), 3.84 (s, 3H) (the NMR spectra were in agreement with those reported).⁴⁵

1,1'-(2-Bromo-5-methoxy-1,3-phenylene)bis(N,N,N-trimethylmethanaminium) bromide

(4b): To a solution of compound **4a** (200 mg, 0.54 mmol) in ethyl acetate (4 mL), 4.2 M trimethylamine solution in ethanol (1.93 mL, 8.11 mmol) was added. The reaction mixture was stirred at rt overnight and then filtrated to afford **4b** as a white solid (250 mg, 0.51 mmol): m. p. 263-264 °C; ¹H NMR (300 MHz, Methanol-*d*₄): δ. 7.55 (s, 2H), 4.89 (s, 4H), 3.97 (s, 3H), 3.31

(s, 18H). ^{13}C NMR (75 MHz, Methanol- d_4): δ . 157.52, 129.42, 122.09, 120.30, 66.77, 54.11, 51.23. HRMS-ESI (+) (m/z): $[\text{M}-2\text{Br}]^{2+}$ calcd. for $\text{C}_{15}\text{H}_{27}\text{N}_2\text{OBr}^{2+}$, 165.0648; found: 165.0638.

5-Methoxyisophthalic acid (11): To a solution of compound **10** (5.0 g, 36.71 mmol) in 150 mL of $^t\text{BuOH}$: H_2O (1:1) solution, KMnO_4 (11.6 g, 73.43 mmol) was added. The mixture was refluxed for 2 h and cooled to rt, then the second portion of KMnO_4 (11.6 g) was added. The reaction mixture was refluxed for another 16 h. The insoluble byproducts were removed by hot filtration. Then, $^t\text{BuOH}$ was removed, and the concentrated HCl (100 mL) was added. The resulting white solid **11** (3.93 g) was collected by filtration and dried overnight under vacuum. ^1H NMR (300 MHz, $\text{DMSO}-d_6$): δ . 13.23 (s, 2H), 8.08 (s, 1H), 7.65 (s, 2H), 3.87 (s, 3H) (the NMR spectra were in agreement with those reported).⁵⁴

Dimethyl 5-methoxyisophthalate (12): A solution of **11** (3.92 g, 20 mmol) in methanol (70 mL) was added concentrated H_2SO_4 (4.0 mL) dropwise at 0 °C. The reaction mixture was refluxed overnight, then poured to ice cold water (50 mL) and extracted with ethyl acetate (3×50 mL). The organic phases were combined, washed with water (30 mL), NaHCO_3 (5%) and brine, and dried over anhydrous Na_2SO_4 . Solvent was removed to provide the crude product that was precipitated with ethyl acetate and hexane to afford pure **12** as a white solid (2.75 g, 12.27 mmol). ^1H NMR (300 MHz, CDCl_3): δ . 8.30 (s, 1H), 7.77 (s, 2H), 3.96 (s, 6H), 3.91 (s, 3H) (the NMR spectra were in agreement with those reported).⁵⁴

(5-Methoxy-1,3-phenylene)dimethanol (13): To a solution of compound **12** (2.25 g, 10 mmol) in THF, LiAlH_4 (835 mg, 22 mmol) was slowly added at 0°C. The reaction mixture was stirred for 2 h, quenched with water, and washed with ethyl acetate (3×40 mL). The organic phases were combined, washed with brine, and dried over anhydrous Na_2SO_4 . Solvent was removed to provide the crude product as a colorless oil that was purified by column chromatography

(Hexane: Ethyl acetate = 1:1, R_f = 0.15) to obtain **13** as a white solid (1.46g, 8.69 mmol). ^1H NMR (300 MHz, CDCl_3): δ . 6.94 (s, 1H), 6.85 (s, 2H), 4.67 (s, 4H), 3.83 (s, 3H), 2.04 (a, broad, 2H) (the NMR spectra were in agreement with those reported).⁴⁶

1,3-Bis(bromomethyl)-5-methoxybenzene (3a): A solution of **13** (1.0 g, 5.95 mmol) in DCM (40 mL) was cooled to 0°C under argon. Then, phosphorus tribromide (3.54 g, 13.09 mmol) was added at 0°C under argon. The reaction mixture was warmed to rt, stirred for 4 h, and diluted with DCM (3 \times 40 mL). The organic phases were combined, washed with brine, and dried over anhydrous Na_2SO_4 . Solvent was removed, and the residue was purified by column chromatography (Hexane: Ethyl acetate = 20:1, R_f = 0.58) to obtain **3a** as a white solid (1.2 g, 4.11 mmol). ^1H NMR (300 MHz, CDCl_3): δ . 7.03 (s, 1H), 6.89 (s, 2H), 4.46 (s, 4H), 3.85-3.84 (d, J = 3.0, Hz, 3H) (the NMR spectra were in agreement with those reported).⁵⁵

1,1'-(5-Methoxy-1,3-phenylene)bis(*N,N,N*-trimethylmethanaminium) bromide (3b): To a solution of compound **3a** (200 mg, 0.68 mmol) in ethyl acetate (6 mL), 4.2 M trimethylamine in ethanol (2.43 mL, 10.2 mmol) was added. The reaction mixture was stirred at rt overnight, and then filtrated to provide **3b** as a white solid (266 mg, 0.65 mmol): m. p. 254-255 °C; ^1H NMR (300 MHz, Methanol- d_4): δ . 7.48 (s, 1H), 7.37 (s, 2H), 4.65 (s, 4H), 3.95 (s, 3H), 3.21 (s, 18H). ^{13}C NMR (125 MHz, Methanol- d_4): δ . 160.58, 130.17, 129.03, 120.53, 68.20, 55.23, 52.15. HRMS-ESI (+) (m/z): $[\text{M}-2\text{Br}]^{2+}$ calcd. for $\text{C}_{15}\text{H}_{28}\text{N}_2\text{O}^{2+}$, 126.1095; found: 126.1088.

5-Methoxy-1,3-dimethyl-2-nitrobenzene (14): To a solution of compound **10** (13.6 g, 100 mmol) in DCM (250 mL), concentrated HNO_3 (10 mL, 68-70%) in 100 mL DCM) was added dropwise at -20 °C. The reaction mixture was stirred at rt for 4 h. Solvent was removed and the residue was purified by column chromatography (Hexane: Ethyl acetate = 10:1, R_f = 0.5) to

afford **14** as a light yellow solid (2.4 g, 13.19 mmol). ^1H NMR (300 MHz, CDCl_3): δ . 6.62 (s, 2H), 3.84 (s, 3H), 2.35 (s, 6H) (the NMR spectra were in agreement with those reported).⁵⁶

5-Methoxy-2-nitroisophthalic acid (15): To a solution of compound **14** (2.0 g, 10.99 mmol) in water (70 mL), NaOH (0.88 g, 21.98 mmol) was added. The reaction mixture was heated to reflux and KMnO_4 (6.94 g, 43.96 mmol) was added. The reaction mixture was refluxed for 6 h, then the second portion of KMnO_4 (8 g, 50 mmol) and NaOH (1 g, 25 mmol) were added. The resulting mixture was refluxed for another 20 h, then the third portion of KMnO_4 (80 g, 50 mmol) was added. The reaction mixture was refluxed overnight, cooled to rt, and filtrated. The filtrate was acidified with concentrated HCl, and extracted with ethyl acetate (3×50 mL). Solvent was removed to afford **15** as a white solid (1.06 g, 4.4 mmol) (1:1 MeOH: Ethyl acetate, $R_f = 0.5$): m.p. 218-219 °C; ^1H NMR (75 MHz, Methanol- d_4): δ . 7.62 (s, 2H), 3.96 (s, 3H). ^{13}C NMR (300 MHz, DMSO- d_6): δ . 164.84, 161.38, 160.34, 128.21, 118.64, 56.92. HRMS-ESI (+) (m/z): $[\text{M}+\text{Na}]^+$ calcd. for $\text{C}_9\text{H}_7\text{NNaO}_7^+$, 264.0115; found: 264.0102.

(5-Methoxy-2-nitro-1,3-phenylene)dimethanol (16): A solution of compound **15** (1.0 g, 4.15 mmol) in THF (20 mL) was cooled to 0 °C, followed by addition of borane tetrahydrofuran complex solution (1.0 M in THF, 20.75 mL, 20.75 mmol). The reaction mixture was allowed to warm up to rt and stirred at rt for 48 h. Then, the second portion of borane tetrahydrofuran complex solution (1.0 M in THF, 15 mL, 15 mmol) was added and stirred for another 36 h. Solvent was removed and the resulting mixture was quenched with water, and diluted with ethyl acetate (3×40 mL). The organic layers were combined, washed with brine, and dried over anhydrous Na_2SO_4 . Solvent was removed and the residue was purified by column chromatography (Hexane: Ethyl acetate = 1:1, $R_f = 0.3$) to afford **16** as a light yellow solid (0.54 g, 2.53 mmol): m.p. 125-126 °C; ^1H NMR (300 MHz, Methanol- d_4): δ . 7.15 (s, 2H), 4.70 (s, 4H),

3.91 (s, 3H). ^{13}C NMR (75 MHz, Methanol- d_4): δ . 161.63, 140.50, 137.87, 111.69, 60.02, 54.82.

HRMS-ESI (+) (m/z): $[\text{M}+\text{Na}]^+$ calcd. for $\text{C}_9\text{H}_{11}\text{NNaO}_5^+$, 236.0529; found: 236.0522.

1,3-Bis(bromomethyl)-5-methoxy-2-nitrobenzene (5a): Into a solution of compound **16** (426 mg, 2 mmol) in DCM (20 mL), phosphorus tribromide (1.19 g, 0.42 mL, 4.4 mmol) was added at 0 °C under argon. The reaction mixture was stirred for 2 h. Then, the second portion of phosphorus tribromide (0.6 g, 0.21 mL, 2.2 mmol) was added. The reaction mixture was stirred for another 2 h and diluted with DCM (3×25 mL). The organic layers were combined, washed with brine, and dried over anhydrous Na_2SO_4 . Solvent was removed, and the residue was purified by column chromatography (Hexane:Ethyl acetate = 10:1, R_f = 0.15) to obtain **5a** as a light yellowish solid (300 g, 0.89 mmol): m.p. 116-117 °C; ^1H NMR (300 MHz, CDCl_3): δ . 6.98 (s, 2H), 4.54 (s, 4H), 3.91 (s, 3H). ^{13}C NMR (75 MHz, CDCl_3): δ . 160.83, 142.81, 133.62, 116.73, 55.97, 27.31. HRMS-ESI (+) (m/z): $[\text{M}+\text{Na}]^+$ calcd. for $\text{C}_9\text{H}_9\text{NNaO}_3\text{Br}_2^+$, 359.8841; found: 359.8830.

1,1'-(5-Methoxy-2-nitro-1,3-phenylene)bis(N,N,N-trimethylmethanaminium) bromide (5b):

To a solution of compound **5a** (70 mg, 0.21 mmol) in ethyl acetate (3 mL), 4.2 M trimethylamine solution in ethanol (0.74 mL, 3.11 mmol) was added. The reaction mixture was stirred at rt overnight and filtrated to afford **5b** as a light yellow solid (82 mg, 0.18 mmol): m. p. 229-230 °C ^1H NMR (300 MHz, Methanol- d_4): δ . 7.64 (s, 2H), 4.79 (s, 4H), 4.07 (s, 3H), 3.24 (s, 18H). ^{13}C NMR (75 MHz, Methanol- d_4): δ . 159.59, 145.79, 121.96, 121.58, 62.20, 54.65, 51.22. HRMS-ESI (+) (m/z): $[\text{M}-2\text{Br}]^{2+}$ calcd. for $\text{C}_{15}\text{H}_{27}\text{N}_3\text{O}_3^{2+}$, 148.6021; found: 148.6013.

General procedure for trapping assay.

Radical trapping: To a solution of compounds **1a-5a** (1 eq) in CH_3CN (2 mL) or **1b-5b** (1 eq) in MeOH (2 mL), TEMPO (10 eq) were added at rt while stirring. The resulting mixture was

allowed to react upon UV irradiation until all starting material was consumed. Solvent was removed and the residue was purified by chromatography (Hexane: DCM = 10:1 for **1a-5a**, DCM: Methanol = 10:1 for **1b-5b**) to afford the trapping adducts **1e-5e**, **1f-4f**, and **4g**.

1-((3-(Bromomethyl)-2,5-dimethoxybenzyl)oxy)-2,2,6,6-tetramethylpiperidine (1e): ^1H

NMR (300 MHz, CDCl_3): δ . 7.10 (s, 1H), 6.86 (s, 1H), 4.89 (s, 2H), 4.58 (s, 2H), 3.86-3.83 (d, $J = 9.0$ Hz, 6H), 1.58-1.51 (m, 6H), 1.28-1.18 (d, $J = 30$ Hz, 12H). ^{13}C NMR (75 MHz, CDCl_3): δ . 155.82, 149.46, 133.31, 131.55, 115.77, 114.24, 73.25, 62.21, 60.05, 55.55, 39.76, 33.01, 28.12, 20.41, 17.10. HRMS-ESI (+) (m/z): $[\text{M}+\text{H}]^+$ calcd. for $\text{C}_{19}\text{H}_{31}\text{NO}_3\text{Br}^+$, 400.1482; found: 400.1475.

1-((6-(Bromomethyl)-4-methoxy-[1,1'-biphenyl]-2-yl)methoxy)-2,2,6,6-

tetramethylpiperidine (2e): ^1H NMR (300 MHz, CDCl_3): δ . 7.42-7.40 (m, 3H), 7.27-7.21 (m, 3H), 7.00 (s, 1H), 4.48 (s, 2H), 4.23 (s, 2H), 3.91 (s, 3H), 1.62-1.23 (m, 6H), 1.11-1.00 (d, $J = 33$ Hz, 12H). ^{13}C NMR (75 MHz, CDCl_3): δ . 158.88, 138.84, 137.46, 136.92, 133.29, 129.85, 128.28, 127.43, 114.54, 113.51, 59.86, 55.32, 39.67, 39.60, 32.66, 32.37, 20.32, 17.05. HRMS-ESI (+) (m/z): $[\text{M}+\text{H}]^+$ calcd. for $\text{C}_{24}\text{H}_{33}\text{NO}_2\text{Br}^+$, 446.1689; found: 446.1678.

1-((3-(Bromomethyl)-5-methoxybenzyl)oxy)-2,2,6,6-tetramethylpiperidine (3e): ^1H NMR

(300 MHz, CDCl_3): δ . 6.97 (s, 1H), 6.91-6.87 (m, 2H), 4.83 (s, 2H), 4.50 (s, 2H), 3.86 (s, 3H), 1.53-1.51 (m, 6H), 1.27-1.20 (m, 12H). ^{13}C NMR (75 MHz, CDCl_3): δ . 159.82, 140.53, 138.92, 120.12, 113.32, 113.07, 60.05, 55.32, 39.74, 33.63, 33.10, 20.36, 17.13. HRMS-ESI (+) (m/z): $[\text{M}+\text{H}]^+$ calcd. for $\text{C}_{18}\text{H}_{29}\text{NO}_2\text{Br}^+$, 370.1376; found: 370.1370.

1-((2-Bromo-3-(bromomethyl)-5-methoxybenzyl)oxy)-2,2,6,6-tetramethylpiperidine (4e): ^1H

NMR (300 MHz, CDCl_3): δ . 7.19 (s, 1H), 6.94 (s, 1H), 4.89 (s, 2H), 4.63 (s, 2H), 3.86 (s, 3H), 1.6-1.53 (m, 6H), 1.23-1.22 (d, $J = 3.3$ Hz, 12H). ^{13}C NMR (75 MHz, CDCl_3): δ . 158.81, 140.64,

137.65, 114.55, 113.80, 60.10, 55.47, 39.72, 33.99, 32.91, 20.46, 17.10. HRMS-ESI (+) (m/z): [M+H]⁺ calcd. for C₁₈H₂₈NO₂Br₂⁺, 448.0481; found: 448.0475.

1-((3-(Bromomethyl)-5-methoxy-2-nitrobenzyl)oxy)-2,2,6,6-tetramethylpiperidine (5e):

HRMS-ESI (+) (m/z): [M+H]⁺ calcd. for C₁₈H₂₈N₂O₄Br₂⁺, 415.1227; found: 415.1220 (Note: the amount of **5e** obtained was not sufficient to conduct NMR analysis due to an extremely slow reaction).

1-(2,5-Dimethoxy-3-(((2,2,6,6-tetramethylpiperidin-1-yl)oxy)methyl)phenyl)-N,N,N-

trimethylmethanaminium (1f): ¹H NMR (300 MHz, Methanol-*d*₄): δ. 7.28 (s, 1H), 7.09 (s, 1H), 4.94 (s, 2H), 4.55 (s, 2H), 3.86 (s, 3H), 3.79 (s, 3H), 3.14 (s, 9H), 1.55-1.53 (m, 6H), 1.27-1.19 (d, *J* = 24 Hz, 12H). ¹³C NMR (75 MHz, Methanol-*d*₄): δ. 156.04, 151.38, 133.78, 121.61, 117.97, 117.64, 73.10, 64.06, 62.01, 59.87, 54.91, 52.18, 39.39, 32.07, 19.39, 16.64. HRMS-ESI (+) (m/z): [M-Br]⁺ calcd. for C₂₂H₃₉N₂O₃⁺, 379.2955; found: 379.2945.

1-(4-Methoxy-6-(((2,2,6,6-tetramethylpiperidin-1-yl)oxy)methyl)-[1,1'-biphenyl]-2-yl)-

N,N,N-trimethylmethanaminium (2f): ¹H NMR (300 MHz, CDCl₃): δ. 7.48-7.35 (m, 5H), 7.12-7.09 (d, 2H), 4.76 (s, 2H), 4.47 (s, 2H), 3.92 (s, 3H), 3.17 (s, 9H), 1.41-1.40 (m, 6H), 1.08 (s, 6H), 0.97(s, 6H). ¹³C NMR (75 MHz, CDCl₃): δ. 158.89, 139.80, 136.85, 135.27, 130.67, 129.00, 128.22, 126.38, 117.80, 117.07, 66.29, 59.90, 55.93, 53.22, 39.59, 32.96, 32.68, 20.32, 19.89, 16.97. HRMS-ESI (+) (m/z): [M-Br]⁺ calcd. for C₂₇H₄₁N₂O₂⁺, 425.3163; found: 425.3138.

1-(3-Methoxy-5-(((2,2,6,6-tetramethylpiperidin-1-yl)oxy)methyl)phenyl)-N,N,N-

trimethylmethanaminium (3f): ¹H NMR (300 MHz, CDCl₃): δ. 7.23 (s, 1H), 7.06 (s, 1H), 6.99 (s, 1H), 4.94 (s, 2H), 4.80 (s, 2H), 3.84 (s, 3H), 3.45 (s, 9H), 1.53-1.32 (m, 6H), 1.19 (s, 6H), 1.13(s, 6H). ¹³C NMR (75 MHz, CDCl₃): δ. 160.12, 141.25, 128.44, 123.17, 117.19, 115.32,

69.21, 60.01, 55.73, 52.88, 39.63, 33.09, 20.31, 17.03. HRMS-ESI (+) (m/z): $[M-Br]^+$ calcd. for $C_{21}H_{37}N_2O_2^+$, 349.2850; found: 349.2822.

1-(2-Bromo-5-methoxy-3-(((2,2,6,6-tetramethylpiperidin-1-yl)oxy)methyl)phenyl)-N,N,N-trimethylmethanaminium (4f): 1H NMR (300 MHz, Methanol- d_4): δ . 7.38 (s, 1H), 7.27 (s, 1H), 4.94 (s, 2H), 4.81 (s, 2H), 3.92 (s, 3H), 3.26 (s, 9H), 1.57-1.56 (m, 6H), 1.23 (d, 12H). ^{13}C NMR (75 MHz, Methanol- d_4): δ . 159.07, 141.17, 128.70, 118.69, 116.78, 116.09, 78.01, 67.81, 59.94, 54.98, 52.62, 39.36, 31.97, 19.44, 16.63. HRMS-ESI (+) (m/z): $[M-Br]^+$ calcd. for $C_{21}H_{36}N_2O_2Br^+$, 427.1955; found: 427.1931.

1,1'-(((2-Bromo-5-methoxy-1,3-phenylene)bis(methylene))bis(oxy))bis(2,2,6,6-tetramethylpiperidine) (4g): 1H NMR (300 MHz, $CDCl_3$): δ . 7.13 (s, 2H), 4.89 (s, 4H), 3.88 (s, 3H), 1.59-1.53 (m, 12H), 1.22-1.13 (m, 24H). ^{13}C NMR (75 MHz, $CDCl_3$): δ . 158.69, 139.13, 112.29, 111.14, 60.06, 55.33, 39.73, 32.93, 20.44, 17.11. HRMS-ESI (+) (m/z): $[M+H]^+$ calcd. for $C_{27}H_{46}N_2O_3Br^+$, 525.2686; found: 525.2679.

Carbocation trapping: To a solution of $MeONH_2 \cdot HCl$ (40 eq) in DMF (2 mL), trimethylamine (44 eq.) was added. After stirring at rt for 30 min, **2a-4a** (1 eq.) in DMF or **2b-4b** (1 eq.) in MeOH were added. The resulting mixture was stirred for 20 min, then irradiated with 350 nm light until the starting material was consumed. The reaction was quenched by water and extracted with ethyl acetate (3×3 mL). The combined organic phases were washed with brine and dried over anhydrous Na_2SO_4 . After removing solvent, the residue was purified by chromatography (Hexane: ethyl acetate = 5:1) to provide the corresponding trapping adducts **2d-5d**.

***N,N'*-((4-Methoxy-[1,1'-biphenyl]-2,6-diyl)bis(methylene))bis(O-methylhydroxylamine) (2d):** 1H NMR (300 MHz, $CDCl_3$): δ . 7.43-7.40 (m, 3H), 7.25-7.23 (d, $J = 6.0$ Hz, 2H), 7.00 (s,

2H), 5.49 (s, 2H), 3.89 (s, 3H), 3.78 (s, 4H), 3.43-3.42 (d, $J = 3.0$ Hz, 6H). ^{13}C NMR (75 MHz, CDCl_3): δ . 158.75, 138.37, 136.99, 134.46, 129.96, 128.41, 127.36, 114.00, 61.42, 55.31, 53.70. HRMS-ESI (+) (m/z): $[\text{M}+\text{H}]^+$ calcd. for $\text{C}_{17}\text{H}_{23}\text{N}_2\text{O}_3^+$, 303.1703; found: 303.1683.

***N,N'*-((5-Methoxy-1,3-phenylene)bis(methylene))bis(O-methylhydroxylamine) (3d)**: ^1H NMR (300 MHz, CDCl_3): δ . 6.94 (s, 1H), 6.85 (s, 1H), 5.74 (s, 1H), 4.04 (s, 4H), 3.83 (s, 3H), 3.54 (s, 6H). ^{13}C NMR (75 MHz, CDCl_3): δ . 159.84, 139.26, 121.44, 113.38, 61.85, 56.09, 55.27. HRMS-ESI (+) (m/z): $[\text{M}+\text{H}]^+$ calcd. for $\text{C}_{11}\text{H}_{19}\text{N}_2\text{O}_3^+$, 227.1390; found: 227.1380.

***N,N'*-((2-Bromo-5-methoxy-1,3-phenylene)bis(methylene))bis(O-methylhydroxylamine) (4d)**: ^1H NMR (300 MHz, CDCl_3): δ . 6.94 (s, 2H), 5.94 (s, 2H), 4.17 (s, 4H), 3.83 (s, 3H), 3.57 (s, 6H). ^{13}C NMR (75 MHz, CDCl_3): δ . 158.55, 138.28, 116.10, 115.87, 61.64, 56.31, 55.47. HRMS-ESI (+) (m/z): $[\text{M}+\text{H}]^+$ calcd. for $\text{C}_{11}\text{H}_{18}\text{N}_2\text{O}_3\text{Br}^+$, 304.0417; found: 304.0408.

***N,N'*-((5-methoxy-2-nitro-1,3-phenylene)bis(methylene))bis(O-methylhydroxylamine) (5d)**: HRMS-ESI (+) (m/z): $[\text{M}+\text{H}]^+$ calcd. for $\text{C}_{11}\text{H}_{18}\text{N}_3\text{O}_5^+$ 272.1241; found: 272.1228 (Note: the amount of **5d** obtained was not sufficient to conduct NMR analysis due to an extremely slow and complex reaction).

ICL formation with duplex DNA. The ^{32}P -labelled oligonucleotide (0.5 μM) was annealed with 1.5 equiv of the complementary strand by heating to 90 $^\circ\text{C}$ for 5 min in potassium phosphate buffer (pH 7, 10 mM), followed by naturally cooling down to rt in heating block. The ^{32}P -labeled ODN duplex (2 μL , 0.5 μM) was then mixed with 1 M NaCl (2 μL), 100 mM potassium phosphate (2 μL , pH 8), and **1a-5a** or **1b-5b** (concentration range: 10 μM to 10 mM in 6 μL CH_3CN) and autoclaved distilled water to give a final volume of 20 μL . The reaction mixture was irradiated with light at 350 nm until the reaction was completed, followed by quenching with

an equal volume of 90% formamide loading buffer. The resulting mixture was then subjected to 20% denaturing polyacrylamide gel for electrophoresis.

Trapping assay of oligonucleotides. The ^{32}P -labeled oligonucleotide duplex (2 μL , 0.5 μM) was mixed with 1 M NaCl (2 μL) and 100 mM potassium phosphate (2 μL , pH 8). The stock solution of $\text{MeONH}_2\cdot\text{HCl}$ (2 M) was titrated with 5 M NaOH to adjust the pH to ~ 7.0 , which was diluted to the desired concentration (100/3 μM to 2000/3 mM). Then, 3 μL was added to the reaction mixture as appropriate for the desired concentration (final MeONH_2 concentration: 50 μM to 100 mM). Similarly, 3 μL of TEMPO in CH_3CN (100/3 μM to 2000/3 mM) was added to the reaction mixture as appropriate for the desired concentration (final TEMPO concentration: 50 μM to 100 mM). Compounds **1a-5a** (40/3 mM, 3 μL in CH_3CN) or **1b-5b** (40/3 mM, 3 μL in H_2O) and the appropriate amount of autoclaved water and CH_3CN were added to give a final volume of 20 μL (final: 6 μL CH_3CN and 14 μL H_2O). The reaction was irradiated with light at 350 nm for 0.75 h (**1a**), 6 h (**4a** and **1b**), 8 h (**2a**), 12 h (**2b** and **5b**), 24 h (**4b** and **5a**), 35 h (**3a**) or 40 h (**3b**) and quenched by an equal volume of 90% formamide loading buffer, then subjected to 20% denaturing polyacrylamide gel electrophoresis.

Stability study of ICL products formed with 17. The ^{32}P -labeled oligonucleotide duplex **17** (30 μL , 0.5 μM) was mixed with 1 M NaCl (6 μL), 100 mM potassium phosphate (6 μL , pH 8), and 20/3 mM **1a-5a** in CH_3CN (18 μL) or **1b-5b** in H_2O (18 μL). The solution was irradiated with light at 350 nm for 0.75 h (**1a**), 6 h (**4a** and **1b**), 8 h (**2a**), 12 h (**2b** and **5b**), 24 h (**4b** and **5a**), 35 h (**3a**) or 40 h (**3b**). After the cross-linking reaction was done, the DNA ICL products and monoalkylated ODNs were separated by gel electrophoresis. The isolated DNA fragments were dissolved in H_2O (60 μL) and divided into three portions. One portion (20 μL) was incubated with 1.0 M piperidine (10 μL) at 90 $^\circ\text{C}$ for 30 min, and the second portion (20 μL) was incubated

with 0.1 M NaCl and 10 mM potassium phosphate buffer (pH 7, 10 μ L) under the same condition, and the third portion (5 μ L) was used as a control sample. The samples were subjected to electrophoresis on a 20% denaturing polyacrylamide gel.

Synthesis of the adducts formed between 1a and dC, dA, or dG. To a solution of dA, dT, dG, or dC (0.2 mmol, 1.0 eq.) in DMF (1.0 mL), 1,3-bis(bromomethyl)-2,5-dimethoxybenzene (**1a**, 0.4 mmol, 2.0 eq.) was added. The reaction mixture was irradiated with light at 350 nm for 1 day at rt. After removing solvents under reduced pressure, the products were isolated upon purification by column chromatography.

2.4. References

1. Peng X, Greenberg MM. Facile SNP detection using bifunctional, cross-linking oligonucleotide probes. *Nucleic Acids Research*. 2008;36.
2. Sun H, Peng X. Template-Directed Fluorogenic Oligonucleotide Ligation Using “Click” Chemistry: Detection of Single Nucleotide Polymorphism in the Human p53 Tumor Suppressor Gene. *Bioconjugate Chemistry*. 2013;24:1226–34.
3. Ogasawara S, Fujimoto K. SNP Genotyping by Using Photochemical Ligation. *Angewandte Chemie International Edition*. 2006;45:4512–5.
4. Noll DM, Mason TM, Miller PS. Formation and Repair of Interstrand Cross-Links in DNA. *Chemical Reviews*. 2006;106:277–301.
5. Peng X, Ghosh AK, Houten BV, Greenberg MM. Nucleotide Excision Repair of a DNA Interstrand Cross-Link Produces Single- and Double-Strand Breaks. *Biochemistry*. 2010;49:11–9.
6. Peng X, Pigli YZ, Rice PA, Greenberg MM. Protein Binding Has a Large Effect on Radical Mediated DNA Damage. *Journal of the American Chemical Society*. 2008;130:12890–1.
7. Dronkert ML, Kanaar R. Repair of DNA interstrand cross-links. *Mutation Research/DNA Repair*. 2001;486:217–47.

8. Tagawa M, Shohda K-I, Fujimoto K, Sugawara T, Suyama A. Heat-resistant DNA tile arrays constructed by template-directed photoligation through 5-carboxyvinyl-2'-deoxyuridine. *Nucleic Acids Research*. 2007;35.
9. Brulikova L, Hlavac J, Hradil P. DNA Interstrand Cross-Linking Agents and their Chemotherapeutic Potential. *Current Medicinal Chemistry*. 2012;19:364–85.
10. Cao S, Peng X. Exploiting Endogenous Cellular Process to Generate Quinone Methides In Vivo. *Current Organic Chemistry*. 2014;18:70–85.
11. Chen W, Balakrishnan K, Kuang Y, Han Y, Fu M, Gandhi V, et al. Reactive Oxygen Species (ROS) Inducible DNA Cross-Linking Agents and Their Effect on Cancer Cells and Normal Lymphocytes. *Journal of Medicinal Chemistry*. 2014;57:4498–510.
12. Rajski SR, Williams RM. DNA Cross-Linking Agents as Antitumor Drugs. *Chemical Reviews*. 1998;98:2723–96.
13. Zeng Q, Rokita SE. Tandem Quinone Methide Generation for Cross-Linking DNA. *The Journal of Organic Chemistry*. 1996;61:9080–1.
14. Wang H, Wahi MS, Rokita SE. Immobilizing a Transient Electrophile for DNA Cross-Linking. *Angewandte Chemie International Edition*. 2008;47:1291–3.
15. Veldhuyzen WF, Pande P, Rokita SE. A Transient Product of DNA Alkylation Can Be Stabilized by Binding Localization. *Journal of the American Chemical Society*. 2003;125:14005–13.
16. Hong IS, Greenberg MM. DNA Interstrand Cross-Link Formation Initiated by Reaction between Singlet Oxygen and a Modified Nucleotide. *Journal of the American Chemical Society*. 2005;127:10510–1.
17. Peng X, Hong IS, Li H, Seidman MM, Greenberg MM. Interstrand Cross-Link Formation in Duplex and Triplex DNA by Modified Pyrimidines. *Journal of the American Chemical Society*. 2008;130:10299–306.
18. Weng X, Ren L, Weng L, Huang J, Zhu S, Zhou X, et al. Synthesis and Biological Studies of Inducible DNA Cross-Linking Agents. *Angewandte Chemie International Edition*. 2007;46:8020–3.
19. Cao S, Wang Y, Peng X. ROS-Inducible DNA Cross-Linking Agent as a New Anticancer Prodrug Building Block. *Chemistry - A European Journal*. 2012;18:3850–4.

20. Cao S, Wang Y, Peng X. The Leaving Group Strongly Affects H₂O₂-Induced DNA Cross-Linking by Arylboronates. *The Journal of Organic Chemistry*. 2014;79:501–8.
21. Chen W, Han Y, Peng X. Aromatic Nitrogen Mustard-Based Prodrugs: Activity, Selectivity, and the Mechanism of DNA Cross-Linking. *Chemistry - A European Journal*. 2014;20:7410–8.
22. Kuang Y, Balakrishnan K, Gandhi V, Peng X. Hydrogen Peroxide Inducible DNA Cross-Linking Agents: Targeted Anticancer Prodrugs. *Journal of the American Chemical Society*. 2011;133:19278–81.
23. Wang Y, Liu S, Lin Z, Fan Y, Wang Y, Peng X. Photochemical Generation of Benzyl Cations That Selectively Cross-Link Guanine and Cytosine in DNA. *Organic Letters*. 2016;18:2544–7.
24. Wang Y, Lin Z, Fan H, Peng X. Photoinduced DNA Interstrand Cross-Link Formation by Naphthalene Boronates via a Carbocation. *Chemistry - A European Journal*. 2016;22:10382–6.
25. Han Y, Chen W, Kuang Y, Sun H, Wang Z, Peng X. UV-Induced DNA Interstrand Cross-Linking and Direct Strand Breaks from a New Type of Binitroimidazole Analogue. *Chemical Research in Toxicology*. 2015;28:919–26.
26. Kashida H, Doi T, Sakakibara T, Hayashi T, Asanuma H. p-Stilbazole Moieties As Artificial Base Pairs for Photo-Cross-Linking of DNA Duplex. *Journal of the American Chemical Society*. 2013;135:7960–6.
27. Haque MM, Sun H, Liu S, Wang Y, Peng X. Photoswitchable Formation of a DNA Interstrand Cross-Link by a Coumarin-Modified Nucleotide. *Angewandte Chemie International Edition*. 2014;53:7001–5.
28. Sun H, Fan H, Eom H, Peng X. Coumarin-Induced DNA Ligation, Rearrangement to DNA Interstrand Crosslinks, and Photorelease of Coumarin Moiety. *ChemBioChem*. 2016;17:2046–53.
29. Sun H, Fan H, Peng X. Quantitative DNA Interstrand Cross-Link Formation by Coumarin and Thymine: Structure Determination, Sequence Effect, and Fluorescence Detection. *The Journal of Organic Chemistry*. 2014;79:11359–69.
30. Takasugi M, Guendouz A, Chassignol M, Decout JL, Lhomme J, Thuong NT, et al. Sequence-specific photo-induced cross-linking of the two strands of double-helical DNA by a psoralen covalently linked to a triple helix-forming oligonucleotide. *Proceedings of the National Academy of Sciences*. 1991;88:5602–6.

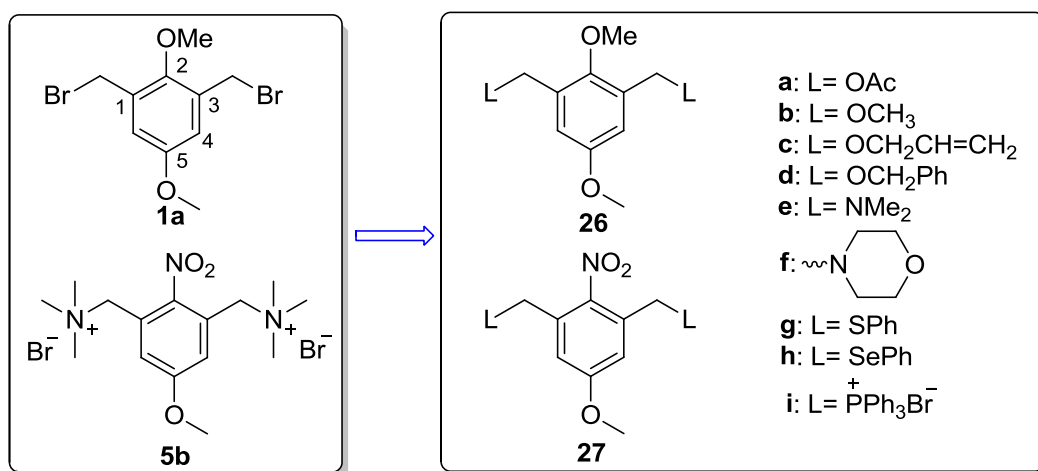
31. Thazhathveetil AK, Liu S-T, Indig FE, Seidman MM. Psoralen Conjugates for Visualization of Genomic Interstrand Cross-Links Localized by Laser Photoactivation. *Bioconjugate Chemistry*. 2007;18:431–7.
32. Fujimoto K, Yamada A, Yoshimura Y, Tsukaguchi T, Sakamoto T. Details of the Ultrafast DNA Photo-Cross-Linking Reaction of 3-Cyanovinylcarbazole Nucleoside: Cis–Trans Isomeric Effect and the Application for SNP-Based Genotyping. *Journal of the American Chemical Society*. 2013;135:16161–7.
33. Sakamoto T, Tanaka Y, Fujimoto K. DNA Photo-Cross-Linking Using 3-Cyanovinylcarbazole Modified Oligonucleotide with Threoninol Linker. *Organic Letters*. 2015;17:936–9.
34. Wang P, Liu R, Wu X, Ma H, Cao X, Zhou P, et al. A Potent, Water-Soluble and Photoinducible DNA Cross-Linking Agent. *Journal of the American Chemical Society*. 2003;125:1116–7.
35. Verga D, Nadai M, Doria F, Percivalle C, Antonio MD, Palumbo M, et al. Photogeneration and Reactivity of Naphthoquinone Methides as Purine Selective DNA Alkylating Agents. *Journal of the American Chemical Society*. 2010;132:14625–37.
36. Richter SN, Maggi S, Mels SC, Palumbo M, Freccero M. Binol Quinone Methides as Bisalkylating and DNA Cross-Linking Agents. *Journal of the American Chemical Society*. 2004;126:13973–9.
37. Colloredo-Mels, S., Doria, F., Verga, D., Freccero, M Photogenerated Quinone Methides as Useful Intermediates in the Synthesis of Chiral BINOL Ligands. *J Org Chem*. **2006**, *71*, 3889-3895.
37. Colloredo-Mels S, Doria F, Verga D, Freccero M. Photogenerated Quinone Methides as Useful Intermediates in the Synthesis of Chiral BINOL Ligands. *The Journal of Organic Chemistry*. 2006;71:3889–95.
38. Fakhari F, Rokita SE. A walk along DNA using bipedal migration of a dynamic and covalent crosslinker. *Nature Communications*. 2014;5.
39. Mccrane MP, Hutchinson MA, Ad O, Rokita SE. Oxidative Quenching of Quinone Methide Adducts Reveals Transient Products of Reversible Alkylation in Duplex DNA. *Chemical Research in Toxicology*. 2014;27:1282–93.
40. Mccrane MP, Weinert EE, Lin Y, Mazzola EP, Lam Y-F, Scholl PF, et al. Trapping a Labile Adduct Formed between anortho-Quinone Methide and 2'-Deoxycytidine. *Organic Letters*. 2011;13:1186–9.

41. Weinert EE, Dondi R, Colloredo-Melz S, Frankenfield KN, Mitchell CH, Freccero M, et al. Substituents on Quinone Methides Strongly Modulate Formation and Stability of Their Nucleophilic Adducts. *Journal of the American Chemical Society*. 2006;128:11940–7.
42. Lin G, Li L. Oxidation and Reduction of the 5-(2'-Deoxyuridinyl)methyl Radical. *Angewandte Chemie International Edition*. 2013;52:5594–8.
43. Weng L, Horvat SM, Schiesser CH, Greenberg MM. Deconvoluting the Reactivity of Two Intermediates Formed from Modified Pyrimidines. *Organic Letters*. 2013;15:3618–21.
44. Wang Y, Fan H, Balakrishnan K, Lin Z, Cao S, Chen W, et al. Hydrogen peroxide activated quinone methide precursors with enhanced DNA cross-linking capability and cytotoxicity towards cancer cells. *European Journal of Medicinal Chemistry*. 2017;133:197–207.
45. Gruter G-JM, Akkerman OS, Bickelhaupt F. Nuclear versus Side-Chain Bromination of Methyl-Substituted Anisoles by N-Bromosuccinimide. *The Journal of Organic Chemistry*. 1994;59:4473–81.
46. González-Bulnes L, Ibáñez I, Bedoya LM, Beltrán M, Catalán S, Alcamí J, et al. Structure-Based Design of an RNA-Bindingp-Terphenylene Scaffold that Inhibits HIV-1 Rev Protein Function. *Angewandte Chemie International Edition*. 2013;52:13405–9.
47. Casal-Dujat L, Rodrigues M, Yagüe A, Calpena AC, Amabilino DB, González-Linares J, et al. Gemini Imidazolium Amphiphiles for the Synthesis, Stabilization, and Drug Delivery from Gold Nanoparticles. *Langmuir*. 2012;28:2368–81.
48. Ozaki T, Nakagawara A. Role of p53 in Cell Death and Human Cancers. *Cancers*. 2011;3:994–1013.
49. Rivlin N, Brosh R, Oren M, Rotter V. Mutations in the p53 Tumor Suppressor Gene: Important Milestones at the Various Steps of Tumorigenesis. *Genes & Cancer*. 2011;2:466–74.
50. Witiak DT, Loper JT, Ananthan S, Almerico AM, Verhoef VL, Filppi JA. Mono and bis(bioreductive) alkylating agents: synthesis and antitumor activities in a B16 melanoma model. *Journal of Medicinal Chemistry*. 1989;32:1636–42.
51. Nishimoto S, Ide H, Wada T, Kagiya T. Radiation-induced Hydroxylation of Thymine Promoted by Electron-affinic Compounds. *International Journal of Radiation Biology and Related Studies in Physics, Chemistry and Medicine*. 1983;44:585–600.
52. Huang J, Su L, Kowalski JA, Barton JL, Ferrandon M, Burrell AK, et al. A subtractive approach to molecular engineering of dimethoxybenzene-based redox materials for non-aqueous flow batteries. *Journal of Materials Chemistry A*. 2015;3:14971–6.

Chapter 3. Substituents and Benzylic Leaving Groups Have a Large Effect on Photo-Induced DNA Cross-Linking

3.1. Introduction

Previous results suggested that the aromatic substituents and benzylic leaving groups affected not only the efficiency of DNA ICL formation but also the mechanism pathway for DNA cross-linking. Among all designed compounds, **1a** and **5b** (Scheme 3-1) showed the highest DNA cross-linking efficiency.¹ However, bromide **1a** is not relatively stable and led to DNA cleavages upon 350 nm irradiation for a long period while the positively charged ammonium salt **5b** has a slow reaction rate and shows poor cell membrane permeability, which hinders further investigation for biological applications. New compounds with improved properties are needed to expand the biological applications of photo-induced DNA cross-linking agents. In this chapter, **1a** and **5b** are used as lead compounds for further modification in order to develop compounds with highly efficient and fast DNA cross-linking therefore having potential biological application. To achieve this goal, we will modify **1a** and **5b** by varying the leaving groups.



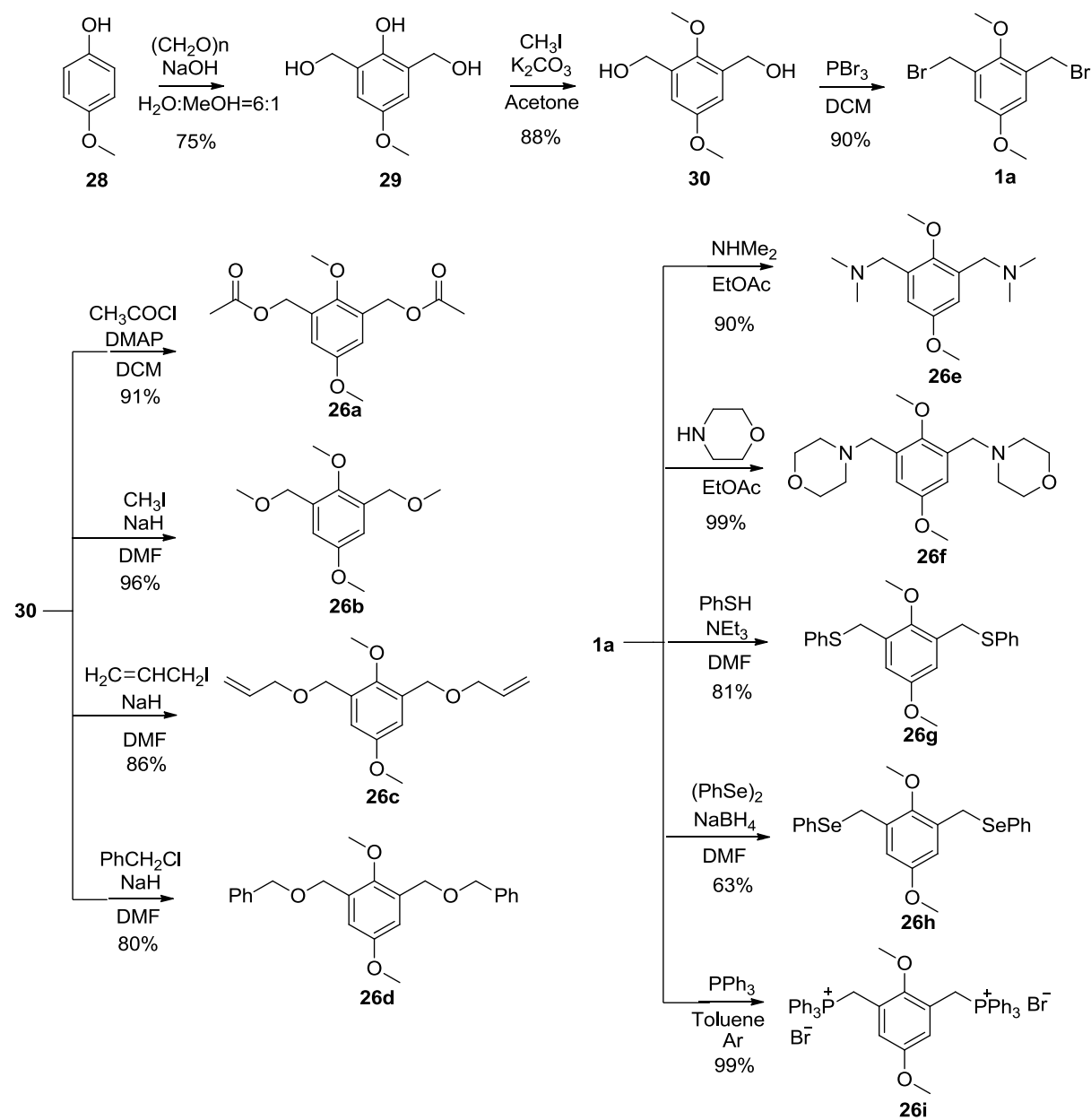
Scheme 3-1. The structures of **26a-i**, and **27a-i**.

Rokita and coworkers found that the benzylic leaving groups have a huge effect on QM formation for the fluoride-cleavable precursors.^{2,3} Peng and coworkers also reported that the leaving group greatly affected DNA cross-linking efficiency, where bromides showed higher photo-reactivity and DNA cross-linking efficiency than the corresponding ammonium salts.⁴ A series of leaving groups have been introduced to different QM precursors, such as -Br, -OAc, -NMe₂, -NMe₃Br, -OH, -COOH, morpholine or amino acids. Among them, -OAc, -NMe₂ and -morpholine groups are reported to be good leaving groups for QM formation.⁵⁻⁸ However, it is not clear how these leaving groups affect photo-induced carbocation formation and subsequent DNA ICL formation. Phenyl sulfide and phenyl selenide were also reported to be good leaving groups which can be activated either by UV or by NaIO₄.^{9,10} Fast-photo-cleaving ether groups were reported that can be cleaved within seconds upon UV irradiation.¹¹ Inspired by the previous work, we used **1a** and **5b** as the parent compounds, designed and synthesized the analogues with a series of different leaving groups, including OAc, NMe₂, morpholine, OCH₃, OCHCH=CH₂, OCH₂Ph, SPh, and SePh. Triphenylphosphonium bromide group was also introduced with the expectation of increasing the UV absorption and improving water solubility (Scheme 3-1). We investigated the effect of the benzylic leaving groups and substituents on the photo-induced DNA cross-linking activity, and determined the mechanism pathways and DNA cross-linking sites.

3.2. Synthesis of compounds with various leaving groups

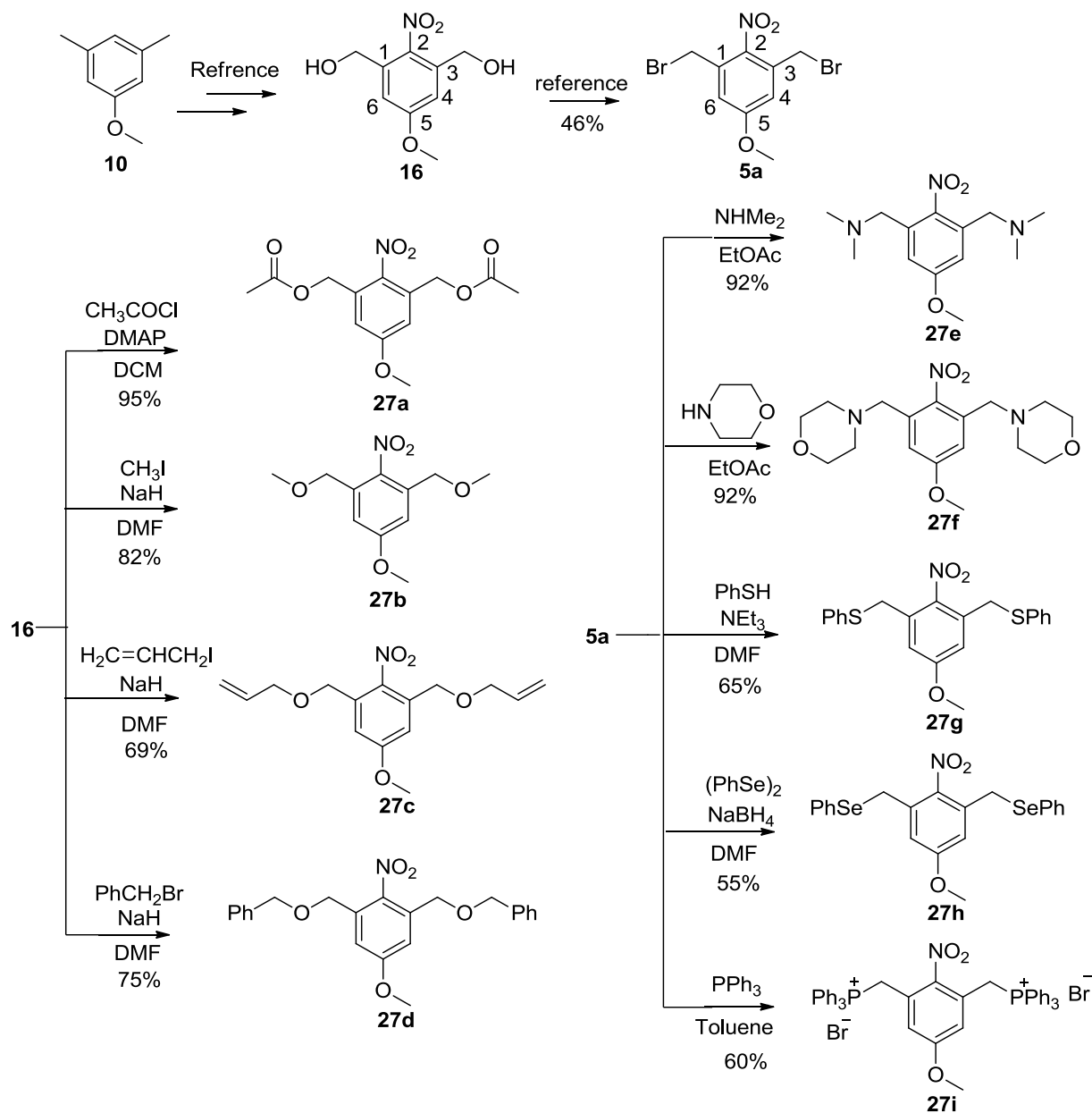
Compounds **26a-i** were synthesized starting from 4-methoxyphenol (**28**) (Scheme 3-2). The reaction of **28** with formaldehyde in the presence of NaOH resulted in 4-methoxy-2,6-bis(hydroxymethyl)phenol (**29**). Methylation of **29** with methyl iodide provided (2,5-dimethoxy-1,3-phenylene)dimethanol (**30**) that was further converted to **1a** via bromination with PBr₃.

Compounds **30** and **1a** were used as starting materials for the synthesis of **26a-d** and **26e-i** through basic nucleophilic substitution reactions.



Scheme 3-2. Synthesis of **26a-i**.

1-Methoxy-3,5-dimethylbenzene (**10**) was used as the starting material to synthesize **27a-i** (Scheme 3-3). Compound **10** was first converted to 2-nitro bifunctional benzyl alcohol **16** via nitrotration, oxidation and reduction.¹ Bromination of **16** was performed with PBr₃ affording **5a**. Compounds **16** and **5a** were then transformed to **27a-d** and **27e-i** via nucleophilic substitution reactions.



Scheme 3-3. Synthesis of **27a-i**.

3.3. DNA interstrand cross-linking assay.

Similar to our previous study, a 49-mer DNA duplex (**17**) was used for the photo reactivity study of compound **26a-i** and **27a-i** in a phosphate buffer (pH 8.0)¹² upon 350 nm irradiation.

Denaturing polyacrylamide gel electrophoresis (PAGE) was used for DNA ICL analysis. The initial study suggested that the UV irradiation is essential for the DNA ICL formation. For all tested compounds, no ICL formation was observed in the absence of UV irradiation, while efficient DNA ICL formation were observed upon UV irradiation. Previous study suggested that both the irradiation time and the concentration of the substrates affect the photo-induced ICL efficiency.¹² So, we optimized the reaction time and concentration for **26a-i** and **27a-i** (Table 3-1 and Appendix A) For all tested compounds, the DNA ICL yield increased gradually with increased reaction time. Then the ICL reaction reached an equilibrium at some point. After that, further increase of the reaction time didn't lead to higher ICL yield. This time was defined as optimal reaction time for the tested compound. The optimal reaction time for all compounds is shown in Table 3-1. Compounds with a strong electron donating group (OMe) as a substituent showed a faster photo-induced DNA cross-linking reaction rate than those with with a NO₂ group as an aromatic substituent. This result indicated that electron donating substituent promoted the cross-linking reaction rate while electron withdrawing substituent suppressed this process. It was also observed that the leaving groups did affect the reaction rate of the DNA ICL formation when comparing those compounds with the same aromatic substituent. For example, among the nitro compounds, **27e** and **27g** showed the fastest reaction rate, followed by **27i**, **27f**, and **27h**, while a very slow reaction rate was observed for **27a-d** with **27a** as the slowest. For compounds with OMe as a substituent, compounds **26g** and **26h** have the fastest reaction rate,

followed by **26i**, **26e** and **26b**, then **26d** and **26f**, while the ICL reaction rate for **26a** and **26c** was much slower.

1 5 6 14 15 18 22 24 25 27 31 40 44 49
 5'-dGCCTAGTTCTTTTAATTACTTTGCAATGCAAGTAATTAAAGCTTGATCTG (**17a**)
 3'-dCGGATCAAGAAAATTAATGAACGTTACGTTTCATTAATTTTCGAACTAGAC (**17b**)

17

Table 3-1. The optimized conditions, ICL yields, and UV absorption data for **26a-i** and **27a-i**.^a

Compound R = OMe (26a-i)	Reaction Time (h)	Con. ^b (mM)	ICL (%) ^c	λ_{\max} (nm)	$\epsilon_{\lambda_{\max}}$ (M ⁻¹ ·cm ⁻¹)
26a (L= OAc)	22	0.5	27 ± 3	286	2600
26b (L= OCH ₃)	6	0.6	34 ± 3	286	2640
26c (L= OCH ₂ CH=CH ₂)	36	2.0	28 ± 2	286	2900
26d (L= OCH ₂ Ph)	12	0.5	37 ± 1	287	3350
26e (L= NMe ₂)	6	0.4	25 ± 3	287	3120
26f (L= N(CH ₂ CH ₂) ₂ O)	12	0.4	18 ± 2	286	2940
26g (L= SPh)	2	0.6	28 ± 3	291	6900
26h (L= SePh)	2	0.6	24 ± 1	299	7050
26i (L= PPh ₃ ⁺ Br ⁻)	5	0.2	34 ± 3	268, 302	7060, 5090
R = NO₂ (27a-i)					
27a (L= OAc)	44	0.4	18 ± 1	282, 347	4340, 2100
27b (L= OCH ₃)	40	0.4	17 ± 2	282, 347,	3190, 1630
27c (L= OCH ₂ CH=CH ₂)	40	0.4	14 ± 1	282, 347	3200, 1600
27d (L= OCH ₂ Ph)	40	0.8	17 ± 2	282, 348	2920, 1400
27e (L= NMe ₂)	24	1	17 ± 2	273, 346	2760, 1040
27f (L= N(CH ₂ CH ₂) ₂ O)	32	0.6	15 ± 1	273, 346	2640, 990
27g (L= SPh)	24	0.6	23 ± 3	345	1750
27h (L= SePh)	36	0.3	21 ± 2	345	2190
27i (L= PPh ₃ ⁺ Br ⁻)	28	0.4	21 ± 1	347	2030

^a The DNA cross-linking reaction was performed in a pH 8 phosphate buffer with 50 nM DNA duplex **17** upon 350 nm irradiation.

^b The minimum compound concentration needed to obtain the highest DNA cross-linking efficiency.

^c The maximum DNA ICL yield obtained for each compound under optimized conditions (all data are the average of three experiments).

After optimizing reaction time for all compounds, the concentration dependent DNA cross-link study was performed with **26a-i** and **27a-i** in order to figure out the optimized concentration (the minimum compound concentration needed to gain the highest DNA cross-linking yield). The cross-linking reaction was performed with the optimized reaction time. For all compounds tested, the DNA ICL yield increased gradually with increasing the compounds concentration, then the ICL reaction reached an equilibrium at a certain concentration (defined as optimal concentration in which the DNA alkylation reaction was complete and the best ICL efficiency was achieved). After that, further increasing compounds' concentration didn't further increase the ICL yield. The optimized concentration was 0.2 mM for **26i**, 0.3 mM for **27h**, 0.4 mM for **26e**, **26f**, **27a-c** and **27i**, 0.5 mM for **26a** and **26d**, 0.6 mM for **26b**, **26g**, **26h**, **27f** and **27g**, 0.8 mM for **27d**, 1.0 mM for **27e**, and 2.0 mM for **26c** (Table 3-1 and Appendix A). In general, compounds with a strong electron donating (OMe) substituent have higher DNA ICL efficiency than those with a strong electron withdrawing (NO₂) substituent. It is likely that the electron donating group (OMe) stabilizes the electron-deficient carbocation intermediate therefore facilitating its formation, while electron withdrawing group (NO₂) decreases its stability thus inhibiting its formation.

For compounds with the same substituent, the leaving group did affect the ICL efficiency.

Among NO₂ substituted compounds (**27a-i**), **27g-i** showed higher cross-linking efficiency, while **27c** and **27f** gave the lowest ICL efficiency and **27a**, **27b**, **27d**, and **27e** had medium cross-linking yield. Similarly, the ICL efficiency of compounds with OMe as a substituent (**26a-i**) also depends on the leaving groups. Compound **26d** with a benzyloxy as a leaving group showed the highest ICL yield, followed by **26b** and **26i**. Compound **26f** with a morpholine as a leaving group had the lowest ICL efficiency, while the rest showed medium ICL efficiency. There is no

general rule about which leaving group is the best as the cross-linking efficiency depends on the combined effect of the aromatic substituent and the leaving groups.

Since different compounds need different optimal concentrations to obtain the highest DNA cross-linking efficiency, it is hard to conclude how the substituent and leaving group affect the ICL efficiency. For better comparison, the DNA cross-linking efficiency was determined at the same concentration (500 μ M) under the optimized reaction time for each compound (Figure 3-1). For both classes of compounds, the trend of ICL yields at 500 μ M was slightly different with that at optimized conditions. The cross-linking efficiency for **27a-i** is in the following order **27g** \approx **27h** \approx **27i** > **27a** \approx **27b** \approx **27d** \approx **27e** > **27f** \approx **27c** while the ICL yields for the bromide **26a-i** is in a different order **26d** > **26b** \approx **26i** > **26a** \approx **26e** \approx **26g** > **26h** > **26f** > **26c**. From these results, we conclude that the electron donating substituent increased the ICL efficiency while the electron withdrawing substituent decreased the ICL efficiency. Although the leaving groups also affect the DNA cross-linking, its overall effect depends on the aromatic substituent. For both cases, compounds with triphenylphosphonium as a leaving group showed higher ICL efficiency in comparison with compounds with same substituent but different leaving groups. As the substituents and leaving groups not only affect the electronic property but also the UV absorption of the compounds, next we investigate the correlation between the photo reactivity of these compounds and their UV absorption.

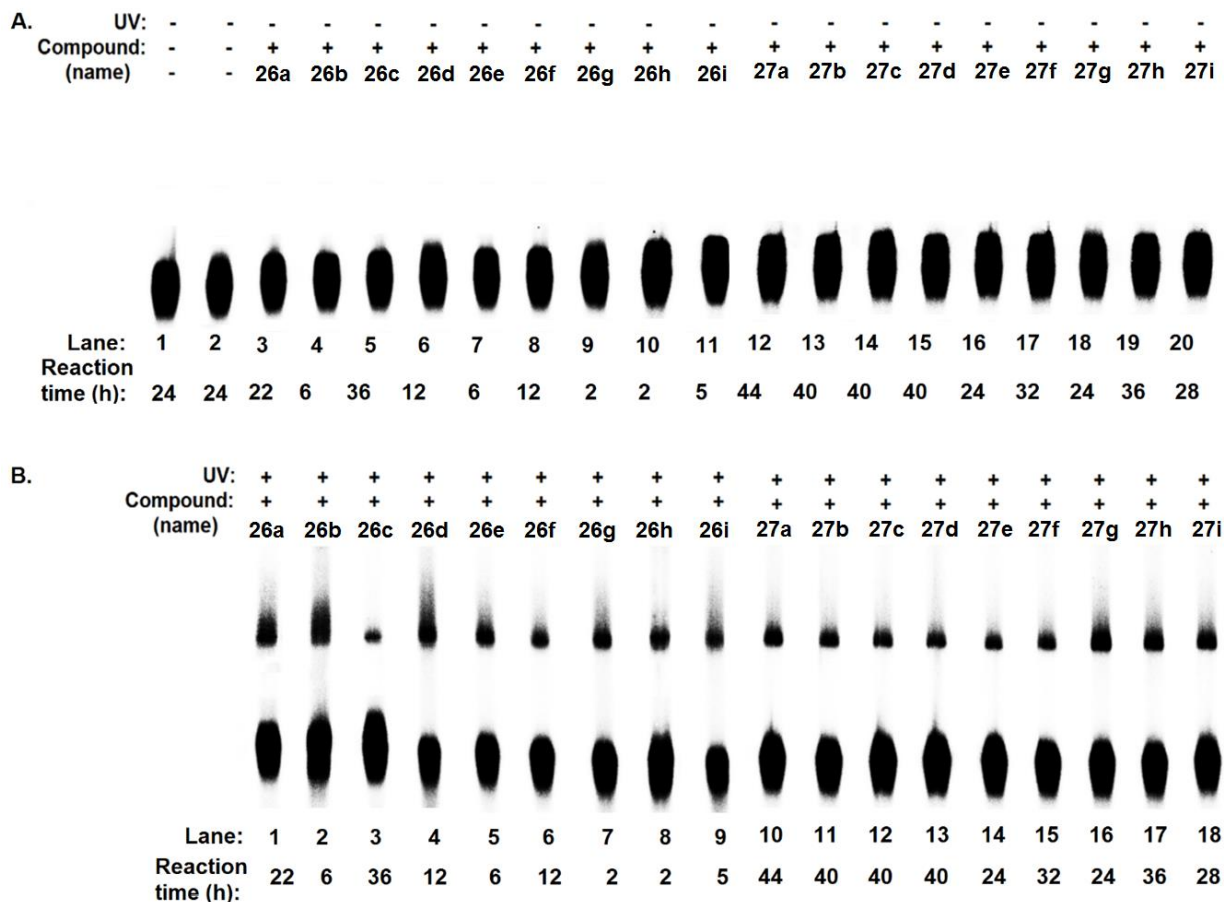


Figure 3-1. Photo-induced DNA ICL formation for **26a-i** and **27a-i**. **A.** Lane 1: DNA without UV irradiation; lane 2: DNA with 24 h UV irradiation at 350 nm; lanes 3-20: DNA with the drug (500 μ M) but no UV irradiation at 350 nm for designed time; **B.** lanes 1-18: DNA with the drug (500 μ M) upon 350 nm irradiation for designed time: lane 1: **26a** (ICL yield, $27 \pm 2\%$); lane 2: **26b** (ICL yield, $32 \pm 4\%$); lane 3: **26c** (ICL yield, $10 \pm 1\%$); lane 4: **26d** (ICL yield, $37 \pm 3\%$); lane 5: **26e** (ICL yield, $26 \pm 2\%$); lane 6: **26f** (ICL yield, $18 \pm 1\%$); lane 7: **26g** (ICL yield, $26 \pm 2\%$); lane 8: **26h** (ICL yield, $21 \pm 2\%$); lane 9: **26i** (ICL yield, $34 \pm 3\%$); lane 10: **27a** (ICL yield, $18 \pm 2\%$); lane 11: **27b** (ICL yield, $17 \pm 2\%$); lane 12: **27c** (ICL yield, $15 \pm 1\%$); lane 13: **27d** (ICL yield, $14 \pm 2\%$); lane 14: **27e** (ICL yield, $12 \pm 1\%$); lane 15: **27f** (ICL yield, $14 \pm 2\%$); lane 16: **27g** (ICL yield, $23 \pm 3\%$); lane 17: **27h** (ICL yield, $22 \pm 2\%$); lane 18: **27i** (ICL yield, $21 \pm$

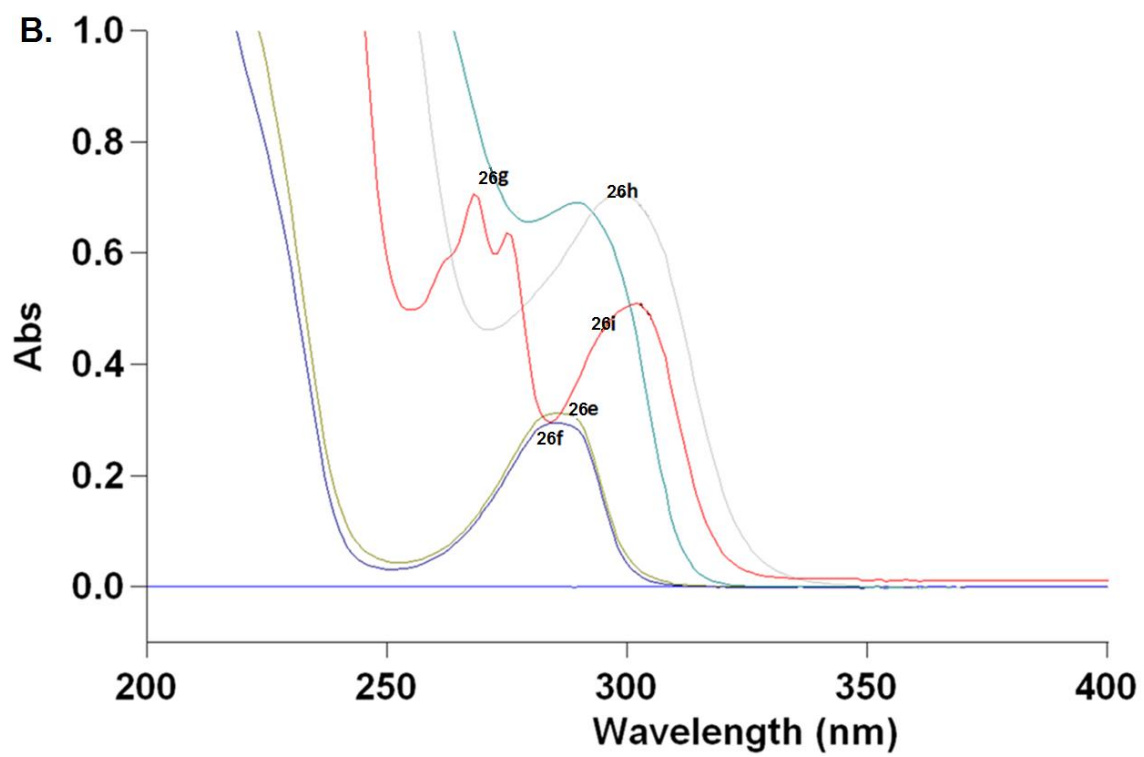
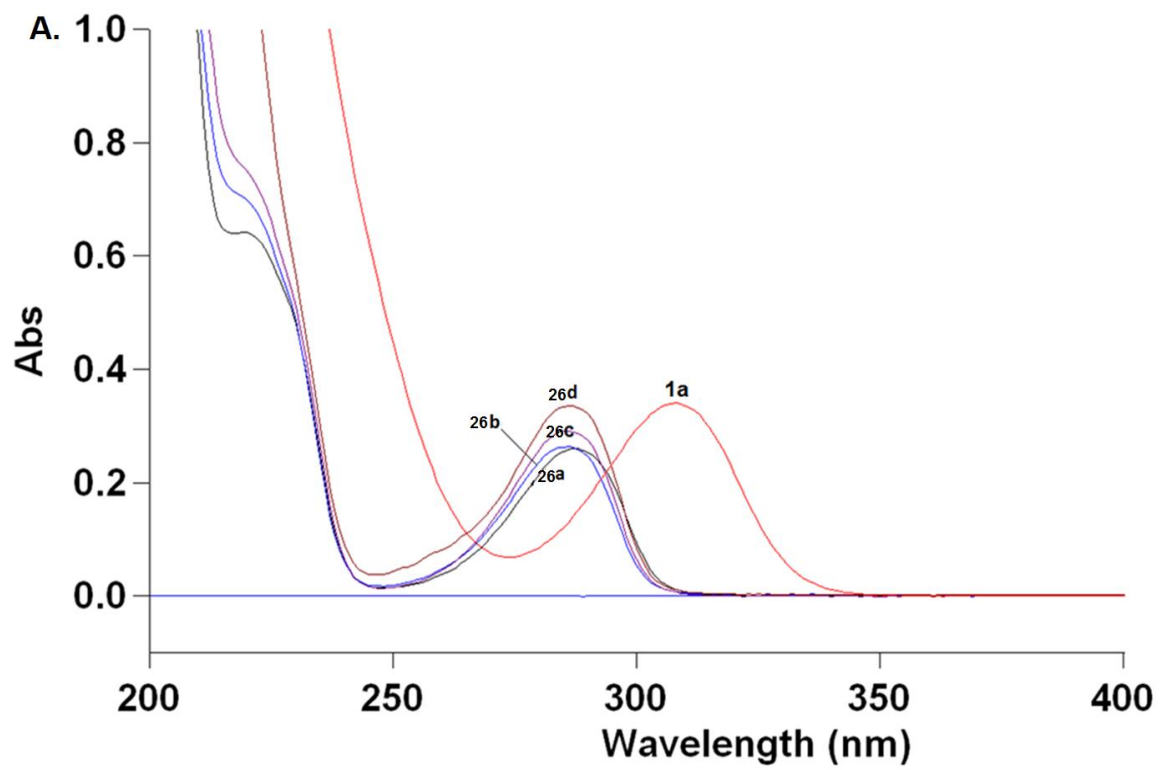
3%); All DNA ICL yields were obtained by triplicate experiments and shown as average \pm standard deviation.

Correlation between UV absorbance and the photo-reactivity.

Our previous study showed that the aromatic substituents and benzylic leaving groups strongly affect the UV absorbance of the compounds, which in turn affect the photo-reactivity of the compounds.¹ So, we tested the UV-Vis spectra of these compounds in acetonitrile at a concentration of 500 μ M (Table 3-1 and Figure 3-2) to check whether there is clear correlation between the UV absorbance and the photo-reactivity of the compounds. In general, the compounds with OMe group showed different UV absorption spectra from those with NO₂ group. Two obvious UV absorption peaks were observed for most compounds containing a NO₂ substituent (**27a-i**) with a major peak at 270-280 nm and a minor one at 340-350 nm. However, only one major UV absorption band was found for most compounds with the OMe group except for **26i** that showed two bands at 268 nm and 302 nm, respectively. The wavelength of maximum UV absorbance (λ_{max}) of the OMe compounds (**26**) is slightly shifted to longer wavelength region than the major band of the nitro compounds (**27**) with the exception of **26g-i**. In addition, the UV absorbance of the OMe compounds is stronger than that of the corresponding NO₂ ones with the exception of **26a-c**. This may explain why the OMe compounds have higher photo-reactivity than the corresponding NO₂ ones.

For each class of compounds, the maximum UV absorption is similar for compounds with the same atom bonded at the benzylic position. For example, compounds **27a-d** with an oxygen at the benzylic position have similar wavelength of maximum UV absorbance, while the maximum UV absorbance of **27e** and **27f** with a benzyl amine group occurs at similar wavelength (273

nm). Similar trend was observed for compounds with OMe as a substituent. For both classes of compounds (**27a-i** or **26a-i**), the leaving groups, such as phenylsulfide, phenylselenide or triphenylphosphonium lead to a red shift of maximum UV absorption (λ_{max}) and stronger UV absorbance (Table 3-1 and Figure 3-2) in comparison with the ester, ether or amine as leaving groups, which in turn led to higher ICL efficiency (**27g-i**) or better photoreactivity (**26g-i**). However, the correlation between the UV absorbance and photo-reactivity is observed for some compounds while no obvious correlation for others. For example, clear correlation was found for **27a-d** and **27e-f**, compounds **27a-d** have similar UV absorption, as a result, they showed similar photoreactivity towards DNA. The wavelength of maximum UV absorbance (λ_{max}) for **27e** and **27f** is similar, while **27e** has slightly stronger UV absorbance leading to higher ICL efficiency. Similar phenomenon was observed for **26e** and **26f**. Compound **26e** showed stronger UV absorption at 287 nm than **26f**. As a result, **26e** showed a faster reaction rate for DNA cross-linking and higher ICL yields than **26f**. However, no clear correlation was found for compound **26a-d**. The UV absorption for **26a-d** are in the order of **26d**>**26c**>**26b**>**26a**, while the photoreactivity of these compounds are in a different order **26b**>**26d**>**26a**>**26c**. There is no general conclusion for the correlation between UV absorption and photoreactivity.



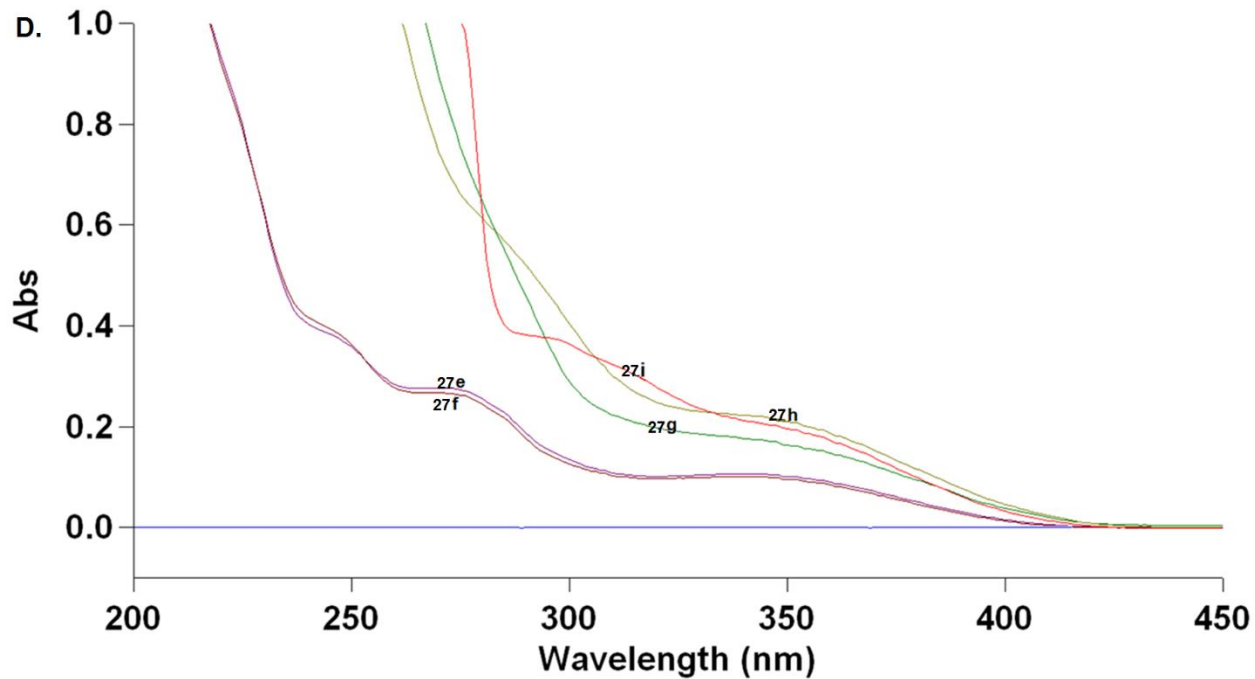
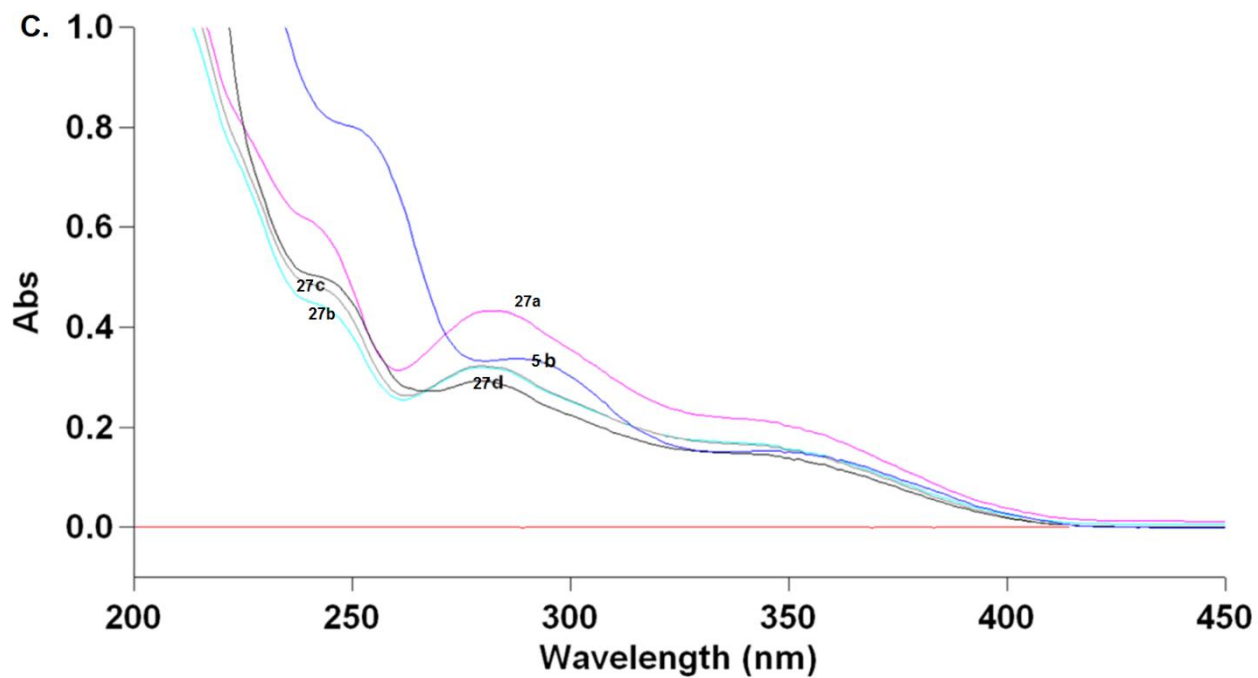
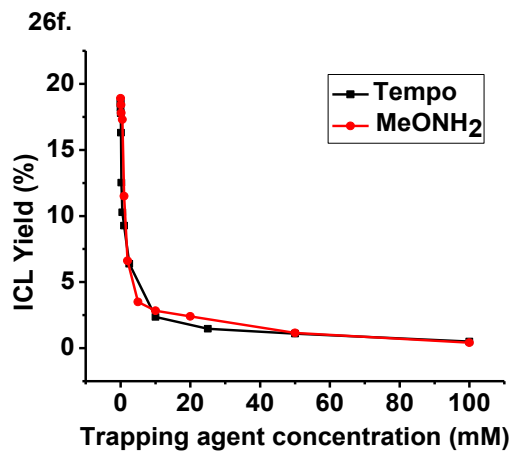
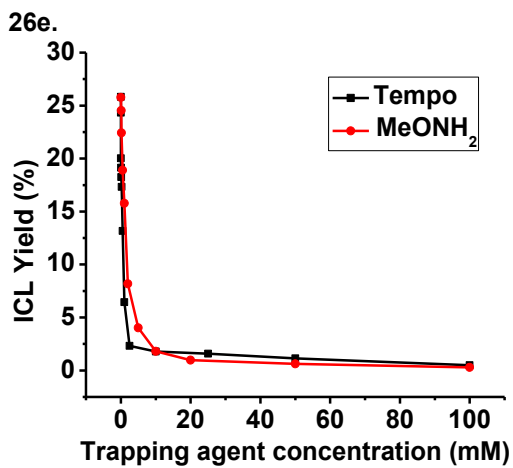
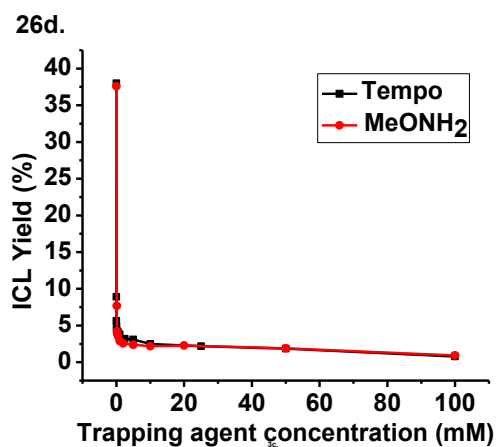
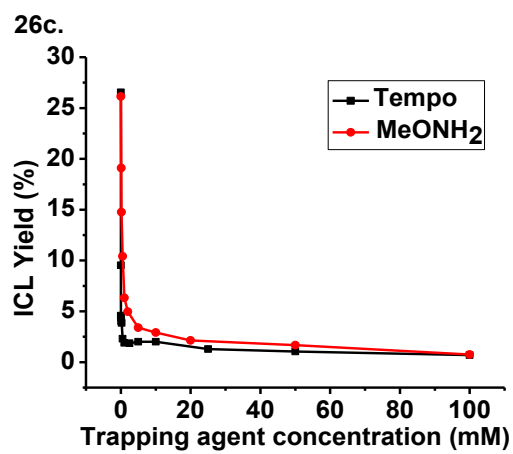
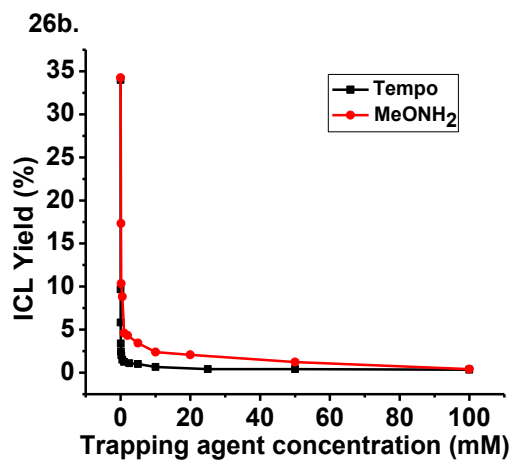
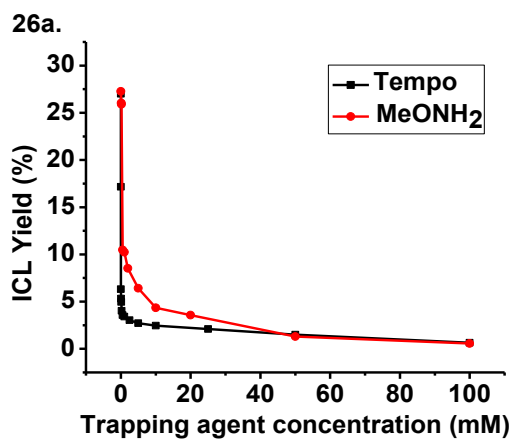
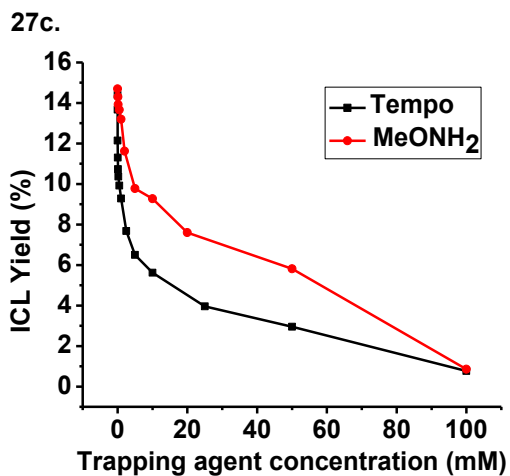
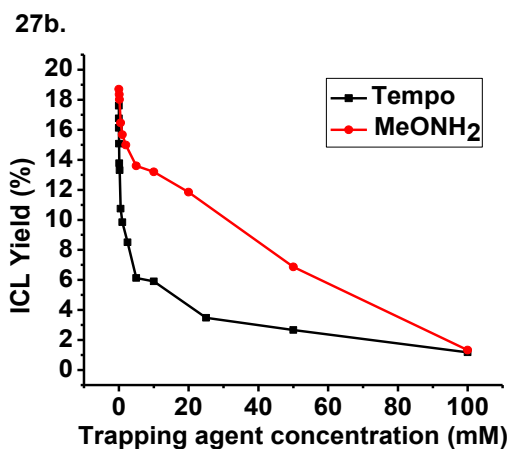
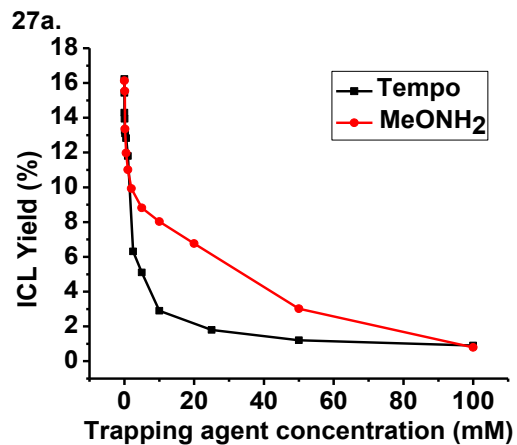
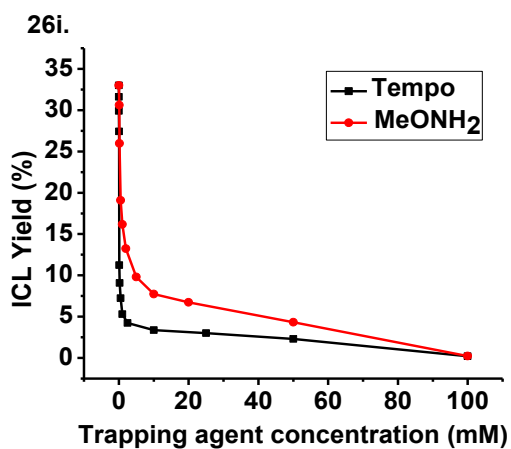
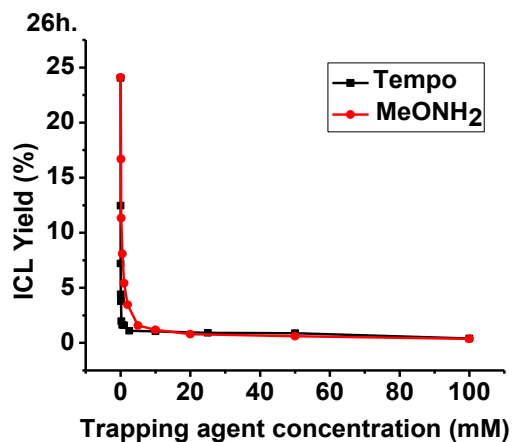
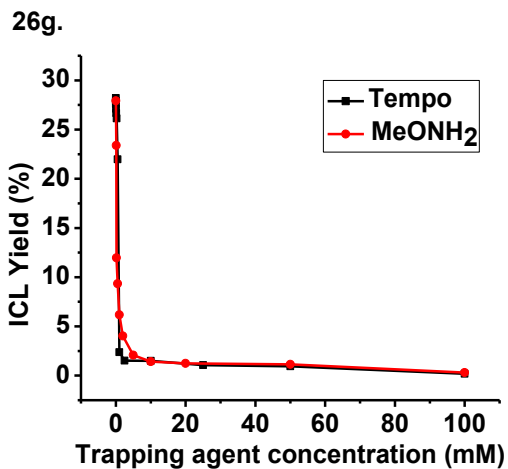


Figure 3-2. UV absorption spectra for 26a-i and 27a-i (500 μ M).

3.4. Mechanism of DNA ICL formation.

Previously, we observed that the photo-induced DNA cross-link formation by compounds containing bromo as leaving group involved generation of free radicals followed by oxidation to carbocations that directly alkylate DNA while the pathway of for compounds with trimethyl ammonium salts as leaving group highly depends on the substitutions.^{1,12} Compounds with an electron donating substituent undergo the radical-cation mechanism (defined as first generate radicals, then radicals converted to cations via free radical oxidation that directly cross-link DNA), while those with a strong electron withdrawing substituent directly generate cations via heterolysis of C-N bond.¹ In order to figure out the generality of such a phenomenon and determine whether benzylic leaving groups affect the pathway for DNA ICL formation, we carried out free radical and carbocation trapping reactions using 2,2,6,6-tetramethylpiperidin-1-oxyl (TEMPO) and methoxyamine as radical and carbocation trapping agents, respectively (Figure 3-3). In all cases, increasing the concentration of methoxyamine led to decreased ICL yields. No DNA ICL formation was observed for all tested compounds when the concentration of methoxyamine reached 100 mM. These data indicated that the carbocations were involved in DNA cross-linking process. To determine whether the cations were generated from heterolysis of C-X bonds or through free radical oxidation, we performed TEMPO trapping experiments. The addition of TEMPO suppressed the DNA ICL formation, and the ICL yield gradually decreased to background level for all tested compounds (**26a-i** and **27a-i**) (Figure 3-3 and Appendix A), suggesting that free radicals (**31**) were involved in the DNA ICL formation process. Overall, these data suggested that both cation and radicals were involved in DNA cross-linking process (Scheme 3-4).





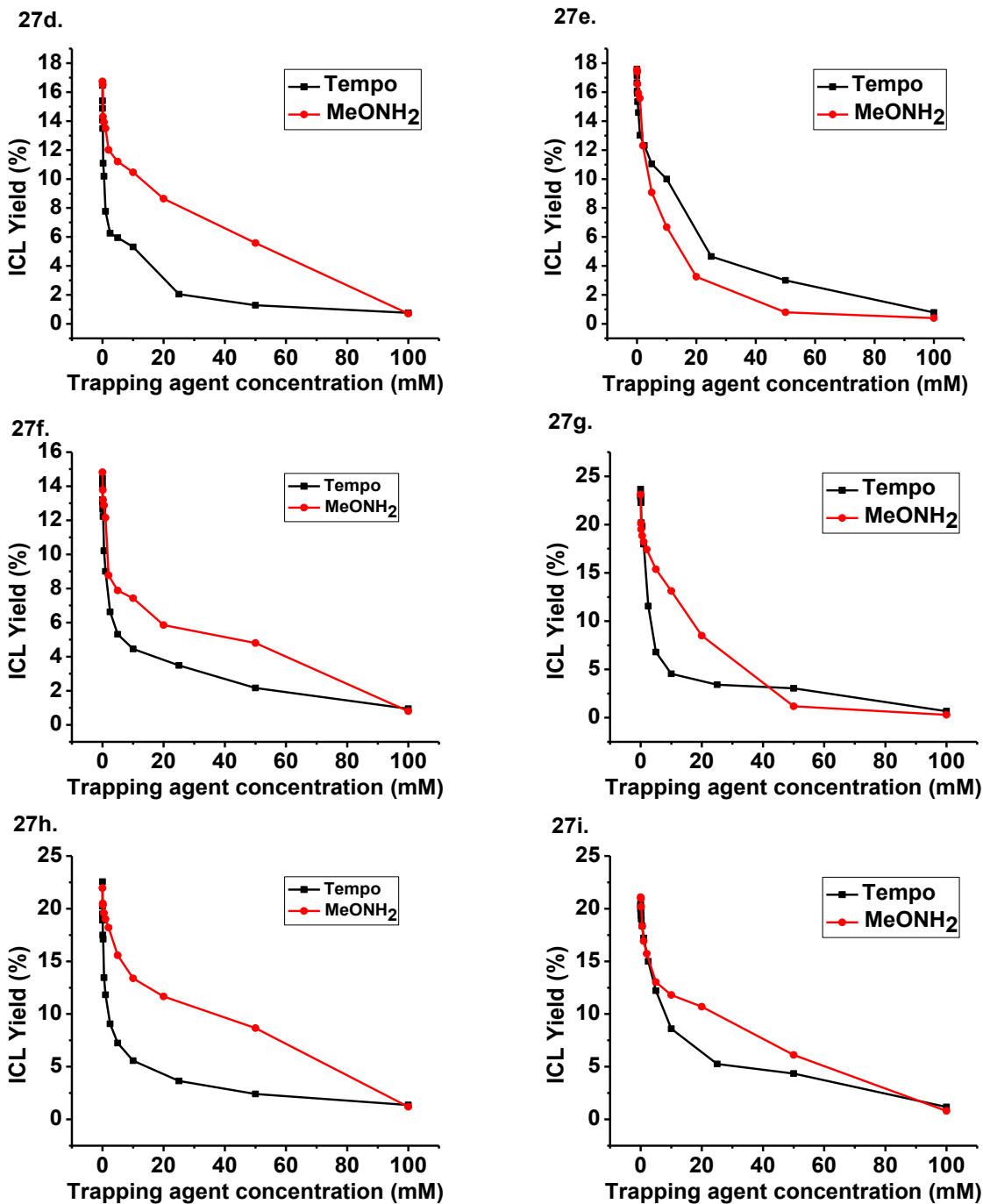
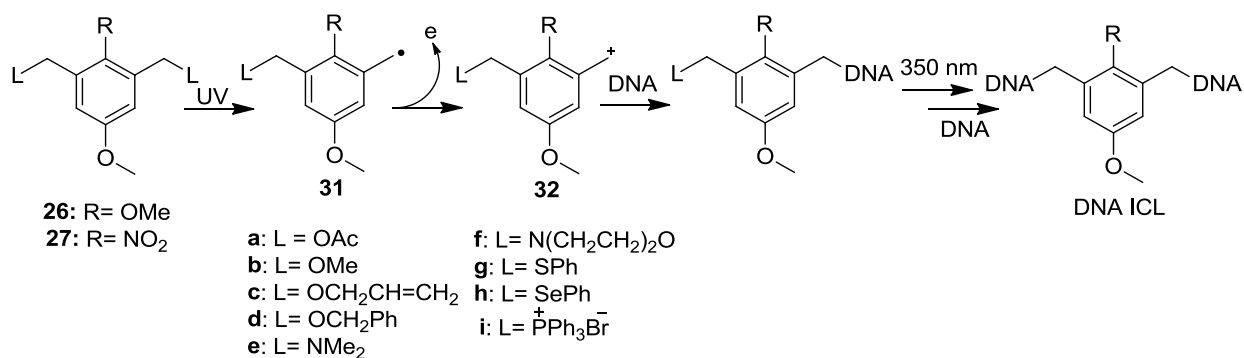
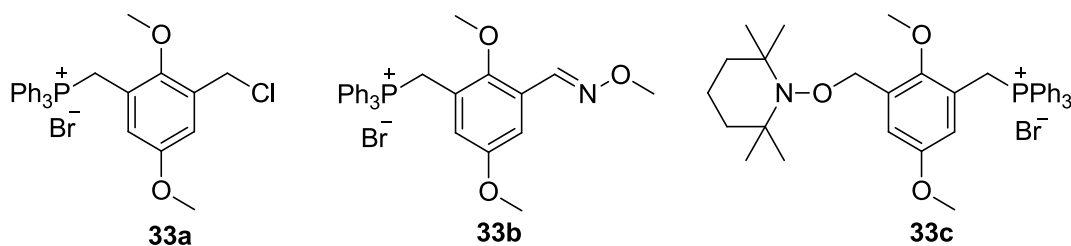


Figure 3-3. Carbocation and radical trapping during DNA ICL formation for **26a-i** and **27a-i**.

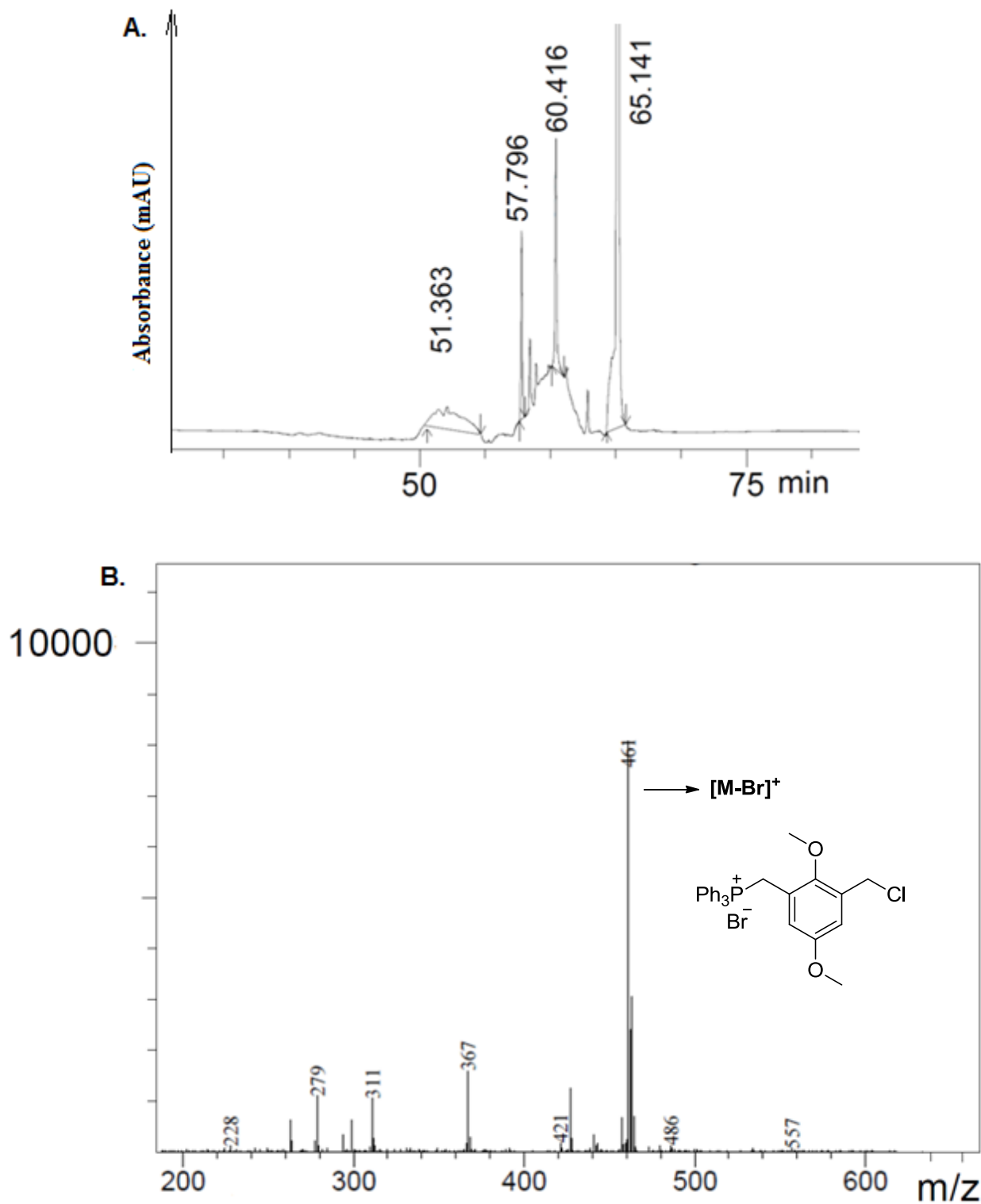


Scheme 3-4. Proposed mechanism for DNA ICL formation.

In order to provide direct evidence for the formation of free radicals and carbocations, we did monomer trapping reactions using methoxyamine and TEMPO as carbocation and free radical trapping agents, respectively. Compound **26i** that is easy to synthesize and showed relatively higher ICL yield, was selected as a representative for this study. TLC showed that the cation trapping reaction resulted in several new spots with similar R_f value, which were impossible to be separated using chromatography. Thus, LC-MS was used for the analysis of the adducts formed in cation trapping reaction (Figure 3-4). Adducts **33a** and **33b** were detected on LCMS 2020 at a retention time of ~57.8 min and ~60.4 min, respectively. Both adducts were further confirmed by HRMS. Formation of **33a** and **33b** indicated that carbocations (**32**) were generated upon UV irradiation. In contrast, the free radical trapping reaction was clean leading to one major product **33c** that was purified by chromatography. The structure of **33c** was determined by NMR and HRMS, suggesting that free radical **31** was generated upon 350 nm irradiation of **26i**. These results provided direct evidences for the proposed mechanism shown in Scheme 3-4.



Scheme 3-5. Cation and free radical trapping products obtained with **26i** upon UV irradiation at 350 nm.



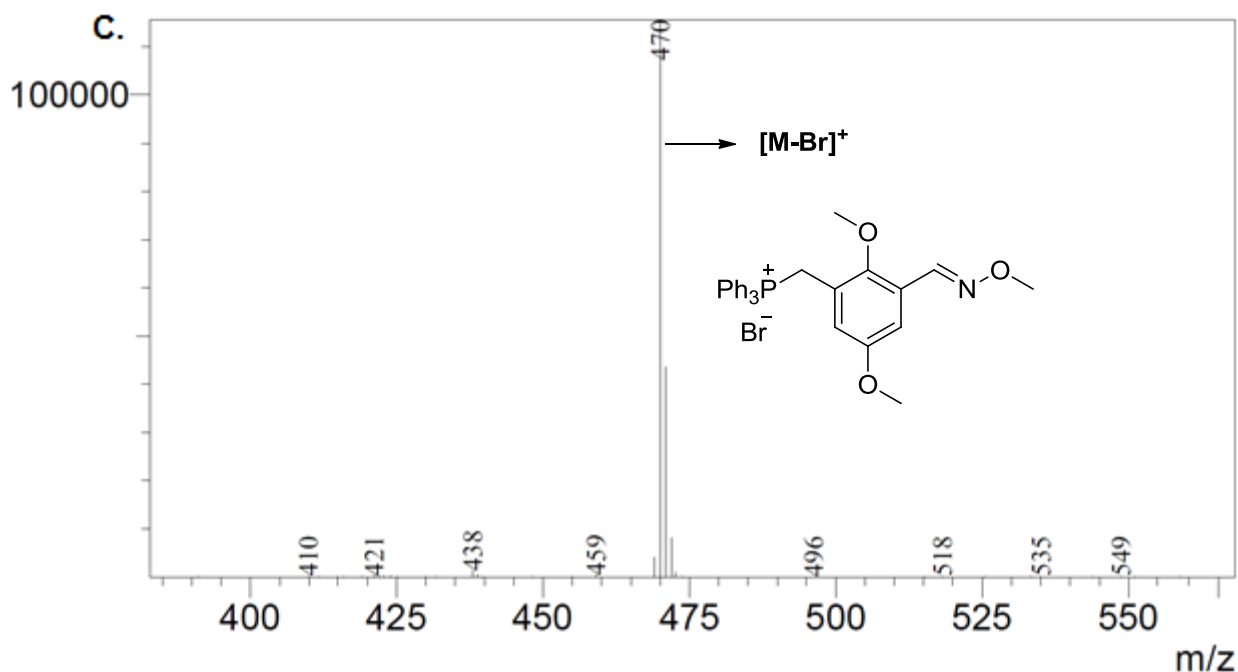


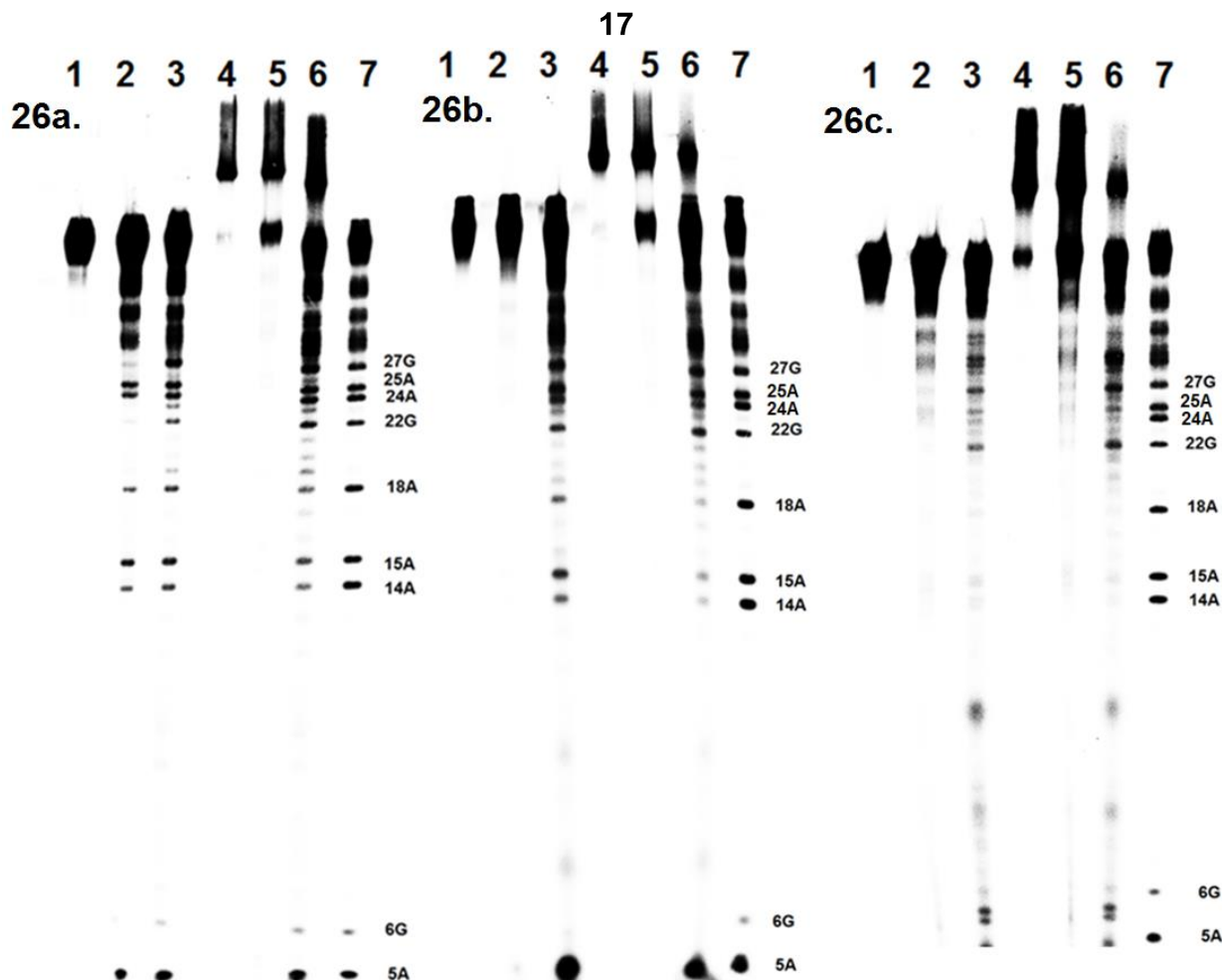
Figure 3-4. LC-MS chromatogram for the reaction mixture of **26i** and methoxyamine hydrochloride upon 350 nm irradiation: A. PDA spectrum of the reaction mixture of **26i** and methoxyamine hydrochloride (reaction time: 24 h) (LCMS 2020); B. Mass spectrum of peak at retention time 57.796 min; C. Mass spectrum of peak at retention time 60.416 min. (analyzed by reversed-phase HPLC, TC-C18 at 256 nm using gradient: 0-30 min 2-20% MeOH in water, 30-35 min 20-50% MeOH in water, 35-42 min 50-100% MeOH in water, 42-50 min 100% MeOH in water, at a flow rate 1.0 mL/min).

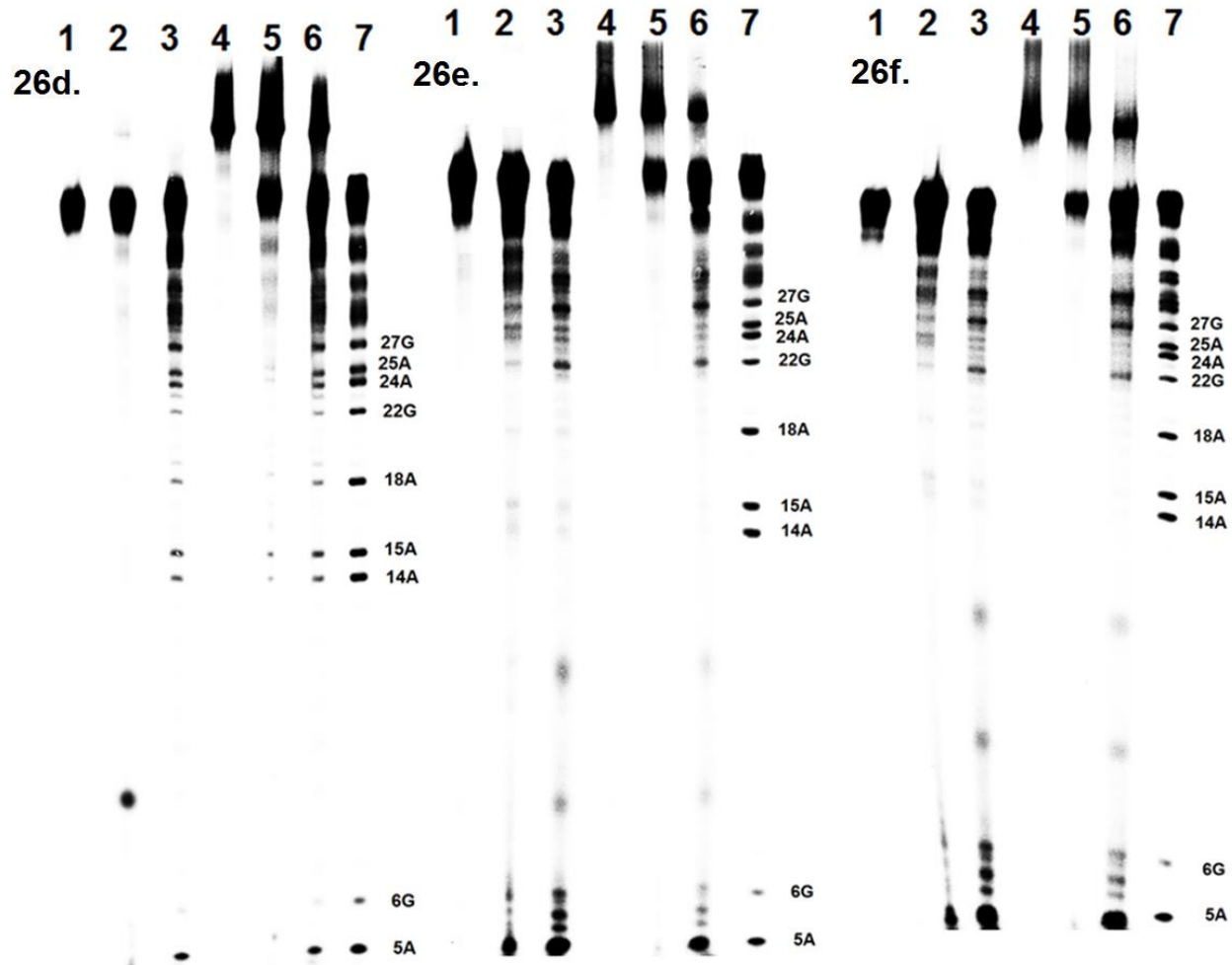
3.5. Determination of DNA alkylation sites.

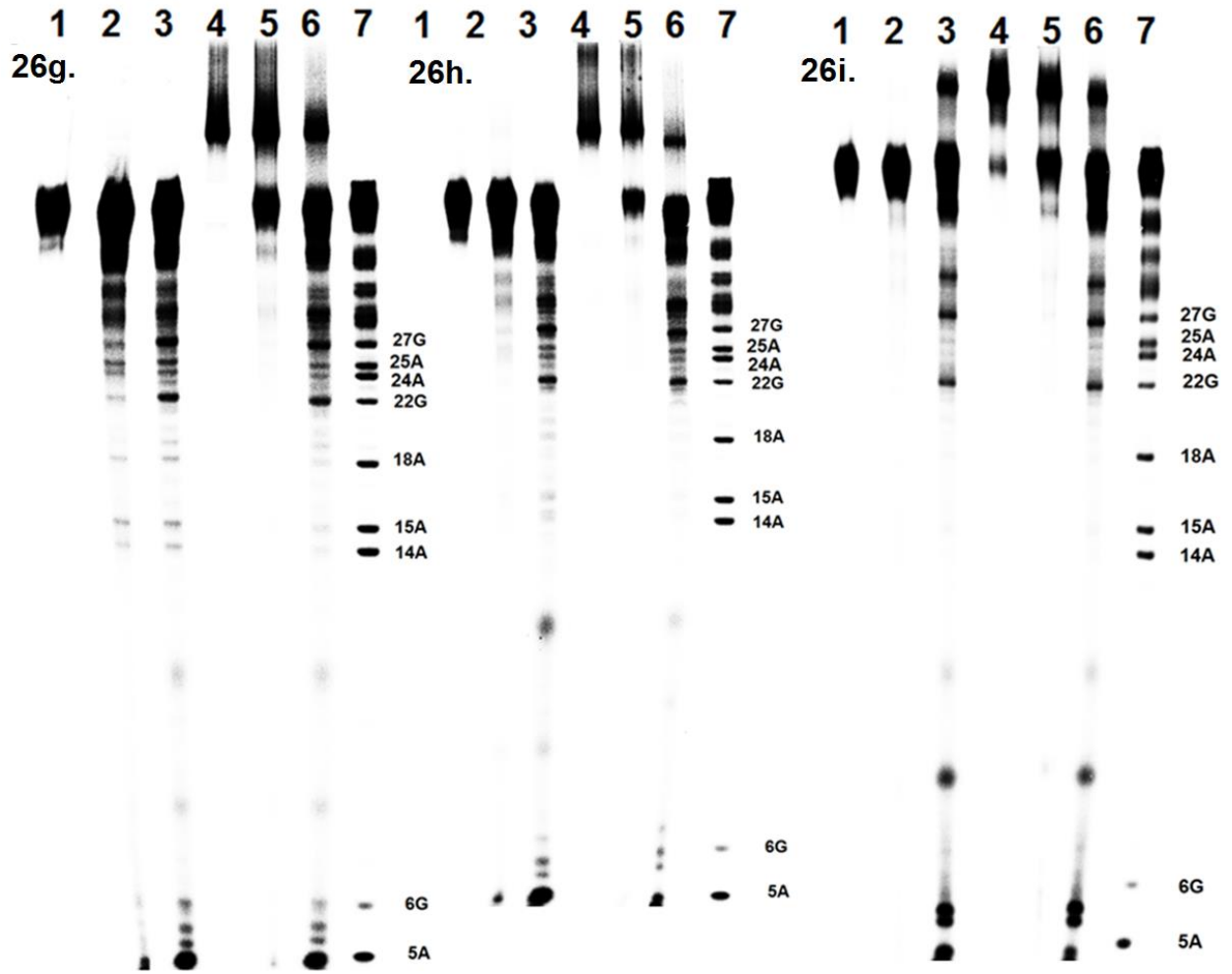
It was reported that the N7-alkylated purines can be cleaved in the presence of piperidine upon heating.¹³⁻¹⁵ The heat stability of the isolated single-stranded DNA and ICL products formed by **27a** and **26a** are shown in Figure 3-5. The ICL products were relatively stable upon heating in a pH 7.0 phosphate buffer for 30 min, while obvious cleavage bands were observed in 1.0 M piperidine. The major cleavage bands were observed at both dA and dG sites for **27a-d**, **27f**, **27h**,

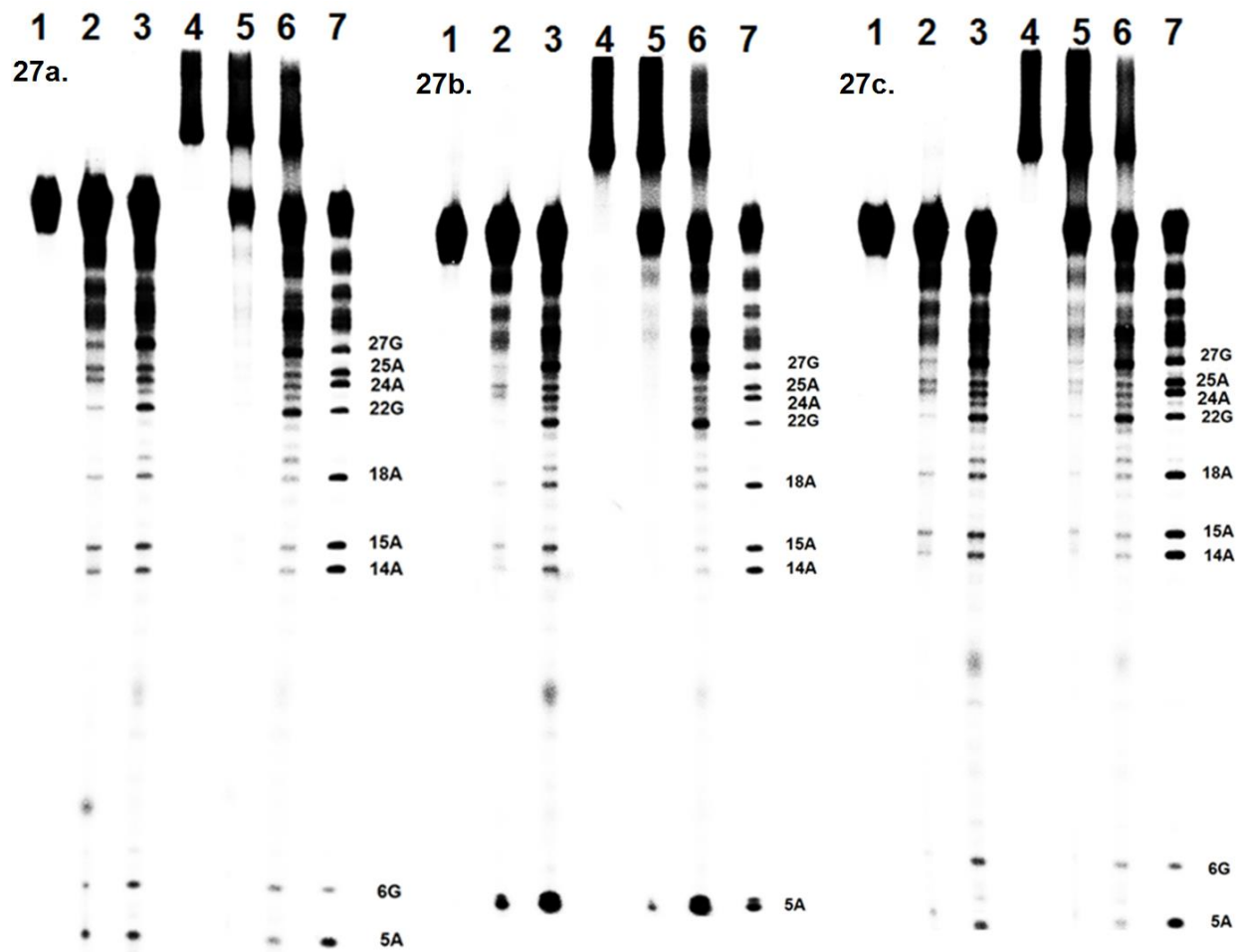
26a, **26b**, and **26d**, while the cleavage mainly occurred at dGs for compounds **27e**, **27g**, **27i** and **26c**, **26e**, **26f-i**. From the heat-stability experiments of the isolated DNA ICL products, we can conclude that compounds **27a-d**, **27f**, **27h**, **26a**, **26b** and **26d** alkylated both dAs and dGs upon photo irradiation while photo-induced alkylation by **27e**, **27g**, **27i**, **26c**, **26e** and **26f-i** mainly occurred with dGs). These data suggested that aromatic substituents and benzylic leaving groups affect the cross-linking site.

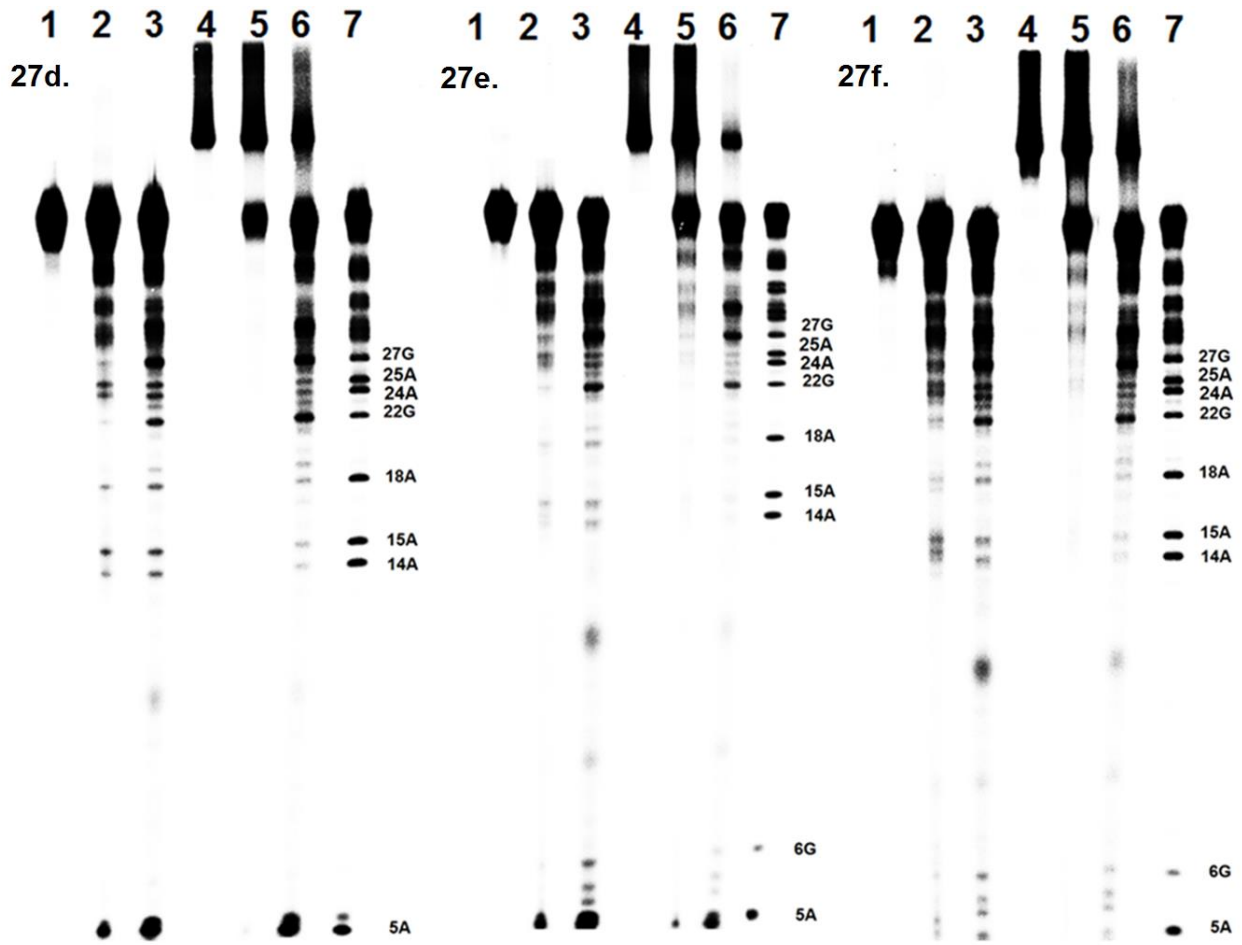
1 5 6 14 15 18 22 24 25 27 31 40 44 49
 5'-dGCCTAGTTCTTTTAATTACTTGCAATGCAAGTAATTAAAGCTTGATCTG (**17a**)
 3'-dCGGATCAAGAAAATTAATGAACGTTACGTTTCATTAATTTTCGAACTAGAC (**17b**)











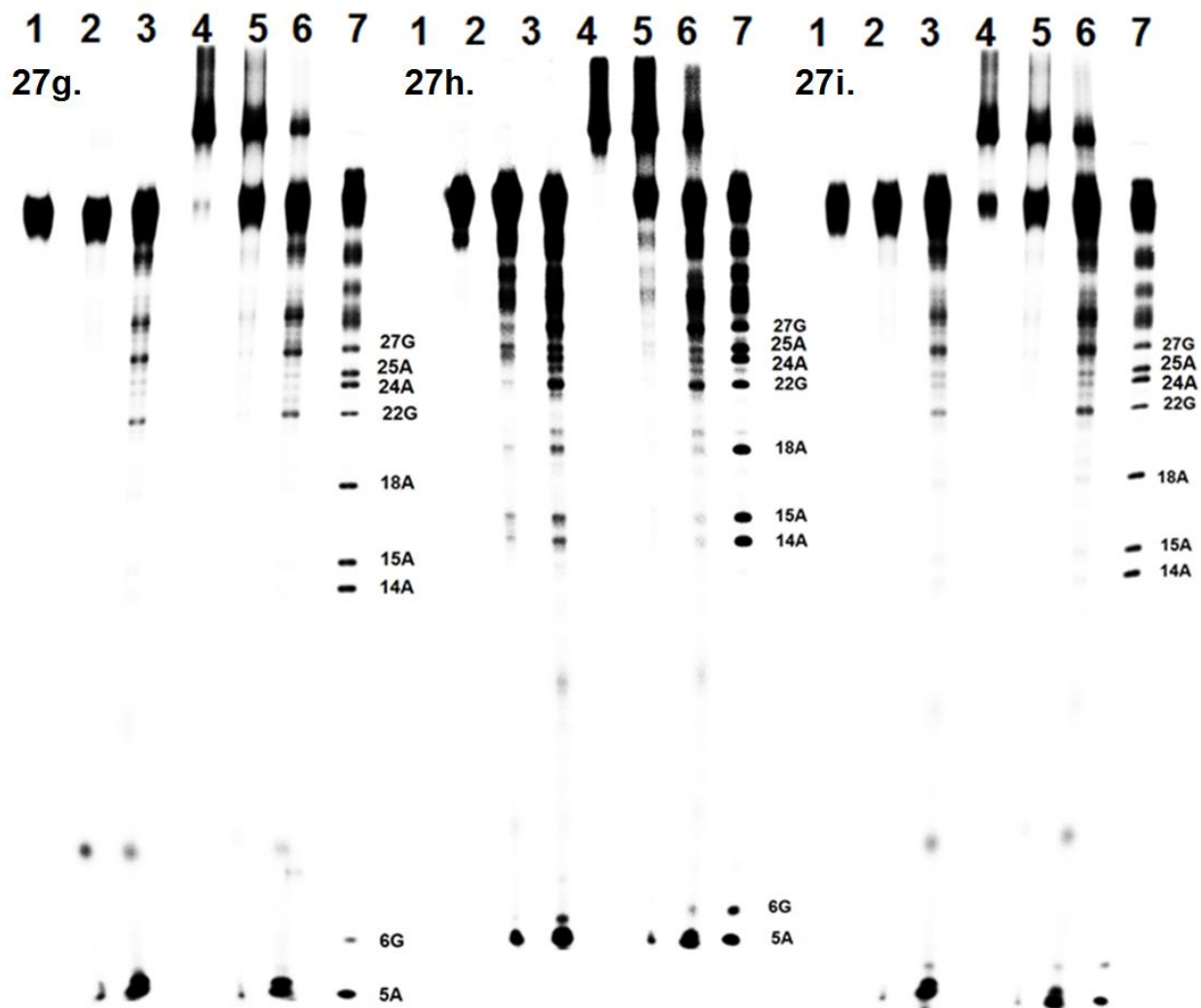


Fig 3-5. Determination of the reaction sites of **26a-i** and **27a-i**. Phosphorimage autoradiogram of 20% denaturing PAGE analysis of the isolated DNA ICL products and alkylated single-stranded DNA (**17a'**) upon heating in piperidine or phosphate buffer. The optimal condition for each compound was used for the ICL reaction and ICL products and **17a'** were isolated via PAGE. **17a** was radiolabeled at the 5'-terminus. Lane 1: isolated alkylated single stranded DNA (**17a'**). Lane 2: **17a'** was heated in a pH 7 phosphate buffer at 90 °C for 30 min. Lane 3: **17a'** was heated

in 1.0 M piperidine at 90 °C for 30 min. Lane 4: Isolated DNA ICL products. Lane 5: the DNA ICL products were heated in a pH 7 phosphate buffer at 90 °C for 30 min. Lane 6: the DNA ICL products were heated in 1.0 M piperidine at 90 °C for 30 min. Lane 7: G+A sequencing.

3.6. Conclusions

In this work, we have synthesized two classes of bifunctional phenyl compounds with OMe or NO₂ aromatic substituent and various benzylic leaving groups. The photo-activity of these compounds towards DNA was determined using 20% denaturing PAGE analysis. Compounds with an electron donating aromatic substituent (**26a-i**) showed higher DNA ICL efficiency than the corresponding compounds with an electron withdrawing group (**27a-i**). Benzylic leaving groups also greatly affect DNA ICL efficiency. Photo-irradiation of **27a-i** and **26a-i** generated the benzyl cations that directly cross-link DNA. The carbocations were produced through free radical oxidation for all tested compounds. The stability of the alkylated DNA was determined upon heating in pH 7 phosphate buffer or in piperidine, which indicated that dAs and/or dGs were the major alkylation sites for all tested compounds. Both aromatic substituents and leaving groups affect the cross-linking sites. This study provides valuable fundamentals for developing photo-induced DNA alkylating agents with higher efficiency. It also provide guidelines for designing potential photo-activated drugs.

3.7. Experimental Section

General Information. All chemicals came from commercial available source were used without further purification. Oligonucleotides were synthesized via standard automated DNA synthesis techniques. Deprotection of the synthesized DNA was performed under mild deprotection conditions using a mixture of 40% aqueous MeNH₂ and 28% aqueous NH₃ (1:1) at room

temperature for 2 h. 20% denaturing polyacrylamide gel electrophoresis was used for DNA purification. [γ - ^{32}P] ATP was used for DNA labeling with standard method. Quantification of radiolabeled oligonucleotides was carried out using a Molecular Dynamics phosphorimager equipped with ImageQuant, version 5.2, software. ^1H NMR and ^{13}C NMR spectra were taken on either a Bruker DRX 300 or DRX 500 MHz spectrophotometer with TMS as internal stander. High-resolution mass spectrometry IT-TOF was used for molecular measurement.

1,3-Bis(bromomethyl)-5-methoxy-2-nitrobenzene (5a): Into a solution of compound **16** (3.0 g, 14.0 mmol) in DCM (50 mL) at 0 °C, phosphorus tribromide (8.72 g, 32.22 mmol) was added. The reaction mixture was allowed to warm to rt and stirred overnight. The reaction mixture was quenched with water (30 mL), diluted with DCM (3 \times 30 mL), washed with brine, and dried over anhydrous Na_2SO_4 . Solvent was removed, and the residue was purified by column chromatography (Hexane: ethyl acetate = 2:1, R_f = 0.65) to afford **5a** as a yellowish solid (2.09 g, 6.44 mmol). ^1H NMR (300 MHz, CDCl_3): δ . 6.98 (s, 2H), 4.54 (s, 4H), 3.91 (s, 3H) (the NMR spectra were in agreement with those reported).¹

(5-Methoxy-2-nitro-1,3-phenylene)bis(methylene) diacetate (27a): Compound **16** (300 mg, 1.41 mmol) and 4-dimethyl aminopyridine (517 mg, 4.23 mmol) in DCM was cooled to 0 °C. Acetyl chloride (443 mg, 5.64 mmol) was added using syringe. The reaction mixture was warmed to rt and stirred overnight. The reaction mixture was quenched with H_2O (10 mL), diluted with DCM (3 \times 15 mL), washed with brine, and dried over anhydrous Na_2SO_4 . Solvent was removed, and the residue was purified by column chromatography (Hexane: Ethyl acetate = 2:1, R_f = 0.35) to obtain **27a** as a light yellowish solid (397 mg, 1.34 mmol): m.p. 95-96 °C. ^1H NMR (300 MHz, CDCl_3): δ . 6.96 (s, 2H), 5.23 (s, 4H), 3.89 (s, 3H), 2.11 (s, 6H). ^{13}C NMR (75

MHz, CDCl₃): δ .170.21, 161.21, 141.72, 132.77, 114.19, 62.43, 55.85, 20.61. HRMS-ESI (+) (m/z): [M+Na]⁺ calcd. for C₁₃H₁₅NO₇Na⁺, 320.0741; found: 320.0717.

5-Methoxy-1,3-bis(methoxymethyl)-2-nitrobenzene (27b): To a solution of compound **16** (300 mg, 1.41 mmol) in DMF (6.0 mL) at 0 °C, NaH (169 mg, 60%, 4.23 mmol) was added. The reaction mixture was stirred at 0 °C for 10 min, and CH₃I (800 mg, 5.64 mmol) was added. The mixture was allowed to warm to rt and stirred overnight. The reaction mixture was quenched with water (10 mL), diluted with ethyl acetate (3 × 15 mL), washed with brine, and dried over anhydrous Na₂SO₄. Solvent was removed, and the residue was purified by column chromatography (Hexane: Ethyl acetate = 2:1, R_f = 0.68) to obtain **27b** as a yellow solid (280 mg, 1.16 mmol): m.p. 39-40 °C. ¹H NMR (300 MHz, CDCl₃): δ . 7.05 (s, 2H), 4.58 (s, 4H), 3.90 (s, 3H), 3.43 (s, 6H). ¹³C NMR (75 MHz, CDCl₃): δ . 161.54, 140.89, 135.27, 112.57, 71.71, 58.82, 55.79. HRMS-ESI (+) (m/z): [M-OMe]⁺ calcd. for C₁₀H₁₂NO₄⁺, 210.0761; found: 210.0737.

1,3-Bis((allyloxy)methyl)-5-methoxy-2-nitrobenzene (27c): To a solution of compound **16** (300 mg, 1.41 mmol) in DMF (6.0 mL) at 0 °C, NaH (169 mg, 60%, 4.23 mmol) was added. The resulting mixture was stirred for 10 min, and then allyl iodide (948 mg, 5.64 mmol) was added. The reaction mixture was allowed to warm to rt and stirred overnight. The reaction mixture was quenched with water (10 mL), diluted with ethyl acetate (3 × 15 mL), washed with brine, and dried over anhydrous Na₂SO₄. Solvent was removed, and the residue was purified by column chromatography (Hexane: Ethyl acetate = 2:1, R_f = 0.8) to obtain **27c** as a yellowish liquid (286 mg, 0.98 mmol). ¹H NMR (300 MHz, CDCl₃): δ . 7.09 (s, 2H), 6.00-5.88 (m, 2H), 5.35 (s, 1H), 5.30 (s, 1H), 5.25-5.22 (d, *J* = 9.0 Hz, 2H), 4.64 (s, 4H), 4.07-4.05 (d, *J* = 6.0 Hz, 4H), 3.89 (s, 3H). ¹³C NMR (75 MHz, CDCl₃): δ . 161.48, 140.98, 135.39, 134.04, 117.58, 112.68, 71.88,

68.21, 55.76. HRMS-ESI (+) (m/z): $[M-OC_3H_5]^+$ calcd. for $C_{12}H_{14}NO_4^+$, 236.0917; found: 236.0915.

(((5-Methoxy-2-nitro-1,3-phenylene)bis(methylene))bis(oxy))bis(methylene)dibenzene

(27d): Compound **16** in (300 mg, 1.41 mmol) in DMF (6.0 mL) was cooled to 0 °C, followed by the addition of NaH (169 mg, 60%, 4.23 mmol). The resulting mixture was stirred for 10 min. Then benzyl bromide (720 mg, 4.23 mmol) was added. The reaction mixture was allowed to warm to rt and stirred overnight. The reaction mixture was quenched with water (10 mL), diluted with ethyl acetate (3 × 15 mL), washed with brine, and dried over anhydrous Na_2SO_4 . Solvent was removed, and the residue was purified by column chromatography (Hexane: Ethyl acetate = 2:1, R_f = 0.76) to afford **27d** as a yellowish oily (414 mg, 1.06 mmol). 1H NMR (300 MHz, $CDCl_3$): δ . 7.42-7.30 (m, 10H), 7.12 (s, 2H), 4.71 (s, 4H), 4.60 (s, 4H), 3.88 (s, 3H). ^{13}C NMR (75 MHz, $CDCl_3$): δ . 161.45, 141.18, 137.55, 135.28, 128.52, 127.91, 127.82, 112.92, 73.15, 68.49, 55.79. HRMS-ESI (+) (m/z): $[M+Na]^+$ calcd. for $C_{23}H_{23}NO_5Na^+$, 416.1468; found: 416.1453.

1,1'-(5-Methoxy-2-nitro-1,3-phenylene)bis(N,N-dimethylmethanamine) (27e): Into a solution of **5a** (150 mg, 0.44 mmol) in ethyl acetate (4.0 mL), dimethylamine solution (2.0 M in methanol) (2.2 mL, 4.4 mmol) was added. The reaction mixture was stirred at rt for 8 h. Solvent was removed, and the residual was purified by column (DCM: Methanol = 10:1, R_f = 0.5) to afford **27e** as a yellowish solid (108 mg, 0.40 mmol): m.p. 44-45 °C. 1H NMR (300 MHz, $CDCl_3$): δ . 7.05 (s, 2H), 3.89 (s, 3H), 3.51 (s, 4H), 2.26 (s, 12H). ^{13}C NMR (75 MHz, $CDCl_3$): δ . 160.50, 144.22, 133.33, 114.58, 59.59, 55.91, 45.22. HRMS-ESI (+) (m/z): $[M+H]^+$ calcd. for $C_{13}H_{22}N_3O_3^+$, 268.1656; found: 268.1633.

4,4'-((5-Methoxy-2-nitro-1,3-phenylene)bis(methylene))dimorpholine (27f): Into a solution of **5a** (150 mg, 0.44 mmol), morpholine (387 mg, 4.40 mmol) was added. The resulting mixture was stirred at rt overnight. Solvent was removed, and the residue was purified by column (DCM: Methanol = 10:1, R_f = 0.72) to afford **27f** as a yellowish solid (143 mg, 0.41 mmol): m.p. 88-89 °C. ^1H NMR (300 MHz, CDCl_3): δ . 6.89 (s, 2H), 3.88 (s, 4H), 3.66 (s, 8H), 3.57 (s, 3H), 2.41 (s, 8H). ^{13}C NMR (75 MHz, CDCl_3): δ . 160.16, 144.30, 133.70, 114.52, 66.84, 59.31, 55.78, 53.33. HRMS-ESI (+) (m/z): $[\text{M}+\text{H}]^+$ calcd. for $\text{C}_{17}\text{H}_{26}\text{N}_3\text{O}_5^+$, 352.1867; found: 352.1865.

((5-Methoxy-2-nitro-1,3-phenylene)bis(methylene))bis(phenylsulfane) (27g): To a solution of compound **5a** (170 mg, 0.5 mmol) in DMF (5.0 mL), thiophenol (165.3 mg, 1.5 mmol) was added, followed by the addition of trimethylamine (0.6 mL). The reaction mixture was stirred at 70 °C overnight. The reaction mixture was quenched with water (10 mL), diluted with ethyl acetate (3×15 mL), washed with brine, and dried over anhydrous Na_2SO_4 . Solvent was removed, and the residue was purified by column chromatography (Hexane: ethyl acetate = 5:1, R_f = 0.45) to afford **27g** as a yellowish solid (130 mg, 0.33 mmol): m.p. 73-74 °C. ^1H NMR (300 MHz, CDCl_3): δ . 7.30-7.26 (m, 10H), 6.65 (m, 2H), 4.15 (s, 4H), 3.64 (s, 3H). ^{13}C NMR (75 MHz, CDCl_3): δ . 160.07, 143.40, 134.65, 133.52, 131.42, 129.04, 127.36, 114.93, 55.56, 36.13. HRMS-ESI (+) (m/z): $[\text{M}+\text{K}]^+$ calcd. for $\text{C}_{21}\text{H}_{19}\text{NO}_3\text{S}_2\text{K}^+$, 436.0438; found: 436.0429.

((5-Methoxy-2-nitro-1,3-phenylene)bis(methylene))bis(phenylselane) (27h): To a solution of diphenyl diselenide (368.3 mg, 1.18 mmol) in DMF (5.0 mL), NaBH_4 (11.2 mg, 0.295 mmol) was added. The reaction mixture was stirred at rt for 2 h. Compound **5a** (100 mg, 0.295 mmol) in DMF (2.0 mL) was added. The resulting mixture was stirred at rt for another 4 h. The reaction mixture was quenched with water (10 mL), diluted with ethyl acetate (3×15 mL), washed with brine, and dried over anhydrous Na_2SO_4 . Solvent was removed, and the residue was purified by

column chromatography (Hexane: ethylacetate = 5:1, R_f = 0.4) to afford **27h** as a light yellowish solid (80.0 mg, 0.16 mmol): m.p. 95-97 °C. ^1H NMR (300 MHz, CDCl_3): δ . 7.50-7.48 (d, J = 6.0 Hz, 4H), 7.30-7.27 (m, 6H), 6.32 (s, 2H), 4.08 (s, 4H), 3.53 (s, 3H). ^{13}C NMR (75 MHz, CDCl_3): 159.54, 135.07, 134.66, 129.03, 128.91, 128.85, 127.81, 114.45, 55.14, 28.28. HRMS-ESI (+) (m/z): $[\text{M}+\text{K}]^+$ calcd. for $\text{C}_{21}\text{H}_{19}\text{NO}_3\text{Se}_2\text{K}^+$, 531.9331; found: 531.9320.

((5-Methoxy-2-nitro-1,3-phenylene)bis(methylene))bis(triphenylphosphonium) bromide

(27i): Compound **5a** (170 mg, 0.5 mmol) and triphenylphosphine (289 mg, 1.1 mmol) in dry toluene (5 mL) was stirred at rt for 2 days under argon. The crude white powder was obtained by filtration, which was further purified by column chromatography (DCM: Methanol = 10:1, R_f = 0.32) to yield **27i** as a yellowish foam (259 mg, 0.30 mmol). ^1H NMR (300 MHz, CDCl_3): δ . 7.83-7.78 (m, 6H), 7.71-7.55 (m, 24H), 7.18 (s, 2H), 5.58-5.53 (d, J = 15.0 Hz, 4H), 3.46 (s, 3H). ^{13}C NMR (75 MHz, CDCl_3): δ . 161.35, 143.10, 135.50, 134.30, 134.16, 130.63, 130.46, 126.91, 126.78, 120.23, 117.31, 116.17, 55.62, 30.93, 29.25, 28.60. HRMS-ESI (+) (m/z): $[\text{M}-2\text{Br}]^{2+}$ calcd. for $\text{C}_{45}\text{H}_{39}\text{NO}_3\text{P}_2^{2+}$, 351.6197; found: 351.6183.

(2-Hydroxy-5-methoxy-1,3-phenylene)dimethanol (29): Into a solution of compound **28** (24.8 g, 0.2 mol) in H_2O (180 mL), NaOH (16 g, 0.4 mol) was added, followed by the addition of paraformaldehyde (18.0 g, 0.6 mol) and methanol (30 mL). The reaction mixture was stirred at 50 °C for 2 days. After addition of hydrochloric acid (5.0 M) to pH 5.0, methanol was removed. The mixture was diluted with ethyl acetate (3×100 mL), washed with brine, and dried over anhydrous Na_2SO_4 . Solvent was removed, and the residue was purified by column chromatography (Hexane: Ethyl acetate = 1:1, R_f = 0.33) to obtain **29** as a white solid (55.2 g, 0.3 mol). ^1H NMR (300 MHz, CDCl_3): δ . 8.04 (s, 1H), 6.76 (s, 2H), 5.24-5.20 (t, J = 6.0 Hz, 2H),

4.54-4.52 (d, $J = 6.0$ Hz, 4H), 3.68 (s, 3H) (the NMR spectra were in agreement with those reported).¹⁶

(2,5-Dimethoxy-1,3-phenylene)dimethanol (30): To a solution of compound **29** (18.4 g, 0.1 mol) in acetone (100 mL), K_2CO_3 (g, 0.2 mol) and CH_3I (g, 0.2 mol) was added. The reaction mixture was stirred at 50 °C overnight. Solvent was removed. The residue was diluted with ethyl acetate (3 × 80 mL), washed with brine, and dried over anhydrous Na_2SO_4 . Solvent was removed, and the residue was purified by column chromatography (Hexane: Ethyl acetate = 1:1, $R_f = 0.3$) to obtain **30** as a white solid (17.4 g, 88 mmol). 1H NMR (300 MHz, $CDCl_3$): δ . 6.87 (s, 2H), 5.12-5.08 (t, $J = 6.0$ Hz, 2H), 4.52-4.50 (d, $J = 6.0$ Hz, 4H), 3.72 (s, 3H), 3.61 (s, 3H) (the NMR spectra were in agreement with those reported).¹⁷

1,3-Bis(bromomethyl)-2,5-dimethoxybenzene (1a): Compound **30** (4.0 g, 20.18 mmol) in DCM (50 mL) was cooled to 0 °C, followed by the addition of phosphorus tribromide (12.02 g, 44.4 mmol). The reaction mixture was allowed to warm to rt and stirred for 4 h. The reaction mixture was quenched with water (30 mL), diluted with DCM (3 × 20 mL), washed with brine, and dried over anhydrous Na_2SO_4 . Solvent was removed, and the residue was purified by column chromatography (Hexane: DCM = 5:1, $R_f = 0.35$) to afford **1a** as a white solid (5.88 g, 18.16 mmol). 1H NMR (500 MHz, $CDCl_3$): δ . 6.92 (s, 2H), 4.56 (s, 4H), 4.00 (s, 3H), 3.82 (s, 3H) (the NMR spectra were in agreement with those reported).¹

(2,5-Dimethoxy-1,3-phenylene)bis(methylene) diacetate (26a): Into a solution of compound **30** (0.99 g, 5 mmol) in DCM (10 mL), 4-dimethylaminopyridine (1.83 g, 15 mmol) was added. After cooling the resulting mixture to 0 °C, acetyl chloride (1.57 g, 20 mmol) was added using syringe. The reaction mixture was warmed to rt and stirred for another 4 h. The reaction mixture was quenched with H_2O (8.0 mL), diluted with DCM (3 × 20 mL), washed with brine, and dried

over anhydrous Na₂SO₄. Solvent was removed, and the residue was purified by column chromatography (Hexane: Ethyl acetate = 1:1, R_f = 0.7) to obtain **26a** as a slightly yellowish liquid (1.28 g, 4.55 mmol). ¹H NMR (300 MHz, CDCl₃): δ. 6.90 (s, 2H), 5.15 (s, 4H), 3.78 (s, 6H), 2.11-2.10 (d, *J* = 3.0 Hz, 6H) (the NMR spectra were in agreement with those reported).¹¹ HRMS-ESI (+) (*m/z*): [M+Na]⁺ calcd. for C₁₄H₁₈O₆Na⁺, 305.0996; found: 305.0985.¹⁸

2,5-Dimethoxy-1,3-bis(methoxymethyl)benzene (26b): To a solution of compound **30** (1.0 g, 5.04 mmol) in DMF (10 mL) at 0 °C, NaH (605 mg, 60%, 15.12 mmol) was added. The reaction mixture was stirred at 0 °C for 10 min, and then CH₃I (2.86 g, 20.16 mmol) was added. The mixture was allowed to warm to rt and stirred for another 4 h. The reaction mixture was quenched with water (20 mL), diluted with ethyl acetate (3 × 30 mL), washed with brine, and dried over anhydrous Na₂SO₄. Solvent was removed, and the residue was purified by column chromatography (Hexane: Ethyl acetate = 1:1, R_f = 0.8) to obtain **26b** as a colorless liquid (1.10 g, 4.86 mmol). ¹H NMR (500 MHz, CDCl₃): δ. 6.92 (s, 2H), 4.51 (s, 4H), 3.81 (s, 3H), 3.76 (s, 3H), 3.44 (s, 6H). ¹³C NMR (125 MHz, CDCl₃): δ. 155.95, 150.02, 132.28, 114.09, 69.44, 62.53, 58.32, 55.59. HRMS-ESI (+) (*m/z*): [M+Na]⁺ calcd. for C₁₂H₁₈O₄Na⁺, 249.1103; found: 249.1094.

1,3-Bis((allyloxy)methyl)-2,5-dimethoxybenzene (26c): To a solution of compound **30** (1.0 g, 5.04 mmol) in DMF (10 mL) at 0 °C, NaH (605 mg, 60%, 15.12 mmol) was added. The resulting mixture was stirred for 10 min, and then allyl iodide (2.54 g, 15.12 mmol) was added. The reaction mixture was allowed to warm to rt and stirred for 3 h. The reaction mixture was quenched with water (10 mL), diluted with ethyl acetate (3 × 30 mL), washed with brine, and dried over anhydrous Na₂SO₄. Solvent was removed, and the residue was purified by column chromatography (Hexane: Ethyl acetate = 3:1, R_f = 0.85) to obtain **26c** as a colorless liquid (1.20

g, 4.31 mmol). ¹H NMR (500 MHz, CDCl₃): δ. 6.95 (s, 2H), 6.03-5.96 (m, 2H), 5.37-5.33 (d, *J* = 20.0 Hz, 2H), 5.24-5.22 (d, *J* = 10.0 Hz, 2H), 4.58 (s, 4H), 4.10-4.09 (d, *J* = 5.0 Hz, 4H), 3.81 (s, 3H), 3.76 (s, 3H). ¹³C NMR (125 MHz, CDCl₃): δ. 155.96, 150.05, 134.75, 132.40, 117.11, 114.18, 71.44, 66.96, 62.56, 55.58. HRMS-ESI (+) (*m/z*): [M+H]⁺ calcd. for C₁₆H₂₃O₄⁺, 279.1591; found: 279.1583.

(((2,5-Dimethoxy-1,3-phenylene)bis(methylene))bis(oxy))bis(methylene)dibenzene (26d):

Compound **30** in (1.0 g, 5.04 mmol) in DMF (10 mL) was cooled to 0 °C, followed by the addition of NaH (605 mg, 60%, 15.12 mmol). The resulting mixture was stirred for 10 min, and then benzyl chloride (1.91 g, 15.12 mmol) was added. The reaction mixture was allowed to warm to rt and reacted for another 3 h. The reaction mixture was quenched with water (10 mL), diluted with ethyl acetate (3 × 30 mL), washed with brine, and dried over anhydrous Na₂SO₄. Solvent was removed, and the residue was purified by column chromatography (Hexane: Ethyl acetate = 3:1, *R_f* = 0.8) to afford **26d** as a colorless liquid (1.52 g, 4.03 mmol). ¹H NMR (500 MHz, CDCl₃): δ. 7.45-7.33 (m, 10H), 7.03 (s, 2H), 4.66 (s, 8H), 3.84 (s, 3H), 3.74 (s, 3H). ¹³C NMR (125 MHz, CDCl₃): δ. 156.01, 150.20, 138.27, 132.41, 128.46, 127.86, 127.70, 114.38, 72.56, 67.07, 62.62, 62.59, 55.66, 55.63. HRMS-ESI (+) (*m/z*): [M+Na]⁺ calcd. for C₂₄H₂₆O₄Na⁺, 401.1723; found: 401.1717.

1,1'-(2,5-Dimethoxy-1,3-phenylene)bis(N,N-dimethylmethanamine) (26e): Into a solution of **1a** (500 mg, 1.54 mmol) in ethyl acetate (5 mL), dimethylamine solution (2.0 M in methanol) (3.85 mL, 7.7 mmol) was added. The reaction mixture was stirred at rt for 2 h. Solvent was removed. The residue was diluted with ethyl acetate (3 × 10 mL), washed with NaOH (1.0 M), brine, and dried over anhydrous Na₂SO₄. Solvent was removed to afford **26e** as a slightly yellowish gel (350 mg, 1.39 mmol). ¹H NMR (500 MHz, CDCl₃): δ. 6.85 (s, 2H), 3.76 (s, 3H),

3.69 (s, 3H), 3.42 (s, 4H), 2.24 (s, 12H). (the NMR spectra were in agreement with those reported).¹¹ HRMS-ESI (+) (*m/z*): [M+H]⁺ calcd. for C₁₄H₂₅N₂O₂⁺, 253.1911; found: 253.1905.¹⁹

4,4'-((2,5-Dimethoxy-1,3-phenylene)bis(methylene))dimorpholine (26f): Into a solution of **1a** (324 mg, 1.0 mmol), was added morpholine (871 mg, 10.0 mmol). The resulting mixture was stirred at rt overnight. The reaction mixture was diluted with ethyl acetate (3 × 10 mL), washed with NaOH (1.0 M), brine, and dried over anhydrous Na₂SO₄. Solvent was removed to afford **26f** as a white solid (333 mg, 0.99 mmol): m.p. 114-115 °C. ¹H NMR (500 MHz, CDCl₃): δ. 6.92 (s, 2H), 3.81 (s, 3H), 3.78 (s, 3H), 3.74-3.72 (t, *J* = 5.0 Hz, 8H), 3.54 (s, 4H), 2.52 (s, 8H). ¹³C NMR (125 MHz, CDCl₃): δ. 155.50, 151.49, 132.07, 114.52, 67.15, 62.18, 57.13, 55.57, 53.72. HRMS-ESI (+) (*m/z*): [M+H]⁺ calcd. for C₁₈H₂₉N₂O₄⁺, 337.2122; found: 337.2113.

((2,5-Dimethoxy-1,3-phenylene)bis(methylene))bis(phenylsulfane) (26g): To a solution of compound **1a** (624 mg, 2.0 mmol) in DMF (10 mL), thiophenol (661.2 mg, 6.0 mmol) was added, followed by the addition of trimethylamine (0.6 mL). The reaction mixture was stirred at 70 °C overnight. The reaction mixture was quenched with water (20 mL), diluted with ethyl acetate (3 × 20 mL), washed with brine, and dried over anhydrous Na₂SO₄. Solvent was removed, and the residue was purified by column chromatography (Hexane: ethyl acetate = 6:1, *R_f* = 0.4) to afford **26g** as a white solid (620 mg, 1.62 mmol): m.p. 63-64 °C. ¹H NMR (500 MHz, CDCl₃): δ. 7.40-7.38 (m, 4H), 7.33-7.30 (m, 4H), 7.25-7.22 (m, 2H), 6.74 (s, 2H), 4.18 (s, 4H), 3.86 (s, 3H), 3.66 (s, 3H). ¹³C NMR (125 MHz, CDCl₃): δ. 155.51, 150.16, 136.51, 131.63, 129.89, 128.95, 126.44, 115.03, 62.65, 55.45, 33.32. HRMS-ESI (+) (*m/z*): [M+K]⁺ calcd. for C₂₂H₂₂O₂S₂K⁺, 421.0693; found: 421.0687.

((2,5-Dimethoxy-1,3-phenylene)bis(methylene))bis(phenylselane) (26h): Diphenyl diselenide (624 mg, 2.0 mmol) in DMF (5.0 mL), NaBH₄ (151 mg, 4.0 mmol) was added. The reaction

mixture was stirred at rt for 10 min. Compound **1a** (324 mg, 1.0 mmol) in DMF (4.0 mL) was added. The resulting mixture was stirred overnight. The reaction mixture was quenched with water (20 mL), diluted with ethyl acetate (3 × 20 mL), washed with brine, and dried over anhydrous Na₂SO₄. Solvent was removed, and the residue was purified by column chromatography (Hexane: DCM = 4:1, R_f = 0.5) to offer **26h** as a white solid (300 mg, 0.63 mmol): m.p. 38-39 °C. ¹H NMR (500 MHz, CDCl₃): δ. 7.55-7.54 (m, 4H), 7.31-7.29 (t, *J* = 5.0 Hz, 6H), 4.16 (s, 4H), 3.86 (s, 3H), 3.59 (s, 3H). ¹³C NMR (125 MHz, CDCl₃): δ. 155.19, 149.75, 133.64, 132.94, 130.71, 129.09, 127.39, 114.90, 62.09, 55.36, 26.46. HRMS-ESI (+) (*m/z*): [M+K]⁺ calcd. for C₂₂H₂₂O₂Se₂K⁺, 516.9586; found: 516.9580.

((2,5-Dimethoxy-1,3-phenylene)bis(methylene))bis(triphenylphosphonium) bromide (26i):

A mixture of **1a** (324 mg, 1.0 mmol) and triphenylphosphine (630 mg, 2.4 mmol) in dry toluene (5.0 mL) was refluxed for 6 h under argon. The crude white powder was obtained by filtration, which was washed with ether (3 × 20 mL) to produce **26i** as a white solid (840 mg, 0.99 mmol). ¹H NMR (500 MHz, CDCl₃): δ. 7.79-7.62 (m, 6H), 7.67-7.64 (m, 24H), 6.53 (s, 2H), 5.18-5.15 (d, *J* = 15.0 Hz, 4H), 3.17 (s, 3H), 2.86 (s, 3H): m.p. 270-271 °C. ¹³C NMR (125 MHz, CDCl₃): δ. 151.46, 135.31, 134.21, 134.17, 134.13, 130.53, 130.48, 130.43, 123.25, 118.05, 117.92, 117.90, 117.86, 117.36, 55.47, 26.03, 25.64. HRMS-ESI (+) (*m/z*): [M-2Br]²⁺ calcd. for C₄₆H₄₂O₂P₂²⁺, 344.1325; found: 344.1319.

Monomer trapping.

Radical trapping: To a solution of compound **26i** (100 mg, 0.118 mmol) in CH₃CN (1.5 mL), TEMPO (184 mg, 1.18 mmol) was added under stirring at rt. The resulting mixture was irradiated under UV at 350 nm for 5 days. Solvent was removed, and the residue was purified by

chromatography. (DCM: MeOH = 10:1) to afford compound **33c** as a white foam (24 mg, 0.036 mmol, 31%). ¹H NMR (300 MHz, CDCl₃): δ. 7.74-7.61 (m, 15 H), 6.97 (s, 1H), 6.69 (s, 1H), 5.23-5.19 (d, *J* = 12.0 Hz, 2H), 4.58 (s, 2H), 3.52-3.49 (d, *J* = 9 Hz, 6H), 1.47 (s, 4H), 1.34 (s, 2H), 1.15-1.11 (d, *J* = 12.0 Hz, 12H). ¹³C NMR (75 MHz, CDCl₃): δ. 155.73, 155.68, 134.86, 134.37, 134.24, 130.08, 129.91, 121.09, 120.97, 118.65, 117.52, 116.51, 114.66, 72.94, 61.96, 60.00, 55.66, 39.66, 32.92, 20.73, 17.01. HRMS-ESI (+) (*m/z*): [M-Br]⁺ calcd. for C₃₇H₄₅NO₃P⁺, 582.3132; found: 582.3115.

Carbocation trapping: To a solution of MeONH₂·HCl (394 mg, 4.72 mmol) in DMF (2 mL), trimethylamine (567 mg, 5.20 mmol) was added. After stirring at rt for 30 min, **26i** (100 mg, 0.118 mmol.) in DMF (1 mL) was added. The resulting mixture was stirred for 20 min, and then irradiated with UV at 350 nm for 2 days. The reaction was quenched with water and the mixture was extracted with ethyl acetate (3×3 mL). The combined organic phases were washed with brine and dried over anhydrous Na₂SO₄. After removing solvent, the residue was redissolved in CH₃CN and analyzed by LCMS. The formation of **33a** and **33b** were confirmed by both LCMS and HRMS. **33a:** HRMS-ESI (+) (*m/z*): [M-Br]⁺ calcd. for C₂₈H₂₇O₂PCl⁺, 461.1432; found: 461.1408. **33b:** HRMS-ESI (+) (*m/z*): [M-Br]⁺ calcd. for C₂₉H₂₉NO₃P⁺, 470.1880; found: 470.1839. (Note: the obtained amount of **33a** or **33b** was not sufficient to conduct NMR spectroscopic analysis due to an extremely slow and complex reaction).

ICL formation with duplex DNA: The ³²P-labeled oligonucleotide (0.5 μM) was annealed with 1.5 equiv of the complementary strand by heating to 90 °C for 5 min in potassium phosphate buffer (pH 7, 10 mM), followed by cooling to rt. The ³²P-labeled ODN duplex (2 μL, 0.5 μM) was then mixed with 1.0 M NaCl (2 μL), 100 mM potassium phosphate (2 μL, pH 8), and **27a-i** or **26a-i** (concentration range: 10 μM to 2 mM in 6 μL CH₃CN) and autoclaved distilled water to

give a final volume of 20 μL . The reaction was irradiated under UV (350 nm) until the reaction was completed, followed by quenching with an equal volume of 90% formamide loading buffer. The resulting mixture was then subjected to 20% denaturing polyacrylamide gel for electrophoresis.

Trapping assay of oligodeoxynucleotides: For carbocation trapping, the stock solution of $\text{MeONH}_2\cdot\text{HCl}$ (2.0 M) was titrated with NaOH (5 M) to adjust the pH to 7.0, which was then diluted to desired concentration (1/3-1000/3 mM). The solution (6 μL) was mixed with ^{32}P -labeled DNA duplex (2 μL , 0.5 μM), NaCl (2 μL , 1 M) potassium phosphate (2 μL , pH 8.0, 100 mM), compound (**27a-i**, **26a-i**) in 6 μL CH_3CN (optimized concentration was used for each compound) and water (2 μL) to give the desired concentration (final MeONH_2 concentration: 100 μM to 100 mM). For radical trapping reaction, 3 μL of TEMPO in CH_3CN (200/3 μM to 2000/3 mM) was mixed with the following solutions: ^{32}P -labeled DNA duplex (2 μL , 0.5 μM), NaCl (2 μL , 1 M), potassium phosphate (2 μL , pH 8.0, 100mM), compound (**27a-i**, **26a-i**) in CH_3CN (3 μL) (optimized concentration was used for each compound) and water (8 μL) as appropriate for the desired concentration (final TEMPO concentration: 10 μM to 100 mM). The reaction mixture was irradiated under UV (350 nm) for desired time (optimized time for each compound was used) and quenched with an equal volume of 90% formamide loading buffer, and then subjected to 20% denaturing polyacrylamide gel electrophoresis.

Stability study of ICL products formed with 17: The ^{32}P -labeled oligonucleotide duplex **17** (60 μL , 0.5 μM) was mixed with NaCl (12 μL , 1 M), 100 mM potassium phosphate (12 μL , pH 8.0) and compounds in CH_3CN (36 μL) (optimized concentration used for all the compounds). The reaction mixture was irradiated under UV for desired time (optimized time). After the cross-linking reaction, the DNA ICLs and the monoalkylated ODNs were purified by gel

electrophoresis. The isolated DNA fragments were dissolved in 60 μ L water, and divided into three portions equally. One portion was incubated with 1.0 M piperidine at 90 $^{\circ}$ C for 30 min, the second portion was incubated with 0.1 M NaCl and 10 mM potassium phosphate buffer (pH 7.0) under the same condition, and the third portion (without treatment) was used as control without heating. Solvent was removed under vacuum after heating. The resulting residue was dissolved in 90% formamide loading buffer, and then subjected to electrophoresis on a 20% denaturing polyacrylamide gel.

3.8. References

1. Fan H, Sun H, Peng X. Substituents Have a Large Effect on Photochemical Generation of Benzyl Cations and DNA Cross-Linking. *Chemistry - A European Journal*. 2018;24:7671–82.
2. Weinert EE, Frankenfield KN, Rokita SE. Time-Dependent Evolution of Adducts Formed between Deoxynucleosides and a Model Quinone Methide. *Chemical Research in Toxicology*. 2005;18:1364–70.
3. Modica E, Zanaletti R, Freccero M, Mella M. Alkylation of Amino Acids and Glutathione in Water by Quinone Methide. *Reactivity and Selectivity. The Journal of Organic Chemistry*. 2001;66:41–52.
4. Wang Y, Lin Z, Fan H, Peng X. Photoinduced DNA Interstrand Cross-Link Formation by Naphthalene Boronates via a Carbocation. *Chemistry - A European Journal*. 2016;22:10382–6.
5. Colloredo-Mels S, Doria F, Verga D, Freccero M. Photogenerated Quinone Methides as Useful Intermediates in the Synthesis of Chiral BINOL Ligands. *The Journal of Organic Chemistry*. 2006;71:3889–95.
6. Verga D, Nadai M, Doria F, Percivalle C, Antonio MD, Palumbo M, et al. Photogeneration and Reactivity of Naphthoquinone Methides as Purine Selective DNA Alkylating Agents. *Journal of the American Chemical Society*. 2010;132:14625–37.
7. Percivalle C, Doria F, Freccero M. Quinone Methides as DNA Alkylating Agents: An Overview on Efficient Activation Protocols for Enhanced Target Selectivity. *Current Organic Chemistry*. 2014;18:19–43

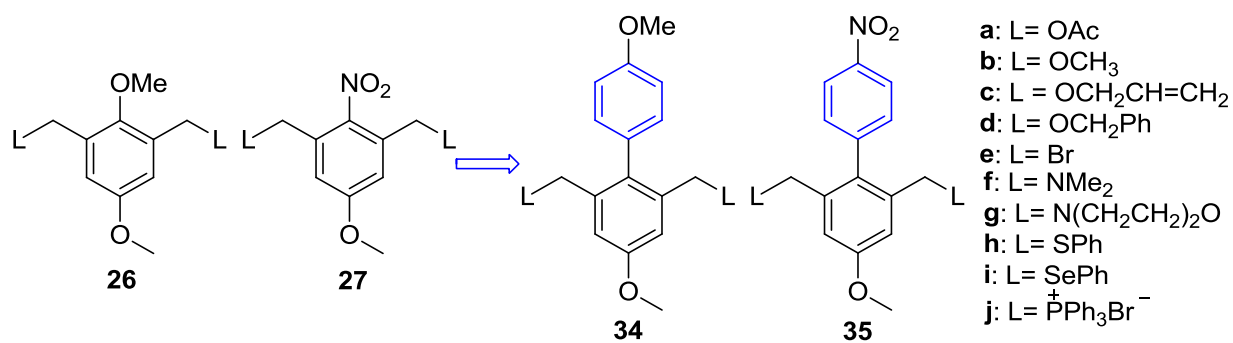
8. Weinert EE, Dondi R, Colloredo-Melz S, Frankenfield KN, Mitchell CH, Freccero M, et al. Substituents on Quinone Methides Strongly Modulate Formation and Stability of Their Nucleophilic Adducts. *Journal of the American Chemical Society*. 2006;128:11940–7.
9. Lin G, Li L. Oxidation and Reduction of the 5-(2'-Deoxyuridinyl)methyl Radical. *Angewandte Chemie International Edition*. 2013;52:5594–8.
10. Weng L, Horvat SM, Schiesser CH, Greenberg MM. Deconvoluting the Reactivity of Two Intermediates Formed from Modified Pyrimidines. *Organic Letters*. 2013;15:3618–21.
11. Stupi BP, Li H, Wang J, Wu W, Morris SE, Litosh VA, et al. Stereochemistry of Benzylic Carbon Substitution Coupled with Ring Modification of 2-Nitrobenzyl Groups as Key Determinants for Fast-Cleaving Reversible Terminators. *Angewandte Chemie International Edition*. 2012;51:1724–7.
12. Wang Y, Liu S, Lin Z, Fan Y, Wang Y, Peng X. Photochemical Generation of Benzyl Cations That Selectively Cross-Link Guanine and Cytosine in DNA. *Organic Letters*. 2016;18:2544–7.
13. Peng X, Hong IS, Li H, Seidman MM, Greenberg MM. Interstrand Cross-Link Formation in Duplex and Triplex DNA by Modified Pyrimidines. *Journal of the American Chemical Society*. 2008;130:10299–306.
14. Maxam AM, Gilbert W. Sequencing end-labeled DNA with base-specific chemical cleavages. *Nucleic Acids Part I Methods in Enzymology*. 1980;65:499–560.
15. Maxam AM, Gilbert W. A New Method for Sequencing DNA. *Proceedings of the National Academy of Sciences of the United States of America*. 1977, 74: 560–564.
16. Samuel APS, Xu J, Raymond KN. Predicting Efficient Antenna Ligands for Tb(III) Emission. *Inorganic Chemistry*. 2009;48:687–98.
17. Jacques SA, Michaelis S, Gebhardt B, Blum A, Lebrasseur N, Larrosa I, et al. Studies on the Total Synthesis of Lactonamycin: Synthesis of the Fused Pentacyclic B-F Ring Unit. *European Journal of Organic Chemistry*. 2012;107–13.
18. Witiak DT, Loper JT, Ananthan S, Almerico AM, Verhoef VL, Filppi JA. Mono and bis(bioreductive) alkylating agents: synthesis and antitumor activities in a B16 melanoma model. *Journal of Medicinal Chemistry*. 1989;32:1636–42.
19. Schmelzeisen-Redeker G, Röllgen FW, Wirtz H, Vögtle F. Thermospray mass spectrometry of diazonium and di-, tri- and tetra-quaternary onium salts. *Organic Mass Spectrometry*. 1985;20:752–6.

Chapter 4. The Effects of Core Structure and Leaving Groups on Photo-induced DNA Cross-linking

4.1. Introduction

Previous studies indicated that both aromatic substituents and benzylic leaving groups affected DNA ICL efficiency. Compounds with OMe as a substituent (**26**) showed higher photo-reactivity and DNA cross-linking efficiency than the corresponding compounds (**27**) with nitro as a substituent (Chapter 3). Among them, compounds with OMe as a substituent and phenyl sulfide or phenyl selenide as a leaving group showed the highest photo-reactivity towards DNA (shortest reaction time: 2 h).

However, there are still some unsolved problems for these two classes of compounds. First, most of the compounds studied have poor UV absorption above 300 nm, which limited their applications in biological context, because many biomolecules have UV absorption under 300 nm. The UV irradiation at or > 350 nm is more compatible in biological systems.¹ Thus, we expect to develop compounds with maximum absorbance (λ_{max}) in longer wavelength period. Second, apart from ICL formation, DNA strand breaks were observed for compounds containing methoxy group with a high concentration or by exposure to UV irradiation for a long time. It is possibly due to the presence of a strong electron donating methoxy group that highly increased the photo-reactivity of these compounds and led to unwanted side reactions. Third, compounds containing NO₂ group showed poor photo-reactivity and low DNA cross-linking efficiency, possibly due to the strong electron withdrawing property of NO₂.



Scheme 4-1. The structures of **34a-j** and **35a-j**.

Herein, we designed and synthesized **34a-j** and **35a-j** by introducing a benzene ring to the existing structure **26** and **27** with the expectation of increasing the wavelength of maximum absorbance (λ_{\max}) and reducing the electronic effects of OMe and NO₂ groups. The extended π system is expected to lead to red shift of the wavelength of maximum absorbance (λ_{\max}). In addition, the reduced inductive effects, bridged by an aromatic ring, may reduce the electronic effects of OMe or NO₂ group. We performed a detailed study on how the substituents, leaving groups, and core structure affect the photo-reactivity of these compounds toward DNA, DNA cross-linking efficiency, mechanism pathways, and DNA cross-linking sites. The information obtained shed light on further design of novel photo-inducible DNA cross-linking agents as potential antitumor drugs and for other biological applications.

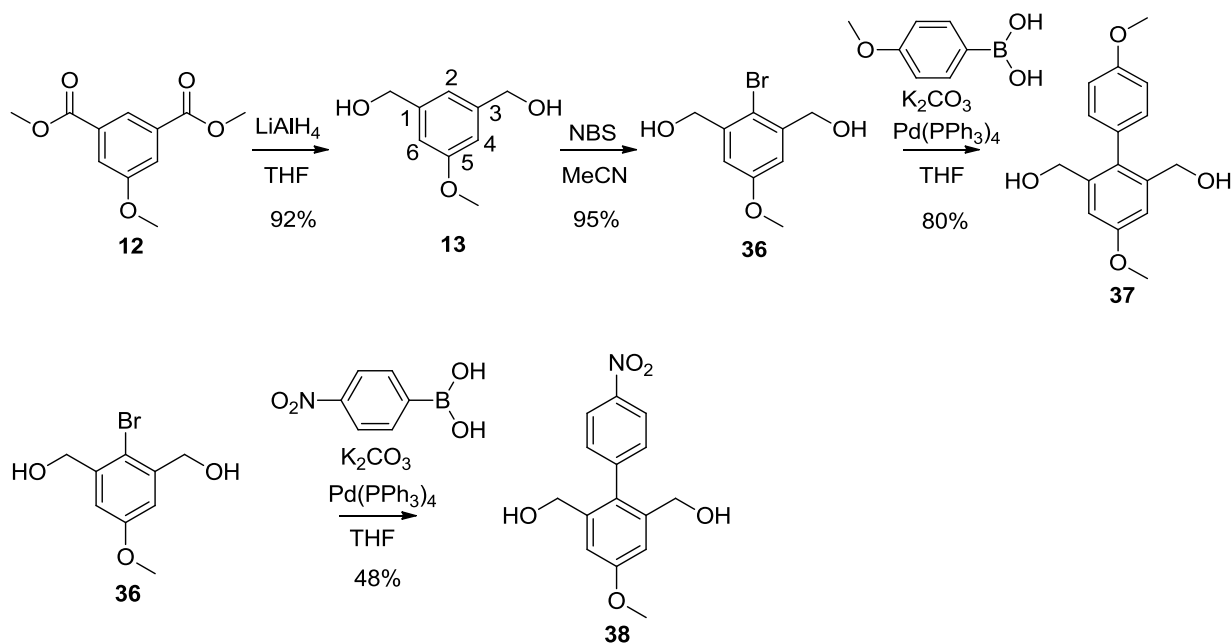
4.2. Modification of core structure to improve DNA cross-linking efficiency

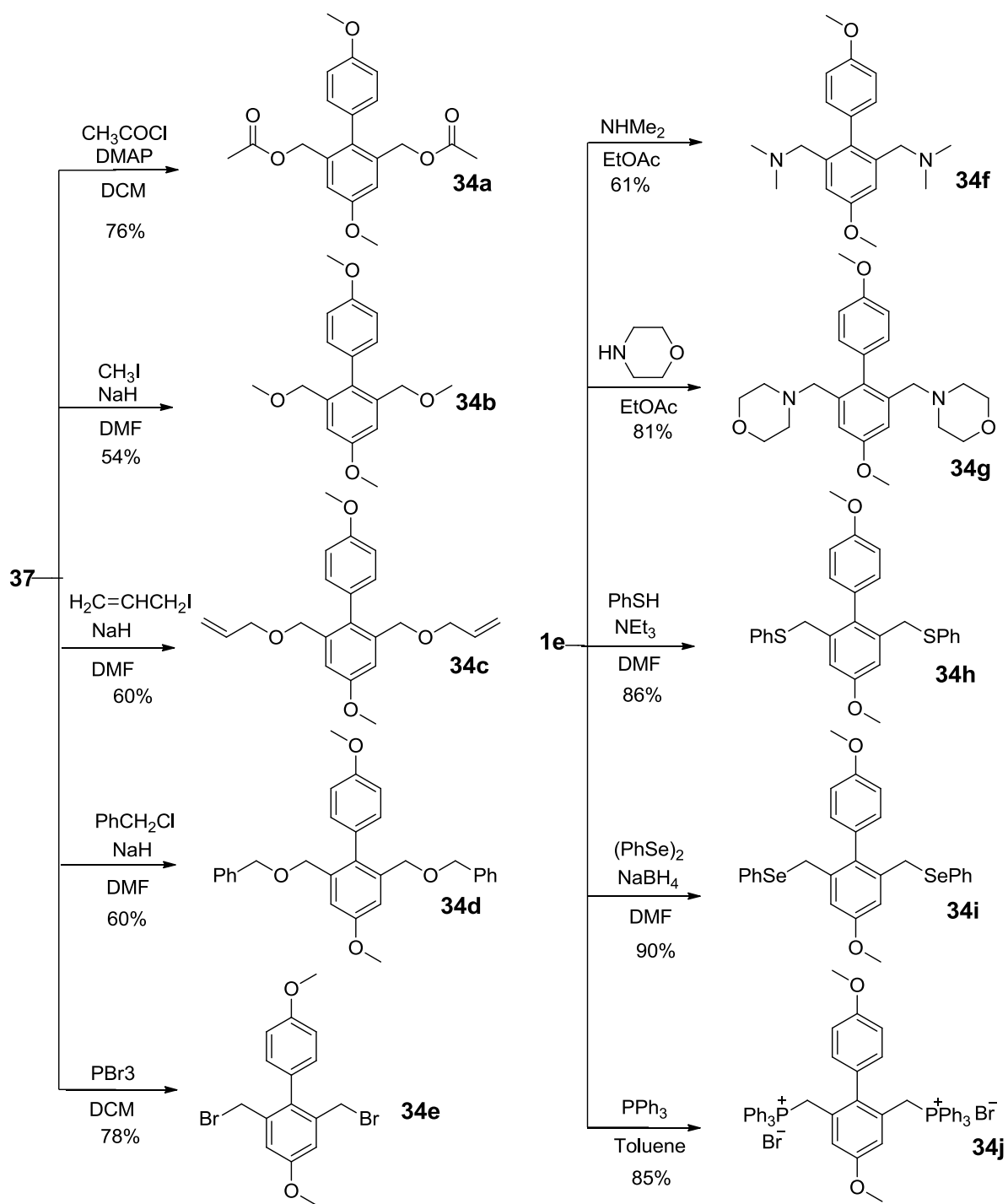
4.2.1. Synthesis of compounds with different core structure and various leaving groups

The general synthetic route is based on our previous work [Chapter 3]. Compound **37** was synthesized starting from compound **12** that was reduced to benzyl dialcohol **13** (Scheme 4-2). Bromination of **13** at the position-2 afforded **36** that was converted to **37** via metal catalyzed Suzuki coupling reaction. Then, compound **37** was transformed to **34a-e** by reacting with the

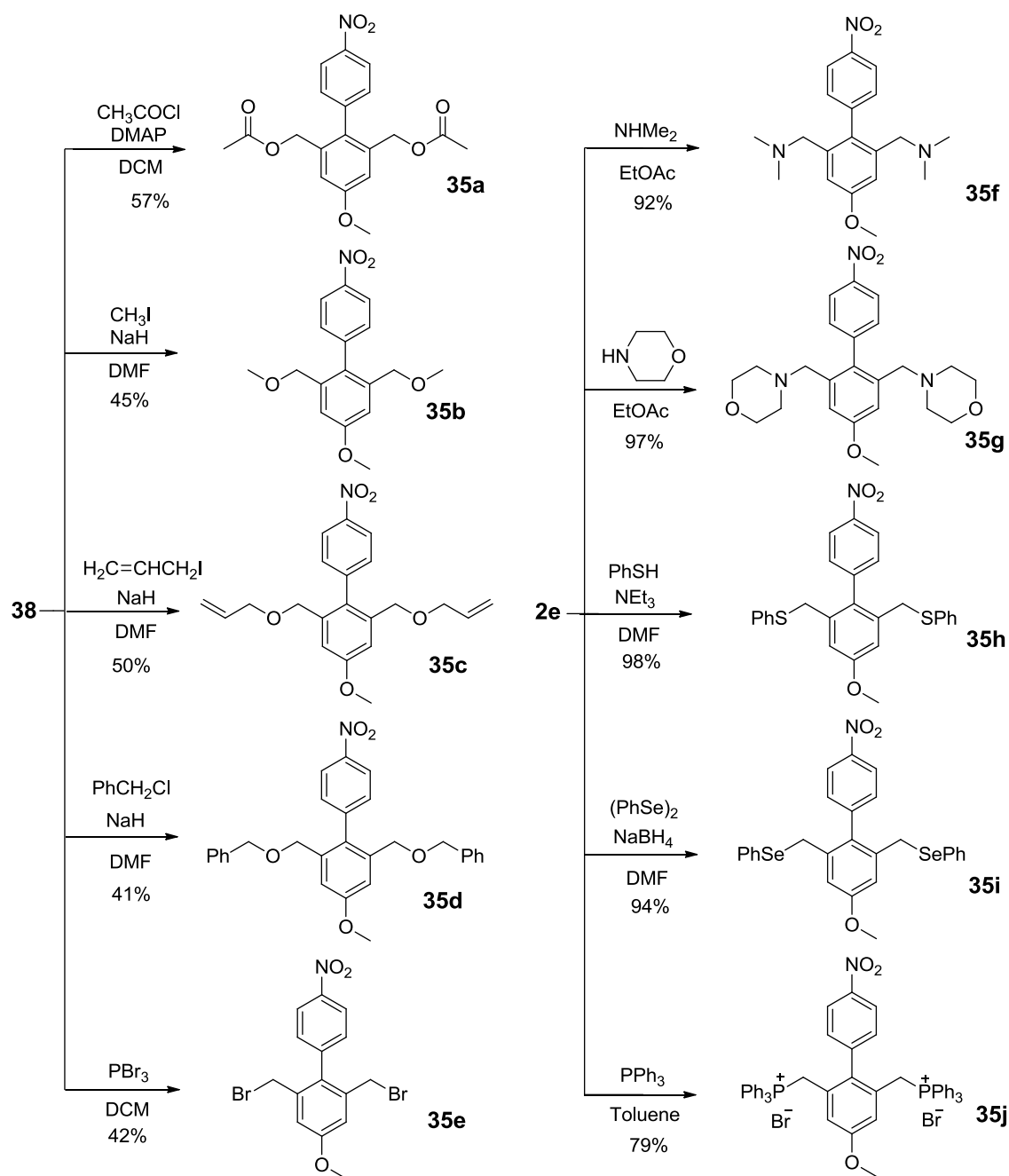
corresponding electrophiles via basic nucleophilic substitution reactions. Finally, compounds **34f-j** were prepared from **34e** by reacting with the corresponding nucleophiles.

A synthetic route similar as **34a-j** was employed to synthesize **35a-j**. Compound **36** was first converted to **38** via metal catalyzed Suzuki coupling reaction, which was then used as starting material to prepare **35a-e** via substitution reactions accordingly. Compounds **35f-j** was synthesized from **35e** by reacting with various nucleophiles. (Scheme 4-3)





Scheme 4-2. Synthesis of **34a-j**.



Scheme 4-3. Synthesis of **35a-j**.

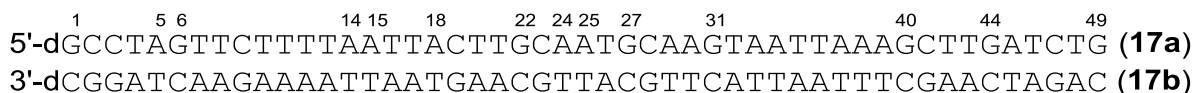
4.2.2. DNA interstrand cross-linking assay.

The photo reactivity of **34a-j** and **35a-j** towards DNA was determined using a 49-mer DNA duplex (**17**) in a phosphate buffer (pH 8.0) upon photoirradiation at 350 nm. Denaturing

polyacrylamide gel electrophoresis (PAGE) was used for DNA cross-linking analysis or adducts purification. No ICL formation was observed without photoirradiation, while efficient DNA cross-linking was obtained upon UV irradiation at 350 nm. Our previous study showed that the photo-induced DNA ICL efficiency highly relied on the irradiation time and the concentration of the corresponding compounds.² In order to obtain the optimized reaction condition for all compounds, we determined the reaction time and concentration required for each compound to complete the DNA cross-linking reaction (Table 4-1 and Appendix A).

In general, the DNA ICL yield increased gradually with increasing irradiation time until reaching the best yield, where the DNA alkylation was completed and further increased irradiation time would not increase the DNA ICL yields. The time-dependent study indicated that both aromatic substituents and benzylic leaving groups affect the reaction rate of the ICL formation. However, to our surprise, most of compounds with a strong electron withdrawing substituent have faster reaction rate for DNA ICL formation than the corresponding compounds with OMe group. Compounds **35a-d** and **35h-j** with an electron withdrawing NO₂ substituent showed faster reaction rate than **34a-d** and **34h-j** with an OMe substituent. However, an opposite trend was observed for **35e-g** and the corresponding **34e-g**. Compounds with the same aromatic substituent but different leaving groups showed different reaction rates, indicating that leaving groups also affected the photo-reactivity of these compounds toward DNA. The reaction rates for **34a-j** follow the order of **34j**>**34a**>**34d-34f**>**34b**>**34g**, **34h**>**34i**>**34c**, while that of **35a-j** is in the order of **35a**, **35j**>**35b**, **35c**>**35d**>**35e**>**35h**, **35i**>**35f**>**35g**. For both classes of compounds, **34a** and **35a** with an ester as a leaving group (OAc) and **34j** and **35j** with triphenylphosphonium as a leaving group showed faster reaction rate than other compounds, which suggested that the good leaving

property of OAc and triphenylphosphonium facilitate the photo-induced cation formation and subsequent DNA cross-linking.



17

Table 4-1. The optimized conditions, ICL yields, and UV absorption data for **34a-j** and **35a-j**.^a

Compound R = OMe (34a-j)	Reaction Time (h)	Con. ^b (mM)	ICL (%) ^c	λ_{\max} (nm)	$\epsilon_{\lambda_{\max}}$ (M ⁻¹ ·cm ⁻¹)
34a L=OAc	12	0.5	30.5 ± 3	278	3500
34b L=OCH ₃	24	0.4	31.2 ± 3	278	3700
34c L=OCH ₂ CH=CH ₂	44	0.6	10.2 ± 1	278	3400
34d L=OCH ₂ Ph	16	0.5	29.7 ± 2	278	3500
34e L=Br	16	0.5	30.4 ± 3	304	3250
34f L=NMe ₂	16	0.05	31.5 ± 4	279	3760
34g L=N(CH ₂ CH ₂) ₂ O	32	0.2	28.1 ± 1	279	3450
34h L=SPh	32	0.5	26 ± 2	295	6720
34i L=SePh	36	0.3	14.6 ± 2	296	7150
34j (L= PPh ₃ ⁺ Br ⁻)	10	0.2	28.0 ± 3	302	4460
R = NO₂ (35a-j)					
35a L=OAc	1.5	0.4	45.5 ± 4	272	11800
35b L=OCH ₃	2.5	0.4	36.0 ± 3	272	10000
35c L=OCH ₂ CH=CH ₂	3	0.3	30.8 ± 3	272	9650
35d L=OCH ₂ Ph	10	0.5	30.6 ± 2	273	9500
35e L=Br	20	0.5	36.0 ± 4	293	8600
35f L=NMe ₂	28	0.6	24.5 ± 2	266	9500
35g L=N(CH ₂ CH ₂) ₂ O	36	0.5	17.6 ± 2	266	8540
35h L=SPh	24	0.5	27.0 ± 3	287	13000
35i L=SePh	24	0.5	15.0 ± 1	292	11000
35j (L= PPh ₃ ⁺ Br ⁻)	1.5	0.5	33.4 ± 3	268, 301	14700, 9070

^a The DNA cross-linking reaction was performed in a pH 8 phosphate buffer with 50 nM DNA duplex **17** upon 350 nm irradiation.

^bThe minimum concentration needed to obtain the highest DNA cross-linking efficiency.

^c The maximum DNA ICL yield obtained for each compound under optimized conditions (all data are the average of three experiments).

In order to determine the optimal concentration for achieving the highest DNA cross-linking efficiency, the concentration-dependent DNA cross-link study was performed with the optimized reaction time for each substrate. In general, the DNA ICL yields increased gradually with increasing concentration of compounds until reaching the maximum yield, where further increased concentration would not obviously alter DNA ICL yields. The optimized concentration is 0.05 mM for **34f**, 0.2 mM for **34g** and **34j**, 0.3 mM **34i** and **35c**, 0.4 mM for **34b**, **35a** and **35b**, 0.5 mM for **34a**, **34d**, **34e**, **34h**, **35d**, **35e**, **35g-j**, and 0.6 mM for **34c** and **35f** (Table 4-1 and Appendix A). For all tested compounds, **35a-j** with a strong electron withdrawing substituent (NO₂) generated a higher ICL yield than corresponding compounds bearing an electron donating substituent (OMe) with the exception of **35f** and **35g** that led to lower ICL yields than **34f** and **34g**, respectively. This indicated that the aromatic substituents have significant effects on ICL formation. On the other hand, compounds with the same substituent but different benzylic leaving groups showed different ICL yields, indicating that benzylic leaving groups also affect DNA ICL formation. For compounds **34a-j**, DNA ICL efficiency is in the following order: most of them showed similar and high ICL yields (26%-32%) with the order **34f**, **34b**>**34a**, **34e**>**34d**>**34g**>**34j**>**34h**>**34i**>**34c**, while **34c** and **34i** showed similar but much lower ICL yields (10%, 15%). For nitro compounds, **35a** showed the highest ICL yield, followed by **35b**, **35e** and **35j**, then **35c**, **35d**, **35h** and **35f**, while **35g** and **35i** have the lowest ICL yield. Since the optimized concentrations for different compounds varied, it is hard to compare the ICL efficiency under optimized concentration. To better understand how the aromatic substitutions and benzylic leaving groups affect the DNA ICL efficiency, further DNA cross-link study was carried out under the same concentration (500 μM) with the optimized reaction time for each

substrate (Figure 4-1). For both classes of compounds, the trend of DNA ICL yields at 500 μM was similar as that obtained with optimized concentration.

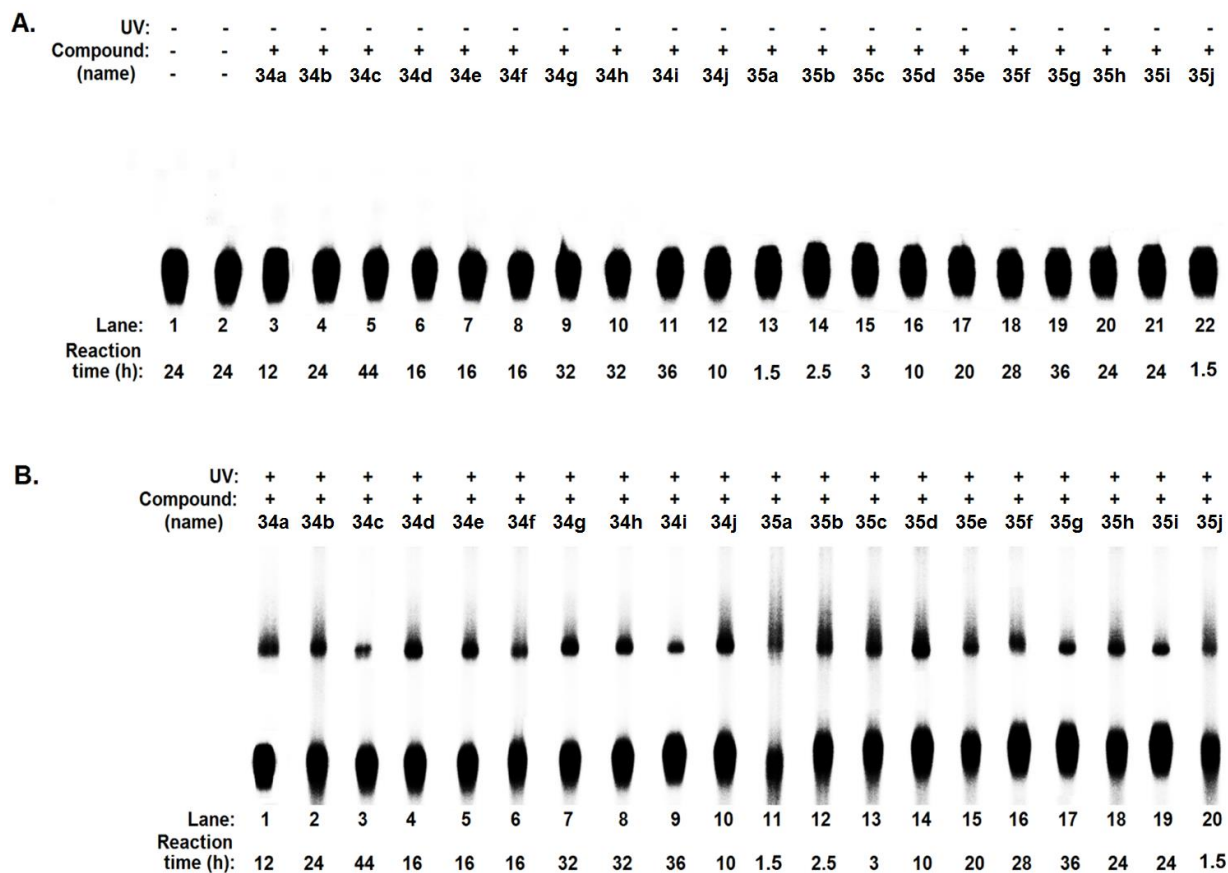


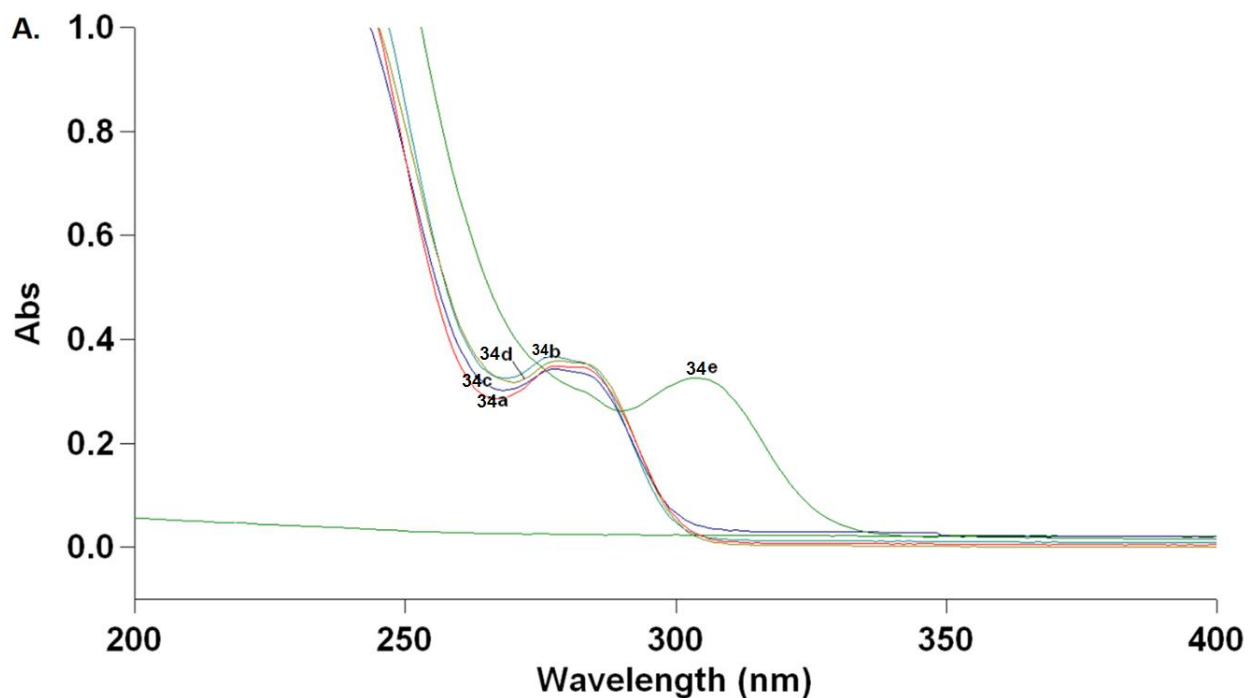
Figure 4-1. Photo-induced DNA ICL formation for **34a-j** and **35a-j**. **A.** Lane 1: DNA without UV irradiation; lane 2: DNA with UV irradiation at 350 nm for 24 h; lanes 3-22: DNA with the drug (500 μM) but no UV irradiation at 350 nm for designed time; **B.** lanes 1-20: DNA with the drug (500 μM) upon irradiation at 350 nm for designed time: lane 1: **34a** (ICL yield, $30.5 \pm 3\%$); lane 2: **34b** (ICL yield, $32.1 \pm 3\%$); lane 3: **34c** (ICL yield, $9.4 \pm 1\%$); lane 4: **34d** (ICL yield, $29.7 \pm 2\%$); lane 5: **34e** (ICL yield, $30.4 \pm 3\%$); lane 6: **34f** (ICL yield, $32.1 \pm 4\%$); lane 7: **34g** (ICL yield, $29.0 \pm 3\%$); lane 8: **34h** (ICL yield, $26.0 \pm 3\%$); lane 9: **34i** (ICL yield, $15.0 \pm 2\%$); lane 10: **34j** (ICL yield, $28.6 \pm 4\%$). lane 11: **35a** (ICL yield, $46.6 \pm 3\%$); lane 12: **35b** (ICL

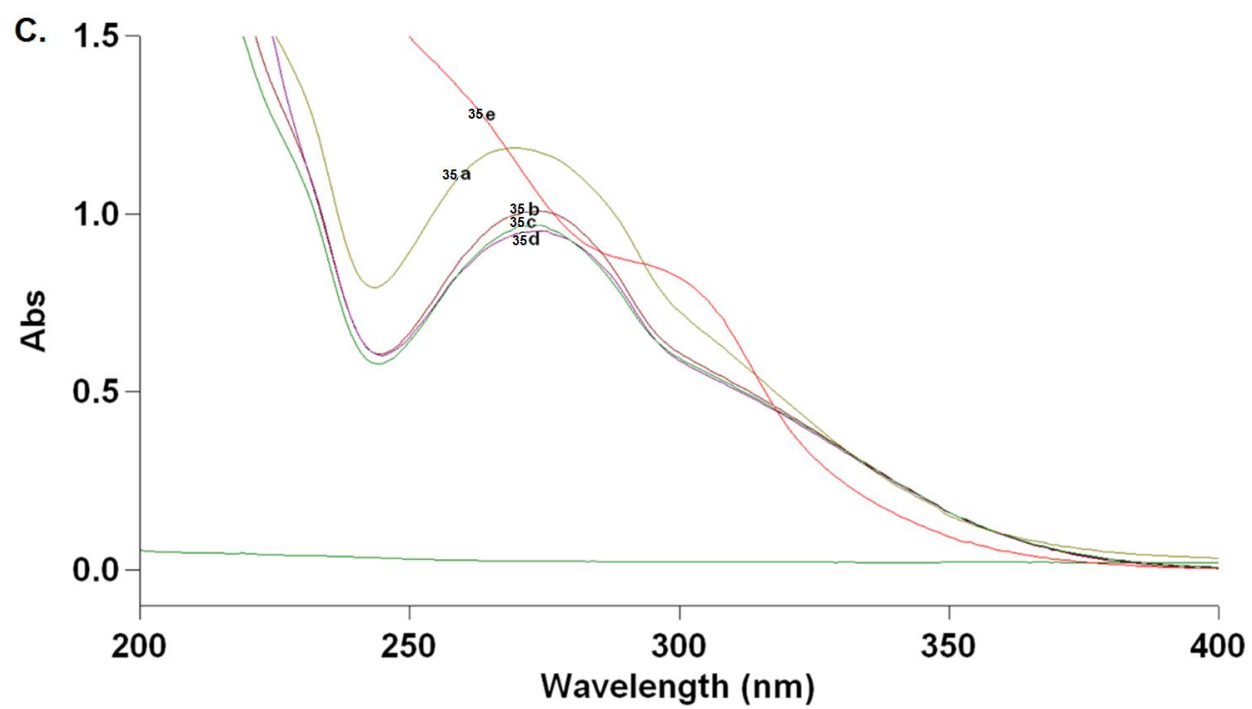
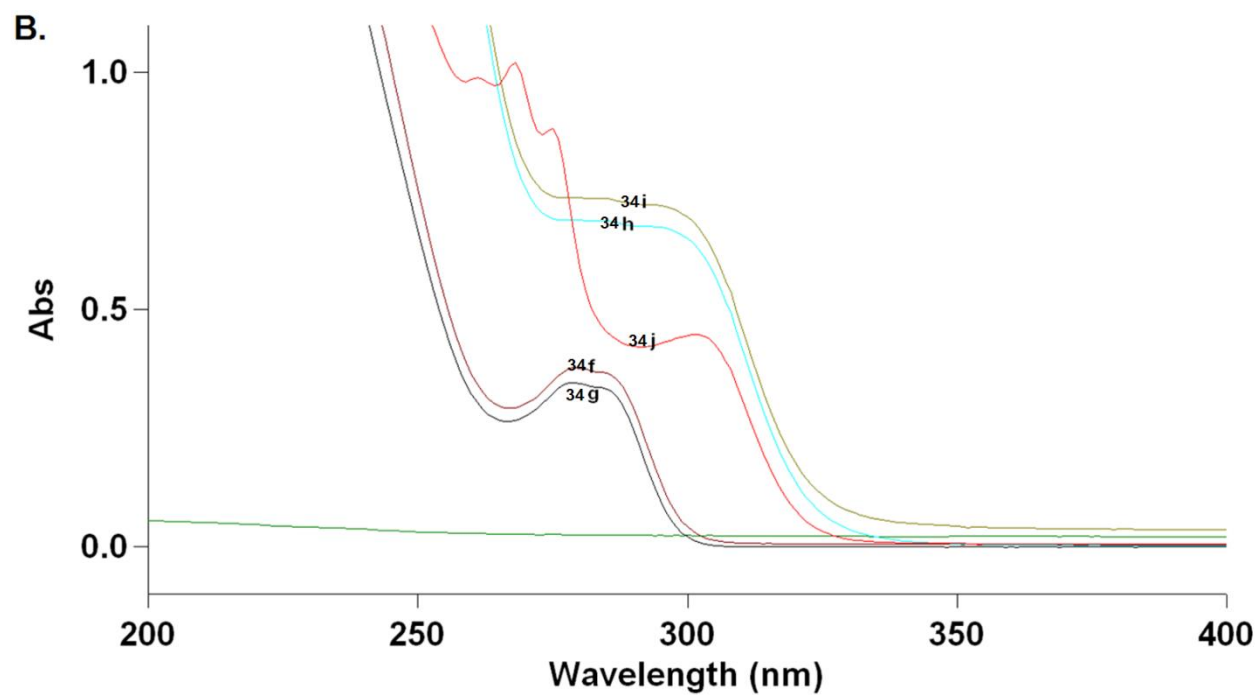
yield, $36.7 \pm 4\%$) ; lane 13: **35c** (ICL yield, $31.4 \pm 2\%$); lane 14: **35d** (ICL yield, $30.6 \pm 3\%$); lane 15: **35e** (ICL yield, $36.0 \pm 2\%$); lane 16: **35f** (ICL yield, $23.4 \pm 2\%$); lane 17: **35g** (ICL yield, $17.6 \pm 1\%$); lane 18: **35h** (ICL yield, $27.0 \pm 3\%$); lane 19: **35i** (ICL yield, $15.0 \pm 2\%$); lane 20: **35j** (ICL yield, $33.4 \pm 3\%$). All DNA ICL yields were obtained by triplicate experiments and shown as average \pm standard deviation.

Correlation between UV absorbance and the photo-reactivity.

UV-Vis spectra of compounds **34a-j** and **35a-j** were measured at a concentration of 500 μ M in acetonitrile (Table 4-1 and Figure 4-2). In general, compounds with a NO₂ group showed slightly shorter wavelength of maximum absorbance (λ_{\max}) but much stronger absorption than the corresponding compounds with OMe group. The stronger UV absorption may explain why the nitro compounds have higher photo-reactivity toward DNA than the OMe ones. For compounds **34a-j**, the UV absorption spectra for **34a-d**, **34f** and **34g** are very similar. They have similar wavelength of maximum absorbance (λ_{\max}) with slightly different strength of UV absorbance. The relationship between UV absorption and reaction rate seems not clear, while the ICL yield is consistent with the strength of the UV absorption with the exception of **34c**. For example, the order of photo-induced DNA ICL yield is **34f** \approx **34b** > **34a** \approx **34d** > **34g**, which is consistent with the order of UV absorption strength **34f** \approx **34b** > **34a** \approx **34d** > **34g**. Absorption spectra of **34e** and **34h-i** are red-shifted. In particular, **34e** and **34j** showed more red-shift than **34h** and **34i**. Accordingly, **34e** and **34j** showed higher photo reactivity toward DNA as shown by faster reaction rate and higher ICL yield than **34h** and **34i**. For nitro compounds, **35a-d** have the same wavelength of maximum absorbance (λ_{\max}) while the strength of the UV absorption ($\epsilon_{\lambda_{\max}}$) follows the order of **35a** > **35b** > **35c** > **35d**, which was consistent with the order of ICL efficiency **35a** > **35b** > **35c** > **35d**. Compounds **35f** and **35g** have shorter wavelength of

maximum absorbance (λ_{max}) (266 nm), which in turn showed lower ICL efficiency (a longer reaction time and a lower ICL yield). Compounds **35e** and **35h-j** showed obvious red-shift with an order of **35j** > **35e** > **35h** for the extent of red shift that is consistent with the order of reaction rates (**35j** > **35e** > **35h**) with the exception of **35i**. However, the order of ICL yields (**35e** > **35j** > **35h** > **35i**) does not match with the order of UV absorbance (**35j** > **35e** > **35i** > **35h**) (Table 4-1 and Figure 4-2).





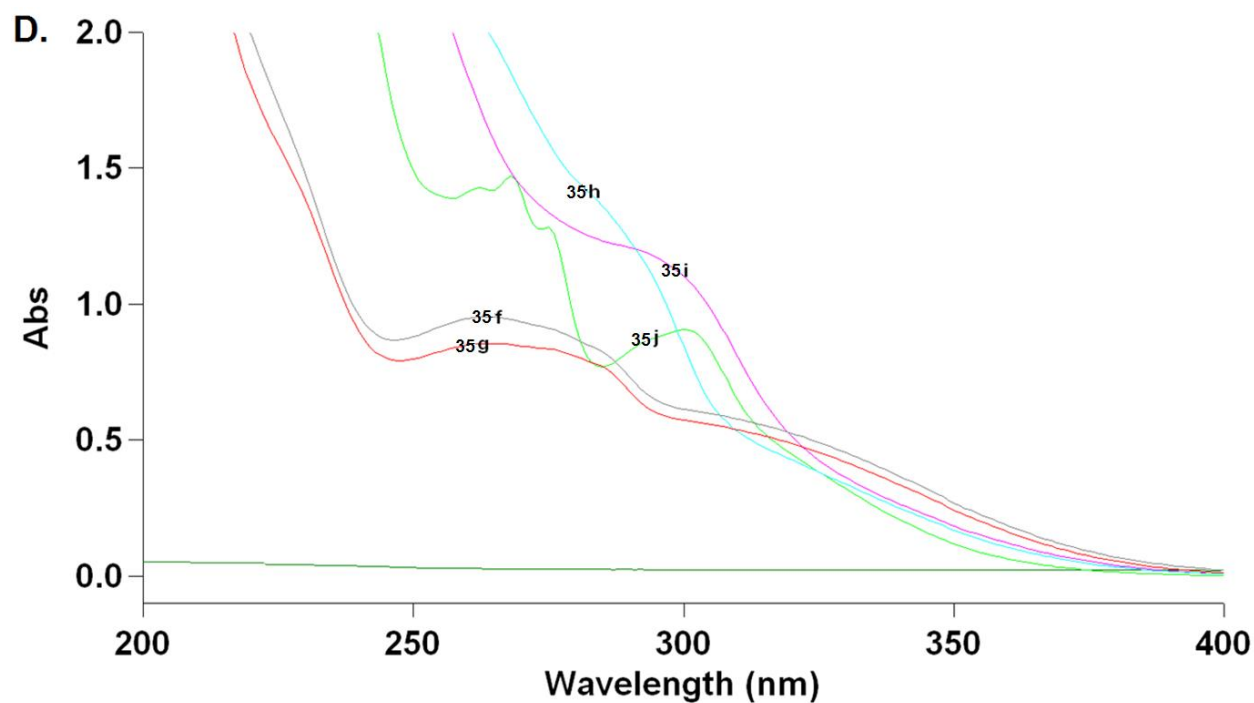
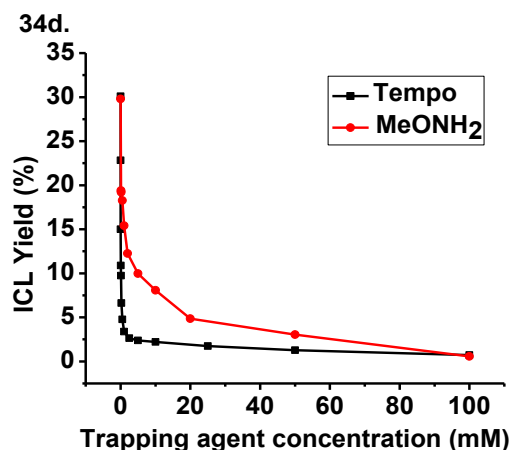
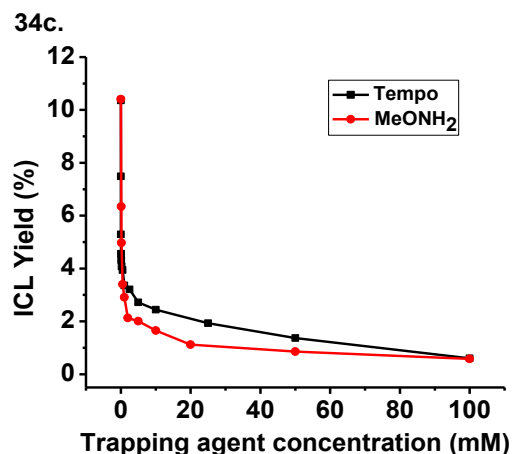
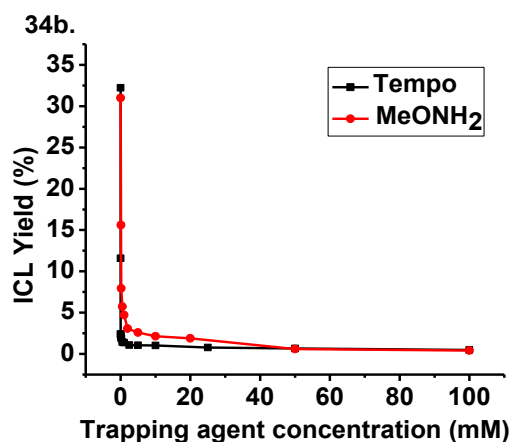
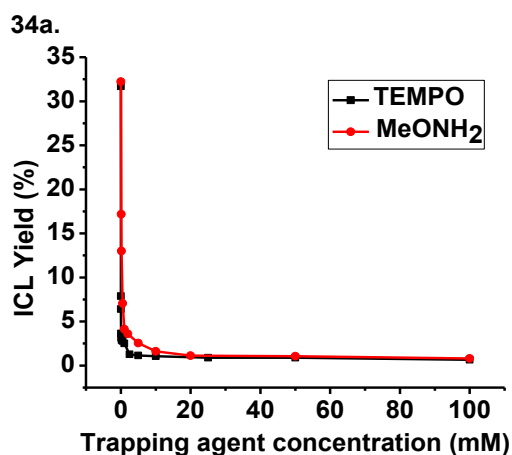


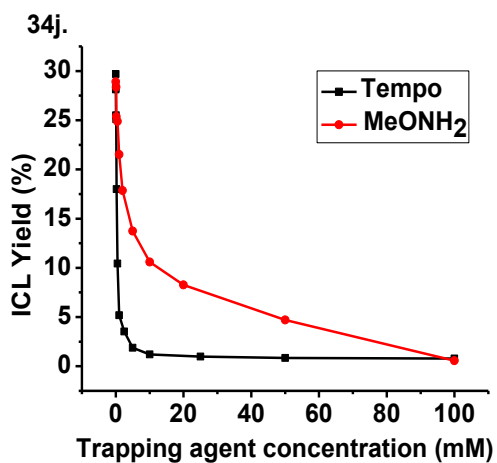
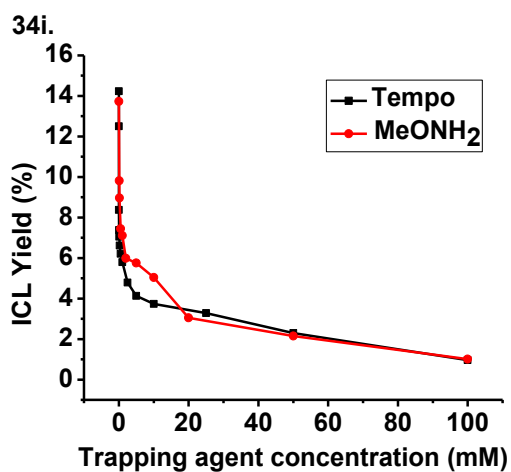
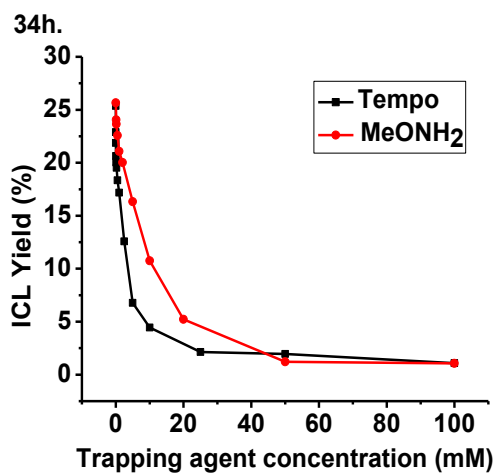
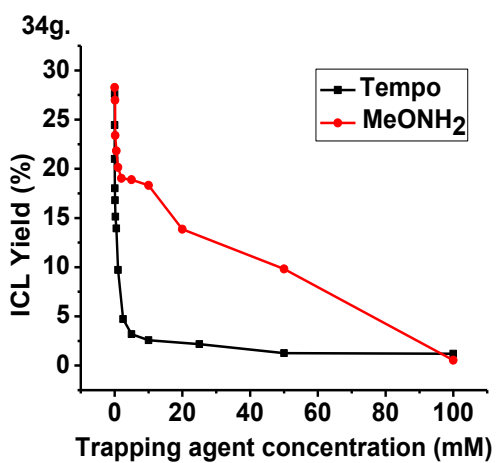
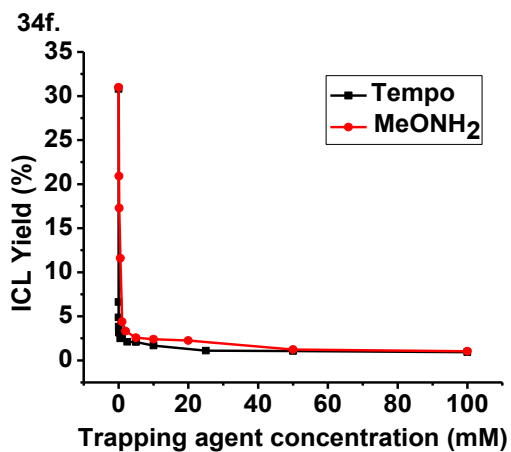
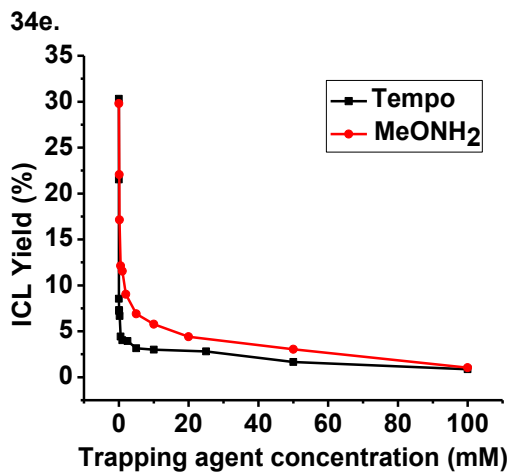
Figure 4-2. UV spectra for **34a-j** and **35a-j** (500 μ M).

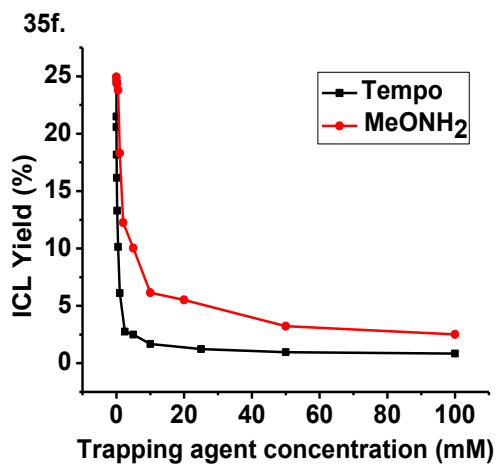
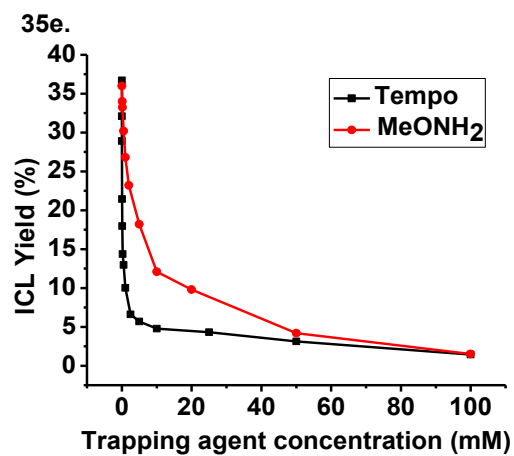
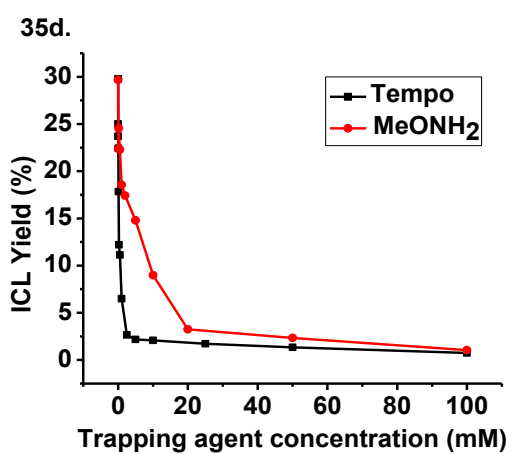
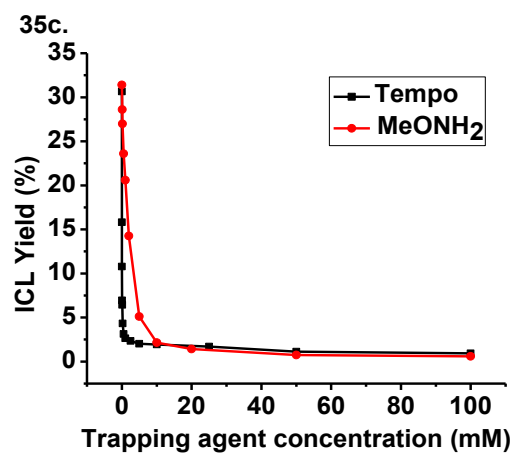
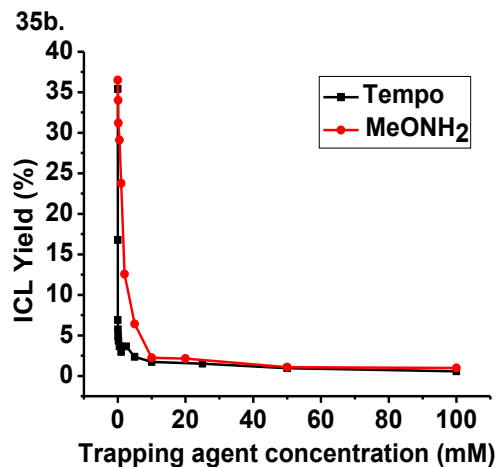
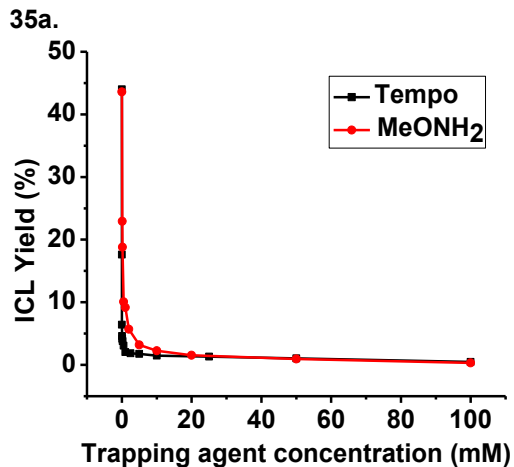
4.2.3. Mechanism of DNA ICL formation.

Previous study showed aromatic substitution greatly affected the photochemical generation of benzyl cations.³ However, there were limited examples about how the benzylic leaving groups and core structure affect the photochemical generation of carbocation and subsequent DNA ICL formation. To further investigate whether the benzylic leaving groups and core structure influence the pathways of ICL formation, we performed free radical and carbocation trapping experiments separately under the optimized DNA cross-linking conditions. Similar to previous study, TEMPO was used to trap free radicals, while methoxyamine was used as a carbocation trapping agent. The effect of TEMPO and methoxyamine on ICL formation was shown in Figure 4-3. The DNA ICL yields decreased gradually for all compounds with increasing concentration of methoxyamine. Almost no ICL was produced when the concentration of methoxyamine went

up to 100 mM. Similar results were observed for TEMPO trapping reactions. The addition of TEMPO suppressed the DNA cross-linking process while 100 mM of TEMPO totally quenched the DNA cross-link reaction. These results suggested that both carbocations and radicals were involved in the photo-induced DNA cross-linking process, and the carbocations were generated via free radical oxidation. The proposed mechanism was shown in Scheme 4-4. Photo-irradiation of compounds **34a-j** or **35a-j** generated free radicals (**39**) that are further oxidized to the corresponding carbocations (**40**) that directly produce DNA ICL formation.







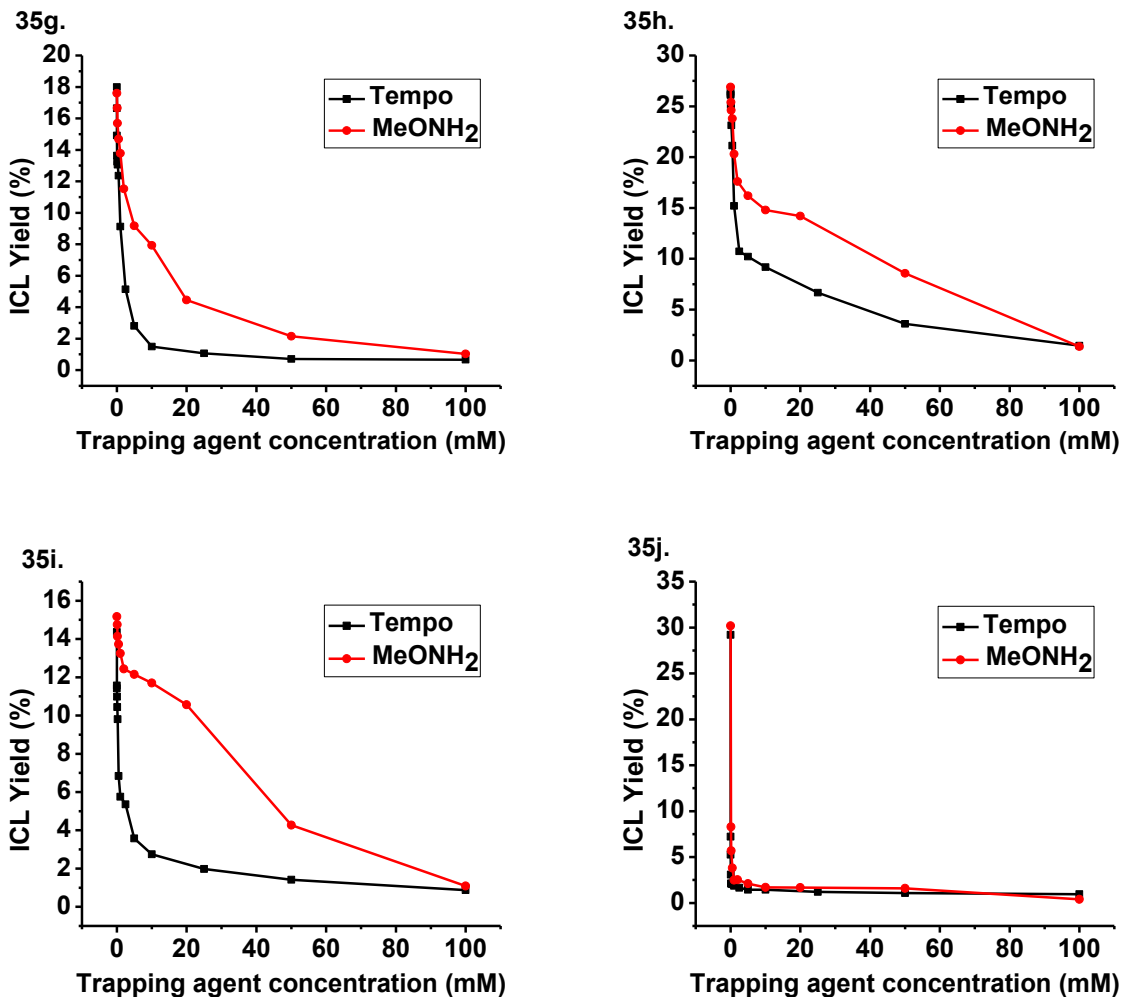
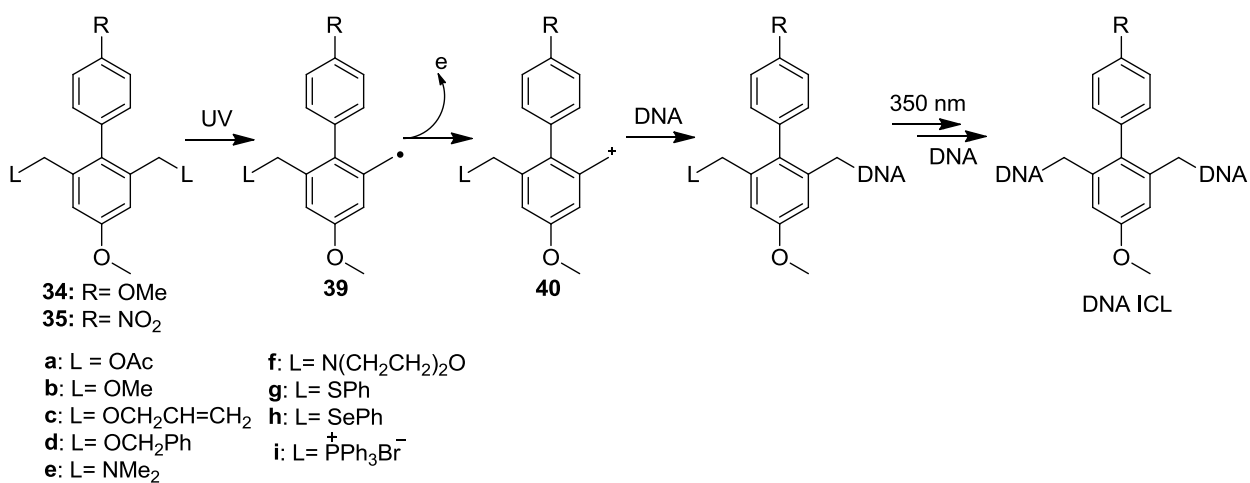


Figure 4-3. Carbocation and radical trapping of DNA ICL formation for **34a-j** and **35a-j**.



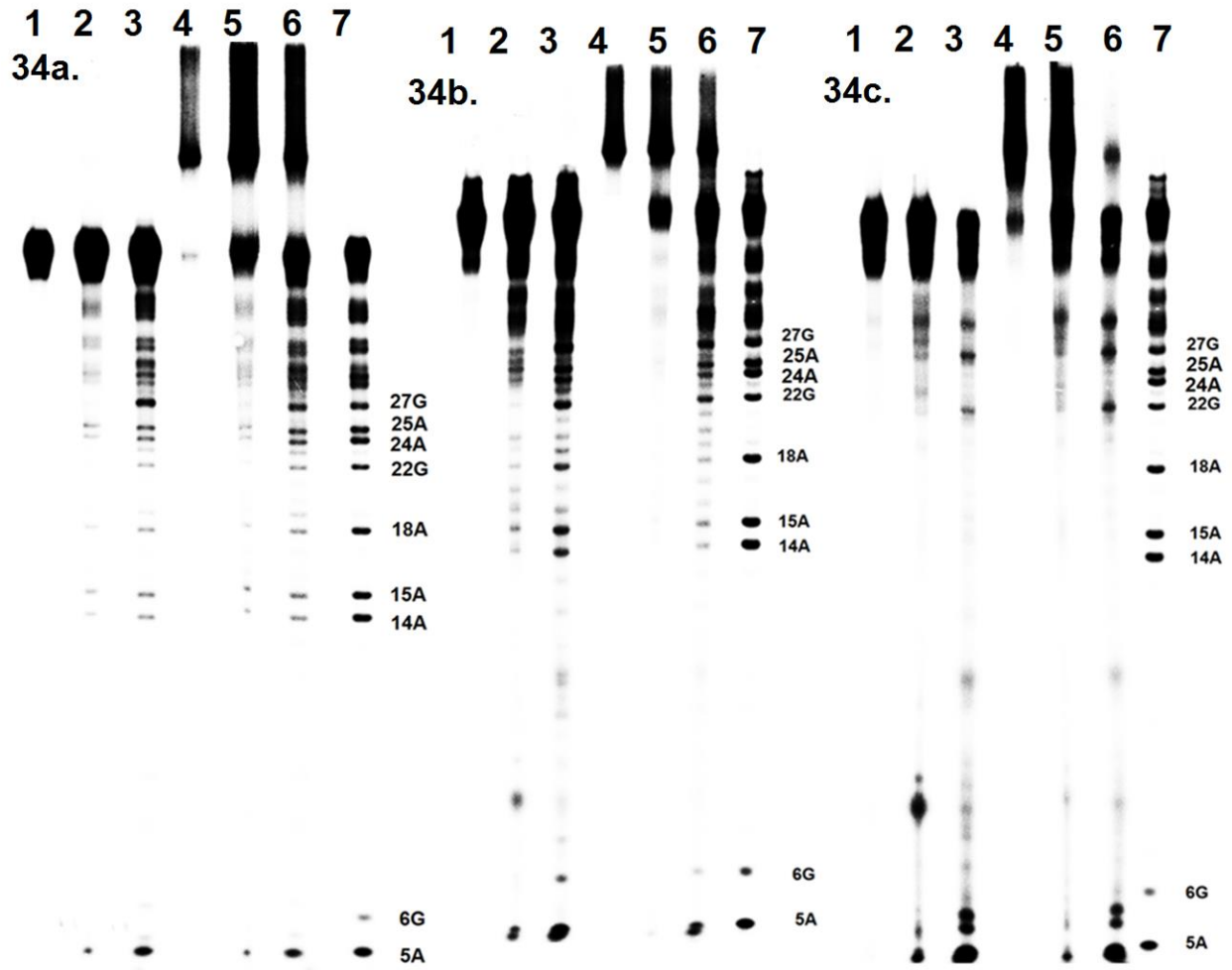
Scheme 4-4. Proposed mechanism for DNA ICL formation.

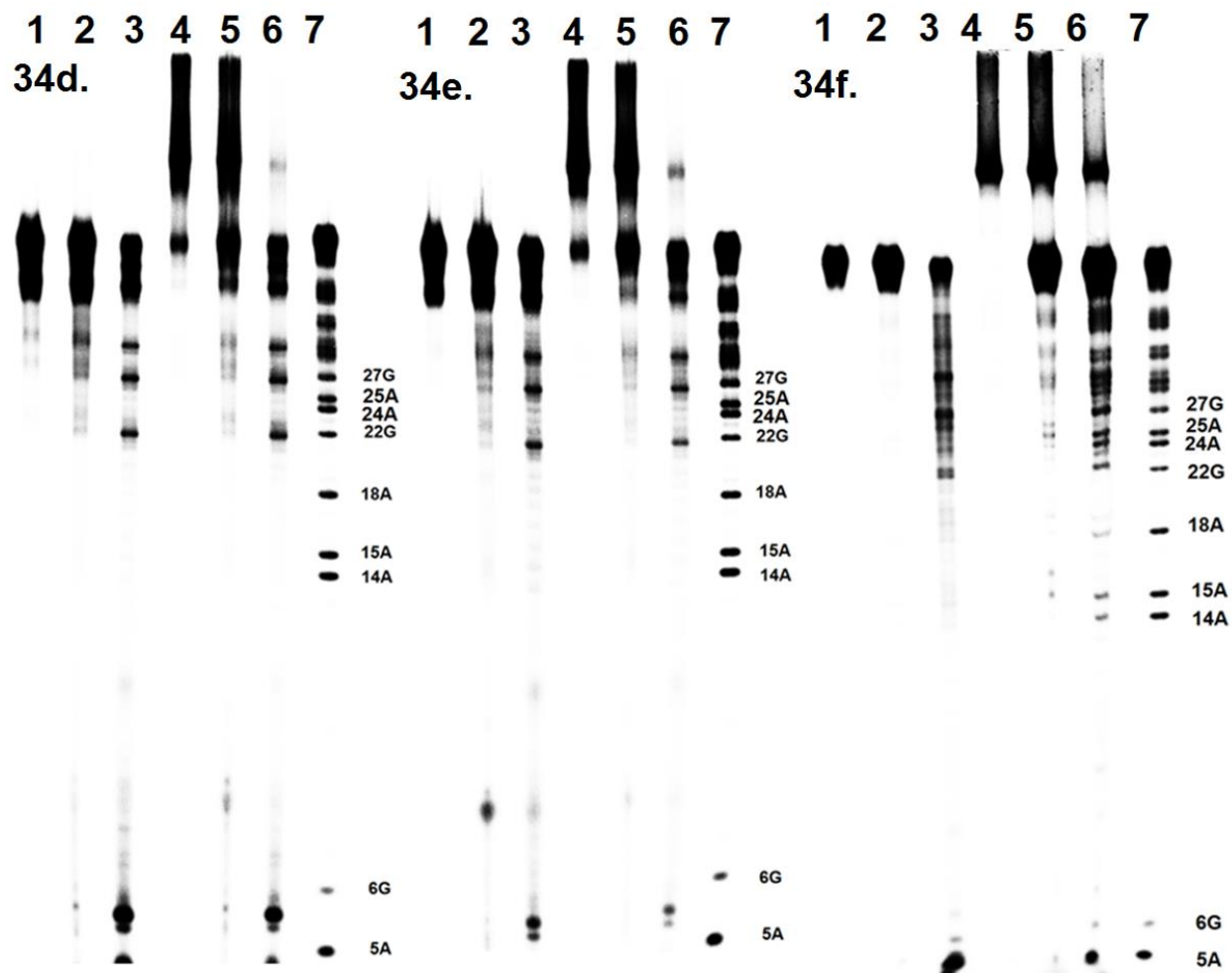
4.2.4. Determination of DNA alkylation sites.

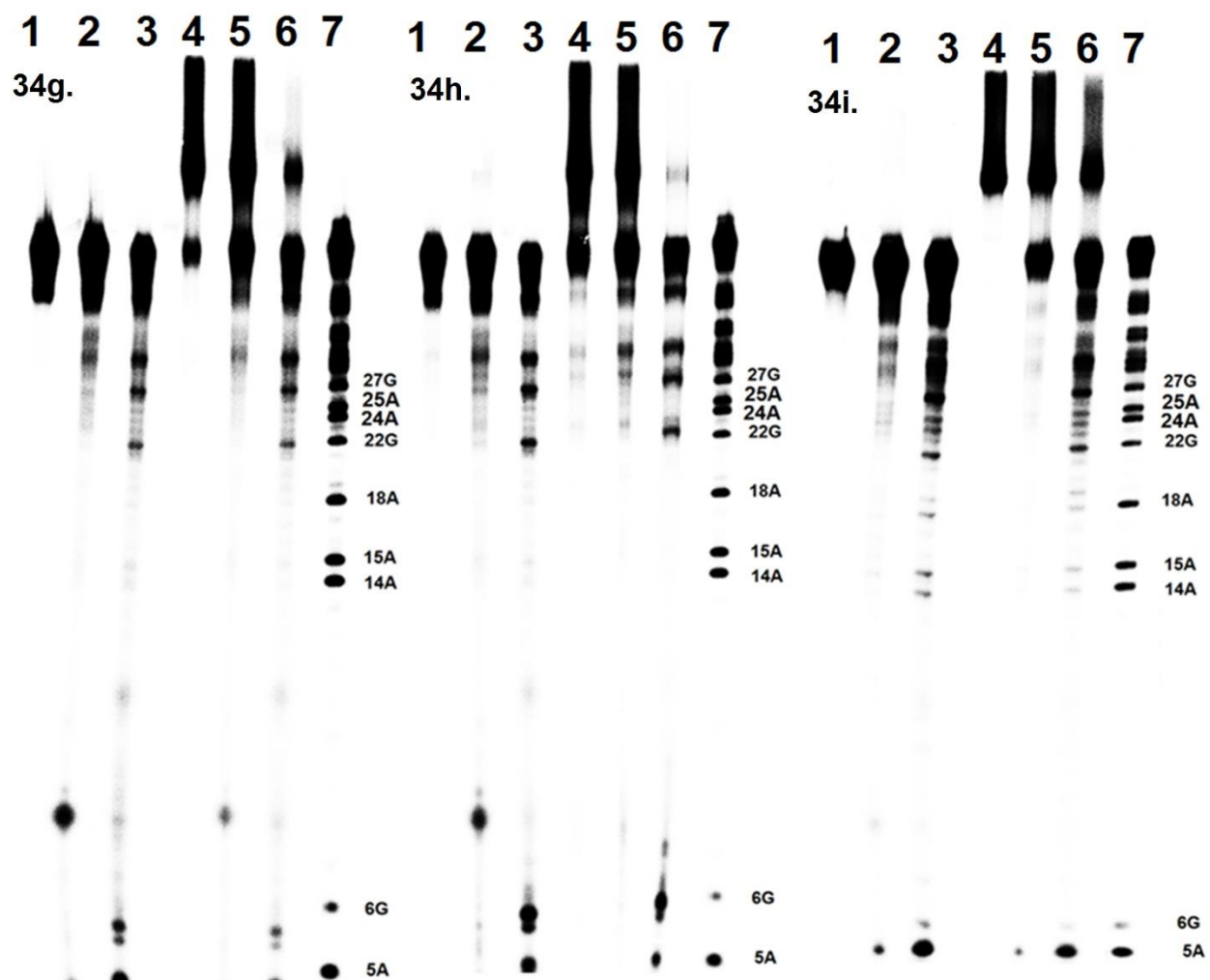
It is well known that N7-alkylated purines can be cleaved upon heating in piperidine.⁴⁻⁶ In order to check whether the benzylic leaving groups and the core structure affect the DNA alkylation sites, heat stability study was performed with DNA ICL products formed with **34a-j** and **35a-j**. Similar to previous study, the ICL products as well as the monoalkylated single stranded DNA were heated in pH 7.0 phosphate buffer or 1.0 M piperidine. The stability of DNA ICL products for **34a-j** and **35a-j** are demonstrated in Figure 4-4. All DNA ICL products are relatively stable upon heating in a pH 7.0 phosphate buffer, while obvious cleavage bands were observed upon heating in 1.0 M piperidine. The major cleavage sites were located at dAs and dGs for compounds **34a**, **34b**, **34f**, **34h-j**, **35c**, **35d** and **35f-i**, while the dGs were the major alkylation sites for compounds **34c-e**, **34g**, **35a**, **35b**, **35e** and **35j**. This indicated that dAs and dGs were the major alkylation sites for **34a**, **34b**, **34f**, **34h-j**, **35c**, **35d** and **35f-i**, while dGs were the major alkylation sites for **34c-e**, **34g**, **35a**, **35b**, **35e** and **35j**.

1 5 6 14 15 18 22 24 25 27 31 40 44 49
5'-dGCCTAGTTCTTTTAATTACTTGCAATGCAAGTAATTAAAGCTTGATCTG (**17a**)
3'-dCGGATCAAGAAAATTAATGAACGTTACGTTCAATTAATTCGAACTAGAC (**17b**)

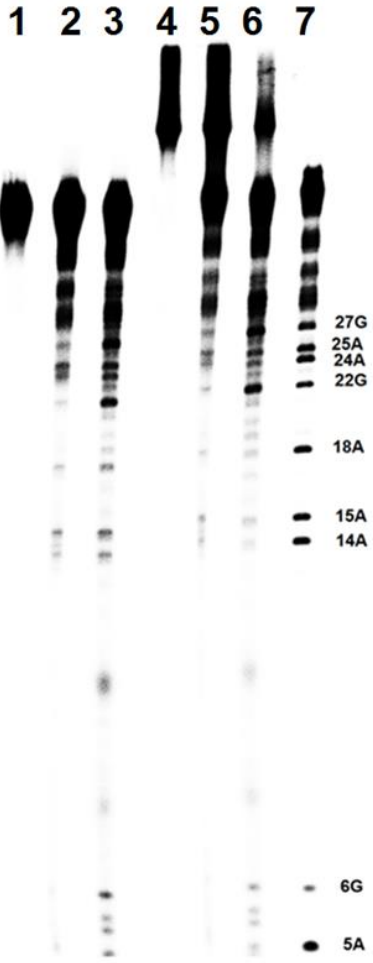
17



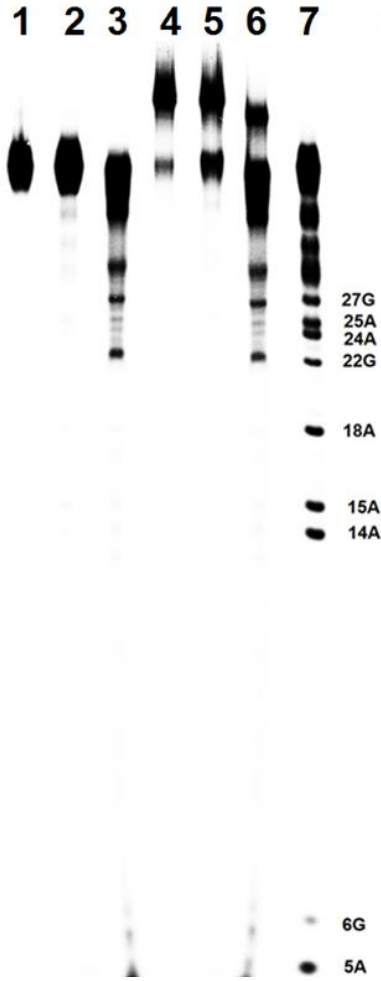




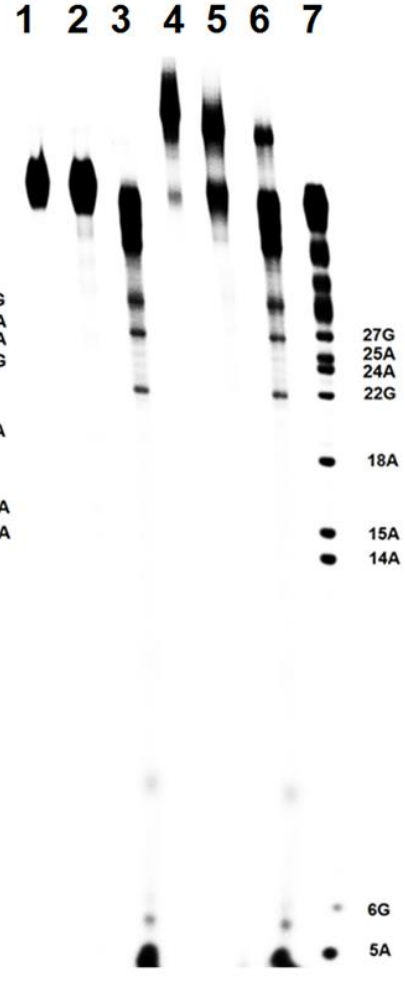
34j.

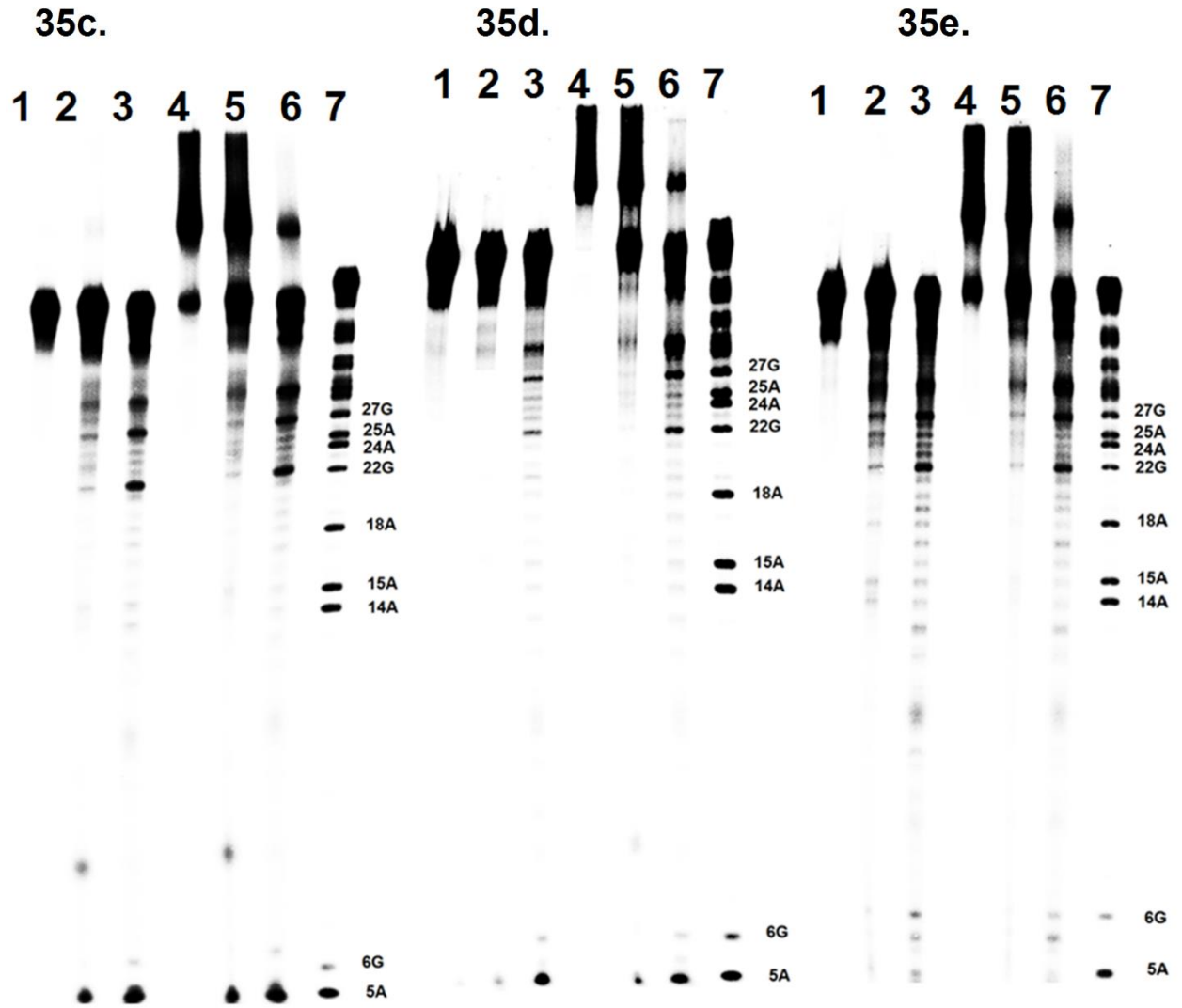


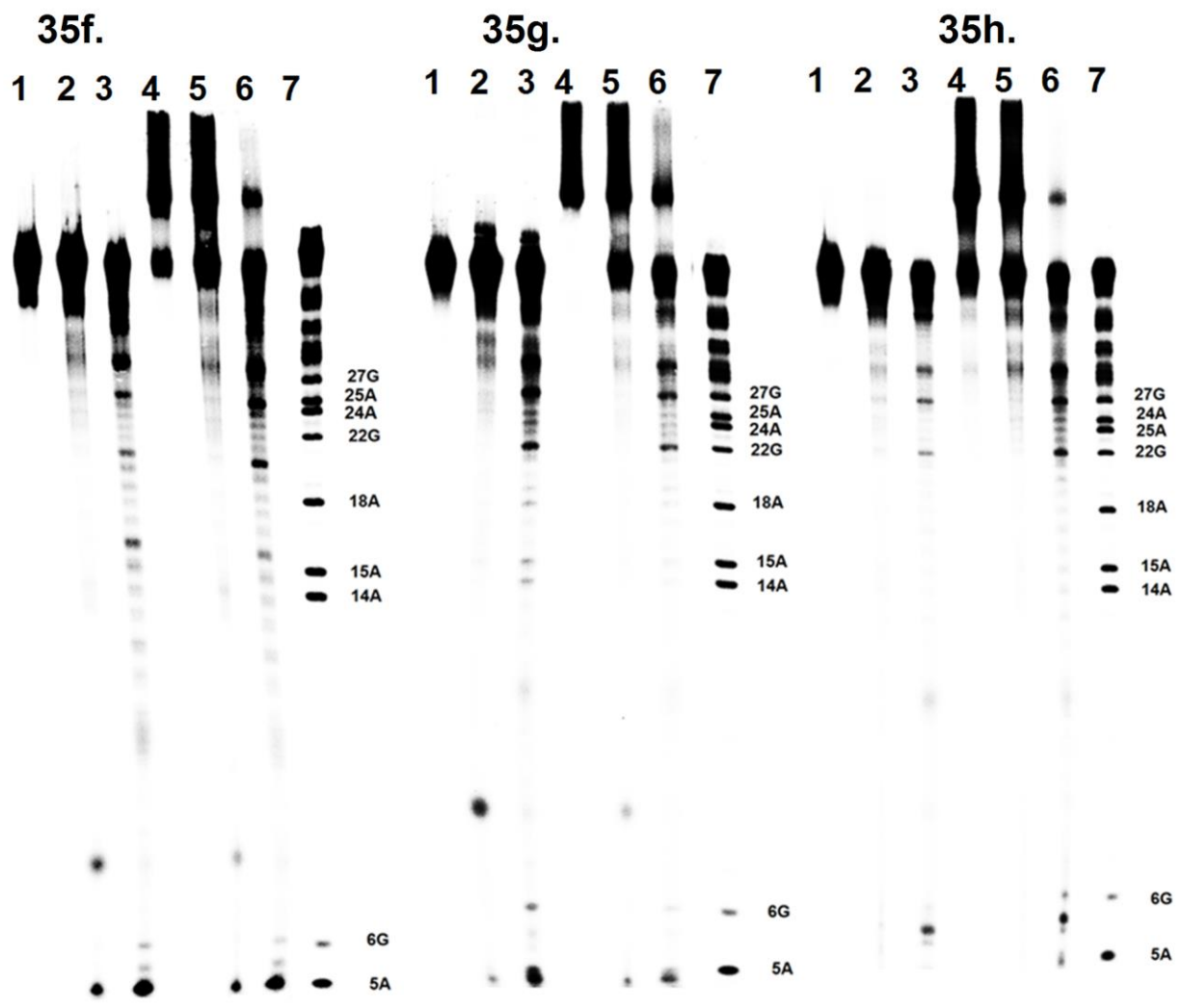
35a.



35b.







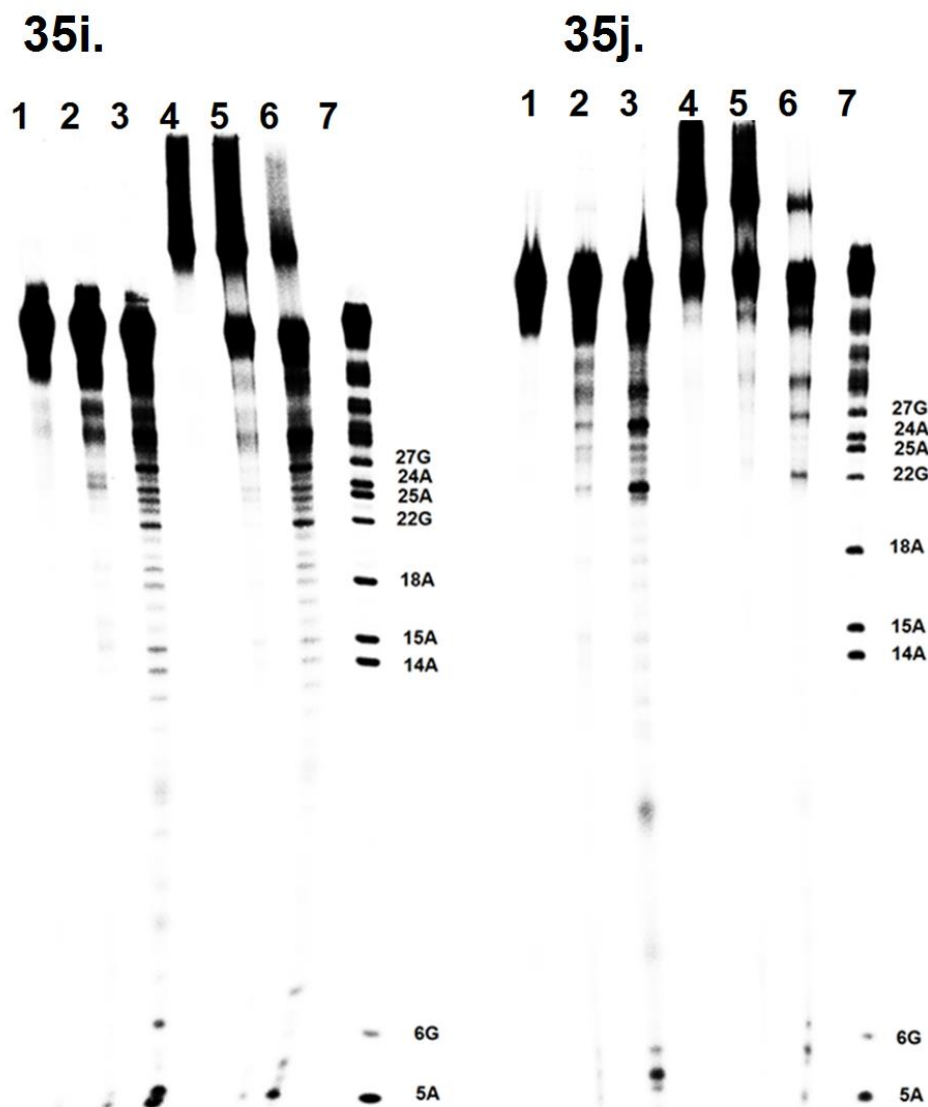


Fig 4-4. Determination of the alkylation sites of **34a-j** and **35a-j**. Phosphorimage autoradiogram of 20% denaturing PAGE analysis of the isolated DNA ICL products and alkylated single-stranded DNA (**17a'**) upon heating in piperidine or phosphate buffer. The ICL product and **17a'** were produced upon irradiation at 350 nm under optimal conditions. **17a** was radiolabeled at the 5'-terminus. Lane 1: isolated alkylated single stranded DNA (**17a'**). Lane 2: **17a'** was heated in a pH 7 phosphate buffer at 90 °C for 30 min. Lane 3: **17a'** was heated in 1.0 M piperidine at 90 °C for 30 min. Lane 4: Isolated DNA ICL products. Lane 5: the DNA ICL products were heated in a

pH 7 phosphate buffer at 90 °C for 30 min. Lane 6: the DNA ICL products were heated in 1.0 M piperidine at 90 °C for 30 min. Lane 7: G + A sequencing.

4.2.5. Conclusions

In this work, we have synthesized two classes of bifunctional biphenyl compounds with an electron donating group -OMe or withdrawing group -NO₂ as an aromatic substituent and various benzylic leaving groups. The UV absorbance and DNA cross-link efficiency of these compounds were investigated, the mechanism for the ICL formation was studied, and their alkylation sites were determined. Compared with the corresponding compounds of chapter 3 with the same leaving group, the introduction of an additional benzene ring in the parent structure (**26**, **27**) did not lead to red shift of the maximum absorption band but led to the enhanced UV absorbance for most compounds (**34a-j**, **35a-j**), especially the NO₂-containing ones. For all tested compounds, compounds **35a-j** with a NO₂ group as a substituent showed better DNA cross-link efficiency than the corresponding ones with OMe group (**34a-j**) except for **35f** and **35g**. Compounds with the same substituent but different leaving groups showed different DNA ICL efficiency suggested that the benzylic leaving groups also have obvious effects on DNA ICL efficiency. All these compounds undergo the same mechanism pathway for DNA cross-linking. The free radicals were first generated upon UV irradiation, which were then converted to the carbocations directly alkylate DNA. The dAs and dGs were the major alkylation sites for compounds **34a**, **34b**, **34f**, **34h-j**, **35c**, **35d** and **35f-i** while dGs were the major alkylation site for others. This work presents insight about the photo reactivities of these aromatic compounds towards DNA, which provides further guidance for development of novel DNA cross-linking agents with potential biological application.

4.3. Experiment Section

General Information. All commercial available chemicals were used without further purification. Oligonucleotides were synthesized via standard automated DNA synthesis techniques. Deprotection of the synthesized DNA was performed under mild deprotection conditions using a mixture of 40% aqueous MeNH₂ and 28% aqueous NH₃ (v/v = 1:1) at room temperature for 2 h. 20% denaturing polyacrylamide gel electrophoresis was used for DNA purification. [γ -³²P] ATP was used for DNA labeling with standard method. Quantification of radiolabeled oligonucleotides was carried out using a Molecular Dynamics phosphorimager equipped with ImageQuant version 5.2. ¹H NMR and ¹³C NMR spectra were taken on a Bruker DRX 300/500 MHz spectrometer with TMS as the internal standard. High-resolution mass spectrometry IT-TOF was used for molecular confirmation.

(5-Methoxy-1,3-phenylene)dimethanol (13): Into a solution of compound **12** (8.52 g, 38.0 mmol) in THF (50 mL) at 0 °C, LiAlH₄ (3.2 g, 83.6 mmol) was added. The reaction mixture was allowed to warm to rt and stirred overnight. The reaction mixture was quenched with water (20 mL) and diluted with ethyl acetate (3 × 50 mL). The combined organic phases were washed with brine, and dried over anhydrous Na₂SO₄. Solvent was removed, and the residue was purified by column chromatography (Hexane: Ethyl acetate = 1:1, R_f = 0.2) to obtain **13** as a white solid (5.86 g, 34.8 mmol). ¹H NMR (500 MHz, CDCl₃): δ . 6.93 (s, 1H), 6.83 (s, 2H), 4.65 (s, 4H), 3.83 (s, 3H), 2.55 (s, 2H). (the NMR spectra were in agreement with those reported).⁷

(2-bromo-5-methoxy-1,3-phenylene)dimethanol (36): Into a solution of compound **13** (5.72 g, 34.0 mmol) in acetonitrile (30 mL) at 0 °C, N-Bromosuccinimide (6.23 g, 35.0 mmol) in acetonitrile (50 mL) was added dropwise. The reaction mixture was allowed to warm to rt naturally and stirred overnight. Solvent was removed. The residue was diluted with ethyl acetate

(3 × 50 mL), washed with brine, and dried over anhydrous Na₂SO₄. Solvent was removed, and the residue was purified by column chromatography (Hexane: Ethyl acetate = 1:1, R_f = 0.5) to obtain **36** as a white solid (8.0 g, 32.4 mmol). ¹H NMR (500 MHz, DMSO-*d*₆): δ. 7.02 (s, 2H), 5.45-5.43 (t, *J* = 3.0 Hz, 2H), 4.51-4.50 (d, *J* = 3.0 Hz, 4H), 3.79 (s, 3H). (the NMR spectra were in agreement with those reported).⁷

(4,4'-Dimethoxy-[1,1'-biphenyl]-2,6-diyl)dimethanol (37): To a solution of compound **36** (2.48 g, 10.04 mmol), 4-Methoxyphenylboronic acid (2.28 g, 15.06 mmol) and Tetrakis(triphenylphosphine)palladium(0) (1.16 g, 1.004 mmol) in THF (72 mL) under argon, potassium carbonate (6.32 g, 45.0 mmol) in H₂O (24 mL) was added. The reaction mixture was refluxed for 20 h. After cooling to rt, the mixture was diluted with ethyl acetate (3 × 75 mL), washed with brine, and dried over anhydrous Na₂SO₄. Solvent was removed, and the residue was purified by column chromatography (Hexane: Ethyl acetate = 1:1, R_f = 0.33) to afford **37** as a brownish oil (2.2 g, 8.02 mmol). ¹H NMR (500 MHz, DMSO-*d*₆): δ. 7.05-6.97 (m, 6H), 5.01-4.99 (t, *J* = 3.0 Hz, 2H), 4.13-4.12 (d, *J* = 3.0 Hz, 4H), 3.80 (s, 6H). ¹³C NMR (125 MHz, DMSO-*d*₆): δ. 158.94, 158.58, 142.05, 130.98, 130.32, 129.89, 114.15, 110.48, 61.35, 55.47, 55.39. HRMS-ESI (+) (*m/z*): [M+Na]⁺ calcd. for C₁₆H₁₈O₄Na⁺, 297.1103; found: 297.1088.

(4-Methoxy-4'-nitro-[1,1'-biphenyl]-2,6-diyl)dimethanol (38): To a solution of compound **36** (5.0 g, 20.2 mmol), 4-Nitrophenylboronic acid (5.07 g, 30.3 mmol) and Tetrakis(triphenylphosphine)palladium(0) (2.33 g, 2.02 mmol) in THF (108 mL) under argon, potassium carbonate (13.9 g, 101 mmol) in H₂O (36 mL) was added. The reaction mixture was refluxed for 20 h. After cooling to rt, the mixture was diluted with ethyl acetate (3 × 75 mL) and washed with brine. The combined organic phases were dried over anhydrous Na₂SO₄. Solvent was removed, and the residue was purified by column chromatography (Hexane: Ethyl acetate =

1:1, $R_f = 0.4$) to obtain **7** as a brownish solid (2.8 g, 9.70 mmol). $^1\text{H NMR}$ (500 MHz, $\text{DMSO-}d_6$): δ . 8.28-8.26 (d, $J = 6.0$ Hz, 2H), 7.48-7.46 (d, $J = 6.0$ Hz, 2H), 7.06 (s, 2H), 5.12-5.10 (t, $J = 3.0$ Hz, 2H), 4.12-4.11 (d, $J = 3.0$ Hz, 4H), 3.83 (s, 3H). $^{13}\text{C NMR}$ (125 MHz, $\text{DMSO-}d_6$): δ . 159.60, 147.06, 146.06, 141.48, 131.67, 128.67, 123.69, 111.30, 61.27, 55.51. HRMS-ESI (+) (m/z): $[\text{M}+\text{Na}]^+$ calcd. for $\text{C}_{15}\text{H}_{15}\text{NO}_5\text{Na}^+$, 312.0848; found: 312.0833.

(4,4'-Dimethoxy-[1,1'-biphenyl]-2,6-diyl)bis(methylene) diacetate (34a): Into a solution of compound **37** (200 mg, 0.73 mmol) in DCM (10 mL), 4-dimethylaminopyridine (268 mg, 2.19 mmol) was added. The resulting mixture was cooled to 0 °C. Acetyl chloride (230 mg, 2.92 mmol) was added using syringe. The reaction mixture was warmed to rt and stirred for another 2 h. The reaction mixture was quenched with H_2O (8.0 mL), diluted with DCM (3×15 mL), and washed with brine. The combined organic phases were dried over anhydrous Na_2SO_4 . Solvent was removed, and the residue was purified by column chromatography (Hexane: Ethyl acetate = 1:1, $R_f = 0.95$) to obtain **34a** as a white solid (200 mg, 0.56 mmol): m.p. 76-77 °C. $^1\text{H NMR}$ (500 MHz, CDCl_3): δ . 7.12-7.11 (d, $J = 5.0$ Hz, 2H), 7.01 (s, 2H), 6.96-6.94 (d, $J = 10.0$ Hz, 2H), 4.83 (s, 4H), 3.89-3.87 (d, $J = 10.0$ Hz, 6H), 2.06 (s, 6H). $^{13}\text{C NMR}$ (125 MHz, CDCl_3): δ . 170.58, 159.03, 158.84, 136.28, 133.67, 130.82, 129.07, 113.82, 64.44, 55.43, 55.26, 20.96. HRMS-ESI (+) (m/z): $[\text{M}+\text{K}]^+$ calcd. for $\text{C}_{20}\text{H}_{22}\text{O}_6\text{K}^+$, 397.1048; found: 397.1062.

4,4'-Dimethoxy-2,6-bis(methoxymethyl)-1,1'-biphenyl (34b): To a solution of compound **37** (200 mg, 0.73 mmol) in DMF (5.0 mL) at 0 °C, NaH (87.6 mg, 60%, 2.19 mmol) was added. The reaction mixture was stirred at 0 °C for 10 min, and CH_3I (624 mg, 4.4 mmol) was added. The mixture was allowed to warm to rt and stirred overnight. The reaction mixture was quenched with water (10 mL), and diluted with ethyl acetate (3×15 mL). The combined organic phases were washed with brine, and dried over anhydrous Na_2SO_4 . Solvent was removed, and the

residue was purified by column chromatography (Hexane: Ethyl acetate = 3:1, R_f = 0.8) to obtain **34b** as a white solid (120 mg, 0.40 mmol): m.p. 70-71 °C. ^1H NMR (500 MHz, CDCl_3): δ . 7.13-7.11 (d, J = 10.0 Hz, 2H), 7.05 (s, 2H), 6.98-6.96 (d, J = 10.0 Hz, 2H), 4.14 (s, 4H), 3.90 (s, 6H), 3.29 (s, 6H). ^{13}C NMR (125 MHz, CDCl_3): δ . 159.04, 158.67, 138.27, 132.17, 130.89, 130.18, 113.52, 112.28, 72.42, 58.28, 55.39, 55.25. HRMS-ESI (+) (m/z): $[\text{M}+\text{Na}]^+$ calcd. for $\text{C}_{18}\text{H}_{22}\text{O}_4\text{Na}^+$, 325.1416; found: 325.1392.

2,6-Bis((allyloxy)methyl)-4,4'-dimethoxy-1,1'-biphenyl (34c): To a solution of compound **37** (200 mg, 0.73 mmol) in DMF (5.0 mL) at 0 °C, NaH (87.6 mg, 60%, 2.19 mmol) was added. The resulting mixture was stirred for 10 min, and then allyl iodide (368 mg, 2.19 mmol) was added. The reaction mixture was allowed to warm to rt and stirred overnight. The reaction mixture was quenched with water (10 mL), and diluted with ethyl acetate (3×15 mL), the combined organic phases were washed with brine, and dried over anhydrous Na_2SO_4 . Solvent was removed, and the residue was purified by column chromatography (Hexane: Ethyl acetate = 3:1, R_f = 0.95) to obtain **34c** as a browish oily (155 mg, 0.44 mmol). ^1H NMR (500 MHz, CDCl_3): δ . 7.14-7.12 (d, J = 10.0 Hz, 2H), 7.10 (s, 2H), 6.98-6.96 (d, J = 10.0 Hz, 2H), 5.93-5.85(m, 2H), 5.28 (d, J = 1.5 Hz, 1H), 5.24 (d, J = 1.5 Hz, 1H), 5.18-5.16 (d, J = 10.0 Hz, 2H), 4.22 (s, 4H), 3.92-3.91 (m, 10H). ^{13}C NMR (125 MHz, CDCl_3): δ . 159.00, 158.68, 138.37, 134.81, 132.36, 130.95, 130.21, 116.83, 113.49, 112.51, 71.36, 70.05, 55.39, 55.29. HRMS-ESI (+) (m/z): $[\text{M}+\text{Na}]^+$ calcd. for $\text{C}_{22}\text{H}_{26}\text{O}_4\text{Na}^+$, 377.1729; found: 377.1709.

2,6-Bis((benzyloxy)methyl)-4,4'-dimethoxy-1,1'-biphenyl (34d): Compound **37** (200 mg, 0.73 mmol) in DMF (5.0 mL) was cooled to 0 °C, followed by the addition of NaH (87.6 mg, 60%, 2.19 mmol). The resulting mixture was stirred for 10 min, and then benzyl chloride (280 mg, 2.19 mmol) was added. The reaction mixture was allowed to warm to rt and stirred overnight.

The reaction mixture was quenched with water (10 mL), and diluted with ethyl acetate (3 × 15 mL). The combined organic phases were washed with brine, and dried over anhydrous Na₂SO₄. Solvent was removed, and the residue was purified by column chromatography (Hexane: Ethyl acetate = 3:1, R_f = 0.9) to afford **34d** as a white solid (200 mg, 0.44 mmol): m.p. 39-40 °C. ¹H NMR (500 MHz, CDCl₃): δ. 7.38-7.30 (m, 10H), 7.16-7.14 (d, *J* = 10.0 Hz, 4H), 6.97-6.95 (d, *J* = 10.0 Hz, 2H), 4.47 (s, 4H), 4.30 (s, 4H), 3.91 (s, 6H). ¹³C NMR (125 MHz, CDCl₃): δ. 159.03, 158.69, 138.37, 138.33, 132.66, 130.98, 130.19, 128.36, 127.71, 127.55, 113.55, 112.88, 72.49, 70.31, 55.42, 55.29. HRMS-ESI (+) (*m/z*): [M+Na]⁺ calcd. for C₃₀H₃₀O₄Na⁺, 477.2036; found: 477.2028.

2,6-Bis(bromomethyl)-4,4'-dimethoxy-1,1'-biphenyl (34e): Into a solution of compound **37** (1.5 g, 5.48 mmol) in DCM (30 mL) at 0 °C, phosphorus tribromide (3.26 g, 12.05 mmol) was added. The reaction mixture was allowed to warm to rt and stirred for 3 h. The reaction mixture was quenched with water (20 mL), and diluted with DCM (3 × 30 mL). The combined organic phases were washed with brine, and dried over anhydrous Na₂SO₄. Solvent was removed, and the residue was purified by column chromatography (Hexane: ethyl acetate = 1:1, R_f = 0.85) to afford **34e** as a white solid (1.71 g, 4.27 mmol): m.p. 107-108 °C. ¹H NMR (500 MHz, CDCl₃): δ. 7.30-7.28 (d, *J* = 6.0 Hz, 2H), 7.04-7.02 (d, *J* = 6.0 Hz, 4H), 4.23 (s, 4H), 3.91-3.89 (d, *J* = 6.0 Hz, 6H). ¹³C NMR (125 MHz, CDCl₃): δ. 159.21, 158.94, 138.41, 134.12, 130.98, 128.59, 115.94, 113.79, 55.49, 55.30, 32.14. HRMS-ESI (+) (*m/z*): [M-Br]⁺ calcd. for C₁₆H₁₆O₂Br⁺, 319.0328; found: 319.0288.

1,1'-(4,4'-Dimethoxy-[1,1'-biphenyl]-2,6-diyl)bis(N,N-dimethylmethanamine) (34f): Into a solution of **34e** (200 mg, 0.50 mmol) in ethyl acetate (4.0 mL), dimethylamine solution (2.0 M in methanol) (2.5 mL, 5 mmol) was added. The reaction mixture was stirred at rt overnight. The

reaction mixture was diluted with ethyl acetate (3 × 10 mL), and washed with brine. The combined organic phases were dried over anhydrous Na₂SO₄. Solvent was removed, and the residue was purified by column chromatography (DCM: Methanol = 5:1, R_f = 0.48) to afford **34f** as a white solid (100 mg, 0.30 mmol): m.p. 64-65 °C. ¹H NMR (500 MHz, CDCl₃): δ. 7.15-7.14 (d, *J* = 5.0 Hz, 2H), 7.03-7.01 (d, *J* = 10.0 Hz, 2H), 6.96-6.94 (d, *J* = 10.0 Hz, 2H), 3.91-3.90 (d, *J* = 5.0 Hz, 6H), 3.18 (s, 4H), 2.18 (s, 12H). ¹³C NMR (125 MHz, CDCl₃): δ. 159.00, 158.38, 138.31, 133.90, 131.43, 131.19, 113.37, 113.10, 61.07, 55.52, 55.23, 45.31. HRMS-ESI (+) (*m/z*): [M+H]⁺ calcd. for C₂₀H₂₉N₂O₂⁺, 329.2224; found: 329.2215.

4,4'-((4,4'-Dimethoxy-[1,1'-biphenyl]-2,6-diyl)bis(methylene))dimorpholine (34g): Into a solution of **34e** (200 mg, 0.5 mmol), morpholine (348 mg, 4.0 mmol) in ethyl acetate (5.0 mL) was added. The resulting mixture was stirred at rt overnight. Solvent was removed. The residue was diluted with ethyl acetate (3 × 15 mL), washed with brine, and dried over anhydrous Na₂SO₄. Solvent was removed, and the residue was purified by column chromatography (DCM: Methanol = 10:1, R_f = 0.86) to obtain **34g** as a colorless gel (167 mg, 0.41 mmol). ¹H NMR (500 MHz, CDCl₃): δ. 7.06-7.04 (m, 4H), 6.94-6.92 (d, *J* = 10.0 Hz, 2H), 3.88 (s, 6H), 3.67-3.65 (t, *J* = 5.0 Hz, 8H), 3.16 (s, 4H), 2.32 (s, 8H). ¹³C NMR (125 MHz, CDCl₃): δ. 158.50, 158.36, 138.24, 134.66, 131.39, 131.13, 113.15, 112.91, 67.14, 60.43, 55.32, 55.24, 53.73, 53.46. HRMS-ESI (+) (*m/z*): [M+H]⁺ calcd. for C₂₄H₃₃N₂O₄⁺, 413.2435; found: 413.2434.

((4,4'-Dimethoxy-[1,1'-biphenyl]-2,6-diyl)bis(methylene))bis(phenylsulfane) (34h): To a solution of compound **34e** (200 mg, 0.5 mmol) in DMF (5.0 mL), thiophenol (165 mg, 1.5 mmol) was added, followed by the addition of trimethylamine (0.6 mL). The reaction mixture was stirred at 70 °C overnight. The reaction mixture was quenched with water (10 mL), and diluted with ethyl acetate (3 × 15 mL). The combined organic phases were washed with brine,

and dried over anhydrous Na₂SO₄. Solvent was removed, and the residue was purified by column chromatography (Hexane: ethyl acetate = 10:1, R_f = 0.5) to offer **34h** as a white solid (198 mg, 0.43 mmol): m.p. 90-91 °C. ¹H NMR (500 MHz, CDCl₃): δ. 7.26-7.19 (m, 10H), 7.13-7.12 (d, *J* = 5.0 Hz, 2H), 6.94-6.92 (d, *J* = 10.0 Hz, 2H), 6.87 (s, 2H), 3.88 (s, 3H), 3.83 (s, 4H), 3.74 (s, 3H). ¹³C NMR (125 MHz, CDCl₃): δ. 158.79, 158.47, 137.56, 136.52, 133.98, 131.31, 130.26, 130.07, 128.79, 126.39, 114.01, 113.63, 55.28, 55.23, 37.69. HRMS-ESI (+) (*m/z*): [M+K]⁺ calcd. for C₂₈H₂₆O₂S₂K⁺, 497.1006; found: 497.1016.

((4,4'-Dimethoxy-[1,1'-biphenyl]-2,6-diyl)bis(methylene))bis(phenylselane) (34i): To a solution of diphenyl diselenide (312 mg, 1.0 mmol) in DMF (5.0 mL), NaBH₄ (75.7 mg, 2.0 mmol) was added. The reaction mixture was stirred at rt for 10 min. Compound **34e** (200 mg, 0.50 mmol) in DMF (2.0 mL) was added. The resulting mixture was stirred at rt overnight. The reaction mixture was quenched with water (10 mL), and diluted with ethyl acetate (3 × 15 mL). The combined organic phases were washed with brine, and dried over anhydrous Na₂SO₄. Solvent was removed, and the residue was purified by column chromatography (Hexane: DCM = 5:1, R_f = 0.25) to afford **34i** s as a light yellowish solid (248 mg, 0.45 mmol): m.p. 101-102 °C. ¹H NMR (500 MHz, CDCl₃): δ. 7.36-7.35 (d, *J* = 5.0 Hz, 4H), 7.27-7.22 (m, 6H), 7.15-7.13 (d, *J* = 10.0 Hz, 2H), 6.95-6.93 (d, *J* = 10.0 Hz, 2H), 6.66 (s, 2H), 3.89 (s, 3H), 3.85 (s, 4H), 3.67 (s, 3H). ¹³C NMR (125 MHz, CDCl₃): 158.75, 158.15, 138.96, 133.83, 133.43, 131.34, 130.78, 130.20, 128.95, 127.29, 113.80, 113.60, 55.29, 55.14, 31.27. HRMS-ESI (+) (*m/z*): [M+K]⁺ calcd. for C₂₈H₂₆O₂Se₂K⁺, 592.9900; found: 592.9913.

((4,4'-Dimethoxy-[1,1'-biphenyl]-2,6-diyl)bis(methylene))bis(triphenylphosphonium) bromide (34j): Compound **34e** (200 mg, 0.5 mmol) and triphenylphosphine (289 mg, 1.1 mmol) in dry toluene (5.0 mL) was stirred at rt for one day under argon. The crude white powder was

obtained by filtration, which was purified by column chromatography (DCM: Methanol = 10:1, R_f = 0.45) to afford **34j** as a white foam (280 mg, 0.42 mmol). ^1H NMR (500 MHz, CDCl_3): δ . 7.78-7.75 (t, J = 7.5 Hz, 6H), 7.64-7.60 (m, 12H), 7.29-7.25 (m, 12H), 6.79 (s, 2H), 6.52-6.50 (d, J = 10.0 Hz, 2H), 5.70-5.68 (d, J = 10.0 Hz, 2H), 5.11-5.09 (d, J = 10.0 Hz, 4H), 3.80 (s, 3H), 3.26 (s, 3H). ^{13}C NMR (125 MHz, CDCl_3): δ . 158.80, 158.33, 136.31, 135.15, 134.20, 134.11, 131.35, 130.44, 130.39, 129.02, 128.92, 127.73, 117.75, 117.07, 114.24, 55.49, 55.32, 53.48, 29.68, 29.48, 29.11. HRMS-ESI (+) (m/z): $[\text{M}-2\text{Br}]^{2+}$ calcd. for $\text{C}_{52}\text{H}_{46}\text{O}_2\text{P}_2^{2+}$, 382.1481; found: 382.1461.

(4-Methoxy-4'-nitro-[1,1'-biphenyl]-2,6-diyl)bis(methylene) diacetate (35a): Into a solution of compound **38** (300 mg, 1.04 mmol) in DCM (10 mL), 4-dimethylaminopyridine (381 mg, 3.12 mmol) was added. The resulting mixture was cooled to 0 °C. Acetyl chloride (327 mg, 4.16 mmol) was added using syringe. The reaction mixture was warmed to rt and stirred for another 4 h. The reaction mixture was quenched with H_2O (8.0 mL), and diluted with DCM (3×15 mL). The combined organic phases were washed with brine, and dried over anhydrous Na_2SO_4 . Solvent was removed, and the residue was purified by column chromatography (Hexane: Ethyl acetate = 1:1, R_f = 0.78) to obtain **35a** as a white solid (220 mg, 0.59 mmol): m.p. 99-100 °C. ^1H NMR (500 MHz, CDCl_3): δ . 8.32-8.30 (d, J = 10.0 Hz, 2H), 7.45-7.43 (d, J = 10.0 Hz, 2H), 7.05 (s, 2H), 4.77 (s, 4H), 3.91 (s, 3H), 2.04 (s, 6H). ^{13}C NMR (125 MHz, CDCl_3): δ . 170.31, 159.66, 147.51, 144.55, 135.60, 131.68, 131.07, 123.51, 114.65, 63.95, 55.52, 20.84. HRMS-ESI (+) (m/z): $[\text{M}-\text{OAc}]^+$ calcd. for $\text{C}_{17}\text{H}_{16}\text{NO}_5^+$, 314.1023; found: 314.1024.

4-Methoxy-2,6-bis(methoxymethyl)-4'-nitro-1,1'-biphenyl (35b): To a solution of compound **38** (300 mg, 1.04 mmol) in DMF (5.0 mL) at 0 °C, NaH (166 mg, 60%, 4.16 mmol) was added. The reaction mixture was stirred for 10 min at 0 °C, and then CH_3I (886 mg, 6.24 mmol) was

added. The reaction mixture was allowed to warm to RT and stirred overnight. The reaction mixture was quenched with water (10 mL), and diluted with ethyl acetate (3 × 15 mL). The combined organic phases were washed with brine, and dried over anhydrous Na₂SO₄. Solvent was removed, and the residue was purified by column chromatography (Hexane: Ethyl acetate = 5:1, R_f = 0.45) to obtain **35b** as a white solid (148 mg, 0.47 mmol): m.p. 69-70 °C. ¹H NMR (500 MHz, CDCl₃): δ. 8.31-8.29 (d, *J* = 10.0 Hz, 2H), 7.44-7.42 (d, *J* = 10.0 Hz, 2H), 7.06 (s, 2H), 4.07 (s, 4H), 3.91 (s, 3H), 3.26 (s, 6H). ¹³C NMR (125 MHz, CDCl₃): δ. 159.69, 147.20, 145.63, 137.47, 131.07, 130.73, 123.21, 113.40, 72.39, 58.31, 55.45. HRMS-ESI (+) (*m/z*): [M+Na]⁺ calcd. for C₁₇H₁₉NO₅Na⁺, 340.1161; found: 340.1143.

2,6-Bis((allyloxy)methyl)-4-methoxy-4'-nitro-1,1'-biphenyl (35c): To a solution of compound **38** (300 mg, 1.04 mmol) in DMF (5.0 mL) at 0 °C, NaH (166 mg, 60%, 4.16 mmol) was added. The resulting mixture was stirred for 10 min, and then allyl iodide (699 mg, 4.16 mmol) was added. The reaction mixture was allowed to warm to rt and stirred overnight. The reaction was quenched with water (10 mL), and diluted with ethyl acetate (3 × 15 mL). The combined organic phases were washed with brine, and dried over anhydrous Na₂SO₄. Solvent was removed, and the residue was purified by column chromatography (Hexane: Ethyl acetate = 5:1, R_f = 0.50) to obtain **35c** as a light yellowish solid (190 mg, 0.50 mmol): m.p. 36-37 °C. ¹H NMR (500 MHz, CDCl₃): δ. 8.29-8.28 (d, *J* = 5.0 Hz, 2H), 7.44-7.42 (d, *J* = 10.0 Hz, 2H), 7.08 (s, 2H), 5.86-5.78 (m, 2H), 5.23-5.20 (d, *J* = 15.0 Hz, 2H), 5.16-5.14 (d, *J* = 10.0 Hz, 2H), 4.14 (s, 4H), 3.90 (s, 3H), 3.87-3.86 (d, *J* = 5.0 Hz, 4H). ¹³C NMR (125 MHz, CDCl₃): δ. 159.65, 147.19, 145.66, 137.53, 134.35, 131.16, 130.96, 123.14, 117.24, 113.63, 71.43, 69.91, 55.43. HRMS-ESI (+) (*m/z*): [M+Na]⁺ calcd. for C₂₁H₂₃NO₅Na⁺, 392.1474; found: 392.1463.

2,6-Bis((benzyloxy)methyl)-4-methoxy-4'-nitro-1,1'-biphenyl (35d): Compound **38** in (300 mg, 1.04 mmol) in DMF (5.0 mL) was cooled to 0 °C, followed by the addition of NaH (166 mg, 60%, 4.16 mmol). The resulting mixture was stirred for 10 min, and then benzyl chloride (527 mg, 4.16 mmol) was added. The reaction mixture was allowed to warm to rt and stirred overnight. The reaction mixture was quenched with water (10 mL), and diluted with ethyl acetate (3 × 15 mL). The combined organic phases were washed with brine, and dried over anhydrous Na₂SO₄. Solvent was removed, and the residue was purified by column chromatography (Hexane: Ethyl acetate = 5:1, R_f = 0.48) to afford **35d** as a yellowish oily (200 mg, 0.44 mmol). ¹H NMR (500 MHz, CDCl₃): δ. 8.19-8.17 (d, *J* = 10.0 Hz, 2H), 7.37-7.29 (m, 8H), 7.24-7.23 (d, *J* = 5.0 Hz, 4H), 7.12 (s, 2H), 4.41 (s, 4H), 4.18 (s, 4H), 3.91 (s, 3H). ¹³C NMR (125 MHz, CDCl₃): δ. 159.66, 147.08, 145.49, 137.72, 137.44, 131.26, 131.05, 128.40, 127.83, 127.78, 123.13, 114.04, 72.63, 69.94, 55.47. HRMS-ESI (+) (*m/z*): [M+Na]⁺ calcd. for C₂₉H₂₇NO₅Na⁺, 492.1787; found: 492.1775.

2,6-Bis(bromomethyl)-4-methoxy-4'-nitro-1,1'-biphenyl (35e): Into a solution of compound **38** (2.1 g, 7.27 mmol) in DCM (30 mL) at 0 °C, phosphorus tribromide (4.34 g, 16.02 mmol) was added. The reaction mixture was allowed to warm to rt and stirred overnight. The reaction mixture was quenched with water (20 mL), and diluted with DCM (3 × 30 mL). The combined organic phases were washed with brine, and dried over anhydrous Na₂SO₄. Solvent was removed, and the residue was purified by column chromatography (Hexane: DCM = 2:1, R_f = 0.45) to afford **35e** as a white solid (1.26 g, 3.05 mmol): m.p. 137-138 °C. ¹H NMR (500 MHz, CDCl₃): δ. 8.38-8.36 (d, *J* = 6.0 Hz, 2H), 7.61-7.60 (d, *J* = 3.0 Hz, 2H), 7.05 (s, 2H), 4.15 (s, 4H), 3.91 (s, 3H). ¹³C NMR (125 MHz, CDCl₃): δ. 159.74, 150.08, 147.74, 143.76, 137.70,

131.22, 123.57, 116.27, 55.59, 31.18. HRMS-ESI (+) (m/z): $[M-Br]^+$ calcd. for $C_{15}H_{13}NO_3Br^+$, 334.0073; found: 334.0061.

1,1'-(4-Methoxy-4'-nitro-[1,1'-biphenyl]-2,6-diyl)bis(N,N-dimethylmethanamine) (35f): Into a solution of **35e** (200 mg, 0.48 mmol) in ethyl acetate (5.0 mL), dimethylamine solution (2.0 M in methanol) (2.41 mL, 4.82 mmol) was added. The reaction mixture was stirred at rt overnight. Solvent was removed. The residue was diluted with ethyl acetate (3×10 mL), washed with brine, and dried over anhydrous Na_2SO_4 . Solvent was removed, and the residue was purified by column chromatography (DCM: Methanol = 10:1, R_f = 0.62) to afford **35f** as a white solid (153 mg, 0.45 mmol): m.p. 135-136 °C. 1H NMR (500 MHz, $CDCl_3$): δ . 8.28-8.26 (d, J = 10.0 Hz, 2H), 7.37-7.35 (d, J = 10.0 Hz, 2H), 7.08 (s, 2H), 3.90 (s, 3H), 3.05 (s, 4H), 2.11 (s, 12H). ^{13}C NMR (125 MHz, $CDCl_3$): δ . 159.46, 146.99, 146.84, 138.08, 132.22, 131.55, 122.92, 113.56, 61.40, 55.49, 45.28. HRMS-ESI (+) (m/z): $[M+H]^+$ calcd. for $C_{19}H_{26}N_3O_3^+$, 344.1969; found: 344.1955.

4,4'-((4-Methoxy-4'-nitro-[1,1'-biphenyl]-2,6-diyl)bis(methylene))dimorpholine (35g): Into a solution of **35e** (200 mg, 0.48 mmol) in ethyl acetate (5.0 mL), morpholine (420 mg, 4.82 mmol) was added. The resulting mixture was stirred at rt overnight. Solvent was removed. The residue was diluted with ethyl acetate (3×15 mL), washed with brine, and dried over anhydrous Na_2SO_4 . Solvent was removed, and the residue was purified by column chromatography (DCM: Methanol = 10:1, R_f = 0.82) to obtain **35g** as a white solid (200 mg, 0.47 mmol): m.p. 121-122 °C. 1H NMR (500 MHz, $CDCl_3$): δ . 8.28-8.26 (d, J = 10.0 Hz, 2H), 7.41-7.39 (q, J = 10.0 Hz, 2H), 7.02 (s, 2H), 3.90 (s, 3H), 3.62-3.60 (t, J = 5.0 Hz, 8H), 3.11 (s, 4H), 2.27 (s, 8H). ^{13}C NMR (75 MHz, $CDCl_3$): δ . 159.06, 146.86, 137.49, 132.95, 131.52, 122.72, 113.83, 67.01, 60.71, 55.40, 53.30. HRMS-ESI (+) (m/z): $[M+H]^+$ calcd. for $C_{23}H_{30}N_3O_5^+$, 428.2180; found: 428.2189.

((4-Methoxy-4'-nitro-[1,1'-biphenyl]-2,6-diyl)bis(methylene))bis(phenylsulfane) (35h): To a solution of compound **35e** (200 mg, 0.48 mmol) in DMF (5.0 mL), thiophenol (159 mg, 1.45 mmol) was added, followed by the addition of trimethylamine (0.5 mL). The reaction mixture was stirred at 70 °C for 2 days. The reaction mixture was quenched with water (10 mL), and diluted with ethyl acetate (3 × 15 mL). The combined organic phases were washed with brine, and dried over anhydrous Na₂SO₄. Solvent was removed, and the residue was purified by column chromatography (Hexane: ethyl acetate = 10:1, R_f= 0.5) to afford **35h** as an orange solid (223 mg, 0.47 mmol): m.p. 114-116 °C. ¹H NMR (500 MHz, CDCl₃): δ. 8.22-8.20 (d, *J* = 10.0 Hz, 2H), 7.35-7.33 (d, *J* = 10.0 Hz, 2H), 7.28-7.22 (m, 6H), 7.18-7.16 (m, 4H), 6.84 (s, 2H), 3.76 (s, 3H), 3.73 (s, 4H). ¹³C NMR (125 MHz, CDCl₃): δ. 159.17, 147.22, 145.27, 136.98, 135.64, 131.88, 131.53, 130.90, 128.95, 127.01, 123.25, 114.55, 55.32, 37.97. HRMS-ESI (+) (*m/z*): [M+NH₄]⁺ calcd. for C₂₇H₂₇N₂O₃S₂⁺, 491.1458; found: 491.1450.

((4-Methoxy-4'-nitro-[1,1'-biphenyl]-2,6-diyl)bis(methylene))bis(phenylselane) (35i): To a solution of diphenyl diselenide (301 mg, 0.96 mmol) in DMF (5.0 mL), NaBH₄ (73 mg, 1.93 mmol) was added. The reaction mixture was stirred at rt for 10 min. Compound **35e** (200 mg, 0.48 mmol) in DMF (2.0 mL) was added. The resulting mixture was stirred at rt for 24 h. The reaction mixture was quenched with water (10 mL), and diluted with ethyl acetate (3 × 15 mL). The combined organic phases were washed with brine, and dried over anhydrous Na₂SO₄. Solvent was removed, the residue was purified by column chromatography (Hexane: DCM = 10:1, R_f= 0.4) to afford **35i** as a light yellowish solid (258 mg, 0.45 mmol): m.p. 105-107 °C. ¹H NMR (500 MHz, CDCl₃): δ. 8.19-8.17 (d, *J* = 10.0 Hz, 2H), 7.34-7.22 (m, 12H), 6.65 (s, 2H), 3.74 (s, 4H), 3.69 (s, 3H). ¹³C NMR (125 MHz, CDCl₃): 158.88, 147.13, 145.39, 138.24, 134.08,

131.50, 131.21, 129.99, 129.08, 127.71, 123.24, 114.15, 55.21, 30.81. HRMS-ESI (+) (m/z): [M+NH₄]⁺ calcd. for C₂₇H₂₇N₂O₃Se₂⁺, 587.0352; found: 587.0345.

((4-Methoxy-4'-nitro-[1,1'-biphenyl]-2,6-diyl)bis(methylene))bis(triphenylphosphonium)

bromide (35j): Compound **35e** (150 mg, 0.36 mmol) and triphenylphosphine (209 mg, 0.8 mmol) in dry toluene (5.0 mL) was stirred at rt for 1 day under argon. The crude white powder was obtained by filtration, which was further purified by column chromatography (DCM: Methanol = 10:1, R_f = 0.46) to afford **35j** as a white solid (268 mg, 0.29 mmol): m.p. 287-288 °C. ¹H NMR (500 MHz, Methanol-*d*₄): δ . 7.92-7.85 (m, 8H), 7.69-7.65 (m, 12H), 7.39-7.34 (m, 12H), 6.67 (s, 2H), 6.46-6.44 (d, J = 10.0 Hz, 2H), 4.69-4.66 (d, J = 15.0 Hz, 4H), 3.31 (s, 3H). ¹³C NMR (125 MHz, Methanol-*d*₄): δ . 159.29, 147.33, 141.83, 135.25, 134.02, 133.95, 133.87, 131.24, 130.25, 130.14, 123.87, 117.89, 117.28, 116.60, 54.62. HRMS-ESI (+) (m/z): [M-2Br]²⁺ calcd. for C₅₁H₄₃NO₃P₂²⁺, 389.6354; found: 389.6338.

ICL formation with duplex DNA: The ³²P-labeled oligonucleotide (0.5 μ M) was annealed with 1.5 equiv of the complementary strand by heating to 90 °C for 5 min in potassium phosphate buffer (pH 7, 10 mM), followed by slowly cooling to rt. The ³²P-labeled ODN duplex (2 μ L, 0.5 μ M) was then mixed with 1 M NaCl (2 μ L), 100 mM potassium phosphate (2 μ L, pH 8), and **34a-j** or **35a-j** in 6 μ L CH₃CN and autoclaved distilled water to give a final volume of 20 μ L (final concentration of compounds ranges from 10 μ M to 1.0 mM). The reaction mixture was irradiated under UV (350 nm) until the reaction was completed, followed by quenching with an equal volume of 90% formamide loading buffer. The resulting mixture was then subjected to 20% denaturing polyacrylamide gel for electrophoresis.

Trapping assay of oligodeoxynucleotides: (1) Carbocation trapping: the stock solution of MeONH₂·HCl (2 M) was titrated with NaOH (5 M) to adjust the pH to 7.0, which was then diluted to desired concentration (1/3-1000/3 mM). MeONH₂ (6 μL) was mixed with ³²P-labeled DNA duplex (2 μL, 0.5 μM), NaCl (2 μL, 1 M), potassium phosphate (2 μL, pH 8.0, 100mM), compound (**34a-j**, **35a-j**) in 6 μL CH₃CN and water (2 μL) to give the desired concentration (final concentration of MeONH₂: 100 μM to 100 mM; final concentration of compounds: optimized concentration). (2) Radical trapping: 3 μL of TEMPO in CH₃CN (200/3 μM to 2000/3 mM) was mixed with the following: ³²P-labeled DNA duplex (2 μL, 0.5 μM), NaCl (2 μL, 1 M), potassium phosphate (2 μL, pH 8.0, 100 mM), compound (**34a-j**, **35a-j**) in CH₃CN (3 μL) and water (8 μL) as appropriate for the desired concentration (final concentration of TEMPO: 10 μM to 100 mM, final concentration of compounds: optimized concentration). The reaction mixture was irradiated under UV (350 nm) for desired time (optimized time) and quenched with an equal volume of 90% formamide loading buffer, and then subjected to 20% denaturing polyacrylamide gel electrophoresis.

Stability study of ICL products formed with 17: The ³²P-labeled oligonucleotide duplex **17** (30 μ, 0.5 μM) was mixed with NaCl (6 μL, 1 M), 100 mM potassium phosphate (6 μL, pH 8.0) and compound in CH₃CN (18 μL) (optimized concentration used for all the compounds). The reaction mixture was irradiated under UV for desired time (optimized time). After the cross-linking reaction, the DNA ICLs and the monoalkylated ODNs were purified by gel electrophoresis. The isolated DNA fragments were dissolved in 45 μL water, and divided into three portions. One portion (15 μL) was incubated with 1.0 M piperidine at 90 °C for 0.5 h, the second portion (15 μL) was incubated with 0.1 M NaCl and 10 mM potassium phosphate buffer (pH 7.0) under the same condition, and the third portion (15 μL) was used as control. Solvent

was removed under vacuum after the treatment. The residue was dissolved in 90% formamide loading buffer, and then subjected to electrophoresis on a 20% denaturing polyacrylamide gel.

4.4. References

1. Percivalle C, Doria F, Freccero M. Quinone Methides as DNA Alkylating Agents: An Overview on Efficient Activation Protocols for Enhanced Target Selectivity. *Current Organic Chemistry*. 2014;18:19–43.
2. Wang Y, Liu S, Lin Z, Fan Y, Wang Y, Peng X. Photochemical Generation of Benzyl Cations That Selectively Cross-Link Guanine and Cytosine in DNA. *Organic Letters*. 2016;18:2544–7.
3. Fan H, Sun H, Peng X. Substituents Have a Large Effect on Photochemical Generation of Benzyl Cations and DNA Cross-Linking. *Chemistry - A European Journal*. 2018;24:7671–82.
4. Peng X, Hong IS, Li H, Seidman MM, Greenberg MM. Interstrand Cross-Link Formation in Duplex and Triplex DNA by Modified Pyrimidines. *Journal of the American Chemical Society*. 2008;130:10299–306.
5. Maxam AM, Gilbert W. Sequencing end-labeled DNA with base-specific chemical cleavages. *Nucleic Acids Part I Methods in Enzymology*. 1980;65:499–560.
6. Maxam AM, Gilbert W. A New Method for Sequencing DNA. *Proceedings of the National Academy of Sciences of the United States of America*. 1977, 74: 560–564.
7. González-Bulnes L, Ibáñez I, Bedoya LM, Beltrán M, Catalán S, Alcamí J, et al. Structure-Based Design of an RNA-Bindingp-Terphenylene Scaffold that Inhibits HIV-1 Rev Protein Function. *Angewandte Chemie International Edition*. 2013;52:13405–9.

Chapter 5. *In vivo* efficacy of hydrogen peroxide activated DNA interstrand cross-linking agents

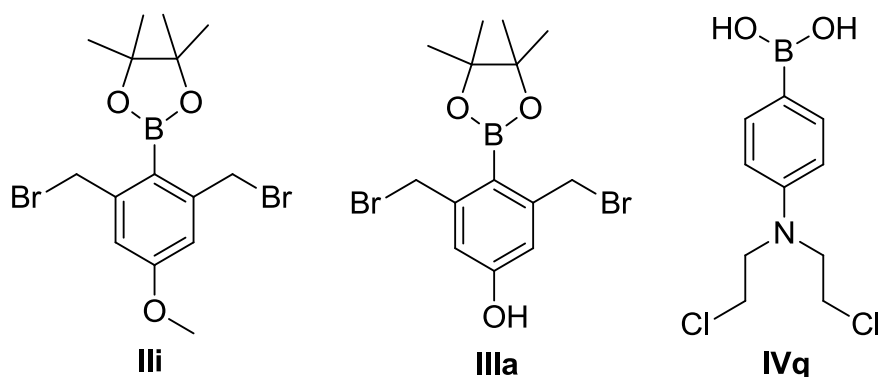
5.1. Introduction

DNA cross-linking (ICL) agents have been an important class of drugs for cancer chemotherapy.¹ They cross-link DNA either within the same strand or between two complementary strands, blocking DNA replication and/or transcription which prevents cell division and finally leads to cell death. A variety of DNA ICL agents have been employed for the treatment of various cancer diseases, such as cisplatin, mitomycin C, nitrogen mustards and psoralens.² However, these traditional DNA ICL agents showed serious side effects towards the host cells due to their poor selectivity towards cancer cells. DNA cross-linking agents targeting cancer cells were expected to reduce side effects. One effective way to reduce the toxicity of DNA cross-linking agents towards host cells is creation of inducible DNA alkylation agents that can only be activated under tumor-specific conditions. Several strategies have been developed for inducing DNA ICL formation under control, including photoirradiation,³⁻¹¹ fluoride induction,¹²⁻¹⁴ oxidation,¹⁵⁻¹⁸ and reduction.¹⁹ Most of these induction methods led to high DNA cross-linking efficiency and selectivity under designed specific conditions. However, most conditions used are not tumor-specific that cannot be employed for targeting cancer cells.

Exploring the intrinsic factor of the cancer cells has been an effective way to develop novel drugs that can be specifically activated in cancer cells. The unique hypoxic condition in tumor offered one possible way for developing selective anticancer agents.²⁰ Recently, several hypoxia-selective DNA cross-linking agents have been developed and showed good selectivity towards cancer cells.²¹⁻²⁵ On the other hand, due to the rapid proliferation and mitochondria malfunction,

cancer cells are believed to be under oxidative stress. Higher level of reactive oxygen species (ROS, such as superoxide (O_2^-), hydroxyl radicals ($OH\cdot$) and hydrogen peroxide (H_2O_2),²⁶⁻²⁸ were observed in cancer cells than in the corresponding normal cells. Thus, DNA cross-linking agents that can be selectively activated by ROS are expected to target cancer cells. Recently, two classes of hydrogen peroxide (H_2O_2) inducible DNA cross-linking agents have been developed in our group,²⁹⁻³⁶ including the quinone methide precursors (QMs)²⁹⁻³³ and nitrogen mustard analogues.³⁴⁻³⁶ Both classes of compounds contain an electron withdrawing boronic acid or pinacol boronate ester as a trigger unit that mask the toxicity of DNA alkylating functional groups while allows its activation by selectively reacting with H_2O_2 . Among all five QM precursors designed (Scheme 1-15 and Scheme 1-27), compounds **IIIi** and **IIIa** (Scheme 5-1) exhibited higher DNA cross-linking efficiency and good selectivity towards H_2O_2 (Figure 5-1). These compounds significantly inhibited cancer cell growth for several cancer cell lines.²⁹⁻³³ They were even more effective than the clinically used DNA alkylating agents such as chlorambucil and melphalan. Compound **IIIi** was more potent than **IIIa** in most cells lines tested, where the inhibitory effect followed the order of MDA-MB-468>UO-31=786-0>A-498.³³ Several classes of H_2O_2 -activated nitrogen mustard precursors have been developed.³⁴ These compounds not only showed good selectivity and activity toward H_2O_2 but also exhibited selective toxicity toward cancer cells and spared normal cells. Among these compounds, neutral molecules **IVq** with the nitrogen mustard moiety directly bonded to the benzene ring showed improved cell membrane permeability and improved cytotoxicity towards cancer cells (Scheme 1-29)³⁵⁻³⁶ For example, compound **IVq** (Scheme 5-1) showed higher DNA ICL efficiency (Figure 5-1) and inhibitory effect for most cell lines tested. In particular, the breast cancer cell line MDA-MB-468 was most sensitive towards **IVq**.³⁵ The *in vitro* study indicated that these ROS-

inducible DNA cross-linking agents (**IIIi**, **IIIa**, **IVq**) are potential and selective anti-cancer prodrugs, which can be used as lead compounds for further drug design. Evaluation of their *in vivo* efficacy will provide further guides for exploring their application and further drug design. In this work, we performed the *in vivo* study in mice to determine the *in vivo* toxicity and efficacy of compounds **IIIi**, **IIIa**, **IVq**.



Scheme 5-1. Compounds used for *in vivo* study.

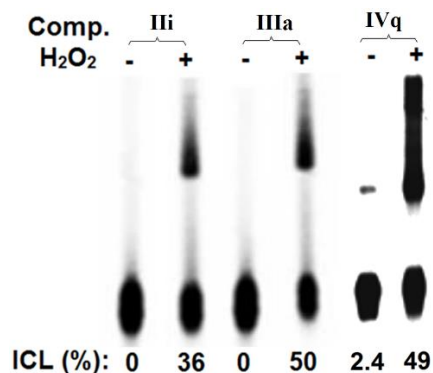


Figure 5-1. DNA ICL formation with/without H₂O₂ for compounds **IIIi**, **IIIa**, **IVq**.

In order to investigate the *in vivo* efficacy of these compounds, the maximum safe dose was first determined using CD-1 mice. The maximum safe dose in this work was defined as maximum dosage that will not lead to weight loss or abnormal behavior. To determine the safe dosage, we carried out two sets of experiments for each compound, including single dose toxicity study and

five dose toxicity tests. Single dose toxicity study was done before five dose treatments. Three mice (4-6 weeks old) were used for each single test.

The *in vitro* study showed that breast cancer cell line MDA-MB-468 was most sensitive towards compounds **III**, **IIIa**, **IVq**.^{33,35} So the breast cancer cell line MDA-MB-468 was the first choice for the *in vivo* efficacy study. Compounds **III** and **IIIa** also showed good inhibitory effect on several renal cancer cell lines where the inhibitory effect follows the order of UO-31 = 786-0 > A-498. Thus, we also determined the *in vivo* efficacy for these renal cancer cell lines.

Cell lines were cultured following the standard protocol (5.5) from one small flask to 16 big flasks (150 cm²). Finally, 16 big flasks of cells were harvested and injected to mice under the skin of the back that is close to the legs. The tumors were allowed to grow in the mice for one week before the drug treatment. On the first day of each week, the body weight and the size of tumor for each mouse were recorded. The mice were euthanized after drug treatment for 6-8 weeks or when the mice weight decreased 20% of the original weight. Tumors were collected, and the weight of tumors was recorded.

5.2. *In Vivo* Efficacy of H₂O₂-activated Nitrogen Mustard Precursor

5.2.1. Toxicity Study with CD-1 Mice

One dose treatment. Four different doses were tested (20, 40, 60 and 80 mg/kg) for nitrogen mustard precursor **IVq**. All mice survived after seven days. No obvious toxicity was observed for mice treated with 20 mg/kg dose, where the weight of mice slightly increased, which was similar to the control mice (Figure 5-2). However, obvious weight loss was observed with the mice treated with 40 mg/kg or higher doses. The mice weight significantly decreased next day

after drug treatment, while the mice weight slightly increased when the injection was discontinued.

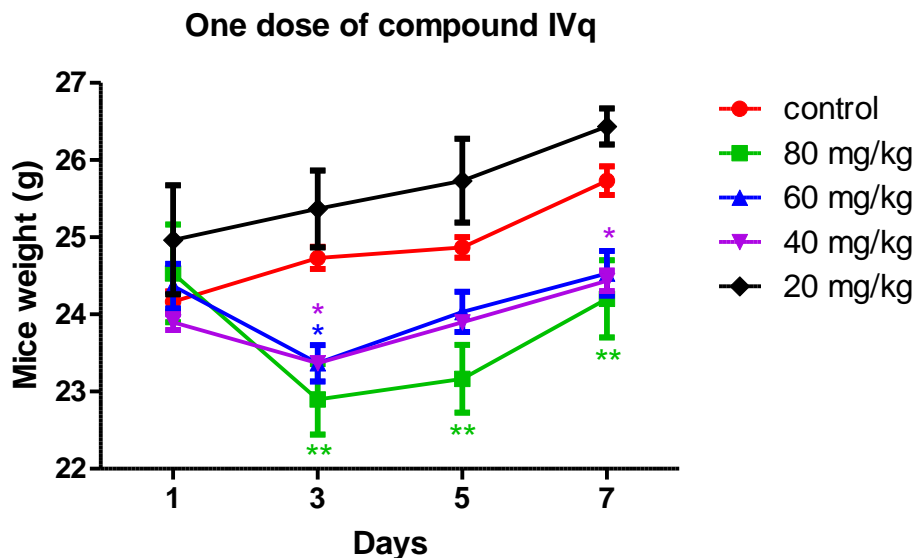


Figure 5-2. The results of one dose treatment for compound **IVq**.

Five dose treatments. The mice were injected with four different dosages of compound **IVq** (10 mg/kg, 20 mg/kg, 40 mg/kg, and 50 mg/kg) and each dose with five continuous injections within five days. All mice treated with lower dosages (10 and 20 mg/kg) of compound **IVq** survived after seven days. Mice treated with 10 mg/kg dose had no obvious weight loss in the first three days, weight loss was observed at the 5th day, while obvious weight loss was observed on the 7th day. Mice treated with 20 mg/kg dosage showed obvious weight loss from the 3rd day. Mice treated with higher dose (40 mg/kg, 50 mg/kg) of compound **IVq** showed obvious weight loss and euthanized on the fifth day.

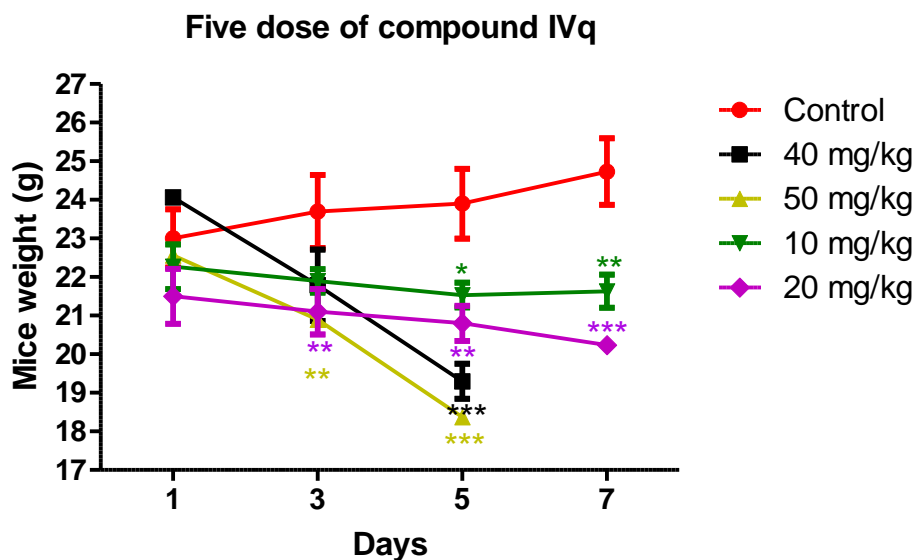


Figure 5-3. The results of five injections per week for compound **IVq**.

5.2.2. *In vivo* efficacy study with athymic nude mice xenografted with breast cancer cell line MDA-MB-468

Twenty four athymic nude mice were employed to investigate the *in vivo* efficacy of compound **IVq**. The mice were xenografted with MDA-MB-468 breast cancer cell line and the tumor were developed in the mice within one week. The mice were equally separated into three groups. One group of mice was used as control treated with vehicle; the second group was treated with 7 mg/kg chlorambucil, while the third group was treated with compound **IVq** with a dosage of 7 mg/kg. The size of tumors and weight of mice were recorded on the first day of each week. After nine weeks, the mice were euthanized, the tumors were harvested, and the weight of tumors was recorded. The tumor size decreased every week for **IVq**- and chlorambucil-treated mice, while the size of tumors in control mice increased. After nine week treatment, the tumor size in **IVq**-treated mice decreased to 6%-26% of the original size, and those in chlorambucil-treated mice decreased to 10%-44% of the original size, while that in the control mice increased to 121%-

480% of the initial size. Normal weight increase was observed for the control mice, while obvious weight loss was observed for mice treated with compound **IVq** or chlorambucil. Weight loss ranged from 1% to 18% for **IVq**-treated mice, while 2% to 11% weight loss was observed for the chlorambucil-treated ones. The size of final harvested tumors was the smallest for **IVq**-treated mice (~ 7% of the ones from control mice), and tumors for chlorambucil-treated mice were slightly bigger those in **IVq**-treated mice (13% of the ones of the control mice). Altogether, these results suggested that both compound **IVq** and chlorambucil greatly suppressed tumor's growth in mice, while the inhibitory effect for compound **IVq** is slightly better than that for chlorambucil. However, compound **IVq** with a dose of 7 mg/kg for nine week treatment is slightly more toxic than chlorambucil at 7 mg/kg dose. Further optimization of dosage is required for a safer treatment.

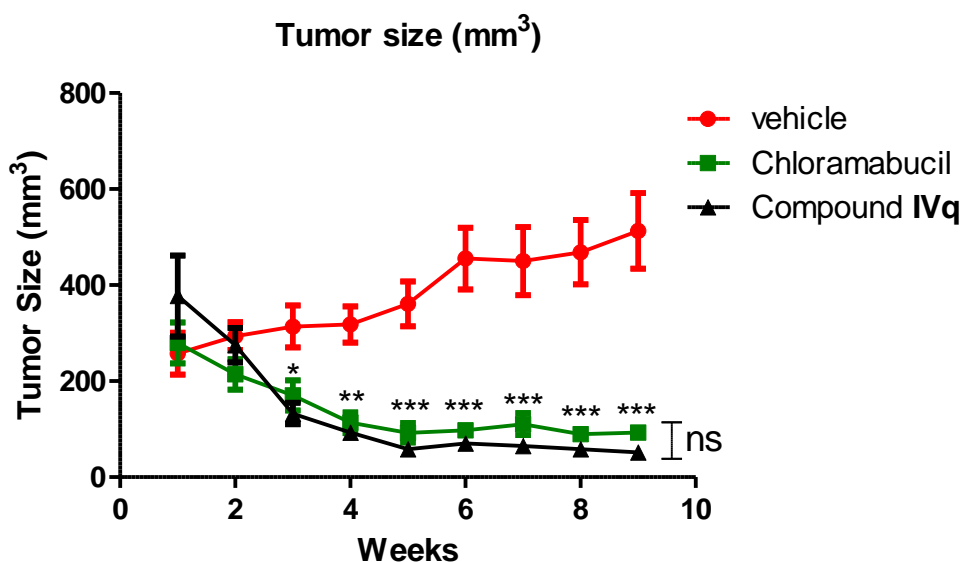


Fig 5-4. The volume of tumors for control and **IVq**-treated mice from 1st to 9th week (7 mg/kg).

[the volume was calculated by $X_{\text{week a}} \cdot Y_{\text{week a}} \cdot X_{(\text{min week a})}$]

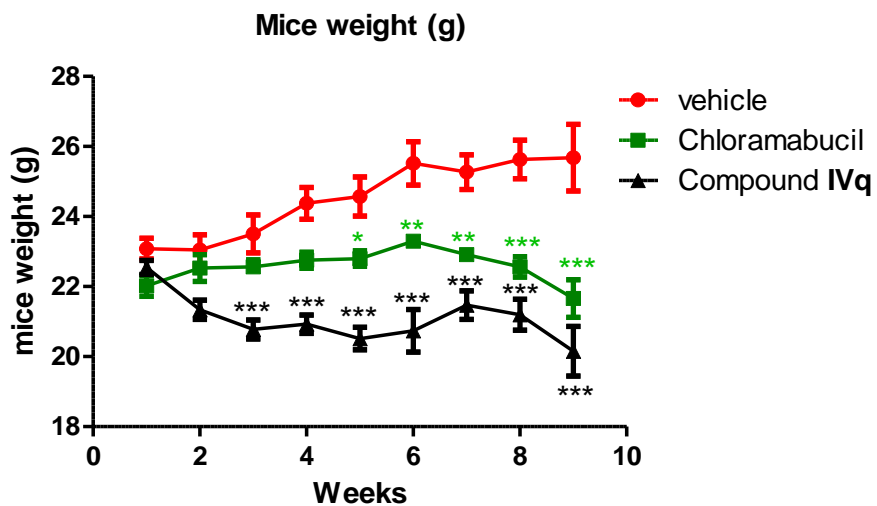


Fig 5-5. Body weight of mice for control and **IVq**-treated mice from 1st to 9th week (7 mg/kg).

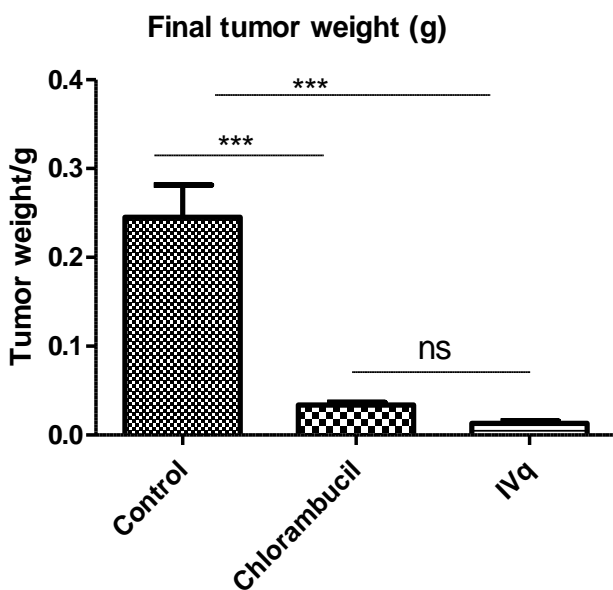


Figure 5-6. Final harvested tumor weight for control, Chlorambucil and **IVq**-treated mice after 9-week's treatment.

5.3. *In Vivo* Efficacy of H₂O₂-activated QM Precursors

5.3.1. Toxicity Study with CD-1 Mice

One dose treatment. For QM precursors **IIIi** and **IIIa**, 10 mg/kg and 20 mg/kg doses were used for single dose treatment. Higher dose was not possible due to the poor solubility of **IIIi** and **IIIa**. All mice survived after one week. No weight loss was observed for the mice treated with 10 mg/kg of **IIIi** and **IIIa** while weight loss was observed for the mice treated with 20 mg/kg of **IIIi** and **IIIa** after first day treatment where body weight gain was observed when the injection was discontinued. The toxicity of compound **IIIi** is similar with that of compound **IIIa** (Figure 5-7).

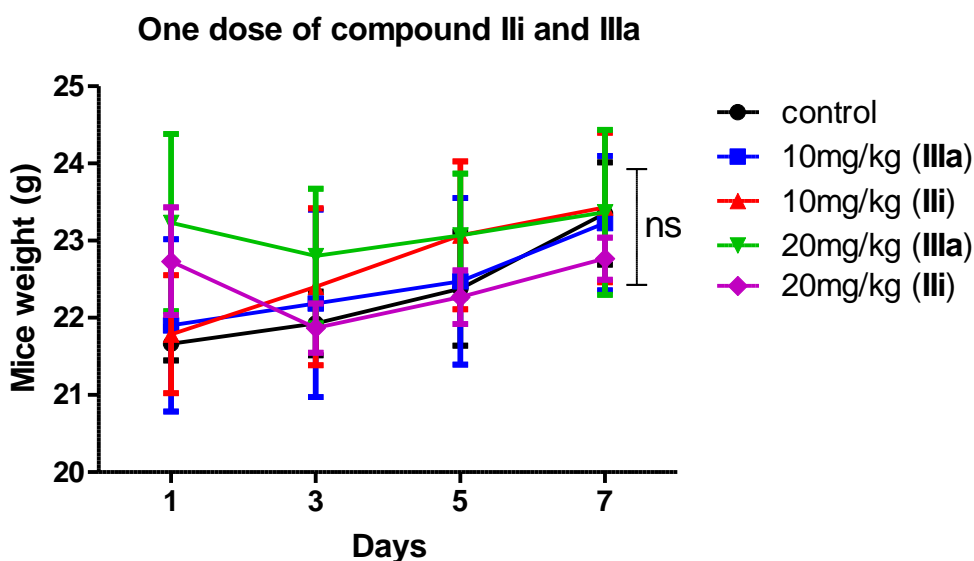


Figure 5-7. The result of one dose treatment for compounds **IIIi** and **IIIa**.

Five doses treatment. Single dose treatment suggested that 10 mg/kg and 20 mg/kg dosages of **IIIi**, **IIIa** were safe for the mice. Thus, we performed five dose treatments with 10 mg/kg and 20 mg/kg of **IIIi**, **IIIa**. All mice survived after seven days. No obvious toxicity was observed for 10 mg/kg dose, while slight weight loss was observed for the mice treated with 20 mg/kg dosage. This suggested that the maximum safe dose for **IIIi** and **IIIa** is 10 mg/kg (no weight loss or abnormal behavior) (Figure 5-8).

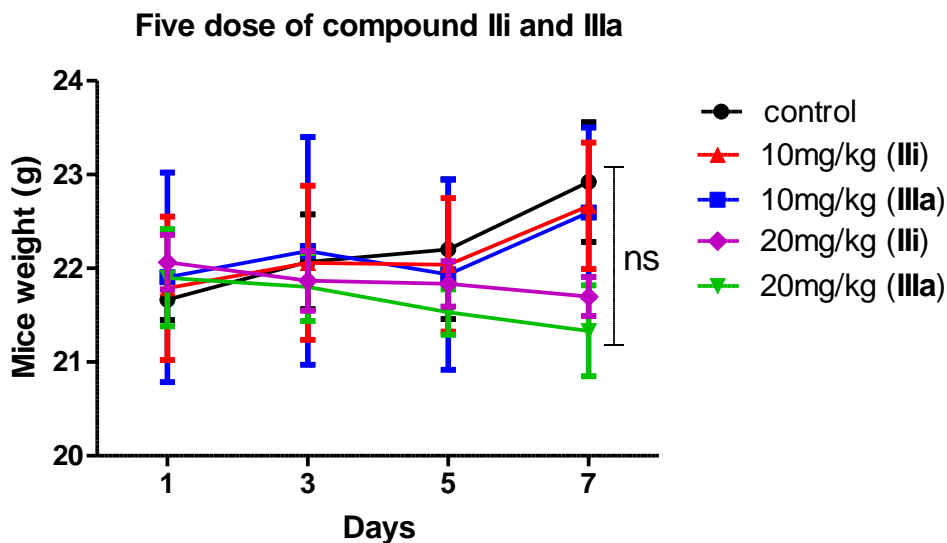


Figure 5-8. The results of five dose treatment for compounds **III** and **IIIa**.

5.3.2. *In Vivo* Efficacy Study with Athymic Nude Mice Xenografted with Breast cancer cell line MDA-MB-468

Initially, the *in vivo* efficacy of compound **III** was tested with mice xenografted with MDA-MB-468 breast cancer cell line. Twenty two mice were used for this study. Eleven of them were treated with compound **III** with a dosage of 5 mg/kg while another eleven were treated with vehicle. The size of tumors and weight of mice were recorded every week. After eight weeks treatment, the tumor size for **III**-treated mice did not increase obviously. The tumor size ranged from 84% to 220% of the initial size, while the control mice showed obvious tumor growth, reaching 256 % to 680% of the initial tumor size. The **III**-treated mice showed normal increase for body weight that was similar to that of the control mice. Tumors harvested from **III**-treated mice are slightly smaller than that from the control mice, which provided evidence that compound **III** inhibited tumor growth in mice. Collectively, these results suggested that compound **III** inhibited tumor growth in xenograft mice with no obvious toxicity.

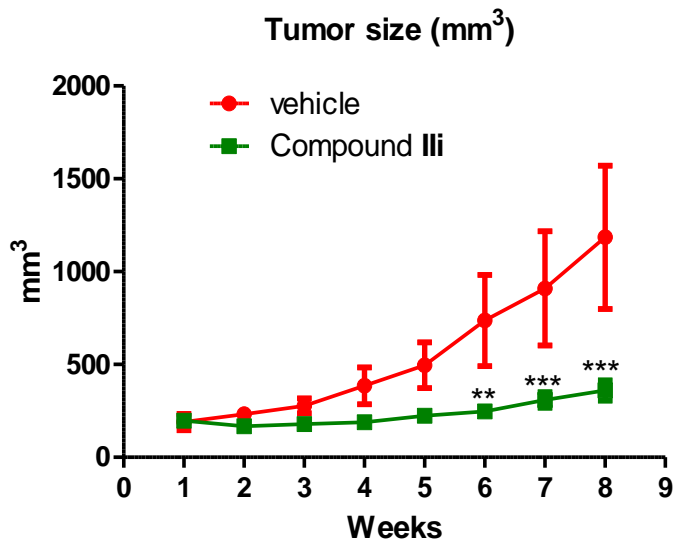


Figure 5-9. The volume of tumors for control and **III**-treated mice from 1st to 8th week.

[Volume was calculated by $X_{\text{week a}} \cdot Y_{\text{week a}} \cdot X_{(\text{min week a})}$]

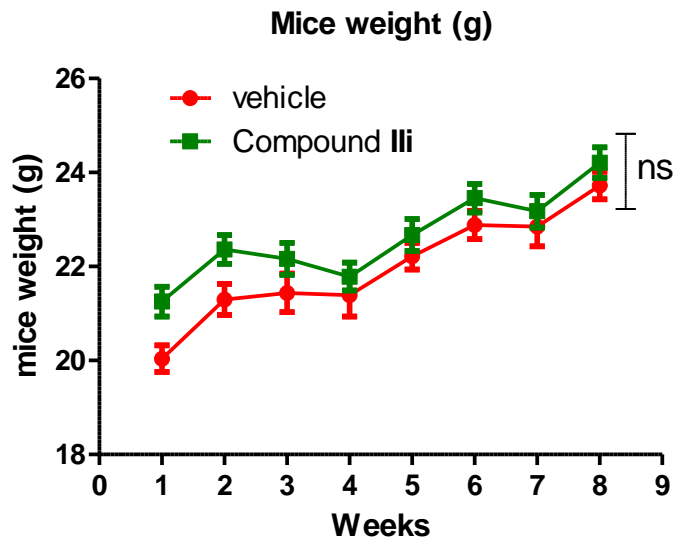


Fig 5-10. Body weight of mice for control and **III**-treated mice from 1st to 8th week.

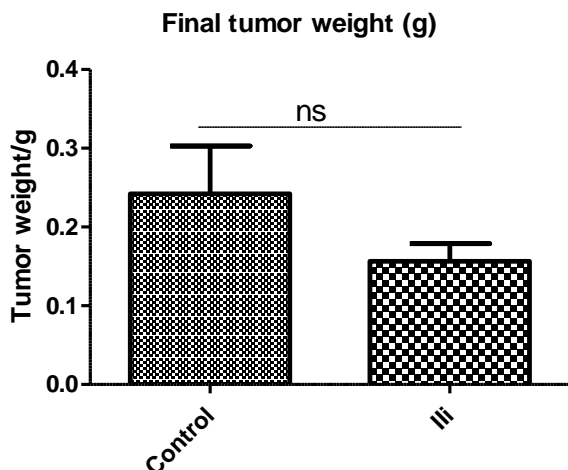


Figure 5-11. Final harvested tumor weight for control and **III**-treated mice after 8 week⁷ treatment. (5mg/kg).

5.3.3. *In Vivo* Efficacy Study with Athymic Nude Mice Xenografted with Renal Cancer Cell Lines (UO-31, 786-O or A-498)

Apart from breast cancer cell line, compound **III** and **IIIa** also showed good inhibitory effect on several renal cancer cell lines where the inhibitory effect follows the order of UO-31 = 786-0 > A-498.³³ Therefore, we determined the *in vivo* efficacy of compounds **III** and **IIIa** toward renal cancer cell lines. Initially, renal cancer cell line UO-31 was chosen for the study since the highest inhibitory effect was observed in this cell line.

The in vivo efficacy of III and IIIa with Renal cancer cell line UO-31. Twenty four UO-31-derived xenograft mice were used to investigate the *in vivo* efficacy of compounds **III** and **IIIa** toward UO-31. The mice were equally separated into three groups. One group of mice was used as control treated with vehicle; the second group was treated with compound **III** at a dose of 7 mg/kg, while the third group was treated with compound **IIIa** with a dose of 7 mg/kg. The tumor size and weight of mice were recorded every week. Obvious tumors were developed in all mice

at the location of tumor cell injection after one week of injection. However, to our surprise, the tumor size decreased significantly for all mice starting from the second week. No obvious tumor was observed after three weeks while the weight of mice increased normally. These results suggested that the UO-31 cell line cannot successfully survive in the xenograft mice used in this study.

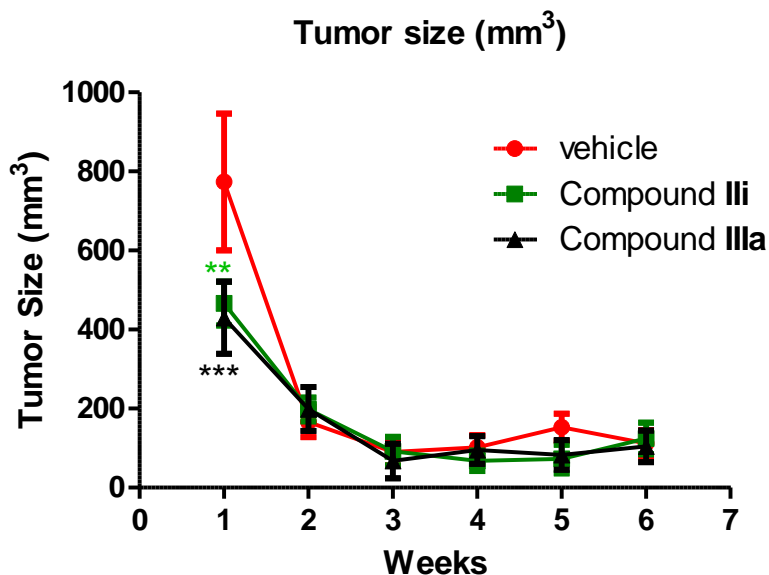


Figure 5-12. The volume of tumors for control, **IIIi** and **IIIa**-treated mice 1st to 6th week.

[Volume was calculated by $X_{\text{week a}} \cdot Y_{\text{week a}} \cdot X_{\text{(min week a)}}$]

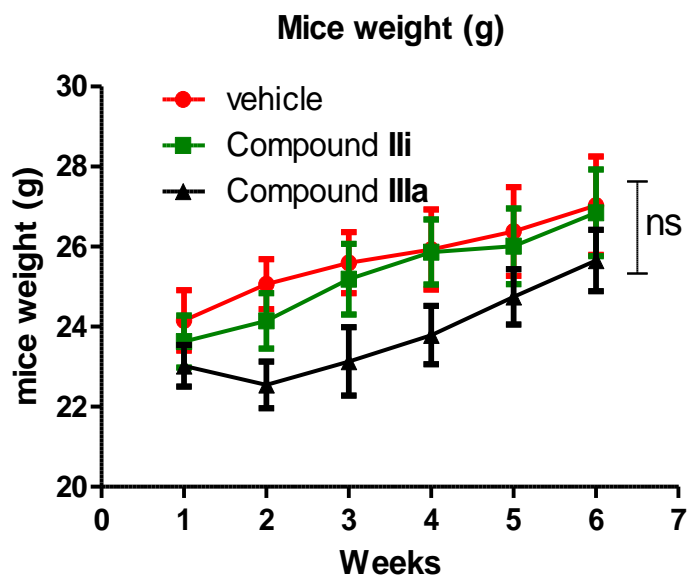


Fig 5-13. Body weight of mice for control, **IIIi** and **IIIa**-treated mice from 1st to 6th week.

The in vivo efficacy of IIIi with Renal cancer cell line 786-O. Since renal cancer cell line UO-31 cannot successfully survive in xenograft mice, renal cancer cells 786-O were chosen for further study. Twenty two mice that were xenografted with 786-O cells line were used for this study, which were separated into two groups equally. One group was used as control while another group was treated with compound **IIIi** with a dosage of 7 mg/kg. The tumor size and weight of mice were monitored every week. Tumors were observed for all mice after one week of the injection of 786-O cells. The tumor size did not change for the first three weeks for the control mice, while slightly decreased size was observed for the ones treated with compound **IIIi**. However, the size of tumors increased rapidly for all mice starting from the fourth week. After seven week treatment, the size of tumors in both group of mice increased significantly, reaching 180% to 420% of the initial size for control mice and 96% to 280% for **IIIi**-treated mice. Normal weight increase was observed for all mice. The weight of final harvested tumor is slightly less for **IIIi**-treated mice than that of the control ones. All data indicated that 786-O xenografted mice

successfully survived, and compound **III** did inhibited the tumor growth for the nude mice xenograft with 786-O cells (Figure 5-14). The dosage of compound **III** at 7 mg/kg is safe for xenograft mice.

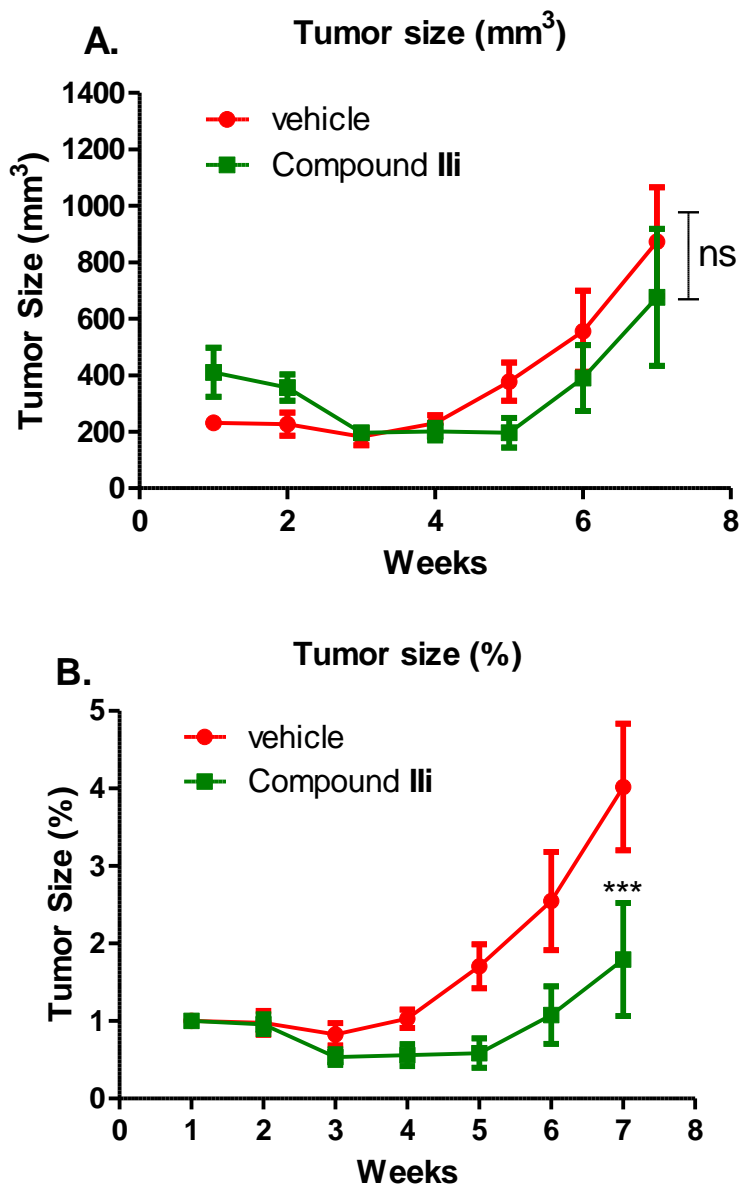


Figure 5-14. The volume (A) or percentage growth (B) of tumors for control and **III**-treated mice from 1st to 7th week. [Volume was calculated by $X_{\text{week } a} \cdot Y_{\text{week } a} \cdot X_{(\text{min week } a)}$; %: $V_{\text{week } a} / V_{\text{week } 0}$]

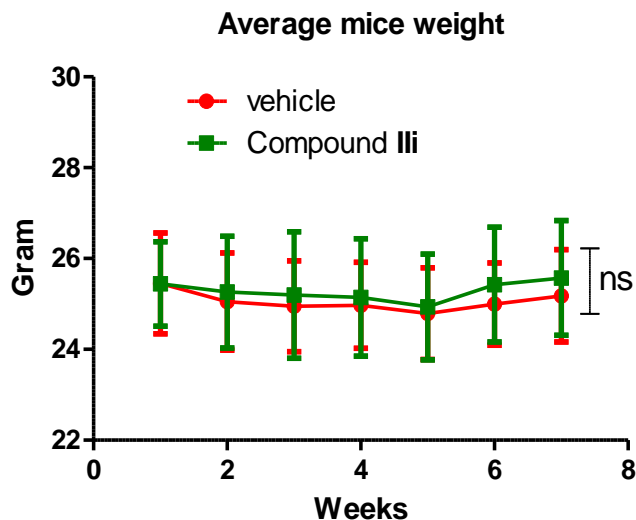


Fig 5-15. Body weight of mice for control and **III**-treated mice from 1st to 7th week.

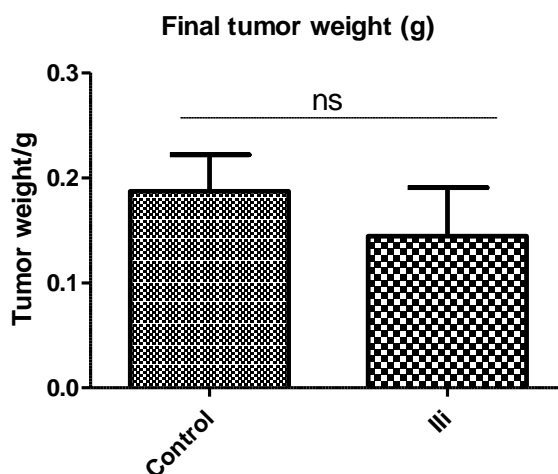


Figure 5-16. Final harvested tumor weight for control and **III**-treated mice after 7 weeks' treatment. (7mg/kg).

The in vivo efficacy of III and IIIa with Renal cancer cell line A-498. Since no satisfactory data was obtained with the renal cell lines **III** and **IIIa**, we further investigated the *in vivo* efficacy of compounds **III** and **IIIa** toward renal cancer cell line A-498. Twenty four A498-derived xenograft mice were used and divided into three groups. One group was used as control, the second group was treated with compound **III** at a dose of 7 mg/kg while the third group was

treated with compound **IIIa** at a dose of 7 mg/kg. The tumor size and body weight of mice were determined in the first day of each week. The tumor was developed in mice at the location of cancer cell injection after one week injection but the tumor size was small. The tumor grew slowly in the first-four weeks but grew rapidly from the fourth to seventh week after treatment with **IIIi** and **IIIa**. Faster growth of tumor size was observed with control mice. After seven weeks, the tumor size increased obviously in all mice, while smaller increase was observed with **IIIi**- or **IIIa**-treated mice (reaching 130%-865% of the original size) than the control mice (reaching 223 % to 1100% of the initial size). All mice had normal weight increase. The weight of harvested tumors provided further evidence that both compounds **IIIi** and **IIIa** showed slight inhibitory effect toward renal cancer A-498. Compound **IIIi** and **IIIa** showed similar inhibitory effect. These results indicated that compounds **IIIi** and **IIIa** can inhibit A-498 tumor growth, but the inhibitory effect is very poor. Compounds **IIIi** and **IIIa** did not show obvious toxicity at a dose of 7 mg/kg.

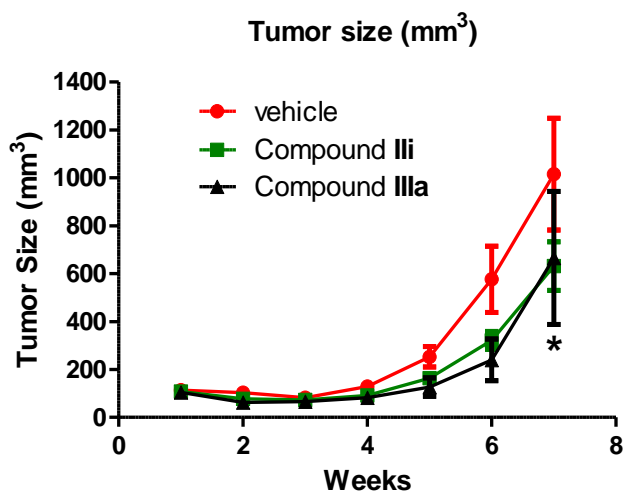


Figure 5-17. The volume of tumors for control, **IIIi** and **IIIa**-treated mice from 1st to 7th week.

[Volume was calculated by $X_{\text{week a}} \cdot Y_{\text{week a}} \cdot X_{(\text{min week a})}$]

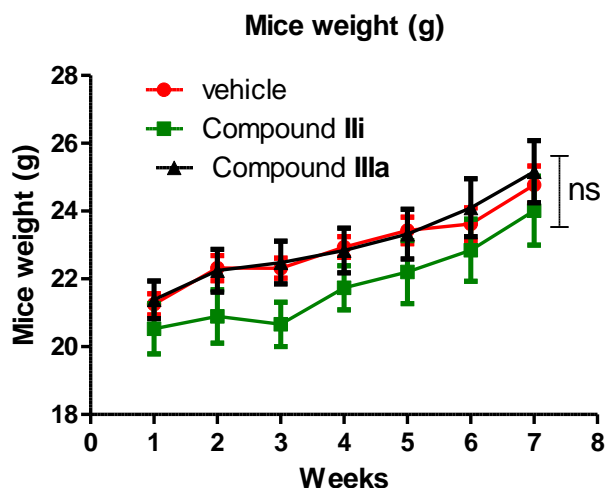


Fig 5-18. Body weight of mice for control, **IIIi** and **IIIa**-treated mice 1st to 7th week.

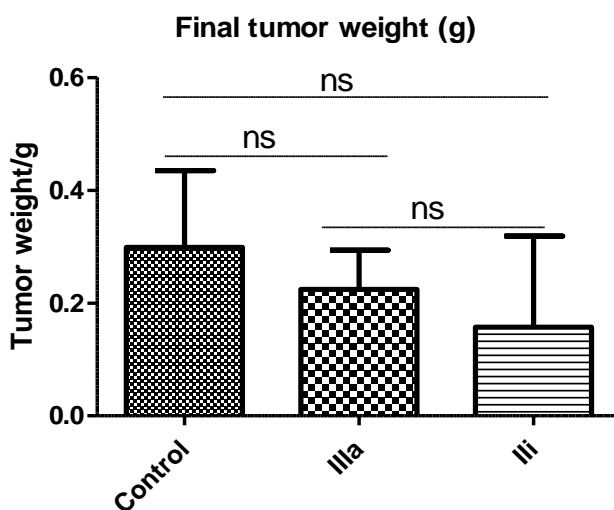


Figure 5-19. Final harvested tumor weight for control, **IIIi** and **IIIa**-treated mice after 7 weeks' treatment. (7 mg/kg).

5.4. Conclusions

In summary, breast cancer cell line MDA-MB-468, renal cancer cell lines 786-O and A-498 can successfully grow in Xenograft nude mice while renal cancer cell line UO-31 cannot. Compound **IIIi** inhibited MDA-MB-468 tumor growth in mice without obvious toxicity, while such inhibitory effect was much lower in renal cancer cell lines 786-O and A-498. Compound **IIIa**

slightly inhibited A-498 tumor growth in mice with no obvious toxicity. Compound **IVq** greatly suppressed MDA-MB-468 tumor growth in mice with slight toxicity.

5.5. Experiment protocol

5.5.1. Protocol for cell preparation

Everything must be done in biosafety hood. The hood was sprayed down with 70% ethanol and cleaned. 16 of big flasks (150 cm²), full of cancer cells, were prepared before xenograft mice study. The matrigel was stored in ice and put in 2-8 °C overnight before xenograft mice study. The media and trypsin (HyClone, cat #: SH30042.01) was pre-warmed at 37 °C and 25 °C respectively for 30 min before the assay.

Breast cancer cell line MDA-MB-468

Media component: 500 mL of L-15 Leibovitz media (cat #: SH30525.01), 50 mL of Fetal bovine serum (MIDSCI Cat#: S01520HI), 5 mL of NEAA (HyClone, cat #: SH30238.01), 5 mL of Penicillin (HyClone, cat #: SV30010). Note: don't need CO₂ for growth (small incubator without CO₂, "VENT" flask)

Preparation of cancer cells in 16 big flasks:

- i. The media and trypsin (HyClone, cat #: SH30042.01) was pre-warmed at 37 °C and 25 °C respectively for 30 min before the assay. Media component: 500 mL of L-15 Leibovitz media (cat #: SH30525.01), 50 mL of fetal bovine serum (MIDSCI Cat#: S01520HI), 5 mL of NEAA (HyClone, cat #: SH30238.01), 5 mL of penicillin (HyClone, cat #: SV30010).
- ii. Coating: add 3.0 mL matrigel solution (0.5 mL matrigel + DMEM/High modified 200 mL) and spread to the whole bottom of the flask, incubate the flask at 37 °C for 10 min. Then,

- remove the matrigel by aspiration.
- iii. Pretreat the flask: prewash the flask with 5.0 mL media and remove the media, then add 25 mL media in the flask; meanwhile, quickly thaw the cancer cells at 37 °C within 1-2 minutes (Note: cells can easily die at r.t. in DMSO).
 - iv. One flask cell growth: transfer the cells to the pre-washed flask (150 cm²) with about 25.0 mL media and incubate the cells at 37 °C for about 2-7 days (the cells are spreading in the bottom of the flask).
 - v. Remove the media in the flask with MDA-MB-468 cell lines by aspiration and 5 mL media was added to wash the bottom of the flask, remove the media carefully not touching the bottom.
 - vi. Add trypsin (SH 30042.01, Hyclone) (4 mL) to the flask and incubate at 37 degree for 5 min.
 - vii. Homogenization of cells solution by pipetting the solution up and down 10 times in the corner of the flask.
 - viii. Transfer 1 mL solution into four new flasks (150 cm²) which were pre-treated with 3 mL of matrigel solution (VWR cat #: 47743-715) (Step ii, coating), and add 25 mL media to the flask for cells growing.
 - ix. Three to seven days later, prepare 16 big flasks of cells by repeating step i to v on every flask which is full cancer cells. The total approximate time is two to three weeks.

Renal cancer cell line (UO-31, 786-O, A-498)

Media component: 500 mL of RPMI 1640, 1X with L-glutamine media (VWR cat #: 45000-396), 50 mL of Fetal bovine serum (MIDSCI Cat#: S01520HI), 5 mL of Penicillin (HyClone, cat

#: SV30010). Note: CO₂ is necessary for cell growth (big incubator with CO₂, flask: not vent).

Other renal cancer cell lines in our lab use the same method for growth.

- i. One flask cell growth: transfer the cells to the flask (don't need coating) (150 cm²) with about 25.0 mL media and incubate the cells at 37 °C for about 2-7 days (the cells are spreading in the bottom of the flask).
- ii. Remove the media in the flask with cell lines by aspiration and 5 mL media was added to wash the bottom of the flask, remove the media carefully not touching the bottom.
- iii. Add the trypsin (SH 30042.01, Hyclone) (4 mL) to the flask and incubate at 37 degree for 5 min.
- iv. Homogenize the cells solution by pipetting the solution up and down 10 times in the corner of the flask.
- v. Transfer 1 mL solution into four new flasks (150 cm²), and add 25 mL media to the flask for cells growing.
- vi. Three to seven days later, prepare 16 big flasks of cell lines by repeating step ii to v on every flask which is full cancer cell lines. The total approximate time is two to three weeks.

5.5.2. Protocol for cell injection to nude mice

1. Store the matrigel on ice and stay in 2-8 °C overnight before xenograft mice study.

Remove the media in the flask containing cancer cell lines by aspiration and 5 mL media was added to wash the bottom of the flask, remove the media carefully not touching the bottom. 4 flasks were done one time.

2. Add trypsin (6 mL) to the flask and incubate at 37 °C for 10 min until all the cells detached from the bottom.
3. Homogenize the cells solution by pipetting the solution up and down 10 time in the corner of the flask and transfer the detached cells (4 flasks) to a 50 mL conical tube (4 X 6 mL), then wash the 4 flasks with 25 mL media, collect in the conical tube (4 X 6 mL+25 mL), total 4 conical tubes.
4. Spin down the cells in the 4 conical tubes (1000 rpm, 5 min) and remove the media carefully.
5. Add 10 mL media to each conical tube mix (up and down 10 times) and combine the solution in 50 mL conical tube, centrifuge (1000 rpm, 5 min) and remove the media again.
6. Add 5 mL media to the cell lines, mix and divided them into 25 small tubes (150-200 uL each tube).
7. Spin down for (1000 rpm, 1 min) and discard half of the supernatant.
8. Mix the cell lines with the same volume of matrigel (100-160 uL) with pipette (keep the matrigel in ice, then put in 4°C refrigerator as the matrigel can easily solidify at room temperature) and inject 100 µL of the mixture to each mice.
9. Injection: 0.1 mL of above solution was injected under skin of the mice, the inject position was on the back close to the legs.

5.5.3. Protocol for compound injection to nude mice

Formulation:

Vehicle: In two of 1.5 mL vials, add 75 μ L of DMSO, 712 μ L of PEG400 and 712 μ L of PBS (1X) (Cat No SH30256.01). Mix well by pipetting 10 times or shaking tube.

Drug solution (Order of adding different solutions is extremely important): (1) In two of 1.5 mL vials, add 75 μ L of drug solution (DMSO); (2) add 712 μ L of PEG400 and mix; (3) add 712 μ L of PBS (1X) (Cat No SH30256.01) and mix well (add half of it and mix, then add remaining); (4)

For a dose of 10 mg/kg, the weight of mice is 20 g in average. Compound (6 mg) was dissolved in 150 μ L of DMSO.

Injection protocol:

0.1 mL of compound solution was injected each day and 5 days/per week in the belly of the mice, the injection position was close to and under the nipple. The treatment lasts for 6-8 weeks.

5.6. References

1. Ralhan R., Kaur J. Alkylating agents and cancer therapy. *Expert Opinion on Therapeutic Patents*. 2007;17:1061-1075.
2. Rajsiki SR, Williams RM. DNA Cross-Linking Agents as Antitumor Drugs. *Chemical Reviews*. 1998;98:2723–96.
3. Verga D, Nadai M, Doria F, Percivalle C, Antonio MD, Palumbo M, et al. Photogeneration and Reactivity of Naphthoquinone Methides as Purine Selective DNA Alkylating Agents. *Journal of the American Chemical Society*. 2010;132:14625–37.
4. Richter SN, Maggi S, Mels SC, Palumbo M, Freccero M. Binol Quinone Methides as Bisalkylating and DNA Cross-Linking Agents. *Journal of the American Chemical Society*. 2004;126:13973–9.
5. Percivalle C, Rosa AL, Verga D, Doria F, Mella M, Palumbo M, et al. Quinone Methide Generation via Photoinduced Electron Transfer. *The Journal of Organic Chemistry*. 2011;76:3096–106.

6. Nadai M, Doria F, Germani L, Richter SN, Freccero M. A Photoreactive G-Quadruplex Ligand Triggered by Green Light. *Chemistry - A European Journal*. 2015;21:2330–4.
7. Colloredo-Mels S, Doria F, Verga D, Freccero M. Photogenerated Quinone Methides as Useful Intermediates in the Synthesis of Chiral BINOL Ligands. *The Journal of Organic Chemistry*. 2006;71:3889–95.
8. Wang P, Liu R, Wu X, Ma H, Cao X, Zhou P, et al. A Potent, Water-Soluble and Photoinducible DNA Cross-Linking Agent. *Journal of the American Chemical Society*. 2003;125:1116–7.
9. Kuang Y, Sun H, Blain JC, Peng X. Hypoxia-Selective DNA Interstrand Cross-Link Formation by Two Modified Nucleosides. *Chemistry - A European Journal*. 2012;18:12609–13.
10. Doria F, Richter SN, Nadai M, Colloredo-Mels S, Mella M, Palumbo M, et al. BINOL–Amino Acid Conjugates as Triggerable Carriers of DNA-Targeted Potent Photocytotoxic Agents. *Journal of Medicinal Chemistry*. 2007;50:6570–9.
11. Wang Y, Liu S, Lin Z, Fan Y, Wang Y, Peng X. Photochemical Generation of Benzyl Cations That Selectively Cross-Link Guanine and Cytosine in DNA. *Organic Letters*. 2016;18:2544–7.
12. Veldhuyzen WF, Pande P, Rokita SE. A Transient Product of DNA Alkylation Can Be Stabilized by Binding Localization. *Journal of the American Chemical Society*. 2003;125:14005–13.
13. Wang H, Rokita SE. Dynamic Cross-Linking Is Retained in Duplex DNA after Multiple Exchange of Strands. *Angewandte Chemie International Edition*. 2010;49:5957–60.
14. Wu J, Huang R, Wang T, Zhao X, Zhang W, Weng X, et al. Fluoride as an inducible DNA cross-linking agent for new antitumor prodrug. *Organic & Biomolecular Chemistry*. 2013;11:2365–9.
15. Hong IS, Ding H, Greenberg MM. Oxygen Independent DNA Interstrand Cross-Link Formation by a Nucleotide Radical. *Journal of the American Chemical Society*. 2006;128:485–91.

16. Hong IS, Greenberg MM. DNA Interstrand Cross-Link Formation Initiated by Reaction between Singlet Oxygen and a Modified Nucleotide. *Journal of the American Chemical Society*. 2005;127:10510–1.
17. Peng X, Hong IS, Li H, Seidman MM, Greenberg MM. Interstrand Cross-Link Formation in Duplex and Triplex DNA by Modified Pyrimidines. *Journal of the American Chemical Society*. 2008;130:10299–306.
18. Weng X, Ren L, Weng L, Huang J, Zhu S, Zhou X, et al. Synthesis and Biological Studies of Inducible DNA Cross-Linking Agents. *Angewandte Chemie International Edition*. 2007;46:8020–3.
19. Antonio MD, Doria F, Mella M, Merli D, Profumo A, Freccero M. Novel Naphthalene Diimides as Activatable Precursors of Bisalkylating Agents, by Reduction and Base Catalysis. *The Journal of Organic Chemistry*. 2007;72:8354–60.
20. Gilkes DM, Semenza GL, Wirtz D. Hypoxia and the extracellular matrix: drivers of tumour metastasis. *Nature Reviews Cancer*. 2014;14:430–9.
21. Tercel M, Lee AE, Hogg A, Anderson RF, Lee HH, Siim BG, et al. Hypoxia-Selective Antitumor Agents. 16. Nitroarylmethyl Quaternary Salts as Bioreductive Prodrugs of the Alkylating Agent Mechlorethamine. *Journal of Medicinal Chemistry*. 2001;44:3511–22.
22. Singleton RS, Guise CP, Ferry DM, Pullen SM, Dorie MJ, Brown JM, et al. DNA Cross-Links in Human Tumor Cells Exposed to the Prodrug PR-104A: Relationships to Hypoxia, Bioreductive Metabolism, and Cytotoxicity. *Cancer Research*. 2009;69:3884–91.
23. Patterson AV, Ferry DM, Edmunds SJ, Gu Y, Singleton RS, Patel K, et al. Mechanism of Action and Preclinical Antitumor Activity of the Novel Hypoxia-Activated DNA Cross-Linking Agent PR-104. *Clinical Cancer Research*. 2007;13:3922–32.
24. Atwell GJ, Yang S, Pruijn FB, Pullen SM, Hogg A, Patterson AV, et al. Synthesis and Structure–Activity Relationships for 2,4-Dinitrobenzamide-5-mustards as Prodrugs for the *Escherichia coli* Nitroreductase in Gene Therapy. *Journal of Medicinal Chemistry*. 2007;50:1197–212.
25. Johnson KM, Parsons ZD, Barnes CL, Gates KS. Toward Hypoxia-Selective DNA-Alkylating Agents Built by Grafting Nitrogen Mustards onto the Bioreductively Activated,

Hypoxia-Selective DNA-Oxidizing Agent 3-Amino-1,2,4-benzotriazine 1,4-Dioxide (Tirapazamine). *The Journal of Organic Chemistry*. 2014;79:7520–31.

26. Szatrowski TP, Nathan C F. Production of large amounts of hydrogen peroxide by human tumor cells. *Cancer Research*.1991;51:794-798.

27. Brown NS, Bicknell R. Hypoxia and oxidative stress in breast cancer Oxidative stress - its effects on the growth, metastatic potential and response to therapy of breast cancer. *Breast Cancer Research*. 2001;3:323-7.

28. Lim SD, Sun C, Lambeth JD, Marshall F, Amin M, Chung L, et al. Increased Nox1 and hydrogen peroxide in prostate cancer. *The Prostate*. 2005;62:200–7.

29. Wang Y, Lin Z, Fan H, Peng X. Photoinduced DNA Interstrand Cross-Link Formation by Naphthalene Boronates via a Carbocation. *Chemistry - A European Journal*. 2016;22:10382–6.

30. Cao S, Wang Y, Peng X. The Leaving Group Strongly Affects H₂O₂-Induced DNA Cross-Linking by Arylboronates. *The Journal of Organic Chemistry*. 2014;79:501–8.

31. Cao S, Wang Y, Peng X. ROS-Inducible DNA Cross-Linking Agent as a New Anticancer Prodrug Building Block. *Chemistry - A European Journal*. 2012;18:3850–4.

32. Cao S, Christiansen R, Peng X. Substituent Effects on Oxidation-Induced Formation of Quinone Methides from Arylboronic Ester Precursors. *Chemistry - A European Journal*. 2013;19:9050–8.

33. Wang Y, Fan H, Balakrishnan K, Lin Z, Cao S, Chen W, et al. Hydrogen peroxide activated quinone methide precursors with enhanced DNA cross-linking capability and cytotoxicity towards cancer cells. *European Journal of Medicinal Chemistry*. 2017;133:197–207.

34. Kuang Y, Balakrishnan K, Gandhi V, Peng X. Hydrogen Peroxide Inducible DNA Cross-Linking Agents: Targeted Anticancer Prodrugs. *Journal of the American Chemical Society*. 2011;133:19278–81.

35. Chen W, Balakrishnan K, Kuang Y, Han Y, Fu M, Gandhi V, et al. Reactive Oxygen Species (ROS) Inducible DNA Cross-Linking Agents and Their Effect on Cancer Cells and Normal Lymphocytes. *Journal of Medicinal Chemistry*. 2014;57:4498–510.

36. Chen W, Han Y, Peng X. Aromatic Nitrogen Mustard-Based Prodrugs: Activity, Selectivity, and the Mechanism of DNA Cross-Linking. *Chemistry - A European Journal*. 2014;20:7410–8.

Chapter 6. The Effect of Triazole-modified Thymidines on DNA and RNA Duplex Stability

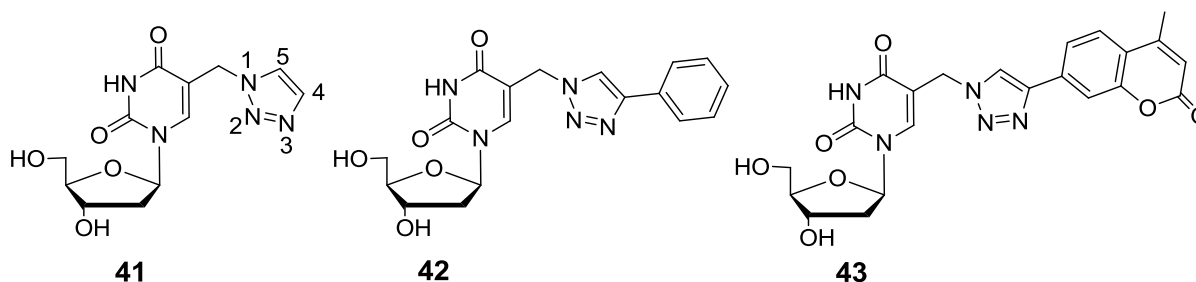
6.1. Introduction

Chemical modification of nucleosides or nucleotides is an important tool to introduce functional or desired group in oligodeoxynucleotides (ODNs). The chemically modified ODNs have wide applications in biological research. For example, they have been used for DNA damage and repair studies,¹⁻² as fluorescent dyes for nucleic acid detection,³⁻⁴ for developing photo-reversible DNA fluorescent switches,⁵ and as building blocks for nanostructure construction.⁶ The chemical modifications have been incorporated either at sugar phosphate backbond, sugar ring or the nucleobase moieties in order to control many important properties of nucleic acids,⁷⁻¹¹ such as nuclease stability, binding affinity for RNA/DNA targeting, thermal stability, and immunostimulatory properties.⁷ The modification at nucleobase is especially important due to its multiple biological applications. Base-modified nucleosides have been applied for reducing immunostimulation, as fluorophores for mutation detection, and to adjust nucleic acid binding efficiency and thermal stabilities.^{7,12} Two major strategies have been used for nucleobase modification, namely by introduction of functional groups or via ring extension.¹³ The incorporation of functional groups can change the property of the nucleobases while ring extension can increase the $\pi - \pi$ stacking, therefore increasing the stability of DNA duplex.¹⁴ One good example for the ring extension is the construction of the phenothiazine tricyclic pyrimidine nucleoside, which greatly improved the thermal stability of the DNA: RNA duplex (up to 5 °C).⁹ Moreover, the [1,2,3]-triazole was considered to be an ideal group for nucleobase modification, not only because the [1,2,3]-triazoles have wide biological activities and industrial

applications,¹⁵ but also because they can be easily incorporated via the Cu(I)-catalyzed “click” reactions. Several triazole-modified nucleosides have been synthesized and their applications have been explored in different areas.^{5,14,16} They are used as DNA interstrand cross-linking agents,⁵ as drugs for the treatment of tuberculosis,¹⁶ and for improving the thermal stability of the ODN duplexes.¹⁴ The effect of triazole-modified 2'-deoxyuridines on the stability of DNA•DNA and DNA•RNA duplexes has been investigated by Nielsen's group.^{17,18} The results showed that even though a single nucleobase modification decreased the stability of the DNA duplexes, the introduction of two or more consecutive modifications did improve the duplex stability due to the additional π - π stacking of triazole moieties. Such stabilizing effect was found even stronger in DNA•RNA duplexes. Most of the triazole-modified pyrimidines were constructed by treating the alkyne-modified 2'-deoxyuridines with azides to form 5-(1,2,3-triazol-4-yl)-2'-deoxyuridines. However, less attention has been paid on the properties of a triazole moiety synthesized from azide-modified nucleosides. In addition, the effect of C4-substituents on the triazole moieties towards the thermal stability of DNA•DNA and DNA•RNA duplexes has not been explored, which limited our understanding about the thermal properties of triazole-modified ODNs.

In this chapter, a systematic investigation was carried out to understand how triazole-modified thymidines affect the thermal stabilities of DNA•DNA and DNA•RNA duplexes. The triazole-modified thymidines were constructed by treating azide-modified thymidine with alkynes to form 5-((1H-1,2,3-triazol-1-yl)methyl)-2'-deoxyuridines (**41-43**) (Scheme 6-1). A detailed study was performed to figure out how the triazole moieties affect pK_a values of the modified thymidines and the thermal stability of DNA•DNA and DNA•RNA duplexes. The pH dependence of the duplex stability was also investigated and DFT computation was used for

DNA modeling and geometry study. Such systematic study provides more information about the thermal properties of triazole-modified ODNs, which is important for further design of biologically functionalized ODNs.

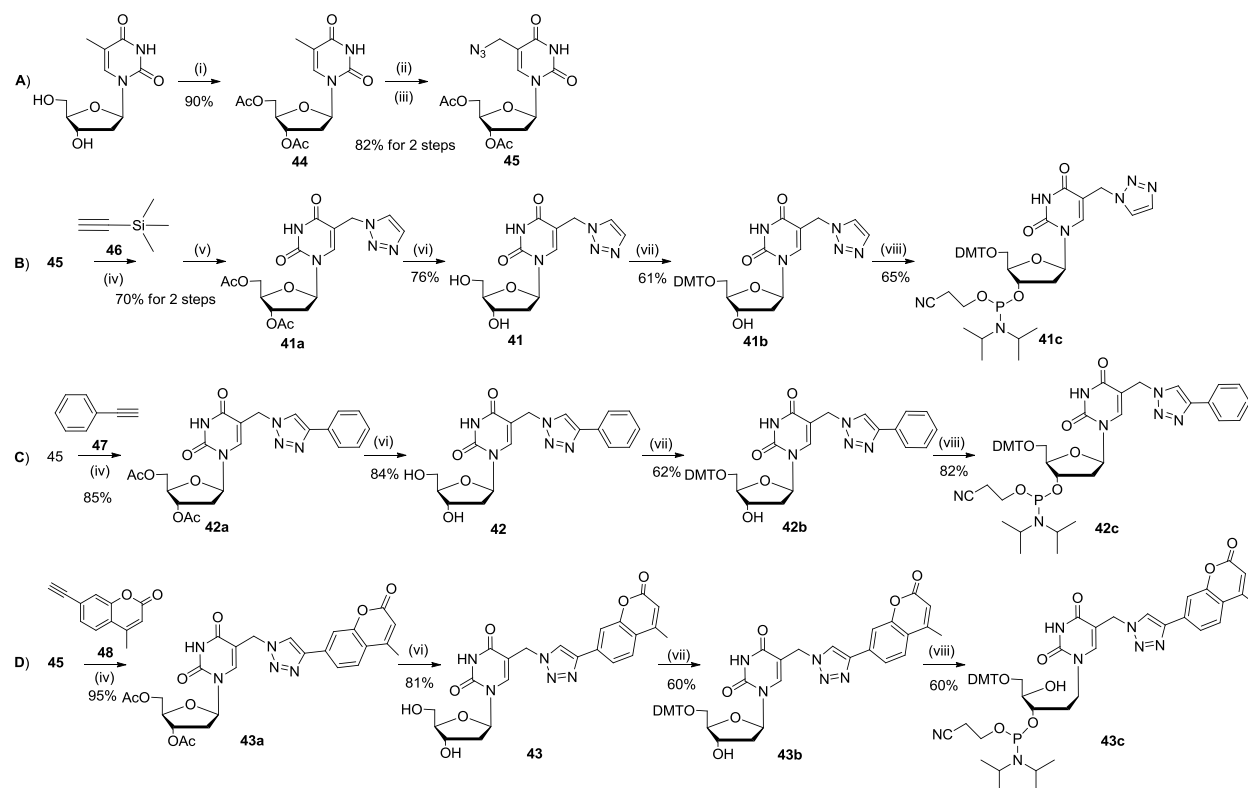


Scheme 6-1. The structure of triazole-modified pyrimidine nucleosides.

6.2. Synthesis of triazole-modified pyrimidine nucleosides and oligodeoxyribonucleotides containing triazole-modified thymidines.

Three triazole-modified thymidines (**41-43**) were designed and synthesized to investigate the effects of triazole ring and C4-substituents of the triazole moiety on stability of DNA:DNA/RNA duplexes. A triazole moiety was introduced to thymidine to form **41** while triazoles with a phenyl or coumarin substituent at the position-4 of triazole ring were incorporated to yield compounds **42** and **43**, respectively (Scheme 6-2). Acetylation of thymidine provided **44** that was further converted to azide-modified thymidine **45** via bromination with *N*-bromosuccinimide (NBS) using azobisisobutyronitrile (AIBN) as an activator, followed by sodium azide treatment (Scheme 6-2A).¹⁹ The Cu (I)-catalyzed “click reaction” was used for the introduction of triazole moiety by treating **45** with different alkynes (**46, 47, 48**) to afford **41a**, **42a** and **43a**, respectively (Scheme 6-2). Deacetylation of **41a**, **42a** and **43a** afforded **41**, **42**, and **43**, respectively. Compounds **41**, **42**, and **43** were converted to **41b**, **42b**, and **43b**, respectively via selective tritylation at 5'-O-position. Finally, the phosphoramidites **41c**, **42c**, and **43c** were

prepared from the corresponding DMT-derivatives **41b**, **42b**, and **43b** by reacting with 2-cyanoethyl-*N,N*-diisopropylchlorophosphoramidite.⁵ The phosphoramidites (**41c**, **42c**, and **43c**) were used for ODN synthesis with the standard solid-phase DNA synthesis method.



Scheme 6-2. Synthesis of compounds **41-43** and the corresponding phosphoramidites **41c-43c**.

Reagents and conditions: (i) Ac_2O , pyridine; (ii) NBS, AIBN, benzene, reflux; (iii) NaN_3 , DMF; (iv) Cu_2SO_4 , sodium ascorbate, MeOH; (v) TBAF, MeOH, 70 °C; (vi) NH_4OH , MeOH; (vii) Dimethoxytrityl chloride (DMTCI), pyridine; (viii) 2-cyanoethyl-*N,N*-diisopropylchlorophosphoramidite, *N,N*-diisopropylethylamine and CH_2Cl_2 .

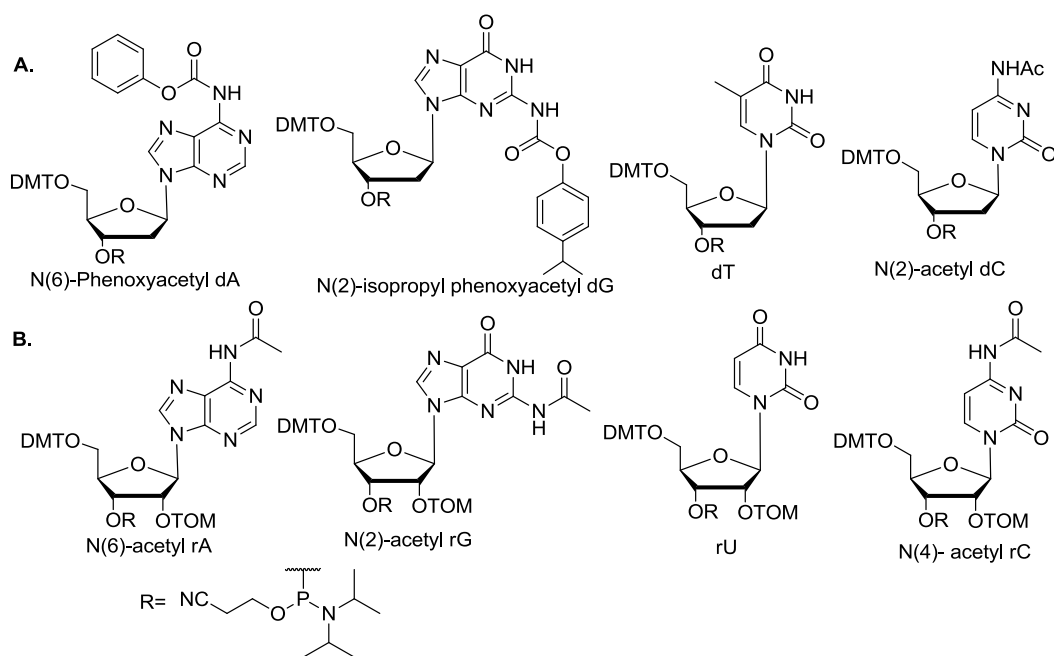
In order to figure out whether the base-pairing properties, π - π stacking, or the stability of the duplex DNAs will be affected by the triazole moieties, we synthesized ODNs with single or consecutive modifications of **41-43** (Scheme 6-4). For better comparison, the native DNA duplex-**49** [3'-d(TCTACCTAAATCCATG) (**49a**) • 5'-d(AGATGGATTAGGTAC (**49b**))] and

native DNA • RNA duplex-**59** [3'-d(UCUACCUAAAUCCAUG) (**59a**) • 5'-

d(AGATGGATTTAGGTAC (**49b**))] were used as reference.

The native ODNs (**49a**, **49b**, **59a**) were synthesized via standard solid-phase ODN synthesis technique (Scheme 2-5) using corresponding phosphoramidites (Scheme 2-5 and Scheme 6-3).

The ODNs (**50b-58b**) containing modified nucleotides (**41-43**) were synthesized using β -cyanoethyl phosphoramidites where the exocyclic amines of dA and dG were protected by phenoxyacetyl groups (Scheme 6-3), which can be deprotected under mild conditions.



Scheme 6-3. Structures of regular phosphoramidites used for DNA (A) or RNA (B) oligonucleotidesynthesis.

Deprotection/cleavage of the native ODNs was carried out in a mixture of 40% aqueous MeNH₂ and 28% aqueous NH₃ (1:1) at room temperature for 2 h. Modified ODNs were deprotected and cleaved under mild conditions using 28% aq. NH₃ at room temperature for 2 h. The deprotection of native RNA was carried out using a mixture of 40% aqueous MeNH₂ and 28% aqueous NH₃

(1:1) at room temperature for 3 h. The desilylation was performed in a mixture of 100 μ L anhydrous DMSO and 125 μ L of TEA·3HF at 65°C for 2.5 h. All ODNs were purified by 20% PAGE and characterized by MALDI-TOF-MS (Appendix B).

3'-dTCTACCTAAATCCATG (49a) 5'-dAGATGGATTTAGGTAC (49b) ds DNA-49	3'-dUCUACCUAAAUCCAUG (59a) 5'-dAGATGGATTTAGGTAC (49b) ds RNA·DNA-59
3'-dTCTACCTA A ATCCATG (49a) 5'-dAGATGGAT 41 TAGGTAC (50b) ds DNA-50	3'-dUCUACCUA A AUCCAUG (59a) 5'-dAGATGGAT 41 TAGGTAC (50b) ds RNA·DNA-60
3'-dTCTACCTA A ATCCATG (49a) 5'-dAGATGGAT 42 TAGGTAC (51b) ds DNA-51	3'-dUCUACCUA A AUCCAUG (59a) 5'-dAGATGGAT 42 TAGGTAC (51b) ds RNA·DNA-61
3'-dTCTACCTA A ATCCATG (49a) 5'-dAGATGGAT 43 TAGGTAC (52b) ds DNA-52	3'-dUCUACCUA A AUCCAUG (59a) 5'-dAGATGGAT 43 TAGGTAC (52b) ds RNA·DNA-62
3'-dTCTACCTA A A TCCATG (49a) 5'-dAGATGGAT 41 41 AGGTAC (53b) ds DNA-53	3'-dUCUACCUA A A UCCAUG (59a) 5'-dAGATGGAT 41 41 AGGTAC (53b) ds RNA·DNA-63
3'-dTCTACCTA A A TCCATG (49a) 5'-dAGATGGAT 42 42 AGGTAC (54b) ds DNA-54	3'-dUCUACCUA A A UCCAUG (59a) 5'-dAGATGGAT 42 42 AGGTAC (54b) ds RNA·DNA-64
3'-dTCTACCTA A A TCCATG (49a) 5'-dAGATGGAT 43 43 AGGTAC (55b) ds DNA-55	3'-dUCUACCUA A A UCCAUG (59a) 5'-dAGATGGAT 43 43 AGGTAC (55b) ds RNA·DNA-65
3'-dTCTACCT A A A TCCATG (49a) 5'-dAGATGGA 41 41 41 AGGTAC (56b) ds DNA-56	3'-dUCUACCU A A A UCCAUG (59a) 5'-dAGATGGA 41 41 41 AGGTAC (56b) ds RNA·DNA-66
3'-dTCTACCT A A A TCCATG (49a) 5'-dAGATGGA 42 42 42 AGGTAC (57b) ds DNA-57	3'-dUCUACCU A A A UCCAUG (59a) 5'-dAGATGGA 42 42 42 AGGTAC (57b) ds RNA·DNA-67
3'-dTCTACCT A A A TCCATG (49a) 5'-dAGATGGA 43 43 43 AGGTAC (58b) ds DNA-58	3'-dUCUACCU A A A UCCAUG (59a) 5'-dAGATGGA 43 43 43 AGGTAC (58b) ds RNA·DNA-68

Scheme 6-4. Double-stranded DNAs and RNA·DNAs used for this study.

6.3. Determination of pK_a values by UV spectroscopy.

The base-pairing strength of DNA duplexes highly depends on the acid ionization/dissociation constants (pK_a) of the nucleobases. The greater the pK_a difference (ΔpK_a) between two matched

nucleobases, the stronger the base pairing.²⁰ To investigate whether the triazole moiety influences the pK_a value of thymine, we tested the pK_a values of **42-43** using UV spectroscopy (Figure 6-1 to Figure 6-9). The pK_a values obtained for compounds **41** and **43** are 8.4 and 10.7, respectively, possibly due to deprotonation of thymine moiety. Interestingly, two pK_a values (4.3 and 8.4) were observed for compound **42**. The pK_a value of 8.4 possibly arose from deprotonation of thymine base, which is similar to that of compound **41** and **43**, while the pK_a value of 4.3 might result from protonation of triazole moiety. In comparison with native thymidine (pK_a 9.8), the introduction of triazole or 4-phenyltriazole moiety slightly decreased the pK_a value of thymidine. On the other hand, the incorporation of coumarin-modified triazole moiety led to increased pK_a value. It was reported that the strong base-pairing can be formed only when the ΔpK_a value between two complementary nucleobases is 5 or greater.²⁰ For example, the ΔpK_a between native deoxyadenosine (dA) (pK_a of 3.8) and deoxythymidine (dT) (pK_a 9.8) is 6.0, so a strong A-T base pair can be formed. Similar to that of native dA-dT, the ΔpK_a between compound **43** and deoxyadenosine (dA) is 6.9, greater than 5, therefore the base pairing between them is expected to be strong. The ΔpK_a of **41**-dA and **42**-dA is 4.6, which is smaller than 5, so the base pairs' strength should be smaller than that of native dT-dA.

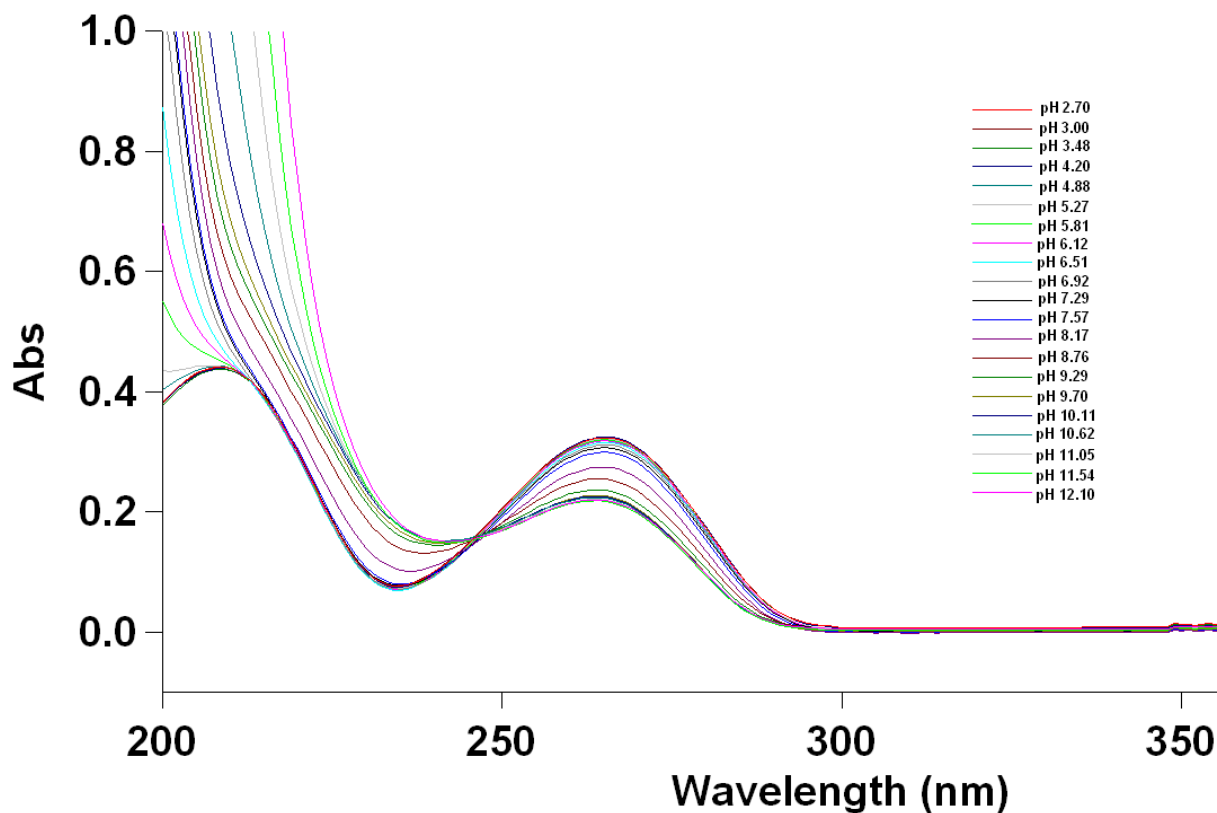


Figure 6-1. UV-Spectra changes of compound 41 in phosphate buffer solution from pH 2.7 to 12.1.

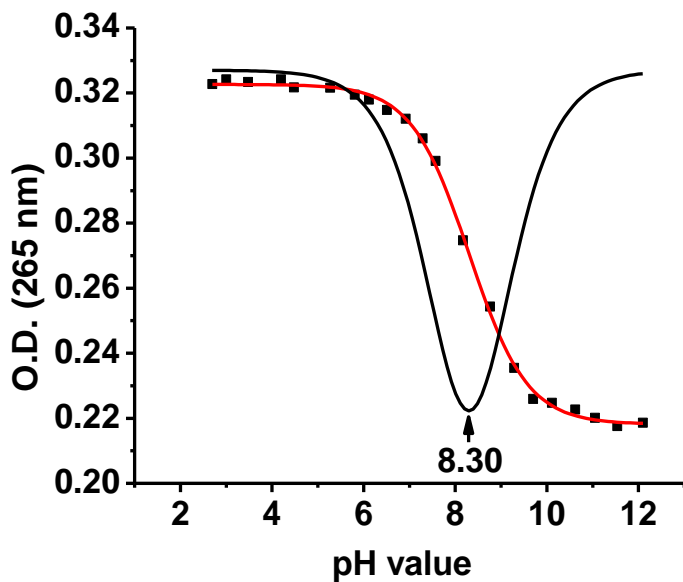


Figure 6-2. UV-absorbance of compound 41 as a function of pH values measured at 265 nm.

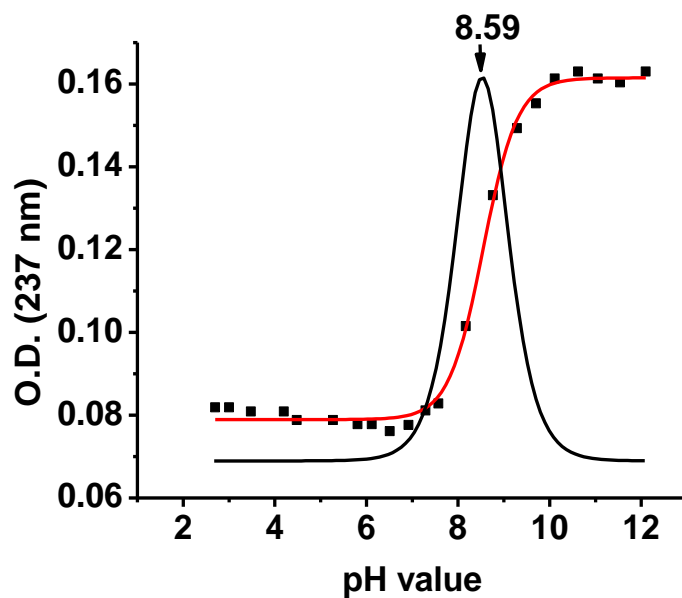


Figure 6-3. UV-absorbance of compound **41** as a function of pH values measured at 237 nm.

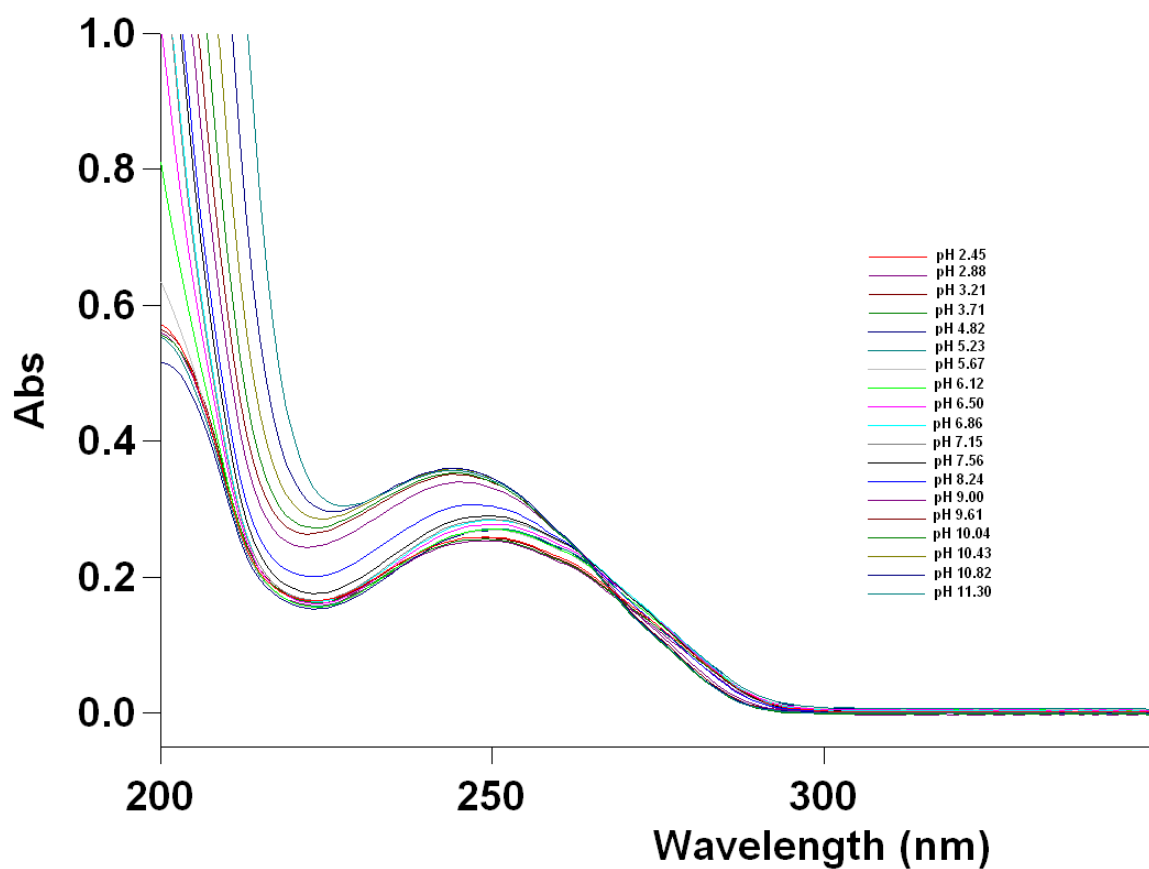


Figure 6-4. UV-Spectra changes of compound **42** in phosphate buffer solution from pH 2.4 to 11.3.

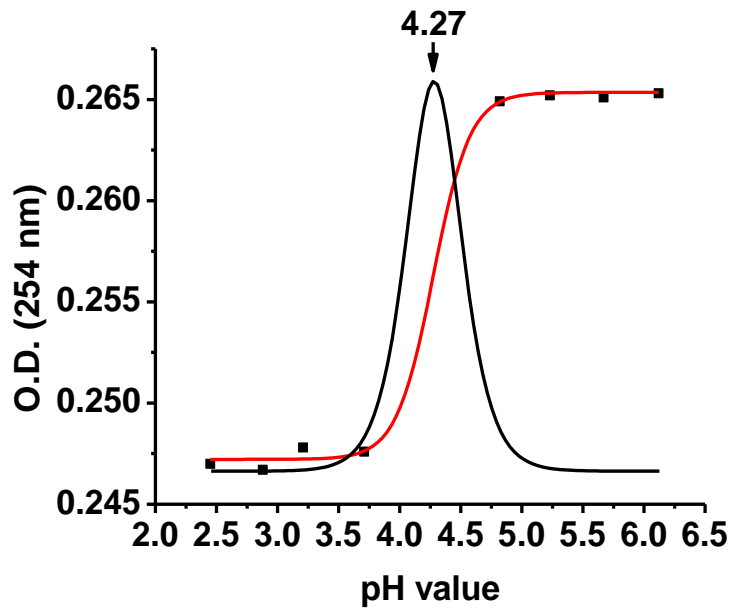


Figure 6-5. UV-absorbance of compound 42 as a function of pH values measured at 254 nm.

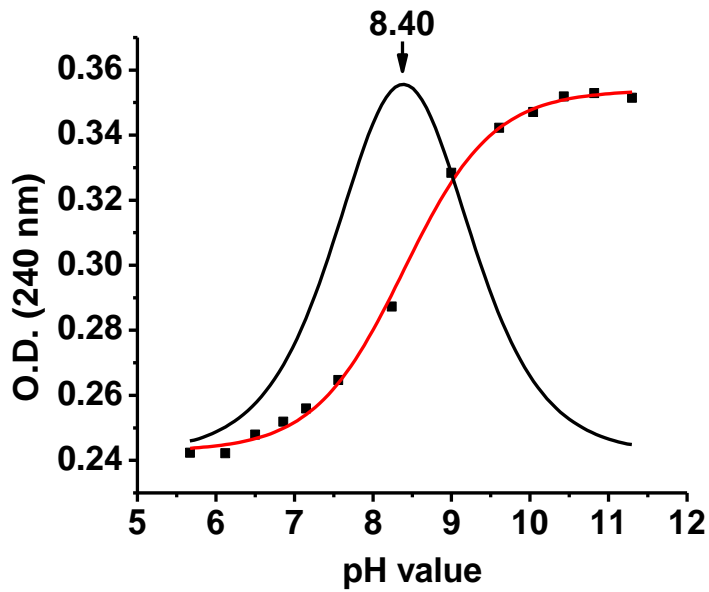


Figure 6-6. UV-absorbance of compound 42 as a function of pH values measured at 240 nm.

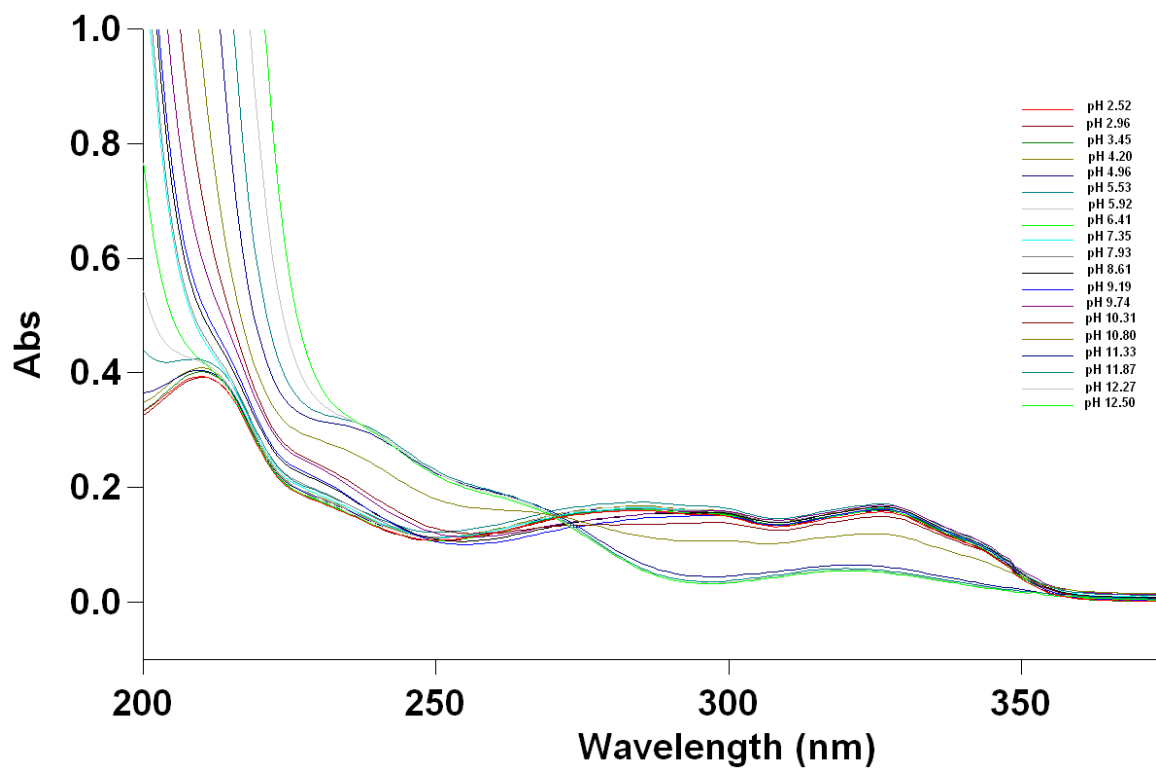


Figure 6-7. UV-Spectra changes of compound **43** in phosphate buffer solution from pH 2.5 to 12.5.

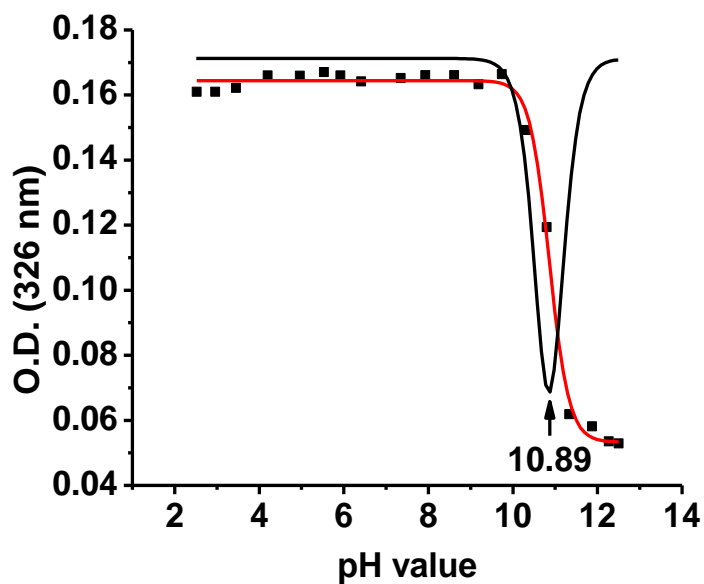


Figure 6-8. UV-absorbance of compound **43** as a function of pH values measured at 326 nm.

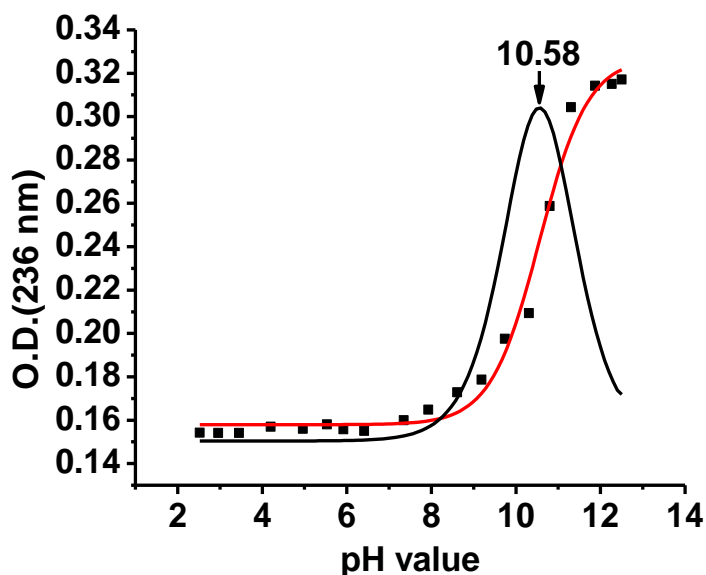


Figure 6-9. UV-absorbance of compound **43** as a function of pH values measured at 236 nm.

6.4. The effect of pH values on the stability of DNA duplexes.

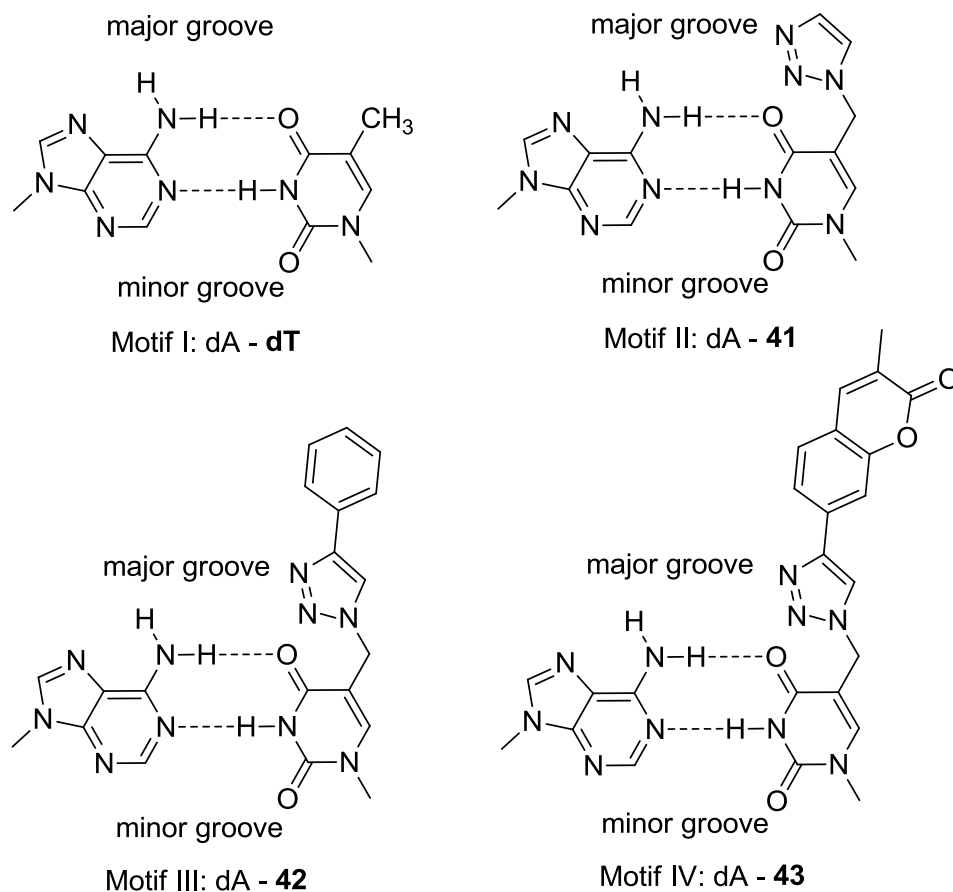
It was reported that the pH value of the medium has a large effect on the stability of DNA duplexes.²¹ Thus, we investigated the stability of DNA duplexes in phosphate buffer of different pH (pH 5-9). The ODN duplexes' thermal stability was determined by testing the melting temperature (T_m), defined as the temperature at which half of a double helix dissociates into single strands. For better comparison, the melting temperature of the native DNA duplex (duplex-**49**) was determined first in different buffers (pH 5-9) (Table 6-1). The results showed that the pH value of the medium has a large effect on the stability of duplex **49**. The stability of DNA duplex was found to be the highest at pH 7, slightly reduced at pH 6 and 8, and significantly decreased at pH 5 and 9. This phenomenon is explainable from pK_a . The pK_a values of dA and dT are 3.8 and 9.8, respectively. Protonation of dA is possible at pH 5 (about 6%) while deprotonation of thymine may occur at pH 9 (about 16%), which both could in turn disrupt the dA-dT base pairs formation, destabilizing the DNA duplexes (Scheme 6-5). Then, we tested

the melting temperature of the ODNs containing artificial bases (**41-43**) by incubating in buffers with different pH (5-9). Similar trends were observed for the modified ODN duplexes-**50**, **51**, and **52** containing **41-43** in buffers with different pH values (pH 5-9). The DNA duplexes are the most stable in neutral condition, while the stability slightly decreased at weak acidic or basic conditions, and significantly reduced at strong acidic or basic conditions. Even though the introduction of triazole moieties slightly alters the pK_a values of thymidine, the stability response of the modified ODNs toward pH value of the media is consistent to that of regular DNA duplex. Since the highest DNA duplex stability was found at pH 7.0 (highest T_m), further experiments were carried out in the pH 7.0 phosphate buffer.

Table 6-1. T_m -Values of oligonucleotides in different pH values^{a,b}

Duplex DNA	pH 5		pH 6		pH 7		pH 8		pH 9	
	T_m (°C)	ΔT_m (°C)	T_m (°C)	ΔT_m (°C)	T_m (°C)	ΔT_m (°C)	T_m (°C)	ΔT_m (°C)	T_m (°C)	ΔT_m (°C)
ds DNA-49	48.7±0.2	---	51.8±0.3	---	52.0±0.2	---	52.0±0.3	---	50.9±0.1	---
ds DNA-50	45.1±0.1	-3.6	48.0±0.2	-3.8	48.8±0.2	-3.2	48.5±0.1	-3.5	47.3±0.3	-3.6
ds DNA-51	41.9±0.2	-6.8	45.4±0.2	-6.4	45.9±0.3	-6.1	45.7±0.3	-6.3	43.8±0.2	-7.1
ds DNA-52	39.5±0.2	-9.2	43.3±0.1	-8.5	43.8±0.1	-8.2	43.3±0.1	-8.7	42.0±0.2	-8.9

^a The melting temperatures were determined in 10 mM potassium phosphate buffer (pH 5.0-9.0), 100 μ M ethylenediaminetetraacetic acid (EDTA), and 100 mM NaCl, with 4 μ M + 4 μ M single-strand concentration. ^bAll data are the average of three experiments.



Scheme 6-5. Watson-Crick base pair motifs of dA-dT/**41/42/43**.

6.5. Substituent effects on the thermal stability of DNA duplexes.

The regular DNA duplex-**49** has a melting temperature (T_m) of 52.0 °C, which decreased to 48.8 °C ($\Delta T_m = -3.3$ °C) by replacing one thymidine with a triazole-modified dT (**41**) (Table **6-2** and Figure **6-10**). This is consistent with previous reports that a single introduction of a triazole-modified dU decreases the stability of the DNA duplex.^{22,23} The introduction of a phenyl group at the position-4 of triazole moiety (**42**) further destabilized the stability of the DNA duplex. For instance, single introduction of 4-phenyltriazole-modified dT (**42**) decreased the DNA melting temperature by 6.1 °C (duplex-**51** vs duplex-**49**). From the electronic effect point of view, the reduced stability of the modified DNA duplexes (duplex-**50**, **51**) might be caused by the lower

pK_a of **41** and **42** than that of native thymidine leading to a weaker base pair with dA. However, the situation for duplex-**52** seemed more complex. Although the pK_a value of **43** is higher than that of thymidine, which in turn should lead to a stronger base pair with dA, a destabilizing effect was observed for the coumarin-modified triazole moiety **43**. The introduction of **43** reduced the DNA duplex stability by 8.2 °C (duplex-**52** vs duplex-**49**). These results indicated that apart from electronic effect, steric effect may also play an important role for the stability of DNA duplex. The substituents with a larger size led to more steric hindrance than the smaller ones, which in turn lead to further decrease for the stability of the ODN duplex. Collectively, the incorporation of triazole moieties to thymidine destabilized the stability of ODN duplexes, and the steric hindrance induced by the substituents at the 4-position of the triazole further decreased the stability of the DNA duplexes. The bigger size the substituent is, the less stable the DNA duplex is.

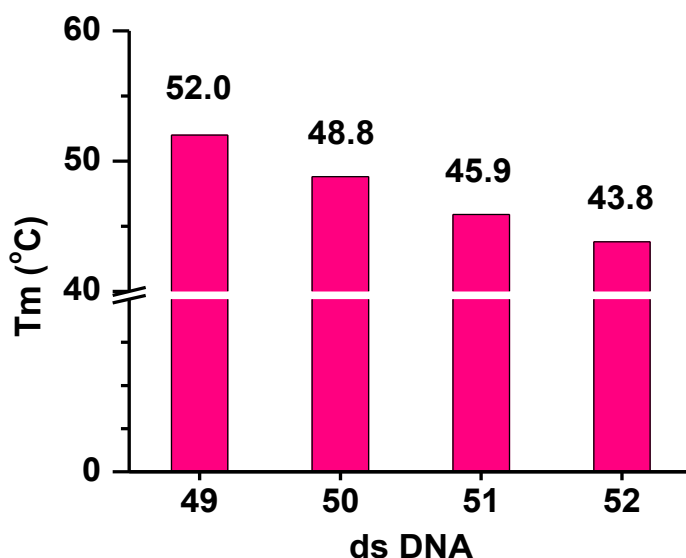


Figure 6-10. Comparison of the melting temperatures of ds DNAs containing **41**, **42**, or **43** in a buffer (pH = 7.0).

6.6. Thermal stability of the DNA duplexes with multiple incorporations.

Apart from Watson-Crick base pairing, π - π stacking also plays an important role for DNA duplexes stability. The research of Nielson's group demonstrated that single replacement of dT with 5-(1,2,3-triazol-4-yl)-2'-deoxyuridine led to decreased stability of the ODN duplex, while the introduction of two to four consecutive modifications increased the stability of duplexes. The increased stability arises from the additional π - π stacking of triazole moieties in the major groove.^{14,23} To check the generality of such a phenomenon, two or three consecutive modifications were incorporated by replacing thymidine with **41-43** to provide ODNs **53b-58b** (Scheme 6-4 and Table 6-2). The results we obtained with **41-43** are different from Nielson's. Two or three consecutive modifications further destabilized the DNA duplexes (ΔT_m of -6 to -12.7) in comparison with that of single modification (Table 6-2). On the other hand, we did notice that ΔT_m per modification ($\Delta T_m/\text{mod}$) increased as increasing number of modifications. For instance, single replacement of dT with **43** reduced the DNA duplex stability by 8.2 °C ($\Delta T_m/\text{mod}$ -8.2), two modification result in a $\Delta T_m/\text{mod}$ of -4.8 °C, while three modifications led to a $\Delta T_m/\text{mod}$ of -4.2 °C. Similar trend was observed for **42**-modified ODNs, while $\Delta T_m/\text{mod}$ for **41** is less dependent on the number of modifications. The data indicated that the additional π - π stacking caused by consecutive phenyl or coumarin substituent at the 4-position of triazole ring lead to extra stability for ODN duplexes. The effect of the π - π stacking followed the order **43** > **42** > **41** which is consistent with the size of the triazole moiety [Coumarin-modified triazole (**43**) > 4-Phenyltriazole (**42**) > triazole (**41**)].

Table 6-2. T_m -Values of oligonucleotides in pH 7.0 buffer^{a,b}

ODNs	DNA			RNA		
	49a: 3'-dTCTACCTAAATCCATG			59a: 3'-dUCUACCUGAAAUCCAUG		
	T_m (°C)	ΔT_m (°C)	$\Delta T_m/\text{mod}$ (°C) ^c	T_m (°C)	ΔT_m (°C)	$\Delta T_m/\text{mod}$ (°C) ^c
49b: 5'-dAGATGGATTTAGGTAC	52.0	---	---	48.4	---	
50b: 5'-dAGATGGAT41TAGGTAC	48.8	-3.2	-3.2	44.3	-4.1	-4.1
51b: 5'-dAGATGGAT42TAGGTAC	45.9	-6.1	-6.1	42.1	-6.3	-6.3
52b: 5'-dAGATGGAT43TAGGTAC	43.8	-8.2	-8.2	39.3	-9.1	-9.1
53b: 5'-dAGATGGAT4141AGGTAC	46.0	-6	-3.0	41.7	-6.7	-3.4
54b: 5'-dAGATGGAT4242AGGTAC	45.0	-7	-3.5	39.7	-8.7	-4.4
55b: 5'-dAGATGGAT4343AGGTAC	42.3	-9.7	-4.8	38.8	-9.6	-4.8
56b: 5'-dAGATGGA414141AGGTAC	44.5	-7.5	-2.5	38.7	-9.7	-3.2
57b: 5'-dAGATGGA424242AGGTAC	42.8	-9.2	-3.1	36.9	-11.5	-3.8
58b: 5'-dAGATGGA434343AGGTAC	39.3	-12.7	-4.2	35.5	-12.9	-4.3

^a The melting temperatures were determined in 10 mM potassium phosphate buffer (pH 7.0), 100 μM ethylenediaminetetraacetic acid (EDTA), and 100 mM NaCl, with 4 μM + 4 μM single-strand concentration.

^b All data are the average of three experiments.

^c ΔT_m increase per modification.

It was reported that the consecutive modifications caused even larger effect on the stability of DNA•RNA duplexes than that of DNA•DNA duplexes.^{17,18} To investigate the generality of such a phenomenon, a complementary RNA strand **59a** was synthesized and the DNA•RNA hybridization studies were carried out by recording UV absorbance at 260 nm. The results are shown in Table 6-2. In general, the melting temperature for all DNA•RNA duplexes is lower (~4 °C) than that of DNA•DNA duplex. Apart from that, we found that the stability trend of DNA•RNA duplexes is similar to that of DNA•DNA duplexes. The introduction of **41-43** decreased the stability of the DNA•RNA duplexes with single or multiple modifications (Table

6-2). Two or three consecutive modifications further decreased the stability of the DNA•RNA duplexes in comparison with that of single modification, but the $\Delta T_m/\text{mod}$ decreased with increasing number of modifications for all compounds. This data indicated that π - π stacking did stabilize ODN duplex. However, the stabilizing effect caused by π -stacking is smaller than destabilizing effect caused by the steric hinderance for all triazole-modified thymidines. Collectively, these data indicated that the introduction of triazole moieties at the C5-methyl group of thymidines decreased the stability of the DNA duplexes. The bigger the substituent was, the less stable the ODN duplexes were.

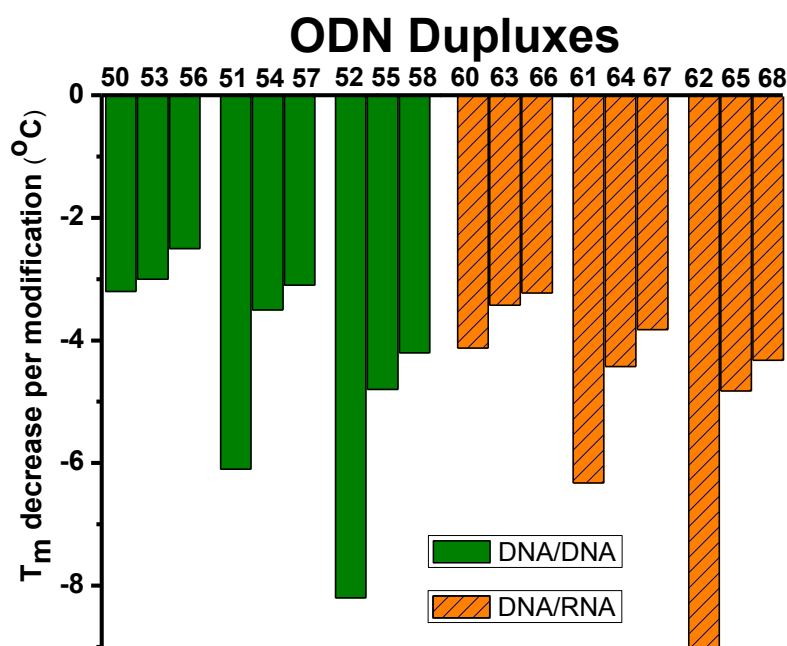


Figure 6-11. T_m decrease per modification in different DNA•DNA or DNA•RNA duplexes in phosphate buffer (pH = 7).

6.7. DNA computational Study.

To gather evidence that the additional π - π stacking did occur and figure out the possible reason for destabilizing effect of the triazole-modified thymidines on DNA duplexes, we carried out computational study (Figure 6-13). To simplify density functional theory (DFT) computation, model systems containing substituted-dT₃/dA₃ base pairs were constructed. All geometries were optimized using M06-2x functional, in combination with 6-31G basis set. Solvent effects of water were accounted using SMD solvation model and all computations were performed using Gaussian 09 (revision D.01) program package.²⁴ The optimized geometries of DNA duplexes containing three consecutive modifications supported that the stability of DNA duplexes depended on the combined effects of π -stacking and steric hinder resulted from nonplanar conformation between substituted triazole moieties and thymine group (Figure 6-13).

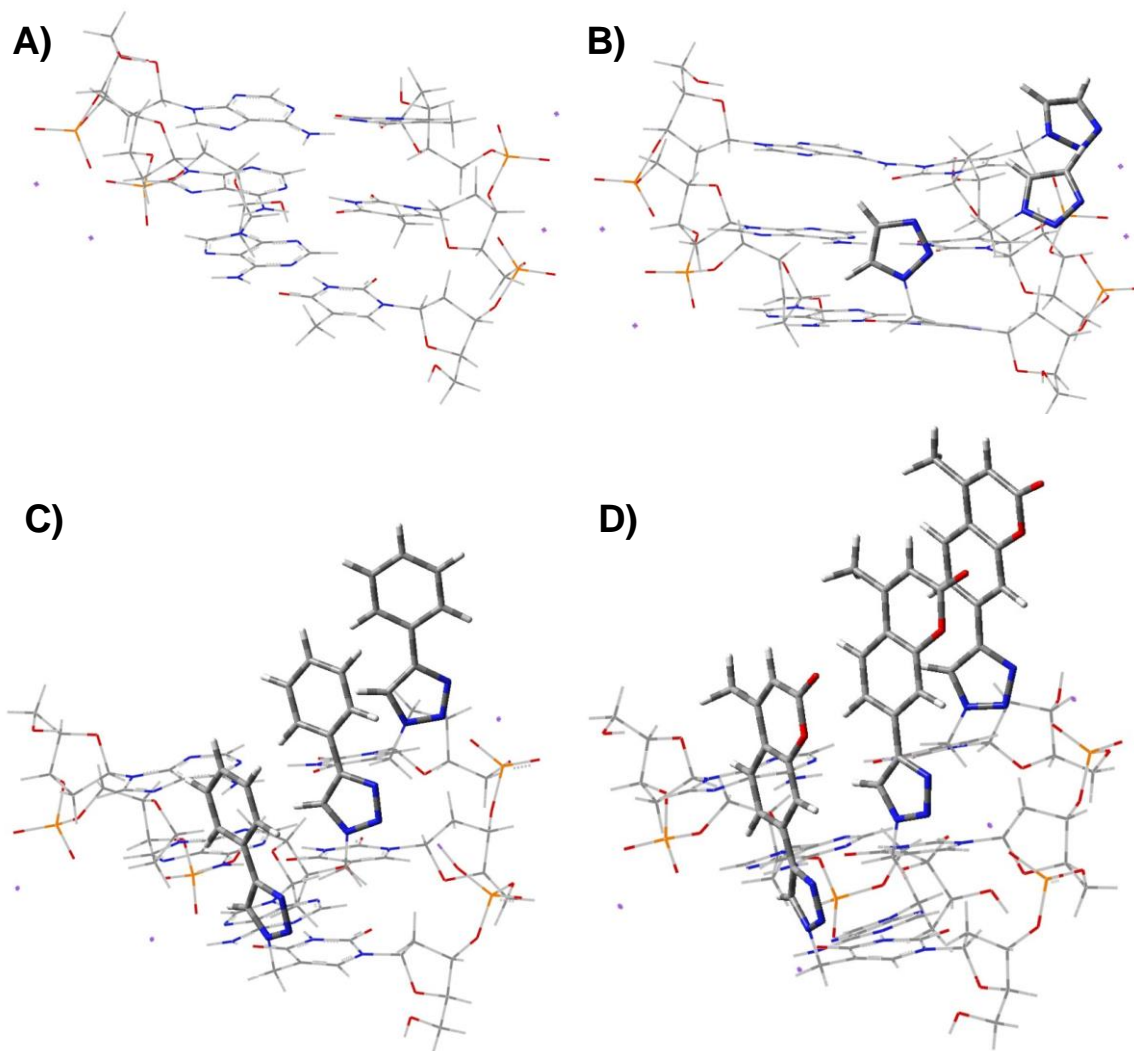


Figure 6-12. Geometries of (un)substituted-dT₃/dA₃ in duplexes **49** (A), **56** (B), **57** (C) and **58** (D) optimized by DFT computation.

Consecutive incorporations of triazole modified thymidine did not significantly change geometries of DNA duplexes. Meanwhile, the increased size of the substituents' π -conjugated system in the major grooves led to more efficient π - π stacking among substituents, which is in favor of stabilizing duplex helices. However, the steric hinderance towards nearby base pairs, arising from flipped conformation of 5-substituents and thymine, increased with increased size of substituents. Both are combined to contribute to the thermal stability of duplexes. Considering

total effects from stacking interaction and steric hinderance, the stability of DNA duplex decreased as a function of substituents' size, if noncoplanar group was introduced in nucleotides of DNA.

6.8. Conclusions

It was reported that multiple consecutive incorporation of 5-(1,2,3-triazol-4-yl)-2'-deoxyuridines increased DNA duplexes' stability due to the π -stacking of triazole-moieties in the major groove. Our detailed study provided novel insights in their effects that the introduction of triazole-modified thymine decreased the stability of DNA•DNA and DNA•RNA duplexes containing single or multiple consecutive modifications. The additional π - π stacking effect among substituents increased the duplexes' stability while the steric effects, arising from flipped conformation of 5-substitutents and thymine, decreased the stability of the duplexes. In addition, the pH values of the medium/buffers also affect ODN duplexes' stability. Much lower melting temperature was observed under acidic or basic condition (pH 5.0, or 9.0), arising from protonation or deprotonation of nucleobases, which disturbed efficient base-pair formation.

6.9. Experiment Section

General Methods. All chemicals from commercially available source were used without further purification. Oligodeoxyribonucleotides (ODNs) were synthesized via standard automated DNA synthesis techniques. Cyanoethyl phosphoramidites with phenoxyacetyl protecting groups on the exocyclic amines of dA and dG were used for the synthesis of modified ODNs.

Deprotection/cleavage of the synthesized normal ODNs was performed under mild conditions using a mixture of 40% aqueous MeNH₂ and 28% aqueous NH₃ (1:1) at room temperature for 2 h. Functionalized ODNs were deprotected and cleaved using 28% aq. NH₃ at room temperature

for 2 h. 20% Denaturing polyacrylamide gel electrophoresis was used for DNA purification. The RNA resin was transferred into a sealable polypropylene vial. Added 1.0 mL solution of Ammonium hydroxide/Methyl Amine (AMA, v/v = 1:1) and incubated at room temperature for 3 h. After centrifuging and cooling to 0 °C, transfer the supernatant using a sterile pipette to a new sterile polypropylene tube. Rinse the resin with 2 × 0.25 mL RNase free water and add to the tube. The supernatant was dried under reduced pressure and subjected to desilylation with a mixture of 100 µL anhydrous DMSO and 125 µL of TEA·3HF at 65 °C for 2.5 h. After cooling in freezer briefly, add 25 µL of 3 M sodium acetate in RNase free water and 1 mL butanol. Mix well by vortexing and cool by dry ice for 30 min. The mixture was centrifuged at 13.2 K RPM for 30 min at 4 °C. Decant the supernatant and rinse the precipitate with 2 × 0.75 mL cold ethanol (- 20 °C). The white solid was dried under reduced pressure and purified by 20% denaturing PAGE gel. Melting temperatures (T_m) were measured on a UV/vis spectrometer equipped with a thermo electrical temperature controller via changing the temperature of DNA duplex at a rate of 1 °C/min. ^1H NMR and ^{13}C NMR, and ^{31}P NMR spectra were taken on a Bruker DRX 300 MHz spectrophotometer with TMS (^1H and ^{13}C) or H_3PO_4 (^{31}P) as internal standard. High-resolution mass spectrometry IT-TOF was used for molecular analysis.

Determination of DNA duplex thermal stability. All measurements were carried out in 10 mM potassium phosphate buffer (pH 5.0-9.0), 100 µM ethylenediaminetetraacetic acid (EDTA), and 100 mM NaCl, with 4 µM + 4 µM single-strand concentration. Samples were heated at 1 °C min^{-1} from 20 °C to 80 °C and the absorbance of ODNs at 260 nm was measured at 1.0 °C steps.

Determining of pK_a value of compounds 41-43. Compounds **41-43** (2.0 mg) were dissolved in 5 mL methanol, followed by the addition of phosphate buffer solution (45 mL, pH 4.8) (7.8 g $\text{NaH}_2\text{PO}_4\cdot\text{H}_2\text{O}$ in 500 mL water). An aliquot (25 mL) was placed in an erlenmeyer flasks (25

mL) and the pH was adjusted to the different values (pH 2.0-13.0) using 1 M H₃PO₄ and 10 M NaOH. The UV spectra were recorded between 200-400 nm. The absorbance data vs. pH values were plotted with Origin software 8.0 and the first derivative of the absorption (dA/dpH) was calculated.²⁵

Experimental procedures and characterizations.

(2R,3S,5R)-3-Acetoxy-5-(5-methyl-2,4-dioxo-3,4-dihydropyrimidin-1(2H)-

yl)tetrahydrofuran-2-yl)methyl acetate (44). A solution of thymidine (5.0 g, 21.0 mmol) in 50 mL pyridine was cooled to 0 °C, and Ac₂O (5.0 g, 4.6 mL) was added dropwise. The reaction mixture was allowed to warm up to room temperature and stirred overnight. After removing the solvent, the residue was diluted with ethyl acetate (3 × 50 mL). The mixture was washed with hydrochloric acid (1.0 M, 50 mL), water (100 mL), and brine (50 mL). The organic layer was dried over Na₂SO₄. The solvent was removed under reduced pressure. The residue was purified by column chromatography (Hexane: Ethyl acetate = 1:1, R_f = 0.25) to obtain **44** as a white solid (6.5 g, 19.92 mmol, 95%). ¹H NMR (300 MHz, CDCl₃): δ. 9.55 (s, 1H), 6.36-6.31 (t, *J* = 12 Hz, 1H), 5.23-5.21 (d, *J* = 6 Hz, 1H), 4.36 (s, 2H), 4.25 (s, 1H), 2.51-2.44 (m, 1H), 2.22-2.17 (m, 1H), 2.13-2.12 (d, *J* = 3 Hz, 6H), 1.94 (s, 3H). (the NMR spectra were in agreement with those reported).²⁶

(2R,3S,5R)-3-Acetoxy-5-(5-(azidomethyl)-2,4-dioxo-3,4-dihydropyrimidin-1(2H)-

yl)tetrahydrofuran-2-yl)methyl acetate (45). To a mixture of compound **44** (3.26 g, 10 mmol), *N*-bromosuccinimide (2.14 g, 12 mmol) and azobisisobutyronitrile (86 mg, 0.5 mmol) in a 100 mL flask, benzene (40 mL) was added. The reaction mixture was refluxed for 4 h, and cooled to room temperature. The solvent was removed under reduced pressure. The residue was re-dissolved in DMF (10 mL), and then a solution of NaN₃ (3.25 g, 50 mmol) in DMF (25 mL) was

added dropwise. The mixture was stirred at room temperature overnight. After diluting with ethyl acetate (3 × 50 mL), the mixture was washed with water (50 mL) and brine (50 mL). The organic phase was dried over anhydrous Na₂SO₄. The solvent was removed under reduced pressure. The residue was purified by column chromatography (Hexane: Ethyl acetate = 1:2, R_f = 0.4) to provide compound **45** as a white solid (3.0 g, 8.2 mmol, 82%). ¹H NMR (300 MHz, CDCl₃): δ. 9.08 (s, 1H), 7.50 (s, 1H), 6.27-6.22 (q, *J* = 6 Hz, 1H), 5.17-5.15 (d, *J* = 6 Hz, 1H), 4.38-4.04 (m, 5H), 2.51-2.44 (m, 1H), 2.15-2.12 (m, 1H), 2.08-2.06 (d, *J* = 6 Hz, 6H). (the NMR spectra were in agreement with those reported).¹⁹

(2R,3S,5R)-5-(5-((1H-1,2,3-Triazol-1-yl)methyl)-2,4-dioxo-3,4-dihydropyrimidin-1(2H)-yl)-2-(acetoxymethyl)tetrahydrofuran-3-yl acetate (41a). Into a solution of **45** (1.0 g, 2.72 mmol) in methanol (25 mL), ethynyltrimethylsilane (2.5 mL, 14.96 mmol) and sodium ascorbate (aq, 0.296 M, 18 mL) were added, followed by the addition of CuSO₄ (aq, 0.368 M, 11 mL). The reaction mixture was stirred at room temperature for 3 h. After removing the solvent, the residue was diluted with ethyl acetate (3 × 20 mL). The combined organic phase was washed with water (20 mL), brine (20 mL), and dried over anhydrous Na₂SO₄. The solvent was removed under reduced pressure. The residue was re-dissolved in methanol (20 mL), followed by the addition of TBAF (13.6 mL, 1.0 M in THF). The reaction mixture was stirred at 70 °C for 1 h. The solvent was removed, and the residue was diluted with ethyl acetate (3 × 15 mL). The combined organic phase was washed with water (15 mL), brine (15 mL), and dried over anhydrous Na₂SO₄. The solvent was removed under reduced pressure. The residue was purified by column chromatography (pure Ethyl acetate, R_f = 0.25) to yield **41a** as a white solid (1.9 mmol, 747 mg). ¹H NMR (300 MHz, CDCl₃): δ. 9.16 (s, 1H), 7.85 (s, 2H), 7.69 (s, 1H), 6.29-6.24 (q, *J* = 6 Hz, 1H), 5.37-5.22 (m, 3H), 4.50-4.44 (m, *J* = 6 Hz, 1H), 4.35-4.30 (m, 2H), 2.58-2.51 (q, *J* = 6 Hz,

1H), 2.24 (s, 3H), 2.21-2.16 (m, 1H), 2.13 (s, 3H). ¹³C NMR (75 MHz, CDCl₃): δ. 170.66, 170.32, 162.60, 149.78, 140.36, 108.98, 85.87, 82.86, 74.23, 63.73, 46.54, 37.88, 20.98, 20.88. HRMS-ESI (+) (*m/z*): [M+H]⁺ calcd. for C₁₆H₂₀N₅O₇⁺, 394.1357; found: 394.1360.

5-((1H-1,2,3-Triazol-1-yl)methyl)-1-((2R,4S,5R)-4-hydroxy-5-

(hydroxymethyl)tetrahydrofuran-2-yl)pyrimidine-2,4(1H,3H)-dione (41). To a solution of compound **41a** (1.0 g, 2.54 mmol) in methanol (13 mL), NH₄OH (aq, 30% v/v, 18 mL) was added. The reaction mixture was stirred at room temperature overnight. The solvent was removed under reduced pressure. The residue was purified by column chromatography (DCM: methanol = 9:1, R_f = 0.2) to afford **41** as a white solid (600 mg, 1.94 mmol, 76%). ¹H NMR (300 MHz, DMSO-*d*₆): δ. 11.55 (s, 1H), 8.13 (s, 1H), 8.04 (s, 1H), 7.69 (s, 1H), 6.16-6.12 (t, *J* = 6 Hz, 1H), 5.27-5.21 (m, 3H), 5.04-5.01 (t, *J* = 3 Hz, 1H), 4.24 (s, 1H), 3.79 (s, 1H), 3.64-3.51 (m, 2H), 2.13 (m, 2H). ¹³C NMR (300 MHz, DMSO-*d*₆): δ. 163.03, 150.64, 141.32, 133.54, 125.26, 108.25, 87.97, 84.92, 70.62, 61.65, 46.35. (the NMR spectra were in agreement with those reported).¹⁶

5-((1H-1,2,3-Triazol-1-yl)methyl)-1-((2R,4S,5R)-5-((bis(4-methoxyphenyl)(phenyl) methoxy)methyl)-4-hydroxytetrahydrofuran-2-yl)pyrimidine-2,4(1H,3H)-dione (41b).

Compound **41** (500 mg, 1.62 mmol) was azeotropically dried with pyridine (5 mL × 3). Pyridine (5 mL) was added, followed by the addition of 4, 4'-dimethoxytriphenylmethyl chloride (822 mg, 2.42 mmol). The reaction mixture was stirred at room temperature overnight. The mixture was diluted with DCM (45 mL), washed with water (15 mL) and brine (15 mL), and dried over anhydrous Na₂SO₄. The solvent was removed under reduced pressure. The residue was purified by column chromatography (DCM: Methanol: Et₃N = 95:5:2, R_f = 0.2) to yield **41b** as a white solid (600 mg, 0.98 mmol, 61%). Spectrum contains Et₃N peak. ¹H NMR (300 MHz, CDCl₃):

δ .8.08 (s, 1), 7.65 (s, 1), 7.60 (s, 1), 7.45-7.42 (d, $J = 9$ Hz, 2), 7.34-7.32 (m, 6), 7.25-7.20 (m, 1), 6.89-6.86 (d, $J = 9$ Hz, 4), 6.34-6.30 (t, $J = 6$ Hz, 1), 4.71-4.66 (d, $J = 15$ Hz, 2), 4.52-4.47 (d, $J = 15$ Hz, 1), 4.08 (s, 1), 3.79 (s, 6), 3.45 (s, 2), 2.53-2.30 (m, 2). ^{13}C NMR (300 MHz, CDCl_3): δ .162.61, 158.74, 149.96, 144.40, 140.70, 135.41, 135.26, 133.50, 130.19, 130.13, 128.19, 128.11, 127.18, 124.54, 113.42, 108.75, 87.06, 86.28, 85.31, 71.84, 63.40, 55.28, 45.97, 41.30, 10.61. HRMS-ESI (-) (m/z): $[\text{M}-\text{H}]^-$ calcd. for $\text{C}_{33}\text{H}_{32}\text{N}_5\text{O}_7$, 610.2307; found: 610.2298.

(2R,3S,5R)-5-(5-((1H-1,2,3-Triazol-1-yl)methyl)-2,4-dioxo-3,4-dihydropyrimidin-1(2H)-yl)-2-((bis(4-methoxyphenyl)(phenyl)methoxy)methyl)tetrahydrofuran-3-yl (2-cyanoethyl) diisopropylphosphoramidite (41c). A solution of **41b** (200 mg, 0.32 mmol) in DCM (20 mL) was cooled to 0 °C under Ar atmosphere, and then *N,N*-Diisopropylethylamine (106 mg, 0.82 mmol) was added. After 10 min stirring, 2-cyanoethyl *N,N*-diisopropylchlorophosphoramidite (147 mg, 0.62 mmol) was added. The reaction mixture was stirred at room temperature for 1.5 h, then diluted with DCM (45 mL), washed with NaHCO_3 (5%, 20 mL) followed by brine (20 mL), and dried over anhydrous Na_2SO_4 . The solvent was removed under reduced pressure and the residue was purified by column chromatography (DCM: Methanol: Et_3N = 95:5:2, R_f = 0.48) to afford **41c** as a white foam (170 mg, 0.21 mmol, 65%). ^{31}P NMR (CDCl_3 , 300 MHz): δ 148.73, 148.94. HRMS-ESI (-) (m/z): $[\text{M}-\text{H}]^-$ calcd. for $\text{C}_{42}\text{H}_{49}\text{N}_7\text{O}_8\text{P}$, 810.3386; found: 810.3379.

((2R,3S,5R)-3-Acetoxy-5-(2,4-dioxo-5-((4-phenyl-1H-1,2,3-triazol-1-yl)methyl)-3,4-dihydropyrimidin-1(2H)-yl)tetrahydrofuran-2-yl)methyl acetate (42a). To a solution of compound **45** (800 mg, 2.18 mmol) and ethynylbenzene (480.8 mg, 2.62 mmol) in DCM (21 mL), sodium ascorbate (aq, 0.296 M, 14 mL) was added, followed by the addition of aqueous CuSO_4 (0.368 M, 8 mL). The reaction mixture was stirred at room temperature for 1h, and then diluted with DCM (3 \times 20 mL). The combined organic phase was washed with water (20 mL)

and brine (20 mL), and dried over anhydrous Na₂SO₄. The solvent was removed under reduced pressure. The residue was purified by column chromatography (DCM: Methanol = 19:1, R_f= 0.32) to provide **42a** as a white solid (880 mg, 1.85 mmol, 85%). ¹H NMR (300 MHz, DMSO-*d*₆): δ. 11.67 (s, 1H), 8.50 (s, 1H), 8.06 (s, 1H), 7.85-7.83 (d, *J* = 6 Hz, 2), 7.46-7.42 (t, *J* = 6 Hz, 2H), 7.35-7.30 (t, *J* = 6 Hz, 1H), 6.19 (s, 1H), 5.28 (s, 3H), 4.26 (m, 3H), 2.42-2.36 (m, 2H), 2.09-2.05 (m, 6H). ¹³C NMR (300 MHz, DMSO-*d*₆): δ. 170.68, 170.51, 163.00, 150.65, 146.52, 141.63, 131.23, 129.31, 128.26, 125.58, 121.78, 108.40, 85.35, 81.85, 74.30, 64.09, 46.65, 36.55, 21.23, 21.04. HRMS-ESI (+) (*m/z*): [M+H]⁺ calcd. for C₂₂H₂₄N₅O₇⁺, 470.1670; found: 470.1667.

1-((2R,4S,5R)-4-Hydroxy-5-(hydroxymethyl)tetrahydrofuran-2-yl)-5-((4-phenyl-1H-1,2,3-triazol-1-yl)methyl)pyrimidine-2,4(1H,3H)-dione (42). To a solution of compound **42a** (640 mg, 1.36 mmol) in methanol (10 mL), aqueous ammonia (30% v/v, 12 mL) was added. The reaction mixture was stirred at room temperature overnight. The solvent was removed under reduced pressure. The residue was purified by column chromatography (DCM: methanol = 9:1, R_f= 0.2) to afford **42** as a white solid (440 mg, 1.14 mmol, 84%). ¹H NMR (300 MHz, DMSO-*d*₆): δ. 11.57 (s, 1H), 8.47 (s, 1H), 8.21 (s, 1H), 7.86-7.83 (d, *J* = 9 Hz, 2H), 7.46-7.41 (t, *J* = 6 Hz, 2H), 7.35-7.30 (t, *J* = 9 Hz, 1H), 6.19-6.14 (t, *J* = 6 Hz, 1H), 5.28-5.18 (m, 3H), 5.06-5.02 (t, *J* = 6 Hz, 1H), 4.28-4.25 (t, *J* = 6 Hz, 1H), 3.81-3.80 (d, *J* = 3 Hz, 1H) 3.66-3.53 (m, 2H), 2.19-2.15 (t, *J* = 6 Hz, 2H) (the NMR spectra were in agreement with those reported).²⁷

1-((2R,4S,5R)-5-((Bis(4-methoxyphenyl)(phenyl)methoxy)methyl)-4-hydroxytetrahydrofuran-2-yl)-5-((4-phenyl-1H-1,2,3-triazol-1-yl)methyl)pyrimidine-2,4(1H,3H)-dione (42b). Compound **42** (470 mg, 1.22 mmol) was azeotropically dried with pyridine (5 mL × 3). Pyridine (5 mL) was added, followed by the addition of 4,4'-

dimethoxytriphenylmethyl chloride (620.3 mg, 2.95 mmol). The reaction mixture was stirred at room temperature overnight. The mixture was diluted with DCM (3×15 mL). The combined organic phase was washed with water (15 mL), brine (15 mL), and dried over anhydrous Na_2SO_4 . The solvent was removed under reduced pressure. The residue was purified by column chromatography (DCM: Methanol: Et_3N = 95:5:2, R_f =0.20) to afford compound **42b** as a white solid (520 mg, 0.76 mmol, 62%). ^1H NMR (300 MHz, CDCl_3): δ . 8.11 (s, 1H), 7.85 (s, 1H), 7.80-7.77 (d, J = 6 Hz, 2H), 7.45-7.31 (m, 11H), 7.25-7.22 (m, 1H), 6.88-6.85 (d, J = 9 Hz, 4H), 6.36-6.31 (t, J = 6 Hz, 1H), 4.73-4.68 (d, J = 15 Hz, 2H), 4.49-4.44 (d, J = 15 Hz, 1H), 4.09 (s, 1H), 3.76 (s, 6H), 3.46 (s, 2H), 2.53-2.31 (m, 2H). ^{13}C NMR (75 MHz, CDCl_3): δ . 163.24, 158.70, 150.47, 147.40, 144.44, 140.99, 135.47, 135.24, 130.56, 130.17, 128.73, 128.21, 128.06, 127.15, 125.68, 120.71, 113.37, 108.51, 86.97, 86.38, 85.36, 71.59, 63.43, 55.22, 41.29. HRMS-ESI (-) (m/z): $[\text{M}-\text{H}]^-$ calcd. for $\text{C}_{39}\text{H}_{36}\text{N}_5\text{O}_7^-$, 686.2620; found: 686.2620.

(2R,3S,5R)-2-((Bis(4-methoxyphenyl)(phenyl)methoxy)methyl)-5-(2,4-dioxo-5-((4-phenyl-1H-1,2,3-triazol-1-yl)methyl)-3,4-dihydropyrimidin-1(2H)-yl)tetrahydrofuran-3-yl (2-cyanoethyl) diisopropylphosphoramidite (42c). A solution of **42b** (200 mg, 0.29 mmol) in DCM (10 mL) was cooled to 0 °C under Ar atmosphere. Then, *N,N*-diisopropylethylamine (93.1 mg, 0.72 mmol) was added, followed by the addition of 2-cyanoethyl *N,N*-diisopropylchlorophosphoramidite (128 mg, 0.54 mmol). The reaction mixture was stirred at room temperature for 1.5 h, diluted with DCM (3×15 mL), washed with NaHCO_3 (5%, 20 mL) and brine (20 mL), and dried over anhydrous Na_2SO_4 . The solvent was removed under reduced pressure and the residue was purified by column chromatography (DCM: Methanol: Et_3N = 95:5:2, R_f = 0.5) to afford compound **42c** as a white foam (210 mg, 0.24 mmol, 82%). ^{31}P NMR

(CDCl₃, 300 MHz): δ 148.80, 148.94. HRMS-ESI (-) (m/z): [M-H]⁻ calcd. for C₄₈H₅₃N₇O₈P⁻, 886.3699; found: 886.3688.

((2R,3S,5R)-3-Acetoxy-5-(5-((4-(4-methyl-2-oxo-2H-chromen-7-yl)-1H-1,2,3-triazol-1-yl)methyl)-2,4-dioxo-3,4-dihydropyrimidin-1(2H)-yl)tetrahydrofuran-2-yl)methyl acetate (43a). To a solution of compound **45** (700 mg, 1.91 mmol) and 4-methyl-2H-chromen-2-one (422 mg, 2.3 mmol) in methanol (18 mL), sodium ascorbate (aq, 0.296 M, 11.5 mL) was added, followed by the addition of CuSO₄ (aq, 0.368 M, 7.0 mL). The reaction mixture was stirred at room temperature for 1 h. The solvent was removed under reduced pressure. The residue was purified by column chromatography (DCM: Methanol = 19:1, R_f = 0.3) to yield **43a** as a white solid (1.0 g, 1.8 mmol, 95%). ¹H NMR (300 MHz, DMSO-*d*₆): δ . 11.69 (s, 1H), 8.72 (s, 1H), 8.08 (s, 1H), 7.91-7.83 (m, 3H), 6.40 (s, 1H), 6.22-6.17 (t, *J* = 6 Hz, 1H), 5.30 (s, 2H), 5.25-5.23 (t, *J* = 3 Hz, 1H), 4.27-4.21 (m, 3H), 2.46-2.35 (m, 5H), 2.08 (s, 3H), 2.04 (s, 3H). ¹³C NMR (75 MHz, CDCl₃): 177.96, 170.75, 170.41, 163.01, 160.65, 153.73, 152.22, 149.89, 140.82, 140.78, 125.26, 121.64, 119.73, 114.94, 113.73, 108.62, 85.92, 82.83, 74.18, 63.74, 37.90, 29.59, 21.00, 20.87, 18.56. HRMS-ESI (+) (m/z): [M+H]⁺ calcd. for C₂₆H₂₆N₅O₉⁺, 552.1725; found: 552.1713.

1-((2R,4S,5R)-4-Hydroxy-5-(hydroxymethyl)tetrahydrofuran-2-yl)-5-((4-(4-methyl-2-oxo-2H-chromen-7-yl)-1H-1,2,3-triazol-1-yl)methyl)pyrimidine-2,4(1H,3H)-dione (43). To a solution of compound **43a** (500 mg, 0.9 mmol) in methanol (6.0 mL), NH₄OH (aq, 30% v/v, 8.0 mL) was added. The reaction mixture was stirred at room temperature overnight. The solvent was removed under reduced pressure, and the residue was purified by column chromatography (DCM: methanol = 9:1, R_f = 0.2) to afford **43** as a white solid (341 mg, 0.73 mmol, 81%). ¹H NMR (300 MHz, DMSO-*d*₆): δ . 11.58 (s, 1H), 8.70 (s, 1H), 8.23 (s, 1H), 7.91-7.84 (m, 3H), 6.40

(s, 1H), 6.19-6.15 (t, $J = 6$ Hz, 1H), 5.27 (s, 3H), 5.05 (s, 1H), 4.27 (s, 1H), 3.82-3.81 (d, $J = 3$ Hz, 1H), 3.60 (s, 2H), 2.26 (s, 3H), 2.19-2.16 (t, $J = 6$ Hz, 2H). (the NMR spectra were in agreement with those reported).⁵

1-((2R,4S,5R)-5-((Bis(4-methoxyphenyl)(phenyl)methoxy)methyl)-4-hydroxytetrahydrofuran-2-yl)-5-((4-(4-methyl-2-oxo-2H-chromen-7-yl)-1H-1,2,3-triazol-1-yl)methyl)pyrimidine-2,4(1H,3H)-dione (43b). Compound **43** (340 mg, 0.73 mmol) was azeotropically dried with pyridine (5 mL \times 3). Then, pyridine (5 mL) was added, followed by the addition of 4, 4'-dimethoxytriphenylmethyl chloride (370 mg, 1.1 mmol). The reaction mixture was stirred at room temperature overnight, and then diluted with DCM (3 \times 15 mL). The combined organic phase was washed with water (15 mL \times 3), brine (15 mL), and dried over anhydrous Na₂SO₄. The solvent was removed under vacuum. The residue was purified by column chromatography (DCM: Methanol: Et₃N= 95:5:2, $R_f = 0.30$) to afford compound **43b** as a white solid (337 mg, 0.44 mmol, 60%). ¹H NMR (300 MHz, CDCl₃): δ . 8.25 (s, 2H), 7.98-7.95 (d, $J = 9$ Hz, 1H), 7.83 (s, 1H), 7.64-7.62 (d, $J = 6$ Hz, 1H), 7.48-7.23 (m, 9H), 6.91-6.89 (d, 4H), 6.51-6.47 (t, $J = 6$ Hz, 1H), 6.27 (s, 1H), 4.87-4.82 (d, $J = 6$ Hz, 1H), 4.70 (s, 1H), 4.45-4.41 (d, $J = 6$ Hz, 1H), 4.19 (s, 1H), 3.80 (s, 6H), 3.49-3.39 (q, $J = 6$ Hz, 2H), 2.80-2.74 (m, 1H), 2.46-2.35 (m, 4H). (the NMR spectra were in agreement with those reported).⁵

(2R,3S,5R)-2-((Bis(4-methoxyphenyl)(phenyl)methoxy)methyl)-5-(5-((4-(4-methyl-2-oxo-2H-chromen-7-yl)-1H-1,2,3-triazol-1-yl)methyl)-2,4-dioxo-3,4-dihydropyrimidin-1(2H)-yl)tetrahydrofuran-3-yl (2-cyanoethyl) diisopropylphosphoramidite (43c). Compound **43b** (200 mg, 0.26 mmol) in DCM (10 mL) was cooled to 0 °C under Ar atmosphere. *N,N*-Diisopropylethylamine (85.3 mg, 0.66 mmol) was added, followed by the addition of 2-cyanoethyl *N,N*-diisopropylchlorophosphoramidite (117 mg, 0.49 mmol). The reaction mixture

was stirred at room temperature for 1.5 h, and then diluted with DCM (45 mL). The organic phase was washed with NaHCO₃ (5%, 20 mL), brine (20 mL), and dried over anhydrous Na₂SO₄. The solvent was removed under reduced pressure and the residue was purified by column chromatography (DCM: Methanol: Et₃N= 95:5:2, R_f= 0.53) to yield **43c** as a white foam (two isomers isolated) (150 mg, 0.155 mmol, 60%). ³¹P NMR (CDCl₃, 300 MHz): δ 148.89, 148.91. (Two isomers were isolated) (the NMR spectra were in agreement with those reported).⁵

6.10. References

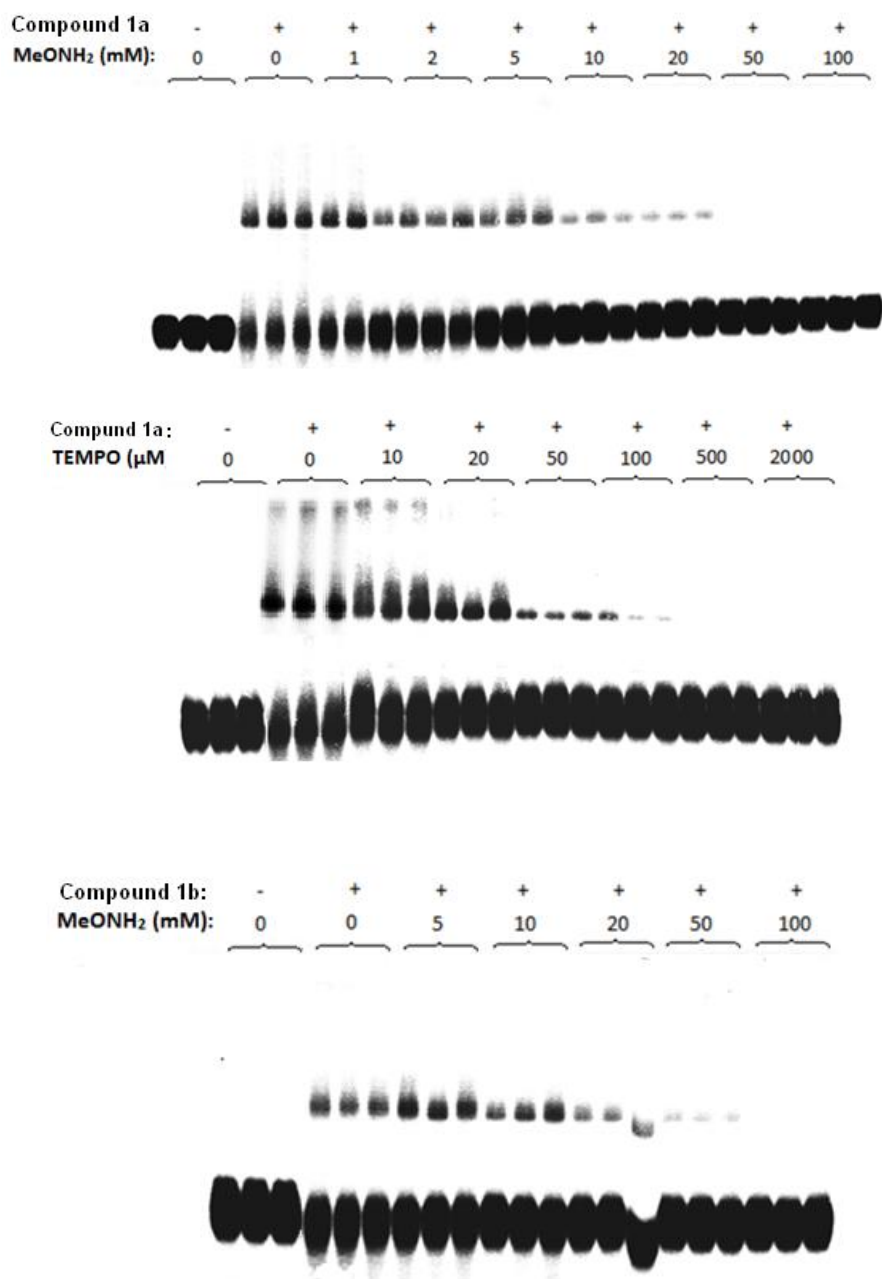
1. Peng X, Ghosh AK, Houten BV, Greenberg MM. Nucleotide Excision Repair of a DNA Interstrand Cross-Link Produces Single- and Double-Strand Breaks. *Biochemistry*. 2010;49:11–9.
2. Peng X, Pigli YZ, Rice PA, Greenberg MM. Protein Binding Has a Large Effect on Radical Mediated DNA Damage. *Journal of the American Chemical Society*. 2008;130:12890–1.
3. Ranasinghe RT, Brown T. Fluorescence based strategies for genetic analysis. *Chemical Communications*. 2005;44:5487-5502.
4. Sun H, Peng X. Template-Directed Fluorogenic Oligonucleotide Ligation Using “Click” Chemistry: Detection of Single Nucleotide Polymorphism in the Human p53 Tumor Suppressor Gene. *Bioconjugate Chemistry*. 2013;24:1226–34.
5. Haque MM, Sun H, Liu S, Wang Y, Peng X. Photoswitchable Formation of a DNA Interstrand Cross-Link by a Coumarin-Modified Nucleotide. *Angewandte Chemie International Edition*. 2014;53:7001–5.
6. Rusling DA, Nandhakumar IS, Brown T, Fox KR. Triplex-directed covalent cross-linking of a DNA nanostructure. *Chemical Communications*. 2012;48:9592-4.
7. Deleavey GF, Damha MJ. Designing Chemically Modified Oligonucleotides for Targeted Gene Silencing. *Chemistry & Biology*. 2012;19:937–54.
8. Gallo M, Montserrat J, Iribarren A. Design and applications of modified oligonucleotides. *Brazilian Journal of Medical and Biological Research*. 2003;36:143–51.

9. Lin K-Y, Jones RJ, Matteucci M. Tricyclic 2-Deoxycytidine Analogs: Syntheses and Incorporation into Oligodeoxynucleotides Which Have Enhanced Binding to Complementary RNA. *Journal of the American Chemical Society*. 1995;117:3873–4.
10. Sinkeldam RW, Greco NJ, Tor Y. Polarity of Major Grooves Explored by Using an Isosteric Emissive Nucleoside. *ChemBioChem*. 2008;9:706–9.
11. Helleday T, Petermann E, Lundin C, Hodgson B, Sharma RA. DNA repair pathways as targets for cancer therapy. *Nature Reviews Cancer*. 2008;8:193–204.
12. Dodd D, Hudson R. Intrinsically Fluorescent Base-Discriminating Nucleoside Analogs. *Mini-Reviews in Organic Chemistry*. 2009;6:378–91.
13. Peacock H, Kannan A, Beal PA, Burrows CJ. Chemical Modification of siRNA Bases To Probe and Enhance RNA Interference. *The Journal of Organic Chemistry*. 2011;76:7295–300.
14. Andersen NK, Døssing H, Jensen F, Vester B, Nielsen P. Duplex and Triplex Formation of Mixed Pyrimidine Oligonucleotides with Stacking of Phenyl-triazole Moieties in the Major Groove. *The Journal of Organic Chemistry*. 2011;76:6177–87.
15. Tornøe CW, Christensen C, Meldal M. Peptidotriazoles on Solid Phase: [1,2,3]-Triazoles by Regiospecific Copper(I)-Catalyzed 1,3-Dipolar Cycloadditions of Terminal Alkynes to Azides. *The Journal of Organic Chemistry*. 2002;67:3057–64.
16. Shmalenyuk ER, Karpenko IL, Chernousova LN, Chizhov AO, Smirnova TG, Andreevskaya SN, et al. New 5-modified 2'-deoxyuridine derivatives: synthesis and antituberculosis activity. *Russian Chemical Bulletin*. 2014;63:1197–200.
17. Kumar P, Hornum M, Nielsen LJ, Enderlin G, Andersen NK, Len C, et al. High-Affinity RNA Targeting by Oligonucleotides Displaying Aromatic Stacking and Amino Groups in the Major Groove. Comparison of Triazoles and Phenyl Substituents. *The Journal of Organic Chemistry*. 2014;79:2854–63.
18. Hornum M, Kumar P, Podsiadly P, Nielsen P. Increasing the Stability of DNA:RNA Duplexes by Introducing Stacking Phenyl-Substituted Pyrazole, Furan, and Triazole Moieties in the Major Groove. *The Journal of Organic Chemistry*. 2015;80:9592–602.
19. Hong IS, Ding H, Greenberg MM. Oxygen Independent DNA Interstrand Cross-Link Formation by a Nucleotide Radical. *Journal of the American Chemical Society*. 2006;128:485–91.
20. Krishnamurthy R. Role of pK_a of Nucleobases in the Origins of Chemical Evolution. *Accounts of Chemical Research*. 2012;45:2035–44.

21. Peng X, Li H, Seela F. pH-Dependent mismatch discrimination of oligonucleotide duplexes containing 2'-deoxytubercidin and 2- or 7-substituted derivatives: protonated base pairs formed between 7-deazapurines and cytosine. *Nucleic Acids Research*. 2006;34:5987–6000.
22. Andersen NK, Chandak N, Brulíková L, Kumar P, Jensen MD, Jensen F, et al. Efficient RNA-targeting by the introduction of aromatic stacking in the duplex major groove via 5-(1-phenyl-1,2,3-triazol-4-yl)-2'-deoxyuridines. *Bioorganic & Medicinal Chemistry*. 2010;18:4702–10.
23. Kočalka P, Andersen NK, Jensen F, Nielsen P. Synthesis of 5-(1,2,3-Triazol-4-yl)-2'-deoxyuridines by a Click Chemistry Approach: Stacking of Triazoles in the Major Groove Gives Increased Nucleic Acid Duplex Stability. *ChemBioChem*. 2007;8:2106–16.
24. Frisch MJ, Trucks G W, Schlegel HB, Scuseria G E, Robb M A.; Cheeseman, J. R.; Scalmani, G.; Barone, V.; Mennucci, B.; Petersson, G. A.; Nakatsuji, H.; Caricato, M.; Li, X.; Hratchian, H. P.; Izmaylov, A. F.; Bloino, J.; Zheng, G.; Sonnenberg, J. L.; Hada, M.; Ehara, M.; Toyota, K.; Fukuda, R.; Hasegawa, J.; Ishida, M.; Nakajima, T.; Honda, Y.; Kitao, O.; Nakai, H.; Vreven, T.; Montgomery, J. A., Jr.; Peralta, J. E.; Ogliaro, F.; Bearpark, M.; Heyd, J. J.; Brothers, E.; Kudin, K. N.; Staroverov, V. N.; Kobayashi, R.; Normand, J.; Raghavachari, K.; Rendell, A.; Burant, J. C.; Iyengar, S. S.; Tomasi, J.; Cossi, M.; Rega, N.; Millam, N. J.; Klene, M.; Knox, J. E.; Cross, J. B.; Bakken, V.; Adamo, C.; Jaramillo, J.; Gomperts, R.; Stratmann, R. E.; Yazyev, O.; Austin, A. J.; Cammi, R.; Pomelli, C.; Ochterski, J. W.; Martin, R. L.; Morokuma, K.; Zakrzewski, V. G.; Voth, G. A.; Salvador, P.; Dannenberg, J. J.; Dapprich, S.; Daniels, A. D.; Farkas, Ö.; Foresman, J. B.; Ortiz, J. V.; Cioslowski, J.; Fox, D. J. *Gaussian 09*, Gaussian, Inc., Wallingford CT, 2010.
25. Seela F, Peng X, Li H. Base-Pairing, Tautomerism, and Mismatch Discrimination of 7-Halogenated 7-Deaza-2'-deoxyisoguanosine: Oligonucleotide Duplexes with Parallel and Antiparallel Chain Orientation. *Journal of the American Chemical Society*. 2005;127:7739–51.
26. Wrigstedt P, Iashin, V, Lagerblom K., Keskiaväli J, Chernichenko K, Repo T. Syntheses of C-6 Aryl- and Alkynyl-Substituted Thymidines from Thymidine trans-5,6-Bromohydrins, *European Journal of Organic Chemistry*. 2017, 880–891.
27. Engels J, Krim J, Taourirte M, Grünewald C, Krstic I. Microwave-Assisted Click Chemistry for Nucleoside Functionalization: Useful Derivatives for Analytical and Biological Applications. *Synthesis*. 2013;45:396–405.

Appendices:

Appendix A: Phosphor Image Autoradiograms



Compound 1b:
 TEMPO (μM):

-	+	+	+	+	+	+	+	+	+
0	0	0.1	0.2	0.5	2	10	20	50	100



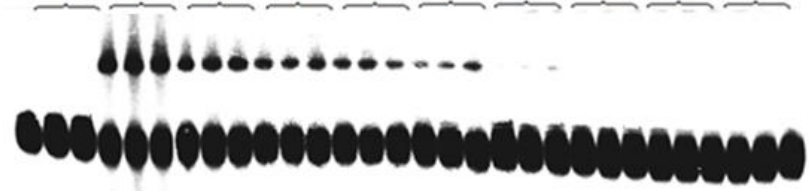
Compound 2a:
 MeONH₂ (mM):

-	+	+	+	+	+	+	+	+	+
0	0	1	2	5	10	20	50	100	100



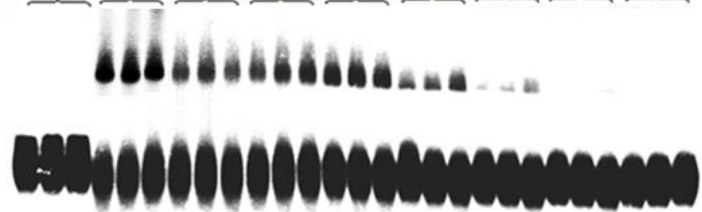
Compound 2a:
 TEMPO (mM):

-	+	+	+	+	+	+	+	+	+
0	0	0.2	0.5	1	2	10	20	50	100



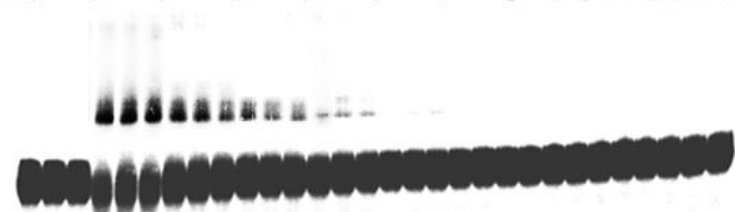
Compound 2b:
 MeONH₂ (mM):

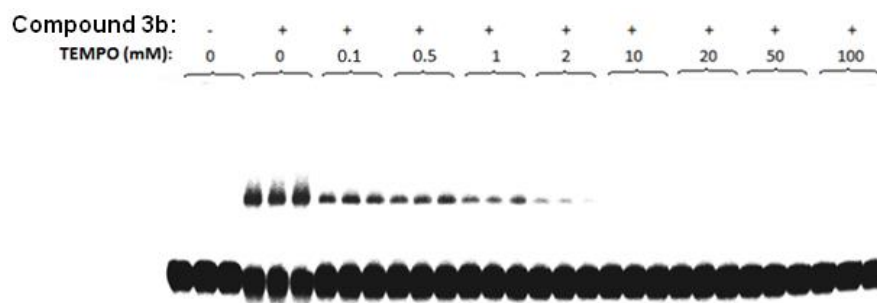
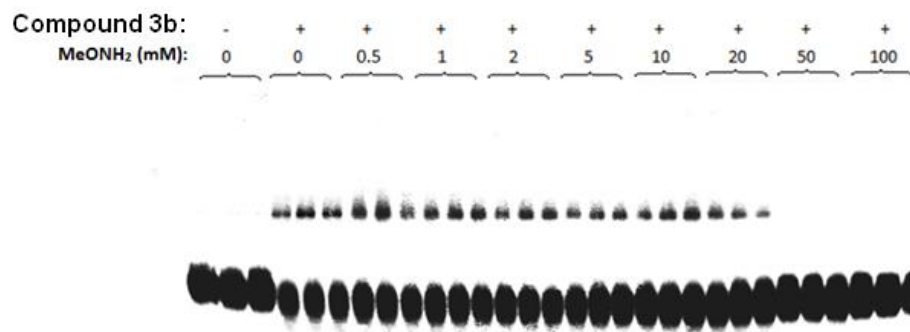
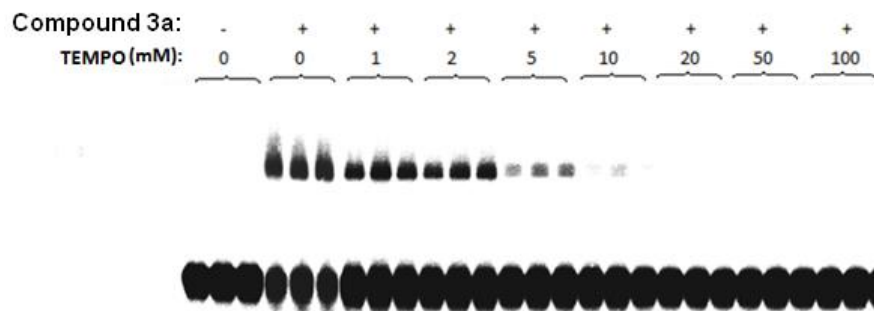
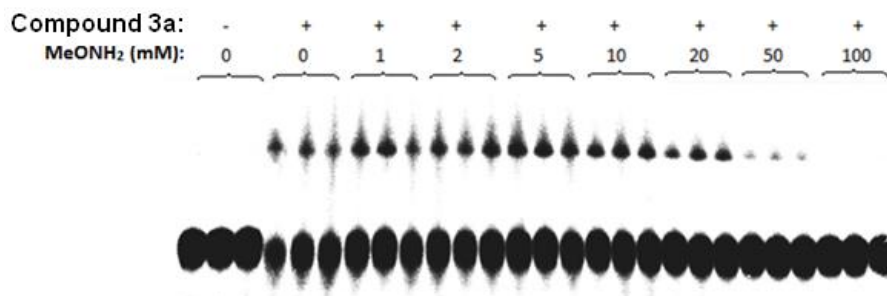
-	+	+	+	+	+	+	+	+	+
0	0	1	2	5	10	20	50	100	100



Compound 2b:
 TEMPO (mM):

-	+	+	+	+	+	+	+	+	+
0	0	0.02	0.05	0.1	1	10	20	50	100





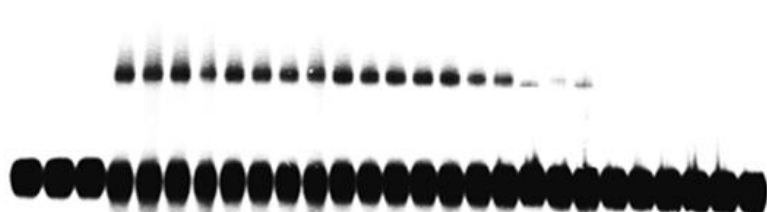
Compound 4a: - + + + + + + + +
 MeONH₂ (mM): 0 0 0.2 0.5 1 5 10 20 50 100



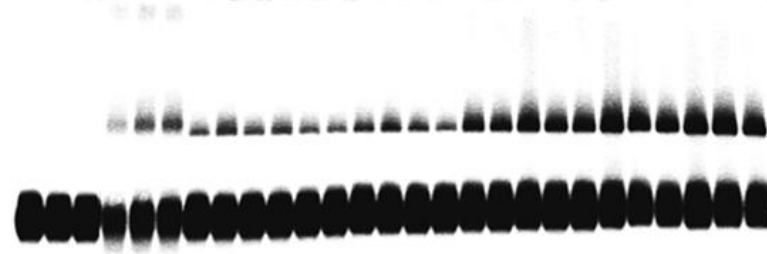
Compound 4a: - + + + + + + + +
 TEMPO (mM): 0 0 0.02 0.1 0.2 1 10 20 50 100



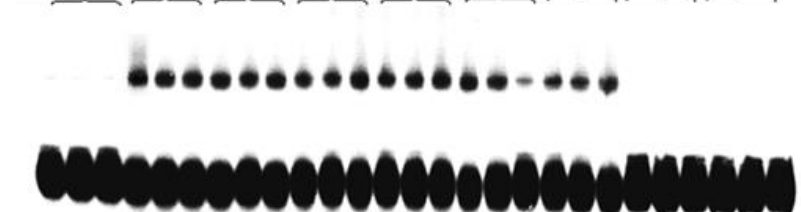
Compound 4b: - + + + + + + + +
 MeONH₂ (mM): 0 0 1 2 5 10 20 50 100

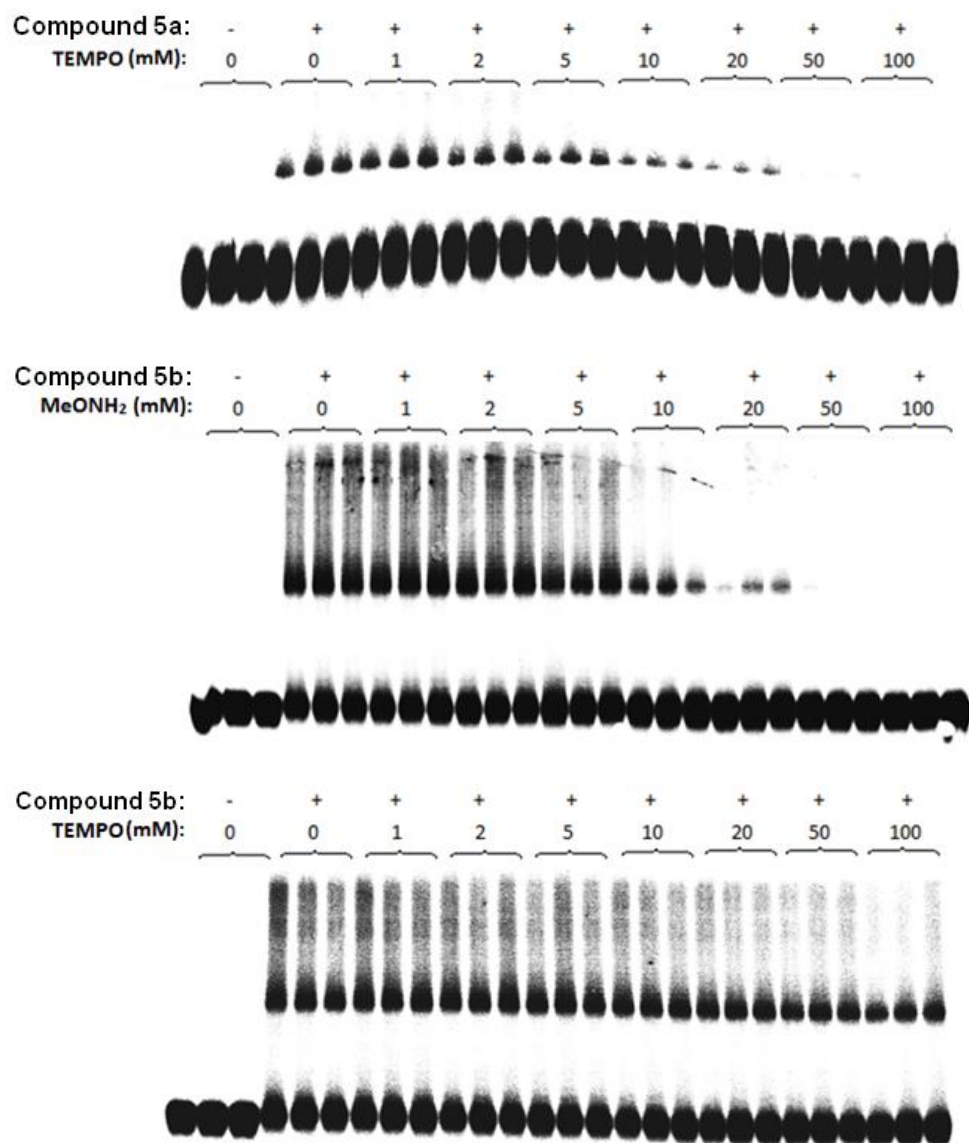


Compound 4b: - + + + + + + + +
 TEMPO (mM): 0 0 1 2 5 10 20 50 100

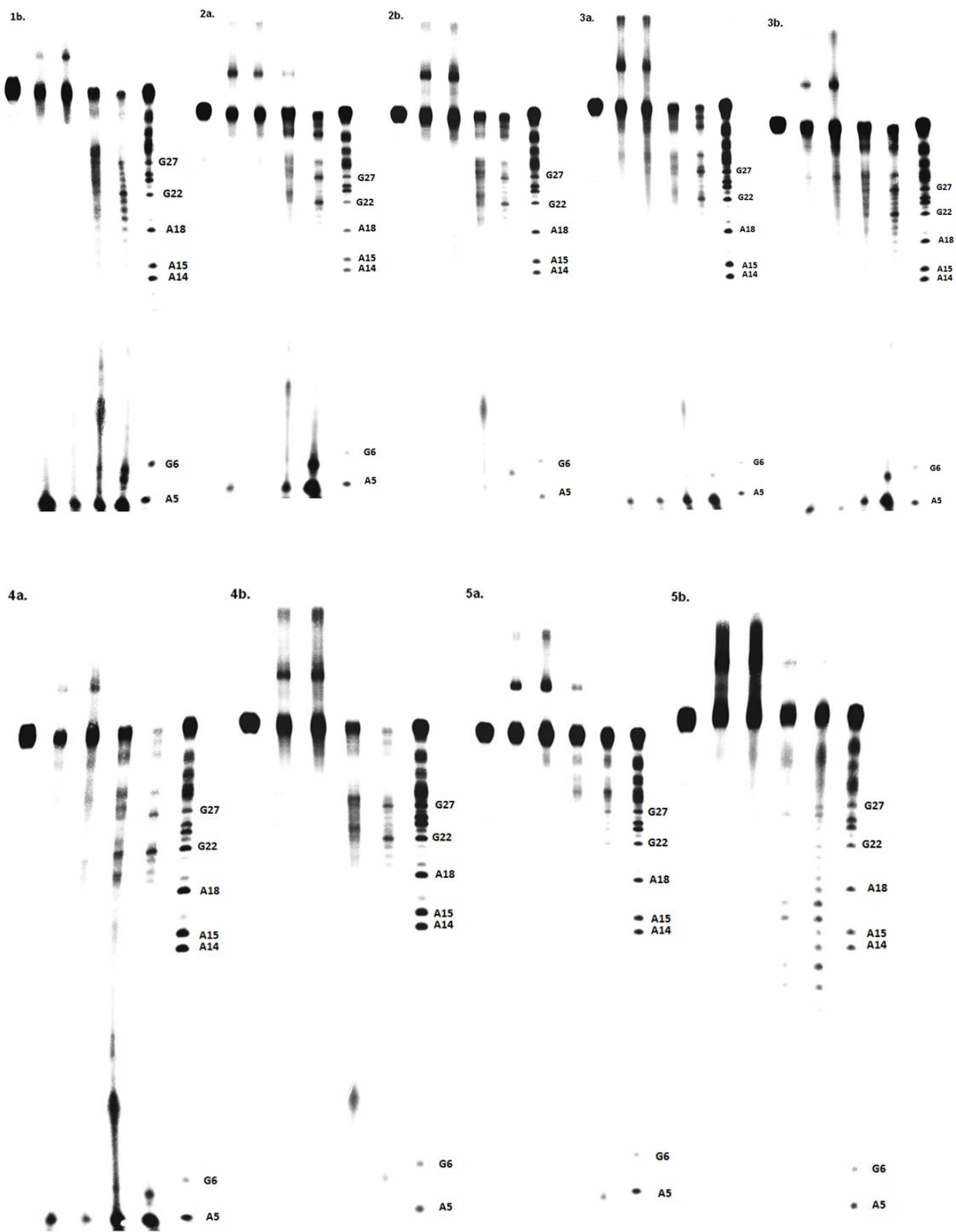


Compound 5a: - + + + + + + + +
 MeONH₂ (mM): 0 0 1 2 5 10 20 50 100

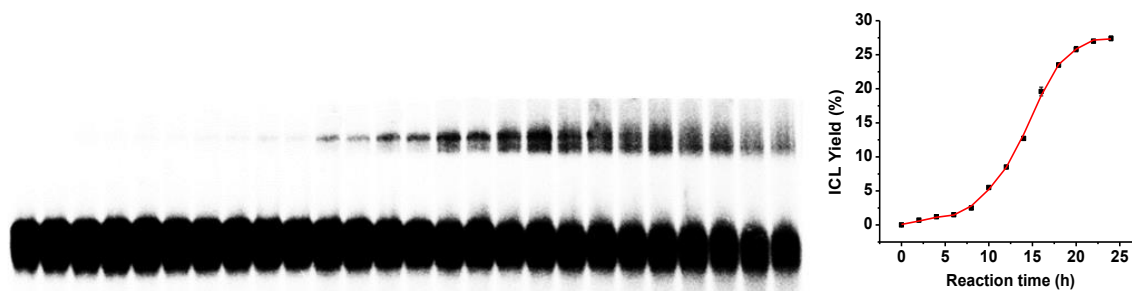




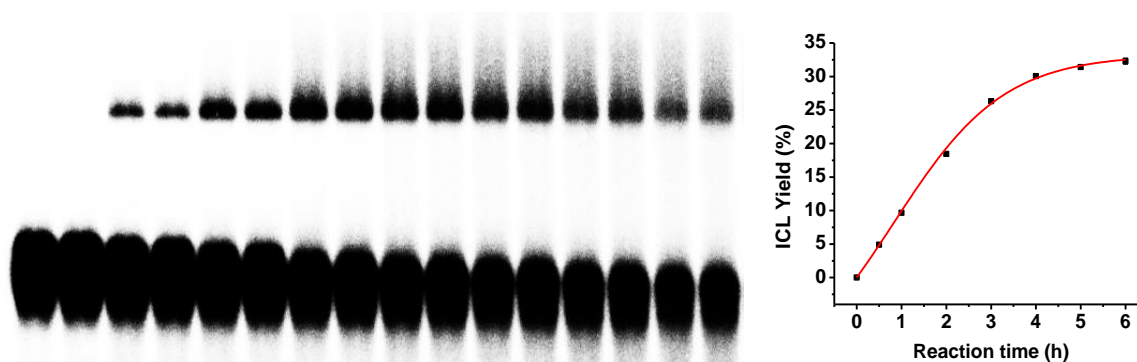
Representative gels for the effect of methoxyamine or TEMPO on DNA cross-link formation induced by **1a-5a** and **1b-5b** upon UV irradiation.



Determination of the reaction sites for **2a-5a** and **1b-5b**.



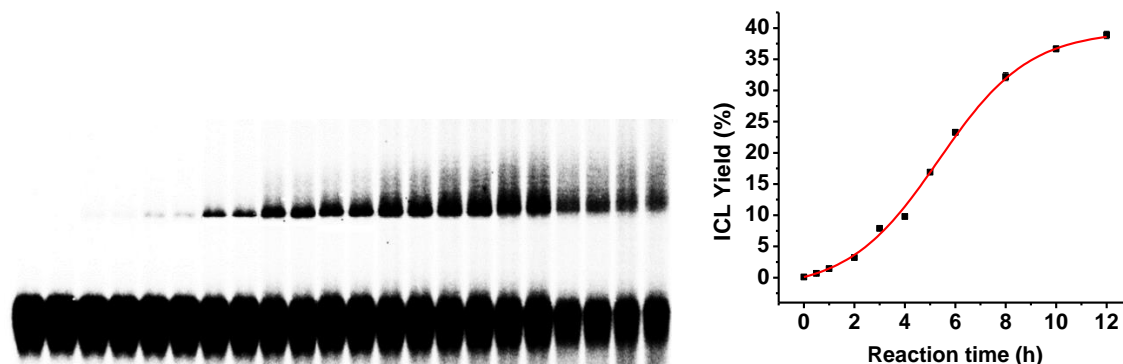
The rate of ICL formation of duplex **17** for **26a** upon photo-irradiation. **A. 26a** at time points 0, 2 h, 4 h, 6 h, 8 h, 10 h, 12 h, 14 h, 16 h, 18 h, 20 h, 22 h, 24 h. [**26a**] = 500 μ M. Reaction mixtures were photo-irradiated under UV (350nm), duplicates was done at each time point.



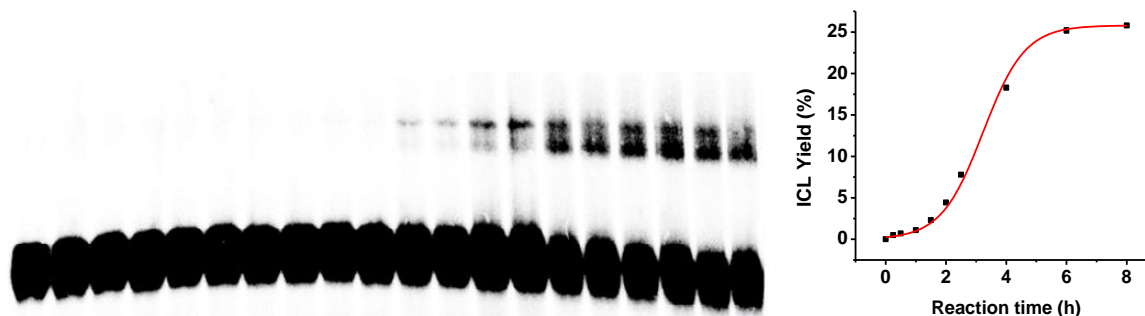
The rate of ICL formation of duplex **17** for **26b** upon photo-irradiation. **A. 26b** at time points 0, 0.5 h, 1 h, 2 h, 3 h, 4 h, 5 h, 6 h. [**26b**] = 500 μ M. Reaction mixtures were photo-irradiated under UV (350nm), duplicates was done at each time point.



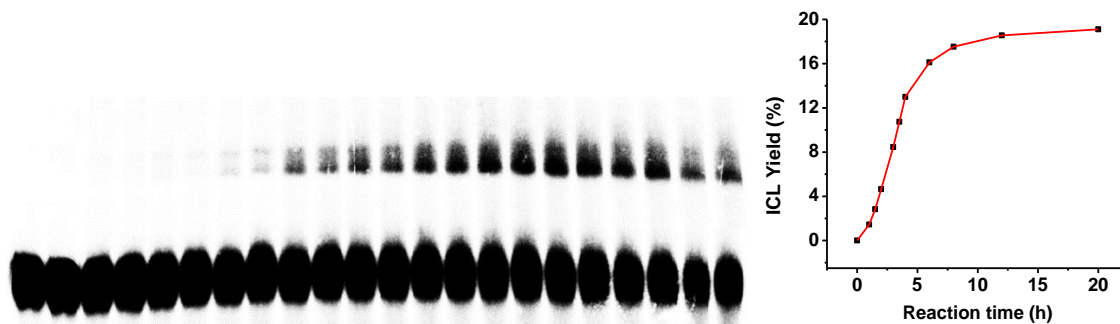
The rate of ICL formation of duplex **17** for **26c** upon photo-irradiation. **A. 26c** at time points 0, 1 h, 3 h, 6 h, 9 h, 12 h, 16 h, 20 h, 24 h, 28 h, 32 h, 36 h, 40 h. [26c] = 500 μ M. Reaction mixtures were photo-irradiated under UV (350nm), duplicates was done at each time point.



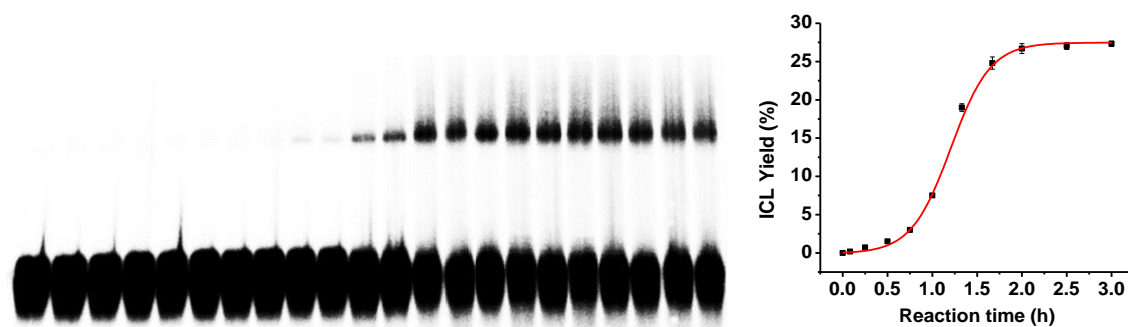
The rate of ICL formation of duplex **17** for **26d** upon photo-irradiation. **A. 26d** at time points 0, 0.5 h, 1 h, 2 h, 3 h, 4 h, 5 h, 6 h, 8 h, 10 h, 12h. [26d] = 500 μ M. Reaction mixtures were photo-irradiated under UV (350nm), duplicates was done at each time point.



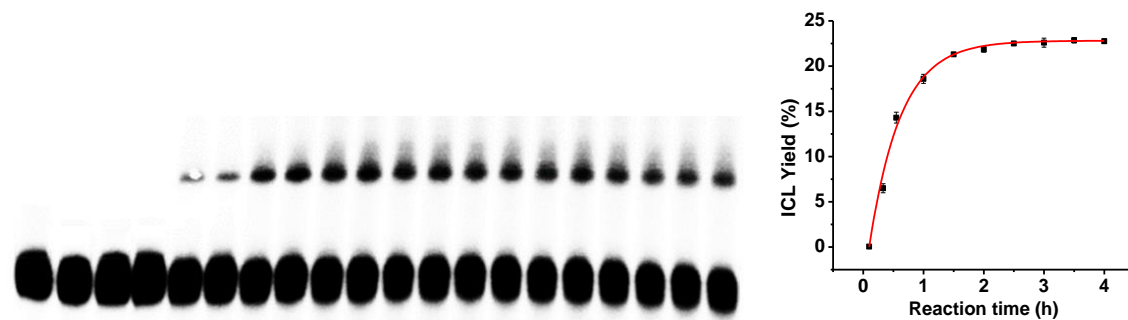
The rate of ICL formation of duplex **17** for **26e** upon photo-irradiation. **A. 26e** at time points 0, 15 min, 30 min, 1 h, 1.5 h, 2 h, 2.5 h, 4 h, 6 h, 8 h. [26e] = 500 μ M. Reaction mixtures were photo-irradiated under UV (350nm), duplicates was done at each time point.



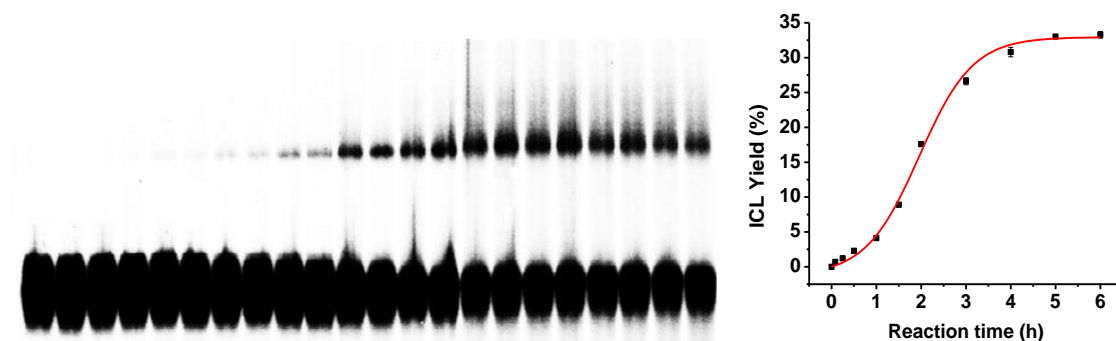
The rate of ICL formation of duplex **17** for **26f** upon photo-irradiation. **A. 26f** at time points 0, 1 h, 1.5 h, 2 h, 3 h, 3.5 h, 4 h, 6 h, 8 h, 12 h, 20 h. $[26f] = 500 \mu\text{M}$. Reaction mixtures were photo-irradiated under UV (350nm), duplicates was done at each time point.



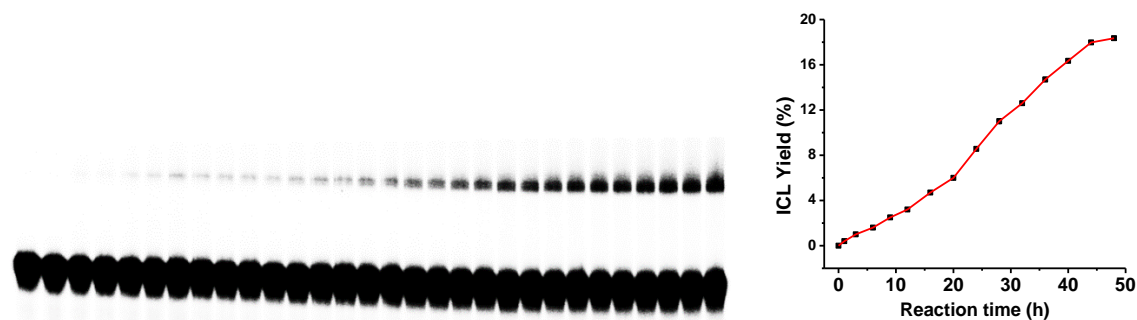
The rate of ICL formation of duplex **17** for **26g** upon photo-irradiation. **A. 26g** at time points 0, 5 min, 15 min, 30 min, 45min, 60 min, 80 min, 100 min, 2 h, 2.5 h, 3 h. $[26g] = 500 \mu\text{M}$. Reaction mixtures were photo-irradiated under UV (350nm), duplicates was done at each time point.



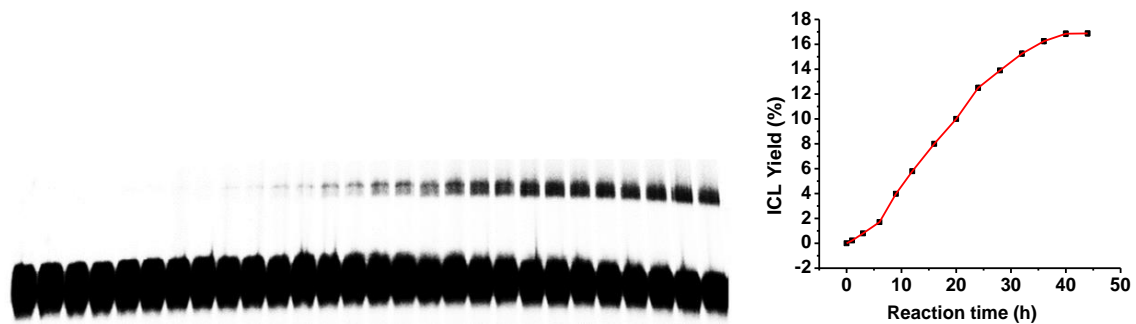
The rate of ICL formation of duplex **17** for **26h** upon photo-irradiation. **A. 26h** at time points 0, 6 min, 20 min, 35 min, 1 h, 1.5 h, 2 h, 3 h, 3.5 h, 4 h. $[26h] = 500 \mu\text{M}$. Reaction mixtures were photo-irradiated under UV (350nm), duplicates was done at each time point.



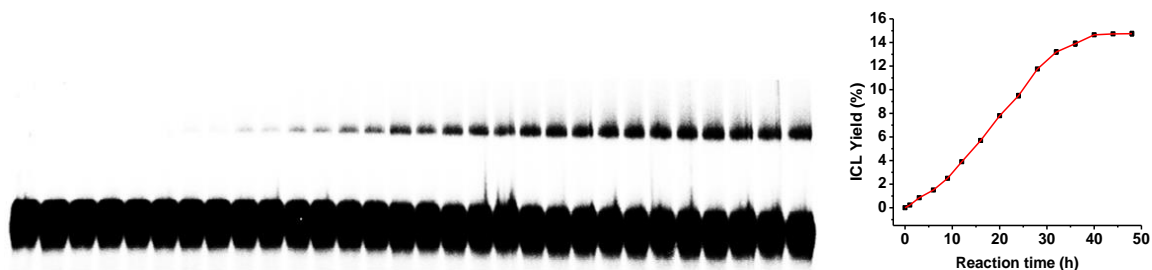
The rate of ICL formation of duplex **17** for **26i** upon photo-irradiation. **A. 26i** at time points 0, 5 min, 15 min, 30 min, 1 h, 1.5h, 2 h, 3 h, 4 h, 5 h, 6 h. $[26i] = 500 \mu\text{M}$. Reaction mixtures were photo-irradiated under UV (350nm), duplicates was done at each time point.



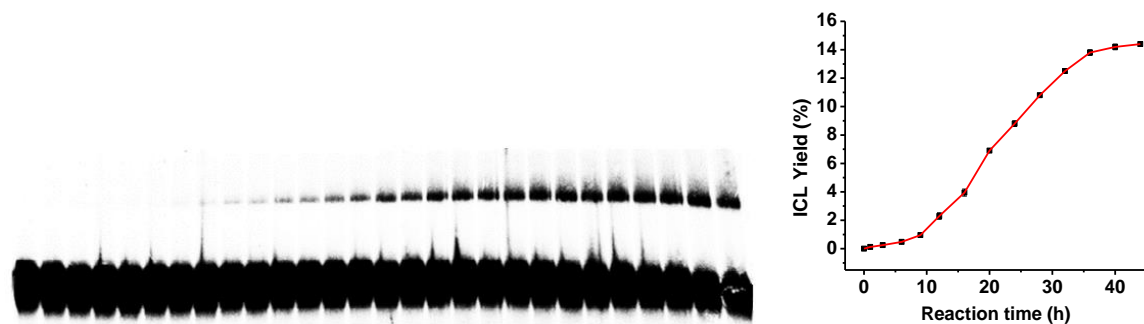
The rate of ICL formation of duplex **17** for **27a** upon photo-irradiation. **A. 27a** at time points 0, 1 h, 3 h, 6 h, 9 h, 12 h, 16 h, 20 h, 24 h, 28 h, 32 h, 36 h, 40 h, 44 h, 48 h. $[27a] = 500 \mu\text{M}$. Reaction mixtures were photo-irradiated under UV (350nm), duplicates was done at each time point.



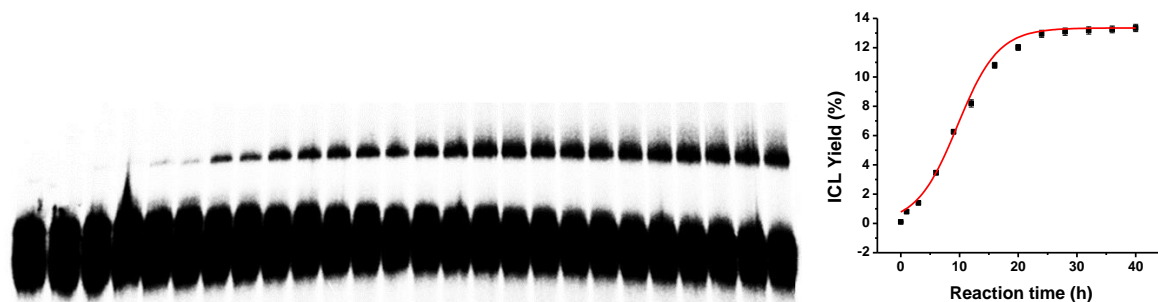
The rate of ICL formation of duplex **17** for **27b** upon photo-irradiation. **A. 27b** at time points 0, 1 h, 3 h, 6 h, 9 h, 12 h, 16 h, 20 h, 24 h, 28 h, 32 h, 36 h, 40 h, 44 h. $[27b] = 500 \mu M$. Reaction mixtures were photo-irradiated under UV (350nm), duplicates was done at each time point.



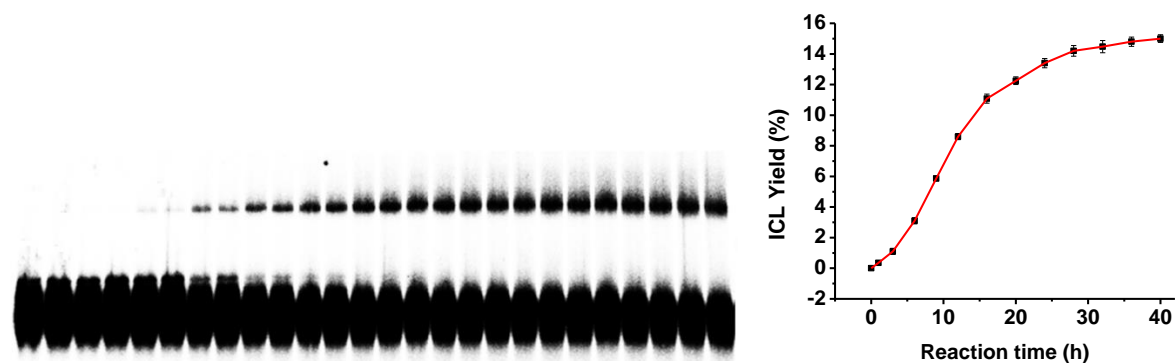
The rate of ICL formation of duplex **17** for **27c** upon photo-irradiation. **A. 27c** at time points 0, 1 h, 3 h, 6 h, 9 h, 12 h, 16 h, 20 h, 24 h, 28 h, 32 h, 36 h, 40 h, 44 h, 48 h. $[27c] = 500 \mu M$. Reaction mixtures were photo-irradiated under UV (350nm), duplicates was done at each time point.



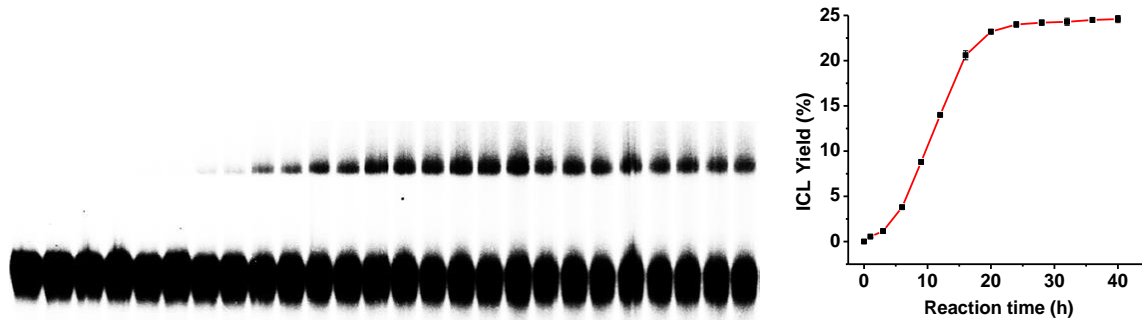
The rate of ICL formation of duplex **17** for **27d** upon photo-irradiation. **A. 27d** at time points 0, 1 h, 3 h, 6 h, 9 h, 12 h, 16 h, 20 h, 24 h, 28 h, 32 h, 36 h, 40 h. [**27d**] = 500 μ M. Reaction mixtures were photo-irradiated under UV (350nm), duplicates was done at each time point.



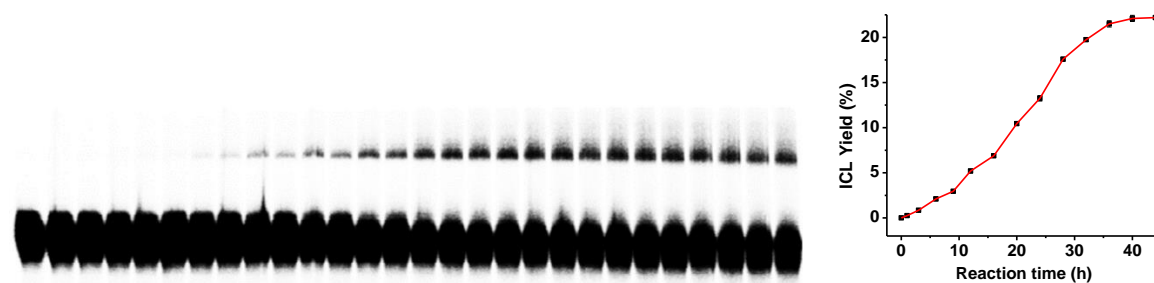
The rate of ICL formation of duplex **17** for **27e** upon photo-irradiation. **A. 27e** at time points 0, 1 h, 3 h, 6 h, 9 h, 12 h, 16 h, 20 h, 24 h, 28 h, 32 h, 36 h, 40 h. [**27e**] = 500 μ M. Reaction mixtures were photo-irradiated under UV (350nm), duplicates was done at each time point.



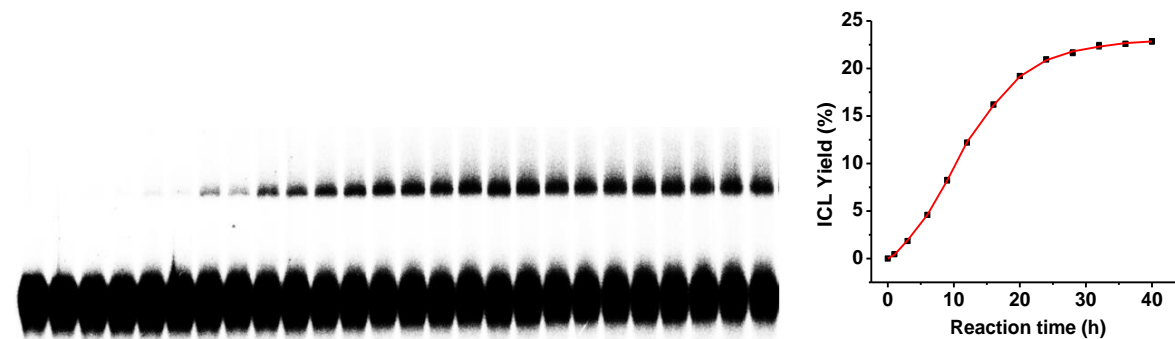
The rate of ICL formation of duplex **17** for **27f** upon photo-irradiation. **A. 27f** at time points 0, 1 h, 3 h, 6 h, 9 h, 12 h, 16 h, 20 h, 24 h, 28 h, 32 h, 36 h, 40 h. [**27f**] = 500 μ M. Reaction mixtures were photo-irradiated under UV (350nm), duplicates was done at each time point.



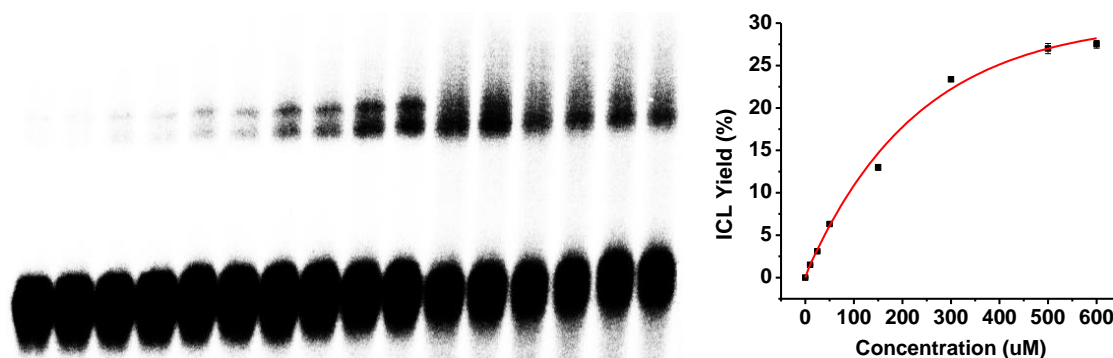
The rate of ICL formation of duplex **17** for **27g** upon photo-irradiation. **A. 27g** at time points 0, 1 h, 3 h, 6 h, 9 h, 12 h, 16 h, 20 h, 24 h, 28 h, 32 h, 36 h, 40 h. $[27g] = 500 \mu\text{M}$. Reaction mixtures were photo-irradiated under UV (350nm), duplicates was done at each time point.



The rate of ICL formation of duplex **17** for **27h** upon photo-irradiation. **A. 27h** at time points 0, 1 h, 3 h, 6 h, 9 h, 12 h, 16 h, 20 h, 24 h, 28 h, 32 h, 36 h, 40 h, 44 h. $[27h] = 500 \mu\text{M}$. Reaction mixtures were photo-irradiated under UV (350nm), duplicates was done at each time point.

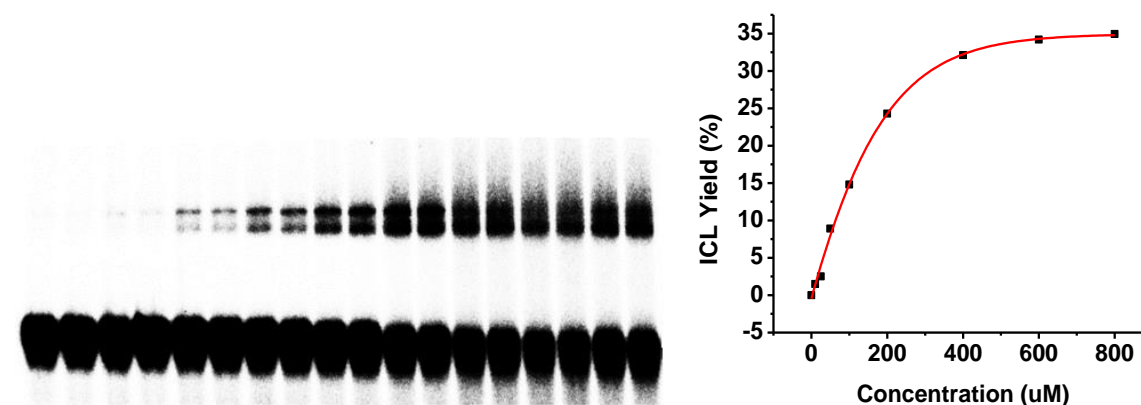


The rate of ICL formation of duplex **17** for **27i** upon photo-irradiation. **A. 27i** at time points 0, 1 h, 3 h, 6 h, 9 h, 12 h, 16 h, 20 h, 24 h, 28 h, 32 h, 36 h, 40 h. [**27i**] = 500 μ M. Reaction mixtures were photo-irradiated under UV (350nm), duplicates was done at each time point.



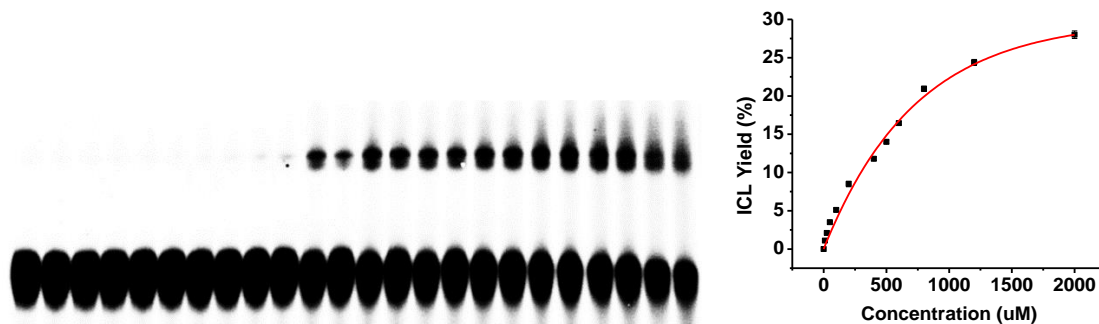
The concentration dependence of ICL formation of duplex **17** for **26a** upon photo-irradiation.

Phosphor image autoradiogram of 20% denaturing PAGD analysis of **26a** under varying concentration. 0, 10 μ M, 25 μ M, 50 μ M, 150 μ M, 300 μ M, 500 μ M, 600 μ M. Reaction mixtures were photo-irradiated under UV (350nm) for 22 h.



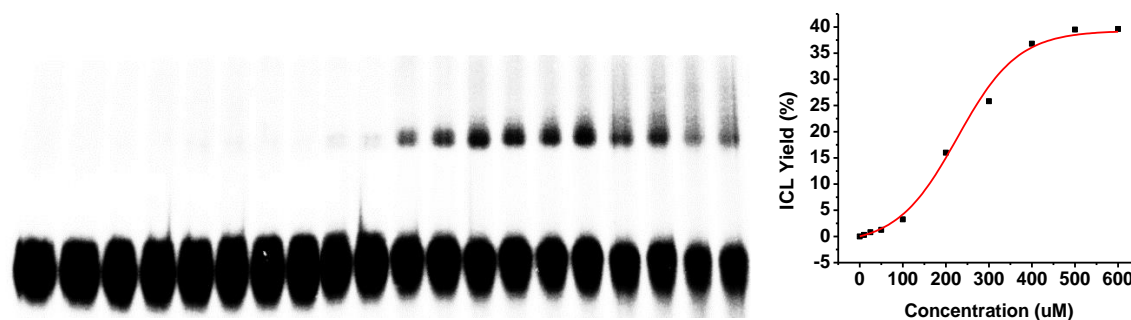
The concentration dependence of ICL formation of duplex **17** for **26b** upon photo-irradiation.

Phosphor image autoradiogram of 20% denaturing PAGD analysis of **26b** under varying concentration. 0, 10 μ M, 25 μ M, 50 μ M, 100 μ M, 200 μ M, 400 μ M, 600 μ M, 800 μ M. Reaction mixtures were photo-irradiated under UV (350nm) for 6 h.



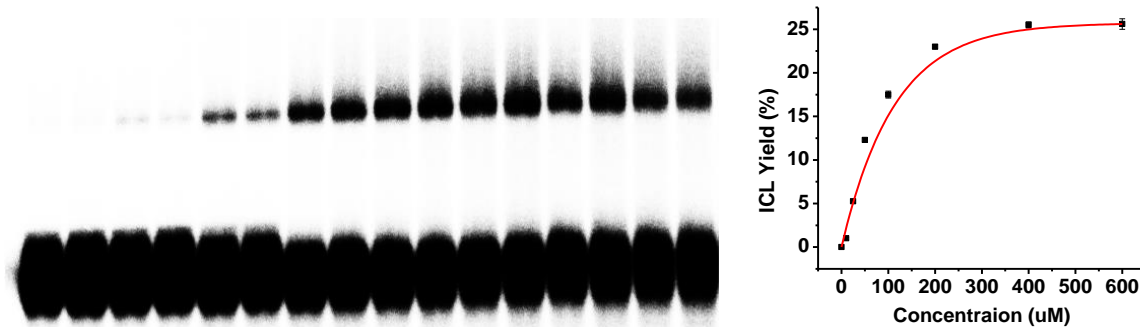
The concentration dependence of ICL formation of duplex **17** for **26c** upon photo-irradiation.

Phosphor image autoradiogram of 20% denaturing PAGD analysis of **26c** under varying concentration. 0, 10 μM , 25 μM , 50 μM , 100 μM , 200 μM , 300 μM , 400 μM , 600 μM , 800 μM , 1.2 mM, 2 mM. Reaction mixtures were photo-irradiated under UV (350nm) for 36 h.



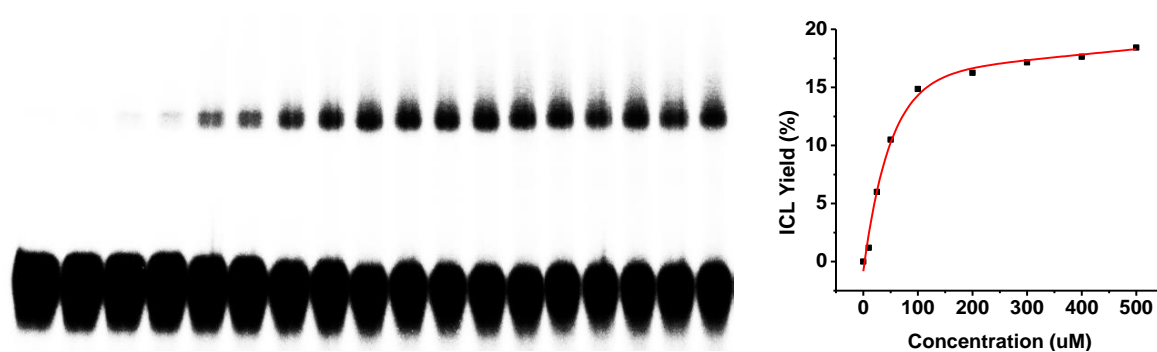
The concentration dependence of ICL formation of duplex **17** for **26d** upon photo-irradiation.

Phosphor image autoradiogram of 20% denaturing PAGD analysis of **26d** under varying concentration 0, 10 μM , 25 μM , 50 μM , 100 μM , 200 μM , 300 μM , 400 μM , 500 μM , 600 μM . Reaction mixtures were photo-irradiated under UV (350nm) for 12 h.



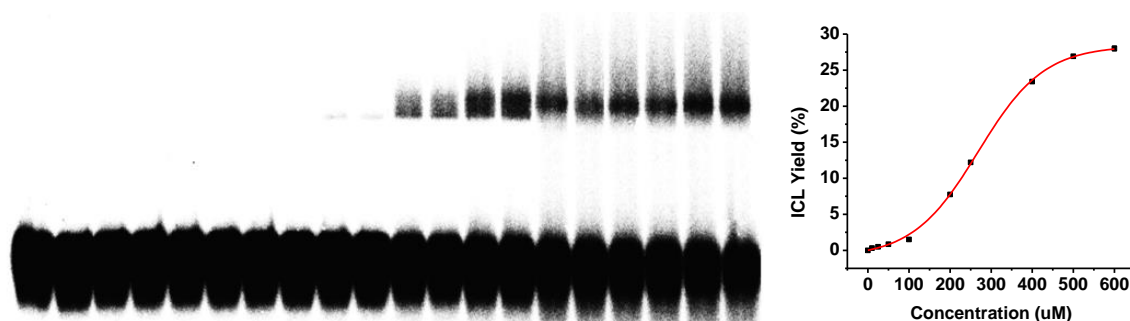
The concentration dependence of ICL formation of duplex **17** for **26e** upon photo-irradiation.

Phosphor image autoradiogram of 20% denaturing PAGD analysis of **26e** under varying concentration 0, 10 µM, 25 µM, 50 µM, 100 µM, 200 µM, 400 µM, 600 µM. Reaction mixtures were photo-irradiated under UV (350nm) for 6 h.



The concentration dependence of ICL formation of duplex **17** for **26f** upon photo-irradiation.

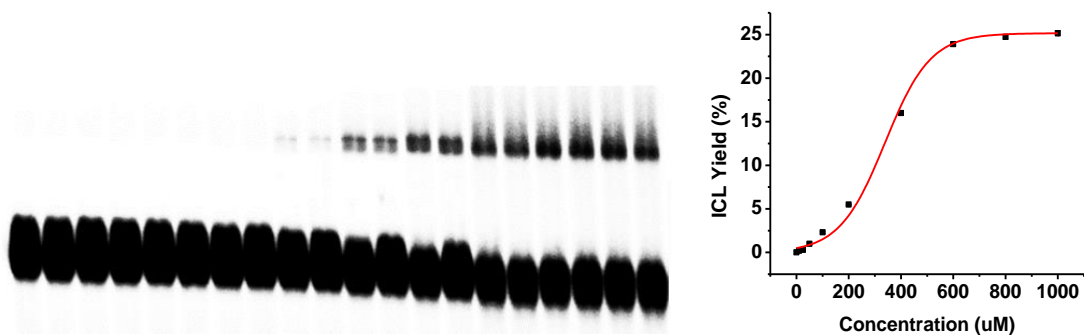
Phosphor image autoradiogram of 20% denaturing PAGD analysis of **26f** under varying concentration 0, 10 µM, 25 µM, 50 µM, 100 µM, 200 µM, 300 µM, 400 µM, 500 µM. Reaction mixtures were photo-irradiated under UV (350nm) for 12 h.



The concentration dependence of ICL formation of duplex **17** for **26g** upon photo-irradiation.

Phosphor image autoradiogram of 20% denaturing PAGD analysis of **26g** under varying concentration 0, 10 µM, 25 µM, 50 µM, 100 µM, 200 µM, 250 µM, 400 µM, 500 µM, 600 µM.

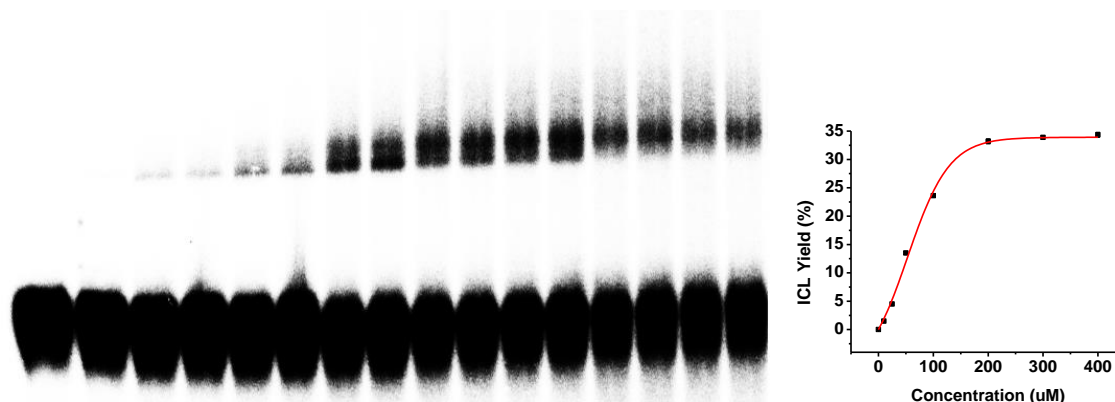
Reaction mixtures were photo-irradiated under UV (350nm) for 2 h.



The concentration dependence of ICL formation of duplex **17** for **26h** upon photo-irradiation.

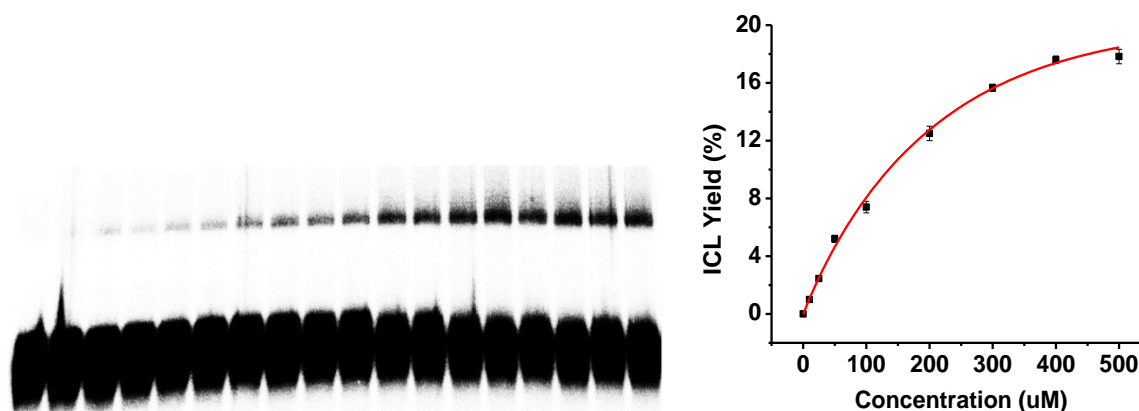
Phosphor image autoradiogram of 20% denaturing PAGD analysis of **26h** under varying concentration 0, 10 µM, 25 µM, 50 µM, 100 µM, 200 µM, 400 µM, 600 µM, 800 µM, 1 mM.

Reaction mixtures were photo-irradiated under UV (350nm) for 2 h.



The concentration dependence of ICL formation of duplex **17** for **26i** upon photo-irradiation.

Phosphor image autoradiogram of 20% denaturing PAGD analysis of **26i** under varying concentration 0, 10 μM , 25 μM , 50 μM , 100 μM , 200 μM , 300 μM , 400 μM . Reaction mixtures were photo-irradiated under UV (350nm) for 5 h.



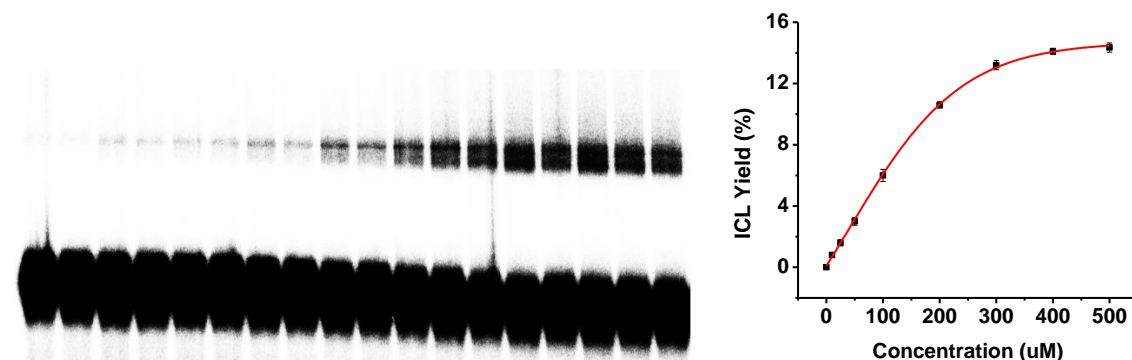
The concentration dependence of ICL formation of duplex **17** for **27a** upon photo-irradiation.

Phosphor image autoradiogram of 20% denaturing PAGD analysis of **27a** under varying concentration 0, 10 μM , 25 μM , 50 μM , 100 μM , 200 μM , 300 μM , 400 μM , 500 μM . Reaction mixtures were photo-irradiated under UV (350nm) for 44 h.



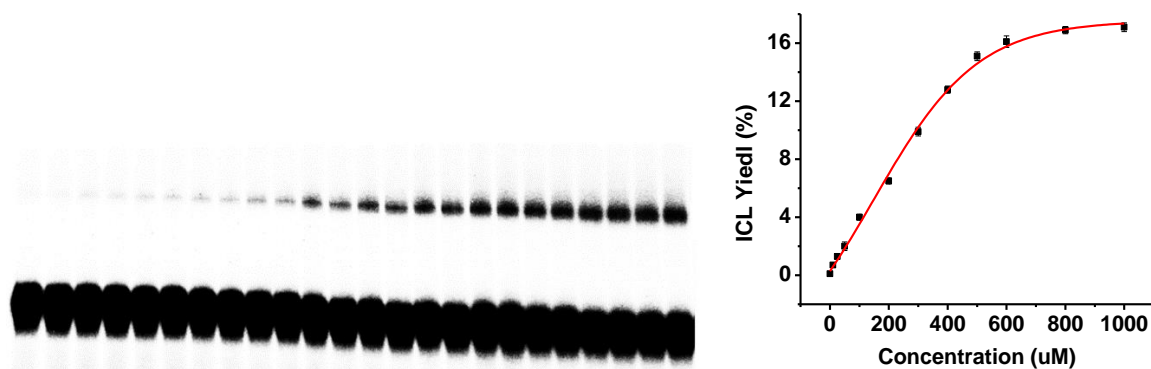
The concentration dependence of ICL formation of duplex **17** for **27b** upon photo-irradiation.

Phosphor image autoradiogram of 20% denaturing PAGD analysis of **27b** under varying concentration 0, 10 µM, 25 µM, 50 µM, 100 µM, 200 µM, 300 µM, 400 µM, 500 µM. Reaction mixtures were photo-irradiated under UV (350nm) for 40 h.



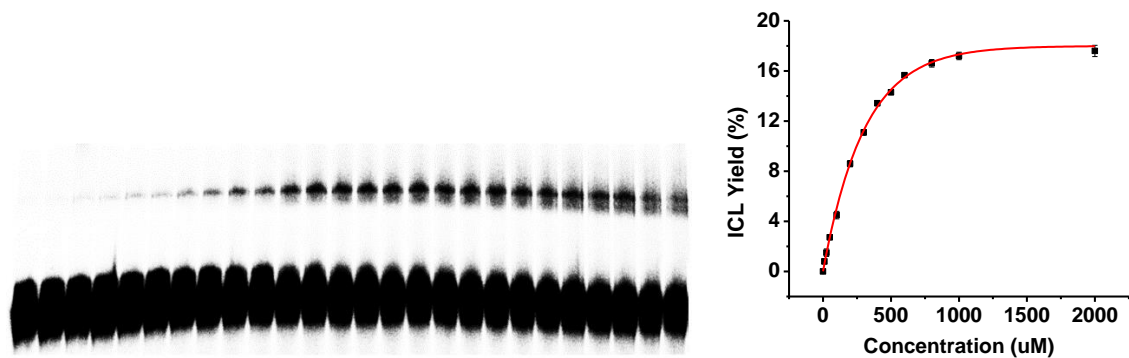
The concentration dependence of ICL formation of duplex **17** for **27c** upon photo-irradiation.

Phosphor image autoradiogram of 20% denaturing PAGD analysis of **27c** under varying concentration 0, 10 µM, 25 µM, 50 µM, 100 µM, 200 µM, 300 µM, 400 µM, 500 µM. Reaction mixtures were photo-irradiated under UV (350nm) for 40 h.



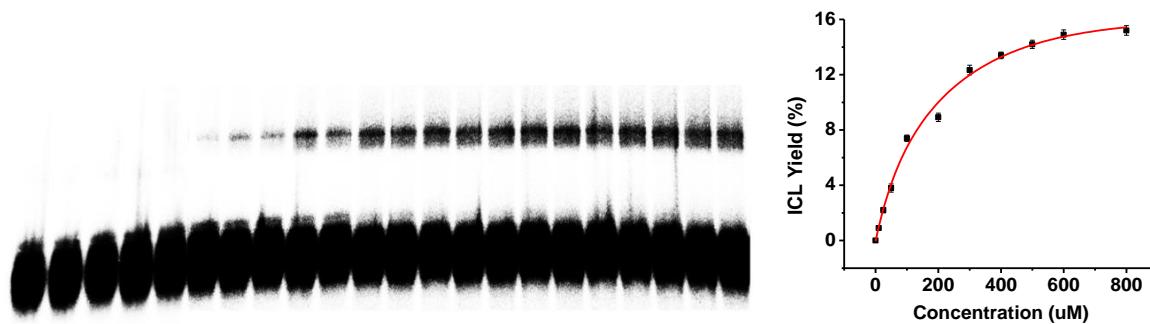
The concentration dependence of ICL formation of duplex **17** for **27d** upon photo-irradiation.

Phosphor image autoradiogram of 20% denaturing PAGD analysis of **27d** under varying concentration 0, 10 µM, 25 µM, 50 µM, 100 µM, 200 µM, 300 µM, 400 µM, 500 µM, 600 µM, 800 µM, 1 mM. Reaction mixtures were photo-irradiated under UV (350nm) for 40 h.



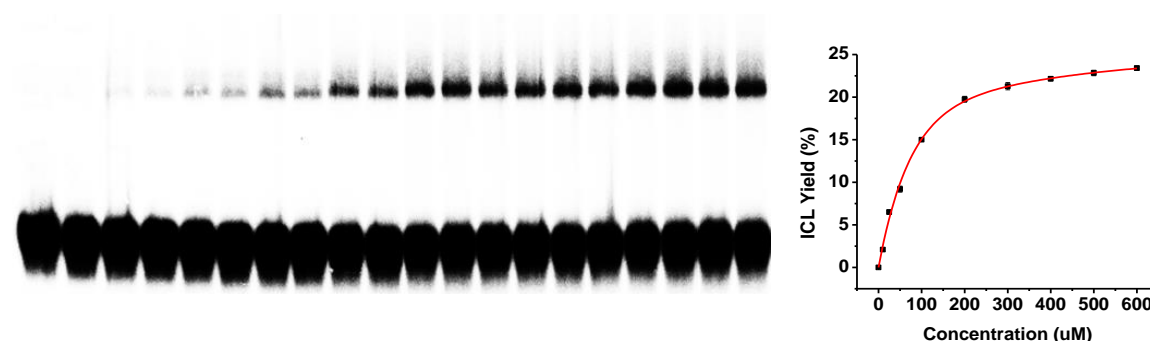
The concentration dependence of ICL formation of duplex **17** for **27e** upon photo-irradiation.

Phosphor image autoradiogram of 20% denaturing PAGD analysis of **27e** under varying concentration 0, 10 µM, 25 µM, 50 µM, 100 µM, 200 µM, 300 µM, 400 µM, 500 µM, 600 µM, 800 µM, 1 mM, 2 mM. Reaction mixtures were photo-irradiated under UV (350nm) for 24 h.



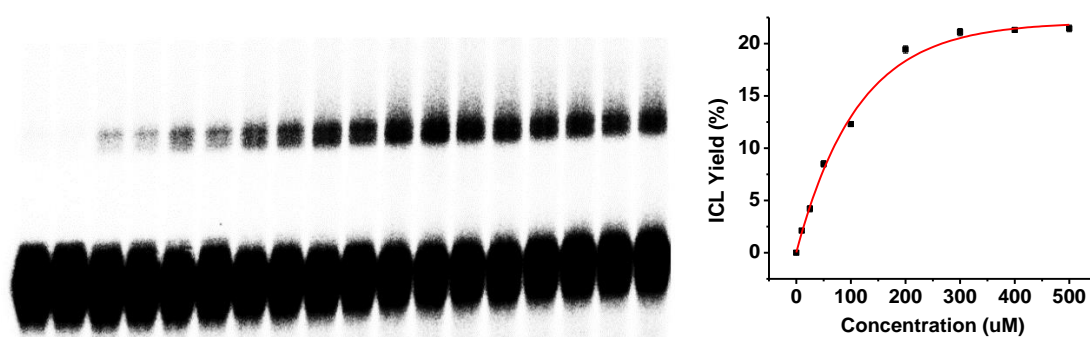
The concentration dependence of ICL formation of duplex **17** for **27f** upon photo-irradiation.

Phosphor image autoradiogram of 20% denaturing PAGD analysis of **27f** under varying concentration 0, 10 µM, 25 µM, 50 µM, 100 µM, 200 µM, 300 µM, 400 µM, 500 µM, 600 µM, 800 µM. Reaction mixtures were photo-irradiated under UV (350nm) for 32 h.



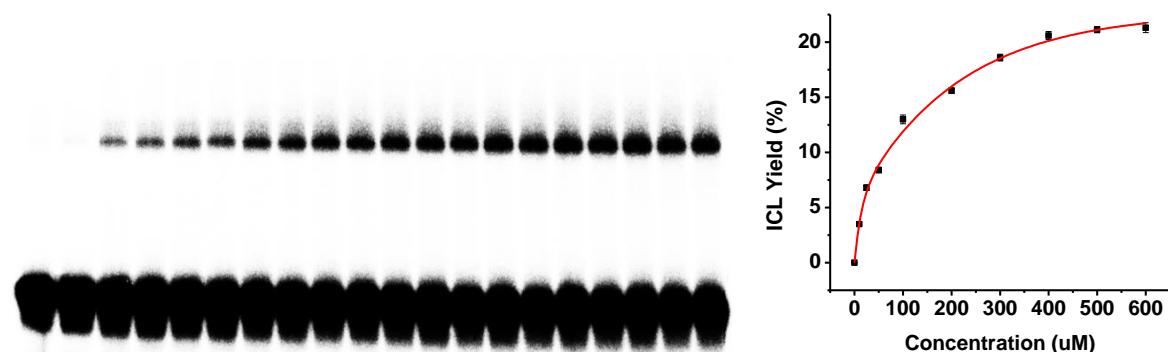
The concentration dependence of ICL formation of duplex **17** for **27g** upon photo-irradiation.

Phosphor image autoradiogram of 20% denaturing PAGD analysis of **27g** under varying concentration 0, 10 µM, 25 µM, 50 µM, 100 µM, 200 µM, 300 µM, 400 µM, 500 µM, 600 µM. Reaction mixtures were photo-irradiated under UV (350nm) for 24 h.



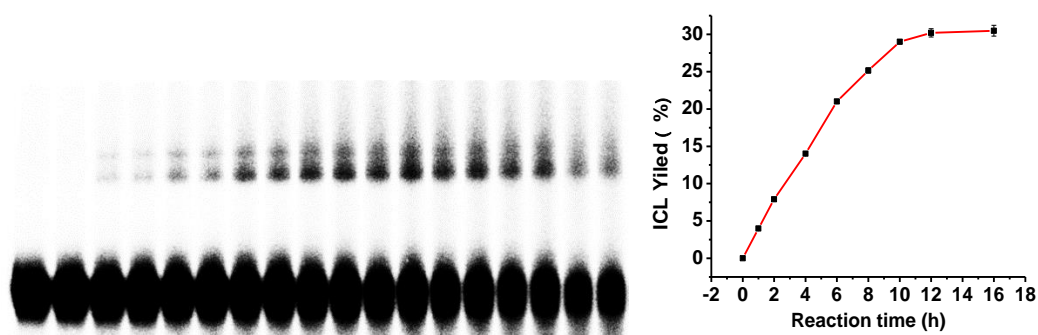
The concentration dependence of ICL formation of duplex **17** for **27h** upon photo-irradiation.

Phosphor image autoradiogram of 20% denaturing PAGD analysis of **27h** under varying concentration 0, 10 µM, 25 µM, 50 µM, 100 µM, 200 µM, 300 µM, 400 µM, 500 µM. Reaction mixtures were photo-irradiated under UV (350nm) for 36 h.

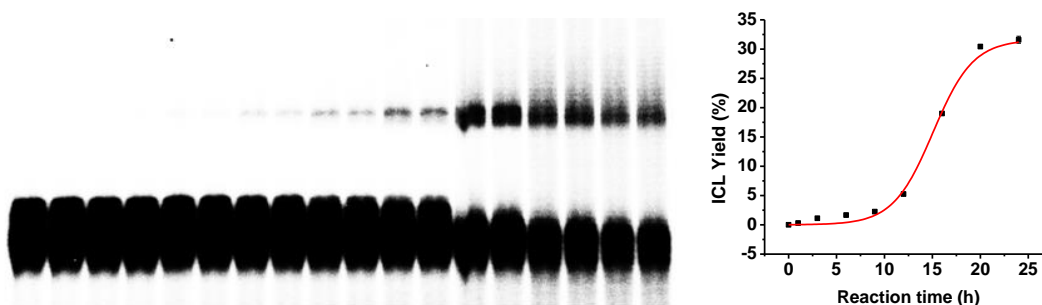


The concentration dependence of ICL formation of duplex **17** for **27i** upon photo-irradiation.

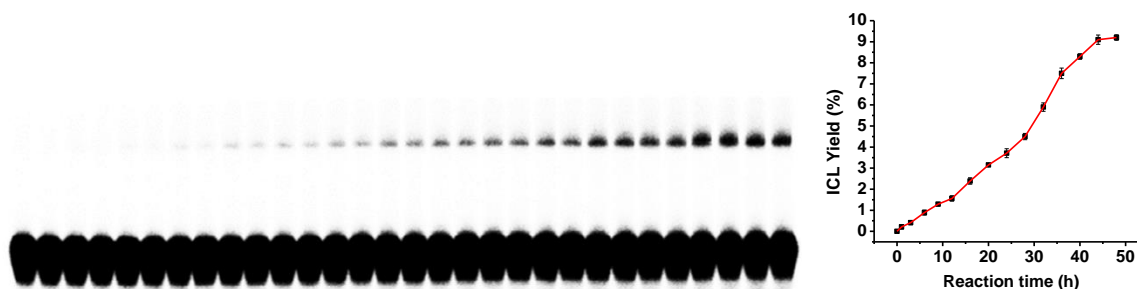
Phosphor image autoradiogram of 20% denaturing PAGD analysis of **27i** under varying concentration 0, 10 µM, 25 µM, 50 µM, 100 µM, 200 µM, 300 µM, 400 µM, 500 µM, 600 µM.



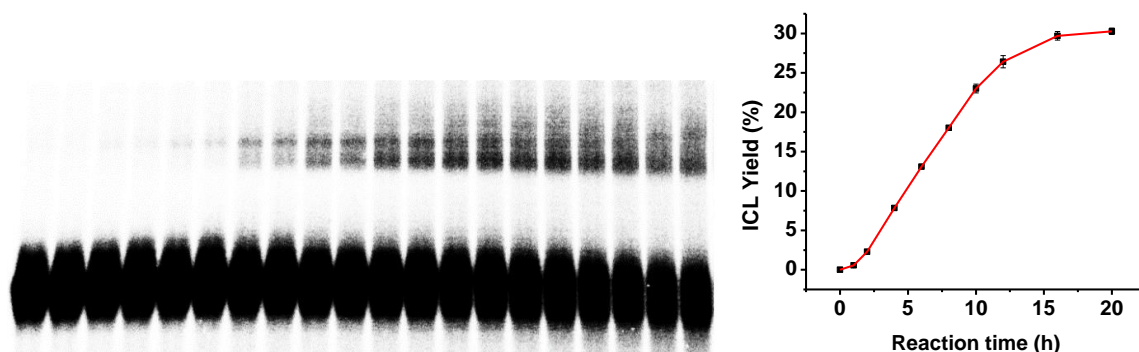
The rate of ICL formation of duplex **17** for **34a** upon photo-irradiation. **A. 34a** at time points 0, 1 h, 2 h, 4 h, 6 h, 8 h, 10 h, 12 h, 16 h. [**34a**] = 500 μ M. Reaction mixtures were photo-irradiated under UV (350nm), duplicates was done at each time point.



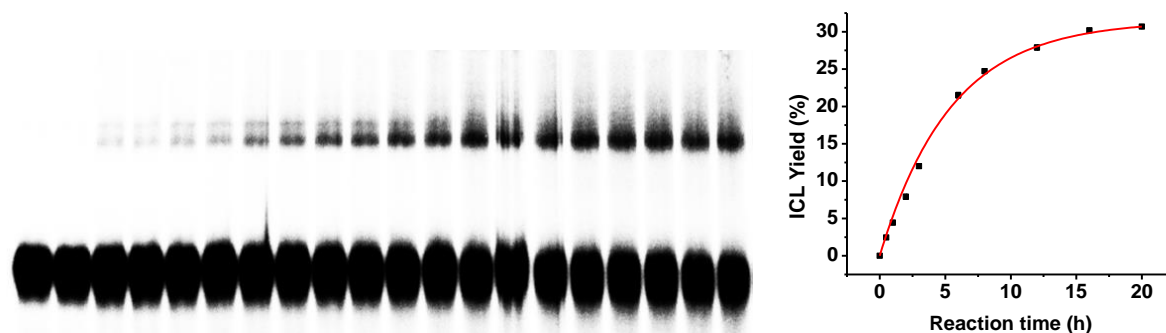
The rate of ICL formation of duplex **17** for **34b** upon photo-irradiation. **A. 34b** at time points 0, 1 h, 3 h, 6 h, 9 h, 12 h, 16 h, 20 h, 24 h. [**34b**] = 500 μ M. Reaction mixtures were photo-irradiated under UV (350nm), duplicates was done at each time point.



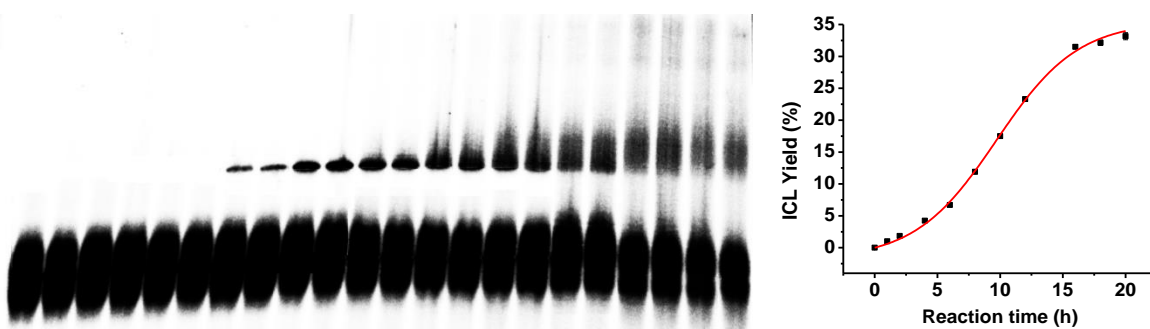
The rate of ICL formation of duplex **17** for **34c** upon photo-irradiation. **A. 34c** at time points 0, 1 h, 3 h, 6 h, 9 h, 12 h, 16 h, 20 h, 24 h, 28 h, 32 h, 36 h, 40 h, 44 h, 48 h. [**34c**] = 500 μ M. Reaction mixtures were photo-irradiated under UV (350nm), duplicates was done at each time point.



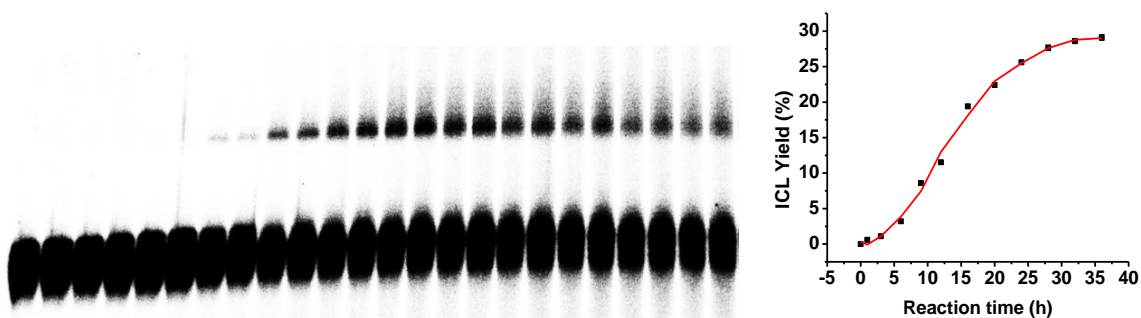
The rate of ICL formation of duplex **17** for **34d** upon photo-irradiation. **A. 34d** at time points 0, 1 h, 2 h, 4 h, 6 h, 8 h, 10 h, 12 h, 16 h, 20 h. [**34d**] = 500 μ M. Reaction mixtures were photo-irradiated under UV (350nm), duplicates was done at each time point.



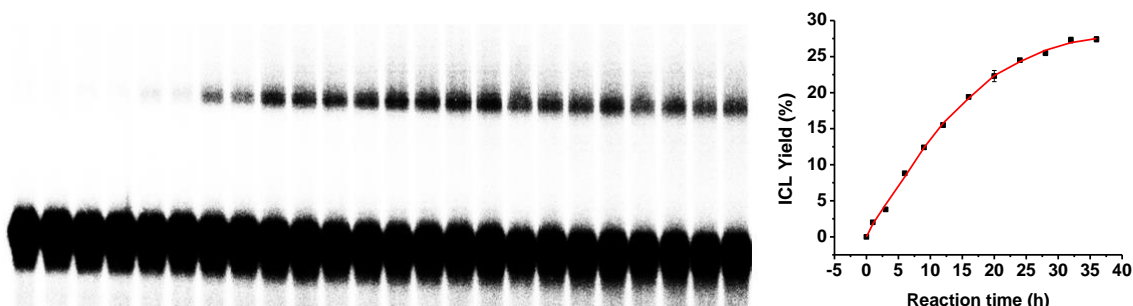
The rate of ICL formation of duplex **17** for **34e** upon photo-irradiation. **A. 34e** at time points 0, 0.5 h, 1 h, 2 h, 3 h, 6 h, 8 h, 12 h, 16 h, 20 h. [**34e**] = 500 μ M. Reaction mixtures were photo-irradiated under UV (350nm), duplicates was done at each time point.



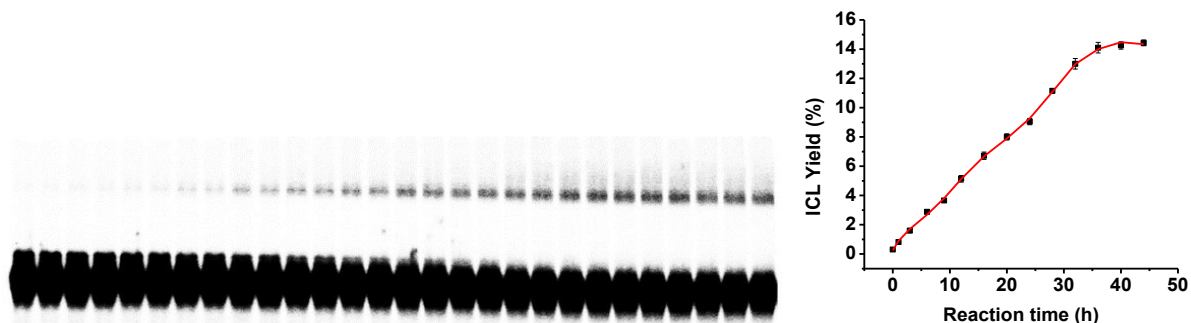
The rate of ICL formation of duplex **17** for **34f** upon photo-irradiation. **A. 34f** at time points 0, 1 h, 2 h, 4 h, 6 h, 8 h, 10 h, 12 h, 16h, 18 h, 20 h. [**34f**] = 500 μ M. Reaction mixtures were photo-irradiated under UV (350nm), duplicates was done at each time point.



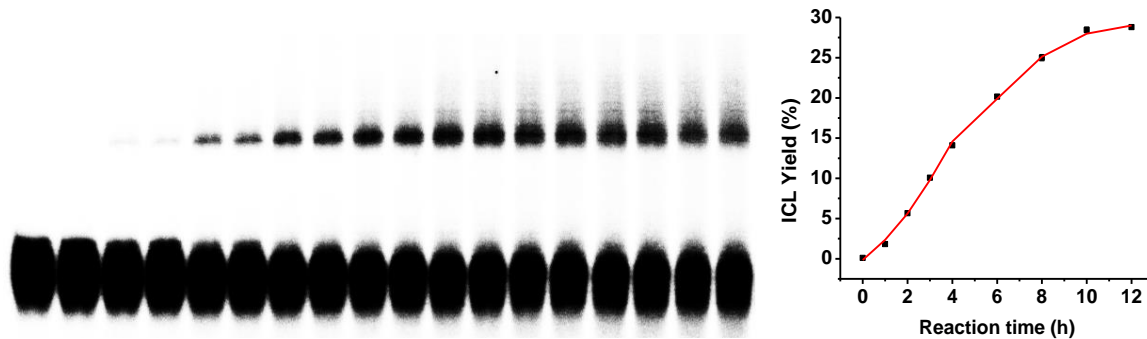
The rate of ICL formation of duplex **17** for **34g** upon photo-irradiation. **A. 34g** at time points 0, 1 h, 3 h, 6 h, 9 h, 12 h, 16 h, 20 h, 24 h, 28 h, 32 h, 36 h. $[34g] = 500 \mu\text{M}$. Reaction mixtures were photo-irradiated under UV (350nm), duplicates was done at each time point.



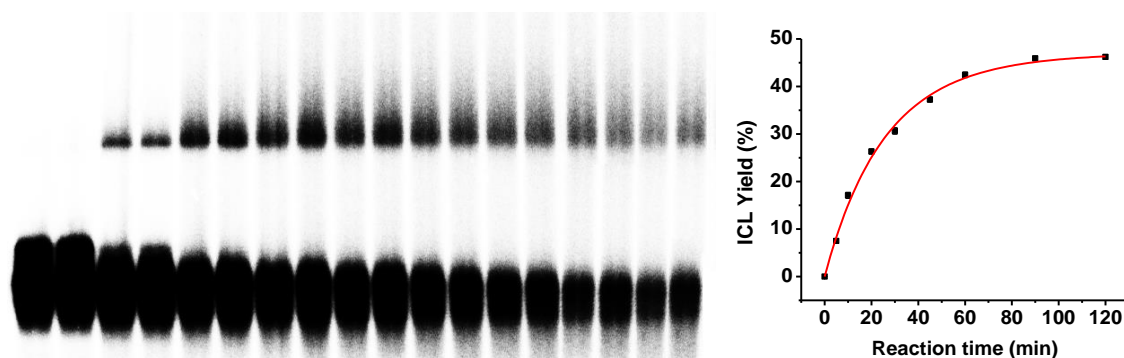
The rate of ICL formation of duplex **17** for **34h** upon photo-irradiation. **A. 34h** at time points 0, 1 h, 3 h, 6 h, 9 h, 12 h, 16 h, 20 h, 24 h, 28 h, 32 h, 36 h. $[34h] = 500 \mu\text{M}$. Reaction mixtures were photo-irradiated under UV (350nm), duplicates was done at each time point.



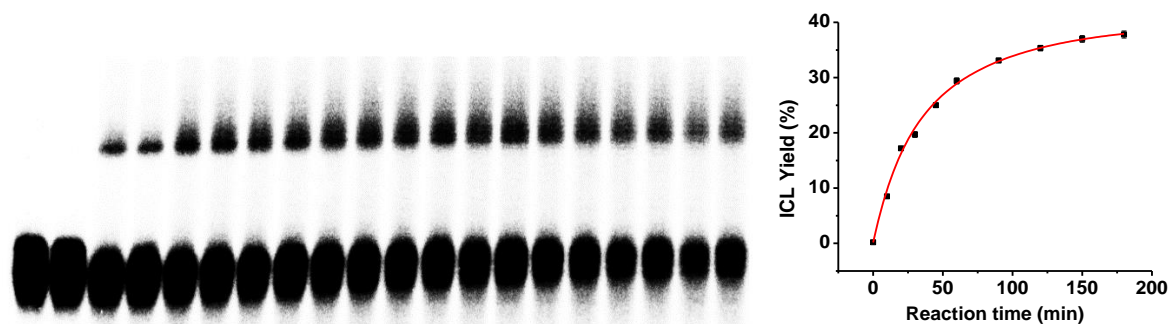
The rate of ICL formation of duplex **17** for **34i** upon photo-irradiation. **A. 34i** at time points 0, 1 h, 3 h, 6 h, 9 h, 12 h, 16 h, 20 h, 24 h, 28 h, 32 h, 36 h, 40 h, 44 h. $[34i] = 500 \mu\text{M}$. Reaction mixtures were photo-irradiated under UV (350nm), duplicates was done at each time point.



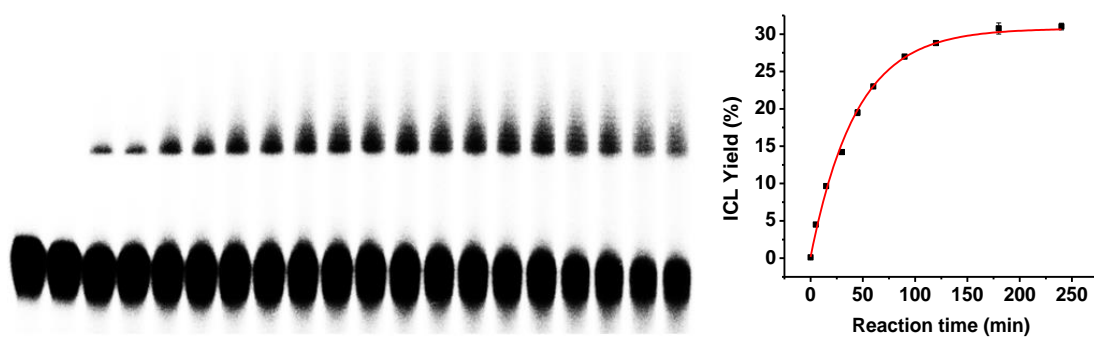
The rate of ICL formation of duplex **17** for **34j** upon photo-irradiation. **A. 34j** at time points 0, 1 h, 2 h, 3 h, 4 h, 6 h, 8 h, 10 h, 12 h. $[34j] = 500 \mu\text{M}$. Reaction mixtures were photo-irradiated under UV (350nm), duplicates was done at each time point.



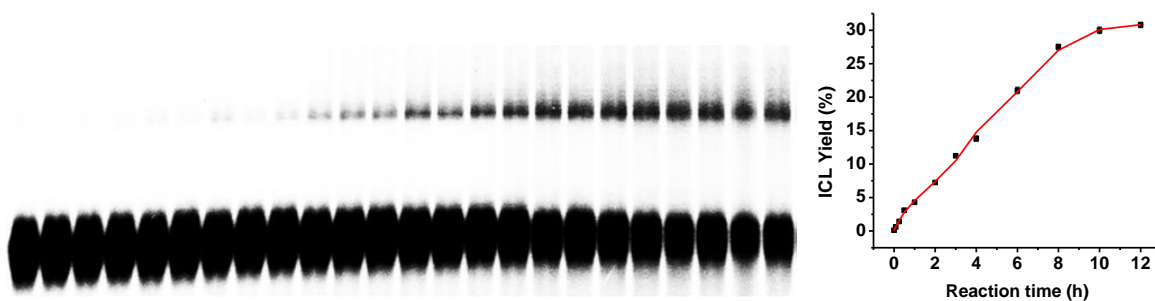
The rate of ICL formation of duplex **17** for **35a** upon photo-irradiation. **A. 35a** at time points 0, 5 min, 10 min, 20 min, 30 min, 45 min, 1 h, 1.5h, 2 h. $[35a] = 500 \mu\text{M}$. Reaction mixtures were photo-irradiated under UV (350nm), duplicates was done at each time point.



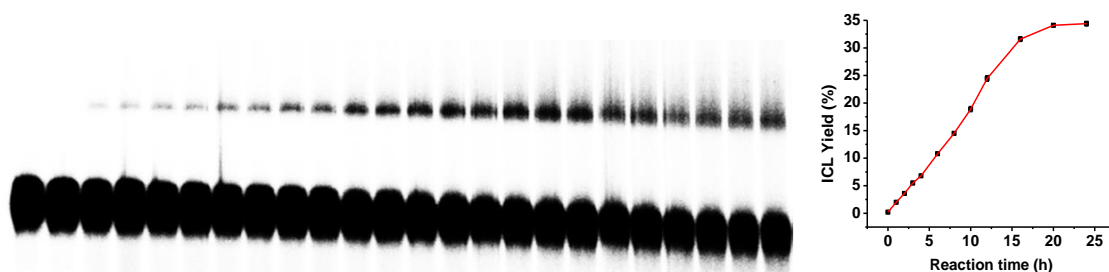
The rate of ICL formation of duplex **17** for **35b** upon photo-irradiation. **A. 35b** at time points 0, 10 min, 20 min, 30 min, 45 min, 1 h, 1.5 h, 2 h, 2.5 h, 3 h. $[35b] = 500 \mu\text{M}$. Reaction mixtures were photo-irradiated under UV (350nm), duplicates was done at each time point.



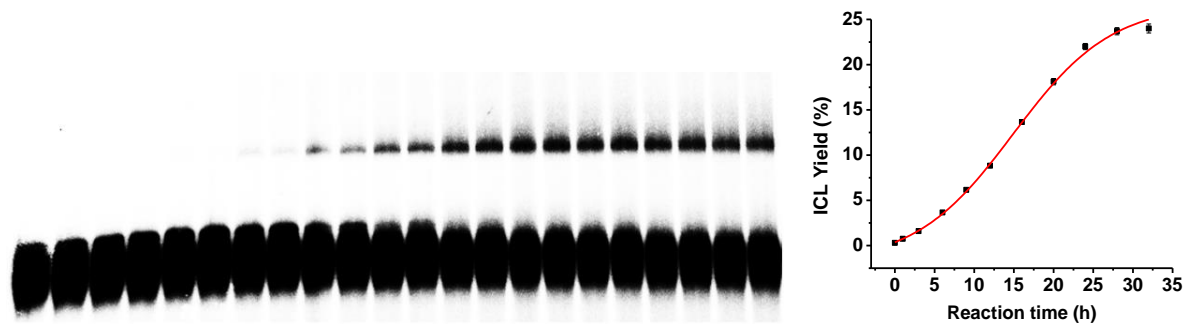
The rate of ICL formation of duplex **17** for **35c** upon photo-irradiation. **A. 35c** at time points 0, 5 min, 15 min, 30 min, 45 min, 1 h, 1.5 h, 2 h, 3 h, 4 h. $[35c] = 500 \mu\text{M}$. Reaction mixtures were photo-irradiated under UV (350nm), duplicates was done at each time point.



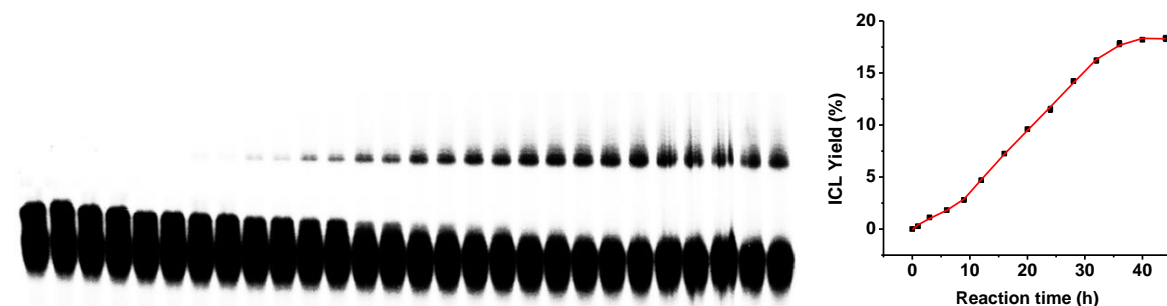
The rate of ICL formation of duplex **17** for **35d** upon photo-irradiation. **A. 35d** at time points 0, 5 min, 15 min, 0.5 h, 1 h, 2 h, 3 h, 4 h, 6 h, 8 h, 10 h, 12 h. $[35d] = 500 \mu\text{M}$. Reaction mixtures were photo-irradiated under UV (350nm), duplicates was done at each time point.



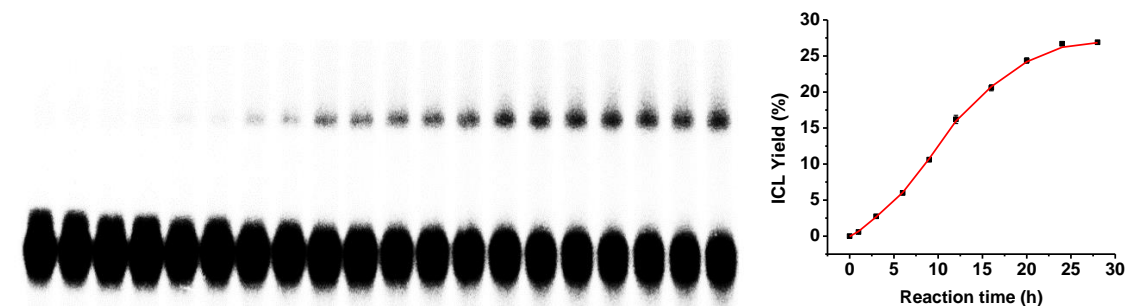
The rate of ICL formation of duplex **17** for **35e** upon photo-irradiation. **A. 35e** at time points 0, 1 h, 2 h, 3 h, 4 h, 6 h, 8 h, 10 h, 12 h, 16 h, 20 h, 24 h. $[35e] = 500 \mu\text{M}$. Reaction mixtures were photo-irradiated under UV (350nm), duplicates was done at each time point.



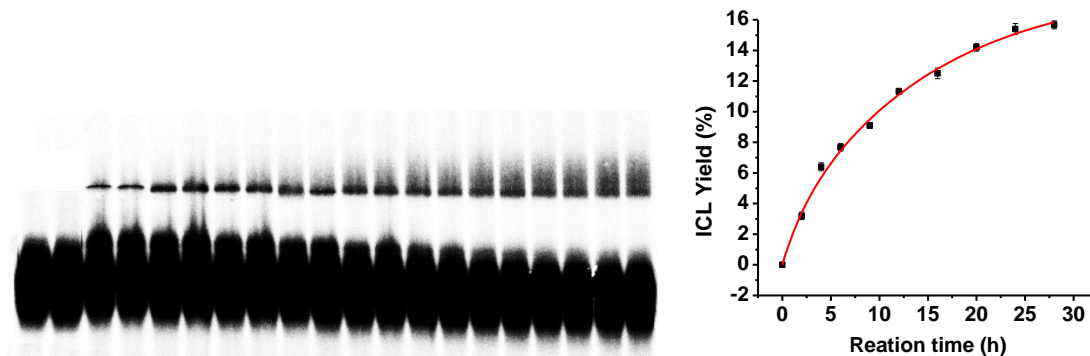
The rate of ICL formation of duplex **17** for **35f** upon photo-irradiation. **A. 35f** at time points 0, 1 h, 3 h, 6 h, 9 h, 12 h, 16 h, 20 h, 24 h, 28 h, 32 h. $[35f] = 500 \mu\text{M}$. Reaction mixtures were photo-irradiated under UV (350nm), duplicates was done at each time point.



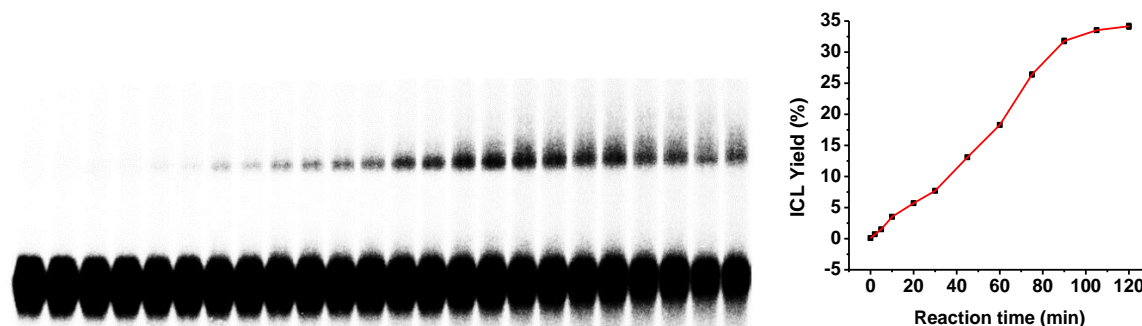
The rate of ICL formation of duplex **17** for **35g** upon photo-irradiation. **A. 35g** at time points 0, 1 h, 3 h, 6 h, 9 h, 12 h, 16 h, 20 h, 24 h, 28 h, 32 h, 36 h, 40 h, 44 h. $[35g] = 500 \mu\text{M}$. Reaction mixtures were photo-irradiated under UV (350nm), duplicates was done at each time point.



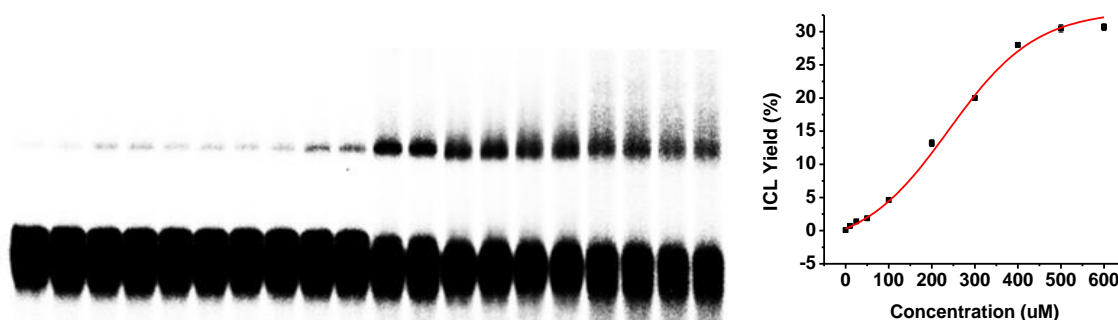
The rate of ICL formation of duplex **17** for **35h** upon photo-irradiation. **A. 35h** at time points 0, 1 h, 3 h, 6 h, 9 h, 12 h, 16 h, 20 h, 24 h, 28 h. $[35h] = 500 \mu\text{M}$. Reaction mixtures were photo-irradiated under UV (350nm), duplicates was done at each time point.



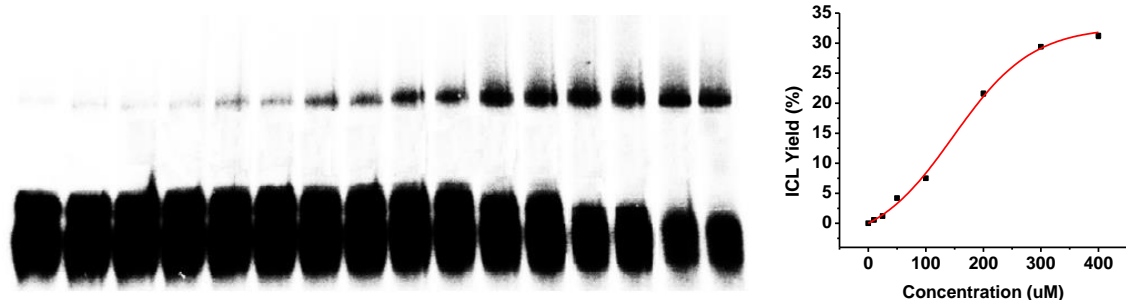
The rate of ICL formation of duplex **17** for **35i** upon photo-irradiation. **A. 35i** at time points 0, 2 h, 4 h, 6 h, 9 h, 12 h, 16 h, 20 h, 24 h, 28 h. $[35i] = 500 \mu\text{M}$. Reaction mixtures were photo-irradiated under UV (350nm), duplicates was done at each time point.



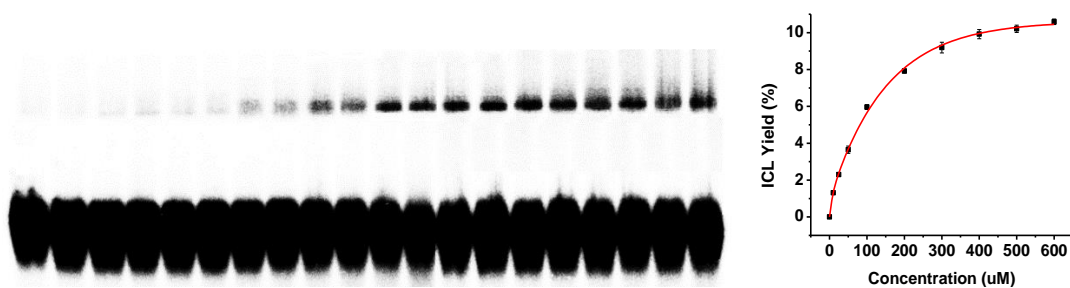
The rate of ICL formation of duplex **17** for **35j** upon photo-irradiation. **A. 35j** at time points 0, 2 min, 5 min, 10 min, 20 min, 30 min, 45 min, 60 min, 75 min, 90 min, 105 min, 120 min. $[35j] = 500 \mu\text{M}$. Reaction mixtures were photo-irradiated under UV (350nm), duplicates was done at each time point.



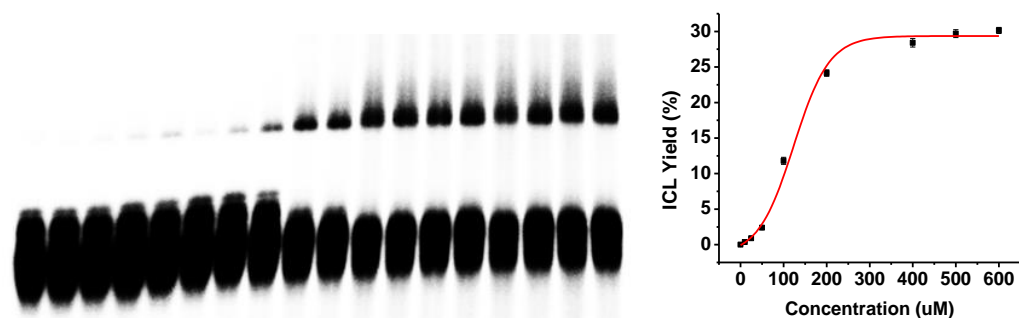
The concentration dependence of ICL formation of duplex **17** for **34a** upon photo-irradiation. Phosphor image autoradiogram of 20% denaturing PAGD analysis of **34a** under varying concentration. 0, 10 μM , 25 μM , 50 μM , 100 μM , 200 μM , 300 μM , 400 μM , 500 μM , 600 μM . Reaction mixtures were photo-irradiated under UV (350nm) for 12 h.



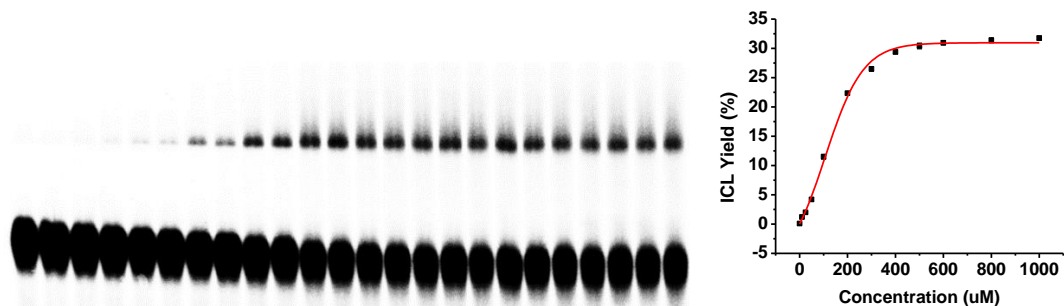
The concentration dependence of ICL formation of duplex **17** for **34b** upon photo-irradiation. Phosphor image autoradiogram of 20% denaturing PAGD analysis of **34b** under varying concentration. 0, 10 μ M, 25 μ M, 50 μ M, 100 μ M, 200 μ M, 300 μ M, 400 μ M. Reaction mixtures were photo-irradiated under UV (350nm) for 24 h.



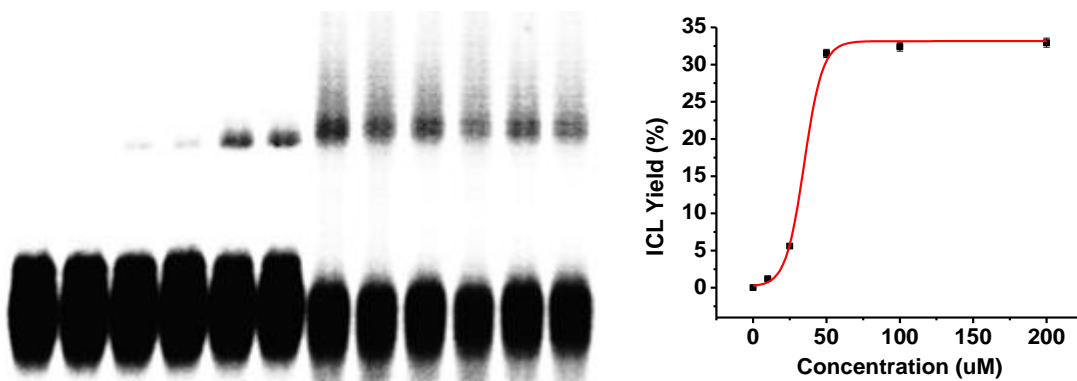
The concentration dependence of ICL formation of duplex **17** for **34c** upon photo-irradiation. Phosphor image autoradiogram of 20% denaturing PAGD analysis of **34c** under varying concentration. 0, 10, 25 μ M, 50 μ M, 100 μ M, 200 μ M, 300 μ M, 400 μ M, 500 μ M, 600 μ M. Reaction mixtures were photo-irradiated under UV (350nm) for 44 h.



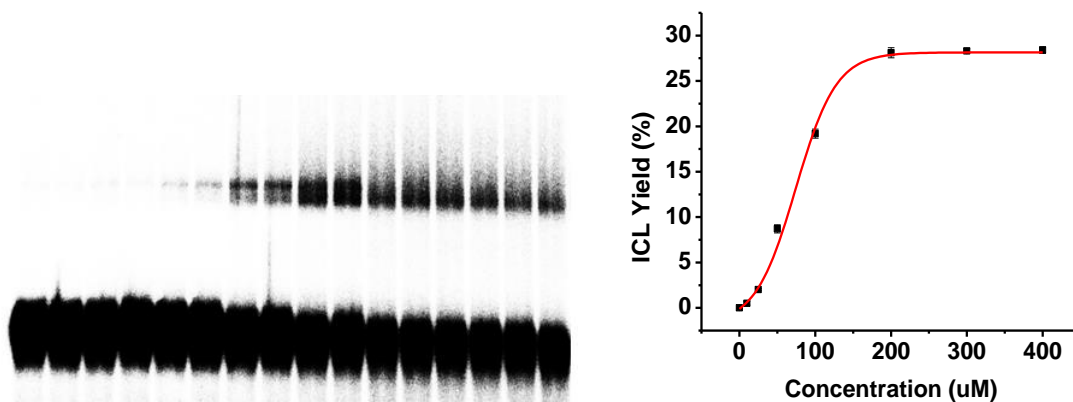
The concentration dependence of ICL formation of duplex **17** for **34d** upon photo-irradiation. Phosphor image autoradiogram of 20% denaturing PAGD analysis of **34d** under varying concentration 0, 10 μ M, 25 μ M, 50 μ M, 100 μ M, 200 μ M, 400 μ M, 500 μ M, 600 μ M. Reaction mixtures were photo-irradiated under UV (350nm) for 16 h.



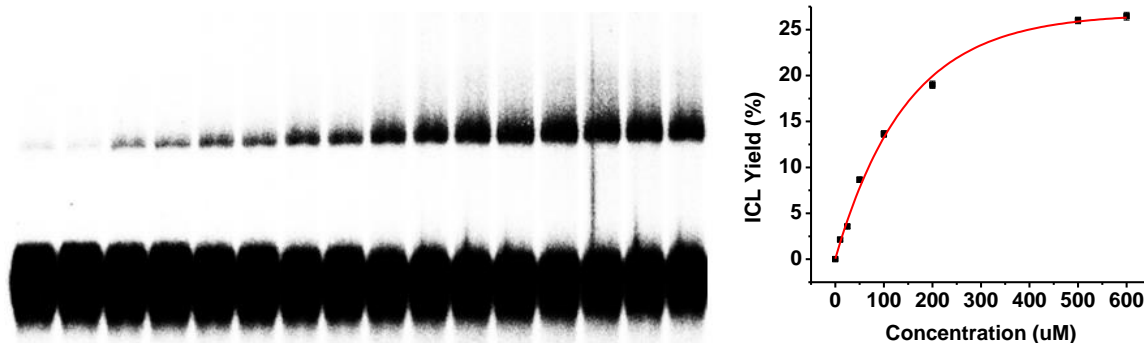
The concentration dependence of ICL formation of duplex **17** for **34e** upon photo-irradiation. Phosphor image autoradiogram of 20% denaturing PAGD analysis of **34e** under varying concentration 0, 10 μM , 25 μM , 50 μM , 100 μM , 200 μM , 300 μM , 400 μM , 500 μM , 600 μM , 800 μM , 1000 μM . Reaction mixtures were photo-irradiated under UV (350nm) for 16 h.



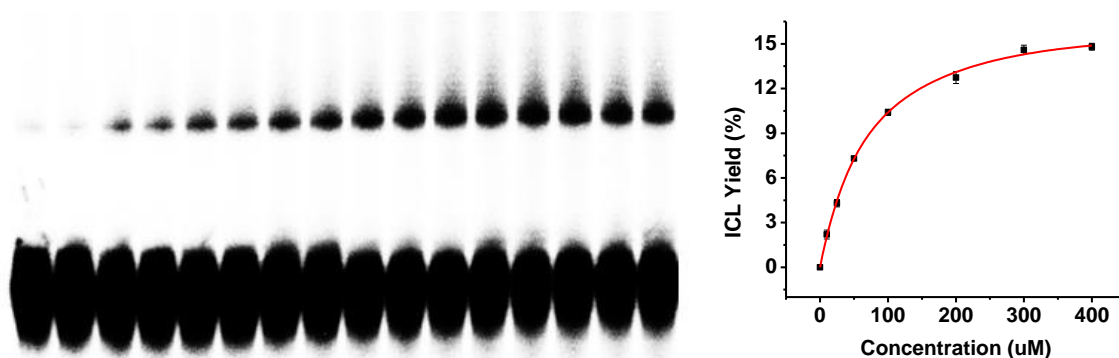
The concentration dependence of ICL formation of duplex **17** for **34f** upon photo-irradiation. Phosphor image autoradiogram of 20% denaturing PAGD analysis of **34f** under varying concentration 0, 10 μM , 25 μM , 50 μM , 100 μM , 200 μM . Reaction mixtures were photo-irradiated under UV (350nm) for 16 h.



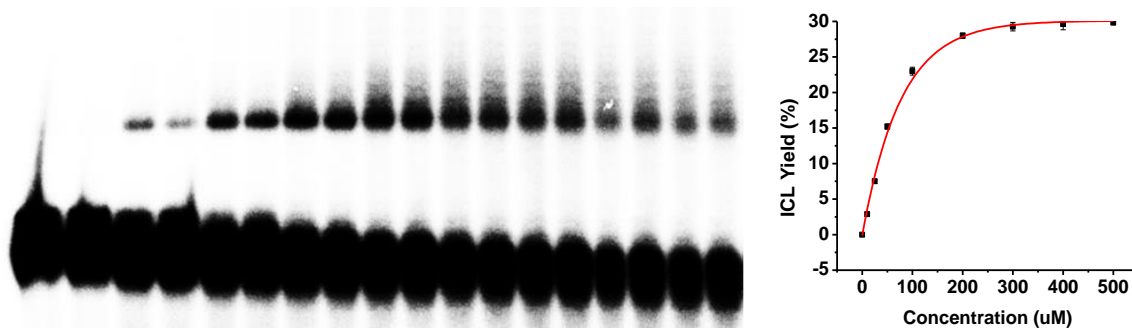
The concentration dependence of ICL formation of duplex **17** for **34g** upon photo-irradiation. Phosphor image autoradiogram of 20% denaturing PAGD analysis of **34g** under varying concentration 0, 10 μM , 25 μM , 50 μM , 100 μM , 200 μM , 300 μM , 400 μM . Reaction mixtures were photo-irradiated under UV (350nm) for 32 h.



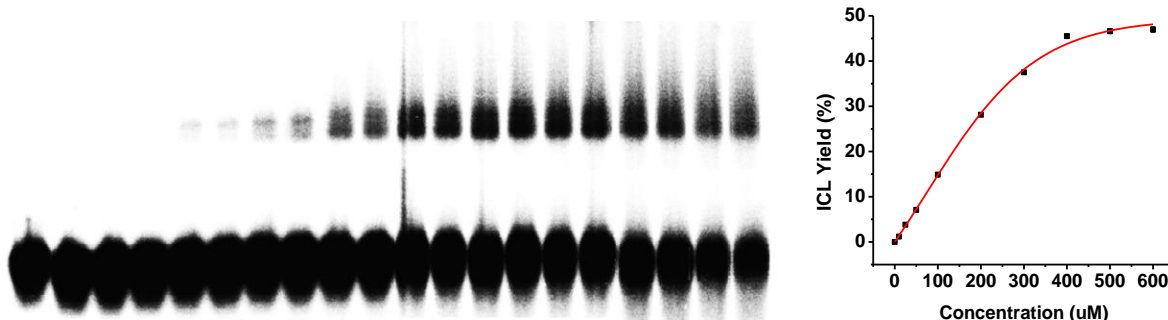
The concentration dependence of ICL formation of duplex **17** for **34h** upon photo-irradiation. Phosphor image autoradiogram of 20% denaturing PAGD analysis of **34h** under varying concentration 0, 10 μM , 25 μM , 50 μM , 100 μM , 200 μM , 500 μM , 600 μM . Reaction mixtures were photo-irradiated under UV (350nm) for 32 h.



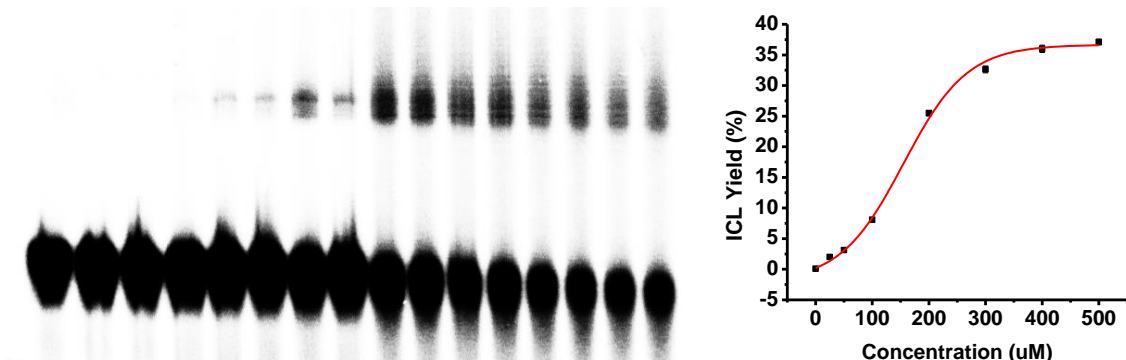
The concentration dependence of ICL formation of duplex **17** for **34i** upon photo-irradiation. Phosphor image autoradiogram of 20% denaturing PAGD analysis of **34i** under varying concentration 0, 10 μM , 25 μM , 50 μM , 100 μM , 200 μM , 300 μM , 400 μM . Reaction mixtures were photo-irradiated under UV (350nm) for 36 h.



The concentration dependence of ICL formation of duplex **17** for **34j** upon photo-irradiation. Phosphor image autoradiogram of 20% denaturing PAGD analysis of **34j** under varying concentration 0, 10 μM , 25 μM , 50 μM , 100 μM , 200 μM , 300 μM , 400 μM , 500 μM . Reaction mixtures were photo-irradiated under UV (350nm) for 10 h.

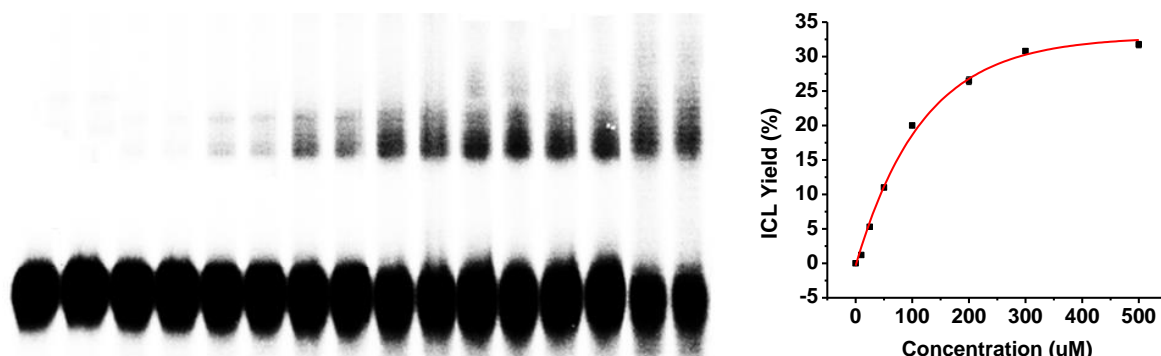


The concentration dependence of ICL formation of duplex **17** for **35a** upon photo-irradiation. Phosphor image autoradiogram of 20% denaturing PAGD analysis of **35a** under varying concentration 0, 10 μM , 25 μM , 50 μM , 100 μM , 200 μM , 300 μM , 400 μM , 500 μM , 600 μM . Reaction mixtures were photo-irradiated under UV (350nm) for 1.5 h.

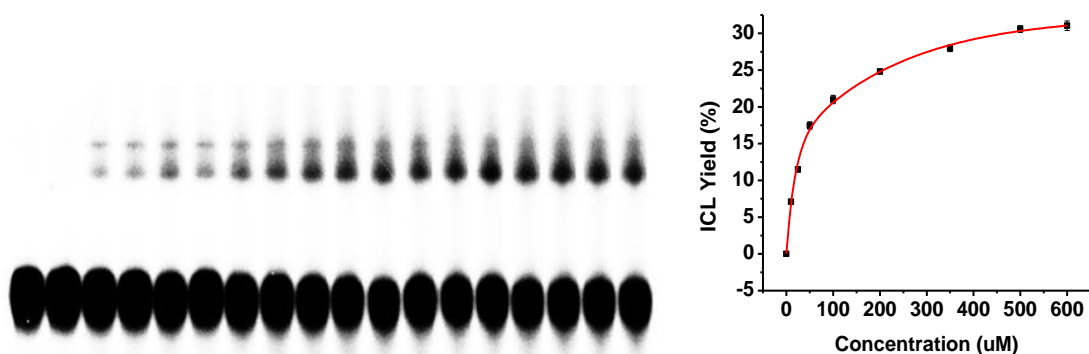


The concentration dependence of ICL formation of duplex **17** for **35b** upon photo-irradiation. Phosphor image autoradiogram of 20% denaturing PAGD analysis of **35b** under varying

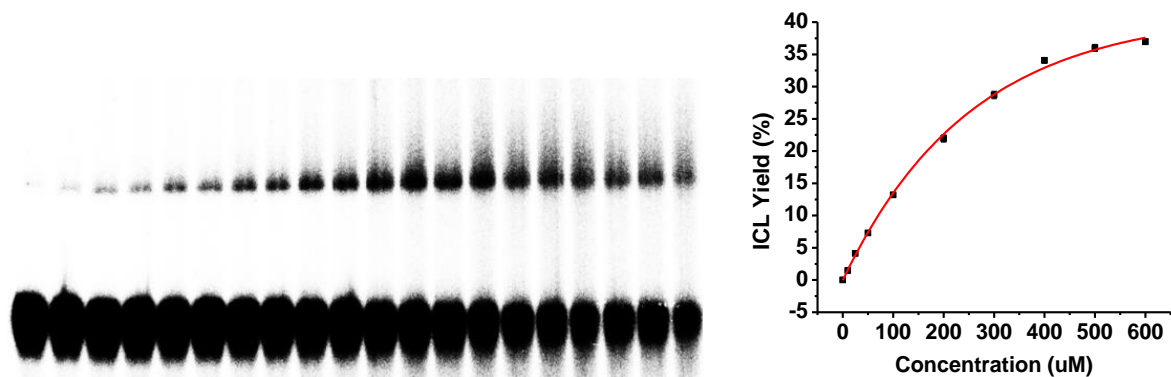
concentration 0, 25 μM , 50 μM , 100 μM , 200 μM , 300 μM , 400 μM , 500 μM . Reaction mixtures were photo-irradiated under UV (350nm) for 2.5 h.



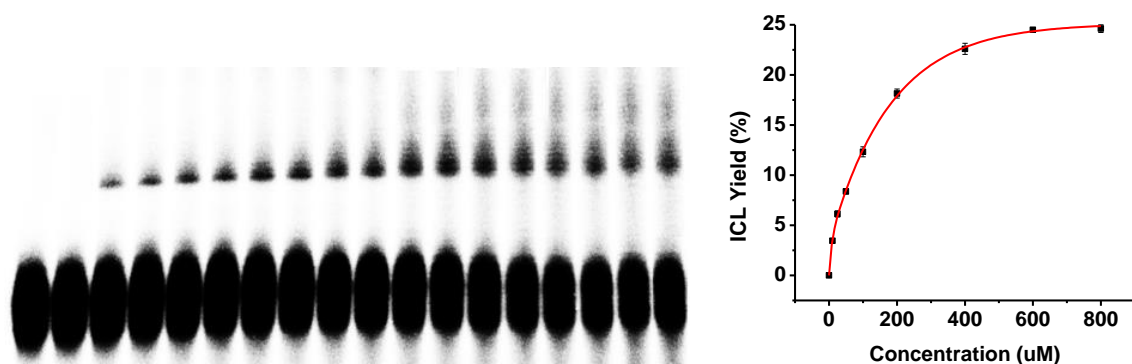
The concentration dependence of ICL formation of duplex **17** for **35c** upon photo-irradiation. Phosphor image autoradiogram of 20% denaturing PAGD analysis of **35c** under varying concentration 0, 10 μM , 25 μM , 50 μM , 100 μM , 200 μM , 300 μM , 500 μM . Reaction mixtures were photo-irradiated under UV (350nm) for 3 h.



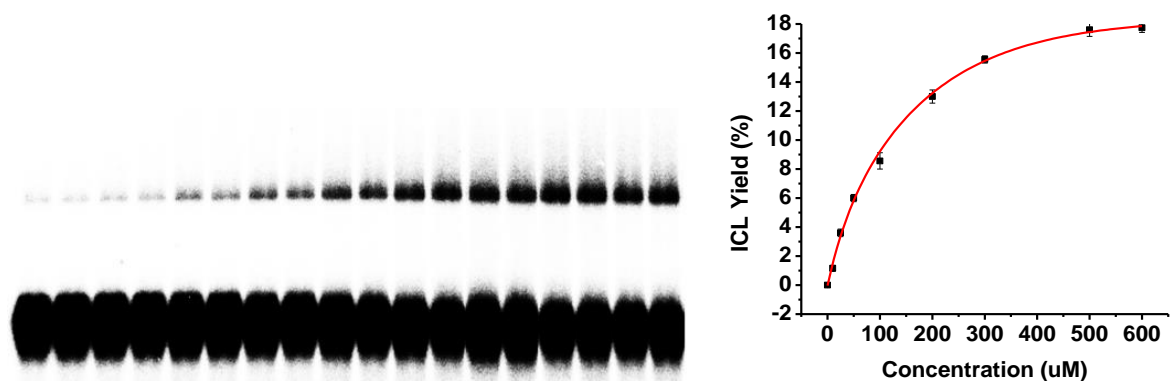
The concentration dependence of ICL formation of duplex **17** for **35d** upon photo-irradiation. Phosphor image autoradiogram of 20% denaturing PAGD analysis of **35d** under varying concentration 0, 10 μM , 25 μM , 50 μM , 100 μM , 200 μM , 350 μM , 500 μM , 600 μM . Reaction mixtures were photo-irradiated under UV (350nm) for 10 h.



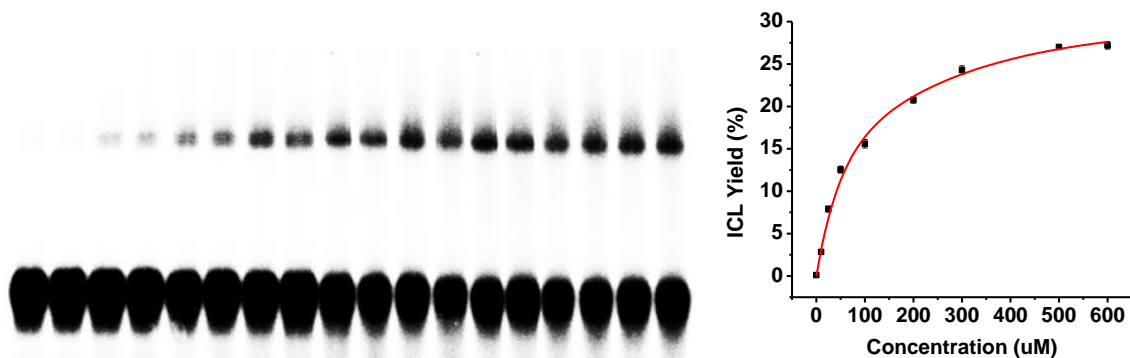
The concentration dependence of ICL formation of duplex **17** for **35e** upon photo-irradiation. Phosphor image autoradiogram of 20% denaturing PAGD analysis of **35e** under varying concentration 0, 10 μM , 25 μM , 50 μM , 100 μM , 200 μM , 300 μM , 400 μM , 500 μM , 600 μM . Reaction mixtures were photo-irradiated under UV (350nm) for 20 h.



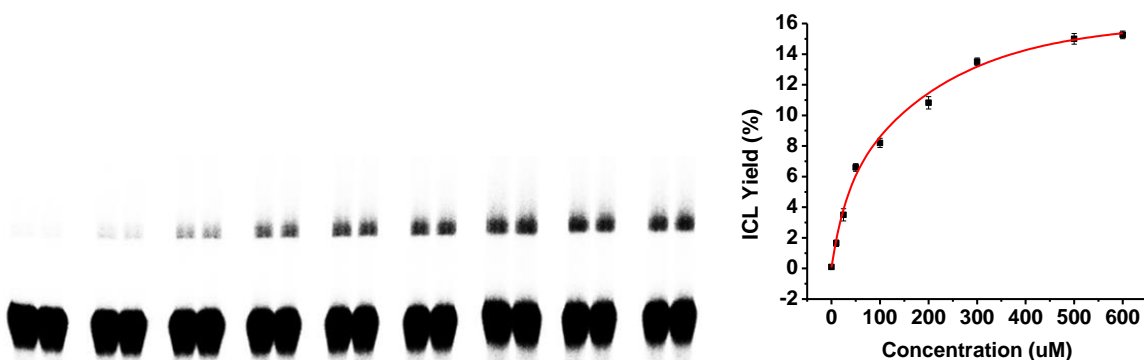
The concentration dependence of ICL formation of duplex **17** for **35f** upon photo-irradiation. Phosphor image autoradiogram of 20% denaturing PAGD analysis of **35f** under varying concentration 0, 10 μM , 25 μM , 50 μM , 100 μM , 200 μM , 400 μM , 600 μM , 800 μM . Reaction mixtures were photo-irradiated under UV (350nm) for 28 h.



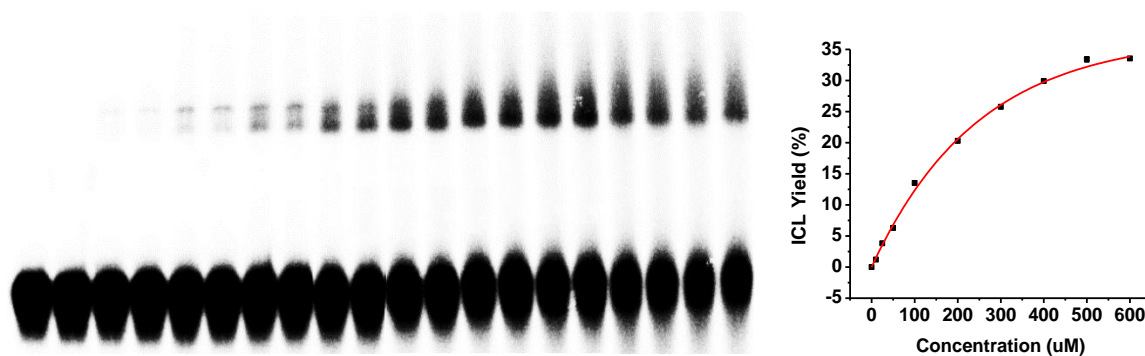
The concentration dependence of ICL formation of duplex **17** for **35g** upon photo-irradiation. Phosphor image autoradiogram of 20% denaturing PAGD analysis of **35g** under varying concentration 0, 10 μM , 25 μM , 50 μM , 100 μM , 200 μM , 300 μM , 500 μM , 600 μM . Reaction mixtures were photo-irradiated under UV (350nm) for 36 h.



The concentration dependence of ICL formation of duplex **17** for **35h** upon photo-irradiation. Phosphor image autoradiogram of 20% denaturing PAGD analysis of **35h** under varying concentration 0, 10 μM , 25 μM , 50 μM , 100 μM , 200 μM , 300 μM , 500 μM , 600 μM . Reaction mixtures were photo-irradiated under UV (350nm) for 24 h.



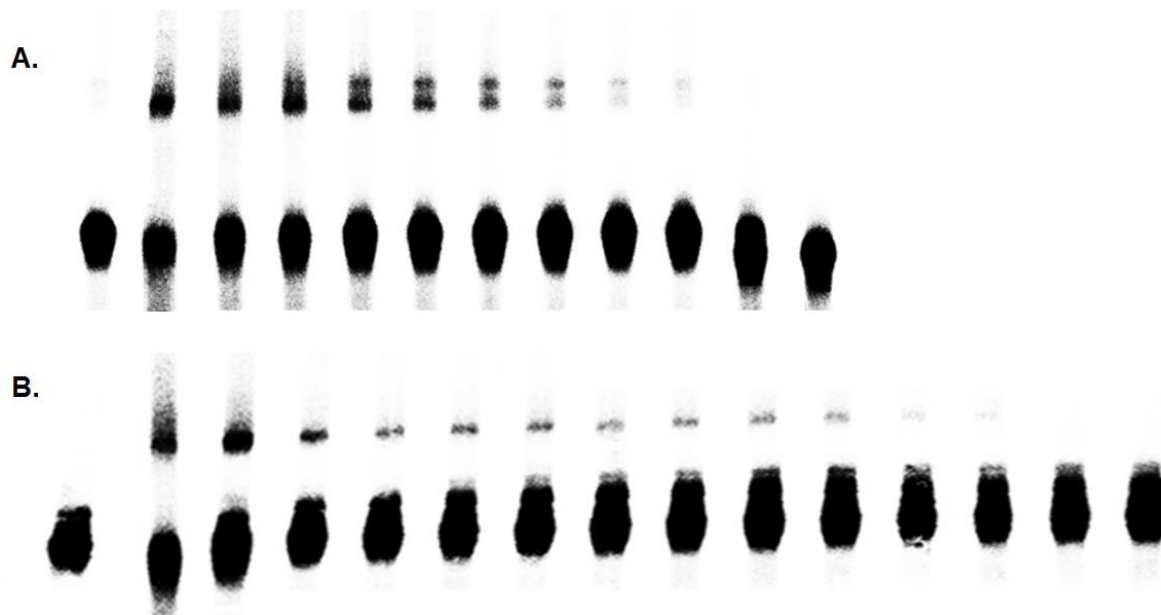
The concentration dependence of ICL formation of duplex **17** for **35i** upon photo-irradiation. Phosphor image autoradiogram of 20% denaturing PAGD analysis of **35i** under varying concentration 0, 10 μM , 25 μM , 50 μM , 100 μM , 200 μM , 300 μM , 500 μM , 600 μM . Reaction mixtures were photo-irradiated under UV (350nm) for 24 h.



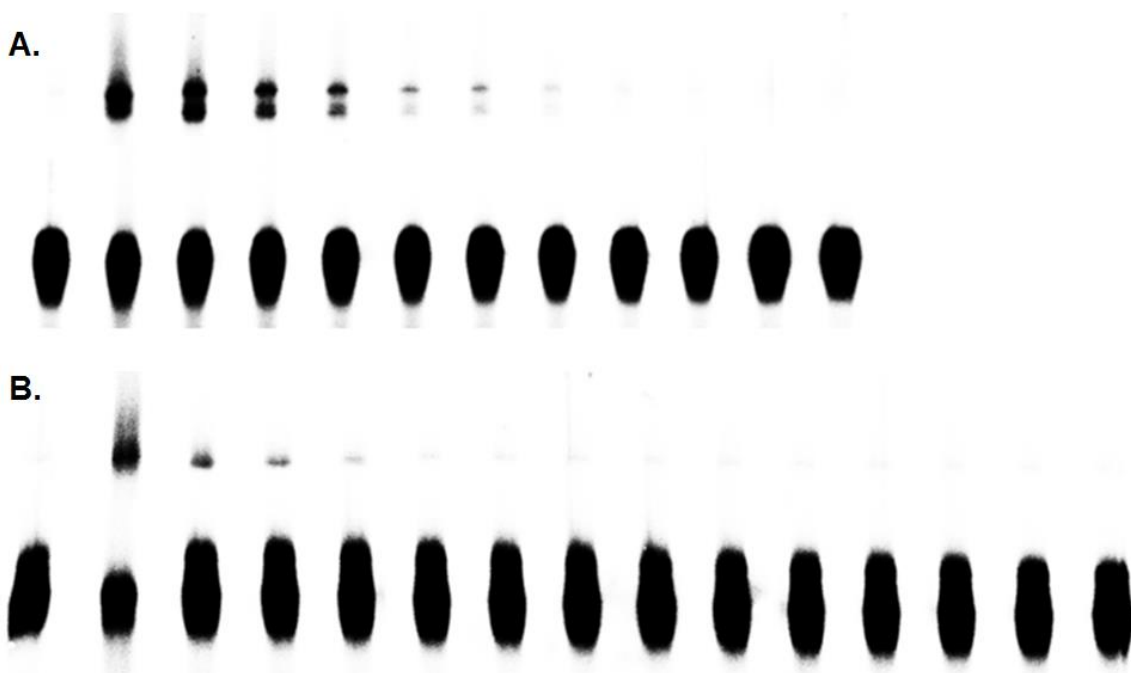
The concentration dependence of ICL formation of duplex **17** for **35j** upon photo-irradiation. Phosphor image autoradiogram of 20% denaturing PAGD analysis of **35j** under varying concentration 0, 10 μM , 25 μM , 50 μM , 100 μM , 200 μM , 300 μM , 400 μM , 500 μM , 600 μM . Reaction mixtures were photo-irradiated under UV (350nm) for 1.5 h.

General condition for cation and radical trapping:

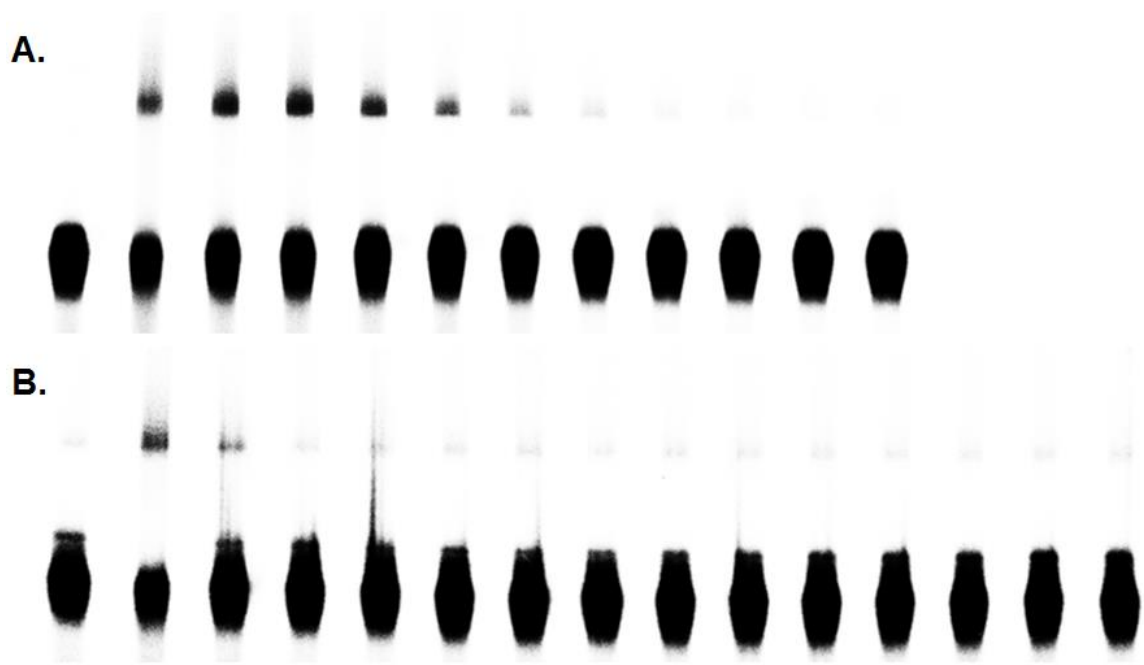
- A. MeONH₂ trapping: lane **1**: No drug with UV. Lane **2-12** with drug with UV. MeONH₂ concentration: lane **2**: 0, lane **3**: 100 μM ., lane **4**: 200 μM , lane **5**: 500 μM , lane **6**: 1 mM, lane **7**: 2 mM, lane **8**: 5 mM, lane **9**: 10 mM, lane **10**: 20 mM, lane **11**: 50 mM, lane **12**: 100 mM.
- B. TEMPO trapping: lane **1**: No drug with UV. Lane **2-15** with drug with UV. Tempo concentration: lane **2**: 0, lane **3**: 10 μM ., lane **4**: 25 μM , lane **5**: 50 μM , lane **6**: 100 μM , lane **7**: 250 μM , lane **8**: 500 μM , lane **9**: 1 mM, lane **10**: 2.5 mM, lane **11**: 5 mM, lane **12**: 10 mM, lane **13**: 25 mM, lane **14**: 50 mM, lane **15**: 100 mM.



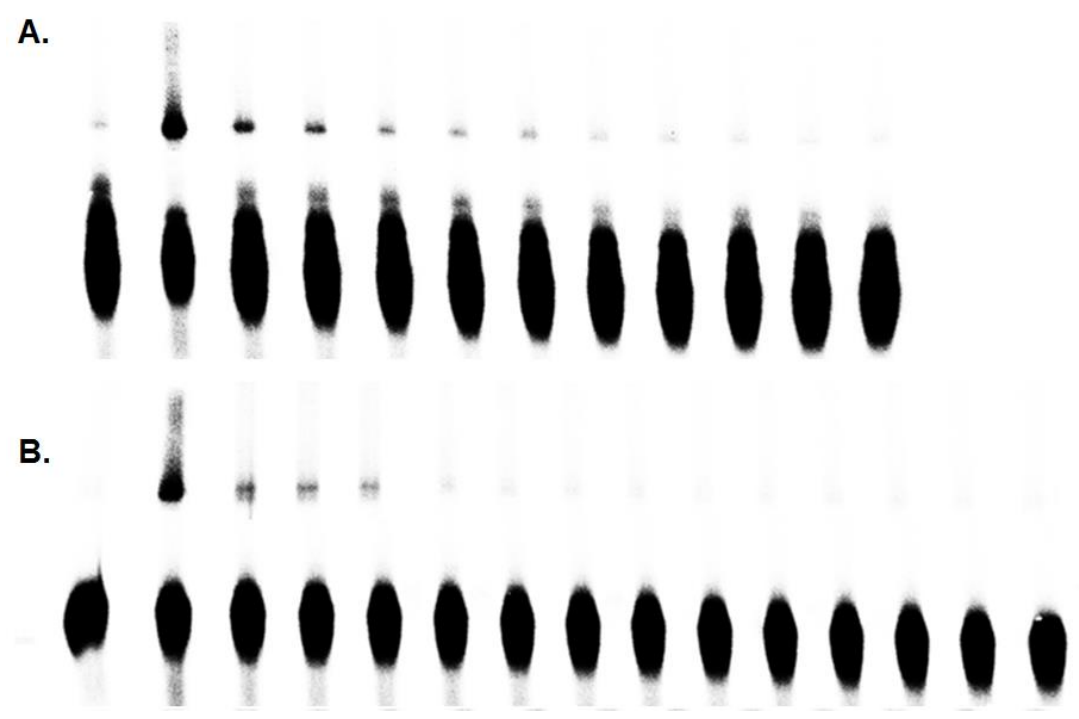
Carbocation and radical trapping with ICL formation of duplex **17** for **26a** at optimized conditions: 500 μM , 22 h.



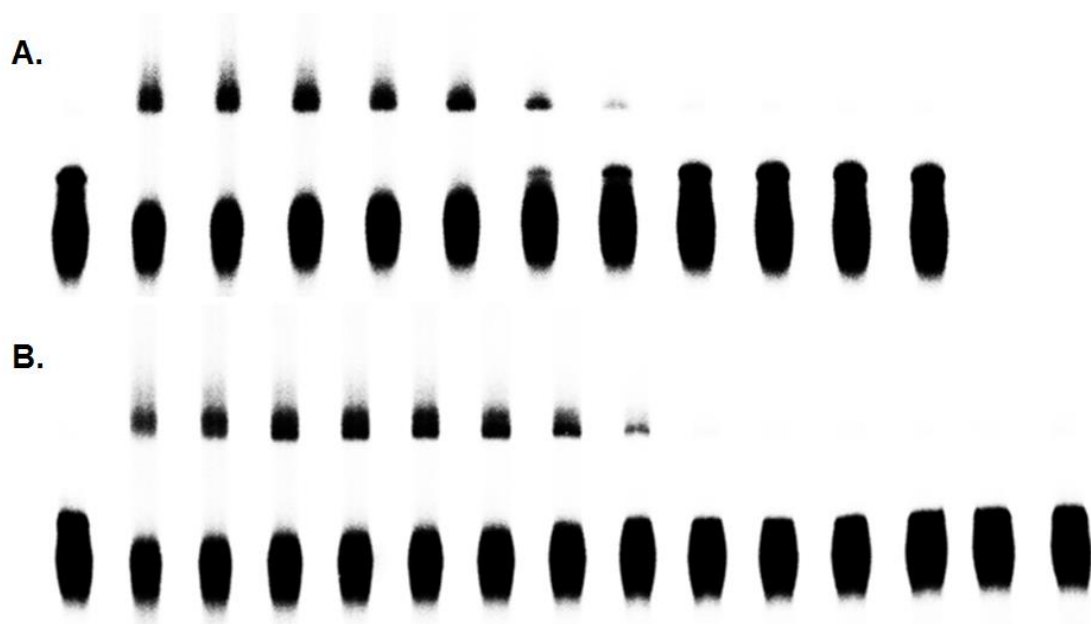
Carbocation and radical trapping with ICL formation of duplex **17** for **26b** at optimized conditions: 600 μM , 6 h.



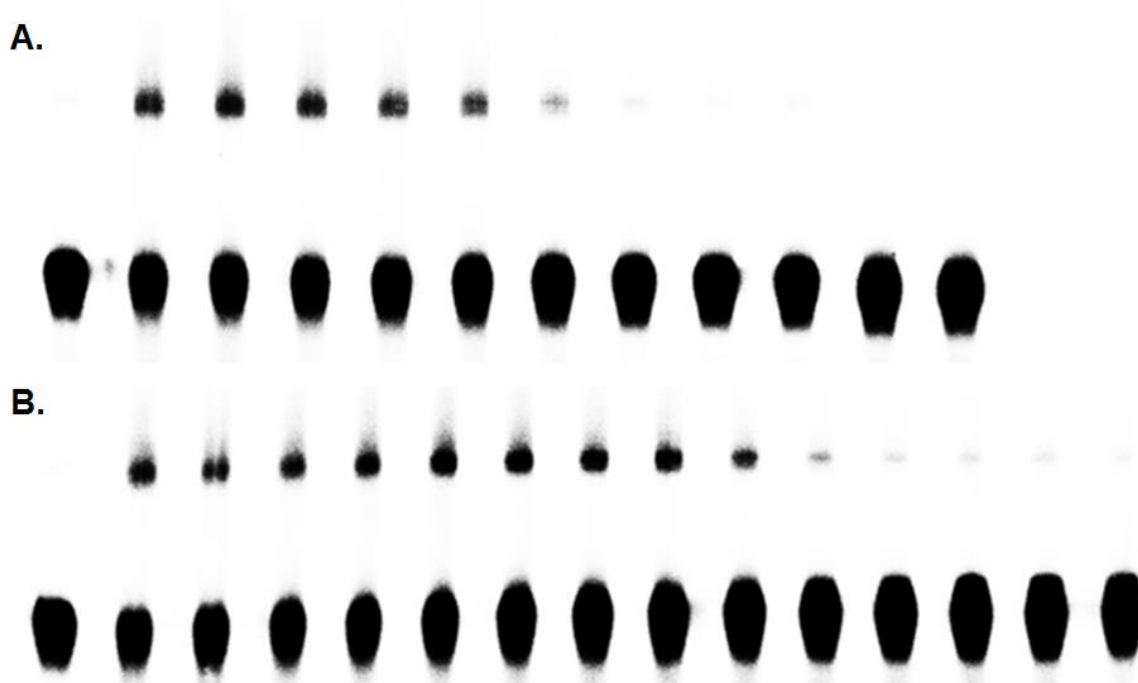
Carbocation and radical trapping with ICL formation of duplex **17** for **26c** at optimized conditions: 2 mM, 36 h.



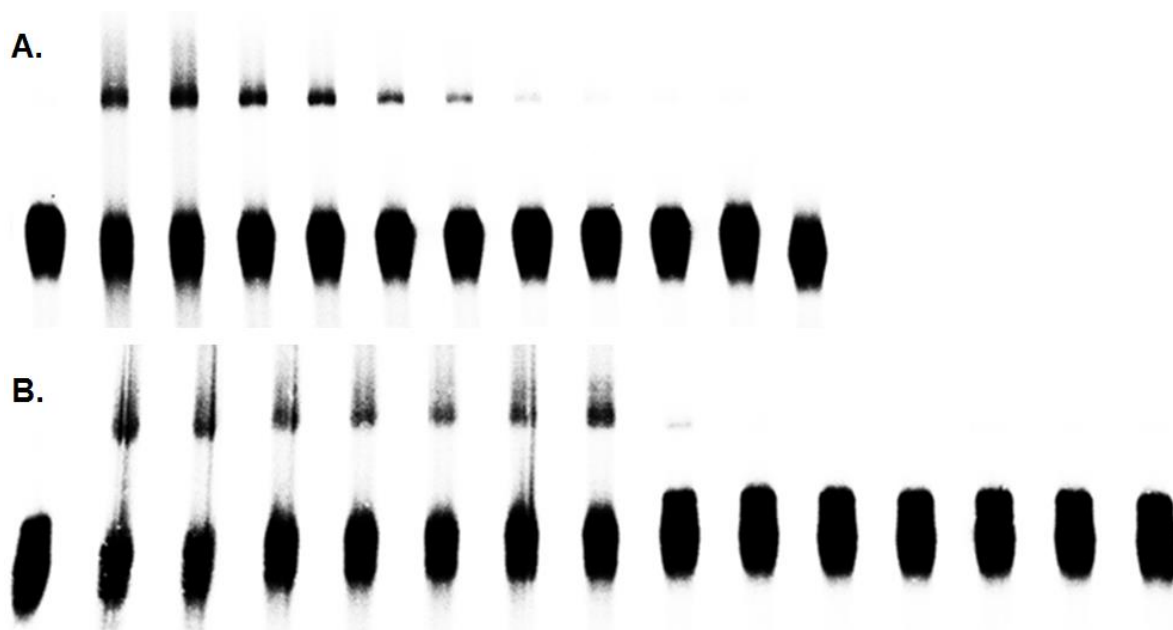
Carbocation and radical trapping with ICL formation of duplex **17** for **26d** at optimized conditions: 500 μ M, 12 h.



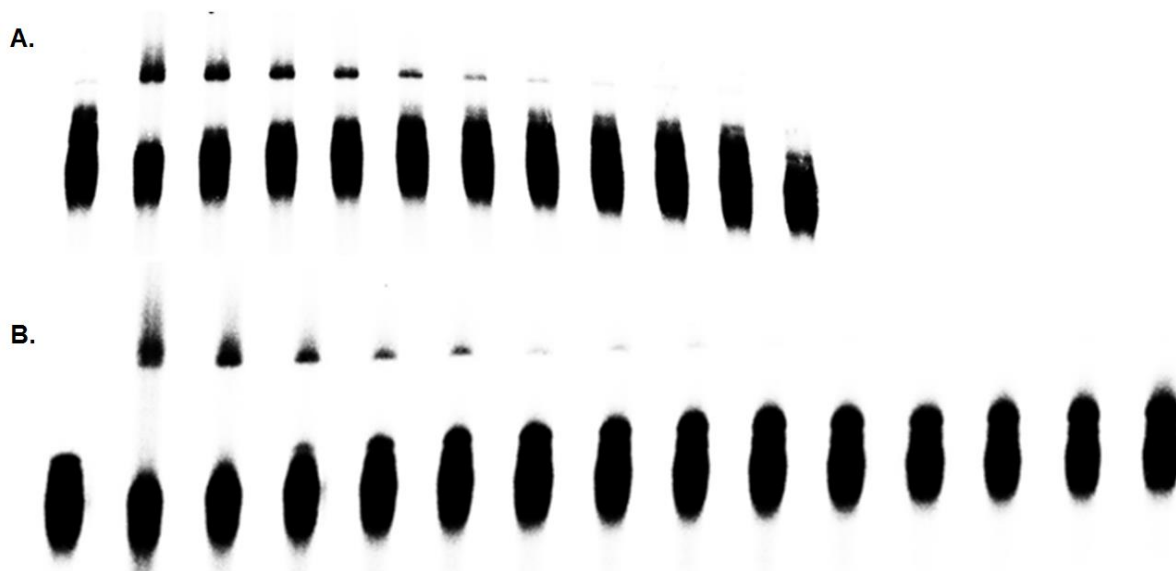
Carbocation and radical trapping with ICL formation of duplex **17** for **26e** at optimized conditions: 400 μ M, 6 h.



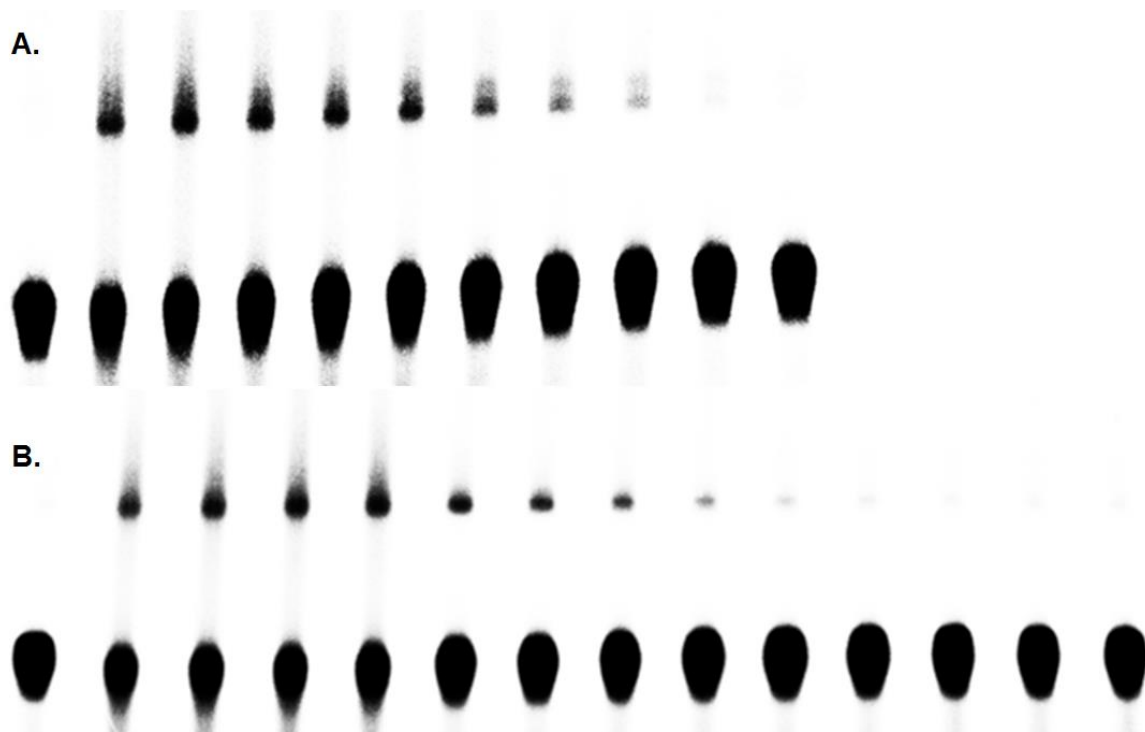
Carbocation and radical trapping with ICL formation of duplex **17** for **26f** at optimized conditions: 400 μ M, 12 h.



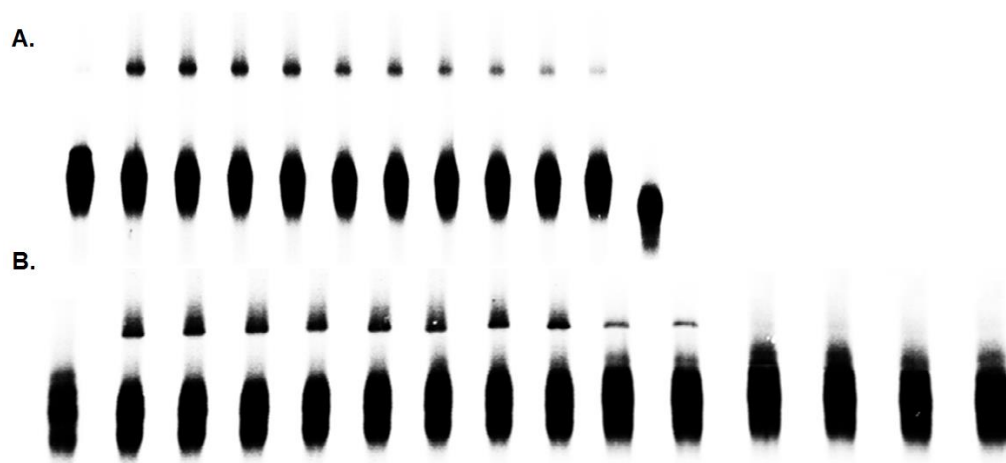
Carbocation and radical trapping with ICL formation of duplex **17** for **26g** at optimized conditions: 600 μ M, 2 h.



Carbocation and radical trapping with ICL formation of duplex **17** for **26h** at optimized conditions: 600 μ M, 2 h.



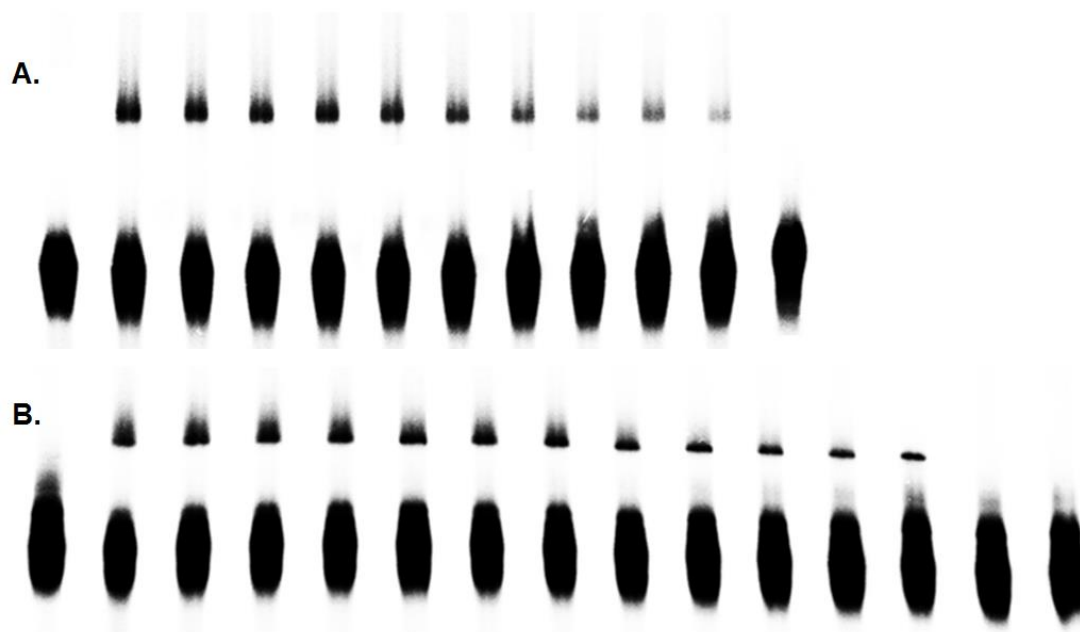
Carbocation and radical trapping with ICL formation of duplex **17** for **26i** at optimized conditions: 200 μM , 5 h.



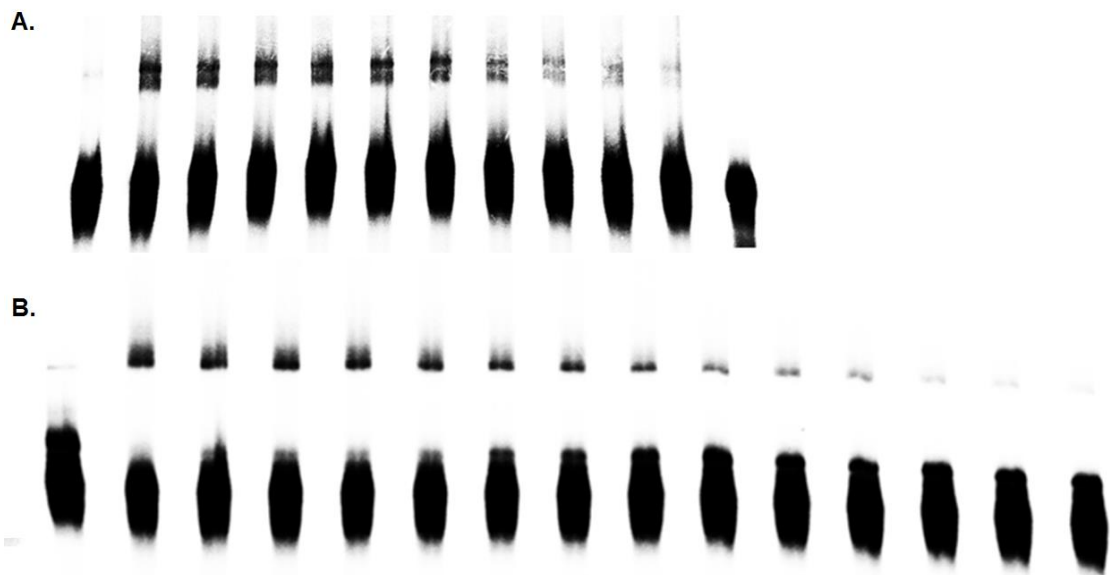
Carbocation and radical trapping with ICL formation of duplex **17** for **27a** at optimized conditions: 400 μM , 44 h.



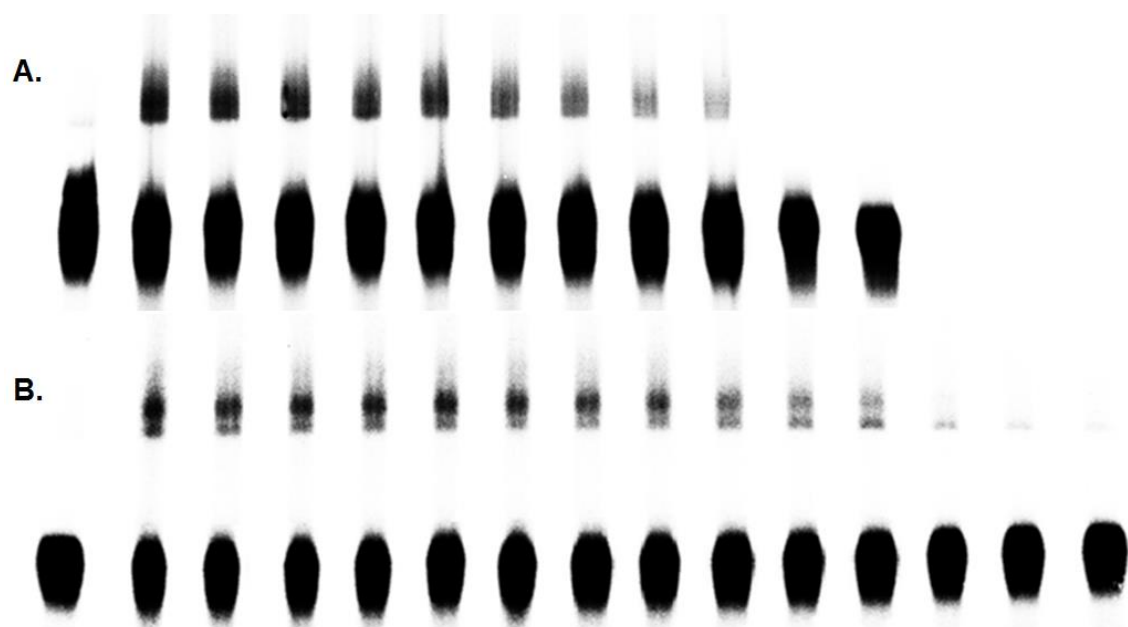
Carbocation and radical trapping with ICL formation of duplex **17** for **27b** at optimized conditions: 400 μM , 40 h.



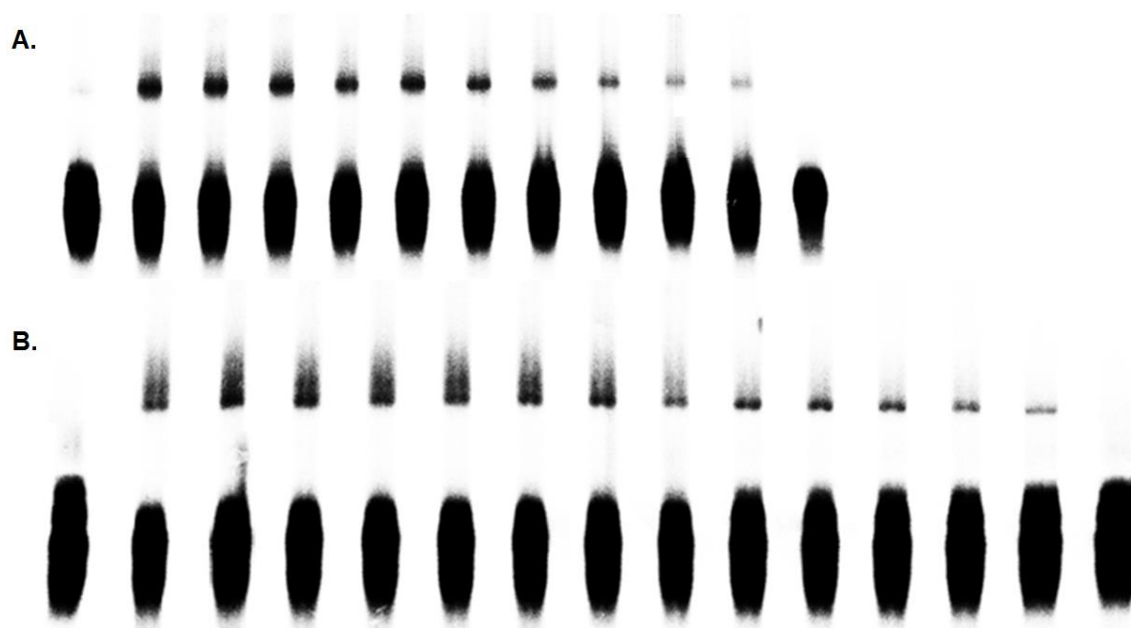
Carbocation and radical trapping with ICL formation of duplex **17** for **27c** at optimized conditions: 400 μM , 40 h.



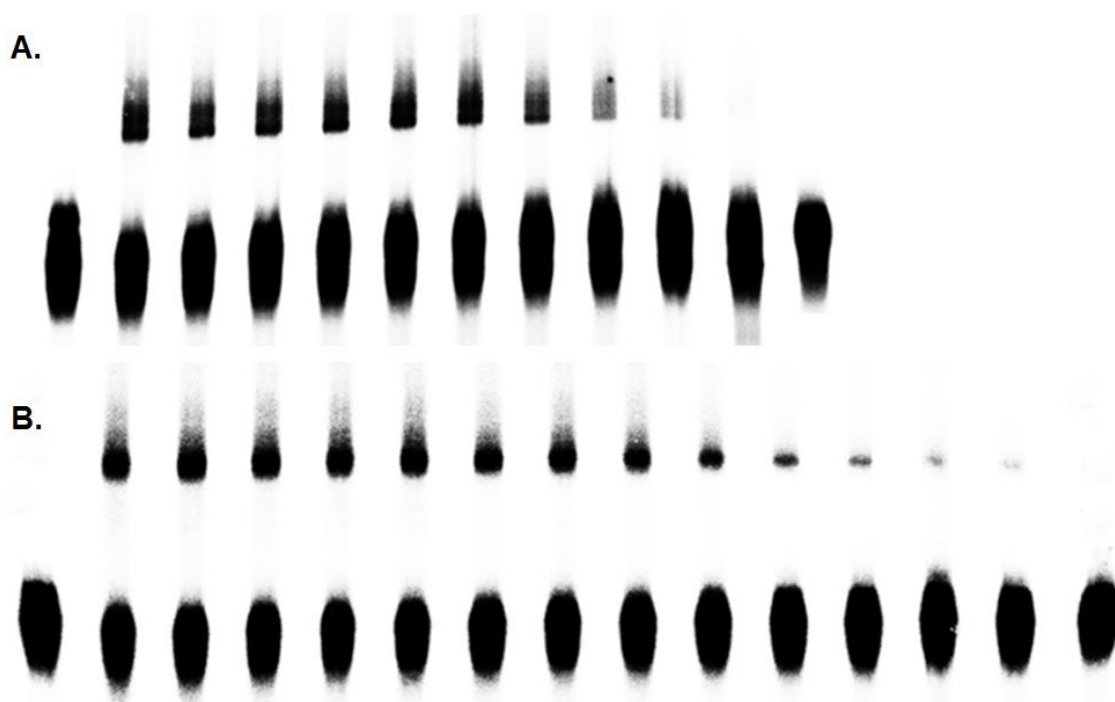
Carbocation and radical trapping with ICL formation of duplex **17** for **27d** at optimized conditions: 800 μ M, 40 h.



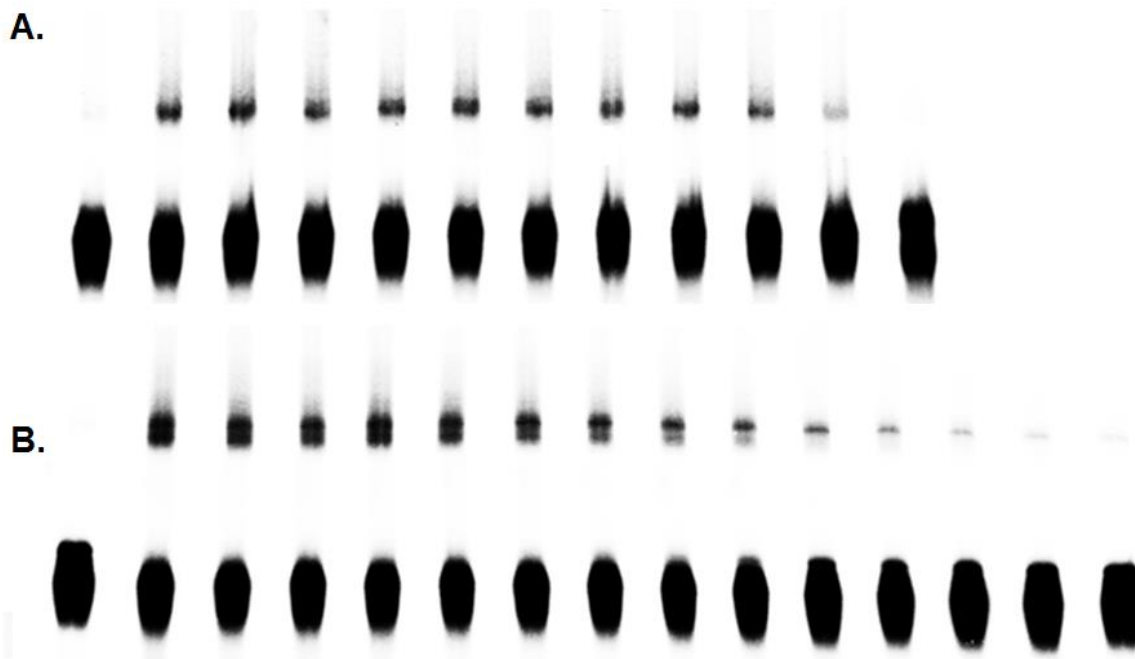
Carbocation and radical trapping with ICL formation of duplex **17** for **27e** at optimized conditions: 1 mM, 24 h.



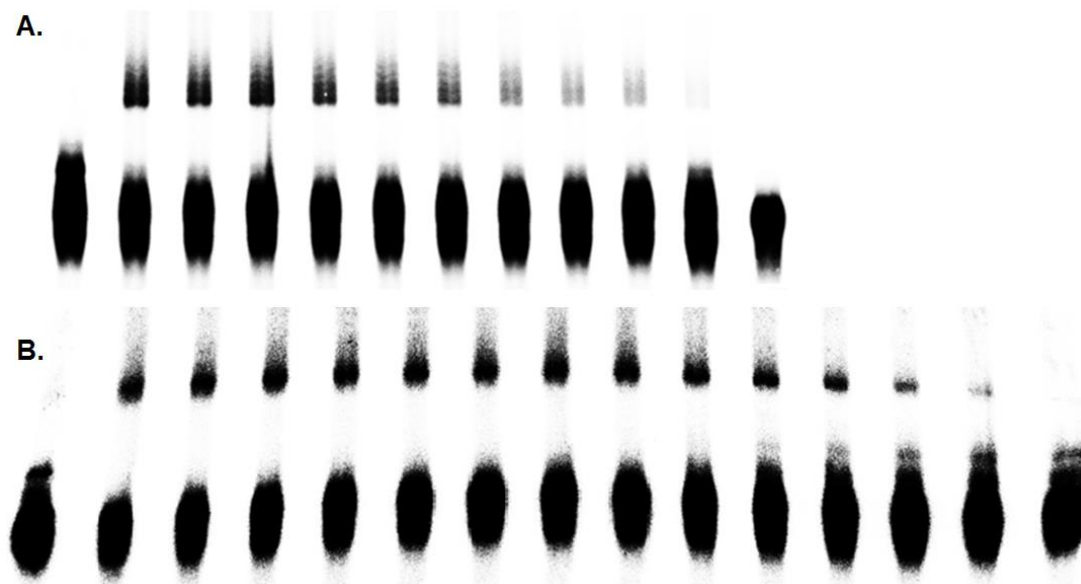
Carbocation and radical trapping with ICL formation of duplex **17** for **27f** at optimized conditions: 600 μ M, 32 h.



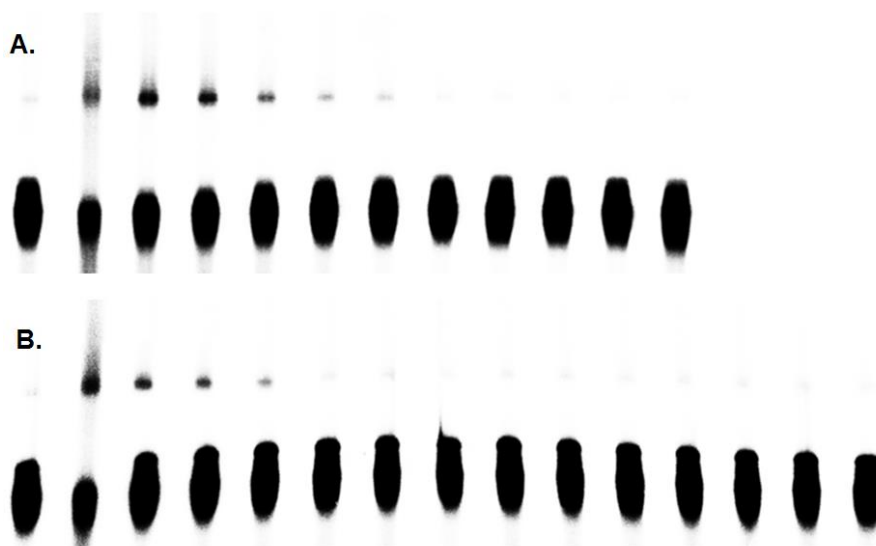
Carbocation and radical trapping with ICL formation of duplex **17** for **27g** at optimized conditions: 600 μ M, 24 h.



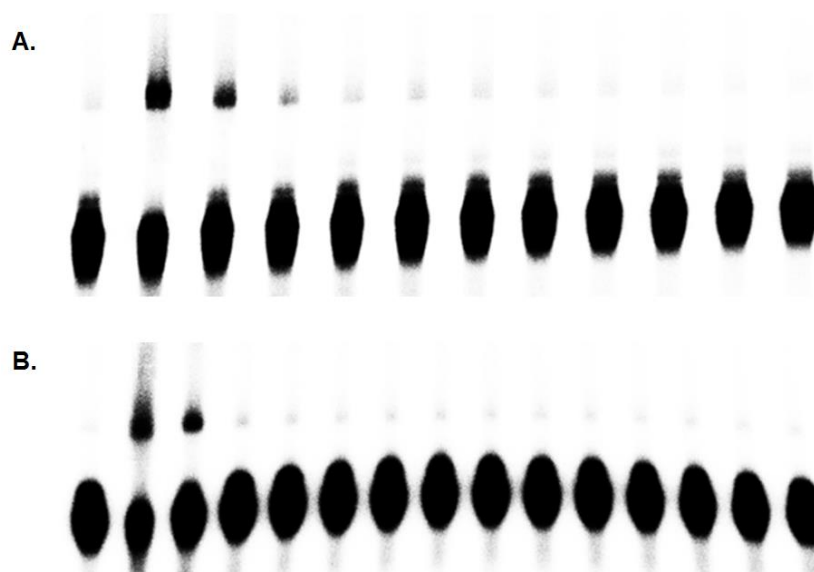
Carbocation and radical trapping with ICL formation of duplex **17** for **27h** at optimized conditions: 300 μ M, 36 h.



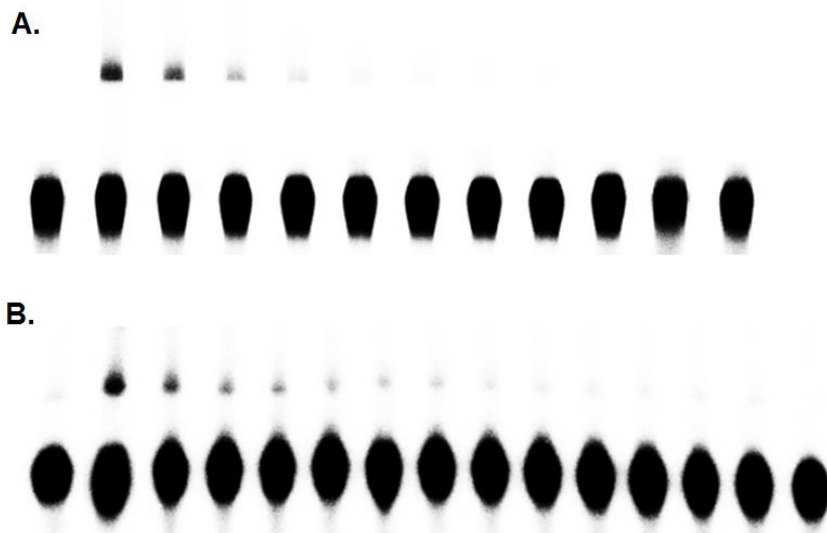
Carbocation and radical trapping with ICL formation of duplex **17** for **27i** at optimized conditions: 400 μ M, 28 h.



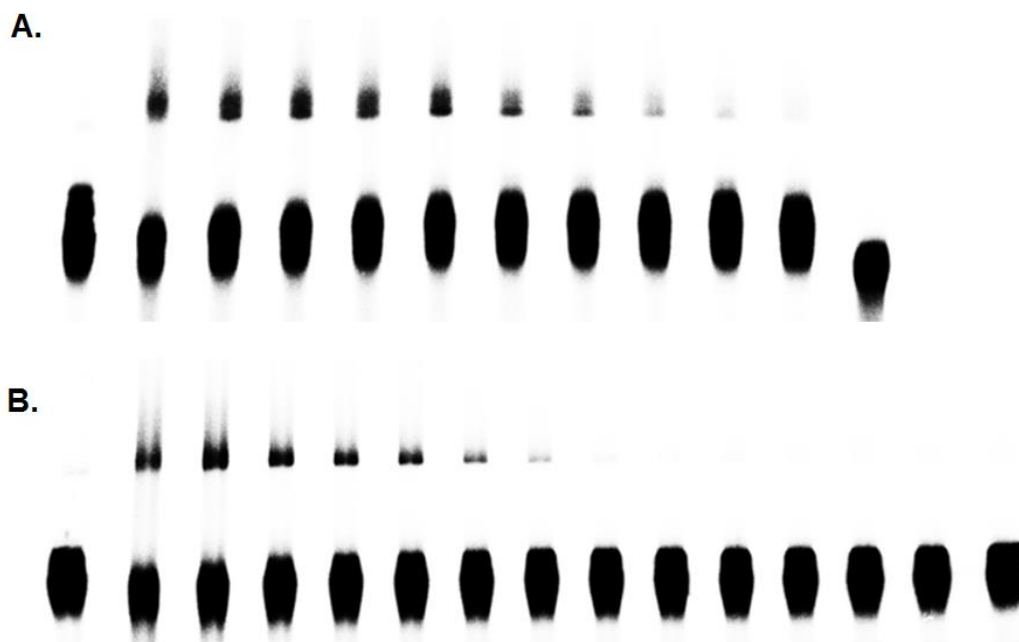
Carbocation and radical trapping with ICL formation of duplex **17** for **34a** at optimized conditions: 500 μ M, 12 h.



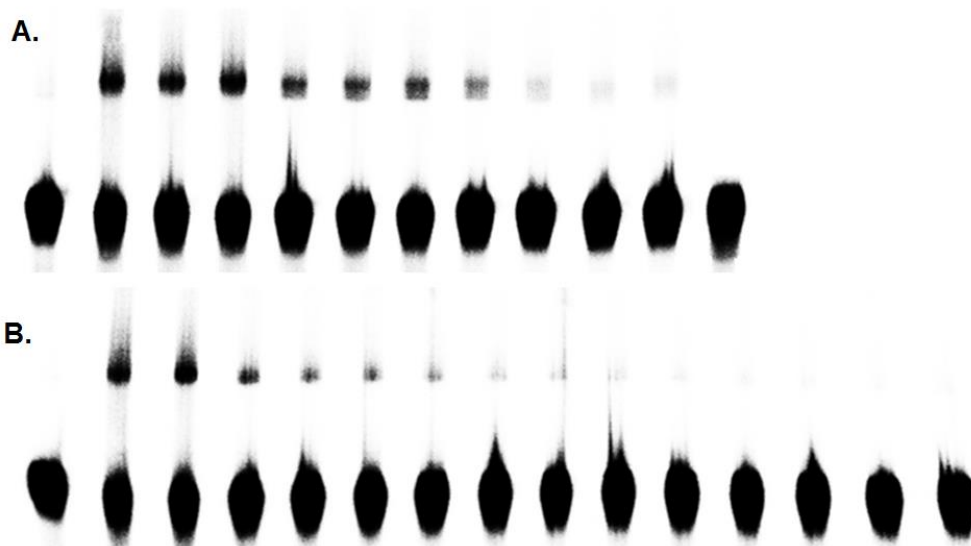
Carbocation and radical trapping with ICL formation of duplex **17** for **34b** at optimized conditions: 400 μ M, 24 h.



Carbocation and radical trapping with ICL formation of duplex **17** for **34c** at optimized conditions: 600 μ M, 44h.



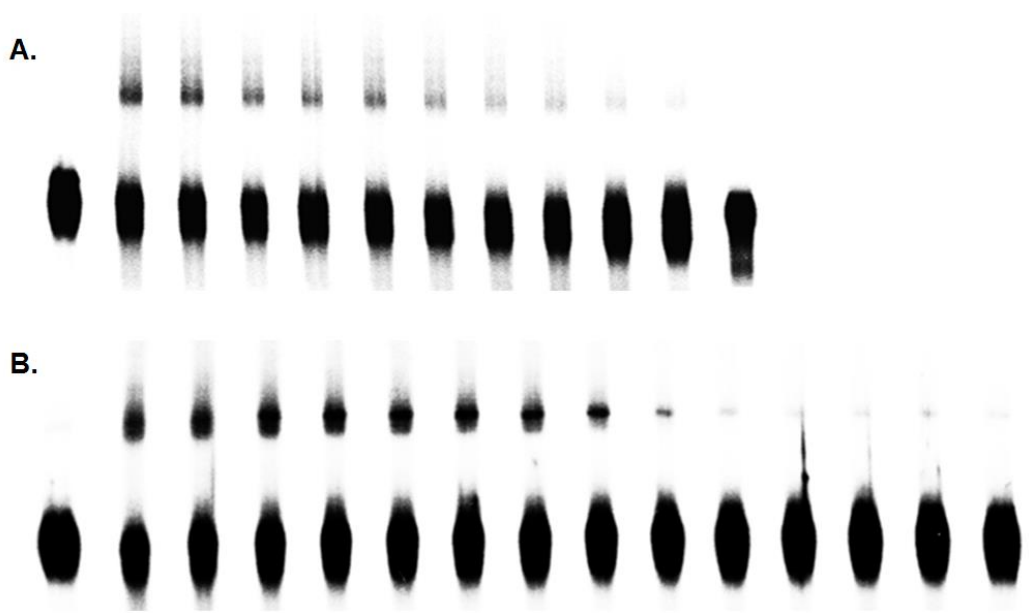
Carbocation and radical trapping with ICL formation of duplex **17** for **34d** at optimized conditions: 500 μ M, 16h.



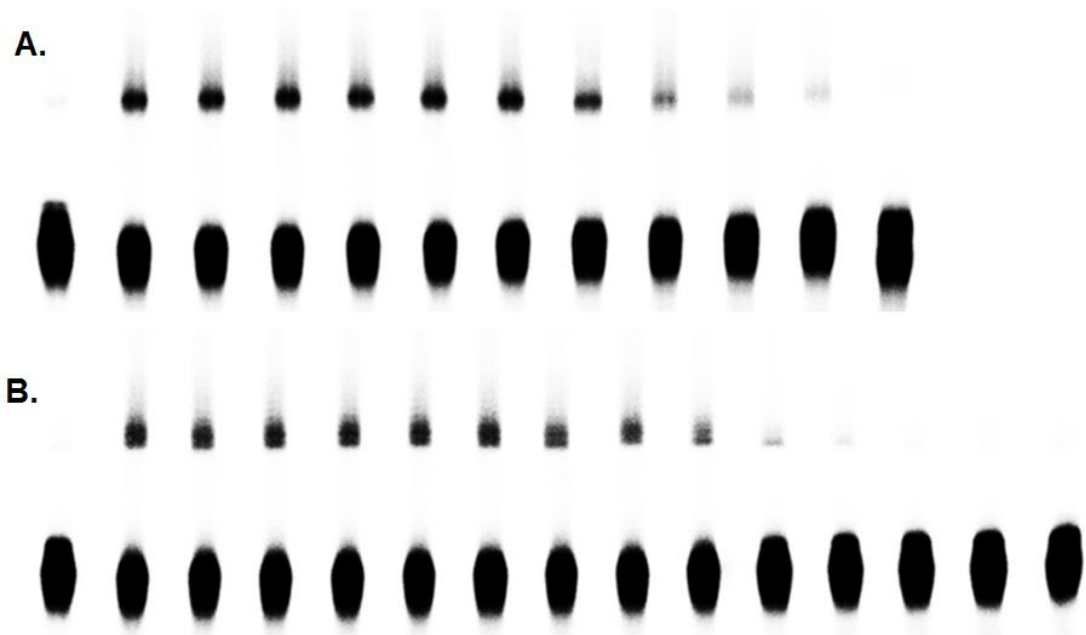
Carbocation and radical trapping with ICL formation of duplex **17** for **34e** at optimized conditions: 500 μ M, 16h.



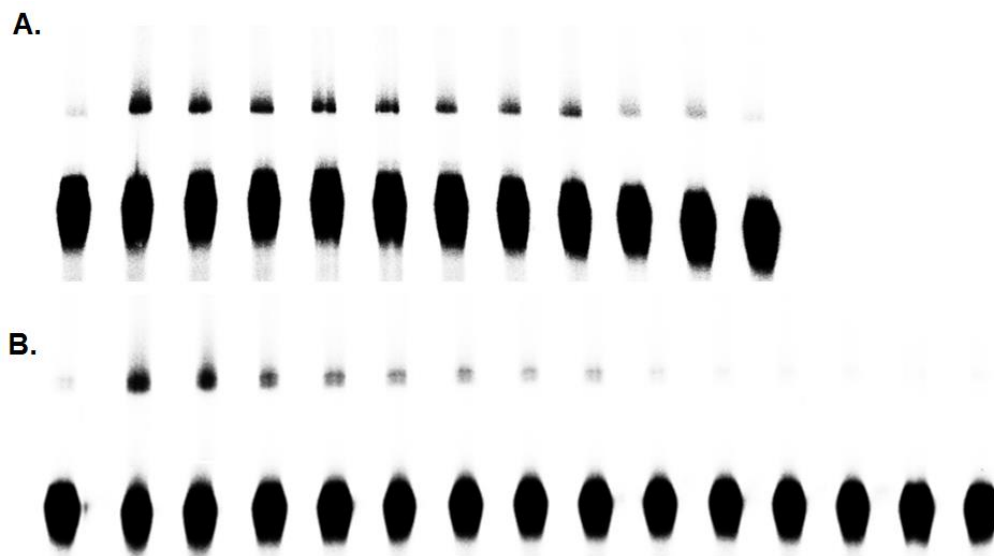
Carbocation and radical trapping with ICL formation of duplex **17** for **34f** at optimized conditions: 50 μ M, 16h.



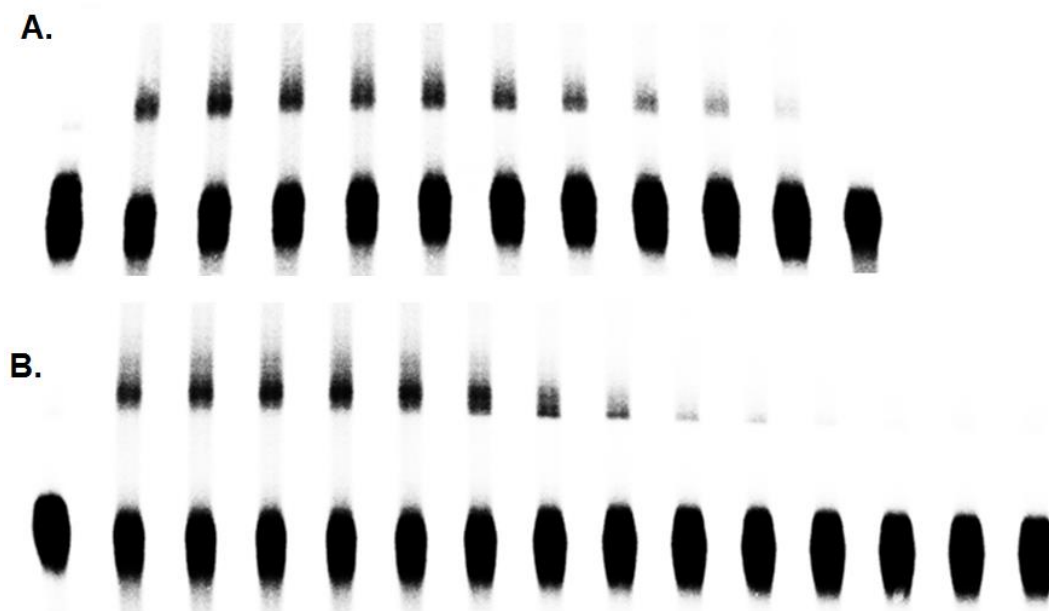
Carbocation and radical trapping with ICL formation of duplex **17** for **34g** at optimized conditions: 200 μ M, 32 h.



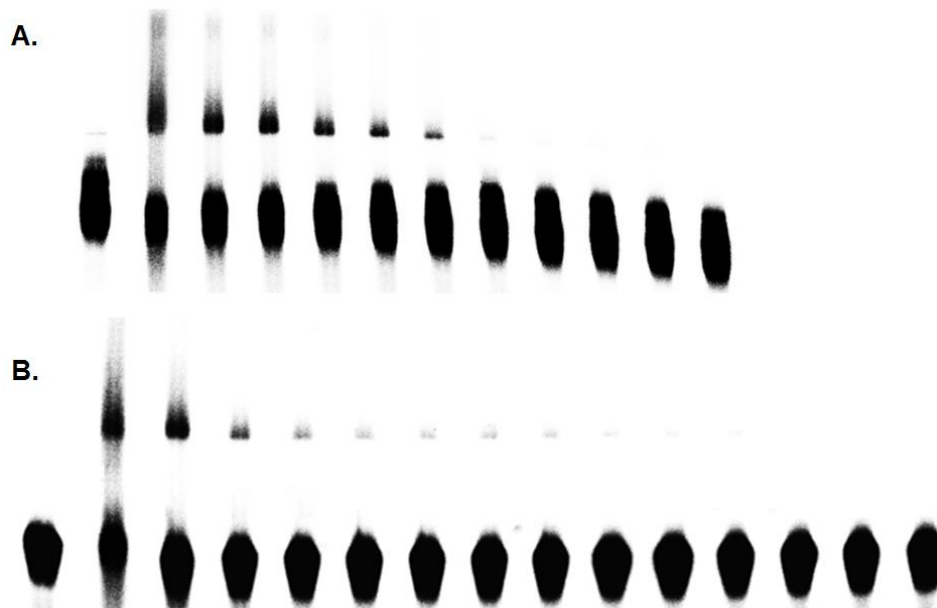
Carbocation and radical trapping with ICL formation of duplex **17** for **34h** at optimized conditions: 500 μ M, 32 h.



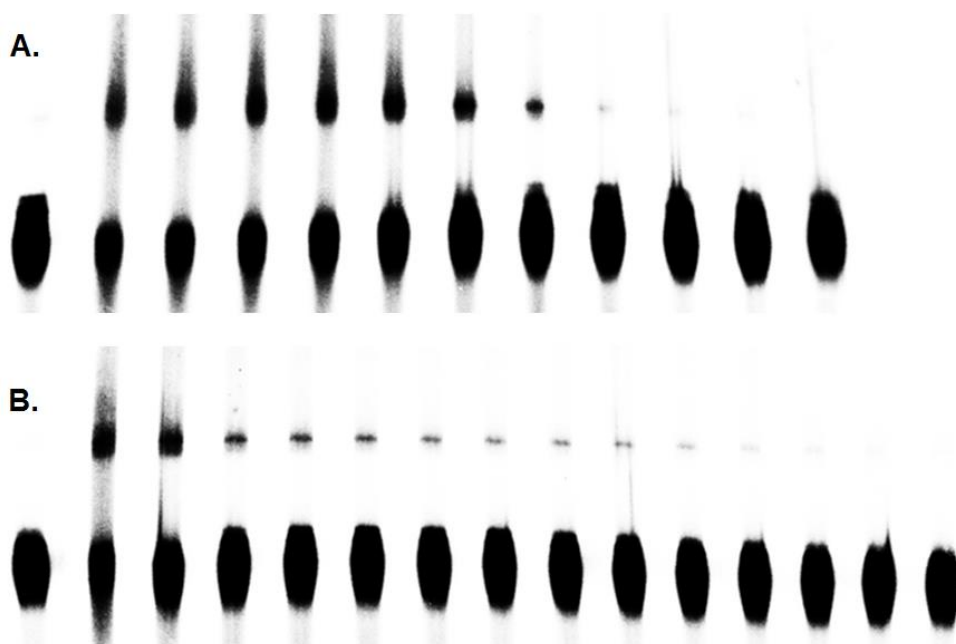
Carbocation and radical trapping with ICL formation of duplex **17** for **34i** at optimized conditions: 300 μM , 36 h.



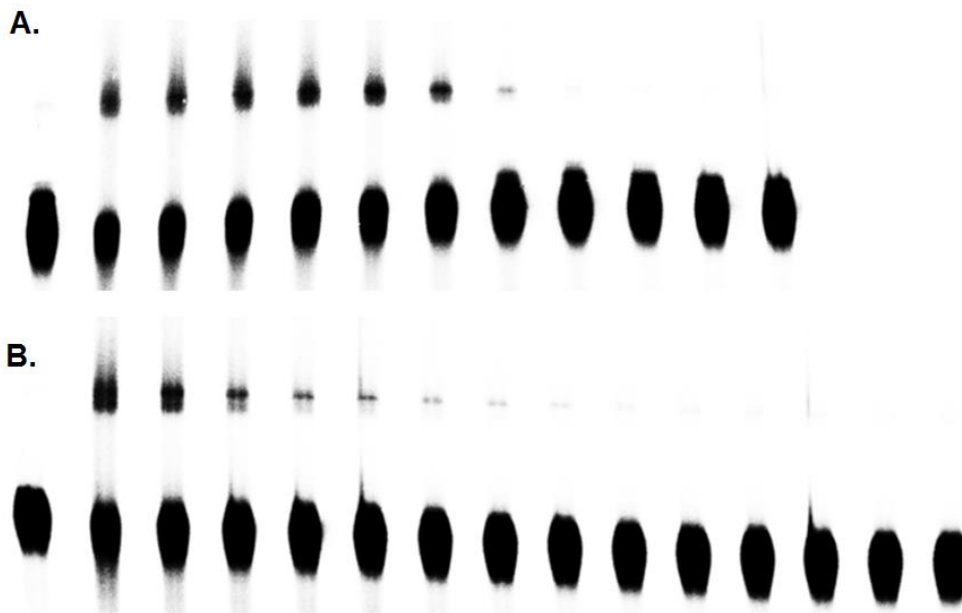
Carbocation and radical trapping with ICL formation of duplex **17** for **34j** at optimized conditions: 200 μM , 10 h.



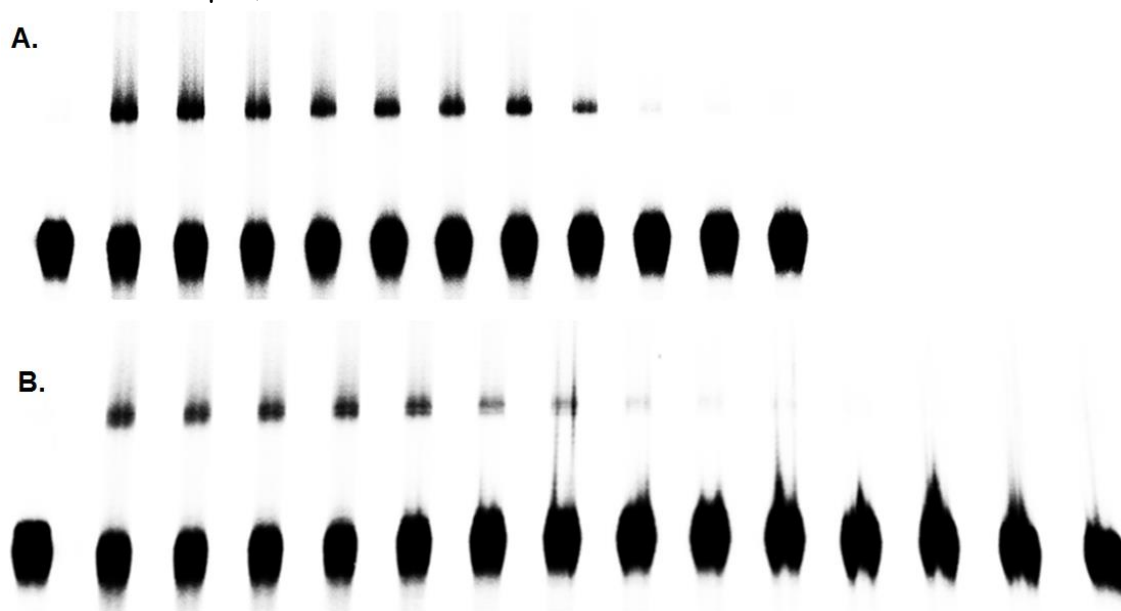
Carbocation and radical trapping with ICL formation of duplex **17** for **35a** at optimized conditions: 400 μ M, 1.5 h.



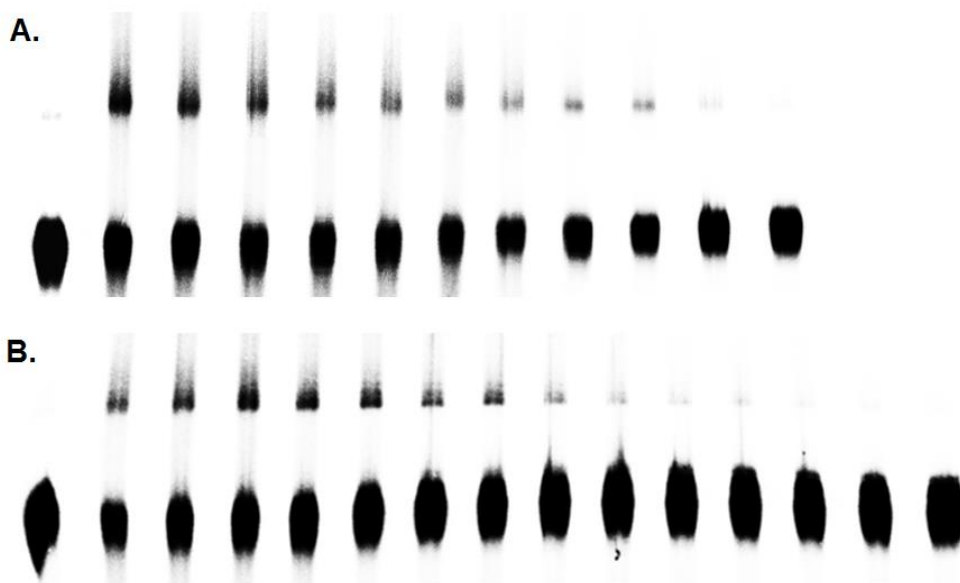
Carbocation and radical trapping with ICL formation of duplex **17** for **35b** at optimized conditions: 400 μ M, 2.5 h.



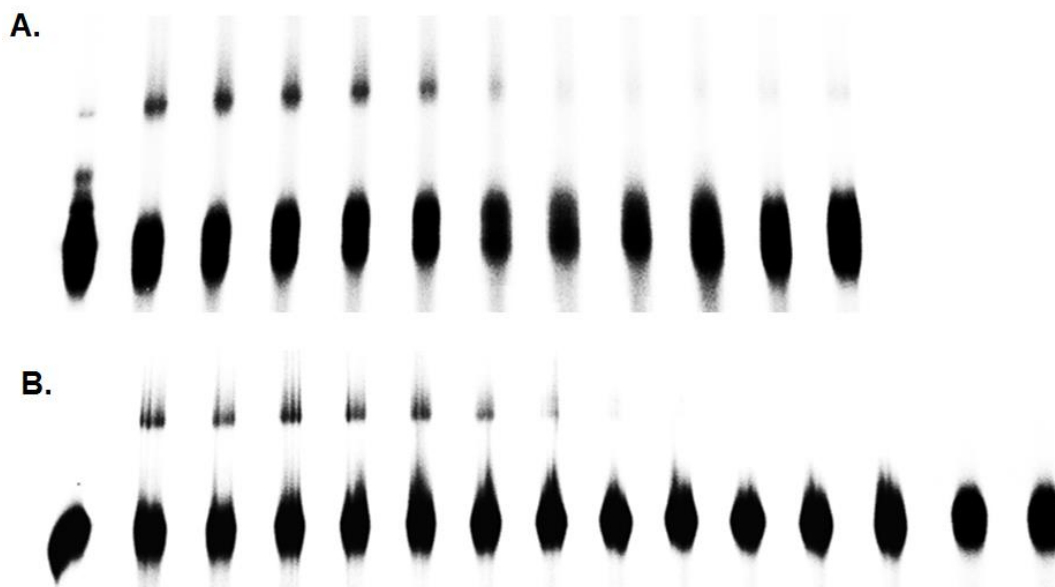
Carbocation and radical trapping with ICL formation of duplex **17** for **35c** at optimized conditions: 300 μM , 3 h.



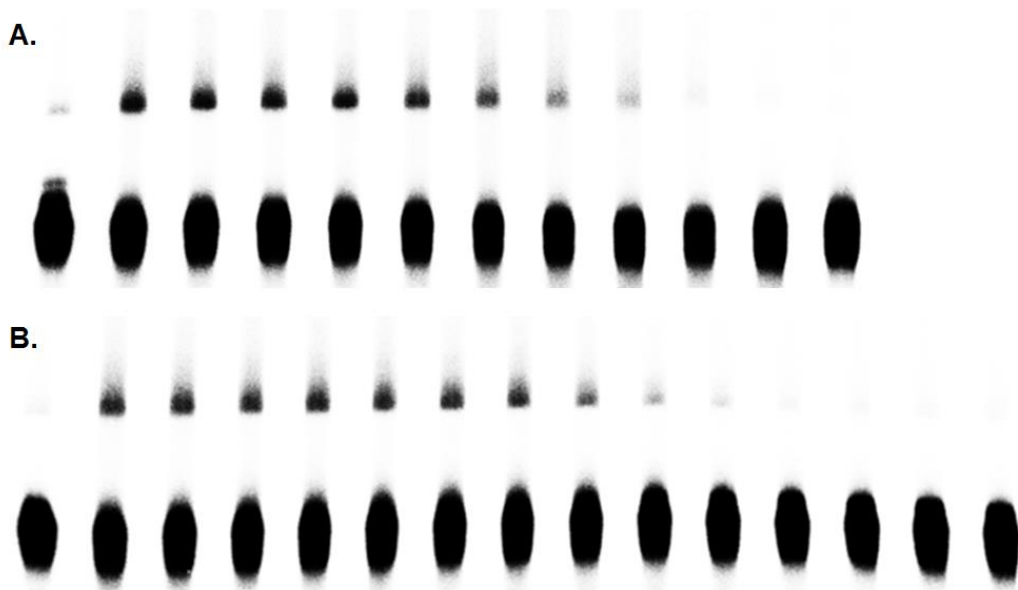
Carbocation and radical trapping with ICL formation of duplex **17** for **35d** at optimized conditions: 500 μM , 10 h.



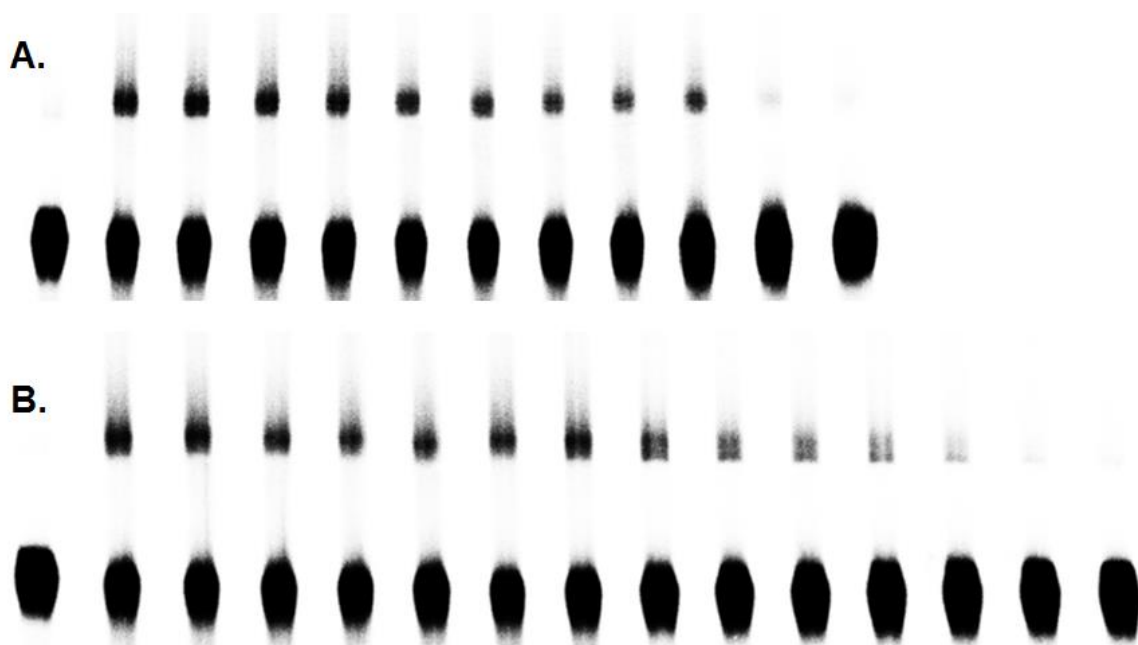
Carbocation and radical trapping with ICL formation of duplex **17** for **35e** at optimized conditions: 500 μM , 20 h.



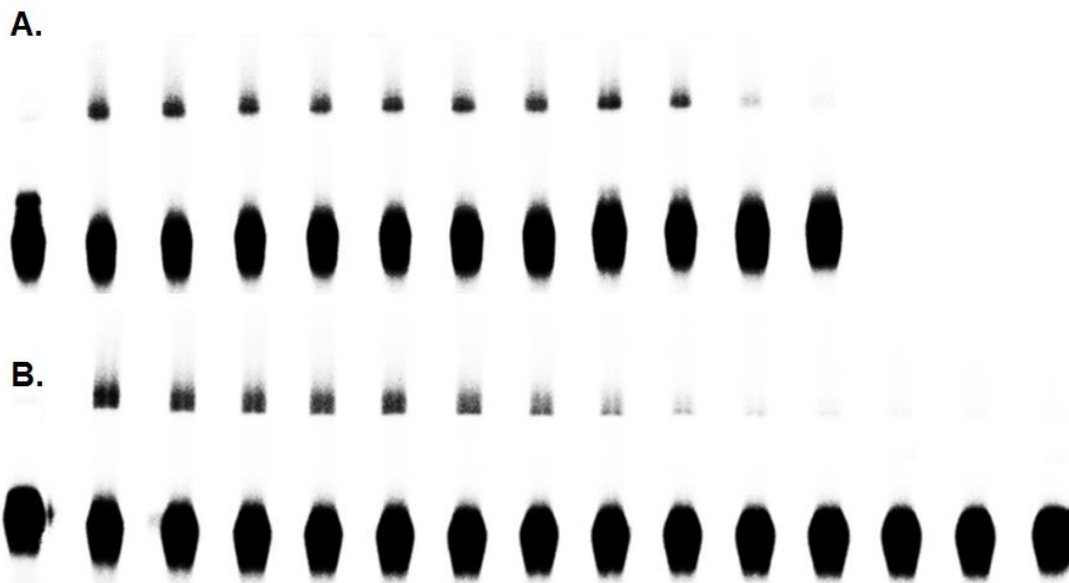
Carbocation and radical trapping with ICL formation of duplex **17** for **35f** at optimized conditions: 600 μM , 28 h.



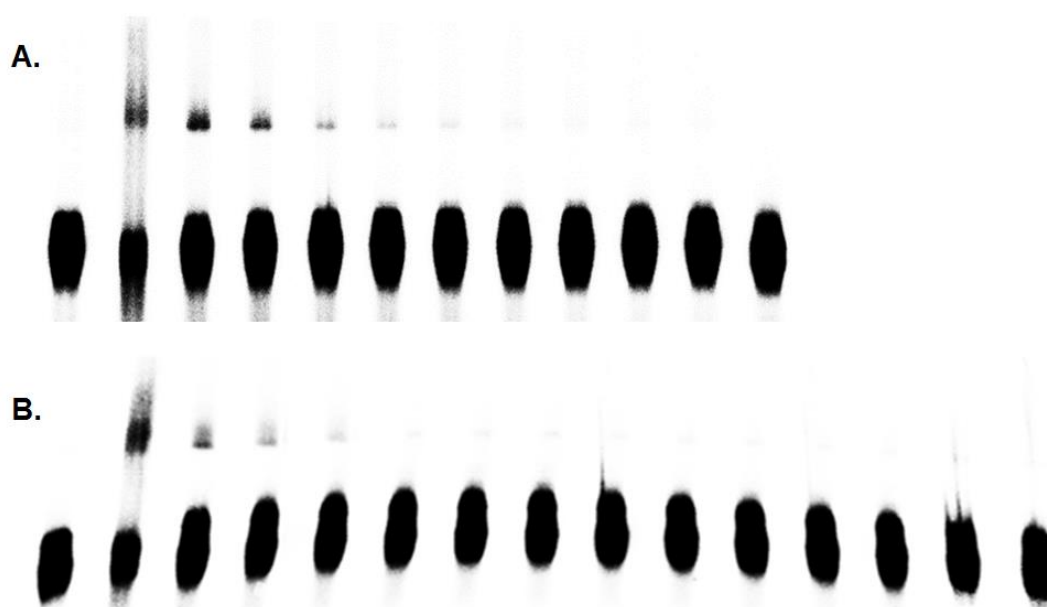
Carbocation and radical trapping with ICL formation of duplex **17** for **35g** at optimized conditions: 500 μ M, 36 h.



Carbocation and radical trapping with ICL formation of duplex **17** for **35h** at optimized conditions: 500 μ M, 24 h.

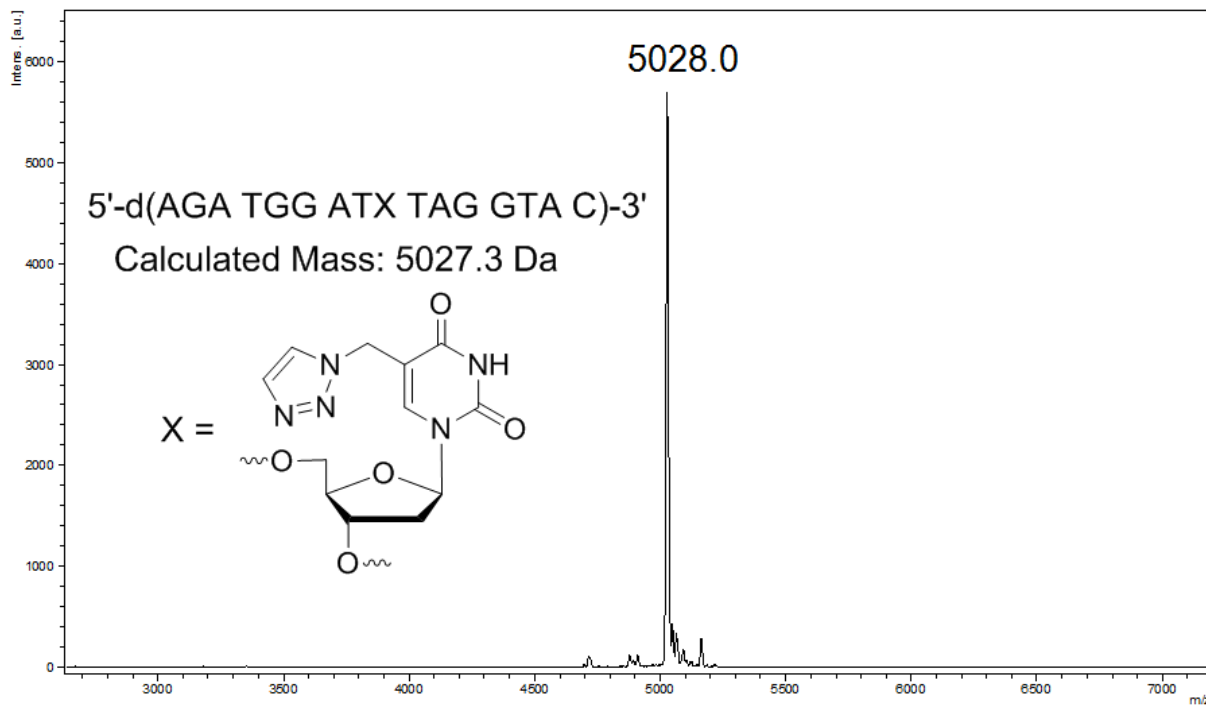


Carbocation and radical trapping with ICL formation of duplex **17** for **35i** at optimized conditions: 500 μ M, 24 h.

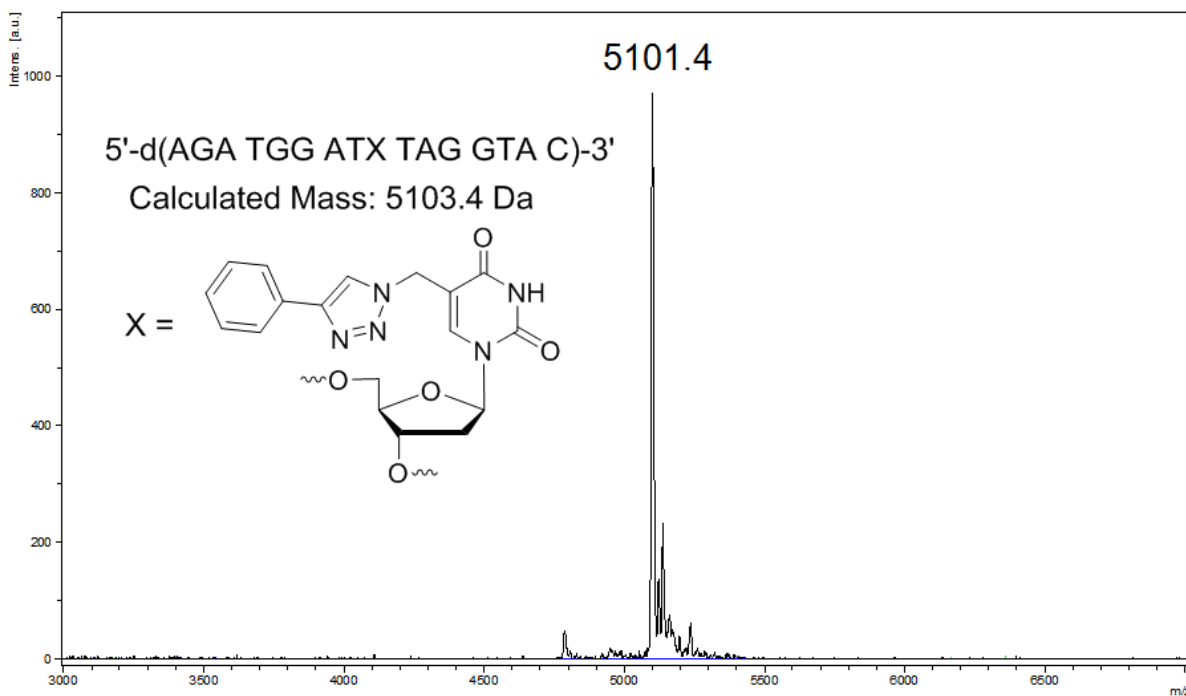


Carbocation and radical trapping with ICL formation of duplex **17** for **35j** at optimized conditions: 500 μ M, 1.5 h.

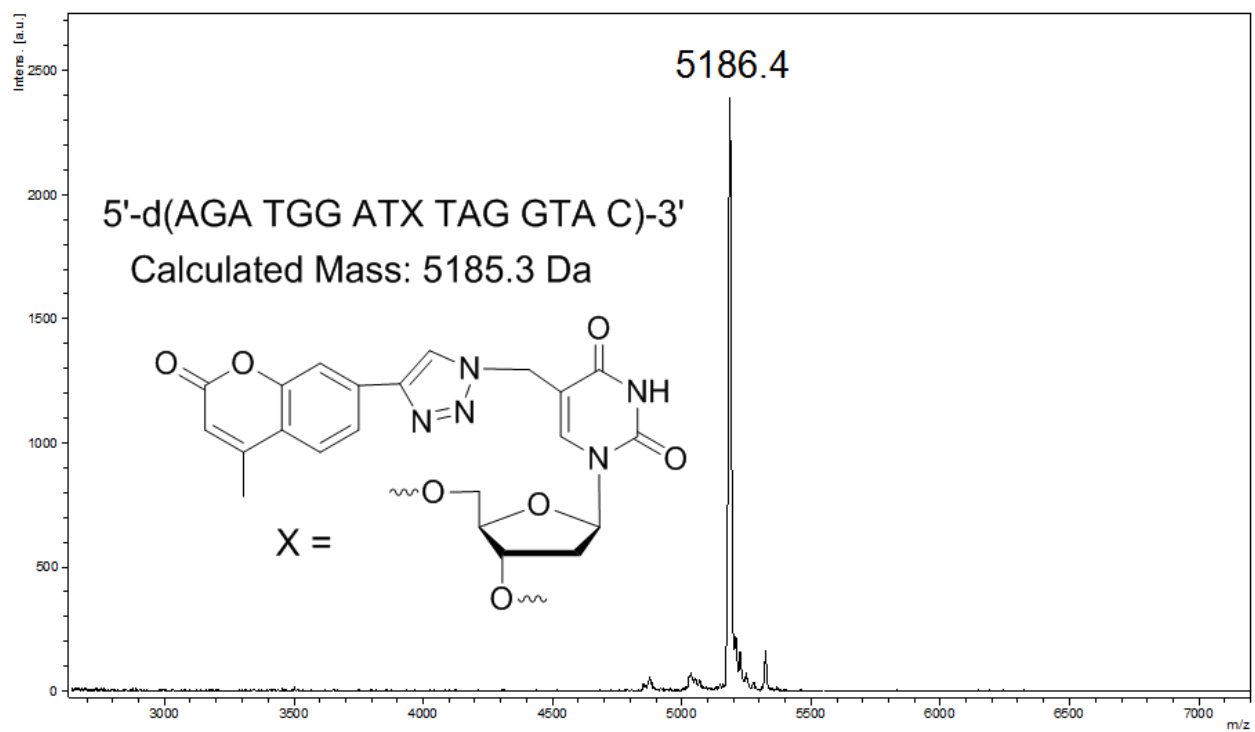
Appendix B: ODN Characterization



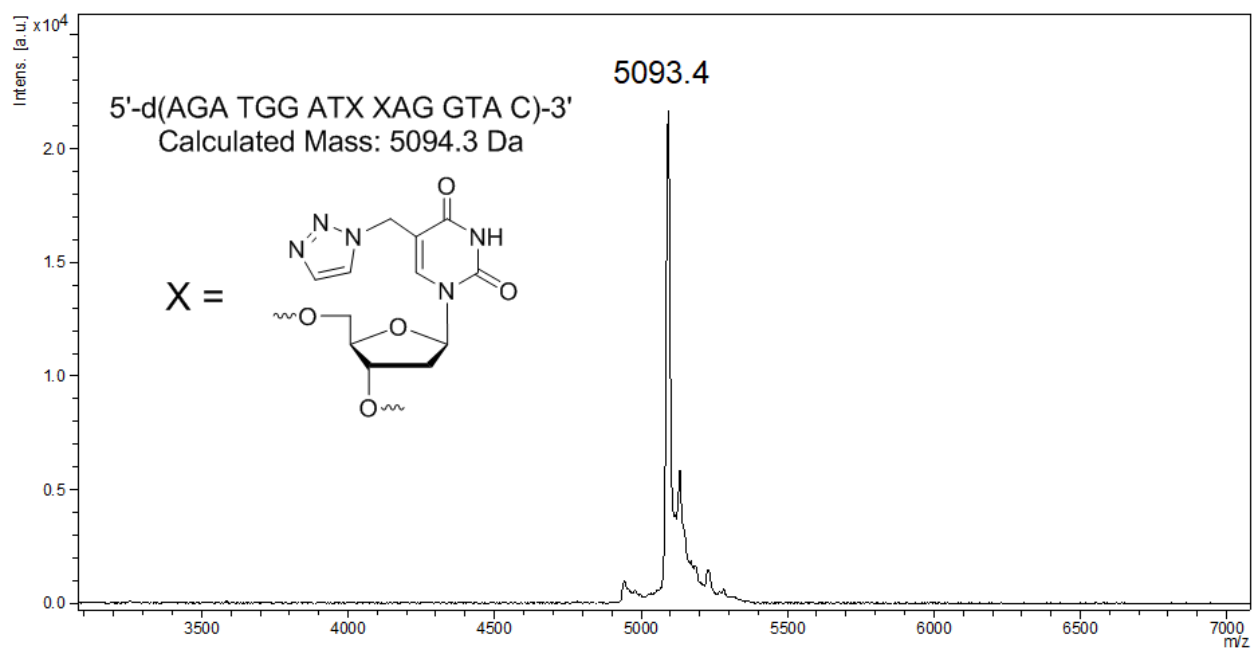
Maldi-TOF-MS spectrum of ODN-50b.



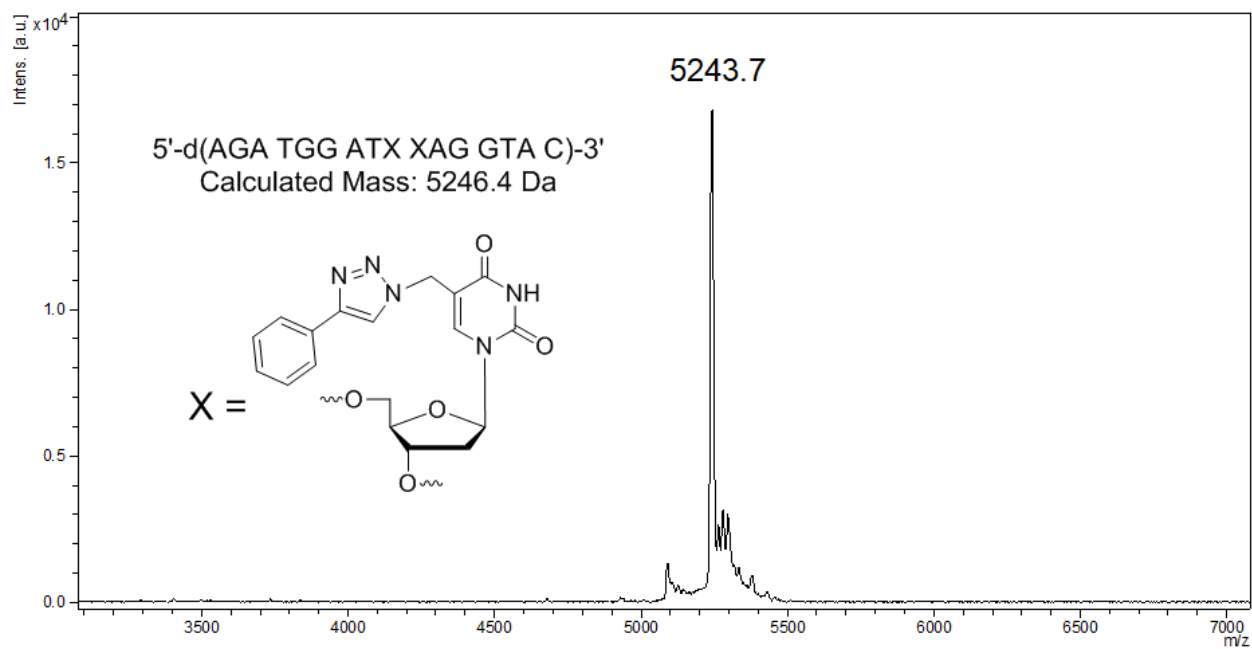
Maldi-TOF-MS spectrum of ODN-51b.



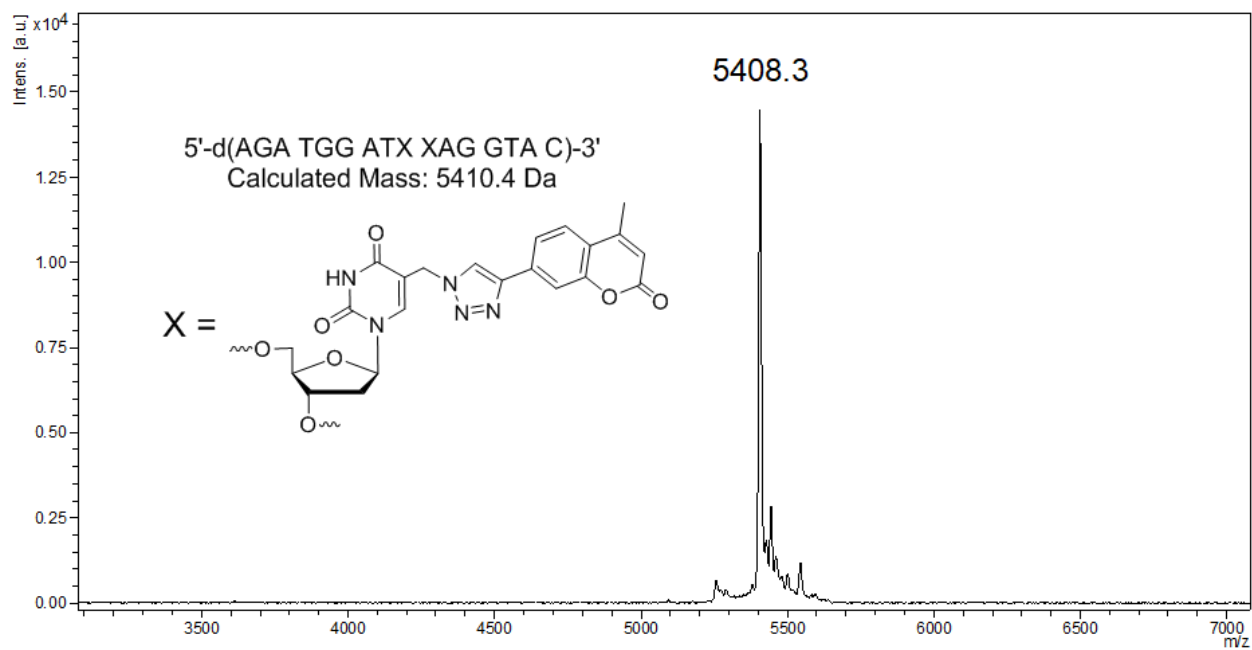
Maldi-TOF-MS spectrum of ODN-52b.



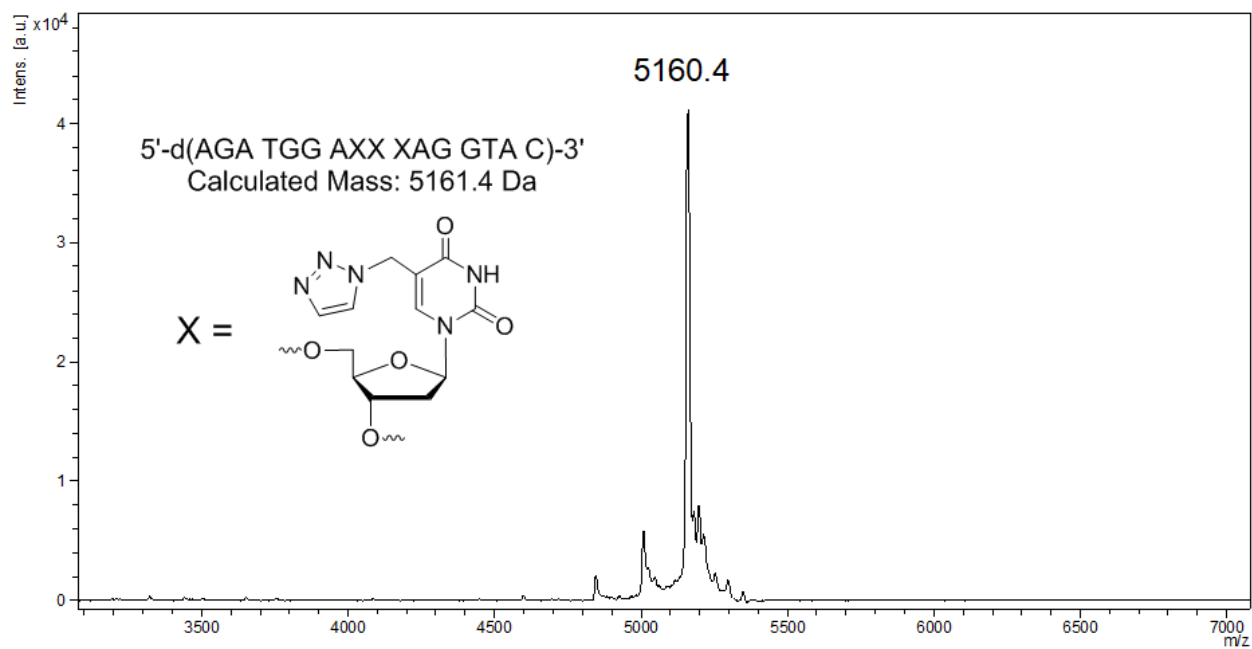
Maldi-TOF-MS spectrum of ODN-53b.



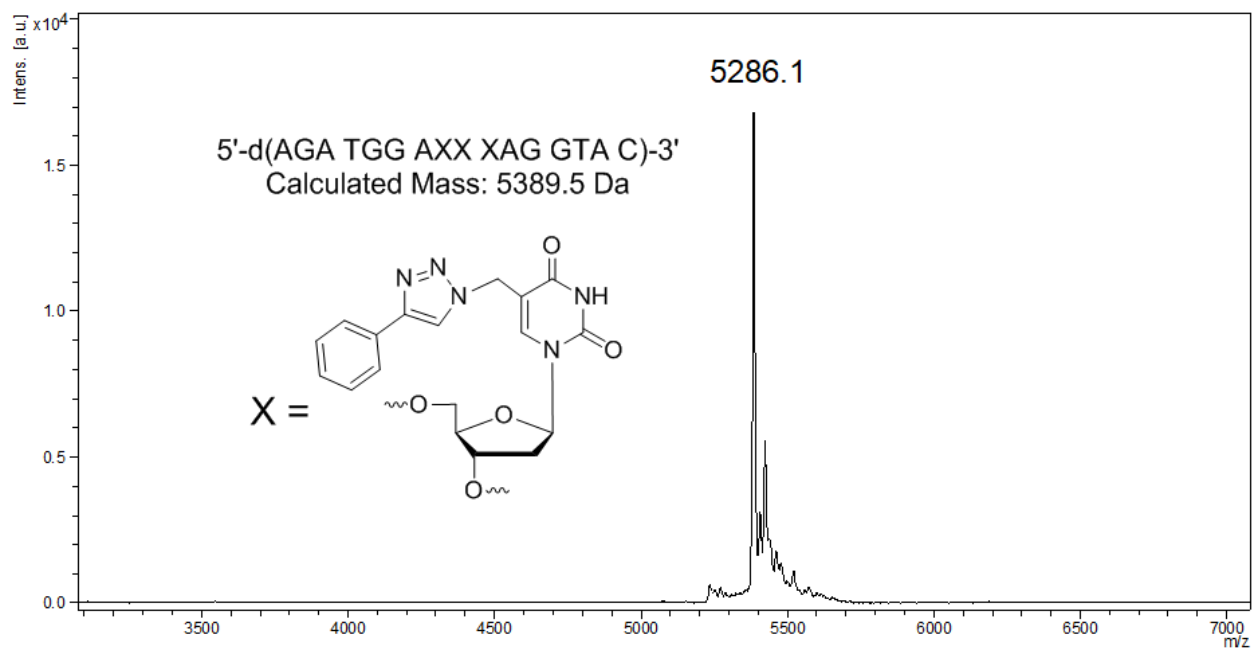
Maldi-TOF-MS spectrum of ODN-54b.



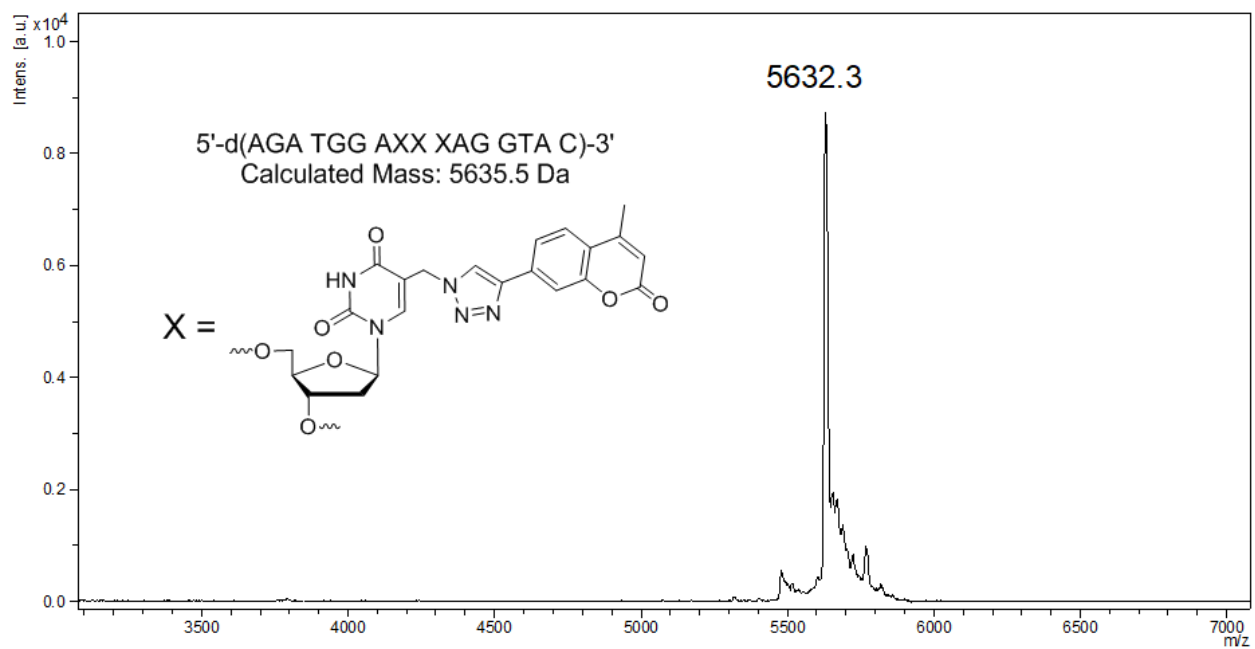
Maldi-TOF-MS spectrum of ODN-55b.



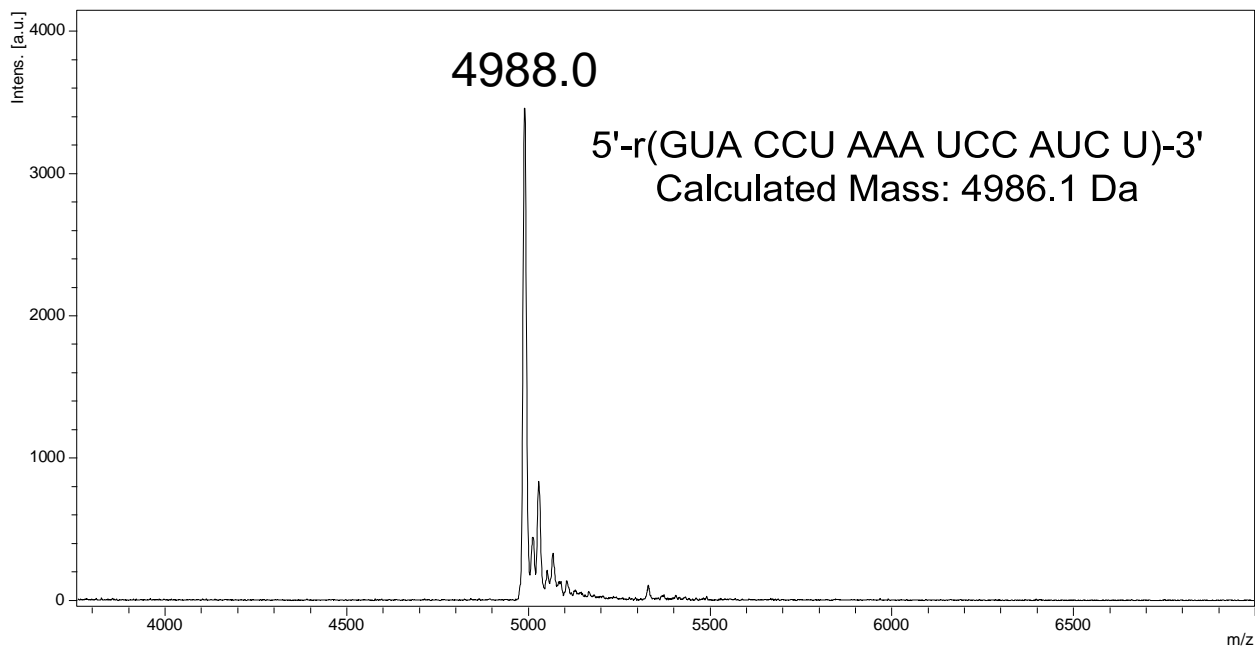
Maldi-TOF-MS spectrum of ODN-56b.



Maldi-TOF-MS spectrum of ODN-57b.



Maldi-TOF-MS spectrum of ODN-58b.



Maldi-TOF-MS spectrum of ODN-59a.

Appendix C: Copy Licenses



RightsLink®

Account Info

Help



Chapter: Chapter Six Novel DNA Cross-Linking Reagents
Book: Advances in Molecular Toxicology
Author: Heli Fan, Xiaohua Peng
Publisher: Elsevier
Date: Jan 1, 2016

Logged in as:
Heli Fan
Account #:
3001358646

LOGOUT

Copyright © 2016 Elsevier B.V. All rights reserved.

Order Completed

Thank you for your order.

This Agreement between Heli Fan ("You") and Elsevier ("Elsevier") consists of your order details and the terms and conditions provided by Elsevier and Copyright Clearance Center.

License number	Reference confirmation email for license number (501440438)
License date	Nov, 01 2018
Licensed Content Publisher	Elsevier
Licensed Content Publication	Elsevier Books
Licensed Content Title	Advances in Molecular Toxicology
Licensed Content Author	Heli Fan, Xiaohua Peng
Licensed Content Date	2016
Licensed Content Volume	10
Licensed Content Issue	n/a
Licensed Content Pages	58
Type of Use	reuse in a thesis/dissertation
Portion	full chapter
Format	electronic
Are you the author of this Elsevier chapter?	Yes
Will you be translating?	No
Order reference number	1
Title of your thesis/dissertation	Inducible DNA Cross-Linking Agents: Design, Synthesis, Mechanism, and Anticancer Activity
Expected completion date	Dec 2018
Estimated size (number of pages)	200
Requestor Location	Heli Fan 1717 E Beverly Rd, #2 MILWAUKEE, WI 53211 United States Attn: Heli Fan
Publisher Tax ID	98-0397604
Billing Type	Invoice

Billing address Heli Fan
1717 E Beverly Rd, #2

MILWAUKEE, WI 53211
United States
Attn: Heli Fan

Total 0.00 USD

CLOSE WINDOW

Copyright © 2018 [Copyright Clearance Center, Inc.](#) All Rights Reserved. [Privacy statement](#). [Terms and Conditions](#).
Comments? We would like to hear from you. E-mail us at customercare@copyright.com

**JOHN WILEY AND SONS LICENSE
TERMS AND CONDITIONS**

Oct 30, 2018

This Agreement between Heli Fan ("You") and John Wiley and Sons ("John Wiley and Sons") consists of your license details and the terms and conditions provided by John Wiley and Sons and Copyright Clearance Center.

License Number	4459070544589
License date	Oct 30, 2018
Licensed Content Publisher	John Wiley and Sons
Licensed Content Publication	Chemistry - A European Journal
Licensed Content Title	Substituents Have a Large Effect on Photochemical Generation of Benzyl Cations and DNA Cross-Linking
Licensed Content Author	Heli Fan, Huabing Sun, Xiaohua Peng
Licensed Content Date	May 7, 2018
Licensed Content Volume	24
Licensed Content Issue	30
Licensed Content Pages	12
Type of use	Dissertation/Thesis
Requestor type	Author of this Wiley article
Format	Electronic
Portion	Full article
Will you be translating?	No
Order reference number	1
Title of your thesis / dissertation	Inducible DNA Cross-Linking Agents: Design, Synthesis, Mechanism, and Anticancer Activity
Expected completion date	Dec 2018
Expected size (number of pages)	200
Requestor Location	Heli Fan 1717 E Beverly Rd, #2 MILWAUKEE, WI 53211 United States Attn: Heli Fan
Publisher Tax ID	EU826007151
Total	0.00 USD
Terms and Conditions	

TERMS AND CONDITIONS

This copyrighted material is owned by or exclusively licensed to John Wiley & Sons, Inc. or one of its group companies (each a "Wiley Company") or handled on behalf of a society with

which a Wiley Company has exclusive publishing rights in relation to a particular work (collectively "WILEY"). By clicking "accept" in connection with completing this licensing transaction, you agree that the following terms and conditions apply to this transaction (along with the billing and payment terms and conditions established by the Copyright Clearance Center Inc., ("CCC's Billing and Payment terms and conditions"), at the time that you opened your RightsLink account (these are available at any time at <http://myaccount.copyright.com>).

Terms and Conditions

- The materials you have requested permission to reproduce or reuse (the "Wiley Materials") are protected by copyright.
- You are hereby granted a personal, non-exclusive, non-sub licensable (on a stand-alone basis), non-transferable, worldwide, limited license to reproduce the Wiley Materials for the purpose specified in the licensing process. This license, **and any CONTENT (PDF or image file) purchased as part of your order**, is for a one-time use only and limited to any maximum distribution number specified in the license. The first instance of republication or reuse granted by this license must be completed within two years of the date of the grant of this license (although copies prepared before the end date may be distributed thereafter). The Wiley Materials shall not be used in any other manner or for any other purpose, beyond what is granted in the license. Permission is granted subject to an appropriate acknowledgement given to the author, title of the material/book/journal and the publisher. You shall also duplicate the copyright notice that appears in the Wiley publication in your use of the Wiley Material. Permission is also granted on the understanding that nowhere in the text is a previously published source acknowledged for all or part of this Wiley Material. Any third party content is expressly excluded from this permission.
- With respect to the Wiley Materials, all rights are reserved. Except as expressly granted by the terms of the license, no part of the Wiley Materials may be copied, modified, adapted (except for minor reformatting required by the new Publication), translated, reproduced, transferred or distributed, in any form or by any means, and no derivative works may be made based on the Wiley Materials without the prior permission of the respective copyright owner. **For STM Signatory Publishers clearing permission under the terms of the [STM Permissions Guidelines](#) only, the terms of the license are extended to include subsequent editions and for editions in other languages, provided such editions are for the work as a whole in situ and does not involve the separate exploitation of the permitted figures or extracts**, You may not alter, remove or suppress in any manner any copyright, trademark or other notices displayed by the Wiley Materials. You may not license, rent, sell, loan, lease, pledge, offer as security, transfer or assign the Wiley Materials on a stand-alone basis, or any of the rights granted to you hereunder to any other person.
- The Wiley Materials and all of the intellectual property rights therein shall at all times remain the exclusive property of John Wiley & Sons Inc, the Wiley Companies, or their respective licensors, and your interest therein is only that of having possession of and the right to reproduce the Wiley Materials pursuant to Section 2 herein during the continuance of this Agreement. You agree that you own no right, title or interest in or

to the Wiley Materials or any of the intellectual property rights therein. You shall have no rights hereunder other than the license as provided for above in Section 2. No right, license or interest to any trademark, trade name, service mark or other branding ("Marks") of WILEY or its licensors is granted hereunder, and you agree that you shall not assert any such right, license or interest with respect thereto

- NEITHER WILEY NOR ITS LICENSORS MAKES ANY WARRANTY OR REPRESENTATION OF ANY KIND TO YOU OR ANY THIRD PARTY, EXPRESS, IMPLIED OR STATUTORY, WITH RESPECT TO THE MATERIALS OR THE ACCURACY OF ANY INFORMATION CONTAINED IN THE MATERIALS, INCLUDING, WITHOUT LIMITATION, ANY IMPLIED WARRANTY OF MERCHANTABILITY, ACCURACY, SATISFACTORY QUALITY, FITNESS FOR A PARTICULAR PURPOSE, USABILITY, INTEGRATION OR NON-INFRINGEMENT AND ALL SUCH WARRANTIES ARE HEREBY EXCLUDED BY WILEY AND ITS LICENSORS AND WAIVED BY YOU.
- WILEY shall have the right to terminate this Agreement immediately upon breach of this Agreement by you.
- You shall indemnify, defend and hold harmless WILEY, its Licensors and their respective directors, officers, agents and employees, from and against any actual or threatened claims, demands, causes of action or proceedings arising from any breach of this Agreement by you.
- IN NO EVENT SHALL WILEY OR ITS LICENSORS BE LIABLE TO YOU OR ANY OTHER PARTY OR ANY OTHER PERSON OR ENTITY FOR ANY SPECIAL, CONSEQUENTIAL, INCIDENTAL, INDIRECT, EXEMPLARY OR PUNITIVE DAMAGES, HOWEVER CAUSED, ARISING OUT OF OR IN CONNECTION WITH THE DOWNLOADING, PROVISIONING, VIEWING OR USE OF THE MATERIALS REGARDLESS OF THE FORM OF ACTION, WHETHER FOR BREACH OF CONTRACT, BREACH OF WARRANTY, TORT, NEGLIGENCE, INFRINGEMENT OR OTHERWISE (INCLUDING, WITHOUT LIMITATION, DAMAGES BASED ON LOSS OF PROFITS, DATA, FILES, USE, BUSINESS OPPORTUNITY OR CLAIMS OF THIRD PARTIES), AND WHETHER OR NOT THE PARTY HAS BEEN ADVISED OF THE POSSIBILITY OF SUCH DAMAGES. THIS LIMITATION SHALL APPLY NOTWITHSTANDING ANY FAILURE OF ESSENTIAL PURPOSE OF ANY LIMITED REMEDY PROVIDED HEREIN.
- Should any provision of this Agreement be held by a court of competent jurisdiction to be illegal, invalid, or unenforceable, that provision shall be deemed amended to achieve as nearly as possible the same economic effect as the original provision, and the legality, validity and enforceability of the remaining provisions of this Agreement shall not be affected or impaired thereby.
- The failure of either party to enforce any term or condition of this Agreement shall not constitute a waiver of either party's right to enforce each and every term and condition of this Agreement. No breach under this agreement shall be deemed waived or

excused by either party unless such waiver or consent is in writing signed by the party granting such waiver or consent. The waiver by or consent of a party to a breach of any provision of this Agreement shall not operate or be construed as a waiver of or consent to any other or subsequent breach by such other party.

- This Agreement may not be assigned (including by operation of law or otherwise) by you without WILEY's prior written consent.
- Any fee required for this permission shall be non-refundable after thirty (30) days from receipt by the CCC.
- These terms and conditions together with CCC's Billing and Payment terms and conditions (which are incorporated herein) form the entire agreement between you and WILEY concerning this licensing transaction and (in the absence of fraud) supersedes all prior agreements and representations of the parties, oral or written. This Agreement may not be amended except in writing signed by both parties. This Agreement shall be binding upon and inure to the benefit of the parties' successors, legal representatives, and authorized assigns.
- In the event of any conflict between your obligations established by these terms and conditions and those established by CCC's Billing and Payment terms and conditions, these terms and conditions shall prevail.
- WILEY expressly reserves all rights not specifically granted in the combination of (i) the license details provided by you and accepted in the course of this licensing transaction, (ii) these terms and conditions and (iii) CCC's Billing and Payment terms and conditions.
- This Agreement will be void if the Type of Use, Format, Circulation, or Requestor Type was misrepresented during the licensing process.
- This Agreement shall be governed by and construed in accordance with the laws of the State of New York, USA, without regards to such state's conflict of law rules. Any legal action, suit or proceeding arising out of or relating to these Terms and Conditions or the breach thereof shall be instituted in a court of competent jurisdiction in New York County in the State of New York in the United States of America and each party hereby consents and submits to the personal jurisdiction of such court, waives any objection to venue in such court and consents to service of process by registered or certified mail, return receipt requested, at the last known address of such party.

WILEY OPEN ACCESS TERMS AND CONDITIONS

Wiley Publishes Open Access Articles in fully Open Access Journals and in Subscription journals offering Online Open. Although most of the fully Open Access journals publish open access articles under the terms of the Creative Commons Attribution (CC BY) License only, the subscription journals and a few of the Open Access Journals offer a choice of Creative Commons Licenses. The license type is clearly identified on the article.

The Creative Commons Attribution License

The [Creative Commons Attribution License \(CC-BY\)](#) allows users to copy, distribute and transmit an article, adapt the article and make commercial use of the article. The CC-BY license permits commercial and non-

Creative Commons Attribution Non-Commercial License

The [Creative Commons Attribution Non-Commercial \(CC-BY-NC\)License](#) permits use, distribution and reproduction in any medium, provided the original work is properly cited and is not used for commercial purposes.(see below)

Creative Commons Attribution-Non-Commercial-NoDerivs License

The [Creative Commons Attribution Non-Commercial-NoDerivs License](#) (CC-BY-NC-ND) permits use, distribution and reproduction in any medium, provided the original work is properly cited, is not used for commercial purposes and no modifications or adaptations are made. (see below)

Use by commercial "for-profit" organizations

Use of Wiley Open Access articles for commercial, promotional, or marketing purposes requires further explicit permission from Wiley and will be subject to a fee.

Further details can be found on Wiley Online Library

<http://olabout.wiley.com/WileyCDA/Section/id-410895.html>

Other Terms and Conditions:

v1.10 Last updated September 2015

Questions? customercare@copyright.com or +1-855-239-3415 (toll free in the US) or +1-978-646-2777.

CURRICULUM VITAE

Heli Fan

Place of birth: Sishui, Shandong, China

Education:

Ph.D., University of Wisconsin-Milwaukee, December 2018

Major: Organic Chemistry, (Advisor: Prof. Xiaohua Peng)

M.S., Nankai University (China), June 2010

Major: Physical Chemistry, (Advisor: Prof. Danhong Wang)

B.S., Liaocheng University (China), June 2007

Major: Chemistry, (Advisor: Bing Liu)

Publications:

Fan, H.; Chen W.; Asad Uz Zaman; Peng, X. H₂O₂-Inducible DNA cross-linking agents and its biological activity investigation. (In preparation)

Fan, H.; Peng, X. The aromatic substituents and the benzylic leaving groups greatly affect DNA interstrand cross-link formation by biphenyl agents. (In preparation)

Fan, H.; Peng, X. Novel prototype compounds as efficient photo-activated DNA cross-linkers: design, synthesis, and mechanistic investigation. (In preparation)

Fan, H.; Sun H.; Haque M.; Peng, X. The effect of triazole-modified thymidines on DNA and RNA duplex stability. (Submitted)

Chen, W.⁺; **Fan, H.**⁺; Balakrishnan, K.; Wang, Y.; Sun, H.; Fan, Y.; Gandhi, V.; Arnold, L.; Peng, X. Discovery and Optimization of Novel Hydrogen Peroxide Activated Aromatic Nitrogen Mustard Derivatives as Highly Potent Anticancer Agents. *J. Med. Chem.* **2018**, *61*, 9132–9145. (+: Equal contribution)

Lin, Z.[‡]; **Fan, H.**[‡]; Zhang, Q.; Peng, X. Design, Synthesis, and Characterization of Binaphthalene Precursors as Photo-Activated DNA Interstrand Cross-Linkers. *J. Org. Chem.*, **2018**, *83*, 8815–8826. (‡: Equal contribution)

Fan, H.; Sun, H.; Peng, X. Substituents Have a Large Effect on Photochemical Generation of Benzyl Cations and DNA Cross-Linking. *Chem. Eur. J.* **2018**, *24*, 7671-7682.

Wang, Y.⁺; **Fan, H.**⁺; Balakrishnan, K.; Lin, Z.; Cao, S.; Chen, W.; Fan, Y.; Guthrie, Q.; Sun, H.; Teske, K.; Gandhi, V.; Arnold, L.; Peng, X. Hydrogen peroxide activated quinone methide precursors with enhanced DNA cross-linking capability and cytotoxicity towards cancer cells. *Eur. J. Med. Chem.* **2017**, *133*, 197-207. (+: Equal contribution)

Sun, H.⁺; **Fan, H.**⁺; Eom, Y.; Peng, X. Coumarin-Induced DNA Ligation, Rearrangement to DNA Interstrand Cross-Links, and Photo-Release of Coumarin Moiety. *ChemBioChem* **2016**, *17*, 2046-2053. (+: Equal contribution)

Fan, H.; Peng, X. Novel DNA Cross-Linking Reagents. *Advances in Molecular Toxicology-Chapter 6*. **2016**, *10*, 235-292.

Wang, Y.; Lin, Z.; **Fan, H.**; Peng, X. Photo-Induced DNA Interstrand Cross-Link Formation by Naphthalene Boronates via a Carbocation. *Chem. Eur. J.* **2016**, *22*, 10382-10386.

Sun, H.; **Fan, H.**; Peng, X. Quantitative DNA Interstrand Cross-Link Formation by Coumarin and Thymine: Structure Determination, Sequence Effect, and Fluorescence Detection. *J. Org. Chem.* **2014**, *79*, 11359-11369.

Awards:

Distinguished Dissertation Fellowship, 2017-2018, UWM.

Distinguished Graduate Student Fellowship, 2016-2017, UWM.

UW-Milwaukee Chancellor's Graduate Fellowship, 2014-2018, UWM.

Scholarship for Academic Achievement, 2003-2007, Liaocheng University, China.